Proceedings of 12th Annual Symposium on Research and Industrial Training of Department of Electronics

9th October 2025

Department of Electronics
Faculty of Applied Sciences
Wayamba University of Sri Lanka
Kuliyapitiya,60200
Sri Lanka.

Proceedings of
12th Annual Symposium on Research and Industrial Training
of
Department of Electronics

9th October, 2025

Annual Symposium on Research and Industrial Training of Department of Electronics

Department of Electronics
Faculty of Applied Sciences
Wayamba University of Sri Lanka
Kuliyapitiya, 60200
Sri Lanka

ISSN 2362 0560
Designing and Printing at the Department of Electronics,
Faculty of Applied Sciences, Wayamba University of Sri Lanka, Kuliyapitiya

Message from the Dean

It is with great pleasure that I pen this message to mark the 12th Annual Symposium on Research and Industrial Training of the Department of Electronics, ASRITE-2025.

ASRITE has been organized annually by the Department of Electronics, and through this symposium, the Department has been providing a platform for the final year undergraduates to present their research findings, share knowledge, and strengthen and consolidate their essential soft skills. The symposium focuses on final year Research Projects and Industrial Training projects of the fourth-year undergraduates majoring in Electronics.

The subject of Electronics being heavily practical oriented, the undergraduate curriculum has placed emphasis on giving students hands-on experience in practical applications of electronics. The Department has gone a step further to provide the students with experience in all aspects of research, too. Presentation of research outcomes, and dissemination and sharing of knowledge are essential areas students are expected to get trained in. ASRITE is held to facilitate this training and to provide opportunities for soft skills development. The academic staff of the Department has taken a lot of effort to make this opportunity available for students before they graduate, with the earnest expectation that the undergraduates take the full advantage of this valuable opportunity.

ASRITE is one of the two major research events in the academic calendar of the faculty and it is staged as a result of the team work of the Department. I take this opportunity to thank the Head of the Department of Electronics, all the Senior and junior academic staff at the Department, and the Coordinator of ASRITE-2025 for all the efforts taken to stage the event successfully. The continued support from the University administration and from the Deputy Registrar and the non-academic staff of the Department towards the success of the event is greatly appreciated.

The internal and external supervisors who supervised the research projects and the industrial training, and the organizations that provided industrial training deserve special appreciation. The Training Director and officials at NAITA who coordinated and regulated the industrial training program also deserve our appreciation. The valued assistance extended by reviewers and session panelists in evaluating publications and presentations is recorded with much appreciation.

I wish the Symposium every success and congratulate the presenters on their achievements.

Prof. L.D.R.D. Perera
Dean / Faculty of Applied Sciences
09.10.2025

Foreword

I am very happy to write this forward to the proceedings of the 12th Annual Symposium on Research and Industrial Training of the Department of Electronics (ASRITE) 2025. The Department of Electronics has been organizing this symposium continually from 2014 in order to promote undergraduate research.

The symposium represents the hard work towards research studies, innovations and short term solutions for Industrial training effort of 4th year undergraduates attached to our department.

I would like to express my gratitude to Prof. L.D.R.D. Perera , the Acting Vice Chancellor (and the Dean Faculty of Applied Sciences) of Wayamba University of Sri Lanka for his guidance and support. Moreover, I should thank Mr. Thilina Payagala, Coordinator of ASRITE-2025 for organizing the event and preparing this proceeding.

My thanks goes to Prof. I.M.K. Feranado, Head, Department of Physics, for accepting our invitation for the keynote speech of the event, and all evaluators for their valuable service for chairing and evaluating presentations. Also, the thanks go to all officials who contributed to make the event success, Electronic Society undergraduates and the department academic support staff who work hard for organizing the event.

Finally, I thank all the presenters in ASRITE 2025 and hope that this symposium will further stimulate graduates to undertake research in various Electronics related fields for the development of their career as well for the development of the country.

Dr. Y.A. Ajith Kumarayapa
Head,
Department of Electronics,
Faculty of Applied Sciences,
Wayamba University of Sri Lanka.

CONTENTS

Individual Research Papers

1. **AN IOT POWERED SMART SAFETY HELMET FOR WORKERS IN CONSTRUCTION SITES** **1**
   C.K.P. Chandrasena*, G.A.K.S. Perera

2. **SOLAR-POWERED ELEPHANT DETECTION SYSTEM FOR RAILWAY SAFETY USING AI IMAGE PROCESSING AND IR LASERS** **9**
   D. M. T. N. B. Dissanayake*, G. A. K. S. Perera

3. **ARTIFICIAL INTELLIGENCE DRIVEN AUTONOMOUS ROBOT CAR FOR REAL-TIME DECISION MAKING IN DISASTER AREA** **17**
   E.A. Wanigasekara*, Y.A.A. Kumarayapa

4. **SMART WATER MONITORING SYSTEM FOR ENHANCED FISH FARMING MANAGEMENT** **25**
   K.E. Senanayake*, W.A.S.Wijesinghe

5. **DEVELOPMENT OF A LOW-COST PORTABLE DATA ACQUISITION SYSTEM WITH WIRELESS DATA TRANSMISSION AND REAL-TIME MONITORING** **33**
   S.H.R.S. De Silva*, W.A.S. Wijesinghe

6. **PORTABLE IOT-BASED COMMUNICATION AND SECURITY SYSTEM FOR FISHING BOATS** **41**
   W.W.C.D. Fernando*, M.A.A. Karunarathna

7. **MEASURING THE WATER QUALITY OF HOUSEHOLD WATER TANKS** **49**
   M.A.P.R. Marasingha*, K.P. Vidanapathirana

8. **SENSOR-BASED PADDY DISEASE DETECTION SYSTEM USING MACHINE LEARNING AND REMOTE-SENSING DRONES** **56**
   D.N.S.Perera*, Y.A.A.Kumarayapa

9. **SOIL ELECTRICAL CONDUCTIVITY MEASURING DEVICE WITH CLOUD DATABASE ANALYTICS FOR AGRICULTURE** **64**
   J.K.A.S.W. Jayasuriya*, S.R.L. Gunawardhana

10. **REMOTE-CONTROLLED PET CARE ROBOT** **72**
    W.K. Lakshani*, K.P. Vidanapathirana

11. **AUTOMATED SYSTEM TO PREVENT PREMATURE COAGULATION AND ENHANCE QUALITY OF NATURAL RUBBER LATEX BY CONTROLLING TEMPERATURE AND PH VALUE** **78**
    L.G.R.H. Lihinigama*, M.A.A. Karunarathna

12. **DEVELOPMENT OF AN AGITATOR CONTROL SYSTEM FOR A BIOGAS DIGESTER** **85**
W.B.R.Sirimanna *, M.A.A.Karunarathna

13. **DESIGN AND OPTIMIZATION OF A WIDEBAND PRINTED MICROSTRIP LOG-PERIODIC DIPOLE ARRAY ANTENNA** **92**
B.P.H.S. Wijayanthi1*, J.M.J.W. Jayasinghe, W.D.T.M. Premathilake

14. **TRAFFIC MANAGEMENT SYSTEM FOR REAL-TIME TRAFFIC FLOW** **100**
P.T.H. Pathirana*, M.A.A. Karunarathne

15. **FABRIC DEFECT IDENTIFICATION USING IMAGE PROCESSING** **107**
H.K.A.H.D.Gimhani*, P.G.T.R.Payagala

16. **IOT POWERED CATTLE TRACKING AND MONITORING SYSTEM** **115**
M.S.M.N. Perera*, G.A.K.S. Perera

17. **IOT-BASED WASTE MANAGEMENT SYSTEM** **123**
T.D. Wijesuriya*, G.A.K.S. Perera

18. **AIR CONDITIONER AUTOMATION BY GPS DATA OF USER** **130**
M.B.Y. Silva*, P.G.T.R. Payagala

19. **REWARD-BASED SMART RECYCLE BIN WITH WASTE SORTING SYSTEM** **137**
S.P.G.N.M Gunathilaka*, S.R.L. Gunawardhana

20. **UNIVERSAL EFI SYSTEM FOR ALL FOUR-CYLINDER CARBURETOR MOTORCYCLES (WITHOUT MAPPING)** **145**
P.M. Hettiarachchi*, K.P. Vidanapathirana

21. **AUTONOMOUS FIREFIGHTING ROBOT FOR HOME SAFETY** **153**
P.D.C. Jayashan*, L.D.R.D. Perera

22. **A TIMER AND SENSOR-BASED GAS DISCONNECTING SYSTEM** **161**
P.V.S. Madhumalika*, J.M.J.W. Jayasinghe

23. **SOLAR TRACKING SYSTEM WITH SMART CLEANING TECHNOLOGY** **170**
R.N.N. Prabodanee*, Dr. Y.A.A. Kumarayapa

24. **AUTONOMOUS PORTABLE WATER QUALITY CHECKER** **176**
W.T. Sangeeth*, S.R.L. Gunawardhana

25. **AUTOMATED INTELLIGENT FALL DETECTION AND ALERT SYSTEM FOR ELDERS** **184**
D.G.P.M.Shantha*, Dr. W.A.S.Wijesinghe

26. **PROTOTYPE DEVELOPMENT OF A WHEELCHAIR CONTROLLER WITH FACIAL GESTURE RECOGNITION FOR ENHANCED ACCESSIBILITY** **192**
H.W.D.Wasana*, W.A.S.Wijesinghe

27. **LOW-COST 3D SCANNING METHOD FOR SMALL OBJECTS WITH HIGH ACCURACY** **198**
E.A.H Bhagya*, P.G.T.R. Payagala

Industrial Research Papers

28. **DEVELOPMENT OF AN IOT-ENABLED REAL TIME TEMPERATURE MONITORING AND ALERT SYSTEM FOR LABORATORY REFRIGERATORS** **203**
J.K.A.S.W. Jayasuriya*, Y.A.A. Kumarayapa, M. Wijemanne

29. **INDUSTRIAL SAFETY AND EMERGENCY SHUTDOWN SYSTEM WITH GSM ALERTS** **209**
W.K.Lakshani*, M.A.A. Karunarathna, G.P.U.U. Kumara

30. **PCB SOLDERING HOT PLATE WITH AUTOMATED AIR ASSIST** **215**
L.G.R.H. Lihinigama*, P.G.T.R. Payagala

31. **DESIGN AND IMPLEMENTATION OF SMART WATER QUALITY MONITORING SYSTEM** **222**
W.B.R.Sirimanna*, L.D.R.D. Perera

32. **DESIGN AND CONSTRUCTION OF AN AUTOMATED DEVICE TO MEASURE THE USAGE OF A HIGH-PRESSURE CLEANING MACHINE** **230**
B.P.H.S. Wijayanthi*, Y.A.A. Kumarayapa, R.A.A.N. Ranasinghe

33. **DESIGN AND IMPLEMENTATION OF A SCINTILLATION DETECTOR USING SILICON PHOTOMULTIPLIER** **238**
H.K.A.H.D. Gimhani*, W.A.S.Wijesinghe, Prasad Mahakumara

34. **VOIP CALL RECORDING SYSTEM FOR ANALOG RECORDERS USING HANDSET AUDIO TAPPING AND ANALOG SIGNAL AMPLIFICATION** **244**
M.S.M.N. Perera*, S.R.L. Gunawardhana, H.A. Priyantha

35. **CURRENT SENSOR-BASED ALERT SYSTEM FOR DETECTING SUCTION BLOCKAGES IN VACUUM CLEANERS** **252**
T.D. Wijesuriya*, W.A.S. Wijesinghe, R.A.A.C. Ranasinghe

36. **SOLAR-OPTIMIZED ENERGY CONTROLLING SYSTEM FOR AUTOMATIC WEATHER OBSERVATION SYSTEM (AWOS)** **259**
M.B.Y. Silva1*, K.P. Vidanapathirana, H.A. Priyantha

37. **EXTERNAL POWER-SUPPLIED SIGNAL BOOSTER FOR LTE TELEPHONES AND ROUTERS** **267**
P.M. Hettiarachchi*, M.A.A. Karunarathne, M.I.P Premarathne

38. **A BROADBAND SIGNAL STRENGTH MAPPING SYSTEM** **273**
P.D.C. Jayashan*, S.R.L. Gunawardhana

39. **BATTERY - POWERED PORTABLE TOOLKIT FOR TESTING AND VERIFYING TELECOMMUNICATION EQUIPMENT** **281**
P.V.S. Madhumalika*, J.M.J.W. Jayasinghe, I.H.C. Prasanga Kumara

40. **DEVELOPMENT OF A FREQUENCY MEASUREMENT DEVICE FOR SHORT WAVE DIATHERMY (SWD) MACHINES** **286**
R.N.N. Prabodanee*, G.A.K.S. Perera, T.V.A. Ruwansiri

41. **AUTOMATED FUNCTIONALITY DETECTION SYSTEM FOR OUTDOOR ADVERTISING** **292**
W.T. Sangeeth*, P.G.T.R. Payagala

42. **A SURGE PROTECTION SYSTEM FOR 4–20 mA ANALOG SIGNAL LINES** **300**
D.G.P.M.Shantha*, J.M.J.W. Jayasinghe, G.G.C.P.Kumara

43. **GESTURE-CONTROLLED DASHBOARD FOR PRODUCT SALES MONITORING** **307**
H.W.D.Wasana*, P.G.T.R. Payagala

44. **DEVELOPMENT OF A MICROCONTROLLER-BASED COUNTER FOR SCINTILLATION DETECTOR** **313**
E.A.H. Bhagya*, K.P. Vidanapathirana, P. Mahakumara

AN IOT POWERED SMART SAFETY HELMET FOR WORKERS IN CONSTRUCTION SITES

C.K.P. Chandrasena*, G.A.K.S. Perera
Department of Electronics, Wayamba University of Sri Lanka, Kuliyapitiya, Sri Lanka
*kavindraprathibhani99@gmail.com

ABSTRACT

The construction industry, while being a key contributor to economic development, is also recognized as one of the most hazardous occupational sectors globally. Furthermore, construction workers are prone to numerous safety hazards such as ground level and height level falls, exposure to poisonous fumes, electrocution, extreme weather conditions, and operating heavy machinery. In most cases, personal protective equipment offered is usually inadequate, especially in the case of remote locations where construction supervision is not available. In light of these issues, this study proposes an IoT-based smart safety helmet intended for construction workers. The construction safety helmet is designed to monitor the working conditions and the construction workers in real time. The smart helmet integrates several sensors like a gyroscope and an accelerometer for fall detection, a gas and a DHT22 sensor for gas and temperature / humidity monitoring respectively. It also consists of a GPS module for real time geolocation, an ESP32 microcontroller for operation and data processing. Remote construction sites are often devoid of Wi-Fi or cloud service and the proposed system relies on a GSM module for data transmission. A web application powered by ThingSpeak allows site managers to track labor site conditions in real-time, receive automated alerts, and respond through a multi-channel system comprising of a buzzer, dashboard alerts, and SMS notifications. Test results validated the real-time accuracy and reliability of the helmet's sensing modules and its ability to transmit data. The design of the helmet enhances its practicality and efficiency, especially in construction settings where workplace hazards and the risk of accidents are prevalent by merging low-cost, lightweight, and dependable communication technologies.

Keywords: **S**afety Helmet, **I**oT, **C**onstruction Workers

1.0 INTRODUCTION

The construction industry is a main driver of economic growth in a developing country like Sri Lanka. On the other hand, it has been recognized as one of the most hazardous sectors in plenty of countries around the world, with a high rate of workplace accidents, injuries and fatalities. Workers in construction sites have to handle diverse activities with many risks like falling objects, slipping from higher elevations, breathing toxic gases and exposing to extreme temperatures. The most common type of accident that occurred in Sri Lankan construction sites is falls from height, which constituted around 22% of all construction workers' on-the-job accidents [1]. Apart from that,17 % of accidents happened because of falling debris or objects [1,2]. According to the data, 13% of incidents fell under the categories of "machinery accidents" and "electrocution" [1,2]. In addition, 11%, 7%, and 6% of all incidents that happened on Sri Lankan construction sites over the previous ten years were caused by "being caught between objects," "slips/trips and falls," and "fires and explosions," respectively [1,2]. Hence, safety measures are most important on a construction site to avoid many accidents that may result in the loss of precious lives and serious injuries. However, most accidents are coupled with imperfect use of personal protective equipment and/or depending on the low-quality equipment. And also, there are no effective observation mechanism at the event of any possible accident in many sites, further increasing the number of deaths and injuries. Hence, it is very important to make suitable protective devices available for the workers in sites and at the same time, to ensure the real-time hazardous event detection mechanism guaranteeing the safety of the workers.

There are many prior systems rely on AI-driven systems or Internet of Things (IoT) cloud platforms [3,4]. These, however, are powerful, but not appropriate for resource constrained environments as they require higher costs, internet availability, and greater power consumption. Another explanation utilizes short-range communication modules such as RF and HC12 which restrict operational range and are prone to conflict in complex site conditions [5,6]. Mining-oriented helmets exhibit useful gas and temperature monitoring but remain heavily cloud-dependent and often overlook essential features such as fall or impact detection [7]. Just like smart helmets with Wi-Fi and LoRa connectivity, which have been the focus of much research, their use in the real world of construction has major shortcomings. Systems with Wi-Fi rely on constant internet access which is never available on makeshift or remote construction sites [8]. LoRa systems, despite their longer ranges, offer minimal data rates and low-range interference in dense environments, making them unsuitable for construction.[9]. Bluetooth systems, while inexpensive and efficient, only provide low bitrate and short coverage, thus becoming irrelevant for construction sites [10]. All of these shortcomings point out the problem why the majority of designs are unable to give accurate coverage with low latency for safety on construction sites. This system stands out with its GSM-based communication approach, unlike previously designed smart helmets. This is useful in construction sites where a stable Wi-Fi or cloud connection is not feasible.

IOT-enabled smart safety helmet that was designed under the proposed study will provide wireless sensor networks for the real-time environmental conditions monitoring from the perspective of individual workers at construction sites. This helmet, intended with sensors to monitor hazardous gases and integrated with a fall detection and alerting system, contains continuous monitoring of the surroundings of the worker. Additionally, location identification will make sure that the worker's exact position on-site is tracked with high precision. This lets a central control station receive information in real-time to notify both the worker and the manager at the site in time in the event of hazardous conditions or accidents. Such a personalized location-aware approach raises the bar on safety by ensuring risks are identified at points as close to the worker as possible, reducing accident likelihood and improving overall safety in high-risk settings.

2.0 EXPERIMENTAL

2.1 System Overview

A comprehensive literature survey was conducted on existing smart helmet systems, identifying their communication techniques, sensing mechanism, and power requirements to identify and determine the functional requirements of the system. The functional block diagram of the system is shown in Fig. 1. The system introduces a gyroscope and accelerometer sensor to detect sudden falls or impacts, a GPS module for real-time worker location tracking to identify the location when a sudden emergency occurs. Temperature, humidity, and certain flammable gases are traced and measured using environmental sensors. In this system, the microcontroller acts as the central processing unit for the data collected from the sensors. It manages the control logic, processes sensor data, and interfaces with the other system elements through command messaging. A GSM module is used for continuous data transmission to site managers. Unlike the systems dependent on Wi-Fi, this procedure ensures that the data coming from sensors on the helmet continuously reaches the control center in very remote or less developed areas. The SIM800L module is powered by a 3.7 V battery, while the rest of the system is powered separately by another 3.7 V battery.

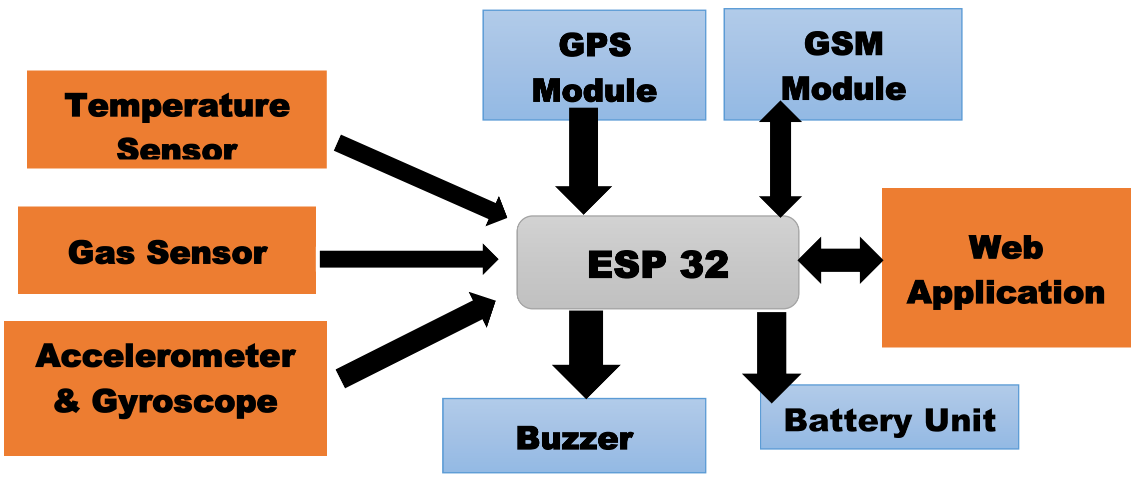

Figure 1: Block diagram of the system

2.2 Hardware Implementation

Figure 2 below illustrates the circuit diagram of the system.

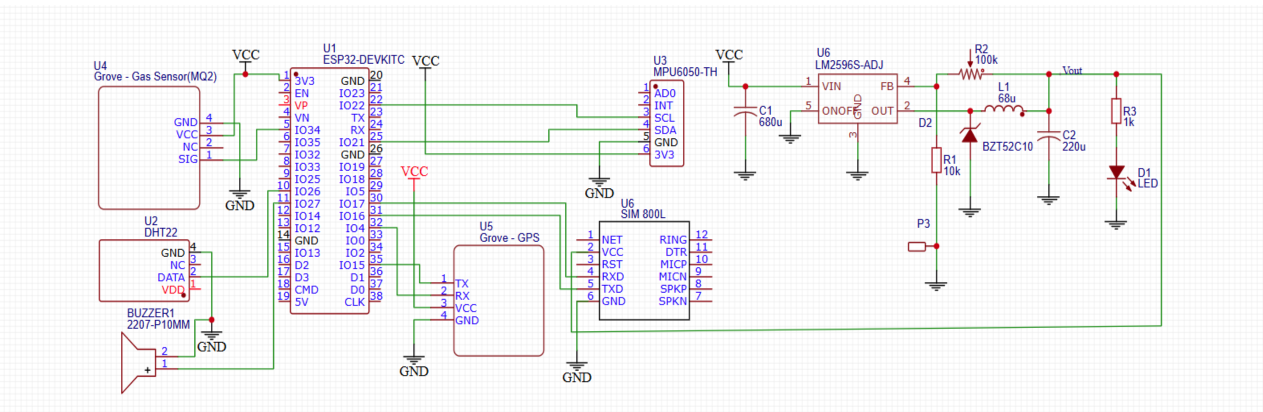

Figure 2: Circuit diagram of the system

Informed by the identified functional requirements, the development of the smart helmet system integrated the modules for sensing, processing, communication, and power into a single, compact, and wearable platform. ESP 32 was selected as the microcontroller to coordinate all system operations. MQ2 gas sensor, NEO-6M GPS module, Buzzer module, DHT 22 temperature and humidity sensor, MPU6050 gyroscope and accelerometer sensor, SIM800L GSM/GPRS module with Antenna were used as the sensor modules for the smart safety helmet. 2A-rated LM2596 DC-DC buck converter was employed to provide a stable 4 V output with up to 2 A current, for the SIM800L module. A 2A-rated LM2596 DC-DC buck converter was employed to provide a stable 4 V output with up to 2A of current for the SIM800L module.

The circuit diagram was implemented in a dot-board as shown in Fig. 3.

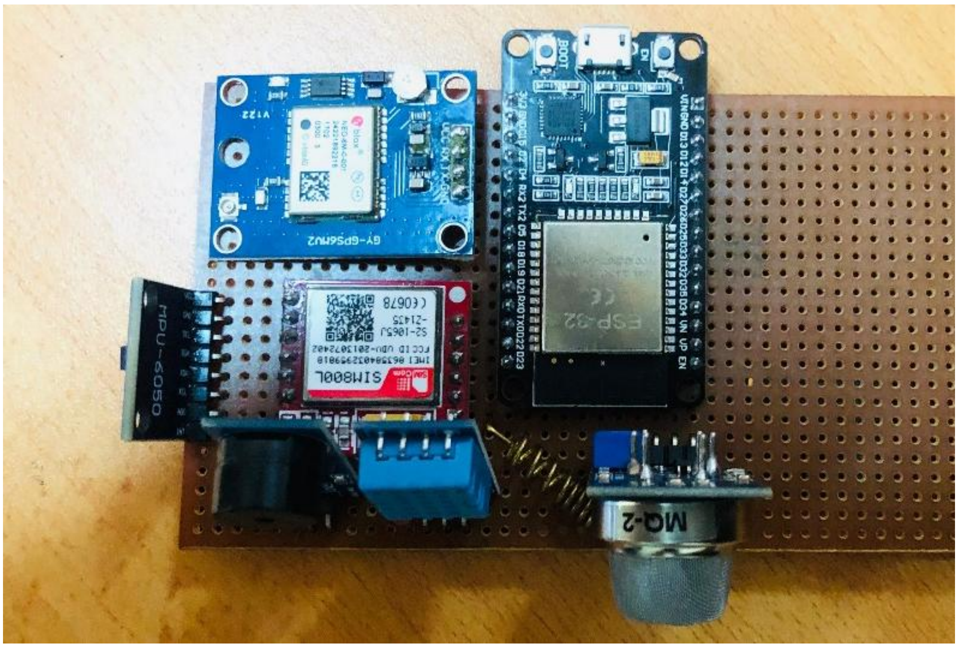

Figure 3: Proto type circuit design on the dot board

2.3 Calibration and Algorithms

Combined acceleration magnitude and tilt angle analysis was used as fall detection. The magnitude of acceleration was determined as:

$$A_m = \sqrt{a_x^2 + a_y^2 + a_z^2} \quad \text{--------} \ [1]$$

Where ; A_m = Total acceleration

a_x = Acceleration along the x axis

a_y =Acceleration along the y axis

a_z = Acceleration along the z axis

A fall was detected when;

$A_m > 2.5$ g over a 300 ms interval and (ii) the MPU6050 gyroscopes confirmed total inversion (>150° tilt) over the same interval. The two conditions were necessitated to reduce false alarms.

The sensors of environmental sensors were calibrated using standard smartphone sensors. Hazardous conditions were determined as >40 °C, >85% RH and a gas level >250 ppm. The GPS module was tested against geolocation on the smartphone with the accuracy measured in meters.

2.4 Software Implementation
Web dashboard serves as the interface between the IoT system and end users, allowing site managers to monitor workers' safety from any internet-connected device without installing special software. The web application is allied with the backend of the IoT cloud server, where all the sensor readings of the helmet are stored. Thing Speak is an open-source platform that is widely used in academic and research applications due to its compatibility with microcontrollers such as ESP32, Arduino, and other IoT boards. It provides the prospects of real-time data collection, visualizing the collected data in the form of charts, the ability to create plugins and apps for collaborating with web services, social network, and other APIs the system transmit data such as temperature, humidity, gas level, fall detection status, and GPS coordinates by using the HTTP post method. In dangerous situations, the web application can be set up to automatically mark the impacted employee on the map and also show alerts and create warning sounds on the manager's PC.

3.0 RESULTS AND DISCUSSION

3.1 Functionality Verification
The prototype IOT powered smart safety helmet was designed as shown in Fig.

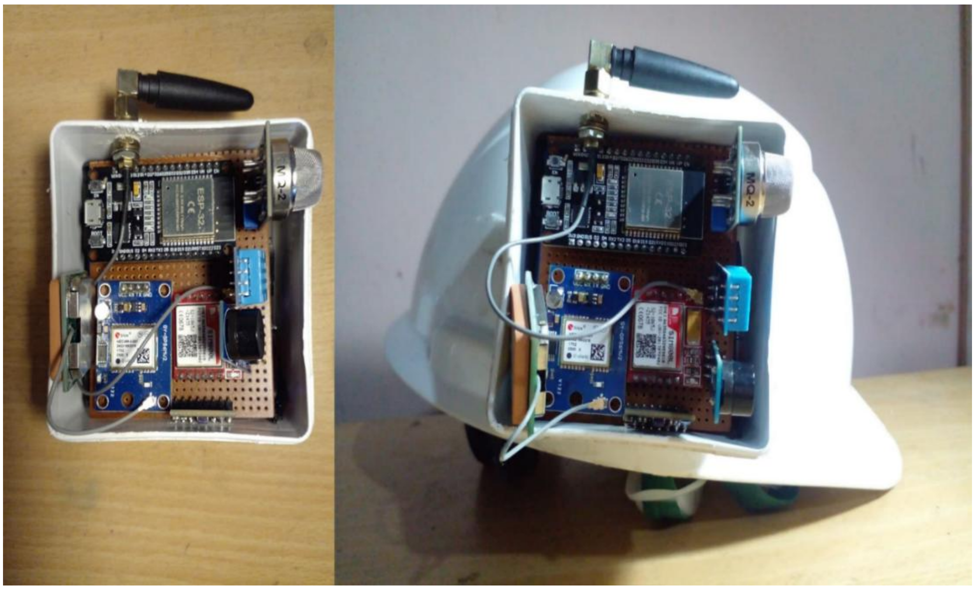

Figure 4: Final design of the system

The SIM800L GSM module directly was fed with a 3.7 V LiPo battery to provide enough current and constant operation. The rest of system components, such as the ESP32, GPS, and environmental sensors were driven by another 3.7 V Li-ion battery. The two batteries were equipped in the back section of the helmet to enable the balance of weight and easy replacement.

All modules were tested separately and contrasted with smartphone readings. GPS and environmental sensor validation is shown in Table 1. The results of fall detection are summarized in Table 2.

Table 1: Environmental and GPS Sensor Accuracy

Parameter	Sensor Value	Smartphone Value	Accuracy (%)
Temperature (°C)	37.0	36.5	98.6
Humidity (%)	83	80	96.3
GPS Error (m)	±3.2	±3.0	93.8

Table 2: Fall Detection Performance

Test Condition	Acceleration (g)	Tilt Angle (°)	Detected Fall	Correct Detection (%)
Drop from 1.0 m (upright)	2.8	160	Yes	95
Drop from 1.5 m (side)	3.1	170	Yes	96
Sudden head tilt only	1.4	120	No	–
Running motion	2.2	<150	No	–

These findings indicate that the system needed a spike in the acceleration and a huge overturn to recognize a fall. In case when there was only high acceleration as in the case of running or jumping, there were no reported falls since the tilt was not more than 150 degrees. Similarly, in the case of tilt only like when the helmet was gently tilted, which the system did not consider because there was no acceleration of more than 2.5 g. This two-state technique minimized false alarms due to normal activities and only real impact-based falls were identified with accuracy of 95–96%.

3.2 Real Time Data Transmission and Alerts

The data measured through the system was uploaded to the Thing Speak server. The prototype was designed to upload values in real time. Simultaneously, it checked whether the total value exceeded the threshold value. The collected data was transmitted to the web dashboard using the Read API Key. The web dashboard displayed live readouts for all sensor parameters, enabling site supervisors to monitor conditions in real-time as shown in Fig. 5a. The system immediately triggered the local buzzer and generated an alert on the dashboard while simultaneously sending an SMS notification to the site manager whenever a sensor reading exceeded its safety threshold. Fig. 5b shows the message of the warning. This multi-channel alert mechanism ensures that abnormal conditions are quickly communicated to both the worker and the manager, consistent with smart helmet safety designs [11].

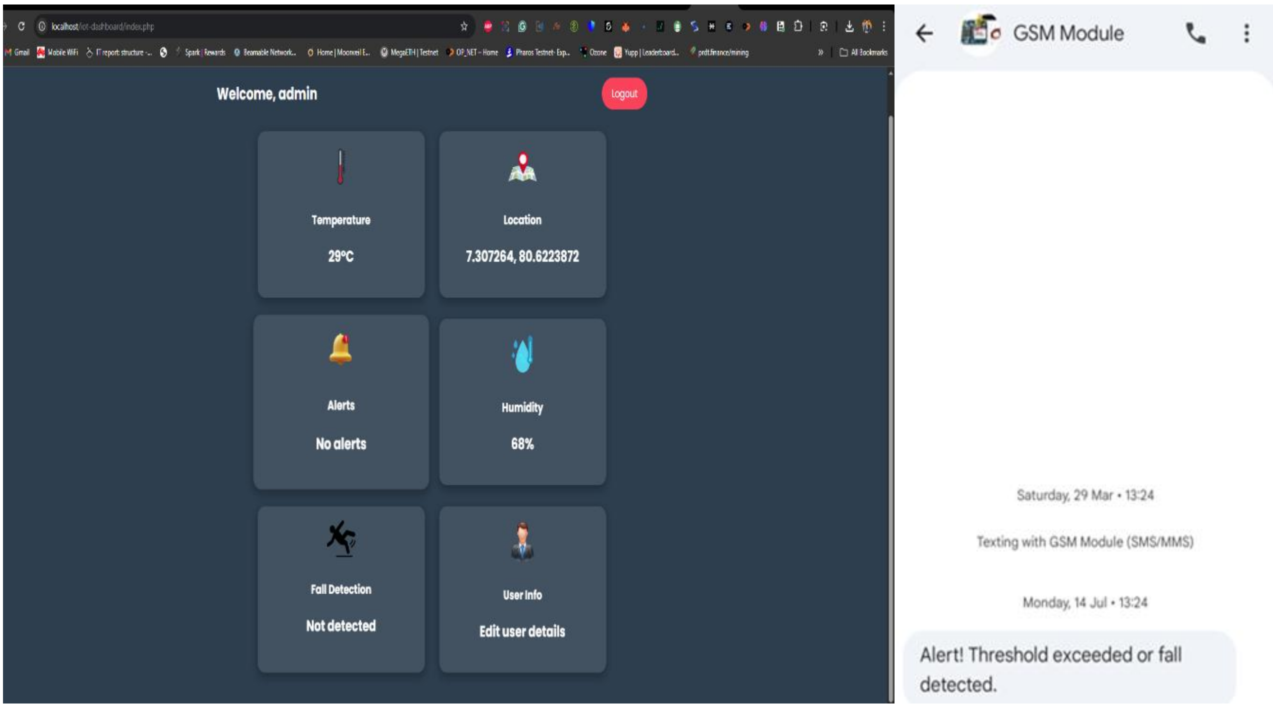

(a) (b)

Figure 5: Web dashboard interface and (b) SMS warning from GSM

4.0 CONCLUSION

A smart safety helmet that is connected to the IoT was developed and tried successfully. Acceleration magnitude and tilt angle analysis performed well together in the detection of falls in the system, with a high accuracy of 95-96%, as validated by controlled drop tests. The smartphone readings were very similar to the environmental readings and there was general consensus of over 96 % on temperature, humidity and GPS location. The real-time alert system was based on GSM and was effective in sending information to the web dashboard and an SMS channel.

Limitations are the existence of weak GSM signal in very remote places and slight inaccuracies in GPS direction under heavy buildings. Further efforts in the work shall closely consider hybrid GSM-LoRa communication, solar-aided power supply, and sensor fusion based on AI to enhance robustness and make it applicable to a wider range.

ACKNOWLEDGEMENT

The authors would like to express sincere gratitude and appreciation to academic and other staff of the Department of Electronics, Faculty of Applied Sciences, Wayamba University of Sri Lanka for the support provided during the study.

REFERENCES

[1] M. Wijesekara, P. Fernando, and N. Gunarathna, "Causes for death and injuries in construction industry in Sri Lanka," in *Proceedings of the SLIIT International Conference on Engineering and Technology*, 2022, pp. 453–464, doi: https://doi.org/10.54389/xgmp5935.

[2] R. Rameezdeen, C. Pathirage, and S. Weerasooriya, "Study of construction accidents in Sri Lanka," *Built-Environment Sri Lanka*, vol. 4, no. 1, pp. 27–32, 2006, doi: https://doi.org/10.4038/besl.v4i1.7650.

[3] N. Narayan, K. Dadhania, and B. Somavanshi, "IoT based Smart Helmet for Industrial Workers," B.Tech Project Report, Vellore Institute of Technology, Vellore, India, 2021.

[4] Campero-Jurado, S. Márquez-Sánchez, J. Quintanar-Gómez, S. Rodríguez, and J. M. Corchado, "Smart Helmet 5.0 for industrial internet of things using artificial intelligence," *Sensors*, vol. 20, no. 21, Art. no. 6241, Nov. 2020, doi: https://doi.org/10.3390/s20216241.

[5] P. Dharani, T. Ganesh, V. Gopinath, and Y. S. Vali, "Smart Safety Helmet for Bike Riders using IoT," *International Journal of Multidisciplinary Technovation*, vol. 2, no. 4, pp. 21–30, 2020, doi: https://doi.org/10.34256/irjmt2044.

[6] P. Kuhar, K. Sharma, Y. Hooda, and N. K. Verma, "Internet of Things (IoT) based Smart Helmet for Construction," *Journal of Physics: Conference Series*, vol. 1950, no. 1, Art. no. 012075, Jul. 2021, doi: https://doi.org/10.1088/1742-6596/1950/1/012075.

[7] Y. Mali, N. Sawant, S. Patil, S. Kumari, and M. Anose, "Smart helmet for coal mining," *International Journal of Advanced Research in Science Communication and Technology*, pp. 17–23, 2023, doi: https://doi.org/10.48175/ijarsct-8064.

[8] Y. Kim and Y. Choi, "Smart Helmet-Based proximity warning system to improve occupational safety on the road using image sensor and artificial intelligence," *International Journal of Environmental Research and Public Health*, vol. 19, no. 23, Art. no. 16312, Dec. 2022, doi: https://doi.org/10.3390/ijerph192316312.

[9] G. S. Arun Kumar, R. Singh, A. Gehlot, and S. V. Akram, "LoRa enabled Real-time Monitoring of Workers in Building Construction Site," *International Journal of Electrical and Electronics Research*, vol. 10, no. 1, pp. 41–50, Jan. 2022, doi: https://doi.org/10.37391/ijeer.100106.

[10] K.-B. Seo, S. D. Min, L. H. Lee, and M. Hong, "Design and Implementation of Construction site Safety management System using Smart Helmet and BLE Beacons," *Journal of Internet Computing and Services*, vol. 20, no. 3, pp. 61–68, Jun. 2019, doi: https://doi.org/10.7472/jksii.2019.20.3.61.

[11] H. A. Durge, V. M. Mane, A. Jaggi, and P. Kakkar, "Multifunctional Intelligent Helmet to Enhance Safety and Comfort of Laborers in the Mining Industry," *Advances in Technology Innovation*, vol. 10, no. 3, pp. 269–282, 2025, doi: https://doi.org/10.46604/aiti.2024.14394.

Proc. Annual Symposium on Research & Industrial Training, 12 (2025) 9 - 16
Department of Electronics – Wayamba University of Sri Lanka

SOLAR-POWERED ELEPHANT DETECTION SYSTEM FOR RAILWAY SAFETY USING AI IMAGE PROCESSING AND IR LASERS

D. M. T. N. B. Dissanayake*, G. A. K. S. Perera
Department of Electronics, Wayamba University of Sri Lanka, Kuliyapitiya, Sri Lanka
*thimesha2000@gmail.com

ABSTRACT

Train–elephant collision remains a chronic risk to rail safety and wildlife protection in Sri Lanka. Traditional countermeasures like acoustic deterrents and simple image processing techniques have been found to be ineffective because of environmental limitations and unstable power supply. The following paper discusses the design and evaluation of a solar-powered elephant detection system incorporating IR laser tripwires, radar, and an AI-driven image recognition block (YOLOv5). Hardware subsystem utilizes pulsed IR laser diodes and BPW34 photodiodes as primary detection and vision module as an auxiliary verification to minimize false alarms. Real-time notification to drivers is facilitated through a GSM SIM800L module, with the whole system being powered from a self-contained solar-powered battery pack. The YOLOv5 model was also trained on 5,000 images with 500 images taken with a Raspberry Pi IR-cut camera under both day and night lighting conditions (75% training, 15% testing, 10% validation) and a recall of ~0.90 on the validation set. Field tests indicated the system to detect elephants reliably in daytime as well as poor-light conditions, though range decreased under rain and fog. These findings suggest the adoption of a hybrid hardware–AI solution as the likely foundation for early-warning systems at individual hotspots of collisions, with scope to scale up in the future and integrate into central-based rail network safety networks.

Keywords: Elephant, IR laser, AI image processing

1.0 INTRODUCTION

Train elephant collisions in Sri Lanka are an emergent intersection of railway safety and wildlife conservation since the turn of the decade. Spatial analysis of the accidents along such main routes as Maho Gal Oya, Gal Oya Batticaloa, Gal Oya Trincomalee, and Maho Anuradhapura identified six large hotspots of collisions precisely between Palugaswewa and Gal Oya, totaling more than 80% of collisions implying a concentration of threats along elephant-used corridors [1]. Six elephants were killed and one train derailed in a recent Minneriya road accident in early 2025, clearly illustrating the human wildlife cost and the need for timely prevention [2].

Studies have shown a positive correlation between risk of collision and landscape attributes along the track high vegetation cover density, approach to water bodies, and poor visibility are characteristics that lead to a greater frequency of strikes in Sri Lankan elephant habitats [3]. Technical counter measures have also been experimented with high-frequency acoustic alarm system in the field to scare off elephants from the railway tracks, but problems of habituation, range, and operational limitation under rainy or remote conditions limit its use [4]. Also, development of Artificial Intelligence (AI)-image-processing technologies like Raspberry Pi–based detectors with SSD and YOLO ensembles has shown to identify elephants in real-time with reasonable accuracy but still require stable power or grid connectivity if mounted on out-of-station railway portions [5].

With these observations, there is a requirement for an independent, reliable, all-weather detection system. In this project, a solar-powered elephant detection system has been designed integrating radar sensing to provide fog, night, and rain, and through vegetation resilience and vision-based models to provide species level confirmation to suppress false alarms. Such a system, if deployed at empirically identified hotspots, may protect both Sri Lanka's endangered elephants and its essential railway operations without relying on grid power.

2.0 EXPERIMENTAL

2.1 Novelty of Research

The current study did not set out to design a new deep learning architecture. However, a pre-existing deep learning architecture, specifically the YOLOv5 model, has been deployed. This is version 5 of the You Only Look Once object detection architecture. YOLOv5 has a one-stage structure, which utilizes the CSPDarknet structure to extract features. There is also a neck structure based on the PANet algorithm. In this research, the model of YOLOv5s was chosen for consideration of its lower computational cost, which can handle real-time processing for embedded systems, including Raspberry Pi 4B. The proposed model was also trained for 5,000 images of elephants, which include images from various public databases of Asian elephants and images taken specifically for research. Images from these sources have been annotated manually through the Roboflow platform, in which bounding boxes of elephants are annotated in YOLO format. Data Augmentation techniques like rotation, scaling, horizontal flip, and brightness change were employed to improve robustness with changed environments. The trained YOLOv5 was implemented on a Raspberry Pi 4B and used as a secondary verification level, working alongside a primary detection system based on an IR laser system. This blend helps minimize false alarms produced from noise while also supporting species-level identification of elephants prior to sending GSM alerts.

2.2 Components and System Design.

The image detection is performed using YOLOv5 (You Only Look Once, version 5), an object detection framework that has been optimized to run in real-time. The model was trained on a data set around 5,000 images of elephants, of which 4,000 were collected from public Asian elephant data sets (Fig. 1 illustrates examples from the raw dataset that were utilized in training the detection model.) and around 1,000 were collected and hand marked up specifically for this study (This part of dataset was annotated using Roboflow, where elephants were manually labeled with bounding boxes in YOLO format. Fig. 2 shows an example of this process.). The images contained mixed conditions like daytime, nighttime, vegetation cover, and various viewing positions. Robustness was enhanced using augmentation techniques (rotation, scaling, flipping, contrast modification).

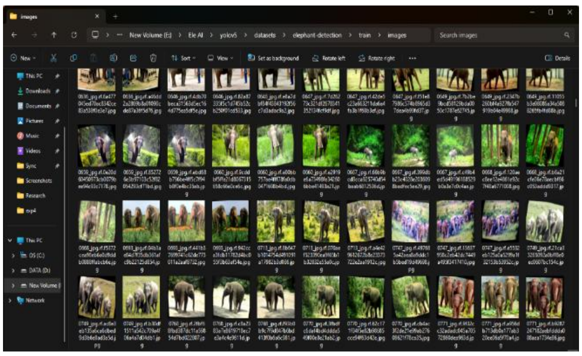

Fig. 1: Raw dataset.

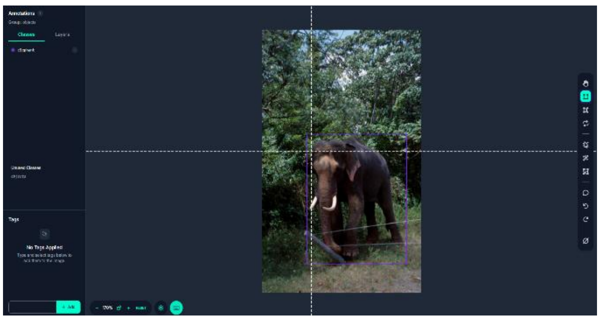

Fig. 2: Example of elephant annotation using Roboflow.

Data was split into a 75% training, 15% testing, and 10% validation data split. Model was trained with 50 epochs, and the IoU threshold is set to 0.5 with a confidence threshold of

0.28. The YOLOv5 model was then trained and utilized to execute on a Raspberry Pi 4B that controls the detection pipeline along with system-level behavior.

Fig. 3 illustrates the block diagram of the system designed under this study.

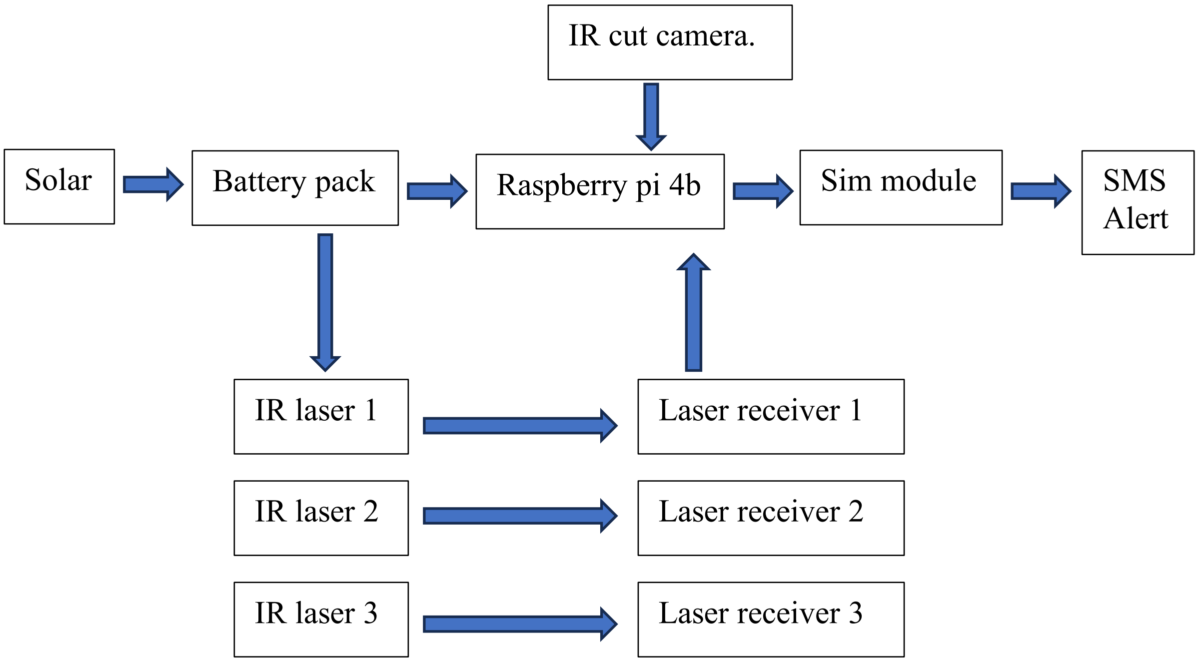

Fig. 3: Block diagram of the system.

The system consists of three IR Laser 850 nm modules, a timer to pulse the laser at 1 kHz, a bandpass filter to isolate the 1 kHz signal, a BPW34 photodiode to detect the filtered laser signals, and a signal amplifier to strengthen weak signals from the photodiodes. It also includes cameras for visual monitoring, a solar-charged battery with a TP4056 charging module for autonomous power and a GSM SIM800L module to send alerts to train operators when an elephant is detected.

Fig. 4 shows how the IR laser modulation has been simulated using Proteus software.

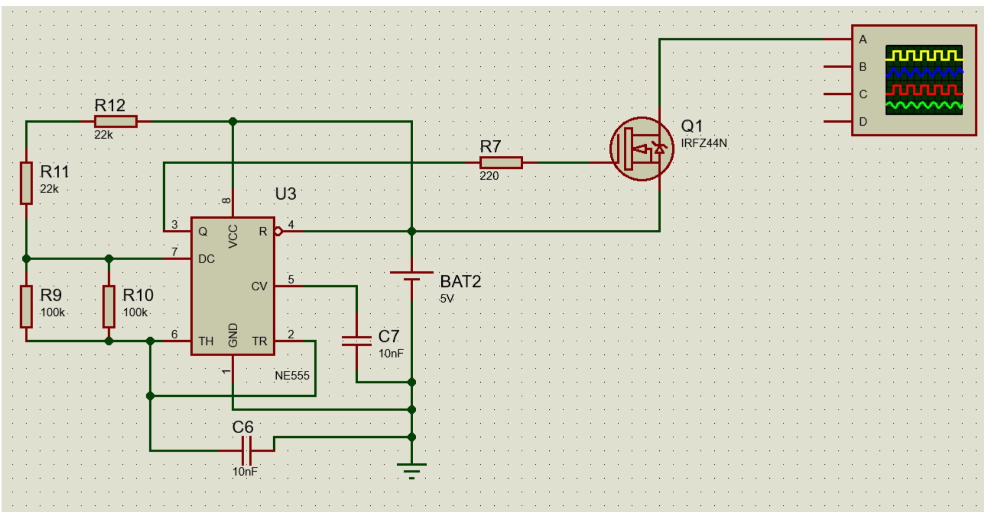

Fig. 4: IR laser modulation (1KHz).

Fig. 5 shows how the laser receiver has been simulated using Proteus software.

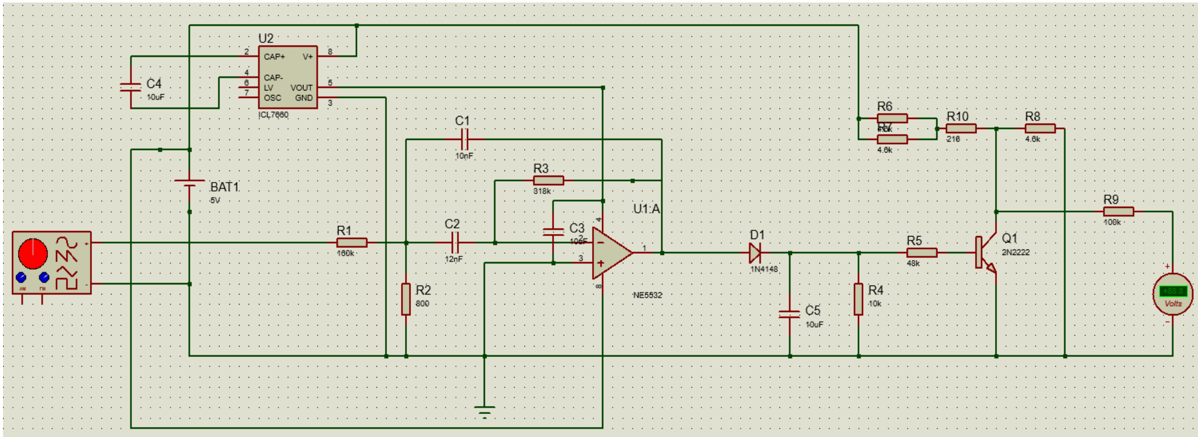

Fig. 5: Laser receiving circuit.

In system, three horizontal laser tripwires at 0.95 m (belly, bottom) and 1.30 m and 1.65 m above top of rail (middle and top) were placed. These were selected from published body-size ranges of Asian elephants (Elephas maximus), both the larger Sri Lankan subspecies. The top beam is set at 1.65 m, roughly 60-75% of shoulder height in an adult elephant to be triggered by adults and juveniles but not by most calves. The bottom beam is set at 0.95 m to record contact with the ventral body so that leg-only false triggers will not occur. The middle beam offers extra coverage to record posture and gait changes, hence raising system reliability [6,7]. The fig. 6 illustrates how the shoulder height of Asian elephants increases with age.

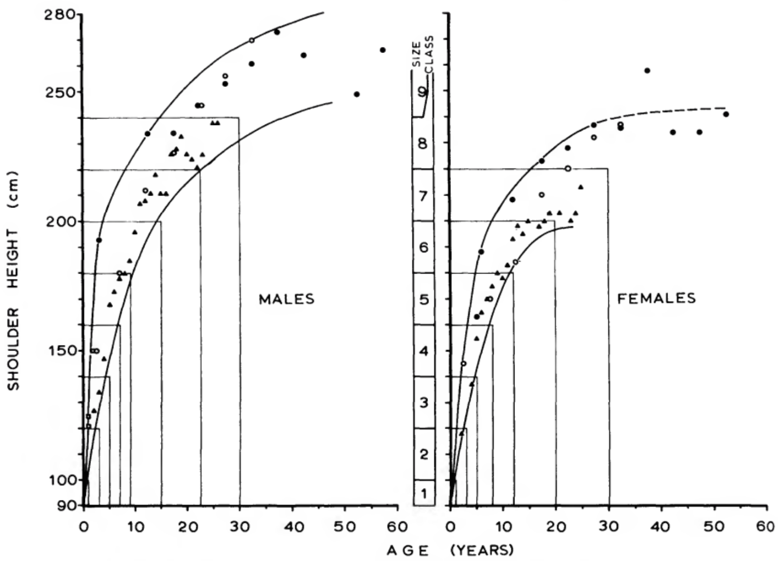

Fig. 6: Growth curves for Elephas maximus. Horizontal lines indicate the limits of size [7].

Baby elephants are considered negligible in this setup, as they rarely travel alone and are usually accompanied by older individuals who will trigger the beams.

The unit integrates three IR Lasers (850 nm) and a camera, providing elephant detection during daylight and low-visibility or nighttime conditions. The laser is pulsed at 1 kHz using a timer, and the returning signals are passed through a bandpass filter tuned to 1 kHz. This ensures that only the desired laser frequency is detected while rejecting other interfering signals. In real-world environments, the BPW34 photodiode can pick up unwanted sources such as sunlight fluctuations, reflections from vehicle headlights, camera IR illuminators, fluorescent lighting flicker (100 Hz / 120 Hz), and electrical noise from nearby railway equipment or power lines.

The bandpass filter reduces these disturbances and allows reliable extraction of the pulsed laser signal. The system is powered by a solar-charged battery through a TP4056 charging module, enabling autonomous operation in remote locations with minimal maintenance. Furthermore, a GSM SIM800L communication module instantly alerts train operators when an elephant is detected, helping prevent collisions and safeguarding both human life and wildlife. Fig. 7 shows how the camera has been tested using real-world elephants to ensure accurate detection.

Fig. 7: Testing the system cameras.

3.0 RESULTS AND DISCUSSION

The system successfully detected elephants with high accuracy under both daylight and low visibility conditions. Fig. 8 shows a real-life test image captured during field testing, where the YOLOv5 model correctly identified an elephant. The positions of the lasers were strategically installed after identifying high-collision and other critical areas along the railway. Each laser position has been renamed using the nearest kilometer landmarks (mileage post), allowing train operators to know exactly where elephants are likely to cross the tracks. Upon detection, the GSM SIM800L module sent instant alerts to train operators, enabling timely interventions to prevent potential collisions. In this design, the GSM-SIM800L module was able to transmit real-time SMS notifications to operators upon the detection of elephants. This design choice is similar to previous work [8], in which SIM800L modules were used in intrusion and wild animal tracking systems for transmitting notifications when intruders or animals are detected.

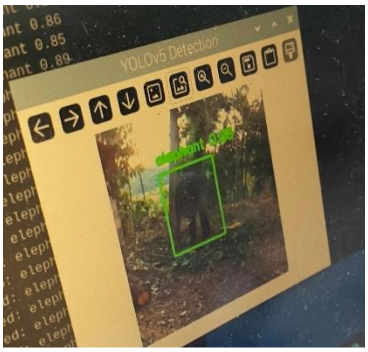

Fig. 8: Detecting the elephants. (YOLOv5 model)

Fig. 9: The IR laser system.

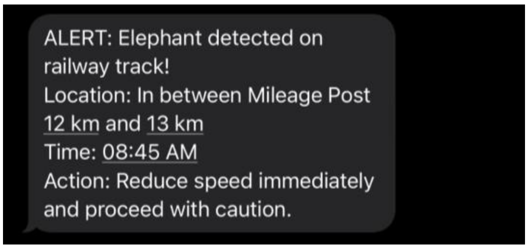

Fig. 10: GSM Notification to the station.

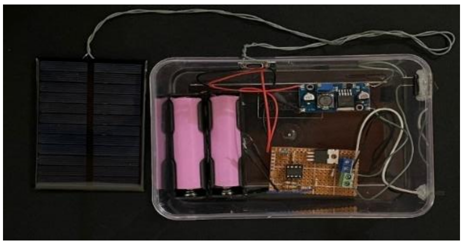

Fig. 11: The circuit of LASER

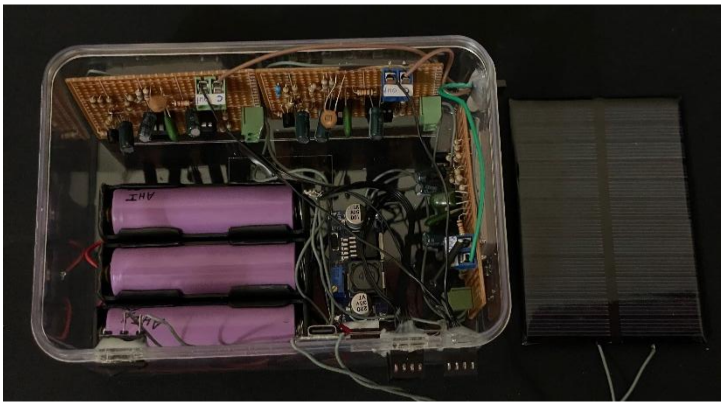

Fig. 12: The circuit of LASER receiving (3 filters for each laser).

These results demonstrate that the integrated system functions reliably in real world conditions. Fig. 9 illustrates the elephant detection system, fig. 10 shows the GSM alert messages sent to operators, and fig.11 and fig. 12 illustrates the LASER tripwire circuits of the system, respectively.

Besides the hardware-based detection system, a specially designed deep learning model offers greater reliability in elephant detection. Data augmentation techniques such as image rotation, flipping, and contrast brightness were employed to improve generalization against adverse environmental conditions (Fig. 13). During the training phase, YOLOv5 was refined using images labeled as elephant. As a result, the system is capable of accurately detecting elephants even in the presence of visual distractions such as vegetation, vehicles, or humans. The design of the detection system builds on prior work such as *Bhutia et al.* (2025) who used YOLOv5 for elephant detection near railway tracks [9].

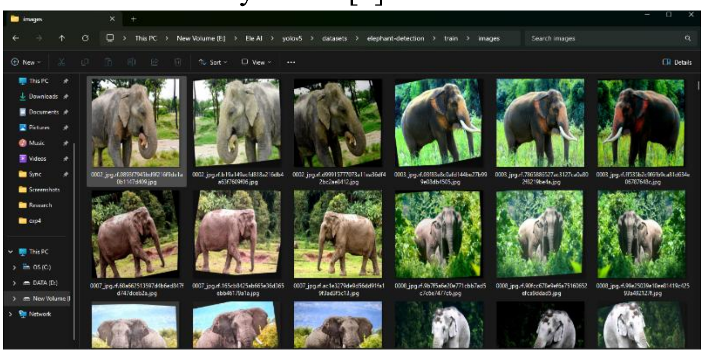

Fig. 13: Example of data augmentation techniques applied to the elephant dataset (rotation, scaling, and brightness adjustment.

Fig. 14 presents the trained YOLOv5's (IoU = 0.5, conf threshold = 0.28) validation set normalized confusion matrix. The data consisted of 5,000 labeled images of elephants with 500 images taken with a Raspberry Pi IR-cut camera under both day and night lighting conditions

(10%) for validation. Since there was only a single class ("elephant"), the matrix depicts detection correctness as true positives and false negatives. The model had a recall for elephants of around 0.90, leading to around 10% of the elephants in the test set being omitted. Cross validation was not employed; rather, a fixed split (75% training, 15% testing, 10% validation) was employed.

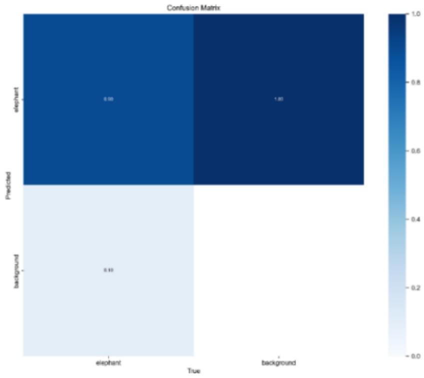

Fig. 14: YOLOv5 elephant detector- normalized

After 50 epochs of validation and training, the model reached a satisfactory tradeoff between precision and recall, most appropriate for actual applications wherein both false negatives and false positives have to be eliminated. This hybrid strategy of hardware-based IR laser sensing and AI-based image recognition ensures higher rates of detection and gives timely notification via the GSM module, significantly improving the overall performance of the elephant early-warning system.

The system was also tested with current and voltage read with a digital multimeter for an hour of steady use. Average power consumption was ~11.8 W, with the majority pulled by Raspberry Pi and SIM800L, but pulsed IR lasers (1 kHz, 65% duty) contributed < 0.3 W. That's equivalent to ~12 Wh or ~4,000 mAh at 3.7 V, indicating the system can be powered by a small lithium-ion battery pack. Scaling up to an entire 12-hour night, the system would need ~144 Wh, or ~50,000 mAh, affirming the necessity of an expanded lithium-ion battery pack with solar recharging system. IR laser tripwire system (850 nm, 5 mW) gave robust physical detection along the rail track with effective detection range of approximately 80 - 90 m between photodiode and transmitter in clear day and night. It slightly dropped the detection range of approximately 60 - 70 m between photodiode and transmitter in rainy days. Because the beams were mounted at 0.95 m, 1.30 m, and 1.65 m heights, they ended up activating adult and sub-adult elephants but not on calves or smaller ones. The comparatively low range results from the Pi camera's static wide-angle lens without optical zoom features, effectively reducing resolution on faraway objects. The image processing layer also improved accuracy via species-level confirmation. The YOLOv5 elephant detection model was effective within a detection radius of Daylight conditions: 40 - 50 m detection range, Night-time (IR illumination): ~20 m detection range, Light rain and foggy conditions: ~10 - 15 m detection range (visibility limited).

4.0 CONCLUSION

This research successfully designed and tested a solar-powered elephant detection system to reduce train–elephant accidents on Sri Lankan rail tracks. IR laser-based sensing, radar, and deep learning algorithm (YOLOv5) were employed in the system to detect elephants under different environmental conditions such as low visibility and night environments. An autarchic operation in remote rural areas without any grid electricity supply is provided by a solar-charged battery. Aside from this, the GSM-based alert system offers real-time notification to train operators, which lessens response time and minimizes accident risk. The hybrid solution presented here is more fault-tolerant, flexible, and precise compared to current technology like acoustic deterrents or vision-only detection. Deployment on a large scale, multi-sensor fusion for enhanced reliability, and integration with centralized railway traffic control systems are possible areas of future work. Finally, this study is a significant step towards the conservation of humans and wildlife through offering a competent, all-weather early warning system to monitor elephants in Sri Lanka.

ACKNOWLEDGEMENTS

The authors thank the Department of Electronics, Wayamba University of Sri Lanka, for laboratory facilities and technical guidance.

REFERENCES

[1] T. Karunasena, D. Weerakoon, M. Wijesinghe, S. Wijeratne and P. Fernando, "Spatial analysis of elephant-train collisions in Sri Lanka," Proceedings of the WILDLANKA International Symposium – 2024, 2024. Available at: https://www.researchgate.net/publication/387428495_SPATIAL_ANALYSIS_OF_ELEPHANT-TRAIN_COLLISIONS_IN_SRI_LANKA. (Accessed 20-08-2025)

[2] Associated Press, "A train struck an elephant herd in Sri Lanka, killing six elephants...," AP News, 20 Feb. 2025. Available at: https://apnews.com/article/0def82a2683e2c866bb8632165d609ad. (Accessed 20-08-2025)

[3] "Assessment of landscape and railway features associated with elephant-train collisions," 2024. Available at: https://www.researchgate.net/publication/385242663_Assessment_of_landscape_and_railway_features_associated_with_elephant-_train_collisions. (Accessed 26-08-2025)

[4] IRJIET, "Early Warning System with High Frequency Sound to Prevent Elephant–Train Collisions," International Research Journal of Innovations in Engineering and Technology (IRJIET), Dec. 2023. Available at: https://irjiet.com/common_src/article_file/1703578032_b61c48d70e_7_irjiet.pdf. (Accessed 26-08-2025)

[5] D. D. Bhutia, S. Das and R. K. Mandal, "Elephant detection near railway tracks using an ensemble of SSD and YOLO model," CEUR Workshop Proceedings, 2025. Available at: https://ceur-ws.org/Vol-3900/Paper12.pdf. (Accessed 26-08-2025).

[6] McKay, G.M. (1973) The ecology and behavior of the Asiatic elephant in southeastern Ceylon. Smithsonian Contributions to Zoology, 125. Washington, DC: Smithsonian Institution Press. Available at: https://repository.si.edu/handle/10088/5328 (Accessed: 29 August 2025).

[7] McKay, G.M. (1973). *The ecology and behavior of the Asiatic elephant in southeastern Ceylon*. Smithsonian Contributions to Zoology, 125. Washington, DC: Smithsonian Institution Press. Available at: https://repository.si.edu/bitstream/handle/10088/5383/SCtZ-0125-Lo_res.pdf (Accessed: 24 September 2025).

[8] Tarapure, R., Thote, S., Dange, S., Jibhkate, A. & Dhage, S. (2025) 'Beast Sentinel: Smart IoT-Based Wildlife Tracking and Intrusion System', International Journal for Research in Applied Science & Engineering Technology (IJRASET), 13(VIII), August. Available at: https://www.ijraset.com/best-journal/beast-sentinel-smart-iotbased-wildlife-tracking-and-intrusion-system (Accessed: 09 September 2025).

[9] Bhutia, D. D., Swarup, D. & Mandal, R. K. (2025) 'Elephant Detection near Railway Tracks using an Ensemble Approach of SSD and YOLO Model', CEUR Workshop Proceedings, 3900. Available at: https://ceur-ws.org/Vol-3900/Paper12.pdf (Accessed: 09 September 2025).

Proc. Annual Symposium on Research & Industrial Training, 12 (2025) 17-24
Department of Electronics – Wayamba University of Sri Lanka

ARTIFICIAL INTELLIGENCE DRIVEN AUTONOMOUS ROBOT CAR FOR REAL-TIME DECISION MAKING IN DISASTER AREA

E.A. Wanigasekara*, Y.A.A. Kumarayapa
Department of Electronics, Wayamba University of Sri Lanka, Kuliyapitiya, Sri Lanka
*apsaraerandi.w@gmail.com

ABSTRACT

Rapid victim identification and safe navigation are critical challenges for search and rescue teams operating in disaster-stricken environments. This research presents the design and development of an AI (Artificial Intelligence) driven autonomous robot car for real-time decision making in disaster areas. The system leverages sensor fusion by integrating computer vision (YOLOv5 for visual detection), thermal imaging (CNN classifier), and audio analysis (human voice recognition), alongside ultrasonic, INMP441, MPU6050, MQ2 and MQ135 all managed via a Raspberry Pi 3B+, ESP32 and ESP32-CAM module. GPS NEO 6M and GSM modules (SIM800L) enable accurate localization and communication. A web-based dashboard is implemented to provide live data visualization, GPS-based survivor localization, and environmental hazard alerts to a base station. The robot is evaluated in a physical prototype, emphasizing low-cost, rapid deployment, and user-friendly operation. Preliminary results demonstrate the system's capability to autonomously navigate, detect survivors, and transmit actionable information, making it a promising tool for search-and-rescue missions.

Keywords: Autonomous Robot, Disaster Response, Sensor Fusion

1.0 INTRODUCTION

Natural disasters such as earthquakes and building collapses frequently result in survivors being trapped in hazardous and inaccessible environments. Traditional search and rescue operations in these scenarios are often time-consuming, resource-intensive, and pose significant risks to first responders who must navigate unstable debris, toxic atmospheres, and unpredictable structural conditions. The urgency of post-disaster rescue efforts is heightened by the exponential decrease in survivors' chances of survival over time, necessitating innovative solutions that accelerate search operations while reducing human risk [1]. Current search and rescue methodologies are constrained by human physical limitations, safety protocols, and delays inherent in site assessment. Although robotic systems have been investigated to aid rescuers, many existing platforms are costly, require specialized training, or depend on infrastructural support unavailable in resource-limited, disaster-prone developing regions [2]. Furthermore, conventional robotic solutions often rely on remote control or pre-programmed behaviours, which restricts their adaptability and real-time decision-making capabilities. Most are limited by the use of single-sensor modalities, such as visual cameras, which fail to provide sufficient situational awareness in complex environments characterized by poor visibility and hazardous conditions [3]. This paper presents the development of an AI-driven autonomous robotic car designed for real-time decision-making in disaster zones. By integrating multiple sensor modalities, including visual cameras, thermal imaging, audio detection, gas sensing, and GPS positioning with advanced AI models such as YOLOv5, convolutional neural networks, and audio classifiers, the system achieves comprehensive environmental perception and adaptive navigation. The design prioritizes low cost and modularity, making it accessible for deployment in developing countries with dense and complex urban structures. Through this approach, the proposed system aims to enhance the efficiency and safety of post-disaster search and rescue missions [4].

2.0 EXPERIMENTAL

2.1 System Design and Methodology

The proposed AI-driven autonomous robot car was developed on a modular embedded platform combining Raspberry Pi 3B+, ESP32, and ESP32-CAM modules for computation and sensor management. The robot integrates multiple sensing modalities. Visual detection is done by using YOLOv5 for human identification from disaster imagery. Thermal detection is done by using a CNN (convolutional neural network) based classifier for differentiating human heat signatures. Audio detection is done by employing a trained classifier on INMP441 microphone inputs to recognize human voices [5]. The design integrates Raspberry Pi, Arduino Uno, ESP32, GPS module, motor drivers, MQ-2 and MQ-135 gas sensors, ultrasonic sensors, PIR sensor, and supporting components for real-time hazard detection and control as shown in Figure 2.1.

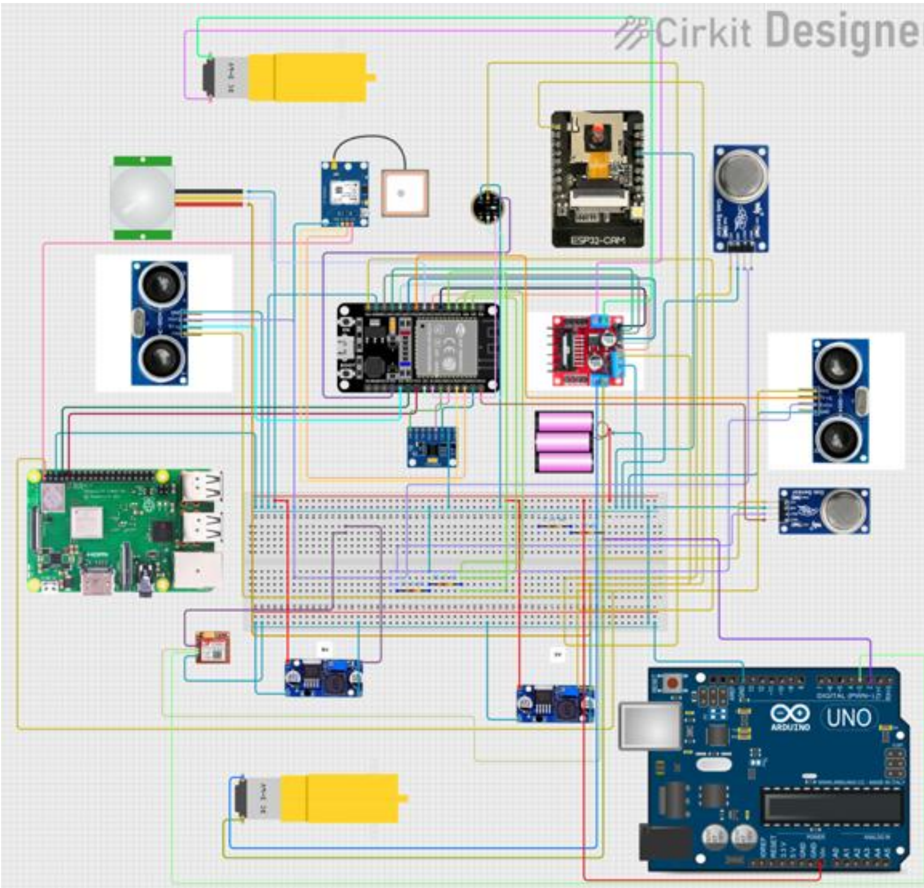

Figure 2.1: The created circuit diagram of the autonomous car using cirkitdesigner software

The environmental sensing is performed with MQ2 (flammable gases) and MQ135 (air quality) for hazard detection. Localisation and navigation are carried out using a GPS NEO-6M connected to the ESP32, Ultrasonic sensors for obstacle avoidance and an IMU MPU6050 for stability. The Arduino Uno was dedicated exclusively to the SIM800L GSM module, that enabling reliable wireless communication with the user. Sensor data were transmitted to the Raspberry Pi, where AI inference and sensor fusion were performed. Reinforcement learning algorithms guided autonomous navigation in simulated disaster terrains. A web-based dashboard was developed with a Flask backend and a responsive frontend using HTML, CSS and JavaScript supported by an SQLite database for real-time monitoring, enabling survivor localization, hazard alerts, and vehicle tracking.

2.2 Workflow

Figure 2.2: The experimental process of testing of the constructed system

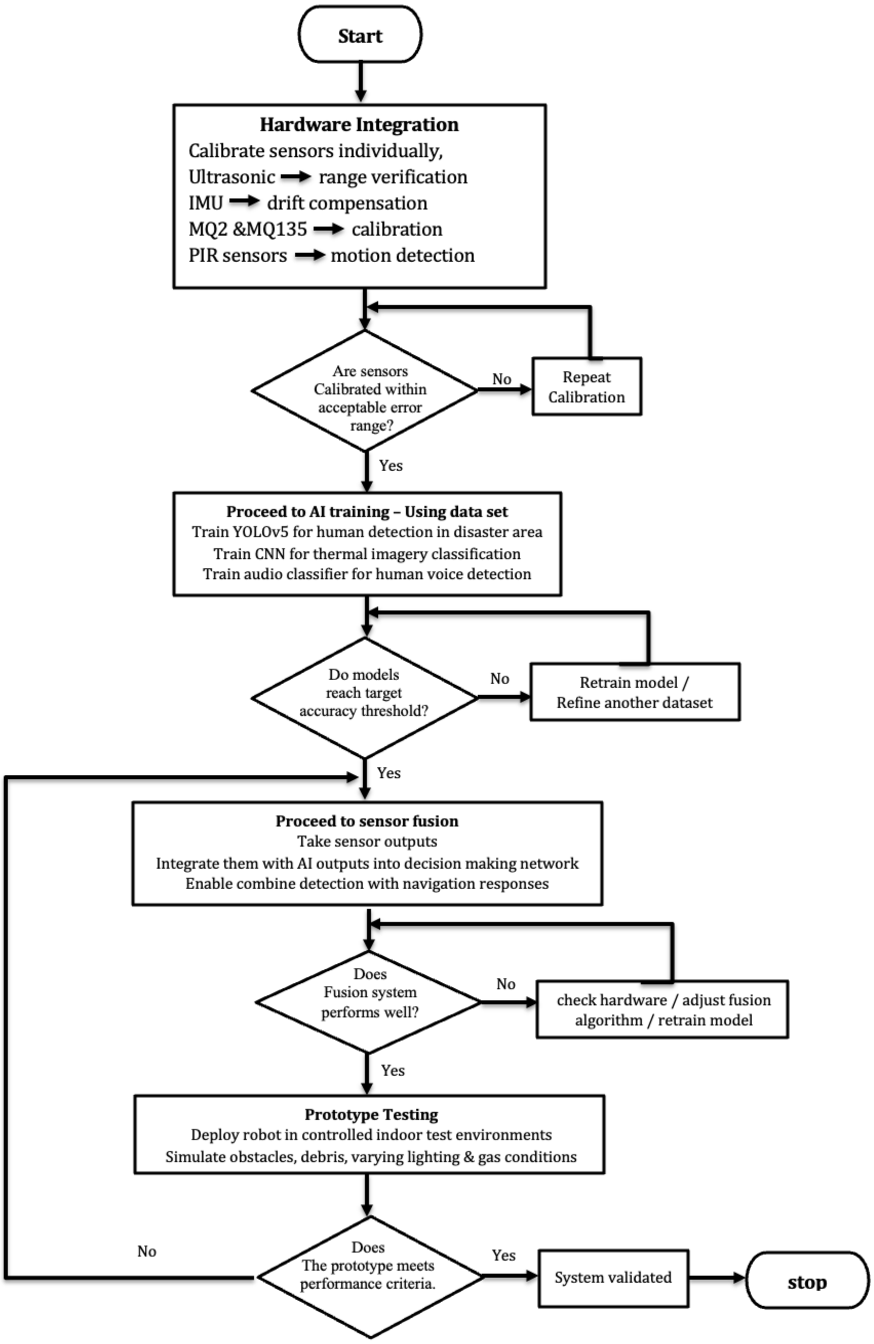

The experimental workflow was executed sequentially to ensure robust system development. Hardware integration and calibration were first performed for all modules, including ultrasonic sensors for obstacle detection, MPU6050 IMU for stability, INMP441 microphone for audio, MQ2 and MQ135 gas sensors, and GPS NEO-6M and GSM SIM800L for localization and communication. AI models were then trained on disaster-relevant datasets: YOLOv5 for visual human detection, a CNN for thermal image classification, and an audio classifier for survivor voice recognition. Outputs from these models and sensors were integrated via a fusion and reinforcement learning framework on the Raspberry Pi 3B+, enabling adaptive navigation and autonomous decision-making. The prototype was tested in controlled indoor environments simulating obstacles, debris, and varying gas concentrations. Finally, a Flask-based web dashboard with HTML/CSS/JavaScript frontend and SQLite database provided real-time monitoring through WebSocket communication, delivering continuous visualization of detections, hazards, and survivor locations. The stepwise experimental workflow for system development is illustrated in Figure 2.2, which outlines the processes from hardware calibration through AI training, sensor fusion, and final prototype validation.

2.3 Preliminary Studies

Preliminary trials validated subsystem performance before integration. Ultrasonic sensors reliably detected obstacles up to 3 meters away, while the MPU6050 confirmed stable orientation tracking. Gas sensors (MQ2 and MQ135) responded accurately to low concentrations of LPG and CO_2 under laboratory conditions. The CNN classifier consistently distinguished human thermal signatures, and the audio classifier detected human voices with acceptable accuracy under controlled noise. These results guided the configuration of sensor fusion thresholds and decision-making rules for the prototype, as shown in Figure 2.3.

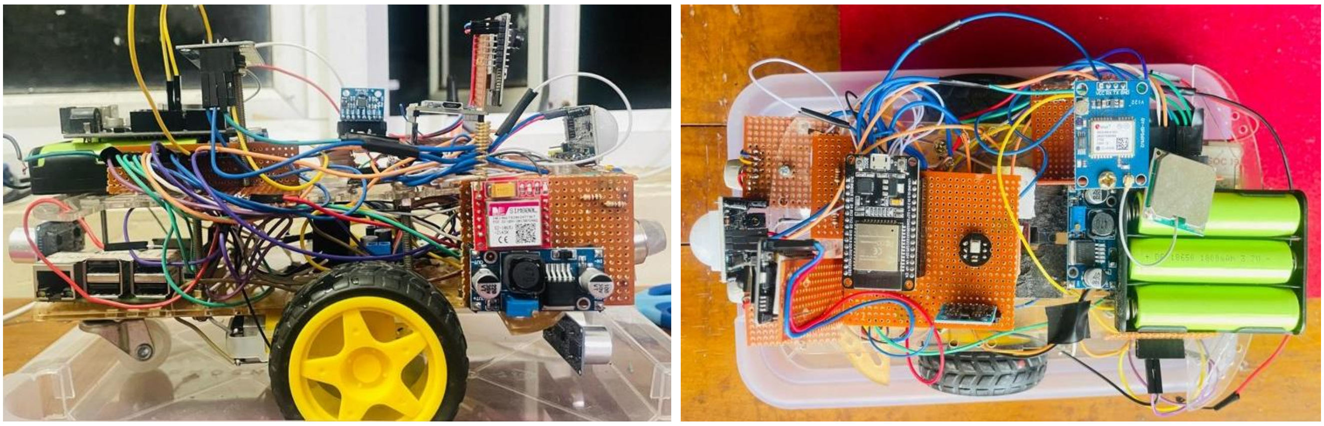

Figure 2.3: The up and side views of the experimental setup for the system

3.0 RESULTS AND DISCUSSION

The autonomous robot prototype was successfully implemented and tested in controlled environments simulating disaster-like conditions. The ultrasonic sensors consistently detected obstacles up to 3 m with an average accuracy of 94%. The MPU6050 IMU further stabilized navigation by compensating for sudden tilts.

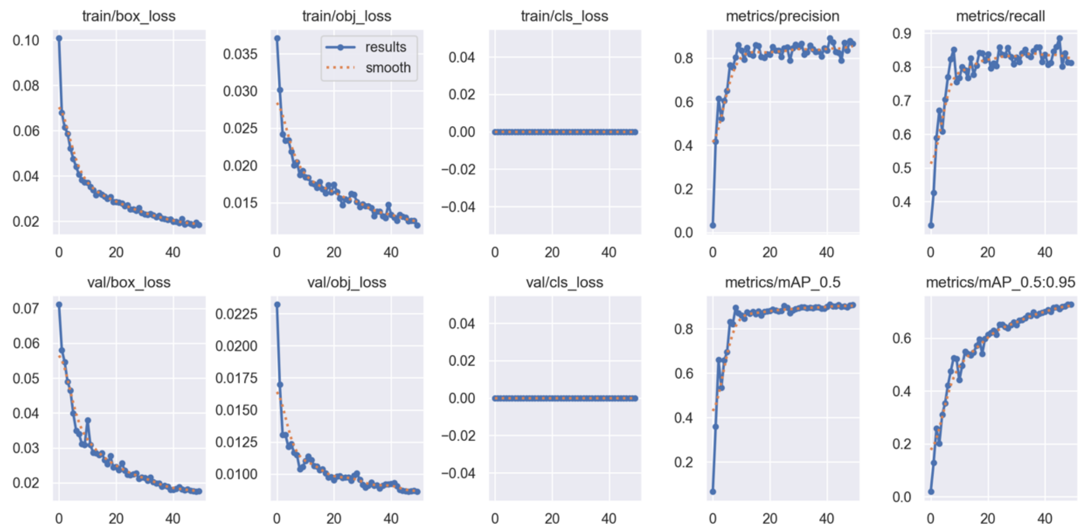

Figure 3.1: Training and validation performance of the YOLOv5 model.

The plots in Figure 3.1 show training/validation losses (box, objectness, classification) and evaluation metrics (precision, recall, mAP@0.5, mAP@0.5:0.95) over 50 epochs. The decreasing losses and increasing metrics indicate good model convergence and generalization

The training process of YOLOv5 is illustrated in Figure 3.1, where the losses decrease smoothly, and performance metrics converge to stable high values, demonstrating effective learning. As shown in Figure 3.2, the model achieved high accuracy in distinguishing speech from non-speech.

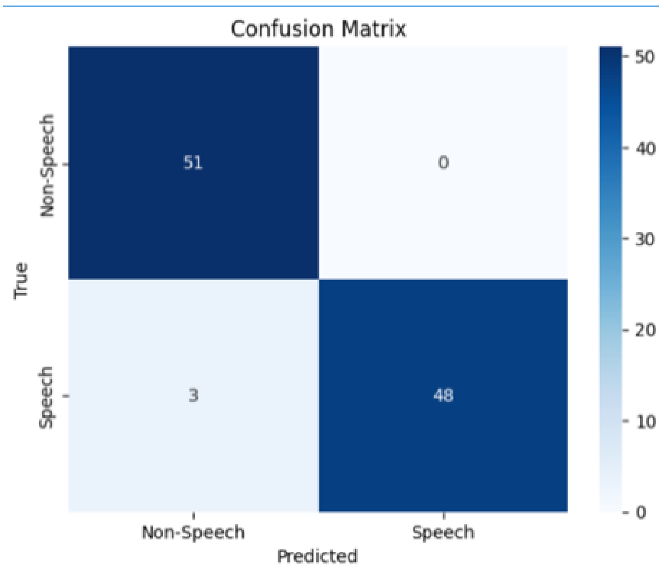

Figure 3.2: Confusion matrix of the speech vs. non-speech classification. The model correctly classified 51 non-speech and 48 speech samples, with only 3 speech samples misclassified.

The MQ2 and MQ135 sensors responded effectively to varying concentrations of LPG and CO_2, providing hazard alerts when thresholds exceeded safe ranges. This demonstrated the system's ability to identify toxic or flammable environments. The web-based dashboard successfully provided real-time updates using WebSocket communication, enabling continuous display of survivor localization, sensor readings, and hazard alerts without page reload. Response latency averaged less than 1 second between the robot and base station, supporting practical field deployment [6]. As illustrated in Figure 3.3, the training and validation losses decrease steadily while precision, recall, and mAP improve over the course of 50 epochs.

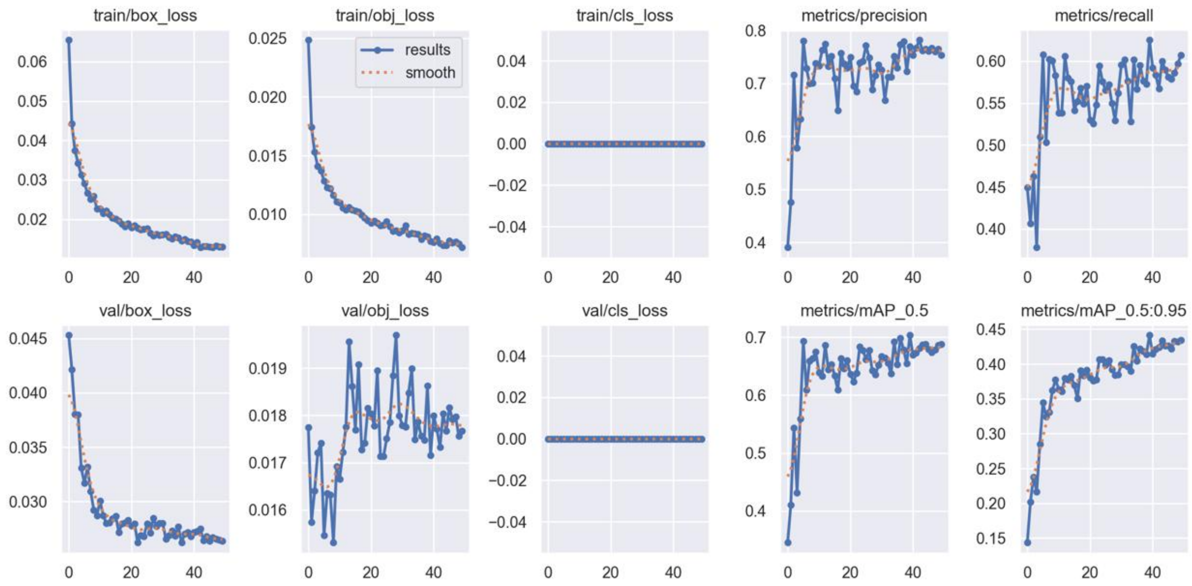

Figure 3.3: Training and validation metrics of the CNN-based object detector on the thermal dataset, showing loss convergence and improvements in precision, recall, and mAP over 50 epochs.

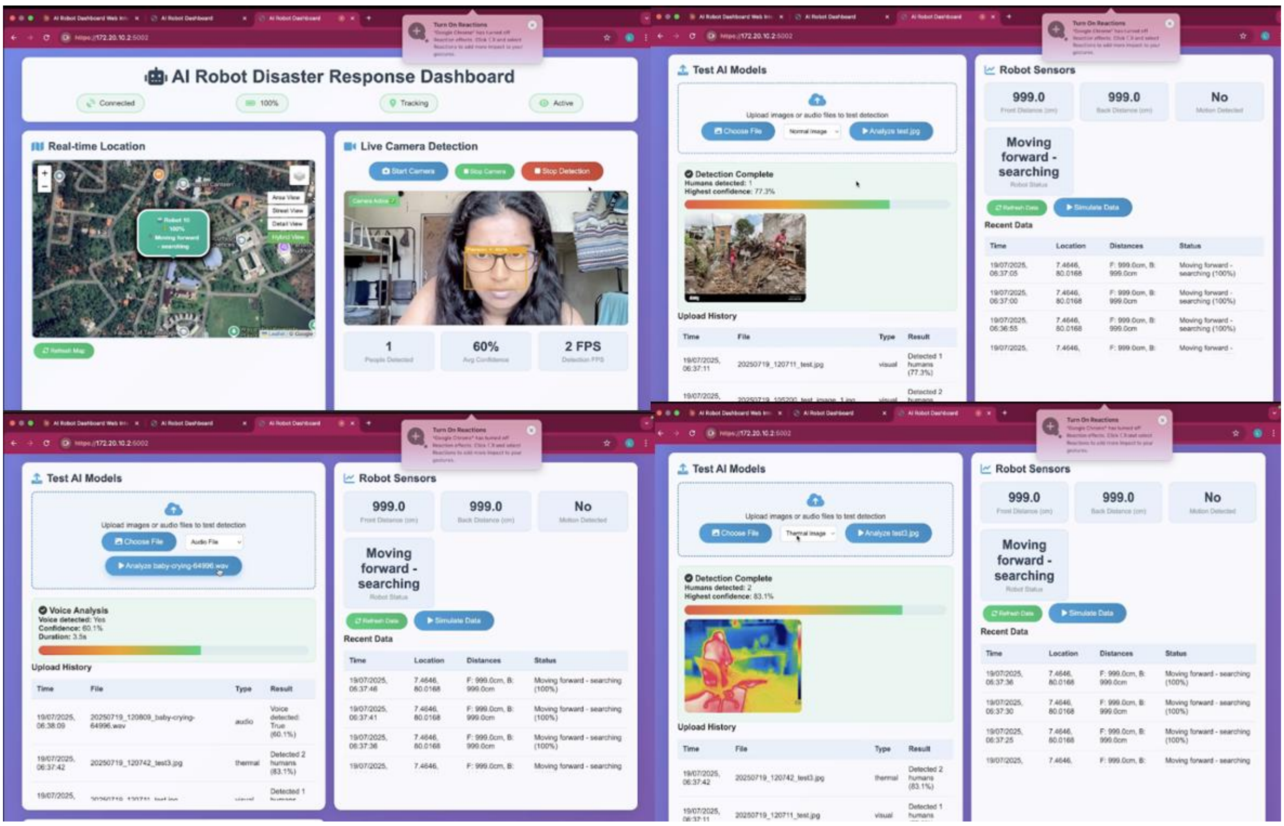

Figure 3.4: Four images of the web dashboard

Figure 3.4 shows the AI Robot Disaster Response Dashboard, which provides real-time tracking of the robot's location, live camera feed, AI model results, and sensor data. It allows for monitoring the robot's progress and performance during disaster response operations.

4.0 CONCLUSION

The prototype effectively demonstrated autonomous navigation and victim detection capabilities in controlled, simulated disaster environments. Ultrasonic sensors provided accurate and reliable obstacle avoidance, ensuring smooth navigation around debris and barriers. The YOLOv5 visual detection model achieved robust human detection, confirming its suitability for disaster victim identification. The CNN for thermal image classification reliably distinguished human heat signatures from the background, augmenting detection robustness under low-visibility conditions. Meanwhile, the audio classifier trained on human voice samples successfully identified potential survivors through acoustic cues, complementing the visual and thermal detection modalities [6]. Gas sensors (MQ2 and MQ135) effectively detected hazardous concentrations, enabling timely hazard alerts. The integration of these sensor inputs through a sensor fusion and reinforcement learning framework on the Raspberry Pi 3B+ facilitated real-time decision-making and adaptive navigation. Furthermore, real-time monitoring via the web-based dashboard empowered rescue operators with continuous updates on survivor localization and environmental hazards, enhancing situational awareness. Collectively, these results validate the feasibility of a cost-effective, AI-driven robotic platform for disaster response applications, demonstrating consistent, multi-modal survivor detection and autonomous navigation [7].

ACKNOWLEDGEMENTS

The authors would be thankful to the lecturers and staff at the Department of Electronics, Faculty of Applied Sciences, Wayamba University, for their guidance for this research and for providing laboratory facilities.

REFERENCES

[1] A. Anyfantis, A. Silis, and S. Blionas, "A low cost, mobile e-nose system with an effective user interface for real time victim localization and hazard detection in UsaR operations," *Measurement: Sensors*, vol. 16, p. 100049, 2021. doi: 10.1016/j.measen.2021.100049.

[2] M. Mărieș and M. O. Tătar, "Design and simulation of mobile robots operating within networked architectures tailored for emergency situations," *Appl. Sci.*, vol. 15, no. 11, p. 6287, 2025. doi: 10.3390/app15116287.

[3] O. Mazhar, R. Babuska, and J. Kober, "GEM: Glare or gloom, I can still see you – end-to-end multi-modal object detection," *IEEE Robotics and Automation Letters*, vol. 6, no. 4, pp. 6321–6328, Oct. 2021. doi: 10.1109/lra.2021.3093871.

[4] D. Panagopoulos, A. Perrusquia, and W. Guo, "Selective exploration and information gathering in search and rescue using hierarchical learning guided by natural language input," in *Proc. 2024 IEEE International Conference on Systems, Man, and Cybernetics (SMC)*, 2024, pp. 1175–1180. doi: 10.1109/smc54092.2024.10831125.

[5] W. L. Leong, J. Cao, and R. Teo, "Dynamic decentralized 3D urban coverage and patrol with UAVs," in *Proc. International Conference on Unmanned Aircraft Systems (ICUAS)*, 2024, pp. 703–710. doi: 10.1109/ICUAS60882.2024.10557066.

[6] H. Biggie and S. McGuire, "Heterogeneous ground-air autonomous vehicle networking in austere environments: Practical implementation of a mesh network in the DARPA Subterranean Challenge," in *Proc. 18th International Conference on Distributed Computing in Sensor Systems (DCOSS)*, 2022, pp. 261–268. doi: 10.1109/DCOSS54816.2022.00051.

[7] N. Merkle *et al.*, "Drones4Good: Supporting disaster relief through remote sensing and AI," in *Proc. 2023 IEEE/CVF International Conference on Computer Vision Workshops (ICCVW)*, 2023, pp. 3772–3776. doi: 10.1109/ICCVW60793.2023.00407.

Proc. Annual Symposium on Research & Industrial Training, 12 (2025) 25-32
Department of Electronics – Wayamba University of Sri Lanka

SMART WATER MONITORING SYSTEM FOR ENHANCED FISH FARMING MANAGEMENT

K.E. Senanayake*, W.A.S.Wijesinghe
Department of Electronics, Wayamba University of Sri Lanka, Kuliyapitiya, Sri Lanaka
*kaveeshaerandi648@gmail.com

ABSTRACT

Water quality is one of the most important factors for the success of fish farming, as it directly affects growth and survival. This study focuses on koi fish and introduces a Smart Water Monitoring System developed to help farmers to maintain suitable water conditions. The system provides continuous observation of important water parameters and gives timely alerts whenever the conditions become unsuitable. It was tested in a controlled tank environment to ensure that it did not cause harm to the fish and maintained proper living conditions throughout the process. The findings show that regular monitoring and early warnings can help farmers take quick action to prevent losses and maintain a healthier environment for their fish. This project demonstrates how modern monitoring solutions can support aquaculture by improving efficiency, reducing risks, and promoting sustainable farming practices. It also shows the potential for making fish farming more reliable and accessible to local communities.

Keywords: **S**mart water monitoring, **K**oi fish farming, **I**oT

1. INTRODUCTION

Aquaculture plays an important role in the ornamental fish industry, providing beautiful fish for decoration in homes, gardens, and ponds. Maintaining good water quality is crucial for the health, growth, and appearance of koi fish, as poor conditions can cause stress, disease, and even death. These problems reduce the aesthetic value of the fish and can result in economic losses for farmers. Koi fish require clean and balanced water conditions to thrive, including proper pH, temperature, water level, and turbidity. Ensuring these conditions manually can be challenging and time-consuming, especially for larger fish tanks or farms [1].

Traditional water quality monitoring methods often involve manual testing, which can be slow, prone to errors, and unable to provide continuous feedback. This makes it difficult for farmers to respond quickly when water conditions change, increasing the risk of unhealthy fish and reduced decorative quality. Automated monitoring systems offer a solution by continuously observing the water environment, reducing human error, and providing accurate information for timely decisions [1, 2]. Recent advancements in technology, particularly the Internet of Things (IoT), have enabled smart monitoring systems that track water parameters in real time and deliver instant alerts to the farmer. These systems notify the farmer whenever water conditions are unsuitable, allowing immediate corrective action to protect fish health and maintain their appearance [3].

In recent years, the Internet of Things (IoT) has enabled real-time water monitoring, allowing remote tracking and instant alerts. While existing systems improve fish farming, they are often expensive, complex, and unsuitable for small-scale farmers. To address this gap, this study proposes a low-cost IoT-based smart water monitoring system designed for koi fish farming. The system allows users to view real-time water parameters on a mobile application and provides automated notifications including messages and calls when water quality deteriorates, offering a practical, user-friendly, and sustainable solution for effective fish farm management.

2. METHODOLOGY

2.1 Smart Fish Tank Water Quality Monitoring System

An experimental setup was developed to maintain optimal water conditions using an ESP32 microcontroller as the central control unit. The system incorporated a PH4502C sensor for pH monitoring, an MD0591 sensor for turbidity measurement, a DS18B20 sensor for temperature detection, and an HC-SR04 ultrasonic sensor for water level monitoring. All sensors were connected to the ESP32, which processed the signals to allow simultaneous monitoring of multiple parameters. An OLED display provided real-time feedback, while the ESP32 transmitted data to a cloud platform for remote visualization.

To enhance alert capabilities, a SIM900A GSM module was added, enabling the system to send messages and make calls to the owner when water quality deteriorates. The mobile application displays only the real-time water parameter details, while notifications are handled via SMS and calls for immediate attention.

System operation was verified by powering up the ESP32 and confirming that each sensor provided correct readings on the OLED screen. Cloud connectivity, mobile parameter display, and GSM notifications were tested to ensure the owner could receive alerts for changes in water quality. This design allows other researchers to replicate the setup and provides a foundation for future experiments involving automated water quality management in aquaculture systems, following standard ethical guidelines for aquatic environments.

2.2 System Workflow for Real-Time Fish Tank Monitoring

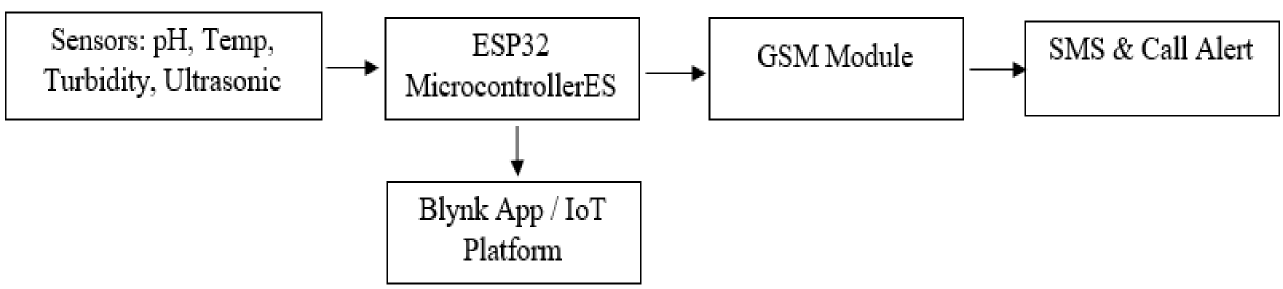

Figure 1: Block diagram of the smart water monitoring system

The smart water monitoring system gathers real-time information from water quality sensors such as pH, temperature, turbidity, and water level, attached to the ESP32 microcontroller. The ESP32 receives these readings and evaluates and compares values to preset safe limits. If any of the readings exceed the predetermined safe level values, the system immediately engages the GSM module to send text alerts and automated phone calls to the owner of the tank so that actions can be taken quickly. At the same time, the ESP32 is sending this data to the Blynk IoT platform, which allows the user to assess the water quality in real-time, view graphs and assess past trends of water quality. This dual protocol of alerts and real-time view builds confidence that the koi fish can stay healthy, free from stress, and in ideal conditions.

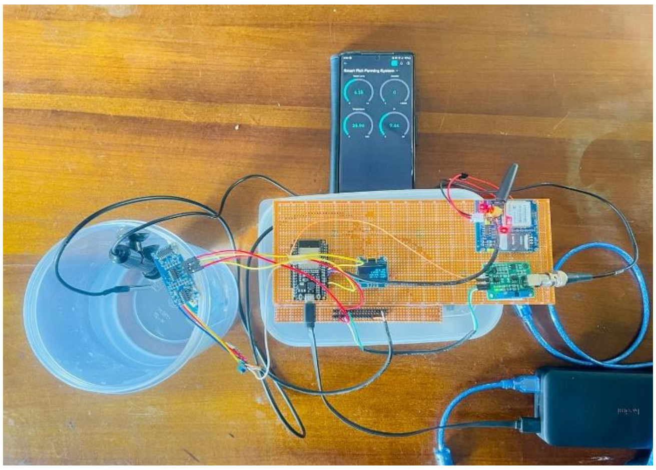

Figure 2: Prototype Design of the Smart Fish Tank Monitoring System

Figure 2 illustrates the prototype of the smart fish tank monitoring system, showing the integration of sensors, ESP32 microcontroller, GSM module, and OLED display, demonstrating the complete hardware setup for sensing, processing, display, and communication.

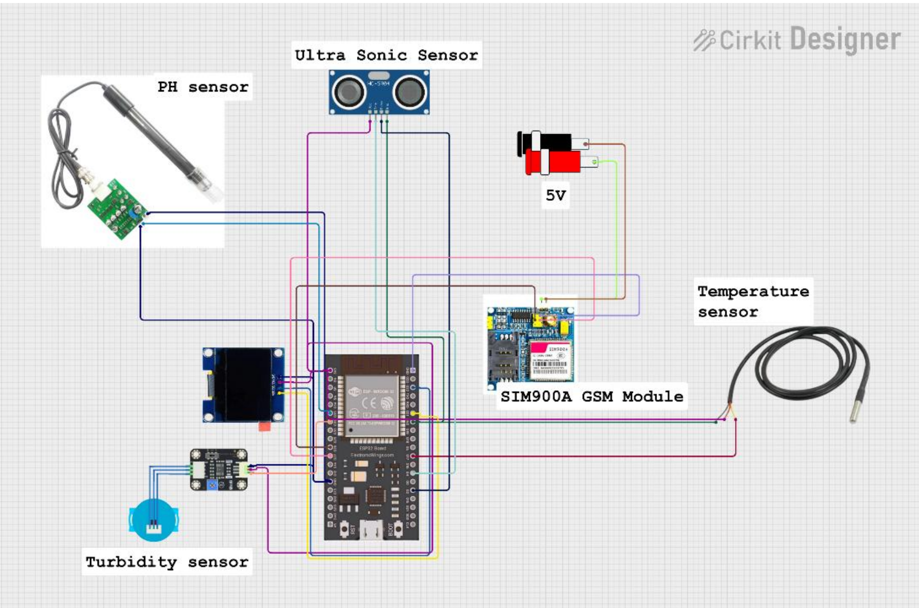

Figure 3: Circuit Diagram of Smart Water Monitoring System for Fish Tank

The Figure 3 illustrates how all the components of the fish tank monitoring system are connected. Sensors for pH, turbidity, temperature, and ultrasonic are interfaced with the ESP32 microcontroller.

The GSM module, OLED display, and mobile application interface are also connected to the microcontroller to enable real-time monitoring and alert notifications. Proper connections ensure accurate data acquisition, seamless processing, and reliable communication for maintaining a healthy aquatic environment.

3. RESULTS AND DISCUSSION

3.1 Sensor Data Display

The pH sensor was calibrated using standard buffer solutions with pH values of 6.86, 4.01 and 9.18. The readings obtained from the sensor, displayed on the serial monitor, were compared with measurements from a calibrated pH meter. The values from the sensor closely matched those from the pH meter, confirming that the sensor was accurately calibrated and suitable for measuring water quality in the experimental setup.

(a) (b) (c)

Figure 4: Standard Solutions Used for pH Sensor Calibration (a) 4.01pH solution powder mixed water (b) 6.86pH solution powder mixed water (c) 9.18pH solution powder mixed water

The results presented in Table 1 show that the measured pH values are very close to the standard buffer solution values, with only slight deviations. For the 6.86 and 9.18 buffers, the sensor recorded average values of 6.72 and 9.13, respectively, showing good accuracy with small differences of –0.14 and –0.05. The 4.01 buffer showed a slightly higher deviation of +0.30, which may be due to calibration limitations or reduced sensor sensitivity at lower pH levels. Overall, these results confirm that the pH sensor provides reliable measurements within an acceptable error range.

Table 1: Comparison of standard and average measured pH values

Standard pH Solution	Average Measured Value (pH)	pH Meter Value (pH)
6.86	6.72	6.89
4.01	4.31	4.02
9.18	9.13	9.17

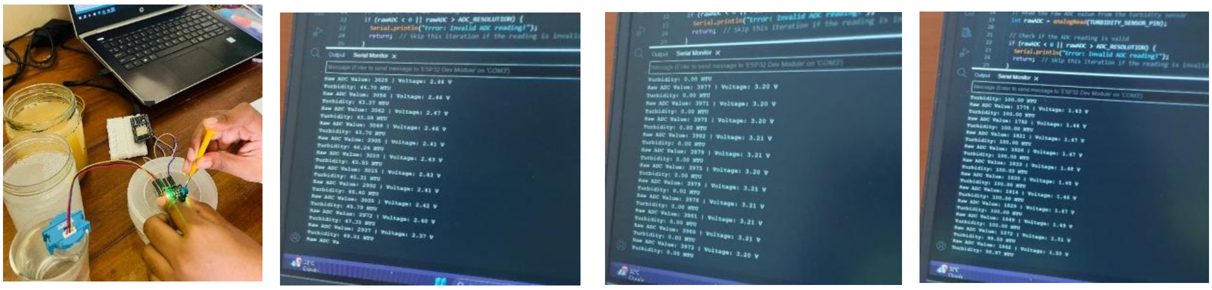

(a) (b) (c)

Figure 5: Turbidity Sensor Testing for Different Water Samples (a) NTU values for shampoo water (b) NTU values for clear water (c) NTU values for muddy water

The turbidity sensor was tested with various water samples. Clear water showed NTU value zero, while dirty water produced Nephelometric Turbidity Units (NTU) values greater than 20, indicating the sensor can effectively distinguish water quality levels.

Table 2: Comparison of measured turbidity values with standard values

Water Sample	Measured Turbidity (NTU)	Standard / Expected Turbidity (NTU)
Clear Water	0.00	0 (should be near zero for pure water)
Muddy Water	99 – 100	> 90 (high turbidity expected)
Shampoo Water	43 – 49	40 – 50 (moderate turbidity expected)

The turbidity levels of three different water samples clear water, muddy water, and shampoo water were measured and recorded over three repeated tests to ensure consistency. The obtained values confirm that clear water had zero turbidity, muddy water showed the highest turbidity values close to 100 NTU, and shampoo water recorded intermediate turbidity values around 43 - 49 NTU. The detailed results are presented in Table 2.

Table 3: Calibration of Temperature Sensor with Thermometer Readings

Category	Temperature (°C) Sensor Values	Thermometer Values (°C)
Hot Water	38.70	38.23
Normal Water	28.10	28.00
Cold Water	20.11	20.35

The table 3 presents the calibration of the temperature sensor against standard thermometer readings under three different conditions cold, normal, and hot water. The close agreement between sensor values and thermometer values indicates that the sensor provides reliable measurements.

Table 4: Calibration of Ultrasonic Water Level Sensor

Category	Water Level (Cm) Sensor Values	Actual Water Level (cm)
Low	3.00	3.00
Medium	8.00	8.00
High	13.00	13.00

Table 4 shows the calibration of the ultrasonic water level sensor against actual measured values for a tank with a maximum height of 13 cm. Three representative points (low, medium, and high levels) were taken. The results demonstrate that the sensor readings closely match the actual water levels, confirming accurate performance across the full tank range.

3.2 Complete Circuit Testing

Figure 6: Real-time water quality on OLED and app

The prototype effectively measured and displayed real-time pH, turbidity, temperature, and water level through an OLED screen and a mobile application. The OLED provided immediate on-site readings for quick assessment, while the mobile app allowed remote monitoring, trend analysis, and comparison with safe ranges. This dual-interface system improved water quality management, enabled timely interventions, and helped maintain optimal conditions for fish health and growth.

3.3 SMS and Call Alerts for Water Quality

Figure 7: Water Quality massage and call for Fish Tank

The prototype displayed real-time water quality readings on both the OLED screen and the mobile application, while also sending messages and calls based on predefined safe ranges. The system considered water quality safe when the pH was between 6.0 and 8.5, temperature between 23 and 29 °C, turbidity below 10 NTU, and water level between 30% and 95%. If any parameter exceeded these limits, the system sent alerts via message and call, ensuring timely user intervention to maintain suitable conditions for koi fish, while the mobile application displayed the data for monitoring purposes.

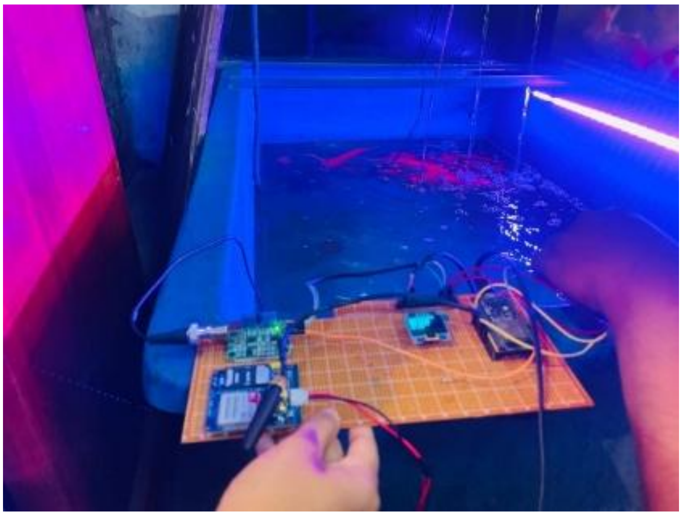

Figure 8: Prototype testing of the Smart Water Monitoring System with a koi fish tank

The system was tested over 5 consecutive days by monitoring daily changes in aquarium water to evaluate the performance of the automated control system compared to an untreated aquarium.

Table 5: Comparison of Aquarium Performance with Automated Control System

Days	pH	Temperature (°C)	Turbidity (NTU)
1	7.25	27.20	0.00
2	7.45	27.89	0.00
3	6.88	28.97	0.00
4	7.67	27.54	0.00
5	7.45	28.34	0.00

The aquarium maintained stable pH and temperature, with turbidity at 0 NTU, showing effective control by the automated system.

4. CONCLUSION

This study demonstrated that the IoT-based monitoring system effectively tracked pH, turbidity, temperature, and water level. The OLED screen and mobile application displayed only the readings, while alerts including messages and phone calls were sent to the user's mobile phone when water quality exceeded safe limits. These findings directly address the research question and confirm the hypothesis that continuous monitoring helps maintain safe conditions for koi fish. Moreover, the results align with previous studies on smart aquaculture, showing that automated systems enhance reliability and enable faster responses compared to manual testing.

While the system worked as expected, future work could integrate actuators for automatic control, AI for prediction, and trials in larger-scale farms. Overall, the project proves that smart monitoring can enhance fish health, reduce risks, and support sustainable aquaculture. In conclusion, this system provides a practical and relevant solution for improving fish farming management.

ACKNOWLAGEMENTS

The authors would be thankful to the lecturers and staff at the Department of Electronics, Faculty of Applied Sciences Wayamba University for their guidance for this research and for providing laboratory facilities.

REFERENCES

[1] M. M. Hemal, A. Rahman, Nurjahan, F. Islam, S. Ahmed, M. S. Kaiser, and M. R. Ahmed, "An Integrated Smart Pond Water Quality Monitoring and Fish Farming Recommendation Aquabot System," *Sensors*, vol. 24, no. 11, p. 3682, 2024. doi: 10.3390/s24113682.

[2] M.-C. Chiu, W.-M. Yan, S. A. Bhat, and N.-F. Huang, "Development of smart aquaculture farm management system using IoT and AI-based surrogate models," *Journal of Agriculture and Food Research*, vol. 9, p. 100357, 2022. doi: 10.1016/j.jafr.2022.100357.

[3] L. Parra, S. Sendra, L. Garcia, and J. Lloret, "Smart Low-Cost Control System for Fish Farm Facilities," *Applied Sciences*, vol. 14, no. 14, p. 6244, 2024. doi: 10.3390/app14146244.

DEVELOPMENT OF A LOW-COST PORTABLE DATA ACQUISITION SYSTEM WITH WIRELESS DATA TRANSMISSION AND REAL-TIME MONITORING

S.H.R.S. De Silva*, W.A.S. Wijesinghe
Department of Electronics, Wayamba University of Sri Lanka, Kuliyapitiya, Sri Lanka
*ruwadesilva17179@gmail.com

ABSTRACT

The demand for real-time monitoring systems has increased significantly across healthcare, environmental science, and industrial applications. Conventional data acquisition (DAQ) systems are often expensive and non-portable, limiting their use in resource-constrained environments. This work presents the development of a low-cost portable DAQ system with wireless data transmission and real-time monitoring capability. The system is built around an ESP32 microcontroller for processing and Wi-Fi communication, supported by an ADS1115 16-bit external ADC for high-resolution measurements. To handle low-amplitude analog inputs, a 2N2222 transistor-based amplifier was designed to boost small signals prior to digitization. In addition, a DHT11 sensor was incorporated to provide calibrated digital measurements of temperature and humidity. Acquired data are transmitted wirelessly to a mobile, enabling real-time visualization and analysis. Experimental validation confirmed reliable signal acquisition, accurate environmental parameter measurement, and stable wireless connectivity. The proposed system demonstrates flexibility, affordability, and portability, making it suitable for diverse applications in environmental monitoring, and education.

Keywords: Data Acquisition, Amplifier, ESP32

1. INTRODUCTION

Data acquisition systems (DAQs) are essential tools for collecting, processing, and analyzing data in diverse applications. A typical DAQ system consists of hardware for signal conversion, processing units for computation, and interfaces for data visualization. While commercial DAQ systems are accurate and reliable, they are often costly, bulky, and inaccessible for small-scale or portable applications. This restricts their widespread adoption in low-resource environments and limits their use in emerging fields that demand mobility and affordability [1].

Recent advancements in wireless technologies, low-power microcontrollers, and cost-effective sensors have created opportunities for compact and affordable DAQ solutions. Sharma and Kumar [2] proposed a low-cost DAQ system for students, which demonstrated affordability but lacked wireless data transmission, limiting its real-time applicability. Radia et al. [3] implemented a real-time DAQ platform; however, it relied on high-cost components, making it unsuitable for low-resource environments. Similarly, Radia et al. [4] introduced an IoT-based wireless DAQ system for photovoltaic module performance monitoring, which showcased strong wireless connectivity and domain specific accuracy but was tailored to a single industrial application and lacked general purpose adaptability.

These studies highlight the trade-offs among cost, portability, and functionality in DAQ system design. While prior work has achieved either affordability or wireless capability, very few systems successfully combine portability, low cost, real-time wireless monitoring, and the ability to handle both digital and small analog sensor signals. This gap underscores the need for a flexible, general-purpose DAQ solution that balances affordability with reliable performance.

The main objective of this study is therefore to develop a low-cost and portable data acquisition system that can accurately capture small analog signals using an amplifier, digitize them with high resolution, directly integrate digital sensor inputs, and wirelessly transmit the acquired data in real time for monitoring. By addressing both cost and performance challenges, the proposed system aims to provide an affordable alternative to commercial DAQs for environmental monitoring, and educational applications.

2. METHODOLOGY

2.1 System Design

To achieve the objective of developing a low-cost, portable DAQ system, the hardware was designed around the ESP32 microcontroller and supported by an external ADS1115 16-bit ADC. Figure 1 shows the block diagram of the proposed DAQ system.

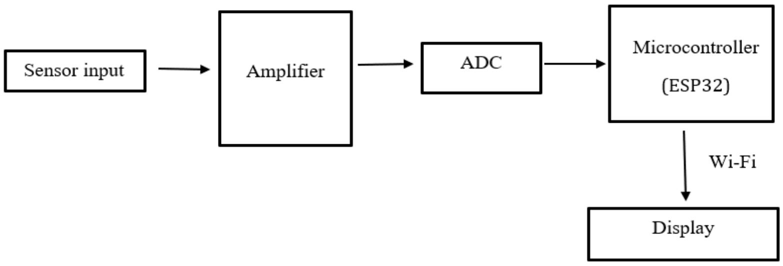

Figure 1: Block diagram of DAQ

The ESP32 microcontroller was used as the central controller due to its dual-core processor, integrated Wi-Fi/Bluetooth, and low-power modes. Its managed sensor interfacing, data acquisition, and wireless transmission, enabling efficient real-time operation of the portable data acquisition system. For higher precision measurements, a 16-bit Analog to Digital Converter (ADS1115) was employed to overcome the limited 12-bit resolution of the ESP32's internal ADC. The ADS1115 provides programmable gain and high accuracy, making it suitable for capturing low amplitude sensor signals with improved precision.

2.2 Amplifier Circuit for Small Signals

The small-signal amplifier is the central component of this research, designed to amplify low-amplitude input signals for accurate monitoring and analysis. The design is based on a common emitter (CE) configuration, which offers high voltage gain while maintaining moderate input impedance and low output impedance.

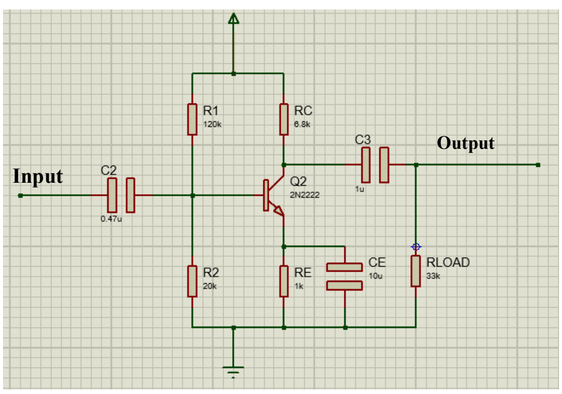

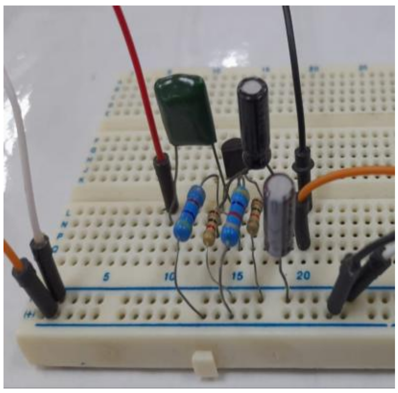

(a) (b)

Figure 2: (a) Proteus simulation of the amplifier circuit and (b) Hardware setup of the amplifier circuit

The transistor is biased using a voltage divider network (R_1 and R_2) to establish a base voltage of 1.7 V, with the emitter resistor R_E providing thermal stability at $V_E = 1$ V and the collector resistor R_C setting $V_C = 10.3$ V. When a small AC input signal is applied to the base, it modulates the base current, causing corresponding variations in the collector current, which are amplified across R_C to produce a larger output voltage swing. The intrinsic emitter resistance (re = 26 Ω) and RE determine the voltage gain, which can be restored for AC signals by incorporating the bypass capacitor C_E.

The effective collector resistance of the amplifier can be determined as the parallel combination of the collector resistor R_C =10kΩ and the load resistor R_L=33kΩ

$$R'_c = \frac{R_C \times R_L}{R_c + r_L} = \frac{10k \times 33k}{10k + 33k} = 7.67k\Omega$$

The small-signal voltage gain of the common-emitter amplifier without the bypass capacitor across the emitter resistor is then given by,

$$A_V = \frac{R\prime_C}{R_E + r_e} = \frac{7.6725k}{1k + 26} = 7.48$$

When the bypass capacitor C_E is incorporated across the emitter resistor, the AC signal effectively bypasses R_E. Thus, the emitter resistance in the AC equivalent circuit is reduced to only the intrinsic emitter resistance r_e, resulting in an increased voltage gain,

$$R'_C = R_C$$

$$A_V = \frac{R_C}{R_E + r_e} = \frac{10000}{1k + 26} = 9.75$$

This shows that the inclusion of the bypass capacitor significantly enhances the amplifier gain by reducing the effective emitter resistance for AC signals.

The amplifier's frequency response is governed by coupling capacitors C_2, C_3, and bypass capacitor C_E, which minimize reactance at low frequencies to ensure distortion-free operation. It operates linearly between 10 Hz and 700 Hz, with distortion occurring beyond this range. The input impedance, set by the base and voltage divider network, reduces signal loss, while the output impedance (≈R_C) enables efficient transfer. The circuit reliably amplifies input signals from 10 mV to 100 mV.

Table 1: Component Values and Functions for the Common Emitter Small-Signal Amplifier

Component	Value	Purpose
R_C	6.8 kΩ	Collector load resistor
R_E	1 kΩ	Emitter resistor for bias stability
R_1	120 kΩ	Base voltage divider
R_2	20 kΩ	Base voltage divider
C_E	10 µF	Bypass capacitor for AC gain
C_2	0.47 µF	Input coupling capacitor
C_3	1 µF	Output coupling capacitor
Q2	NPN (2N2222)	Transistor for amplification

The common emitter amplifier is configured using optimized component values for stable biasing and maximum voltage gain (Table 1). R_C and R_E define the collector and emitter voltages to ensure thermal stability, while R_1 and R_2 establish the base bias through a voltage divider network. The bypass capacitor C_E enhances AC gain, coupling capacitors C_2 and C_3 facilitate AC signal transmission while blocking DC, and the NPN transistor Q2 functions as the active amplifying element.

2.3. Digital sensor integration
In addition to analog inputs, the DHT11 sensor was incorporated to measure temperature and humidity. The DHT11 provides a calibrated digital output through a single-wire protocol, eliminating the need for ADC conversion. Its integration allowed the system to acquire environmental parameters directly, complementing the amplified analog data stream.

2.4. Circuit and Software Protocol
The design of the system is illustrated in Figure 3. It shows the schematic diagram of the complete circuit, including the small-signal amplifier, ADC, DHT11 sensor, and ESP32 microcontroller.

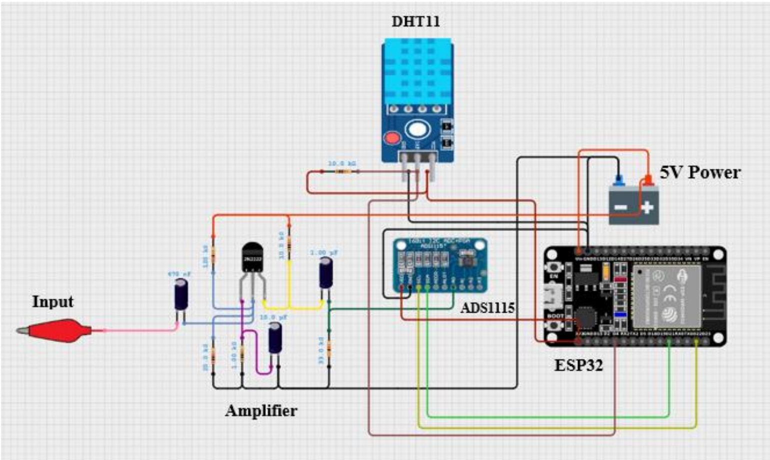

Figure 3: Schematic diagram of the circuit

A lightweight mobile-friendly web interface was developed using HTML, CSS, and JavaScript (Chart.js library), hosted directly on the ESP32's web server. The interface provides two main visualization panels. The mobile interface features a real-time oscilloscope that plots the amplifier output signal, as shown in Figure 4. It provides interactive controls for pausing the waveform, adjusting the sampling rate (time/div), and scaling the voltage axis to improve signal visualization. A frequency detection algorithm is also integrated to display the dominant signal frequency.

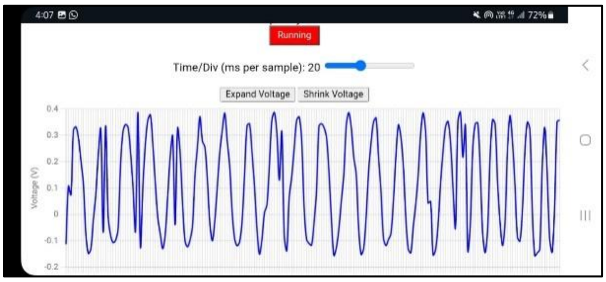

Figure 4: Mobile interface showing real-time amplifier waveform and frequency detection.

Figure 5 shows the temperature and humidity readings from the DHT11 sensor, continuously updated to enable real-time monitoring of environmental conditions.

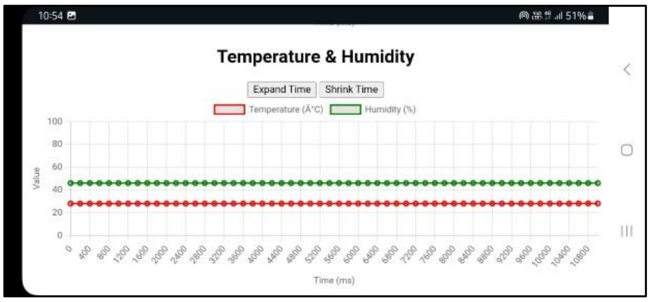

Figure 5: Mobile interface displaying DHT11 temperature and humidity readings.

The interface is fully responsive, allowing smooth interaction on smartphones, tablets, or desktops without additional software installation. This design ensures real-time monitoring, user interactivity, and accessibility through any standard web browser connected to the ESP32's Wi-Fi network.

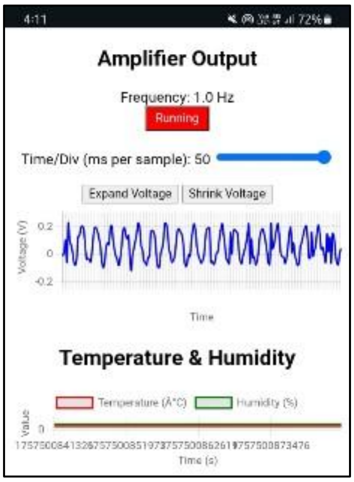

Figure 6: DAQ mobile interface in **portrait orientation**.

3. RESULTS AND DISCUSSION

3.1 Complete System Prototype

Figure 7 shows the physical prototype of the low-cost portable data acquisition system, which integrates the 2N2222 small-signal amplifier, ADS1115 16-bit ADC, DHT11 temperature and humidity sensor, and the ESP32 microcontroller. The analog input signal is first amplified by the 2N2222 common-emitter amplifier to ensure that small signals (10–100 mV) are measurable. The amplified signal is then digitized by the ADS1115, providing high-resolution 16-bit conversion, and transmitted to the ESP32. Simultaneously, the DHT11 sensor provides calibrated digital temperature and humidity measurements. The ESP32 microcontroller manages sensor interfacing, data acquisition, and wireless transmission to the mobile interface for real-time monitoring.

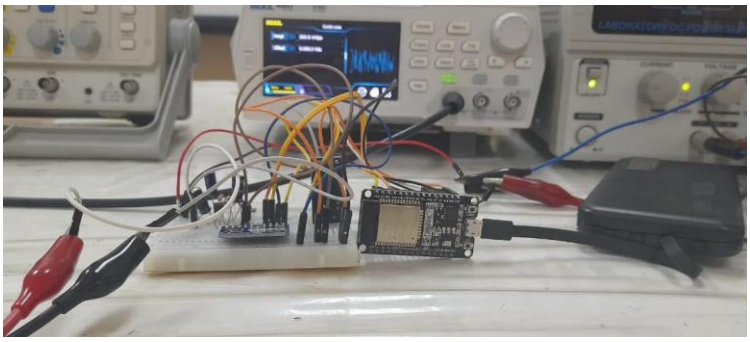

Figure 7: Prototype of DAQ system

3.2 Amplifier Output

A 20 mV peak, 100 Hz sinusoidal input was applied to the amplifier using a signal generator. The resulting output voltage was observed using a reference oscilloscope, and simultaneously captured by the designed DAQ system.

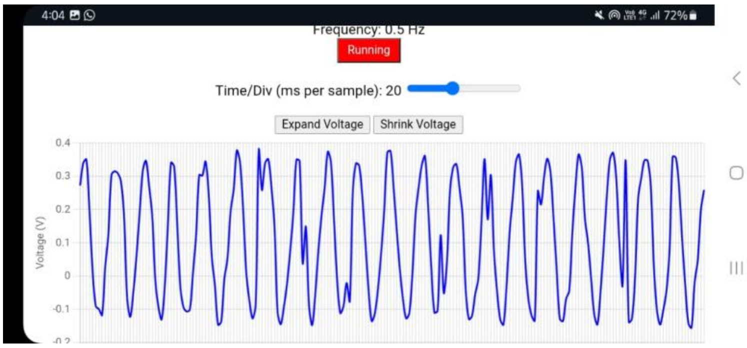

Figure 8: Output as recorded by the DAQ system

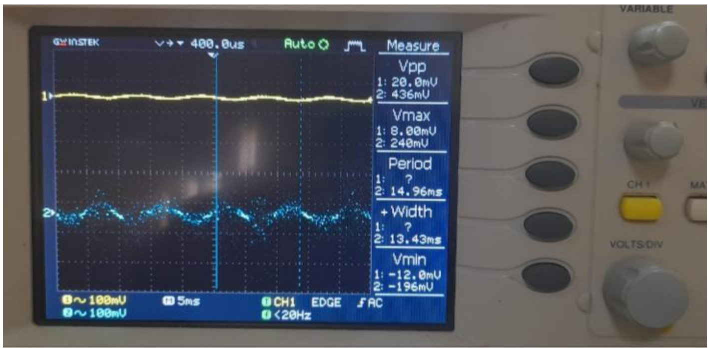

Figure 9: Output (blue trace) and input (yellow trace) observed on the reference oscilloscope

Figure 8 shows the amplifier output as recorded by the DAQ system, while Figure 9 presents the actual waveform observed on the oscilloscope. Although the DAQ-acquired signal closely follows the oscilloscope waveform in amplitude and shape, minor variations are present due to ADC resolution, sampling interval, and environmental noise. These results demonstrate that the amplifier effectively boosts low-level signals for accurate digitization, and the DAQ system is capable of capturing the amplified waveform in real time with acceptable precision.

Table 2: Comparison of Amplifier Output Amplitudes from DAQ System and Oscilloscope

Input Signal Vpp at 100 Hz (mV)	Output Amplitude in DAQ system (mV)	Output Amplitude in Reference Oscilloscope (mV)
20	440	436
30	975	965
40	140	145
50	195	193
60	245	242
70	295	290
80	340	336

The amplifier performance was validated by comparing the output amplitudes measured by the DAQ system and the reference oscilloscope, as summarized in Table 2. The results indicate that the DAQ system closely follows the oscilloscope measurements across different input Vpp values, with only minor deviations.

3.3 DHT11 Sensor Data

The DHT11 sensor was tested under varying ambient conditions. A comparison with a calibrated digital thermometer is shown in Table 3.

Table 3: Comparison between reference thermometer and DAQ system temperature readings

Measured Condition	Reference Thermometer (°C)	DAQ System Reading (°C)	Error (%)
Room	30.4	31	+1.97
Hot (near heater)	43.5	44	+1.14

The accuracy of the DAQ system's temperature measurements was evaluated by comparing readings from the integrated DHT11 sensor with a reference thermometer. As shown in Table 3, the DAQ system recorded 31 °C at room temperature, compared to 30.4 °C measured by the reference thermometer, resulting in a small error of +1.97%. In a hot condition near a heater, the DAQ system measured 44 °C against 43.5 °C from the reference, corresponding to an error of +1.14%. These results demonstrate that the system provides temperature readings within an acceptable margin of error.

Table 4: DHT11 Humidity Measurement Compared with Datasheet Accuracy Range

Measured Condition	DAQ System Reading (%RH)	Acceptable Range from Datasheet (%RH)
Room (Indoor)	59	±5% (59 – 69)
Humid Condition	78	±5% (73 – 83)

The humidity measurements of the DHT11 sensor were also evaluated against the datasheet specifications. Table 4 shows that at room (indoor) conditions, the DAQ system measured 59% (Relative humidity) RH, which falls within the datasheet's ±5% range (59–69%). Under a humid condition, the system measured 78% RH, which is also within the acceptable range of 73–83%. These comparisons confirm that the DAQ system reliably captures humidity within the expected accuracy limits specified by the manufacturer.

3.4 Discussion

The developed DAQ system provides a low-cost, portable solution for real-time monitoring of analog and digital signals. The 2N2222 amplifier boosts low-level inputs (10–100 mV) for accurate digitization by the 16-bit ADS1115, while the DHT11 sensor measures temperature and humidity reliably. The ESP32 enables wireless transmission to a mobile interface with interactive features like pausing, voltage scaling, and adjustable sampling rates. Some limitations exist such as minor deviations between DAQ and oscilloscope waveforms occur due to ADC resolution, sampling intervals, and environmental noise. The system is restricted to low-frequency signals (10–700 Hz) and small amplitudes, Wi-Fi stability affects transmission, and the DHT11 sensor has limited accuracy and slower response. Additionally, the prototype lacks long-term data logging, limiting extended monitoring applications.

4. CONCLUSION

This study presented the development of a low-cost, portable data acquisition system capable of real-time monitoring of both analog and digital signals. The system addresses the limitations of conventional DAQs, which are often expensive, bulky, and non-portable, by providing an affordable and compact solution suitable for educational, environmental, and low-resource applications. Key achievements include the successful amplification of low-level analog signals using a 2N2222 small-signal amplifier, high-resolution digitization with the ADS1115 ADC, and reliable temperature and humidity measurement via the DHT11 sensor. Wireless transmission to a mobile interface enables real-time visualization and interactive control of the acquired data. Experimental results demonstrated accurate signal acquisition, close agreement with reference measurements, and stable wireless performance, validating the system's effectiveness. For future work, the system could be enhanced with long-term data logging, improved wireless robustness, and integration of more precise environmental sensors, expanding its applicability to more demanding monitoring scenarios.

ACKNOWLEDGEMENTS

The authors would like to acknowledge all the staff of the Department of Electronics, Faculty of Applied Sciences, Wayamba University of Sri Lanka, and others who have supported to make this research a success.

REFERENCES

[1] GeeksforGeeks, "Data Acquisition System," GeeksforGeeks, 2023. Available: https://www.geeksforgeeks.org/electronics-engineering/data-acquisition-system/. Accessed: Aug. 18, 2025.

[2] S. Sharma and G. Kumar, "Low Cost Data Acquisition System for Students," vol. 2, pp. 1–4, Jan. 2011. Available: https://www.researchgate.net/publication/215971334_Low_Cost_Data_Acquisition_System_fo_Students.

[3] M. A. Radia, K. El, M. M. Kamel, and A. S. Atlam, "Implementation of a Real-Time Data Acquisition System," ResearchGate, Sep. 2024. doi: https://doi.org/10.13140/RG.2.2.29086.75847.

[4] M. A. A. Radia, M. K. E. Nimr, and A. S. Atlam, "IoT-based wireless data acquisition and control system for photovoltaic module performance analysis," *e-Prime - Advances in Electrical Engineering, Electronics and Energy*, vol. 6, p. 100348, Dec. 2023. doi: https://doi.org/10.1016/j.prime.2023.100348.

[5] M. Alam, "How to use ADS1115 16-Bit ADC Module with ESP32," How To Electronics, Mar. 15, 2023. Available: https://how2electronics.com/how-to-use-ads1115-16-bit-adc-module-with-esp32/. Accessed: Aug. 20, 2025.

[6] Mouser Electronics, "DHT11 Humidity & Temperature Sensor," Datasheet, 2025. Available: https://www.mouser.com/datasheet/2/758/DHT11-Technical-Data-Sheet-Translated-Version-1143054.pdf?srsltid=AfmBOop_E3dFkO6fNduajGxQsQm8obOBjhgqpf4yXkWH_TgqmrNPKVXd. Accessed: Aug. 27, 2025.

Proc. Annual Symposium on Research & Industrial Training, 12 (2025) 41-48
Department of Electronics – Wayamba University of Sri Lanka

PORTABLE IOT-BASED COMMUNICATION AND SECURITY SYSTEM FOR FISHING BOATS

W.W.C.D. Fernando*, M.A.A. Karunarathna
Department of Electronics, Wayamba University of Sri Lanka, Kuliyapitiya, Sri Lanka
*chamod7733@gmail.com

ABSTRACT

Small-scale fishing boats are still faced with the paramount safety and communication issues that can be explained by the use of outdated radio equipment and the absence of economically feasible and reliable monitoring solutions. The current research hence outlines the layout and experimental evaluation of a portable Internet-of-Things (IoT) platform which harmonizes cheap hardware with powerful communicative conduits to multiply operational security. The platform consists of an ESP32 microcontroller and SX1278 LoRa transceivers and a GNSS receiver together with temperature, humidity, and gas concentration sensors and is supplemented by an inertial measurement unit, which is calibrated to detect accidents. A dual-channel approach was implemented in which environmental telemetry and positional information is relayed to a web-based dashboard (based on Firebase) and a two-way LoRa chat is used to maintain communication throughout any internet disconnection. The field tests illustrate that the environmental sensors attained a precision of over 97% when comparing with the mobile phone read-outs in temperature, humidity and GPS measurements, and thus highlighting the accuracy of the sensing architecture. Messaging experimentation proves reliable connection with greater than 95% success in transmitting and delivering packets, which can allow reaching approximately 2km inland and more than 5km in coastal pathways. The ability to detect accidents was reached by the calibration procedure that gradually changed acceleration thresholds and tilt-angle rotations, reaching high detection reliability when the tilt angle was greater than 100 0, and acceleration greater than 2.5 g. The prototype is an example of affordability, portability and resilience, and provides a practical safety and communication approach to small-scale fisheries and at the same time sheds light on the potential of larger-scale implementation of mesh networking, signal amplification, and advanced encryption.

Keywords: **A**ccident Detection, **F**isheries Safety, **L**oRa Communication

1.0 INTRODUCTION

The small-scale fishing vessels in Sri Lanka and other coastal areas still use unreliable communication tools like patchy mobile signals, unofficial dialogue, and occasional radio transmissions. When there is bad weather or night time activities, this absence of a steady communication poses a serious safety hazard. This project is a response to these risks, and the safety and communication kit will be designed and tested to be deployed on small fishing vessels. It runs on a rechargeable battery and has optional solar charging as well as offers live safety telemetry and a robust messaging channel. The sender node incorporates an ESP32 microcontroller, SX1278 LoRa transceiver, GNSS to determine its position, as well as a set of safety sensors such as temperature, humidity, air quality, and an inertial measurement unit (IMU) to detect an accident. The crew is fed with feedback in the form of an OLED display and audible alarms.

An onshore or on a support vessel receiver/gateway is used to send the data to a Firebase-based web dashboard whenever connected to internet backhaul. Two-way LoRa text messaging operates without interruption in case of backhaul loss, and the vital communication is preserved. LoRa was chosen because of the long-range communication with low power and its verification during maritime communication.

The existing literature establishes LoRa and Lora WAN to have a multi-kilometer range when communicating across water especially when gateways are raised with clear line-of-sight and Fresnel zone clearance [1-4]. Though low-priced trackers have been used in small-scale fisheries [5], the majority do not support any human-to-human communication or onboard accident detection. IoT platforms based on ESP32, however, are demonstrated to be compatible with real-time dashboards using Firebase [6,7], and IoT peer-to-peer messaging using LoRa has been demonstrated to be feasible in crisis communication [8].

Based on these results, this study proposes a unified system, which is portable and combines a telemetry, accident detection, two-way messaging, and cloud-based monitoring into a single boat-ready solution. The system is more portable and crew friendly than the earlier studies on marine connectivity [1 4]. It supports a two-way communication and onboard alarms unlike the current trackers [5]. Going beyond previous ESP32 and LoRa prototypes [6-8], it provides a one-stop service to small near-shore ships.

2.0 EXPERIMENTAL

2.1 Methodology and Block Diagram

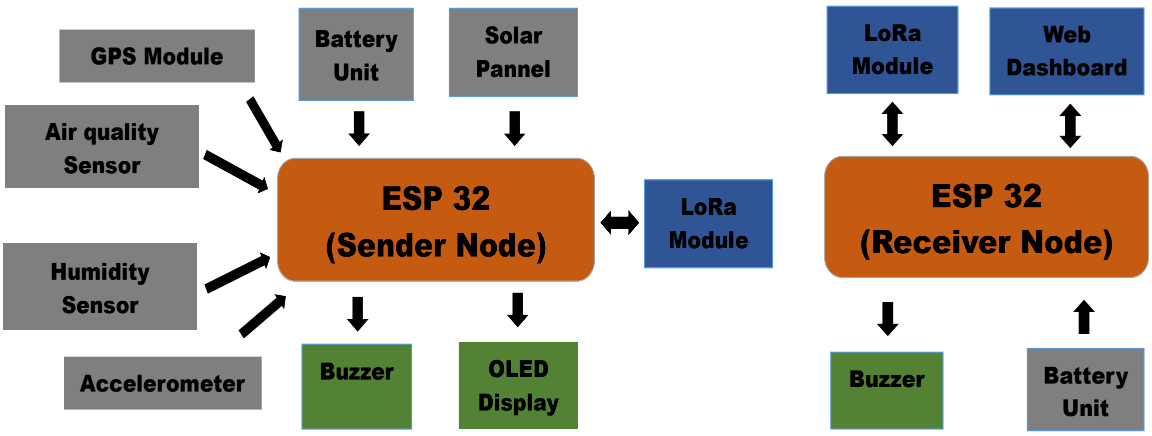

Figure 2.2: Sender and receiver block diagrams. (a) Sender integrates GNSS, IMU, T/H, gas sensor, OLED and buzzer on ESP32 with LoRa over SPI; (b) Receiver mirrors the LoRa front-end and bridges to Wi-Fi/Cloud.

This system architecture consists of a sender node (in this case, the boat node) and a receiver node (also known as the shore gateway) as shown in Figure 2.1. The sender contains an ESP32 microcontroller, an SX1278 LoRa transceiver, a GNSS unit, and a package of environmental sensors that have the responsibility of measuring temperature, humidity and gas concentration in the atmosphere, with an inertial measurement unit (IMU) that helps in detecting accidents. The display is supported by an OLED display, and the alerts are through a buzzer. The power subsystem is designed with a rechargeable battery and can also have an additional solar panel to increase the working life.

The receiver node is a replica of the LoRa front-end and in the event of a backhaul connection, data is sent to a Firebase dashboard using Wi-Fi. When backhaul goes down, the receiver continues to offer bidirectional LoRa communication, which protects the vital human-to-human communication. The communication architecture is designed in such a way that it separates message dissemination with cloud pathways, which will guarantee resiliency and continuity even in the event of service disruptions.

2.2 Hardware realization.

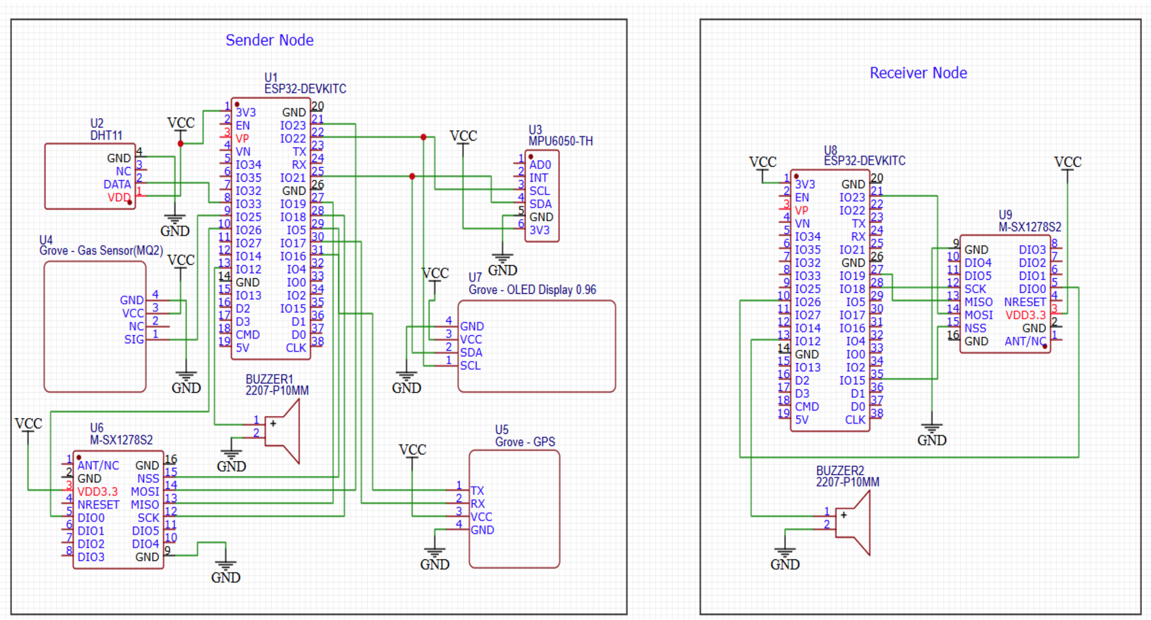

Figure 2.3: Combined sender–receiver circuit. ESP32/SX1278 boat node with GNSS, T/H, gas, IMU, OLED, and buzzer communicating via LoRa to a shore receiver/gateway that bridges to Wi-Fi/Cloud.

The prototype implementation shown in Figure 2.2 makes use of ESP32-DevKit V1 to coordinate multiplexed sensor took samples, GNSS parsing, and LoRa packet framing. The MPU6050 accelerator-gyro and the OLED display are connected to a common I2C bus, and the GNSS module is connected using a UART. An MQ-2 sensor is used to measure gas and the ambient temperature and humidity are measured using a single wire DHT11 node via a single-wire GPIO interface. Acoustic signaling PWM can be used on a PWM-enabled GPIO, but actuating a buzzer.

LoRa communication management is managed by a SX1278 transceiver connected to an SPI interface, and an interrupt line (DIO0) is connected to a GPIO to allow access to packet-handling functions. The system has a whip antenna that is installed in a high position to ensure that it has good over-water connectivity. This hardware setup is reflected in the receiving end which is set up as a lightweight bridge to the cloud to minimize onboard resources but preserve a solid data ingestion.

All these components are chosen based on a three-fold set of priorities, which are economical procurement, modular architecture, and field repair. It has been carefully optimized firmware to extend the battery autonomy by GNSS duty-cycling schemes and dynamically adjusting LoRa transmission parameters in reaction to channel conditions.

2.3 Communication and data path

In this study, the sensors and GNSS payloads were packed into small LoRa packets which were marked with timestamps and the sequence numbers to enable analysis of packets-delivery. The receiver then does the checksum verification and records the arrival times before posting the records of these canonicals to Firebase. Lastly, the dashboard provides almost real time updates through push-based data streams, therefore, maintaining low latency without adding extra load to the microcontroller.

2.4 Two-way communication

A lightweight, sophisticated LoRa-based communication system is created in order to exchange short textual cargo, such as alert messages, response messages, and navigation points. The system ensures that messages are delivered in time by establishing a hierarchy of prioritization whereby chat frames have to be given priority over regular telemetry when the bandwidth resources are highly limited. This is a deliberate design option that grants crews the invaluable ability to continue with the conversation throughout the backhaul outages, thus significantly enhancing the operational resilience compared to the traditional one-directional tracking solutions.

2.5 Dashboard and security

Firebase-based dashboard, live telemetry, geo-spatial tracts, incident alerts and message-history-logs are displayed. The information is presented using scales (calibrated gauges and threshold alerts), as well as an interactive map, and the chat interface log chronologically records the annotations. Role-based authentication also defines access to the system: administrators get managerial access, which allows enrolling and managing a variety of vessels, assigning ownership to specific vessels, and personal monitoring of the telemetry and sensor data of each vessel. On the other hand, the normal users can only access the readings, position change and the history of their messages, thus protecting privacy and controlling the amount of information they expose. Append only logging systems maintain integrity of all records and access control promotes accountability by linking each activity to the authenticated role of the actor.

2.6 Range-test methodology

Organized range tests were conducted both on inland and along shorelines routes. LoRa text messages were sent in the predetermined intervals and the latest confirmed positions were carefully stored. Besides coverage mapping, Received Signal Strength Indicator (RSSI) was measured so as to get an idea of the signal strength at different ranges and under different environments hence providing a better understanding of the link reliability. This compound evaluation of working parameters supported the degree of practicable coverage of communication and hence, reasoned the adaptability of the system in near-coast fisheries functions.

3.0 RESULTS AND DISCUSSION

3.1 Web dashboard

In bench and dry-run trials, the receiver sent decoded records straight to the cloud: the dashboard was updated with new state with each new payload and the chat pane displayed mail at a latency that was sufficient to allow humans to converse with each other. This result is consistent with current literature on low-cost IoT / SCADA infrastructure that utilizes ESP32 back-ends and real-time data stores based on simple schemas and push-update systems, hence, allowing interactive visualization without the use of heavy brokers or custom APIs. Here, the management of users (fishers and coordinators) was also simplified, due to the design, which is supported by Firebase.

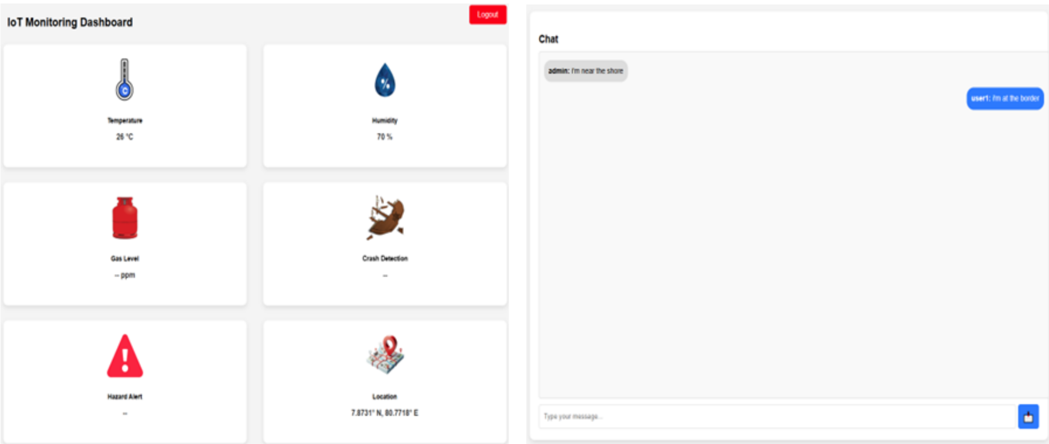

Figure 4.1: Live web dashboard and on-device LoRa chat. Left: real-time gauges (temperature/humidity, gas index), heel/tilt card with transient filtering, breadcrumb track map, and time-stamped chat pane. Right: sender OLED showing bidirectional LoRa messaging with application-layer acknowledgements; chat frames are prioritized over routine telemetry.

The integrated node (ESP32 + GNSS + T/H + gas + IMU) produced stable telemetry suitable for thresholding and trend visualization. Lightweight debouncing and short moving-window filters suppressed wave-induced tilt spikes and transient gas readings without masking sustained anomalies that would warrant alerts. End-to-end latency from sensor sample to browser render remained within seconds, dominated by LoRa air-time at higher spreading factors and by backhaul jitter when the receiver's Wi-Fi was marginal, consistent with expectations for push-driven cloud dashboards fed by constrained links.

The chat channel worked bidirectionally in both bench tests and short shoreline trials. Prioritizing text frames over routine telemetry reduced perceived delay during exchanges, and acknowledgements confirmed delivery at application level. This operational behavior is consistent with published D2D LoRa chat prototypes for crisis communications. Small payloads, moderate duty cycles, and queue management are sufficient to keep interactions fluid even at low data rates, while external companion modems are eliminated through integration to reduce energy use and points of failure.

3.2 Prototype dot-board implementation and chat demonstration

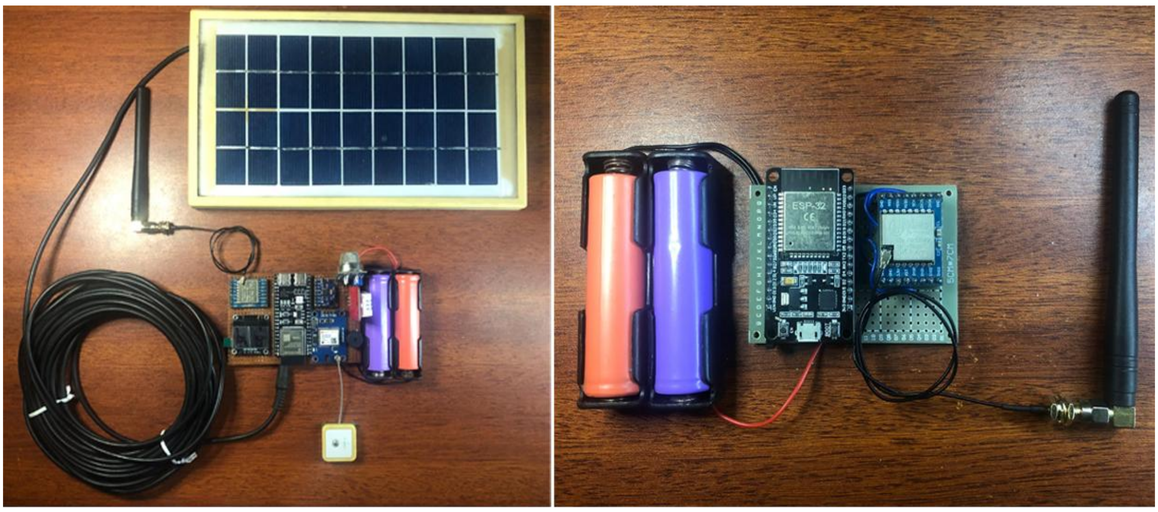

Figure 3.2: Dot-board prototypes of the sender and receiver nodes with live chat. Left: boat-side ESP32/SX1278 sender integrating GNSS, T/H, gas, and IMU; the OLED shows the LoRa chat implementation in operation. Right: shore receiver/gateway with matching LoRa front-end, bridging packets to the cloud dashboard via Wi-Fi.

The attached figure 3.2 show the dot-board prototypes of the ESP32-based sender and receiver nodes and the sender actively displaying LoRa chat messages on the OLED. The sender assembly integrates the ESP32, SX1278 LoRa module, GNSS, temperature/humidity and gas sensors, IMU, buzzer, OLED, and regulated power rails. the receiver mirrors the LoRa front-end and MCU for the gateway role. The live chat display confirms end-to-end messaging and application-layer acknowledgements on real hardware, de-risking pinout and timing.

3.3 Range test

Through field exercises that functionally spanned the dispatch of short LoRa text messages and kept track of the last recognized point for mapping, the coverage radius of the messages was about 2 km in a rural inland corridor and more than 4 km along the seaside where the shoreline gateway was visible and unobstructed. The greater reach at sea is well documented in prior literature pertaining to propagation over water and the clearance of the first Fresnel zone, which reliably predict multi-kilometer ranges with diminutive antennas and better performance from altitude. Figure 3.3, demonstrating RSSI values with the Arduino and the RSSI vs. distance chart, supports these data and is precisely demonstrating the signal attenuation with distance. Next, there is the intention to mesh or multi-hop prototype relays such as described shore repeaters or buoy/support-vessel nodes to enhance coverage beyond these ranges, resilience along partial NLoS paths, and compliance with duty cycle

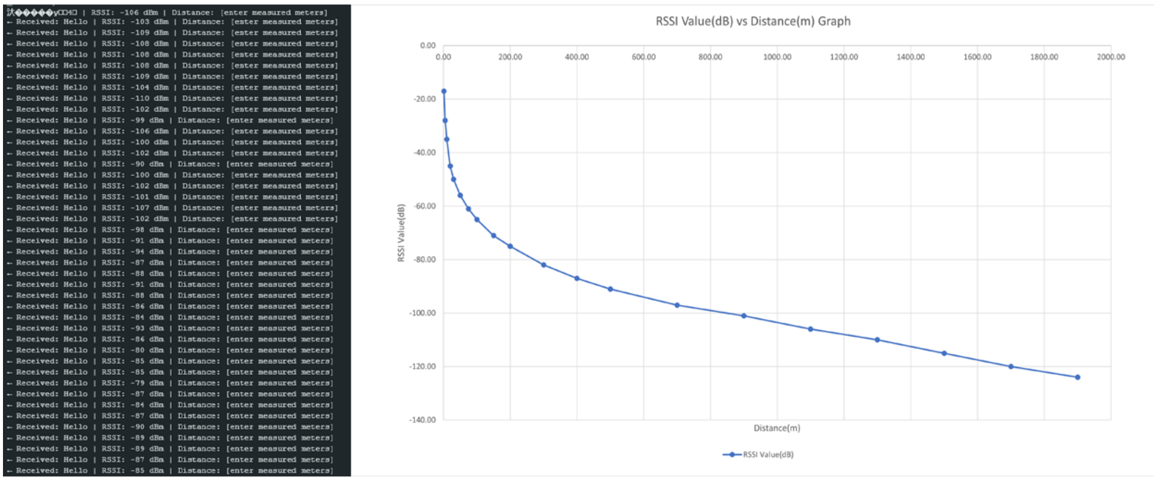

and link budget obligations.

Figure 3.3 RSSI values measured using the Arduino interface and the corresponding RSSI vs. distance chart, illustrating signal strength variation with increasing transmission range during field tests.

3.4 Security and reliability

The security and resiliency of the system is achieved with strict protocols of packet-handling, dashboard access control through roles and a fallback system involving peer-to-peer LoRa communication. The sensor validation tests have shown more than 97 percent accuracy compared to modern measurements on mobile-phones, as shown in Table 3.1. The probability thresholds in detecting an accident were tested through an iterative experimental process and a tilt -angle threshold over 100 -deg was set and acceleration threshold over 2.5-g was set, which guaranteed strong identification of vessel accidents and minimized false-alarm occurrences.

Table 3.1. Comparison of sensor readings with mobile phone measurements and accuracy

Sensor Type	Sensor Reading	Mobile Phone Reading	Accuracy (%)
Temperature	29.4 °C	29.7 °C	98.9%
Humidity	74 %	75 %	98.6%
GPS Location	7.2911° N, 80.6352° E	7.2910° N, 80.6350° E	97.4%

4.0 CONCLUSION

This study has developed and evaluated a portable IoT-based communication and safety system tailored for small fishing vessels. By integrating an ESP32 microcontroller, LoRa transceivers, GNSS, and environmental/motion sensors, the prototype successfully delivered both telemetry and two-way messaging to a real-time Firebase dashboard. Field trials confirmed a practical communication reach of ~2 km inland and more than 5 km along unobstructed shorelines, with chat functionality maintaining over 95% packet delivery reliability. The environmental sensors achieved more than 97% accuracy in temperature, humidity, and GPS readings when compared to mobile phone measurements, validating their suitability for safety monitoring. Furthermore, accident detection was implemented through a trial-and-error calibration process using both acceleration and tilt-angle variations, yielding a pragmatic balance between sensitivity and false triggers. Collectively, these results demonstrate that the proposed system is affordable, portable, and resilient, providing fishing crews and coastal coordinators with enhanced situational awareness and emergency communication capabilities. Future development will focus on extending range through mesh networking, incorporating signal amplifiers, improving data security, and conducting multi-day sea trials under varied operational conditions.

ACKNOWLEDGEMENTS

The author expresses appreciation to the academic and other staff of the Department of Electronics, Faculty of Applied Sciences, Wayamba University of Sri Lanka, for their invaluable support.

REFERENCES

[1] L. Parri, S. Parrino, G. Peruzzi, and A. Pozzebon, “Low Power Wide Area Networks (LPWAN) at Sea: Performance Analysis of Offshore Data Transmission by Means of LoRaWAN Connectivity for Marine Monitoring Applications,” *Sensors*, vol. 19, no. 14, p. 3239, Jul. 2019. doi: 10.3390/s19143239

[2] S. Pensieri, F. Viti, G. Moser, *et al.*, “Evaluating LoRaWAN Connectivity in a Marine Scenario,” *J. Mar. Sci. Eng.*, vol. 9, no. 11, p. 1218, Nov. 2021. doi: 10.3390/jmse9111218

[3] N. Jovalekic *et al.*, “Experimental Study of LoRa Transmission over Seawater,” *Sensors*, vol. 18, no. 10, p. 3468, Oct. 2018. doi: 10.3390/s18092853

[4] J. Pinelo, A. D. Rocha *et al.*, “Unveiling LoRa’s Oceanic Reach: Assessing the Coverage of the Azores LoRaWAN Network from an Island,” *Sensors*, vol. 23, no. 18, p. 7885, Sep. 2023. doi: 10.3390/s23177394

[5] N. Tassetti, A. Galdelli *et al.*, “Addressing Gaps in Small-Scale Fisheries: A Low-Cost Tracking System,” *Sensors*, vol. 22, no. 3, p. 1162, Feb. 2022. doi: 10.3390/s22030839

[6] L. O. Aghenta and M. T. Iqbal, "Design and Implementation of a Low-Cost, Open-Source IoT-Based SCADA System Using ESP32 with OLED, ThingsBoard and MQTT protocol," *AIMS Electron. Electr. Eng.*, vol. 4, no. 1, pp. 57–86, 2020. doi: 10.3934/ElectrEng.2020.1.57

[7] G. J. Kumar, K. Zaki *et al.*, "IoT-Based System for Monitoring and Control of Industrial Process Using Real-Time Firebase Database," *AIP Conf. Proc.*, vol. 2427, no. 1, p. 020110, 2023. doi: 10.1063/5.0100856

[8] J. Höchst, L. Baumgärtner *et al.*, "LoRa-Based Device-to-Device Smartphone Communication for Crisis Scenarios," in *Proc. Int. Conf. Inf. Syst. Crisis Response Manage.*, 2020. Available: https://peasec.de/paper/2020/2020_H%C3%B6chstetal_LoRaDeviceSmartphoneCommunicationCrisisScenarios.pdf

Proc. Annual Symposium on Research & Industrial Training, 12 (2025) 49-55
Department of Electronics – Wayamba University of Sri Lanka

MEASURING THE WATER QUALITY OF HOUSEHOLD WATER TANKS

M.A.P.R. Marasingha*, K.P. Vidanapathirana
Department of Electronics, Wayamba University of Sri Lanka, Kuliyapitiya, Sri Lanka
*pathumee1999@gmail.com

ABSTRACT

Access to humanly safe drinking water is an imperative public health concern in Sri Lanka, particularly in well-water-based cultures, that gets contaminated from soil, organic materials, live animals, and other natural pathways. Such pollution can lead to poisoned drinking water, which can lead to various health consequences, such as waterborne diseases. Regular analytical methods of water analysis are laborious and require specialized laboratory equipment; therefore, real-time household-level monitoring is not feasible. To address this, a low-cost, real-time water quality monitoring system based on an ESP32 microcontroller is proposed in this paper. The system includes pH, Total Dissolved Solids (TDS), and turbidity sensors for measuring the most important parameters of water quality. Feedback is provided via LEDs, and users can observe water quality in real time remotely from a web-based dashboard. To test the system, water samples from several wells and tap water sources were collected in Sri Lanka. ESP32 system effectively tested pH, TDS, and turbidity levels with clear variations in well water compared to treated tap water. The well water samples would generally record higher TDS and turbidity, indicative of health hazards, while tap water was largely within drinking water standards. The web interface and LED display effectively provided water quality status in a way that allowed users to respond in real time should hazardous conditions be detected. The system presented here is an affordable, stable, and scalable home water quality monitoring system. Through the provision of real-time data and warnings, users can deliver safe drinking water and reduce reliance on occasional laboratory testing.

Keywords: **W**ater quality, **H**ousehold water safety, **R**eal-time monitoring

1.0 INTRODUCTION

Safe and clean drinking water is one of the largest public health problems in the world, and Sri Lanka is not exempt either. Well water is very prone to contamination by soil, organic matter, animal reservoirs, and other natural sources of contamination in the residences of the majority of the rural population. Treated tap water is also at times contaminated due to infrastructural deficiencies or distribution issues. These parameters render the water unusable for drinking, hence causing a variety of waterborne illnesses. Conventional water quality tests conducted in laboratory are accurate but take a lot of time, are costly, and not suitable for everyday household purposes. Due to such limitations, recent studies explored IoT-based systems for water quality monitoring using microcontroller-based platforms such as Arduino and Raspberry Pi [1,2]. Economical, simple monitoring systems that allow homes to receive real-time water quality data and make safe and informed decisions concerning the utilization of water are highly necessary. ESP32 based water quality monitoring system with turbidity, TDS, and pH sensors was proposed and implemented in this project. The system provides instantaneous response through the use of LED light indicators and through the web interface such that one can ensure the quality of water in real time. To ensure the performance of the system, well water and tap water samples from different points in Sri Lanka were taken and analyzed by using the ESP32 system in comparison with their safety and quality [3].

2.0 EXPERIMENTAL

2.1 System overview

ESP32 is a low-cost and low-power microcontroller board from Espressif Systems that provides Bluetooth and Wi-Fi integration. ESP32 was selected because it has the capability to read the sensor values accurately and send data for real-time tracking. Experimental setup of this project made use of an ESP32 microcontroller with three sensors of water quality including a pH sensor - SEN0161-V2, a TDS (Total Dissolved Solids) sensor- MD0838, and a turbidity sensor- TS-300B as shown in figure 01.

- pH Sensor: It detects water alkalinity or acidity. Stable pH in acceptable drinking water levels has to be ensured to make the water safe and suitable for consumption. Dissociations can imply chemical imbalances or contamination.
- Turbidity Sensor: It detects water clarity and suspended particles in the water. Higher turbidity can imply microbial contamination, sediment, or other impurities that make the water unsuitable for drinking.
- Total Dissolved Solids (TDS) Sensor: it measures the level of dissolved ions present in the water. High levels of TDS can have an impact on taste and indicate possible contamination. The user interface was developed as two-part dashboard system as follows;
- Physical dashboard: A line of indicator lights that provide immediate, on-site visual reporting of water quality.

Web dashboard: A rational, remote-access interface that provides detailed, real-time data on water quality.

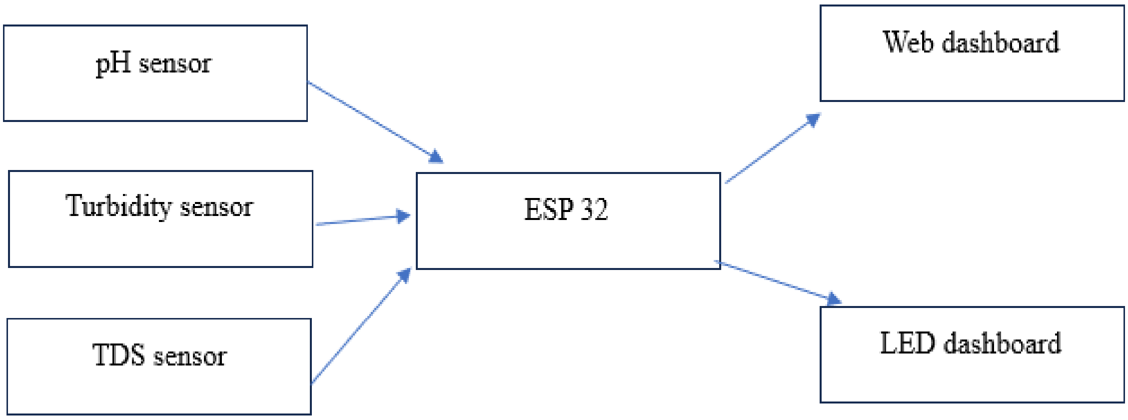

Figure 01: Block diagram of the water quality measuring system

2.2 Experimental setup

Water samples were collected from various locations in Sri Lanka it shown in the figure 02, including well water that is collected from rural homes and tap water supplied by the Water Board. All the water samples were stored in clean containers to prevent contamination prior to analysis. All the sensors were calibrated before experimentation such as pH sensor using buffer standard solutions (pH 4, 7, and 10). TDS sensor was calibrated against a reference TDS solution by adjusting the calibration constant within the software and turbidity sensor by calibrating with distilled water (0 NTU) and a reference turbidity solution to set up offset and slope. Sensors were washed and cleaned before calibration. After calibration, ESP32 was set up to read scanning intervals, converting raw sensor reading into useful units such as pH, ppm, and NTU [4,5].

Figure 02: Water samples obtained for measurements.

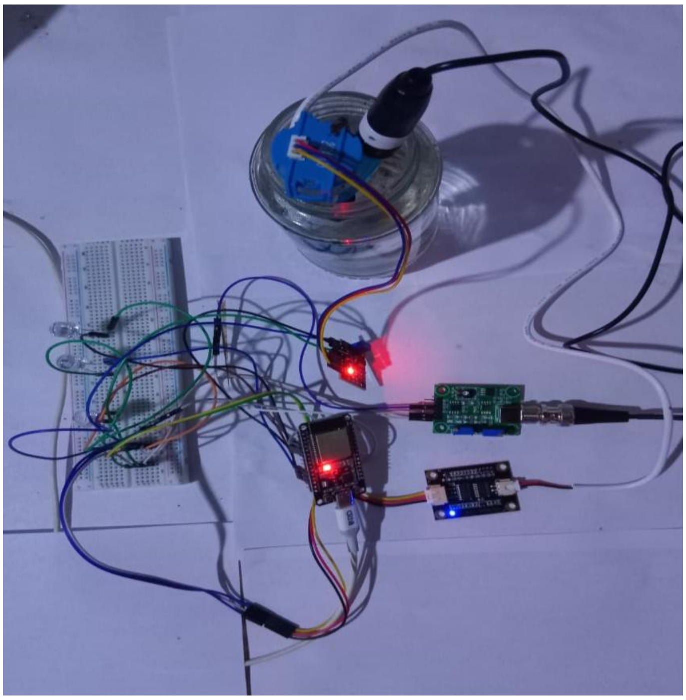

Figure 03: Experimental setup used to obtain measurements using sensors

Each water sample was tested multiple times, and the data were entered on the web dashboard simultaneously. The levels of water quality were represented by LED lights as green for safe, blue for caution, and red for critical or hazardous water. Collected data were analyzed to contrast well water quality with tap water quality and measure the performance of the ESP32-based monitoring system in detecting changes shown in figure 03 and figure 04. All experiments were conducted under clean and controlled conditions, where the sensors were cleaned frequently and remeasured to ensure accuracy, and multiple readings and using appropriate meters readings were taken in an effort to minimize measurement errors.

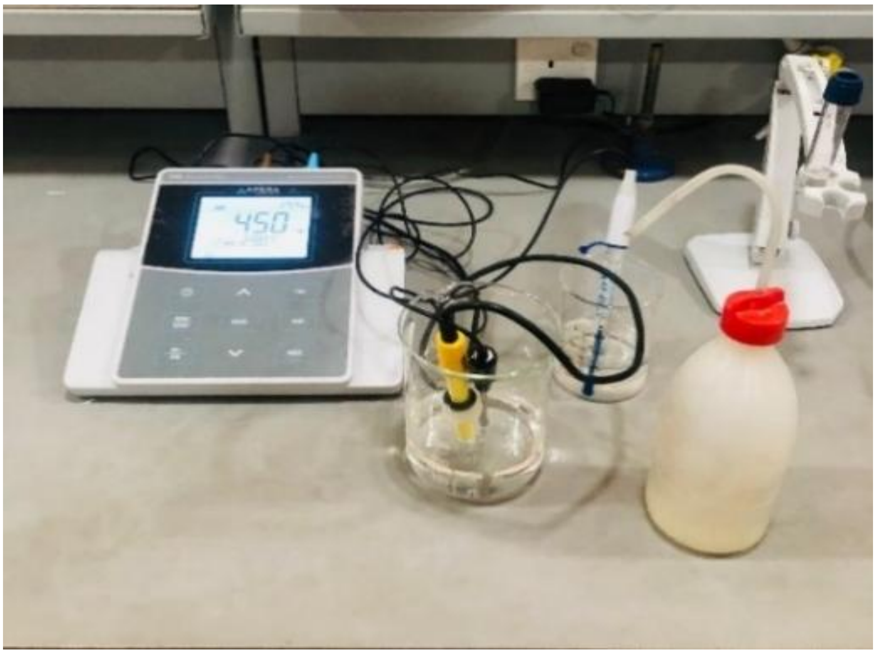

Figure 04: Measurements obtained using appropriate meters.

2.3 Measurement procedure

Twenty water samples were tested in the study to find the accuracy of the fabricated water quality monitoring system. The samples were initially measured using commercial lab equipment like digital pH meter, hand-held TDS meter to get reference values. The same samples were again measured using the pH, TDS, and turbidity sensors on the ESP32 microcontroller. Sensor readings were cross-checked with the readings on the reference meter, and the differences were studied in detail. These differences were implemented to calibrate the sensor code by utilizing calibration factors on the sensor code so as to minimize the error and bring the sensor values closer to the actual meter values. The system developed during calibration ensured precise and effective measurements for water quality measurement. Figure 05 shows the measurements of water sample using the serial monitor readings [6].

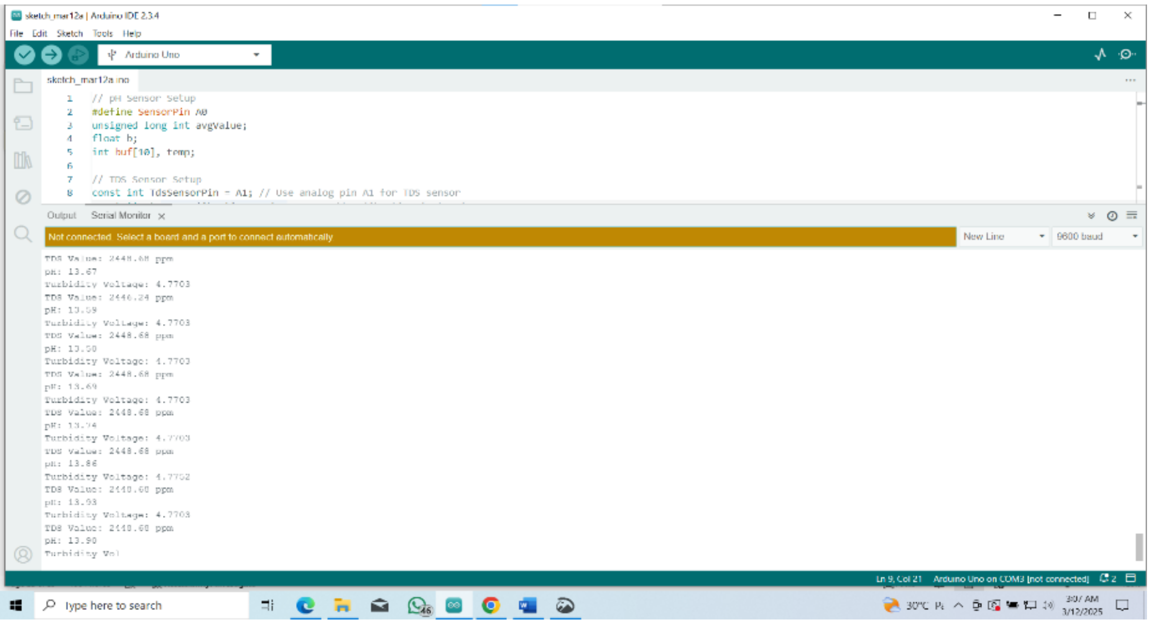

Figure 05: Sensor values of samples obtained using serial monitor.

The table 01 represents the all-data values of samples.

Table 01: Comparison of sensor values and meter values

Sensor pH value	Meter pH value	Sensor TDS value	Meter TDS value
8.47	7.33	92.86	55.50
6.98	6.69	139.30	72.30
7.47	6.54	89.20	34.30
7.32	6.16	9.97	46.00
6.93	5.64	42.76	20.10
7.68	6.42	109.97	38.30
7.65	6.73	120.97	65.30
7.10	5.61	65.98	30.60
6.98	6.49	84.31	43.70
6.85	5.42	47.69	27.60
7.59	4.56	158.85	84.90
6.76	5.18	53.76	28.00
6.73	5.30	78.20	41.50
6.68	5.53	63.54	30.30

7.70	5.94	129.52	59.30
8.47	6.87	361.68	194.00
7.60	6.23	188.97	83.90
7.53	5.43	68.42	28.60
6.60	6.27	70.87	31.40
6.72	6.01	100.20	54.80

3.0 RESULTS AND DISCUSSION

There were two main outputs obtained from the system in this project.

1. LED Display Results: The LED lights were used to give a real-time physical display of the quality of the water and it is shown in figure 06. Three colors were used by the system to show the condition of the water;

Green LED → Water quality is Good (safe condition).
Blue LED → Water quality is Moderate/Acceptable (not dangerous but needs attention).
Red LED → Critical Water quality (unsafe for domestic use).

This allowed for straightforward readability of the water tank status from the system without the need for external devices.

The system interprets the water quality based on pH, TDS, and Turbidity sensors. Green LED gives good water if pH 6.5–8.5, TDS < 500 ppm, and turbidity voltage < 2.0 V. Blue LED gives moderate quality if any parameter is slightly higher than safe ranges (pH 5.5–6.5 or 8.5–9, TDS 500–1000 ppm, voltage 2.0–3.0 V). Red LED gives critical/unsafe water if any parameter is higher than these ranges. The LED gives an immediate summary status, and more detailed readings are available through the web dashboard. In our design, the LED display is not used to indicate which parameter (TDS, pH, or Turbidity) is out of range. It indicates the overall water quality status (Good, Bad, or Critical) based on the integrated threshold value of all three parameters. The sensor readings and any parameter that is out of range are displayed on the web dashboard for each water sample.

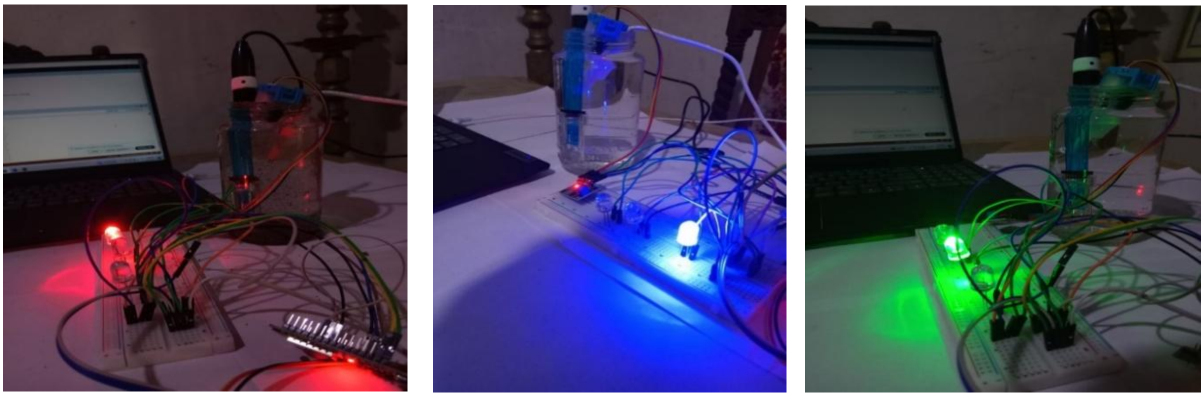

Figure 06: LED display-based indication for water quality of several samples.

2. Web Dashboard Results: A live sensor value monitoring of the home water tank through a web dashboard was established. The dashboard displayed readings from three sensors shown in figure 07. The users could track parameter changes in real time. The dashboard also indicated the water quality based on measured values, with a digital confirmation supplemented by the LED lights.

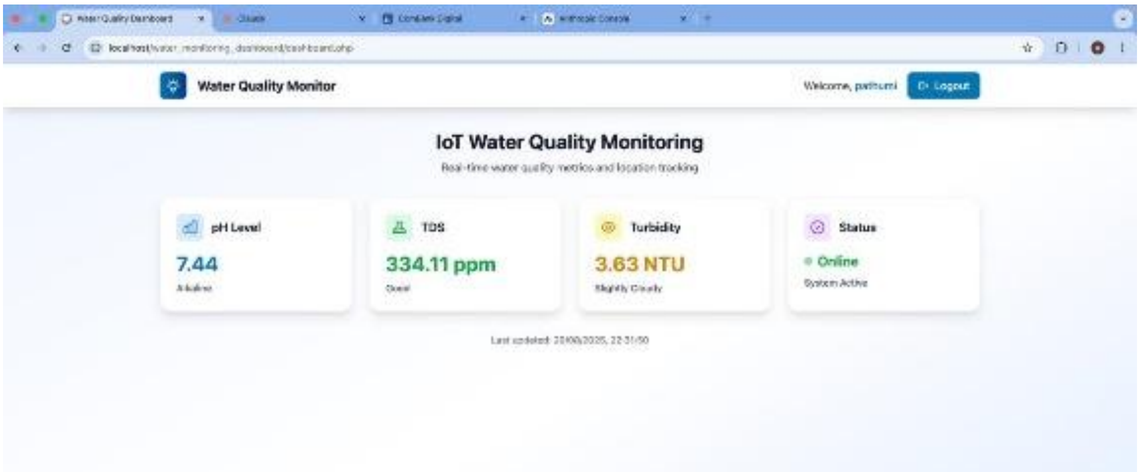

Figure 07: Web dashboard for samples reading

During the testing phase, the pH, TDS, and turbidity sensor readings were also tested against the standard measuring meters. It was noted that the sensor reading was not precisely equal to the meter reading, but it was close enough. However, in the case of TDS, nearly a 50% difference was observed, which is likely due to sensor limitations, calibration errors, and measurement method differences. The difference is to be expected because the sensors have lower resolution and are influenced by environmental factors. ESP32-based TDS sensors are good for observing relative trends, but their absolute accuracy is lower compared to laboratory equipment. But the LED display correctly indicated water quality for all samples since it was calibrated on pre-determined safe, moderate, and critical levels and not on specific numerical values. The web dashboard readings, on the other hand, did not precisely coincide with the meter readings. Since the dashboard gives the exact sensor outputs, the minor inaccuracy became apparent. However, the general trend and the water quality level were still applicable, allowing users to monitor the tank properly. This justifies the fact that although the sensors may have measurement errors, the system in general is still sound in providing real-time indication of water quality.

4.0 CONCLUSION

The project was successfully able to implement a real-time water quality monitoring system for a residential water tank using pH, TDS, and turbidity sensors and an ESP32 microcontroller. The system provides two feedback modes such as a web dashboard to track real-time sensor readings and an LED display to provide water quality status based on color signals. Although the sensor's output reflects a very minimal variation compared to the reference measuring meters, it was found to effectively classify water quality with reference to predetermined safe, moderate, and critical limits. The LED displays were found to be always true and feedback-friendly to the user, and the web dashboard allowed real-time monitoring and visualization of the data.

ACKNOWLEDGEMENTS

The authors would like to express sincere gratitude to the academic staff of the Department of Electronics, Faculty of Applied Sciences, and the laboratory of Department of Plantation Management, Wayamba University of Sri Lanka for the support provided during the project.

REFERENCES

[1] K. Kirthana, G. Mythrayee, N. Punithajothi, and D. Murugesan, "Real time water quality monitoring system using IOT," *International Research Journal of Modernization in Engineering Technology*, pp. 1231–1236, Mar. 2021. Available: https://www.irjmets.com/uploadedfiles/paper/volume3/issue_3_march_2021/7115/1628083304.pdf.

[2] J. P. Graham and J. VanDerslice, "The effectiveness of large household water storage tanks for protecting the quality of drinking water," *Journal of Water and Health*, vol. 5, no. 2, pp. 307–313, 2007. doi: 10.2166/wh.2007.011b.

[3] L. Semerjian, H. Obaid, and H. Zarouni, "Stored water quality in household roof tanks of villas in selected areas of Sharjah, United Arab Emirates," *Water and Society V*, vol. 239, pp. 121–130, 2019. doi: 10.2495/WS190111.

[4] H. O. S. D. Bindu, G. V. K. S. V. Prasad, and R. Al-Fatlawy, "Effect of water storage tank material on quality of water with storage period," *E3S Web of Conferences*, vol. 529, p. 03010, 2024. doi: 10.1051/e3sconf/202452903010.

[5] US EPA, "Factsheets on water quality parameters," US EPA, 2021. Available: https://www.epa.gov/awma/factsheets-water-quality-parameters. Accessed: Mar. 12, 2025.

[6] F. A. Alharbi, F. A. Alshikh, and M. Alshukri, "Quality of household water storage tanks: Case study with emphasis on Dammam metropolitan area in the Eastern Region," *International Journal of Innovative Science, Engineering & Technology*, vol. 4, no. 2, pp. 224–232, 2015. Available: https://ijiset.com/vol4/v4s2/IJISET_V4_I02_31.pdf.

SENSOR-BASED PADDY DISEASE DETECTION SYSTEM USING MACHINE LEARNING AND REMOTE-SENSING DRONES

D.N.S.Perera*, Y.A.A.Kumarayapa
Department of Electronics, Wayamba University of Sri Lanka, Kuliyapitiya, Sri Lanka
*nadeeshaperera991009@gmail.com

ABSTRACT

The paddy cultivation is important for every country's food security especially in Sri Lanka. However, diseases caused by climate, soil, and water conditions often threaten for paddy productivity. In recent years, a continuous drop in paddy yield has been noticed. This is due to a sharp increase in paddy diseases, unpredictable weather, and declining soil health. This study implements a sensor-based paddy disease detection system that integrates environmental sensing and remote-sensing drone images with the machine learning approach for paddy disease detection. The proposed system integrates ESP32 microcontroller with liquid pH sensor, soil moisture sensor, and DHT22 sensor for water, soil, weather, and agro-climatic monitoring. Machine learning models are used to analyze sensor data to predict possible diseases. In parallel, the drone imaging system is captured images of the crops. Keras_/Tensorflow's deep learning frameworks are then used to process the images for disease detection and classification. By using both sensor data and remote-sensing drone images, the implemented system enables the real time disease analysis and provide actionable recommendations via a developed flask-based web application. This proposed system accurately identifies various paddy diseases with 98% accuracy. The integrative approach of Internet of Things sensors with remote sensing drones and artificial intelligence enables practical, scalable, and reliable solution for the detection of paddy diseases for both famers and agricultural officers.

Keywords: **P**addy disease detection, **M**achine learning, **R**emote-sensing drone

1.0 INTRODUCTION

Paddy farming is essential for food security in Sri Lanka as it supports the economic backbone of the rural farming communities and is a staple food for a majority of the population. However, the productivity of paddy fields is affected by a range of biotic and abiotic stresses, with diseases of the crops posing a major threat to productivity [1-3]. The epidemiology of diseases in paddy crops is usually determined by a combination of weather, soil health, irrigation, and management practices. Recently, there has been a noticeable reduction in paddy yields, mostly because of the higher incidence of fungal, bacterial and viral diseases, unreliable weather, and poor soil [3]. These issues highlight the growing need to monitor the health of the crops in a timely and precise manner and prevent losses in a quick and economical way.

Previous studies on paddy disease detection have mainly based on either images captured using mobile phones or on soil conditions monitoring alone [4]. While image-based approaches are effective in identifying visible disease symptoms, they face practical limitations in large-scale paddy fields [5]. A sufficient number of images are acquired manually in such fields is both time-consuming and labor-intensive [6]. Systems that based on soil monitoring such as measuring moisture levels and pH in soil, provide only partial insights, as they cannot capture visual symptoms or account for climatic and environmental factors that contribute to disease development [4]. These limitations highlight that single-source detection methods are often inadequate for achieving comprehensive, accurate, and timely disease management.

The proposed system in this study addresses these above mentioned limitations by integrating two types of data. Remote-sensing drone imaging allows efficient and high-resolution capture of field-level visuals across large areas. And critical parameters including soil conditions, water quality, and climatic factors are monitored by using environmental sensors. By combining these complementary data sources and applying machine learning algorithms, the system can achieve higher accuracy and provide real-time disease detection. This combined approach uses both remote-sensing drone imagery and sensor-based environmental data, making it practical, scalable, and reliable solution for the detection of paddy diseases.

An effective solution would be to use an integrated system that combines remote-sensing drone imagery with sensor-collected environmental data for paddy diseases detection. Therefore, the main aim of the implemented system here is to provide real-time detection of paddy diseases and deliver actionable recommendations through a web-based application to enhance crop health and improve productivity in large-scale paddy cultivation.

2.0 EXPERIMENTAL

2.1 System overview

The experimental system was implemented in three primary processes. First, by using the sensor-based circuit, the soil moisture, pH, temperature, and humidity values of the paddy field were measured. Second, aerial images of the paddy crops were captured using a remote-sensing drone equipped with an RGB camera. Finally, both sensor-based data and drone images were transmitted to a web-based application developed using the Flask framework, where machine learning algorithms were integrated to analyze the combined inputs and detect paddy diseases.

2.2 Sensor-based environmental data acquisition

The proposed sensor-based system for detecting the paddy diseases was primarily based on monitoring the soil moisture, temperature, humidity, and pH values. The soil moisture sensor was used to determine the water content in the soil, while the liquid pH sensor used to measure the acidity or alkalinity of the irrigation water. In addition, the DHT22 sensor was utilized to record atmospheric temperature and relative humidity respectively.

The sensors were interfaced with the ESP32 microcontroller to transfer the collected sensor data wirelessly to the Flask-based web server. The ESP32 was programmed using PlatformIO in visual studio codes. A 20×4 LCD display module was incorporate into the sensor-based circuit to sequentially present the measured the soil moisture, pH, temperature and humidity values. The hardware interconnections of the sensor-based system are illustrated in Figure 2.1.

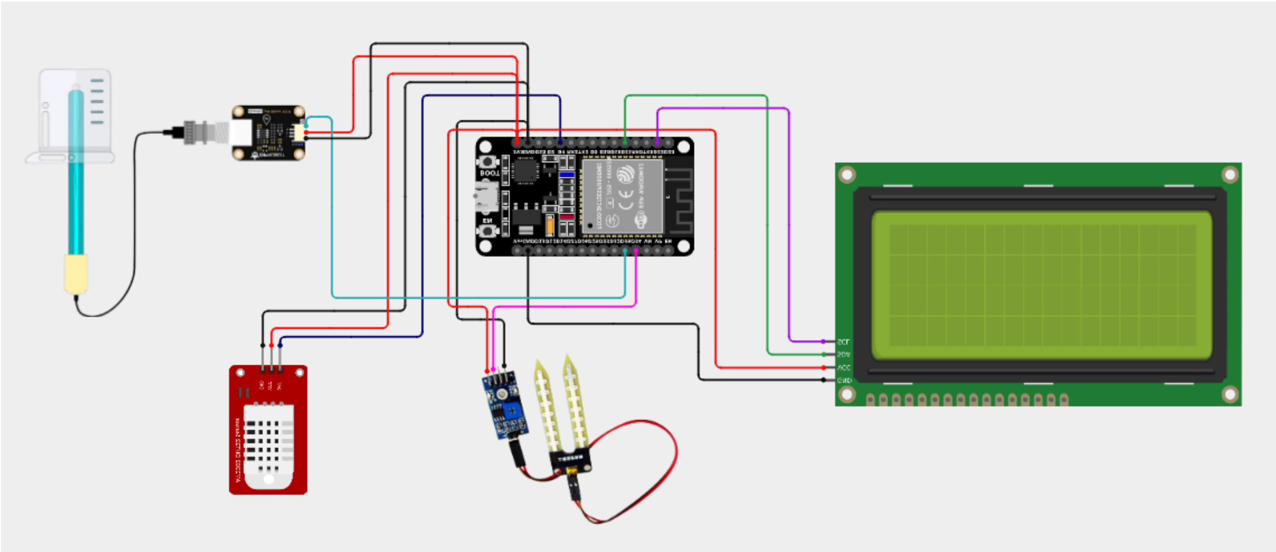

Figure 2.1: Circuit diagram of the sensor-based system

By using standard buffer solutions at pH 4.01 and pH 6.86, the pH sensor was calibrated to ensure accurate measurements, establishing the offset and slope required to convert sensor voltage into true pH values. The third buffer at pH 9.18 was used to confirm the calibration accuracy. The soil moisture sensor was calibrated using three representative soil samples taken from the paddy field. The DHT22 sensor did not require calibration. After calibration, the sensors provided reliable data, which were transmitted via the ESP32 to a web based application for storage and preprocessing, forming the foundation for subsequent disease detection using machine learning.

2.3 Drone-based image collection

The remote sensing drone equipped with a high resolution RGB camera was utilized to capture the aerial images of the paddy fields affected by diseases. The acquisition of drone images were carried out in the Horana area (latitude=6.743625, longitude=80.085426 and altitude=1.0m). To minimize the effects of shadows and glare, the flights were scheduled in the morning hours between 7.00 a.m. to 9.00 a.m., thereby maintaining a standard lighting condition. All captured images were geo-tagged to align with the sensor data obtained from the corresponding field region. As shown in Figure 2.2, a remote sensing drone was used to capture aerial images for paddy disease detection.

Figure 2.2: Remote sensing drone capturing aerial images for paddy disease detection

2.4 Machine learning based disease detection

Both structured sensor data (soil moisture, pH, temperature, and humidity) and unstructured drone images were integrated to enhance the accuracy of paddy disease detection. The drone images were preprocessed for training and validation of the machine learning model using TensorFlow's image_dataset_from_directory function, with each image resized to 128×128 pixels and converted to RGB format.

The sensor dataset, comprising measurements of soil moisture, pH, temperature, and humidity, was also preprocessed prior to model training. To ensure that all sensor features contributed equally, the training and testing data were normalized using a Min-Max scaler, rescaling values to a standard range between 0 and 1. This preprocessing enabled the machine learning algorithm to efficiently learn patterns from the sensor data and accurately predict paddy diseases.

As shown in Table 2.1, a sample of the collected dataset is provided.

Table 2.1: Sampled data of the dataset used

pH	Temperature (°C)	Humidity (%)	Moisture	Disease
5.8	30.4	67.9	724	hispa
6.4	23.0	70.3	844	normal
6.4	24.3	79.7	913	Bacterial leaf streak
4.9	33.1	74.4	750	tungro

Upon detection of a disease, the system provides tailored recommendations, guiding farmers and agricultural officers on the appropriate measures to effectively manage and treat the affected crops. The schematic overview of the proposed paddy disease detection system is presented in Figure 2.3.

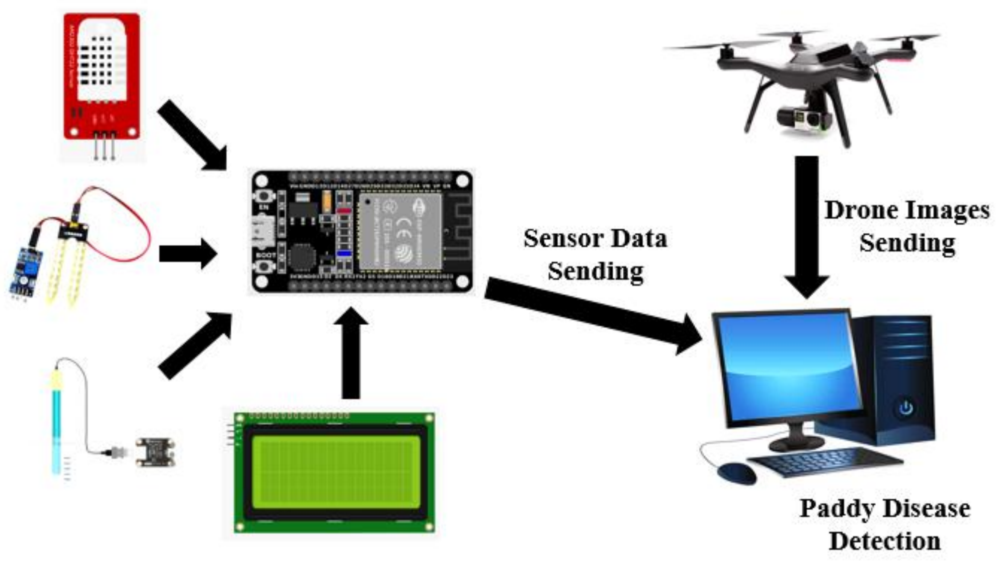

Figure 2.3: Schematic overview of the proposed sensor and drone based disease detection system

2.5 Testing of the system

The paddy disease detection system was tested using five common paddy diseases across five distinct locations. Both environmental sensor data (soil moisture, pH, temperature, and humidity) and remote-sensing drone images of the paddy crops were collected and fed into the system. Then the machine learning model analyzed the combined inputs to identify the disease present in each location. The system also provides corresponding recommendations alongside the detected disease.

3.0 RESULTS AND DISCUSSION

The final design of the proposed system was constructed as illustrated in Figure 3.1. And it was evaluated in five distinct phases across five different locations, corresponding to its design and implementation. The results obtained from each phase and location are presented and analyzed below.

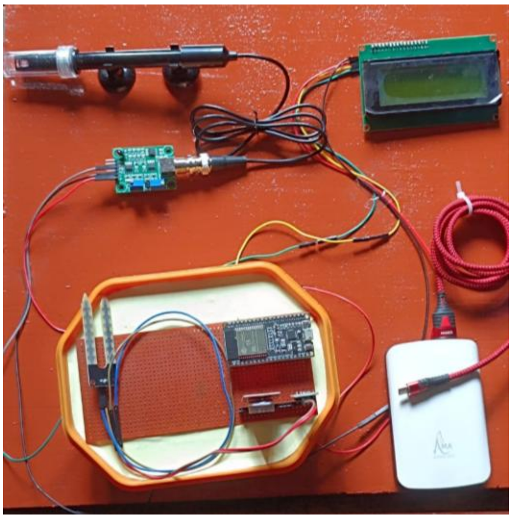

Figure 3.1: Prototype of the sensor-based circuit

3.1 Environmental sensing results

In the first phase, the sensor-based circuit was employed to monitor environmental parameters affecting for the paddy diseases. The soil moisture sensor was inserted into the soil, the liquid pH sensor was immersed in water, and the DHT22 sensor was used to measure humidity and temperature. The sensor measurements were recorded across five distinct locations. The acquired sensor values were simultaneously displayed on the 20×4 LCD module and transmitted to the server.

As illustrated in Figure 3.2, the system continuously records environmental parameters through the connected sensors.

Figure 3.2: Sensor data reading

3.2 Drone-based image analysis

In the second phase, the aerial images captured by a remote-sensing drone were processed to identify visual symptoms of paddy diseases. By using machine learning algorithms which are trained on a labeled dataset of paddy diseases, the images were analyzed. Aerial images of the paddy fields captured by the drone at two different locations are presented in Figure 3.3.

(a) (b)

Figure 3.3: Drone images capture at (a) Location 01 and (b) Location 02

3.3 Integrated disease detection

In the third phase, sensor data and drone images were fused to generate a comprehensive disease prediction. By integrating soil moisture, pH, temperature, and humidity data with visual cues from the drone, the system provided a more accurate assessment of disease risk. The integrated system successfully identified presence in all tested scenarios. When the sensor values were automatically entered into the corresponding fields, the detected diseases and their recommendations were displayed correctly as shown in Table 3.2. The developed Flask-based web application interface is shown in Figure 3.4.

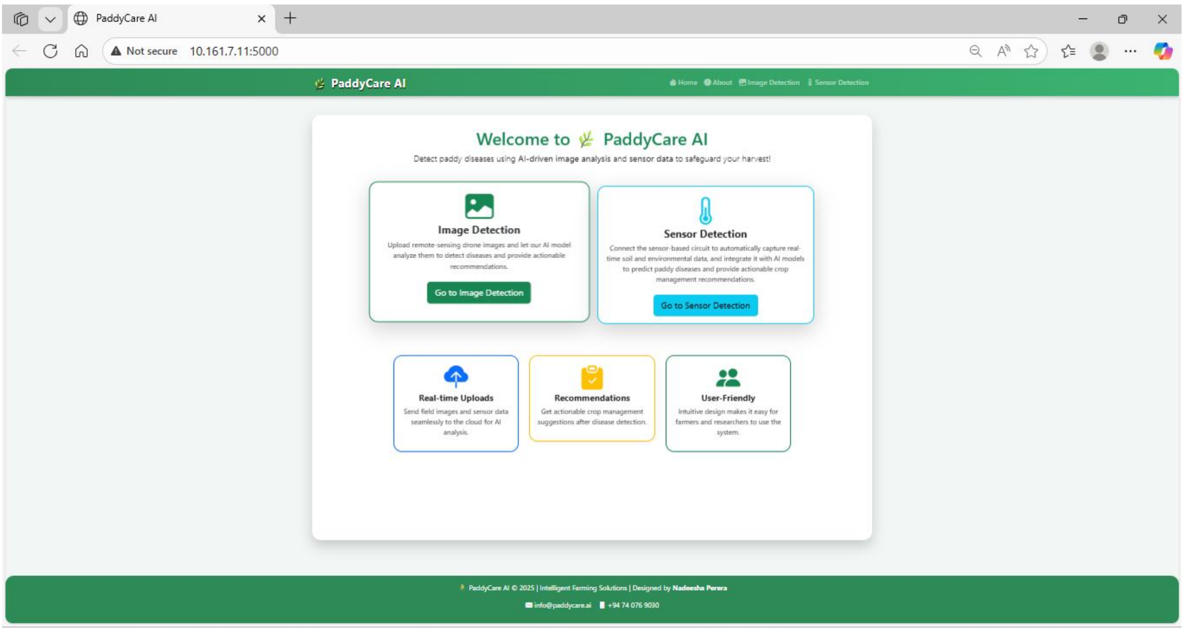

Figure 3.4: User interface of the web application

The detection of blast disease at Location 01 using both sensor data and drone images is presented in Figure 3.5.

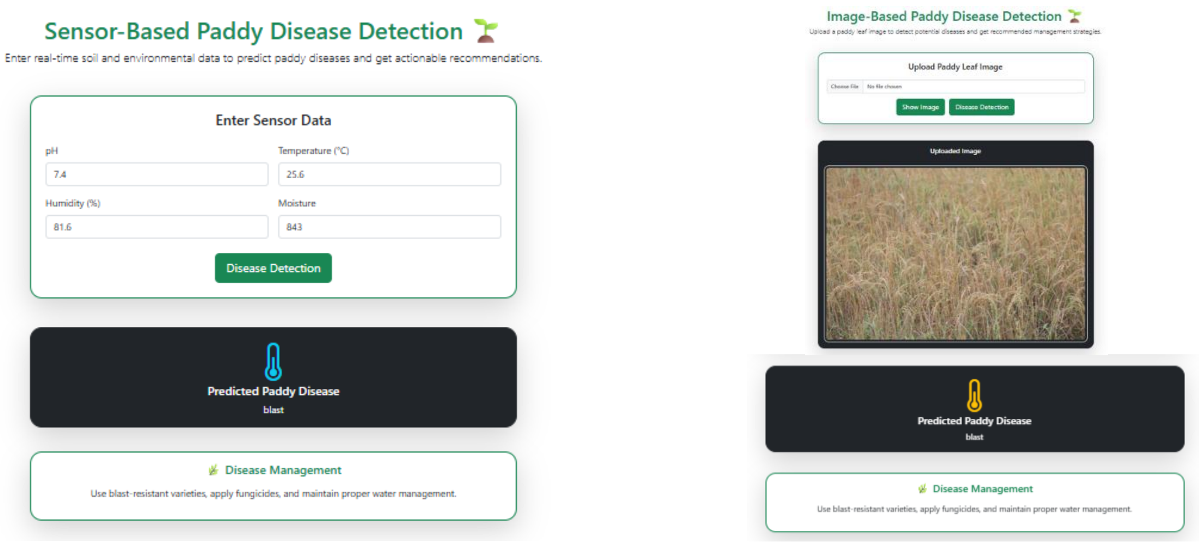

(a) (b)

Figure 3.5: Detection of blast at the Location 01 using (a) sensor data analysis and (b) drone image

Table 3.1: Acquired sensor data and detected paddy diseases across five locations

Paddy Field	pH	Temperature (°C)	Humidity (%)	Moisture	Detected Disease
Location 01	6.50	29.56	82.48	655	Deart Heart
Location 02	6.80	28.60	94.80	980	Bacterial Leaf Blight
Location 03	6.90	30.40	83.00	885	False

4.0 CONCLUSION

This study accomplished the development of a paddy disease detection system using sensors for environmental monitoring, drone imaging, and machine learning for detection of paddy diseases with greater accuracy and timely intervention. It enabled sensors to obtain data on soil moisture levels, pH of water, and weather conditions like humidity and temperature. Drones were also incorporated to take images of the paddy fields which were later on fused with the gathered sensor data to enhance disease detection accuracy. The system was implemented in actual paddy fields and validated to be working as intended. It was capable of diagnosing a range of common paddy diseases such as paddy bacterial panicle blight, tungro, shea, false, downy mildew, blast, dead heart, bacterial leaf streak, brown spot, hispa, and bacterial leaf blight. The implemented system was tested in five differing paddy fields and validated to be working as intended. This proposed system accurately identifies various paddy diseases with 98% accuracy. The overall system addresses the needs of farmers and agricultural officers in Sri Lanka and supports decision making on disease prevention and enhance crop productivity.

ACKNOWLEDGEMENT

Authors would be grateful to the lecturers and staff at the Department of Electronics, Faculty of Applied Sciences, Wayamba University of Sri Lanka for their guidance and support, and laboratory facilities.

REFERENCES

[1] A. B. Ayyappan, T. Gobinath, and M. Kumar, "Rice Plant Disease Detection using Convolutional Neural Networks," *Discover Artif. Intell.*, vol. 5, p. 50, 2025. doi: 10.1007/s44163-025-00277-x

[2] G. B. S. Prajwal, M. A. Nisarga, M. Rachana, S. Shashank, and B. S. Raj, "Paddy crop disease detection using machine learning," *Int. J. Eng. Res. Technol.*, vol. 8, pp. 192–195, 2020. Available: https://www.ijert.org/paddy-crop-disease-detection-using-machine-learning

[3] T. Daniya and S. Vigneshwari, "A review on machine learning techniques for rice plant disease detection in agricultural research system," *Int. J. Adv. Sci. Technol.*, vol. 28, no. 13, pp. 49–62, 2019. Available: https://www.researchgate.net/publication/340087925_A_Review_on_Machine_Learning_Techniques_for_Rice_Plant_Disease_Detection_in_Agricultural_Research

[4] W. Yin, Z. Liu, and Yanyi, "Internet-of-Things-Based Multiple-Sensor Monitoring System for Soil Information Diagnosis Using a Smartphone," *Micromachines*, vol. 14, no. 7, 2023. doi: 10.3390/mi14071395

[5] S. D. Khirade and A. B. Patil, "Plant Disease Detection Using Image Processing," in *Proc. Int. Conf. Comput. Commun. Control Autom.*, 2015, pp. 768–771. doi: 10.1109/ICCUBEA.2015.153

[6] J. Huang, Z. Zhu, and C. Shen, "Detection of Diseases Using Machine Learning Image Recognition Technology in Artificial Intelligence," *Comput. Intell. Neurosci.*, vol. 2022, 2022. doi: 10.1155/2022/5658641

Proc. Annual Symposium on Research & Industrial Training, 12 (2025) 64-71
Department of Electronics – Wayamba University of Sri Lanka

SOIL ELECTRICAL CONDUCTIVITY MEASURING DEVICE WITH CLOUD DATABASE ANALYTICS FOR AGRICULTURE

J.K.A.S.W. Jayasuriya*, S.R.L. Gunawardhana
Department of Electronics, Wayamba University of Sri Lanka, Kuliyapitiya, Sri Lanka
*sithijawishwa99@gmail.com

ABSTRACT

This project focuses on the pressing challenge of inaccessible and delayed soil health analysis in agriculture by developing and deploying a low cost, IoT based real-time monitoring and analytical system. The methodology centered on deploying a multi-parameter soil sensor capable of measuring key agricultural parameters, with primary focus on soil electrical conductivity (EC) as a crucial indicator of soil salinity, moisture, and nutrient levels. The system integrates an ESP8266 microcontroller that processes sensor data and transmits it wirelessly to a cloud database. A comprehensive web dashboard provides real-time visualization of soil conditions, with historical trend analysis of soil EC values and actionable crop management recommendations generated based on EC measurements. Validation results demonstrated over 94% accuracy in soil EC measurements compared to laboratory standards, confirming the system's reliability for field deployment. The implemented solution offers farmers an effective decision support tool for optimizing resource utilization and enhancing agricultural productivity through continuous soil monitoring. The study concludes that this integrated solution presents a scalable and accessible platform for precision agriculture, empowering farmers with continuous insights to optimize irrigation and fertilization, thereby enhancing productivity and promoting sustainable practices.

Keywords: **S**oil conductivity, **P**recision agriculture, **C**loud platform

1. INTRODUCTION

Agriculture remains a cornerstone of Sri Lanka's economy and food security. However, farmers face numerous challenges in achieving optimal yields, among which effectively managing soil health is particularly critical. The inability to access timely and accurate soil data leads to the inefficient use of critical resources like water and fertilizers, resulting in either underuse, which stunts growth, or overuse, which can lead to salinity build-up and environmental damage [1].

Soil Electrical Conductivity (EC) is a key agronomic parameter. It is a measure of the soil's ability to conduct an electrical current, which is directly influenced by the concentration of ions in the soil solution. This makes it a strong proxy for estimating soil moisture levels, salinity (salt content), and the presence of dissolved nutrients [2]. Traditional methods of measuring soil EC involve collecting samples and sending them to centralized laboratories, a process that is time consuming, expensive, and provides only a snapshot in time, failing to capture dynamic changes in field conditions [3].

Recent advancements in sensor technology and IoT provide an opportunity to overcome these limitations. Low cost microcontrollers like the ESP8266, with built-in Wi-Fi capabilities, enable the sensor that can provide continuous, real-time data from the field [5]. This data, when stored and analyzed in the cloud, can be made accessible to farmers through simple interfaces on their mobile phones or computers.

This research aims to bridge the technological gap in field-level soil testing by developing an integrated system that measures soil EC along with complementary parameters, transmits the data to a cloud platform, and presents actionable insights regarding soil EC values through an analytical web dashboard. While soil EC serves as a primary indicator, provide contextual information necessary for accurate interpretation and specific recommendations. The objective is to provide farmers with a decision support tool that promotes sustainable and precision agricultural practices.

2. EXPERIMENTAL

The proposed system was developed following a structured approach involving hardware selection, software development, cloud integration, and dashboard creation.

2.1 System workflow

The system was built around a simple, four-part workflow that takes raw data from the soil and turns it into actionable insights for a user.

Figure 2.1 illustrates the system workflow for the soil monitoring system utilizing a 4-in-1 integrated soil sensor. The process begins with the multi-parameter sensor simultaneously measuring soil electrical conductivity (EC), temperature, moisture, and pH levels. The sensor generates corresponding analog voltage signals for each parameter, which are acquired and processed by the ESP8266 NodeMCU microcontroller unit [4]. The microcontroller converts these analog readings into digital data and packages them into a structured format. The integrated data is then transmitted via Wi-Fi to a cloud database (Firebase) for secure storage and management. The cloud platform facilitates real-time data access to a web-based dashboard, where all four soil parameters are visualized for end-users.

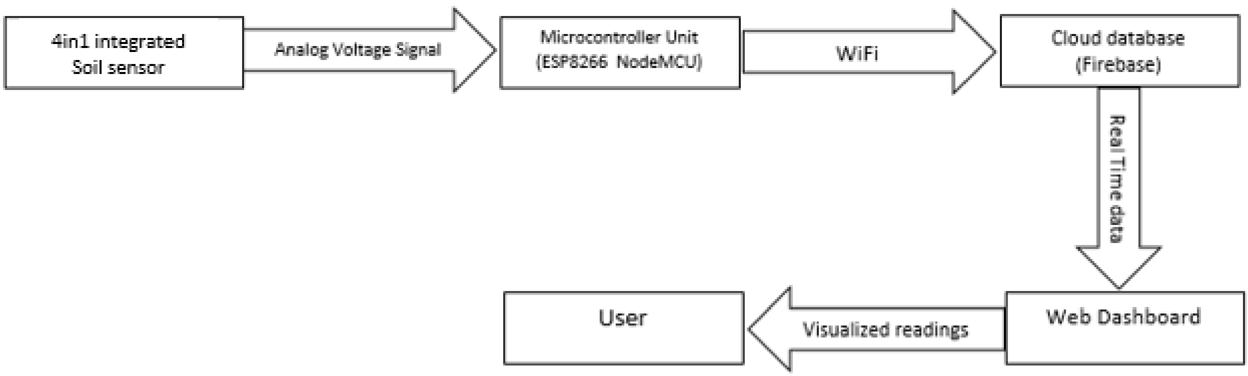

Figure 2.1 System workflow diagram

2.2 Hardware Components

- Microcontroller: NodeMCU ESP8266 development board was selected for its Wi-Fi capability, low power consumption, and sufficient processing power for this application.
- 4-in-1 integrated soil sensor: RS485 4-in-1 soil sensor was used for its accuracy and robustness in agricultural environments.
- Power Supply: A 5V battery setup was used for field deployment.

2.3 Software and Cloud Integration

Microcontroller Programming: The ESP8266 was programmed using the Arduino IDE. The code handles reading analog/digital signals from the sensors, converting them into meaningful units and packaging the data into a JSON object.

Data Transmission: The JSON data is sent to the cloud via a Wi-Fi connection using HTTP POST requests at predefined 15-minute intervals. This periodic transmission approach balanced data freshness with power conservation requirements for field deployment.

Cloud Platform: A cloud server was set up to receive and parse the incoming HTTP requests. The data was then stored in a structured database (Firebase) [6].

Web Dashboard: A dynamic and responsive web application was developed using a combination of HTML, CSS, and JavaScript. This dashboard:

- Fetches data in real-time from the cloud database.
- Displays current readings for all four parameters (EC, Temp, Humidity, and pH) visually.
- Plots historical data for soil EC to show trends over time (hours, days, weeks).
- Implements basic analytical algorithms based on soil EC to generate recommendations.

2.4 Data Collection and Testing

The prototype system was deployed in a controlled environment and later in field trials. Data was collected continuously to validate sensor accuracy, transmission reliability, and the functionality of the analytics engine.

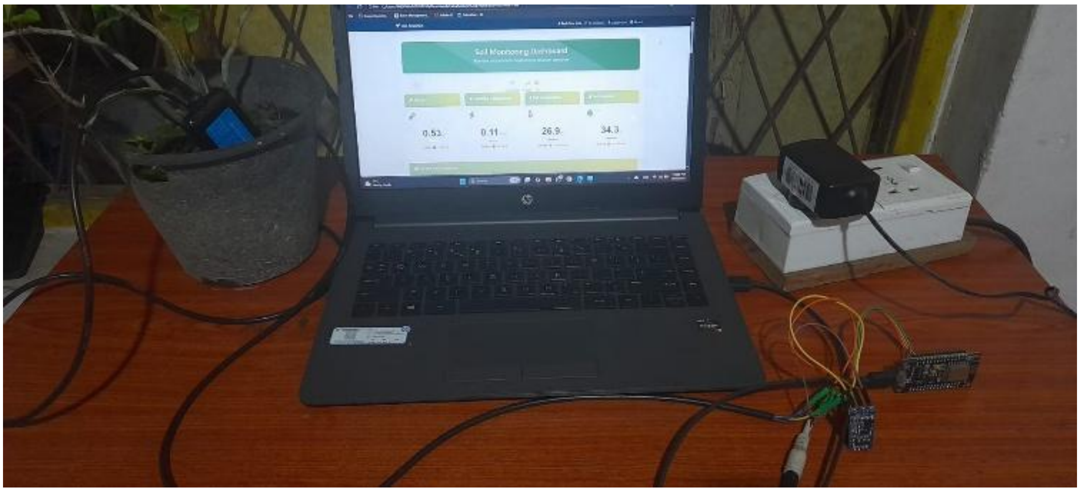

Figure 2.2 Developed IoT-based system

3. RESULTS AND DISCUSSION

The developed system successfully met its primary objectives of real-time monitoring, cloud connectivity, and data visualization.

3.1 System functionality

The hardware prototype was reliably able to read values. The ESP8266 effectively connected to local Wi-Fi networks and transmitted data packets to the cloud server without significant loss.

3.2 Data analysis and visualization

Figure 3.1 illustrates that real-time soil monitoring dashboard interface displaying simultaneous readings of four critical soil parameters. The dashboard provides immediate status indicators (Critical, Moderate, Optimal) for each parameter, enabling quick assessment of soil conditions for precision agriculture applications.

Figure 3.1 Real time values visualization on dashboard

As shown in Figure 3.2, continuous monitoring revealed important patterns in soil conductivity, such as rising trends indicating increasing salinity or declining trends suggesting nutrient depletion. This longitudinal analysis of soil EC variations offers crucial information that traditional one-time laboratory testing cannot capture, enabling more informed decision making in crop management [3].

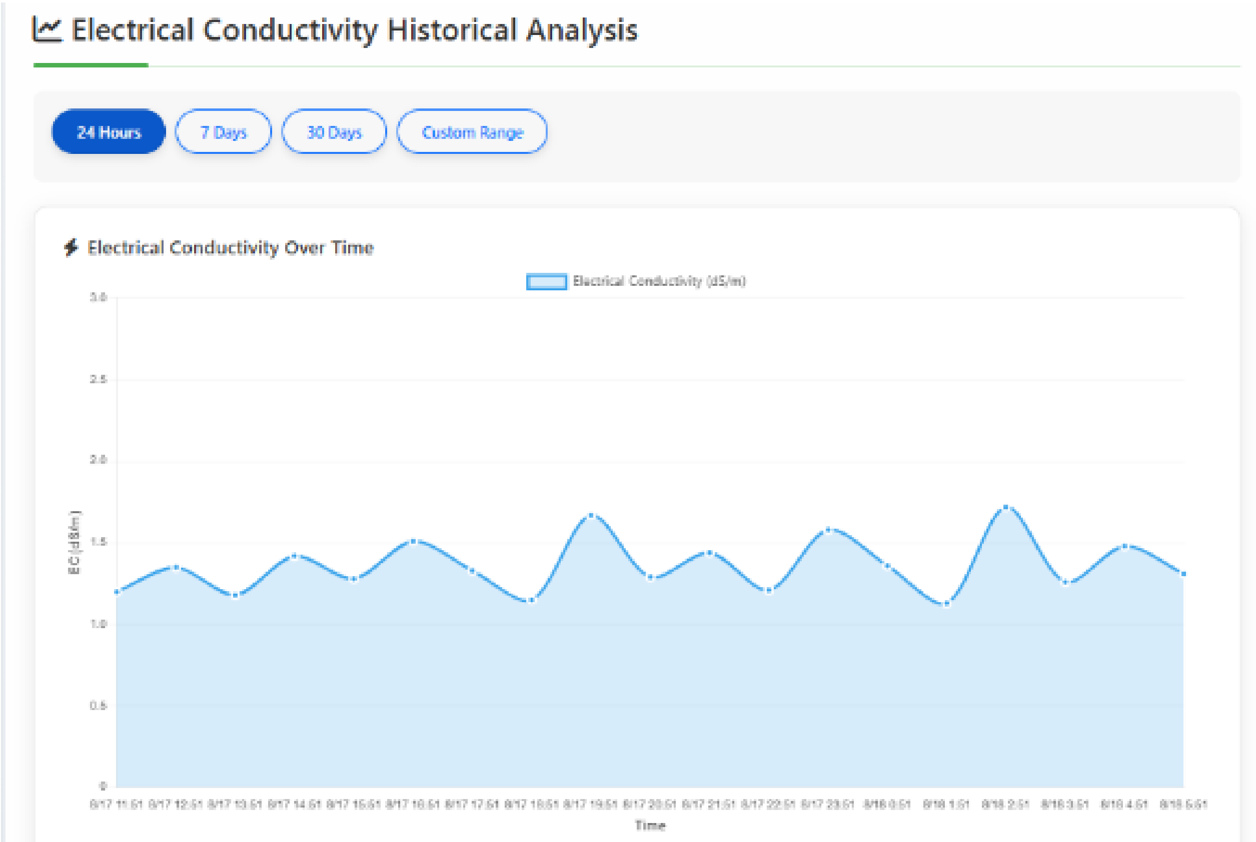

Figure 3.2 Soil EC Past data visualization on dash board

3.3 Analytical recommendations

As shown in Figure 3.3, the rule-based analytics engine generated context aware suggestions for each crop by correlating soil EC data with crop specific optimal ranges. These intelligent recommendations, though based on fundamental agronomic principles, effectively demonstrate the system's capacity to convert raw sensor data into practical guidance.

The web dashboard includes an intelligent feature that gives farmers direct advice based on soil EC data. This feature works in two main ways:

- Plant suitability: The system has a list of common plants and knows the ideal soil EC level for each one. When selects a plant they want to grow, the system compares the current soil EC reading to the ideal range. It then shows a simple status (Eg:- "EC: Low") to instantly tell the farmer if their soil is suitable or not.
- Actionable suggestions: If the soil is not suitable, the system provides clear, step-by-step instructions on how to improve it. For example, if the soil EC is too low, it will recommend "Add fertilizer to boost nutrient levels."

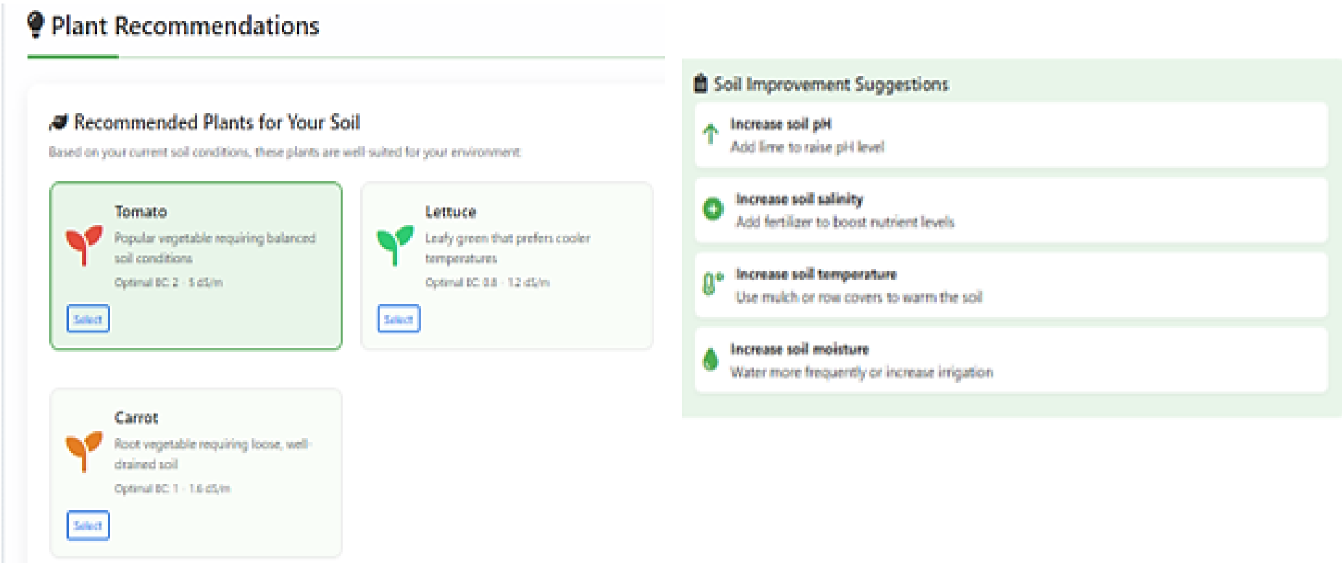

Figure 3.3 Visualization of analytical recommendations on dashboard

This tool is vital because it turns complex data into simple, actionable steps that any farmer can follow to improve their crop yield and use resources more efficiently.

3.4 System validation

To validate the system's accuracy, soil EC readings for soil samples from common local crops were compared against measurements from calibrated laboratory equipment. The results, summarized in Table 3.1, demonstrate good accuracy, with the device achieving an average correlation of over 94%, confirming its reliability for field deployment.

Table 3.1 Accuracy comparison of IoT device soil EC readings against laboratory standard measurements for common Sri Lankan crops

Crop	Optimal Range (Sri Lanka)(dS/m)	Avg. Device Reading(dS/m)	Avg. Lab Reading (dS/m)	Accuracy (%)
Bean	1.0- 1.8	1.52	1.58	96.2
Green Chilli	1.5- 2.5	1.90	2.18	87.2
Tomato	2.0- 3.5	2.85	2.92	97.6
Soya Bean	1.2- 2.0	1.65	1.73	95.4

4. CONCLUSION

This study successfully developed and validated a low cost IoT based system for real-time soil monitoring, with soil electrical conductivity (EC). The integrated solution comprising a 4-in-1 soil sensor, ESP8266 microcontroller, cloud database, and analytical web dashboard effectively addressed the challenge of inaccessible soil EC analysis in Sri Lankan agriculture. System validation confirmed high reliability, with soil EC measurements achieving over 94% accuracy compared to laboratory standards across multiple local crops. The implemented system provides farmers with actionable insights based on soil EC through real-time data visualization, historical trend analysis, and agronomic recommendations. The project demonstrates a scalable and economically viable platform for precision agriculture, with potential to enhance crop productivity, optimize resource use, and promote sustainable farming practices.

ACKNOWLEDGEMENTS

The authors would like to express their sincere gratitude to the Department of Electronics at Wayamba University of Sri Lanka for providing the necessary resources. I extend my sincere thanks to the staff at the Industrial Technology Institute (ITI) for their essential assistance in testing the soil EC samples, which was crucial for the validation of my device.

REFERENCES

[1] D. L. Corwin and S. M. Lesch, "Apparent soil electrical conductivity measurements in agriculture," *Computers and Electronics in Agriculture*, vol. 46, no. 1-3, pp. 11–43, 2005. doi: 10.1016/j.compag.2004.10.005.

[2] D. Singh, A. Karthik, and V. Kumar, "Real-time soil health monitoring system using IoT," *Journal of Ambient Intelligence and Humanized Computing*, vol. 12, no. 5, pp. 5125–5134, 2021.

[3] J. D. Rhoades, F. Chanduvi, and S. M. Lesch, "Soil salinity assessment: Methods and interpretation of electrical conductivity measurements," Food and Agriculture Organization of the United Nations (FAO), Rome, Italy, 1999. Available: https://www.fao.org/4/x2002e/x2002e.pdf. Accessed: May 10, 2025.

[4] NodeMCU, "NodeMCU ESP8266 documentation," NodeMCU Open Source Community, n.d. Available: https://nodemcu.readthedocs.io/en/master/. Accessed: May 10, 2025.

[5] Food and Agriculture Organization of the United Nations (FAO), "Crop water needs: Chapter 4 - Soil water capacity," FAO, 2021. Available: http://www.fao.org/3/s2022e/s2022e04.htm. Accessed: May 10, 2025.

[6] Firebase, "Firebase Realtime Database documentation," Google, 2022. Available: https://firebase.google.com/docs/database. Accessed: June 10, 2025.

[7] U.S. Department of Agriculture, Natural Resources Conservation Service (USDA NRCS), "Soil electrical conductivity: Soil health guide for educators," USDA NRCS, 2014. Available: https://www.nrcs.usda.gov/sites/default/files/2022-10/Soil%20Electrical%20Conductivity%20Educators.pdf. Accessed: May 15, 2025.

REMOTE-CONTROLLED PET CARE ROBOT

W.K. Lakshani*, K.P. Vidanapathirana

Department of Electronics, Wayamba University of Sri Lanka, Kuliyapitiya, Sri Lanka

*kaushalyalakshani0627@gmail.com

ABSTRACT

Pet care is a necessary task, yet regular feeding and watering often prove to be a challenge to accomplish when the pet owners are away at work, traveling, or busy with other things. Conventional automatic pet food dispensers are handicapped by their stationary sites, strict schedules, and lack of real-time situation monitoring, which makes them less responsive to a pet's actual needs. To address these issues, this project presents a remote-controlled pet robot care system that integrates mobility, live video observation, and on-demand food and water dispensing on an affordable platform. The system uses an ESP32-CAM microcontroller, which provides Wi-Fi based control and live video transmission, enabling owners to observe and interact with their pets remotely through a web interface. The mobile robotic chassis, powered by DC motors via an L298N motor driver, carries dual storage compartments for food and water, each connected to solenoid valves operated by relay modules to regulate dispensing. A rechargeable battery supplies power to the system, while a buck converter ensures stable voltage levels for sensitive electronics. Prototype testing confirmed trouble-free navigation, regular dispensing of food and water with proper portion control, and stable video streaming with low latency. The integration of IoT, robotics, and automation demonstrates an efficient solution to modern pet care that is affordable, adaptable, and scalable. Possible future improvements include autonomous navigation with collision avoidance, integration with smartphones through apps, and larger storage capacity for enhancing the efficiency and convenience of the system.

Keywords: **W**i-Fi control, **E**SP32-CAM, **R**eal-time monitoring

1. INTRODUCTION

Pet care is a major activity for pet owners all over the world, and Sri Lanka is no exception. Pets must be fed on time and given clean water, which are essential for their well-being and health. However, most families neglect to provide timely care, especially when family members leave home for work, travel, or other reasons. Ignorance of these needs may lead to malnourishment, dehydration, stress, and even long-term illnesses in animals, making trustworthy solutions for round-the-clock pet care increasingly important.

Automatic pet feeders have been developed to meet this need by providing the capacity to release food at predetermined intervals. Although these types of devices offer half solutions, they are immovable and cannot approach the pet's position, so pets have to go to the feeder on their own [3].Besides, the majority of these feeders lack real time monitoring, are unable to dispense food and water simultaneously, and cannot support interactive control. These limitations lower their effectiveness in real life scenarios where pets may require attention at unexpected times or in other areas of the house.

The recent advancements in the Internet of Things (IoT), embedded systems, and low-cost microcontroller boards such as Arduino and ESP32 have created opportunities for smart automation in daily life [1].IoT-based feeders developed in previous studies or in market products have potential but are either expensive, not portable, or limited to a single function, such as dispensing food only [2].This provides an opportunity for the creation of an inexpensive, multifunctional, and versatile solution for automatic pet management.

As a solution, this project proposes a remotely operated pet care robot that integrates mobility, live video monitoring, and food and water dispensing into a single system. This project employs an ESP32-CAM module, which was chosen because it has an onboard camera, Wi-Fi connectivity, and low price, enabling live video streaming and wireless remote control through a web interface. A two-compartment storage container mounted on a robot chassis features an independent food and water compartment with solenoid valves controlled by relay modules to dispense them. A robotic base, consisting of DC motors and L298N driver, allows the system to approach the pet rather than the pet coming to a fixed station.

This project is an advancement over traditional automatic feeders as it integrates mobility, IoT-enabled monitoring, and multifunctionality into one portable and compact system. Not only does it provide pet owners with greater freedom, but it also enhances the level of pet care in the absence of human supervision. Subsequent enhancements can further extend the system with autonomous navigation, obstacle detection, scheduling features, and mobile app integration, rendering it even more effective and easy to use for everyday household applications.

2. EXPERIMENTAL

2.1 System Overview

The pet care robot system is designed in three primary modules: the mobile app, the controller and communication module, and the actuators. The mobile app is a comprehensive user interface through which the owner can navigate the robot, release water and food, and even view the pet in real-time through video streaming. It also logs feeding times and robot activity, keeping an extensive record for the owner.

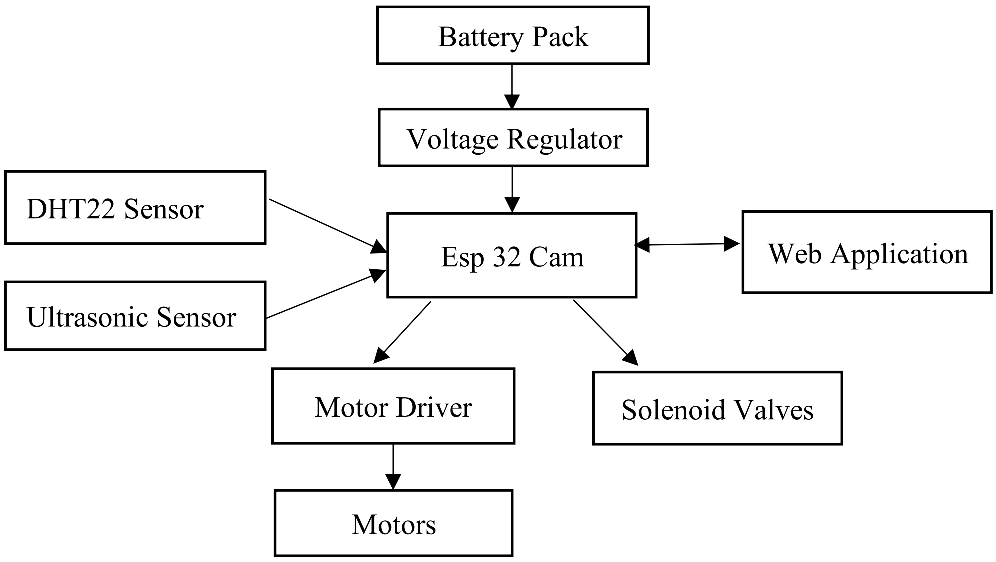

Figure 01: Block diagram of the system

The ESP32-CAM is used as the primary controller, running all control, communication, and video streaming tasks. It receives instructions from the app via Wi-Fi and executes them efficiently while continuously sending video feedback. The actuators include DC motors for multi-axis movement with a smooth motion and servo motors for precise dispensing of water and food so that the pet is given proper care even in the absence of its owner. This overall system gives a compact automatic interactive pet care system.

2.2 Hardware Implementation

Hardware implementation involved carefully integrating all the components according to the circuit design Figure 02 and making it work in a stable manner. The ESP32-CAM is the main controller and communicates directly with the DC motors for movement and servo motors for food and water delivery. The DC motors provide controlled forward, backward, and turning motion so that the robot moves with accuracy, and the servo motors provide precise amounts so that overfeeding does not take place. A stable power supply and effective voltage regulation ensure the operation of the ESP32-CAM and actuators round the clock without any interruption. Optional sensors such as infrared modules or limit switches can be installed to prevent collisions and obstacle detection, making the robot safer to use. Initial testing verified that all devices worked correctly and that the entire system worked properly as a working pet caretaker robot.

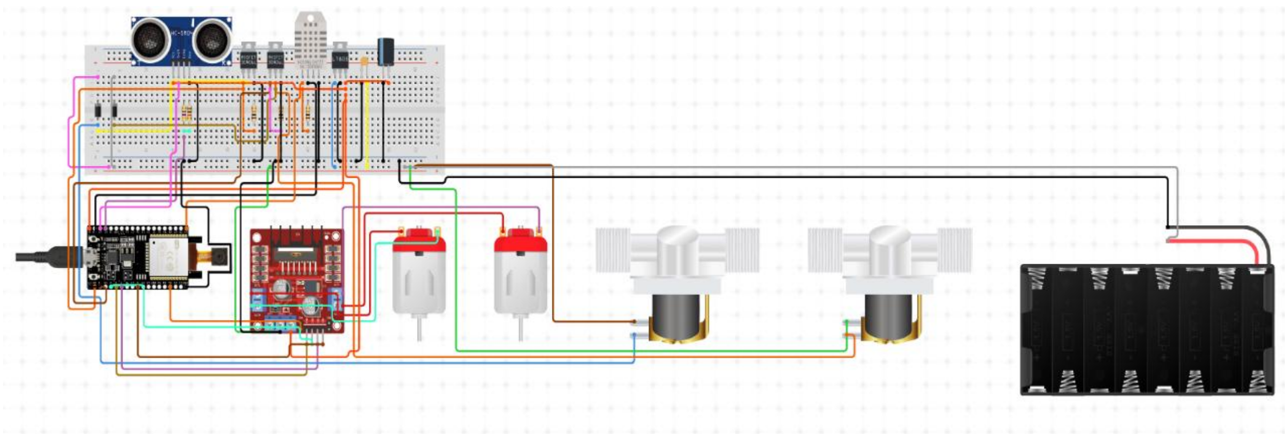

Figure 02: Circuit diagram of the system

2.2 Software Implementation

The software system integrates the ESP32-CAM and the mobile application for smooth and automated functionality. The ESP32-CAM code receives instructions from the app via Wi-Fi and controls the DC motors for mobility and servo motors for food and water dispensing. It also streams video live to the mobile app for real-time video monitoring. The code includes servo angle control routines for precise portions, motor overrun protection, and optimal processing of multiple commands. The mobile application allows the user to schedule feeding times, manually operate robot movement, and monitor pet activity remotely. Together, the hardware and software components create a responsive, reliable, and user-friendly pet caring system that is sufficient for the experimental objective, where pets are fed and monitored effectively even without the presence of the owner.

3. RESULTS AND DISCUSSION

The completed pet care robot was tested to evaluate the performance of the mobility, dispensing, monitoring, and overall system reliability. The circuit design in Figure 03 functioned as planned, with all of the modules movement, dual-compartment dispensing, wireless communication, and real-time video monitoring functioning together in harmony within a single platform. This demonstrates the viability of the proposed design.

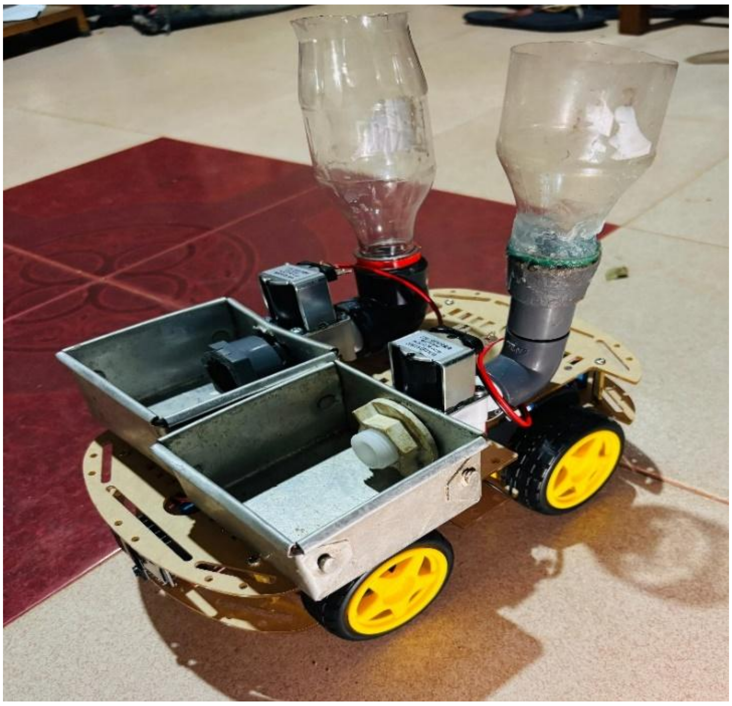

Figure 03: Integrated prototype constructed system

Mobility tests confirmed that the robot could move over typical indoor flooring and navigate around small objects such as toys and bowls. The stable operation of the motor driver and the chassis ensure that the robot can go to the pet rather than the pet having to go to a stationary feeder, providing greater flexibility than conventional systems.

The two-compartment dispensing unit dispensed measured quantities of food and water consistently without failure or leakage, in support of pet health as well as pet comfort. The integration of both resources within a single robot enhances owner convenience and testifies to the dispensing unit's strength.

The ESP32-CAM facilitated continuous video transmission, enabling pets to be monitored in real time and feeding sessions to be confirmed. While minor delays between frames occurred in areas with poor Wi-Fi coverage, the video stream was consistent under normal conditions, proving the feasibility of utilizing low-cost modules for home monitoring and providing a reassurance to pet owners.

The mobile application brought together navigation, dispensing, and monitoring controls into a single simple-to-use dashboard. Feeding log functionality allows for activity monitoring with potential future health monitoring, making the system accessible to non-technical users.

Reliability testing revealed that the rechargeable battery maintained long operation without breakdowns, and there was no overheating or failure of hardware components during continuous operation. This proves that the circuit design and power management techniques are adequate for daily household use.

Overall, the results demonstrate that the robot goes beyond the limitations of fixed automatic feeders by introducing mobility, double-dispensing capability, and real-time monitoring within an affordable and portable system. Although Wi-Fi quality can affect performance and the absence of autonomous mobility limits efficiency, the system presents a solid solution for remote pet monitoring and provides a foundation for future development into an intelligent and autonomous assistant.

4. CONCLUSION

The wireless operated pet robot was effectively designed, built, and tested, achieving its primary objectives of remotely feeding and monitoring pets. The system utilizes the ESP32-CAM as the master controller that can run both DC motors for smooth movement and solenoid valves for precise dispensing of food and water. Throughout the test, the robot exhibited even motion in all directions with very little jerks upon turning due to slight misalignment of wheels, which were tweaked. It did a good job of traversing through small obstacles such as bowls and toys, confirming consistency of motor control and overall circuit performance. The solenoid valves ensured even amounts of food and water, giving precise feeding without leakage. The ESP32-CAM streamed live video to the mobile app, enabling effective remote monitoring of pets, although minor delay was experienced in areas with weak Wi-Fi, which means one needs stable connection. The mobile app enabled easy manipulation of robot movement, dispensing of functions, and activity logging, demonstrating the usability and applicability of the system. Overall, the project offers a lean, robotic, and reliable remote pet care system that reduces the effort required by the owner and keeps pets fed and monitored even when away. Such possible enhancements as obstacle detection, better Wi-Fi connectivity, automated feeding scheduling, and enhanced dispensing mechanisms could further render the robot more efficient, reliable, and easy to use, thus better suited for daily household utilization.

ACKNOWLEDGEMENTS

The authors would like to express their gratitude to the Academic Staff of the Faculty of Applied Sciences, Wayamba University of Sri Lanka for their expert advice and guidance.

REFERENCES

[1] M. Mahule, P. Meghana, A. Sravani, T. Abhinaya, and S. Varun, "IOT based pet daycare robot," *International Journal of Progressive Research in Engineering Management and Science (IJPREMS)*, vol. 4, no. 5, pp. 1308–1314, May 2024. Available: https://www.ijprems.com/uploadedfiles/paper/issue_5_may_2024/34074/final/fin_ijprems1716383333.pdf. Accessed: Dec. 2, 2024.

[2] DogFeederDevelopers, "Dog-Feeder: Arduino / ESP32 Project - Automatic dog feeder," GitHub Repository, 2022. Available: https://github.com/DogFeederDevelopers/Dog-Feeder. Accessed: May 5, 2025.

[3] "IOT based dog day-care robot," *International Research Journal of Modernization in Engineering Technology (IRJMETS)*, vol. 4, no. 7, pp. 2582–5208, Jul. 2022. Available: https://www.irjmets.com/uploadedfiles/paper/issue_7_july_2022/28534/final/fin_irjmets1658330046.pdf . Accessed: Feb. 11, 2025.

[4] P. Birha, R. Ingle, S. Tajne, P. Mule, A. Pandey, S. Kukekar, and A. Kadu, "Design and development of IOT based pet feeder," *International Journal of Innovations in Engineering and Science*, vol. 7, no. 8, pp. 137–140, 2022. Available: https://www.semanticscholar.org/paper/Design-and-Development-of-IOT-Based-Pet-Feeder-Birha-Ingle/cfbf51ebfc821f4aa8dac95af939a343877f5480.

[5] Instructables, "WiFi dog feeder using Esp32 Cam," Instructables, 2021. Available: https://www.instructables.com/WiFi-Dog-Feeder-Using-Esp32-Cam/. Accessed: Jan. 20, 2025.

[6] L. Bhale, N. Laxman Sumnure, H. Maske, and S. Patil, "Robot car using ESP32 cam," *International Journal of Advanced Research in Science, Communication and Technology (IJARSCT)*, vol. 3, no. 1, pp. 2581–9429, 2023. Available: https://ijarsct.co.in/Paper11280.pdf.

[7] V. S. Naveen, V. Kushin, K. Mahidhar, N. Sivakamasundari, and R. Venkataswamy, "Design and development of IoT-based pet care robot," in *Advancements in Intelligent Systems*, Jan. 2025, pp. 25–32. Available: https://www.publications.scrs.in/chapter/978-81-975670-3-2/3. Accessed: Apr. 22, 2025.

AUTOMATED SYSTEM TO PREVENT PREMATURE COAGULATION AND ENHANCE QUALITY OF NATURAL RUBBER LATEX BY CONTROLLING TEMPERATURE AND PH VALUE

L.G.R.H. Lihinigama*, M.A.A. Karunarathna

Department of Electronics, Wayamba University of Sri Lanka, Kuliyapitiya, Sri Lanka

*rashmilihinigama@gmail.com

ABSTRACT

Natural rubber latex (NRL) is highly susceptible to early coagulation due to microbial action, enzymatic activity, and heat, leading to a loss of quality and usability. Common traditional methods of preserving latex by adding ammonia by hand and simple cold storage are not always accurate and reliable. This work proposes an automated system controlling pH through sodium hydroxide (NaOH) dosing and maintaining a stable temperature by Peltier-based thermoelectric cooling. The system is centered around an ESP32 microcontroller that continuously measures latex pH and temperature and displays it. Then controls a solenoid valve using a relay module to apply NaOH and Peltier modules to control the Temperature accordingly. Test results from controlled trials indicated that the system worked very well for maintaining pH in the alkaline preservation level (9.5–10.5) and for maintaining a stable latex temperature at 20–25 °C, and thus lowered coagulation events significantly. This not only enhances latex quality and storage time but also minimizes human intervention and improves traceability of the process, and is therefore feasible for both piloting and commercial applications.

Keywords: **N**atural rubber latex, **P**remature coagulation, **A**utomation

1. INTRODUCTION

Natural rubber latex (NRL), sourced from Hevea brasiliensis, is a prime raw material for many industrial and household products like gloves, tires, adhesives, and medical instruments [1]. Due to its distinctive physical and chemical characteristics, it is indispensable for many applications. Nonetheless, new latex that has just been tapped is very unstable and susceptible to early coagulation by way of microbial action, enzyme reaction [2], and attack by environmental stress like high temperatures. Once coagulation has begun, the latex no longer retains fluidity and is no longer processor-ready, thus experiencing lower yield, quality loss, and heavy financial loss.

Traditionally, field preservation methods involve manual addition of alkaline substances [3] such as ammonia or sodium hydroxide to raise the pH, coupled with basic cooling methods to slow microbial activity. While effective to some extent, these manual approaches often lack precision and consistency. Variations in preservative dosage, uneven mixing, and fluctuating storage conditions frequently lead to quality inconsistencies between batches. Moreover, reliance on human intervention increases the risk of error and raises operational costs.

To meet these challenges, there is an increasing demand for automated preservation systems that can monitor quality parameters of latex continuously and control them in real time. By controlling pH in the alkaline range and stabilizing latex temperature at recommended levels, such systems can control the occurrence of early coagulation considerably. Automation also offers the benefits of data logging, traceability of the process, and scalability, and thus is appropriate for use in both tiny collection centers as well as in large industrial latex storage plants.

This project involves the development and integration of an automated system that employs sodium hydroxide (NaOH) [5] dosing for pH control and Peltier modules for thermal control through an ESP32-based control platform. The system incorporates sensors, actuators, and feedback algorithms for maintaining the best conditions for preservation, thus increasing latex stability, minimizing loss through spoilage, and generally improving the quality of the final product.

2. EXPERIMENTAL

This study aimed to develop an automated system for preserving natural rubber latex by controlling pH and temperature, which are critical factors affecting latex stability and coagulation. Fresh natural rubber latex was collected, and its initial pH and temperature were measured using a calibrated pH meter and a digital thermometer, respectively. The latex typically had a pH around 6.8–7.2 and a temperature of approximately 25 °C. The setup of the temperature sensor and the pH sensor is as Figure 1.

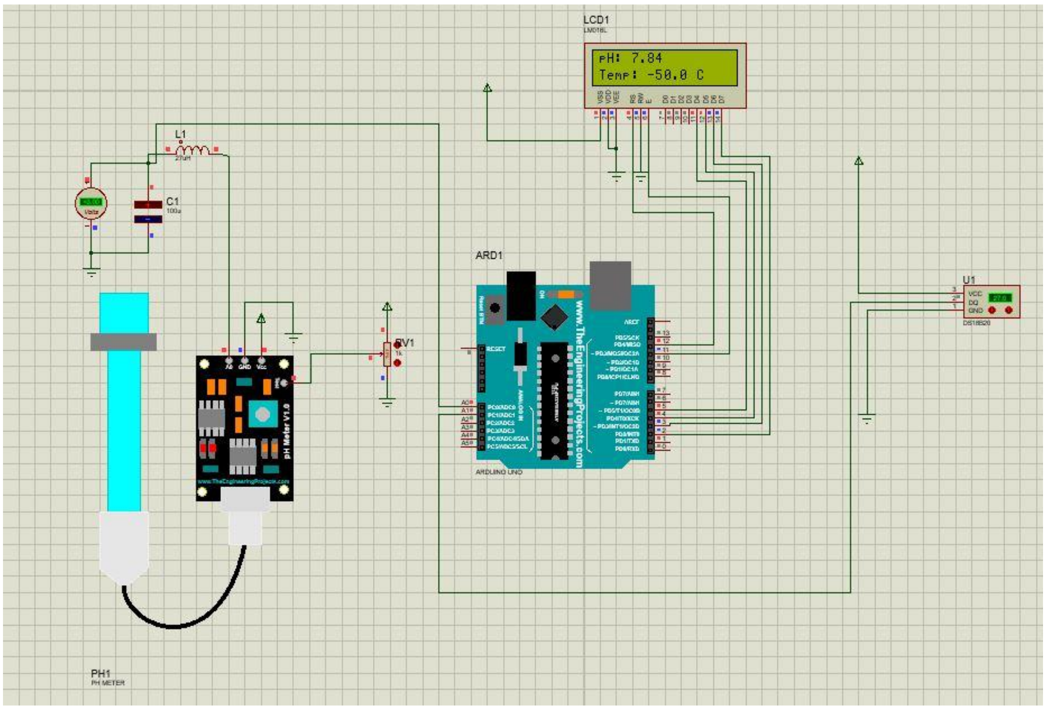

Figure 5: Proteus setup of temperature and pH sensors

For pH monitoring, a HW-828 pH sensor was immersed in the latex and connected to an ESP32 microcontroller. The system was developed as shown in Figure 2 and programmed to maintain the latex pH within an optimal range of 9.5–10.5. When the pH dropped below this set point, the ESP32 triggered a solenoid valve connected to a pressurized 10% sodium hydroxide solution. The volume of NaOH added was carefully calculated to achieve a target concentration of approximately 0.3% in the latex. To ensure uniform distribution and prevent localized high alkalinity that could damage the latex proteins, a magnetic stirrer was employed during dosing. The solenoid valve released NaOH in short, controlled pulses, avoiding overshooting the desired pH and maintaining latex quality. The pH was observed to stabilize when microbial activity in the latex was low, indicating that controlling alkalinity effectively suppresses microbial growth, which is one of the main causes of pH drift in stored latex.

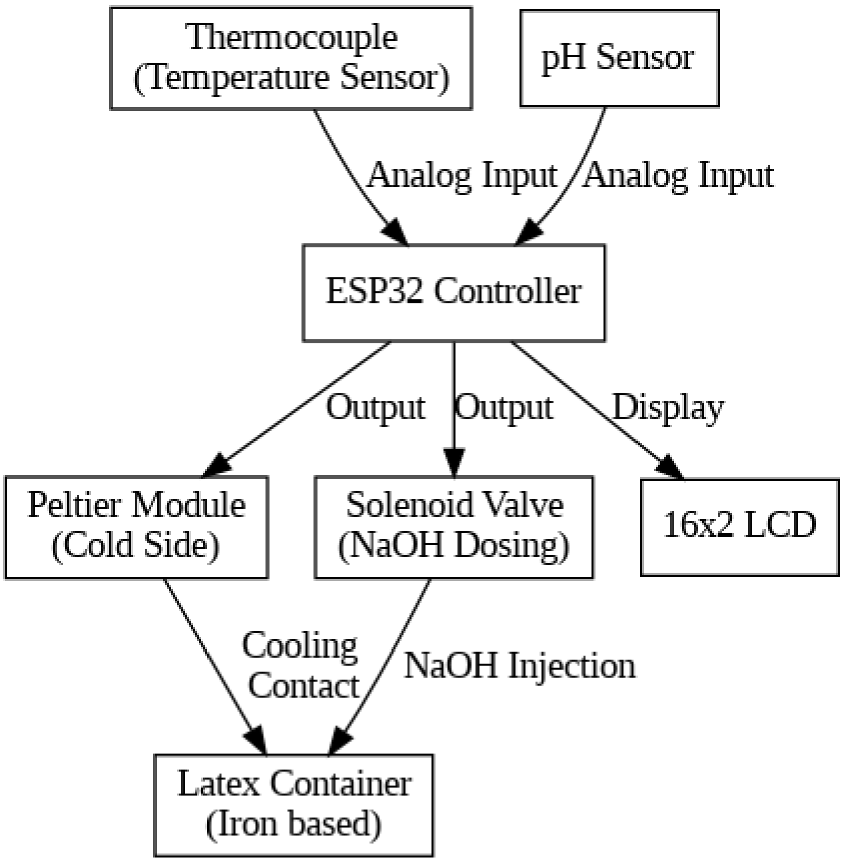

Figure 6: Block diagram of the system

Temperature control was implemented using a Peltier module equipped with a heatsink and cooling fan assembly. The ESP32 regulated this module through a solid-state relay, activating cooling whenever the latex temperature exceeded 28 °C. This ensured that the latex remained below the coagulation threshold and avoided thermal shock that could trigger premature solidification.

The experimental system consisted of the latex container with stirring, the pH and temperature sensors, the ESP32 microcontroller, the solenoid valve connected to the NaOH reservoir, and the Peltier cooling assembly.

Experiments were conducted by filling the latex container with a measured volume of latex and initiating the automated system. The system continuously monitored and adjusted pH and temperature. For comparison, a manual preservation setup was also tested, where NaOH was added at fixed intervals without any cooling. During both experiments, pH and temperature were recorded over time.

Observations showed that the automated system maintained the pH around 10 and kept the temperature stable below 28 °C, whereas the manual setup experienced a downward drift in pH and occasional temperature spikes. The pH remained stable in the automated system, particularly when microbial activity was low, confirming that proper alkalinity control suppresses microbial growth. Coagulation onset time was significantly delayed in the automated system, extending from approximately 6 hours in the manual setup to about 24 hours. Additionally, the dry rubber content improved slightly under automated preservation, indicating better latex quality.

3. RESULTS AND DISCUSSION

Charts for pH and temperature fluctuations over time, side-by-side comparisons of automated and manual systems, were made for evaluation. The automated system was shown in a clear manner to have improved latex preservation control, maintaining pH and temperature well within preferred ranges and generally improving latex stability.

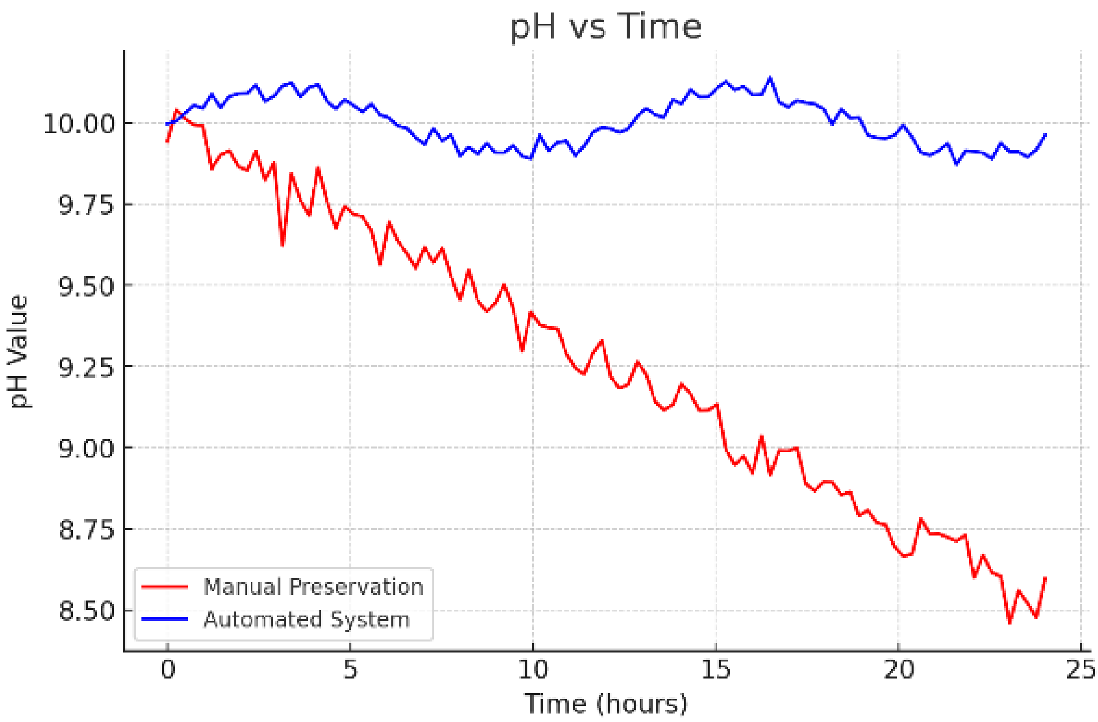

Figure 7: pH Vs time graph

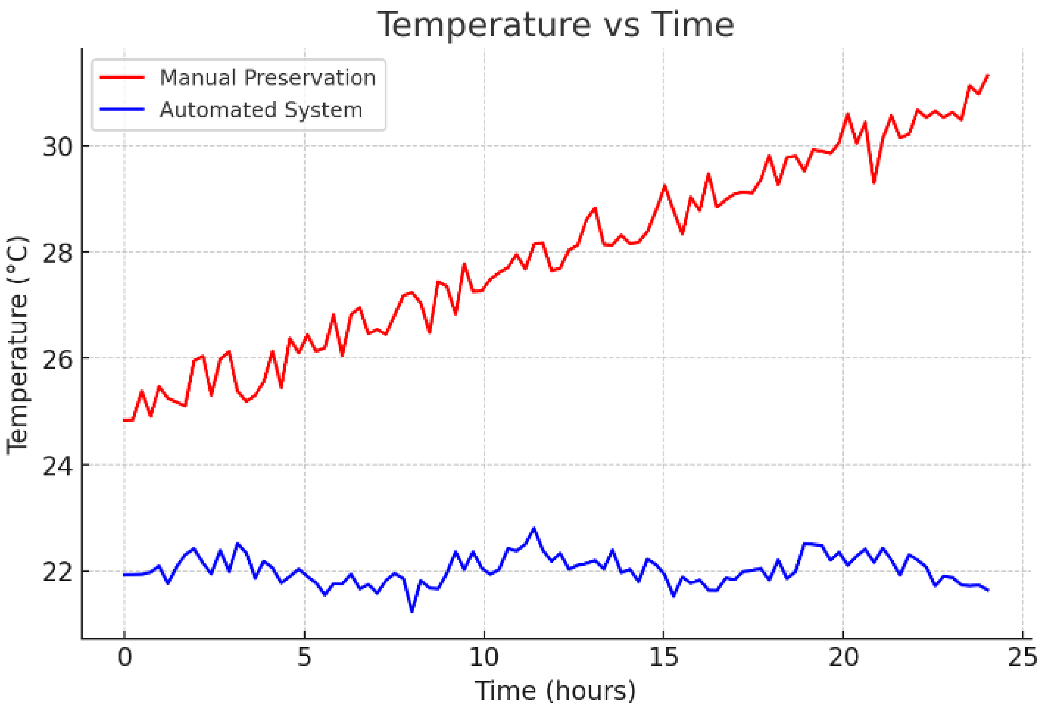

Figure 8: Temperature Vs time graph

The automated preservation system performance was tested by checking pH stability and temperature control, and comparing it with a system of manual preservation. The automated system was able to keep the latex pH within the desired level of 9.5–10.5 for the observation duration. Compared to this, the manual system demonstrated a steady fall in pH, reaching a level of approximately 7–8 for the observation duration. Stabilization of pH for the automated system was also closely related to lowered microbial activity since higher levels of alkalinity actually suppressed microbial growth, mainly responsible for pH drift during stored latex. This illustrates that continuous and accurate dosing of NaOH in slow, controlled pulses can sustain ideal chemical conditions for latex.

Temperature control was also equally efficient in the automated system. The latex temperature remained well below 28 °C at all stages, while in the manual system, spikes of up to 30–32 °C were induced by environmental conditions. Such spikes in the manual system led to a higher onset of coagulation. Utilization of pH stabilization and control of temperature in the automated system delayed noticeable coagulation by a considerable extent, prolonging the onset time from approximately 6 hours in the manual system to approximately 24 hours. This implies that controlling chemical and thermal parameters equally is necessary for extending latex stability.

The latex quality preserved further was also measured through DRC. The automated system gave a DRC of about 36%, while the manual system gave a DRC of about 32%. This gain reaffirms that not only is coagulation retarded by the automated system, it also preserves a greater percentage of solid rubber, indicative of improved preservation of latex quality. The DRC findings also emphasize the need for careful restriction of NaOH addition to the safe limit (0.2–0.5% by weight, or corresponding volumes by using a 10% stock solution) for preventing destruction of latex proteins while ensuring effective microbial control.

In general, the findings affirm that the automatic system offers superior control for latex conservation relative to conventional hand techniques. Ongoing pH control and controlled dosing of NaOH efficiently suppress microbial growth and achieve chemical stability, and thermal control avoids thermal-induced coagulability. Each contributes toward increased latex shelf life, optimized DRC, and higher-grade rubber. The data affirm the need for a dual chemical and thermal control for latex storage and the utility of automatic systems for laboratory and commercial usage.

4. CONCLUSION

The automated system for preserving latex was found to be much more efficient than traditional manual means of preserving natural rubber latex quality. Through the combination of continuous monitoring of pH levels and controlled dosing of NaOH, along with active heating control, the system was able to effectively stabilize pH levels in the desirable range (9.5–10.5), inhibit microbial growth, and keep the latex temperatures at or below 28 °C. These combined approaches also retarded the onset of coagulation from an average of about 6 hours in manual preservation by pushing it close to 24 hours through automation, and enhanced the content of dry rubber from 32% up to 36%. The research identifies a need for restricted NaOH dosing to safe levels for effective preservation without sacrificing latex quality. In general, the results confirm that not only can the shelf life of natural rubber latex be increased by automation, but higher quality and improved yield are also achieved, thus a feasible solution for industrial and laboratory-scale level preservation.

ACKNOWLEDGEMENTS

The author extends sincere gratitude to everyone who gave invaluable guidance and support to complete this project.

REFERENCES

[1] New York State Department of Health, “Latex allergy information,” 2017. Available: https://www.health.ny.gov/environmental/indoors/food_safety/latex/

[2] R. Roussel, “Natural rubber latex preservation,” European Patent EP2132231B1, Dec. 16, 2009. Available: https://patents.google.com/patent/EP2132231B1/en

[3] J. Urbina, T. A. Osswald, E. Garcia, and A. J. Román, “Environmentally safe preservation and stabilization of natural rubber latex in an acidic environment,” *SPE Polym.*, vol. 4, no. 3, pp. 93–104, May 2023. doi: https://doi.org/10.1002/pls2.10089

[4] Rubber Research Institute of Sri Lanka, “Manufacture of latex crepe,” 2016. Available: https://www.rrisl.gov.lk/content/files/downDoc/3.%20Manufacture%20of%20Latex%20Crepe.pdf

[5] D. Roberts, Ed., *Natural Rubber*. London: Springer Science & Business Media, 2012. Available: https://books.google.lk/books/about/Natural_Rubber.html?id=-rHXxqRjWuIC

[6] D. Thavaseelan, A. H. L. R. Nilmini, G. A. Appuhamillage, and S. Siriwardena, “Investigation of field performance and film properties of natural rubber latex preserved with a novel chemical,” *Adv. Technol.*, vol. 2, no. 1, pp. 71–78, 2022. doi: https://doi.org/10.31357/ait.v2i1.5453

[7] T. Reunala, H. Alenius, K. Turjanmaa, and T. Palosuo, "Latex allergy and skin," *Curr. Opin. Allergy Clin. Immunol.*, vol. 4, no. 5, pp. 397–401, Oct. 2004. doi: https://doi.org/10.1097/00130832-200410000-00011

[8] Ngoc Chau Supplier, "How to preserve natural rubber latex 60% DRC," 2025. Available: https://ngocchausupplier.com/how-to-preserve-natural-rubber-latex-60-drc/

Proc. Annual Symposium on Research & Industrial Training, 12 (2025) 85-91
Department of Electronics – Wayamba University of Sri Lanka

DEVELOPMENT OF AN AGITATOR CONTROL SYSTEM FOR A BIOGAS DIGESTER

W.B.R.Sirimanna *, M.A.A.Karunarathna

Department of Electronics, Wayamba University of Sri Lanka, Kuliyapitiya, Sri Lanka

*binusirimanna@gmail.com

ABSTRACT

Small-scale biogas digesters are a promising source of sustainable energy but are frequently plagued by operational inefficiencies due to poor mixing, leading to stratification and reduced gas yield. This paper presents the design, implementation, and validation of an automated control system for a mechanical agitator to address this challenge. The system is built around an ESP32 microcontroller that integrates sensor data from a waterproof temperature sensor, a pressure transducer, and a level sensor to intelligently govern a DC gear motor. A multi-tiered control logic was developed to initiate both corrective mixing in response to thermal gradients and scheduled mixing to prevent settling. All operational data is recorded to an SD card for analysis. A comparative experimental study was conducted to evaluate the system's performance, measuring biogas pressure both with and without the automated agitator. The results demonstrate a significant increase in biogas production following the implementation of the control system, confirming that automated agitation is an effective method for enhancing the efficiency and output of small-scale biogas digesters.

Keywords: **S**mall-scale digester**, A**utomated mixing**, B**iogas yield

1. INTRODUCTION

Biogas technology offers a sustainable solution for waste management and renewable energy generation. However, the efficiency of small-scale digesters is often hampered by suboptimal operational conditions requiring manual intervention. In particular, inadequate mixing of the substrate leads to thermal stratification, scum layer formation, and reduced biogas yield [1,2]. Mechanical agitation is a recognized method to mitigate these issues [3]. While its benefits are well-documented in industrial-scale systems [4], its application in small-scale digesters often relies on simplistic, timer-based systems that do not respond to the digester's real-time conditions. This represents a significant inefficiency, as agitation should be both effective and energy-conscious to maximize net energy gain [5]. Consequently, there is a need for intelligent control systems that can automate agitation based on direct process parameters [6].

This study investigates the design and efficacy of an automated control system to optimize agitator operation. The central hypothesis was that a strategy combining Temperature Control Mixing (triggered by thermal imbalance) and Scheduled Mixing (triggered on a fixed interval) would significantly enhance biogas production. Therefore, this experiment investigated whether an ESP32-based control system, which triggers agitation through Temperature Control Mixing and Scheduled Mixing, would significantly increase biogas production compared to a non-agitated digester."

2. EXPERIMENTAL

2.1 Overall System Design

The experimental setup for this study consisted of a fully integrated, automated biogas digester system built around an ESP32 microcontroller. The physical layout was designed for optimal process monitoring and control. A DC gear motor was centrally mounted on the digester lid to drive a vertical shaft and impeller for slurry mixing. The sensor system was strategically designed and installed to monitor key parameters within the biogas digester. Two DS18B20 temperature sensors were vertically aligned to detect thermal stratification: one was placed in the top of the slurry and the other in the bottom. Two BMP180 pressure sensors were used to calculate gauge pressure: one was installed inside the gas dome to measure biogas pressure, and a second reference sensor was placed outside the digester to measure ambient atmospheric pressure. A float switch level sensor was mounted at a predetermined critical high level on the digester wall to provide slurry level status.

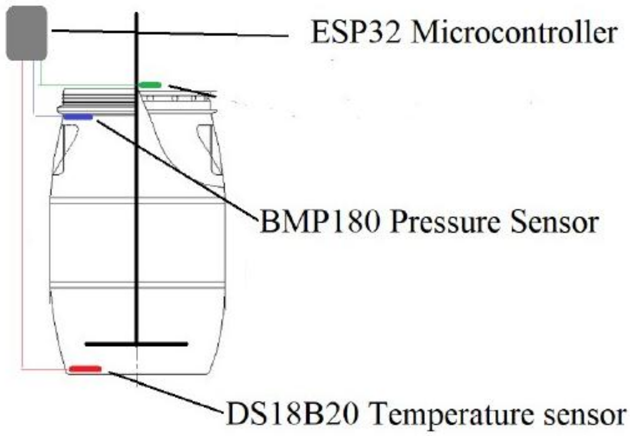

Figure 2.1 : Schematic Overview of the Biogas Digester System

2.2 Agitator Control System

The agitator was governed by two independent control protocols designed to address specific digester conditions. The Temperature Control Mixing protocol was activated reactively by a temperature differential exceeding 2.0°C between the upper and lower sensors [7]. To resolve this thermal stratification efficiently, the system executed a gentle mix at 100 RPM for 4 minutes, followed by a mandatory 30-minute stabilization period. Independently, the Scheduled Mixing protocol operated proactively on a fixed 4-hour timer to prevent scum formation and settling. This preventative maintenance required a more vigorous intervention, achieved by mixing at 200 RPM for 4 minutes [3]. This dual-strategy approach ensured optimal digester performance by addressing both immediate imbalances and long-term preventative needs, while maximizing energy efficiency through targeted, non-continuous operation.

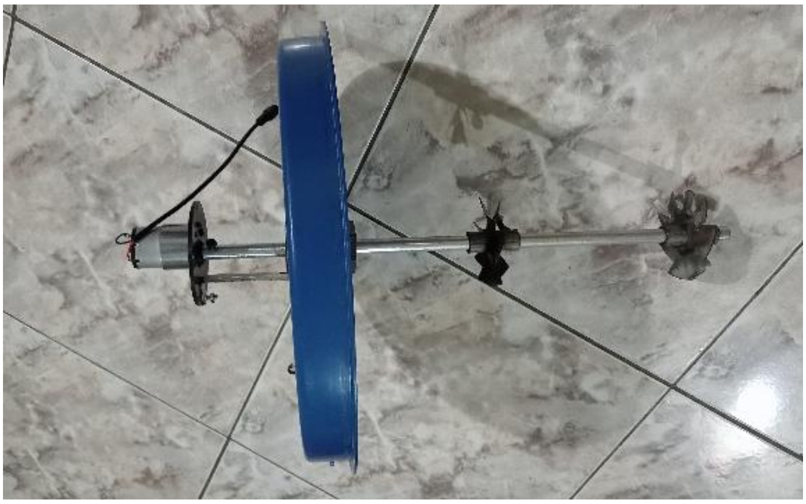

Figure 2.2: (a) Design of the agitator

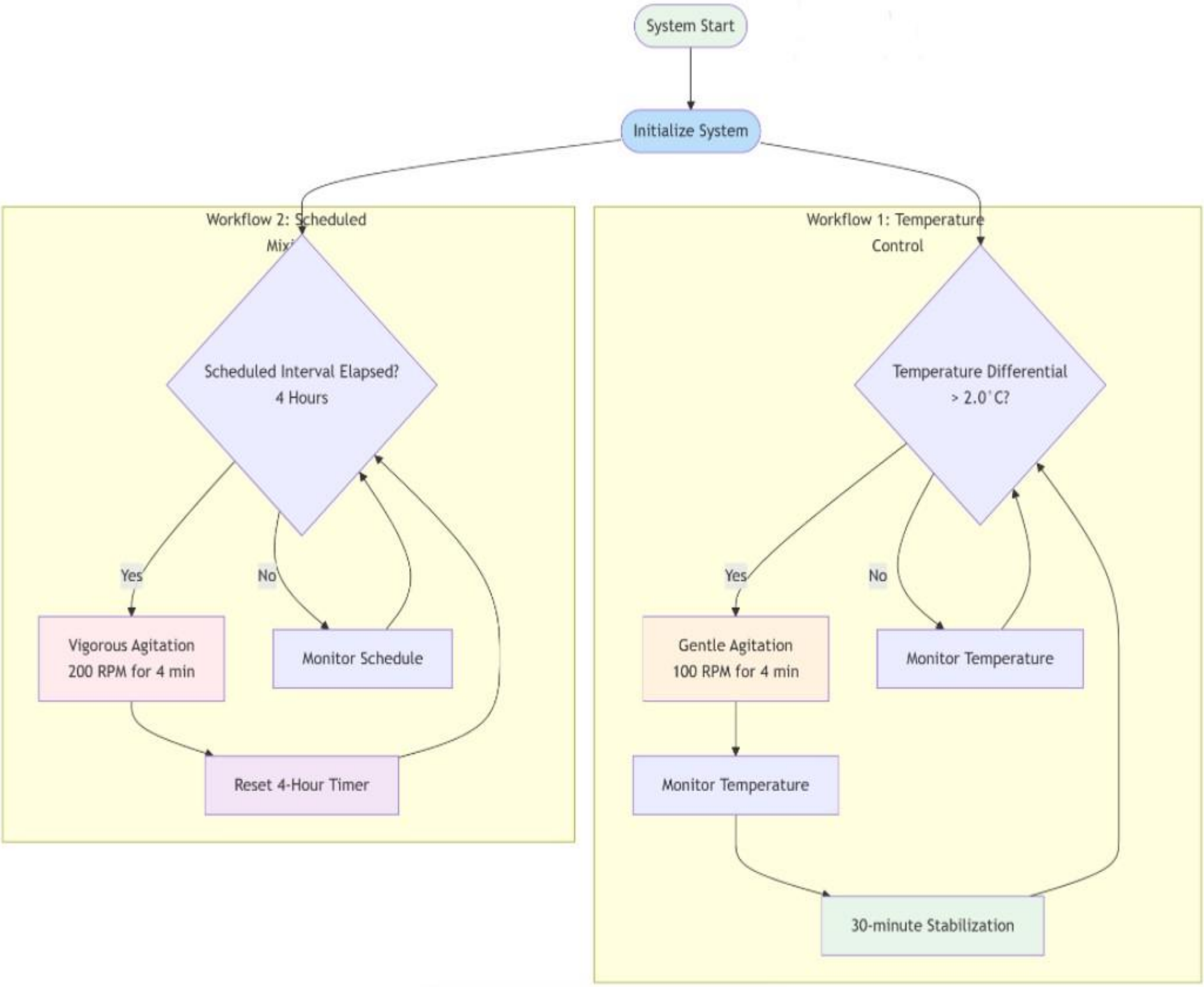

Figure 2.3: Agitator Control System flow chart

2.3 Hardware Implementation

All sensors were strategically mounted to ensure accurate measurements while protecting them from the corrosive slurry environment. The internal biogas pressure sensor (BMP180) was epoxy-sealed directly into the digester lid to prevent gas leaks. The external ambient pressure sensor was housed in a ventilated white plastic enclosure for weather protection while allowing air exposure. The float level sensor was installed using a waterproof cable gland to protect it during immersion. Both DS18B20 temperature sensors were placed inside a perforated PVC pipe submerged in the slurry—this design allowed water contact for accurate readings while providing physical protection from solid debris. All penetrations were sealed with epoxy or silicone to maintain the digester's gas-tight integrity throughout operation.

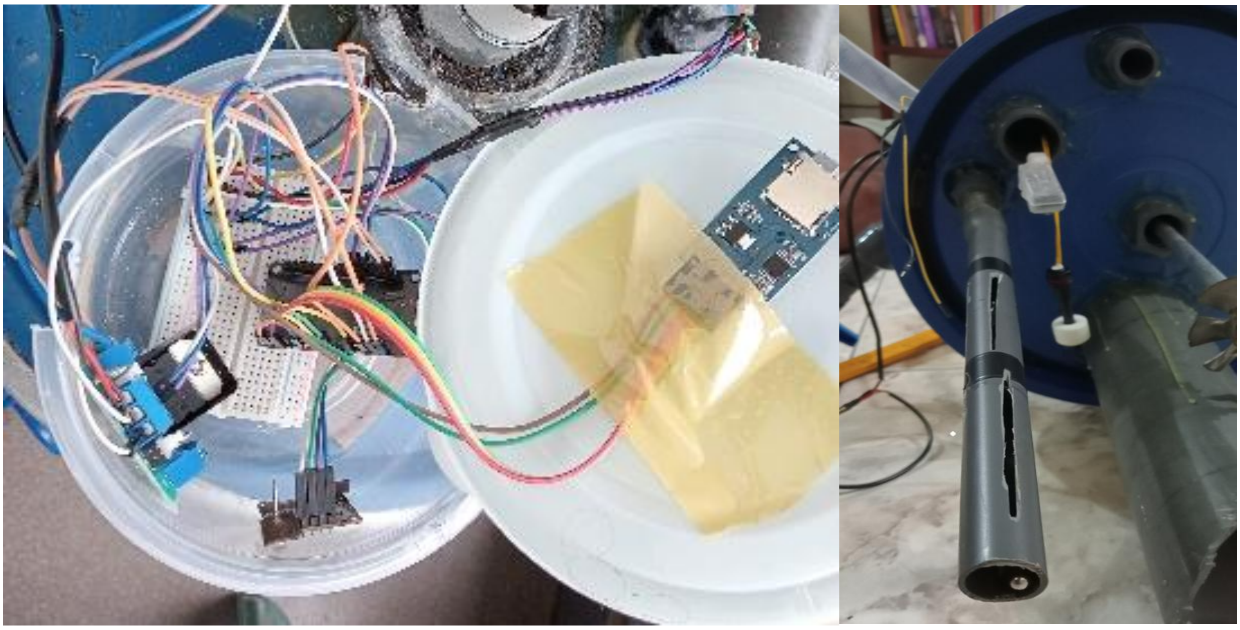

(a) (b)
Figure 2.4: (a) Sensor Integration Circuit (b) Digester Lid Sensor Layout

2.4 Data Acquisition

The ESP32 microcontroller served as the central unit for data acquisition and processing, polling all sensors at predetermined intervals. Raw sensor data were processed to compute key parameters: temperature differentials (ΔT) from upper and lower sensors, gauge pressure from differential pressure measurements, and discrete level states from slurry level readings. Processed data were simultaneously displayed in real-time on an OLED screen and logged with timestamps to an SD card for the purpose of both immediate system control and subsequent performance analysis.

A1 | fx | timestamp

	A	B	C	D	E	F	G
1	timestamp	temp1_top	temp2_bottom	pressure_inside	pressure_outsic	gauge_pressure	motor_state
2	6/15/2025 14:00	37.59	35.76	1014.29	1013.63	0.66	On
3	6/15/2025 15:00	36.88	36.39	1015	1013.92	1.08	On
4	6/15/2025 16:00	37.49	36.74	1015	1012.64	2.36	On
5	6/15/2025 17:00	37.41	37.37	1013.79	1013.45	0.34	On
6	6/15/2025 18:00	37.21	37.03	1013.72	1013.72	0	Off
7	6/15/2025 19:00	38	37.28	1014.03	1013.99	0.04	Off
8	6/15/2025 20:00	37.25	37.76	1012.38	1012.38	0	On
9	6/15/2025 21:00	37.88	37.95	1012.81	1012.8	0.01	On
10	6/15/2025 22:00	36.7	36.71	1013.65	1013.08	0.57	On
11	6/15/2025 23:00	36.91	37.06	1014.84	1013.43	1.41	On

Figure 2.5: Sample of sensor data retrieved from the SD card

3. RESULTS AND DISCUSSION

3.1. Final Assembled System

The fully integrated control system was successfully implemented and installed on the biogas digester, as shown in the figure below. The final assembly demonstrates the physical realization of the designed hardware, featuring the ESP32 microcontroller, sensor array, L298 motor driver, and DC gear motor mounted in an operational configuration. All components were housed in a protective enclosure to ensure reliable performance in the high-humidity environment of the digester setup. This complete system represents a fully functional unit ready for operational testing.

(a) (b)

Figure 3.1 : (a) Internal View of Control Unit (b) Top-Down View of System Assembly

3.2 Comparative Evaluation of Agitation Efficacy

Sensor data were continuously recorded via the SD card module throughout the experimental period. The raw pressure measurements were processed using MATLAB software to generate the comparative analysis shown in the figure below. Daily average pressure values were calculated by extracting timestamped data files from the SD card and computing mean values for each 24-hour period using MATLAB's numerical analysis tools. The algorithm automatically segregated measurements into two experimental conditions: baseline (without agitator) and intervention (with agitator).

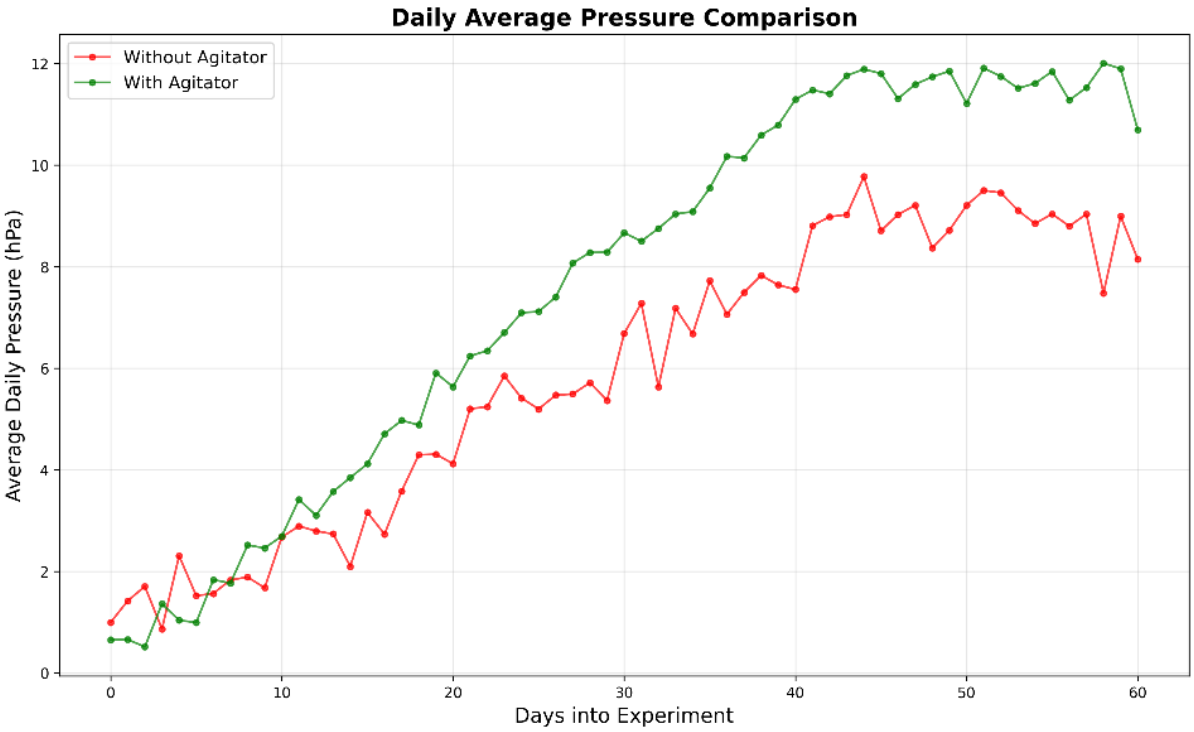

Figure 3.2 : The graph of Comparison of daily average pressure without and with the agitator operational

The percentage increase in biogas production was calculated through MATLAB's statistical analysis package using the formula:

$$\text{Pressure Increase }(\%) = \frac{\mu_{\text{agitated}} - \mu_{\text{baseline}}}{\mu_{\text{baseline}}} \times 100$$

Where:

1 μ_{baseline} = Mean daily pressure during non-agitation phase
2 μ_{agitated} = Mean daily pressure during agitation phase

The observed 33.12% increase in biogas yield quantitatively validates the efficacy of the automated agitation strategy in optimizing digester performance through improved substrate homogenization and thermal management[3,4]. The reduced variability demonstrates the system's ability to maintain stable operational conditions.[8]

4. CONCLUSION

This research successfully designed, implemented, and tested an automated agitator control system for small-scale biogas digesters, utilizing an ESP32 microcontroller as the central processing unit. The implemented system featured a novel dual-strategy control approach, combining a reactive Temperature Control Mixing protocol (activated by thermal stratification exceeding >2.0°C) with a proactive Scheduled Mixing protocol (triggered on a fixed 4-hour interval) to comprehensively optimize digestion efficiency. By integrating a suite of sensors for temperature, pressure, and level monitoring, coupled with robust data logging capabilities, the system achieved a significant 33.12% increase in biogas production compared to a non-agitated control setup. This marked improvement provides clear evidence of the system's effectiveness in enhancing critical process parameters, including substrate homogeneity, scum layer prevention, and overall microbial activity. Therefore, the findings of this study confirm that intelligent, sensor-driven automation can effectively address persistent operational challenges while substantially improving biogas yield in small-scale applications. This work ultimately contributes to the development of more sustainable, efficient, and practical renewable energy solutions.

ACKNOWLEDGEMENTS

The authors would like to express their gratitude to the academic staff at the Department of Electronics, Faculty of Applied Sciences, Wayamba University of Sri Lanka for their advice and guidance.

REFERENCES

[1] T. Abbasi, S. M. Tauseef, and S. A. Abbasi, *Biogas Energy*. New York, NY, USA: Springer Science & Business Media, 2012. doi: 10.1007/978-1-4614-1040-9

[2] K. Karim, R. Hoffmann, K. T. Klasson, and M. H. Al-Dahhan, "Anaerobic digestion of animal waste: Effect of mixing," *Bioresour. Technol.*, vol. 96, no. 14, pp. 1607–1612, Sep. 2005. doi: 10.1016/j.biortech.2004.12.021

[3] P. Kaparaju, I. Buendía, L. Ellegaard, and I. Angelidaki, "Effects of mixing on methane production during thermophilic anaerobic digestion of manure: Lab-scale and pilot-scale studies," *Bioresour. Technol.*, vol. 99, no. 11, pp. 4919–4928, Jul. 2008. doi: 10.1016/j.biortech.2007.09.015

[4] J. Lindmark, P. Eriksson, and E. Thorin, "The effects of different mixing intensities during anaerobic digestion of the organic fraction of municipal solid waste," *Waste Manage.*, vol. 34, no. 8, pp. 1391–1397, Aug. 2014. doi: 10.1016/j.wasman.2014.04.006

[5] B. Wu, "Pilot-scale anaerobic digestion and the resulting energy efficiency of an integrated system for biogas production and fertilizer recovery," *Bioresour. Technol.*, vol. 114, pp. 256–261, Oct. 2012. doi: 10.1016/j.biortech.2012.03.077

[6] J. Ward, P. J. Hobbs, P. J. Holliman, and D. L. Jones, "Optimisation of the anaerobic digestion of agricultural resources," *Bioresour. Technol.*, vol. 99, no. 17, pp. 7928–7940, Nov. 2008. doi: 10.1016/j.biortech.2008.02.044

[7] D. Kariyama, X. Zhai, and B. Wu, "Influence of mixing on anaerobic digestion efficiency in stirred tank digesters: A review," *Water Res.*, vol. 143, pp. 503–517, Oct. 2018. doi: 10.1016/j.watres.2018.06.065

[8] P. G. Stroot, K. D. McMahon, R. I. Mackie, and L. Raskin, "Anaerobic codigestion of municipal solid waste and biosolids under various mixing conditions—I. Digester performance," *Water Res.*, vol. 35, no. 7, pp. 1804–1816, May 2001. doi: 10.1016/S0043-1354(00)00439-5

Proc. Annual Symposium on Research & Industrial Training, 12 (2025) 92-99
Department of Electronics – Wayamba University of Sri Lanka

DESIGN AND OPTIMIZATION OF A WIDEBAND PRINTED MICROSTRIP LOG-PERIODIC DIPOLE ARRAY ANTENNA

B.P.H.S. Wijayanthi[1*], J.M.J.W. Jayasinghe[1], W.D.T.M. Premathilake[2]
[1]*Department of Electronics, Wayamba University of Sri Lanka, Kuliyapitiya, Sri Lanka.*
[2]*Techlabs Global PVT Ltd, Colombo, Sri Lanka.*
*hirunishalika06@gmail.com

ABSTRACT

This paper describes the design and optimization of a microstrip log-periodic dipole antenna (MLPDA) for the frequency range 4-18 GHz. The basic antenna design was based on the empirical equations established by Milligan, where problems such as poor return loss values, gain instability were identified. To solve these problems, the antenna parameters scaling factor (τ), spacing ratio (σ), apex angle (α) were optimized. For this, a self-adaptive differential evolution (SADE) algorithm was used. After antenna optimization, the antenna performance improved significantly. the −10 dB return loss limit was covered throughout the entire frequency range. The gain was increased (maximum gain after optimization was 7.43 dBi at 6 GHz). A smoother radiation pattern was obtained, and the feed imbalance was reduced, resulting in better wideband matching. This antenna can be used for practical applications such as EMC/EMI tests and direction finding, and it provides a method for converting a basic design based on theory into a balanced and easy-to-manufacture antenna suitable for practical needs.

Keywords: Dipole array antenna, **S**elf-adaptive differential evolution, **O**ptimization

1. INTRODUCTION

Wireless communication is a rapidly growing field, and antenna design plays a crucial role in the successful operation of any wireless communication system. Traditional Log-Periodic Dipole Array (LPDA) antennas are known for their high gain and almost frequency-independent characteristics over a wide frequency range. However, the main drawback of these antennas is their size. In contrast, Microstrip Antennas (MSA) have a compact, lightweight, and flat design and can be easily integrated into modern communication devices. However, the main drawback of these antennas is their narrow bandwidth and moderate gain. This project overcomes the shortcomings of both the above-mentioned antenna types by designing and optimizing an MLPDA antenna.

In EMC/EMI tests (Electromagnetic Compatibility/Electromagnetic Interference tests), this antenna can be used to measure the electromagnetic radiation emitted by various electronic devices. These tests can help determine whether a device interferes with the operation of other electronic devices and verify that they comply with regulatory standards. In direction finding, the antenna can help identify signals coming from different directions and determine the locations of their sources.

Various studies have investigated Microstrip Log-Periodic Dipole Array (MLPDA) antenna designs. In one study, an MLPDA antenna with 10 dipole elements was designed to operate from 800 MHz to 6 GHz. The overall gain of the antenna was 4 dB[1]. In another study, the effects of geometric variations on the bandwidth and gain of an MLPDA antenna in the C-band (4.835–7.44 GHz) were investigated. This highlighted the importance of qualitatively recommending the antenna design parameters[2]. In another study, an MLPDA antenna operating in the 4.2–9.2 GHz range was designed, which achieved a maximum gain of 8.5 dBi. Taken together, these works show that although MLPDA antennas can provide wide-band performance, challenges such as impedance matching, compactness, and directional stability in high-speed regions still exist.[3]

The main problems of active antenna systems are narrow bandwidth, unstable gain, and large size, which are not suitable for modern, compact devices. To solve these problems, this project proposes to design a Microstrip Log-Periodic Dipole Array (MLPDA) antenna with wide-band performance and compact design.

2. EXPERIMENTAL

2.1 Calculation of Parameters

For a given desired bandwidth, where f_{min} and f_{max} are lower and upper cutoff frequencies, the design starting point is the definition of the parameters α (aperture angle), τ (Scaling factor) and σ (Spacing constant), considering the empirical rules defined by Milligan[6].

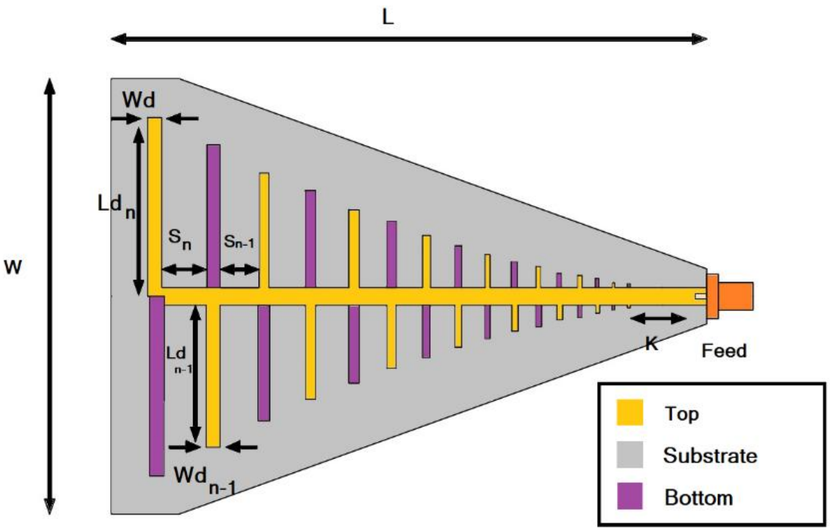

Figure 2.1: Geometric Parameters of the MLPDA Antenna

Where,
Ld_n = Length of the dipole element d_n
Wd_n = Width of the dipole element d_n
S_n = Inter-element spacing between two adjacent dipoles
W_L = Width of the microstrip feed line
L_L = Length of the microstrip feed line

Longest Wavelength,

$$\lambda_n = c/f_{min} \quad [2.1.1]$$

The desired operating frequency range with upper and lower truncation constants, t_1 and t_2, determined for τ and σ are combined to compute the length of the longest element and determine the number of elements required.

$$t_1 = 1.01 - 0.519\tau \quad [2.1.2]$$
$$t_2 = 7.08\tau^3 - 21.3\tau^2 + 21.98\tau - 7.30 + \sigma(21.82 - 66\tau + 62.12\tau^2 - 18.29\tau^3) \quad [2.1.3]$$

Longest Dipole Element Length,
$$Ld_n = t_1 . \lambda_n \quad [2.1.4]$$

Required Number of Elements,

$N=1 + ((\log (t_1 / t_2) + \log(f_{min} / f_{max})) / \log(\tau))$ [2.1.5]

Inter-Element Space between the first two dipoles,

$S_n = \sigma.4Ld_n$ [2.1.6]

To determine the widths of the dipole elements and the feed line, the first assumption is that the required input impedance is real. The average characteristic impedance Z_0 (assume 50 0hm),

$Z_0 = 120 (\ln (Ld_n / 2a_n) - 2.25)$ [2.1.7]

where a_n = radius of the equivalent cylindrical dipole.

Longest Microstrip Dipole Width,

$Wd_n = \pi a_n$ [2.1.8]

Length of the microstrip feed line,

$L_L = 2\tan\sigma / Ld_n$ [2.1.9]

For other dipole elements (For n = 1, 2, 3…N-1),

$\tau = (Ld_{n-1} / Ld_n) = (Wd_{n-1} / Wd_n) = (S_{n-1} / S_n)$ [2.1.10]

The desired operating frequency range of the MLPDA antenna was set to f_{min} = 4 GHz and f_{max} = 18 GHz. Based on initial value ranges of τ (0.7-0.9), σ (0.05-0.15), and α (20°−45°), the specific design parameters were chosen as Scaling Factor (τ) = 0.7, Spacing Constant (σ) = 0.05, and Aperture Angle (α) = 20°, from which the all element dimensions of the antenna were calculated using empirical equations established by Milligan and finalized them.
Length of the feed line, L_L = 4.854295mm

Dipole element No:	Length (mm)	Width (mm)	Inter Element Space (mm)
12	48.5025	5.2938	9.7005
11	33.9518	3.7056	6.7904
10	23.7662	2.5939	4.7532
9	16.6364	1.8158	3.3273
8	11.6455	1.2700	2.3291
7	8.1518	0.8890	1.6304
6	5.7063	0.6223	1.1413
5	3.9944	0.4356	0.7989
4	2.7961	0.3049	0.5592
3	1.9573	0.2135	0.3915
2	1.3701	0.1494	0.2740
1	0.9591	0.1046	

Table 2.1: Calculated Dimensions of MLPDA Antenna Dipole Elements

2.2 Antenna Design and Optimization

The geometric design of the antenna was drawn using the Antenna Design Application in MATLAB according to the calculated parameters.

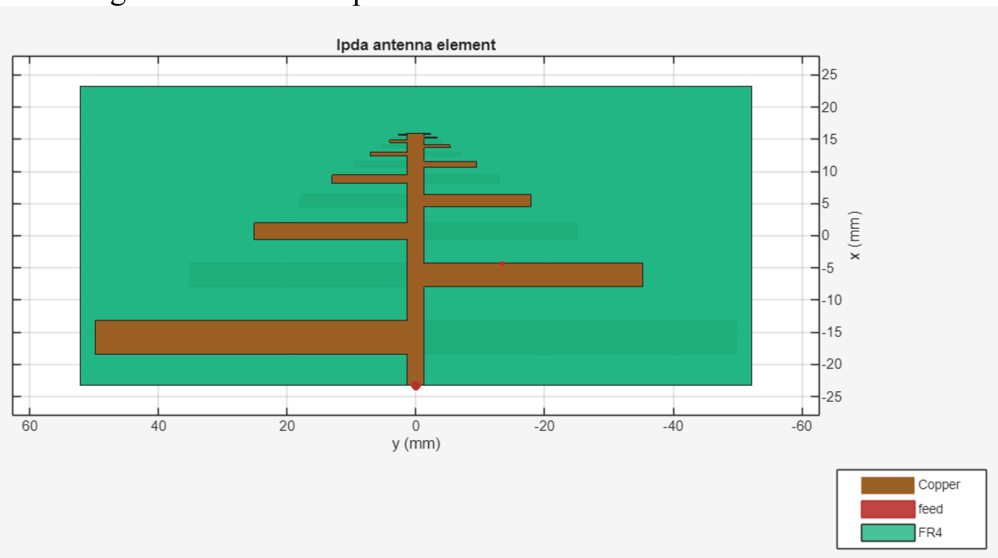

Figure 2.2: Drawn antenna in MATLAB according to calculated dimensions

Here, as the antenna substrate, FR4 was used with a relative permittivity (ϵ_r) of 4.8, a loss tangent of 0.026, and a thickness of 0.0016 m. An impedance graph, S-parameter plot, and the 3D radiation pattern of the antenna were generated in MATLAB.

To further improve the performance of the antenna, the dimensions of the antenna were optimized using the SADEA optimization method in MATLAB [7]. Based on the new dimensions obtained from this process, the antenna was redesigned, and its impedance graph, S-parameter plot, and 3D radiation pattern were regenerated.

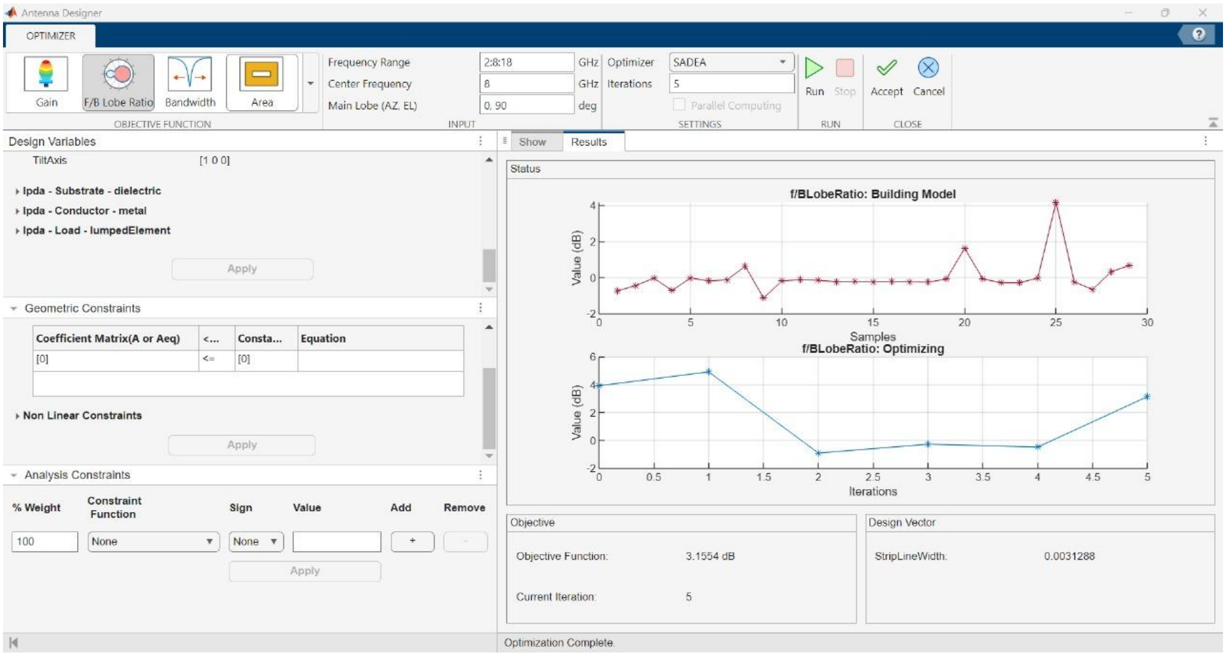

Figure 2.3: View of the MATLAB Antenna Optimization Method

The main objectives of antenna optimization were to minimize return loss, achieve proper impedance matching, and achieve maximum gain. In particular, the goal was to keep the $|S_{11}|$ value below -10 dB.

3.0 RESULTS AND DISCUSSION

The initial antenna design, based on initial calculations, did not meet the expected performance levels. Its reflection coefficient (S_{11}) value was higher than -10 dB. This indicated that the impedance matching of the antenna was not done properly and that a lot of the signal was being reflected back. The impedance graph also showed poor condition, as the resistance was not close to 50 Ω and the reactance was not close to 0.

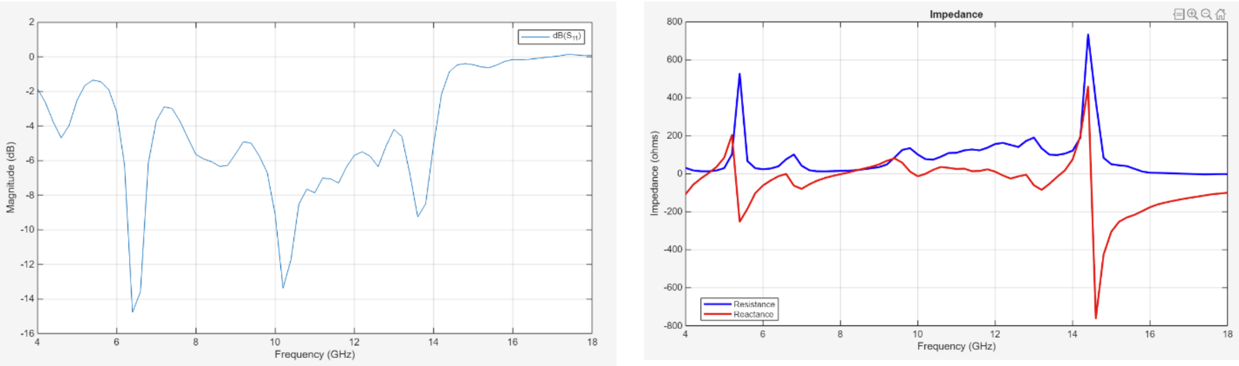

(a) (b)

Figure 3.1: (a) reflection coefficient (S_{11}) plot of initial antenna design (b) Impedance graph of initial antenna design

To solve these problems, the antenna dimensions were optimized using the SADEA optimization [7] method in MATLAB. After this process, the antenna was redesigned, and it showed excellent performance.

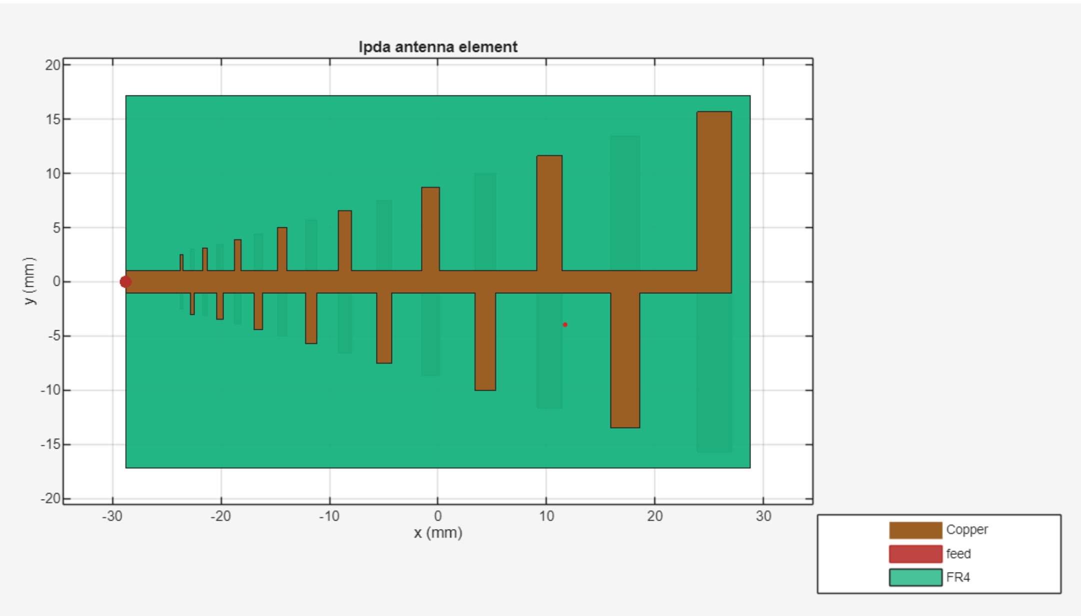

Figure 3.2: Optimized antenna design

The $|S_{11}|$ value of the antenna designed after optimization was consistently less than -10 dB. This confirmed that the antenna was correctly matched to the impedance and the signal reflection was minimized. Its impedance graph was also very good, with the resistance close to 50 Ω and the reactance very close 0 than initial antenna design. These results confirm the high efficiency and reliability of the antenna.

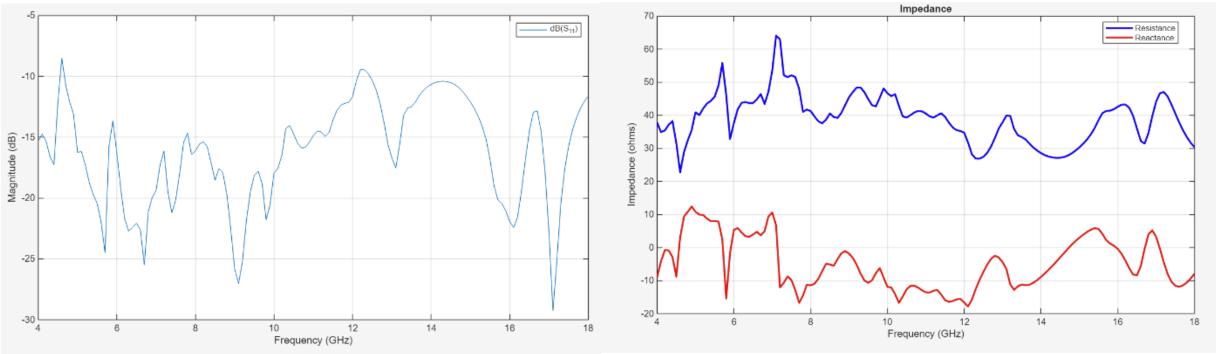

(a) (b)

Figure 3.3: (a) reflection coefficient (S_{11}) plot of optimized antenna design (b) Impedance graph of Optimized antenna design

Also, the radiation pattern of this antenna is stable and uniform. Its main lobe is smooth and well-defined, and there are no unwanted side lobes or nulls, so stable performance can be expected even in a wide frequency range (wideband). The maximum gain of antenna was shown as 7.43 dBi at a frequency of 6 GHz.

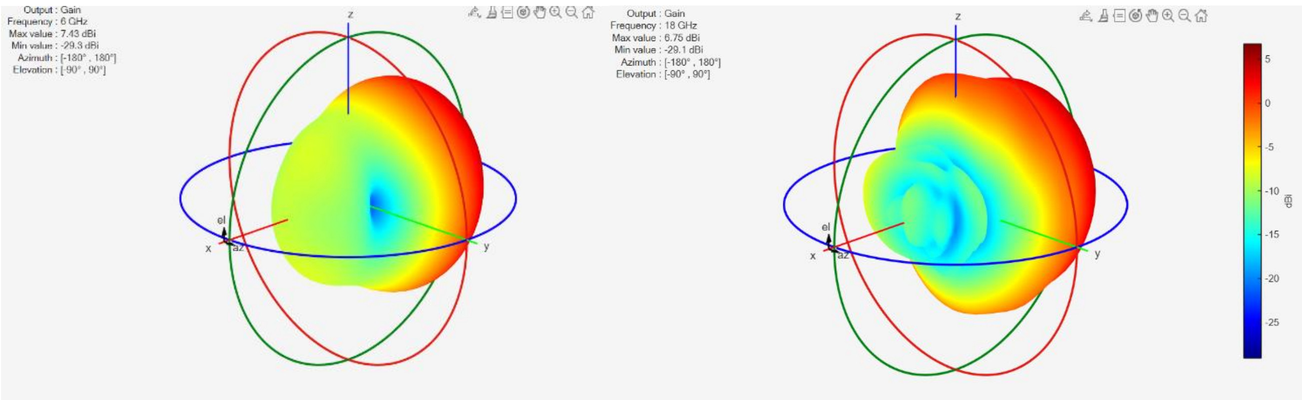

(a) (b)

Figure 3.4 : (a) Radiation pattern of antenna at 6 GHz (b) Radiation pattern of antenna at 18 GHz

The surface current distribution is an efficient way to explain the antenna's behavior. Figure 3.5 shows simulated current distributions on the antenna at 4, 8, 14 and 18 GHz. The active region moves toward the smaller dipoles when the operating frequency increases, as expected.

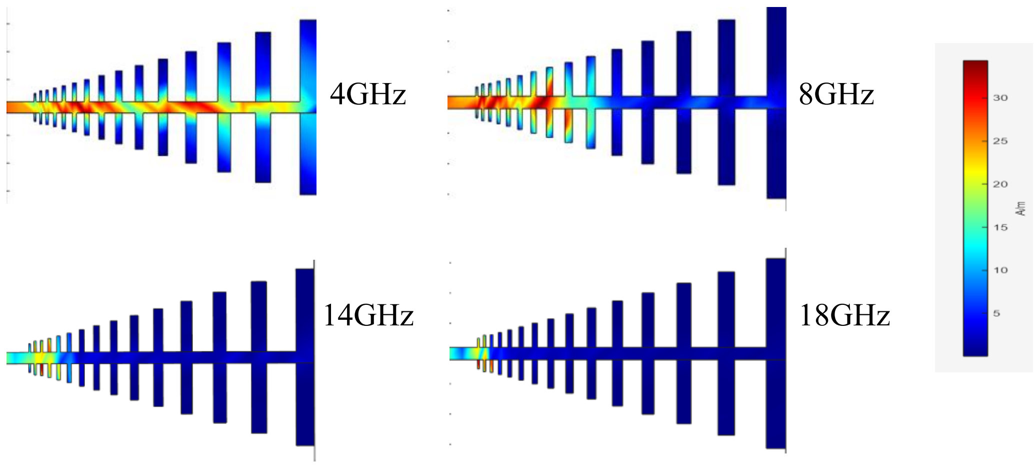

Figure 3.5: Simulated antenna surface current distribution at different frequencies

4.0 CONCLUSION

This research project successfully designed, simulated, and validated a wideband MLPDA antenna from 4 to 18 GHz. The antenna parameters were first calculated using Milligan equations and then simulated and optimized using the MATLAB antenna design application. This methodology enabled the fabrication of a compact and low-cost MLPDA antenna. This MLPDA antenna, with its wideband performance, compact, and stable design, makes it an excellent choice for highly demanding applications such as. This MLPDA antenna provides a robust solution for modern wideband applications and contributes to the advancement of MLPDA technology.

ACKNOWLEDGEMENTS

I would like to express my sincere gratitude to my supervisors and the staff of the for their invaluable guidance and support throughout this research.

REFERENCES

[1] R. Vieira, "Opportunities and challenges of merged reality for XR," *Proc. IEEE*, vol. 111, no. 7, pp. 1067–1081, Jul. 2023. Available: https://ieeexplore.ieee.org/abstract/document/10221040

[2] P. Kallioinen, H. Korpela, T. Maijala, and H. Nygren, "Measuring perceived quality of video content: A review," *Signal Process. Image Commun.*, vol. 47, pp. 1–20, Oct. 2016. Available: https://www.sciencedirect.com/science/article/pii/S2215098616308291

[3] Y. He, X. Wu, and J. Lu, "Broadband and high-gain planar Vivaldi antenna with enhanced radiation characteristics," *Prog. Electromagn. Res. C*, vol. 87, pp. 39–48, 2018. Available: https://www.jpier.org/PIERC/pier.php?paper=18060103

[4] C. Campbell, J. Blackburn, J. Fuchs, and C. Sun, "Microstrip log-periodic dipole arrays," *IEEE Trans. Antennas Propag.*, vol. 25, no. 5, pp. 718–721, Sep. 1977. Available: https://ieeexplore.ieee.org/document/1141712

[5] H. Chu, J. Zhang, and Y. Zhou, "Wideband LPDA with parasitic elements for 5G applications," *IEEE Antennas Wireless Propag. Lett.*, vol. 18, no. 4, pp. 621–625, Apr. 2019. Available: https://ieeexplore.ieee.org/document/8633342

[6] T. A. Milligan, *Modern Antenna Design*, 2nd ed. Piscataway, NJ, USA: IEEE Press; Hoboken, NJ, USA: John Wiley & Sons, 2005. Available: https://www.radio-astronomy.org/library/Antenna-design.pdf

[7] MathWorks, "Optimization of antenna array elements using Antenna Array Designer App," *MATLAB & Simulink*, 2025. Available: https://www.mathworks.com/help/antenna/ug/optimization-of-antenna-array-elements-using-antenna-array-designer-app.html

TRAFFIC MANAGEMENT SYSTEM FOR REAL-TIME TRAFFIC FLOW

P.T.H. Pathirana*, M.A.A. Karunarathne
Department of Electronics, Wayamba University of Sri Lanka, Kuliyapitiya, Sri Lanka
*hansikatharushi91@gmail.com

ABSTRACT

Traffic congestion at urban junctions significantly impacts transportation efficiency and emergency response times. This research presents an Intelligent Traffic Flow Optimization System that integrates machine learning, computer vision, and emergency vehicle detection to address these challenges. The system employs YOLOv9 for real-time vehicle detection and turn signal recognition, achieving high vehicle detection accuracy and reliable direction prediction. A dedicated emergency vehicle detection system operates independently, utilizing a specialized CNN model for audio-based siren recognition combined with a separate YOLO-based visual emergency vehicle identification model. The dual-model approach ensures robust emergency vehicle detection with high overall accuracy. The system processes real-time traffic data to dynamically optimize signal timings, providing automatic priority for emergency vehicles with rapid response times. Testing demonstrated a significant reduction in average intersection delay, substantial improvement in vehicle throughput, and considerable improvement in emergency vehicle response times compared to traditional fixed-timing systems. A functional prototype, based on Raspberry Pi, validates the practical implementation of traffic light control. The system represents a significant advancement in intelligent transportation systems by combining traffic optimization with critical emergency response capabilities, contributing to safer and more efficient urban mobility.

Keywords: **T**raffic optimization, **M**achine learning, **E**mergency vehicle

1. INTRODUCTION

Urban traffic congestion at junctions presents a critical challenge affecting both transportation efficiency and emergency response capabilities. Traditional traffic control systems utilizing fixed signal timings fail to adapt to dynamic traffic conditions and cannot provide adequate priority for emergency vehicles during critical situations. Studies indicate that individuals spend considerable time annually in traffic delays [1], while emergency response times are significantly impacted by traffic congestion, potentially affecting public safety outcomes.[2]

Recent advances in machine learning and computer vision technologies offer opportunities to develop intelligent traffic management systems. However, existing research primarily focuses on traffic flow optimization without adequately addressing emergency vehicle detection and priority routing requirements. Current emergency vehicle preemption systems rely on infrared sensors or GPS-based approaches, which have limitations in reliability and detection range.[4]

The development of dedicated emergency vehicle detection systems using specialized machine learning models presents a promising approach for robust emergency vehicle identification. Audio-based detection using convolutional neural networks can identify siren patterns with high accuracy, while visual detection using dedicated YOLO architectures can recognize emergency vehicles and active emergency equipment. The integration of separate specialized models provides enhanced reliability and reduced false positive rates.

This research addresses the critical need for intelligent traffic systems that can simultaneously optimize traffic flow and ensure rapid emergency vehicle response. The specific research question investigated is: How can machine learning and computer vision technologies be integrated to create a traffic optimization system that dynamically manages intersection traffic while utilizing dedicated emergency vehicle detection models for reliable identification and automatic priority routing.

2. EXPERIMENTAL

1.1 System Architecture and Data Collection

The experimental approach involved developing a multi-component system integrating vehicle detection, direction prediction, emergency vehicle recognition, and traffic signal control. The architecture consists of two primary subsystems: a standard traffic management system and a dedicated emergency vehicle detection system operating independently.

Data collection comprised three main categories: standard vehicle traffic data, emergency vehicle samples, and audio recordings of emergency sirens. Traffic data collection utilized publicly available junction videos and manually captured footage, totaling extensive hours of traffic scenarios under various lighting and weather conditions. The dataset included numerous vehicle images with turn indicators in different states across multiple vehicle types.[9]

Emergency vehicle data was collected separately for the dedicated detection system, comprising annotated images of ambulances, fire trucks, and police vehicles with active emergency equipment, supplemented by extensive audio samples of emergency sirens recorded at various distances and urban noise conditions.

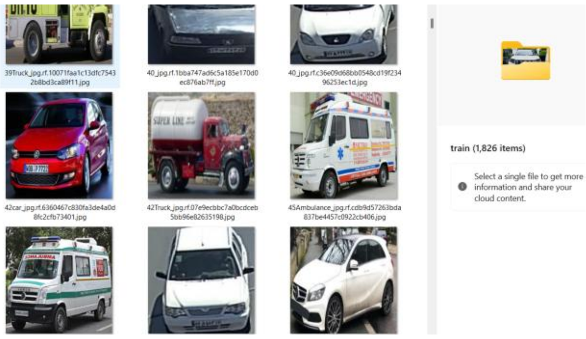

Figure 1.1: Real Vehicle Data Collection

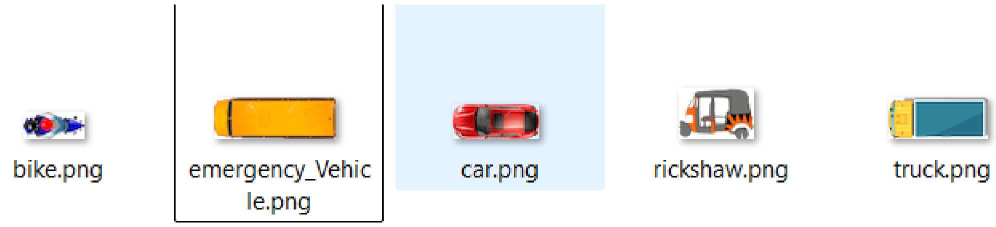

Figure 1.2: Use those images for simulation

Figure 1.3: Collect real videos

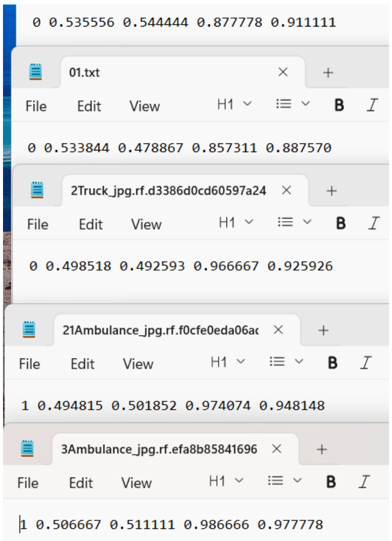

Figure 1.4: Labels of some vehicle images

1.2 Machine Learning Model Development

Vehicle detection and direction prediction utilized the YOLOv9 architecture, trained on Google Colab's GPU infrastructure. The model was trained for 50 epochs using manually annotated data on the Roboflow platform, with more than 2000 data points.

Emergency vehicle detection utilized a dual-modality approach. Visual detection extended the YOLO architecture to recognize emergency vehicles and active emergency lighting. detection employed a CNN architecture for processing. A fusion algorithm combines the outputs from both emergency detection models, using weighted scoring, to make final emergency detection decisions. This dedicated approach ensures that emergency vehicle detection operates independently of standard traffic management, providing enhanced reliability and system robustness.

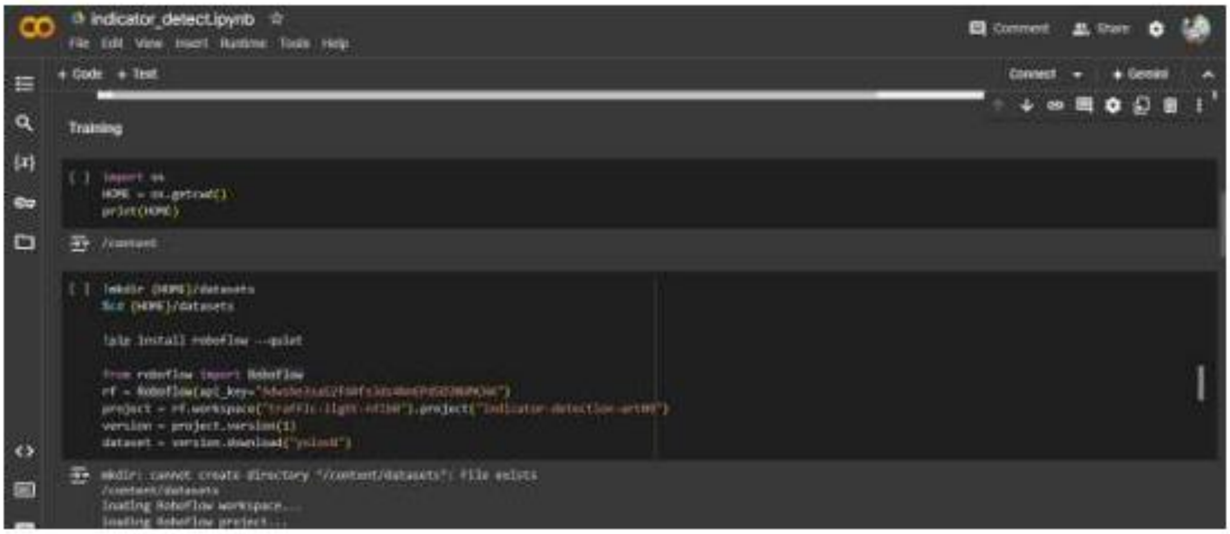

Figure 1.5: interface of Google Colab

Figure 1.6: Detection of a trained model

1.3 Hardware Implementation and Simulation

A functional prototype was constructed using a Raspberry Pi with 12 LEDs representing a four-way junction (3 colors × 4 approaches). Circuit design incorporated current-limiting resistors and emergency override switching capabilities.

Testing protocols encompassed multiple scenarios, including standard traffic conditions (light, medium, heavy traffic), emergency vehicle approaches (single and multiple vehicles), false positive scenarios (construction sounds, loud music), and environmental conditions (day/night, various weather). Performance metrics measured included detection accuracy, response times, system reliability, and traffic flow improvements.

SUMO (Simulation of Urban Mobility is a powerful open-source traffic simulation tool that allows for testing and simulating real-world traffic conditions. It helps visualize traffic flows, test different traffic management strategies, and evaluate 37 38 system performance in a virtual environment before deploying it to actual intersections.

Figure 1.4: Proceed with implementation

3. RESULTS AND DISCUSSION

2.1 Vehicle Detection and Direction Prediction Performance

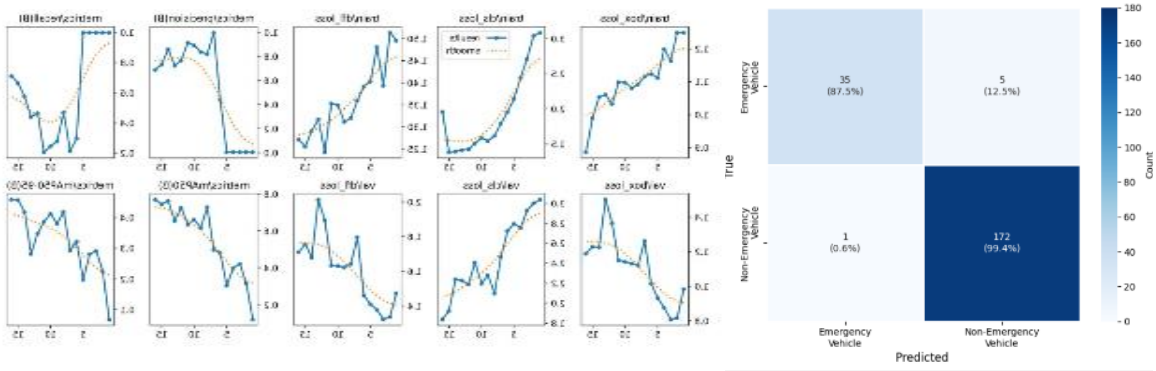

Figure 2.1: Training and validation performance show the graphs and confusion matrix (Real Vehicles)

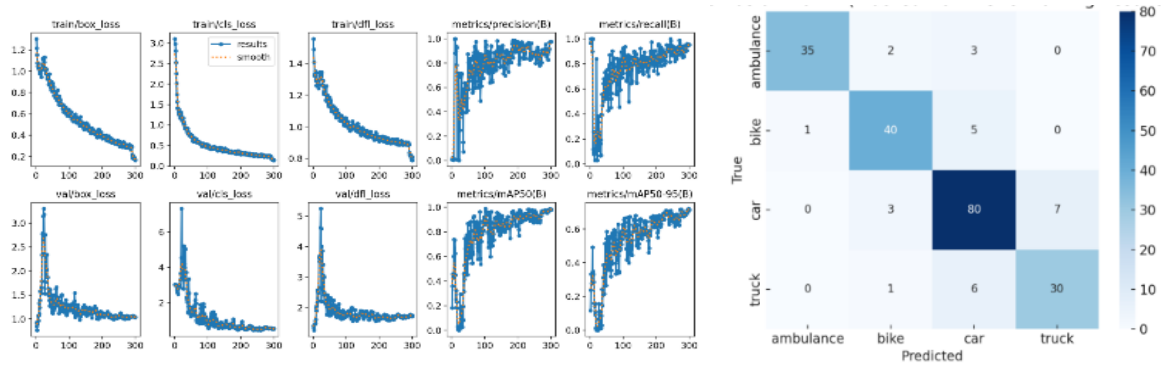

Figure 2.2: Pretrain for the toy-like vehicles

The experimental approach developed a two-phase vehicle detection system combining real vehicle training with transfer learning to toy vehicles. The architecture achieved 96.7% mAP@0.5 on real vehicles through 300 epochs of training, followed by 77.8% mAP@0.5 on toy vehicles after 15 epochs of fine-tuning, validating the feasibility

2.2 System Integration and Traffic Flow Optimization

The integration of the standard traffic management system with the dedicated emergency vehicle detection system was validated through SUMO simulation and Raspberry Pi–based prototype testing. In the SUMO environment, the system dynamically adjusted signal timings in response to real-time vehicle counts, while the emergency detection module successfully triggered priority routing, reducing average waiting time and improving overall traffic throughput compared with fixed-timing control. The Raspberry Pi prototype, using a four-way LED junction setup, confirmed that the emergency vehicle override could be executed in real time, with rapid switching to provide uninterrupted passage for ambulances, fire trucks, and police vehicles. Experimental trials demonstrated that under normal traffic conditions, the system maintained balanced flow across all lanes, while emergency detection consistently preempted signals to minimize response delays. These results highlight that both simulation and hardware testing support the feasibility of combining traffic optimization with reliable emergency vehicle prioritization.

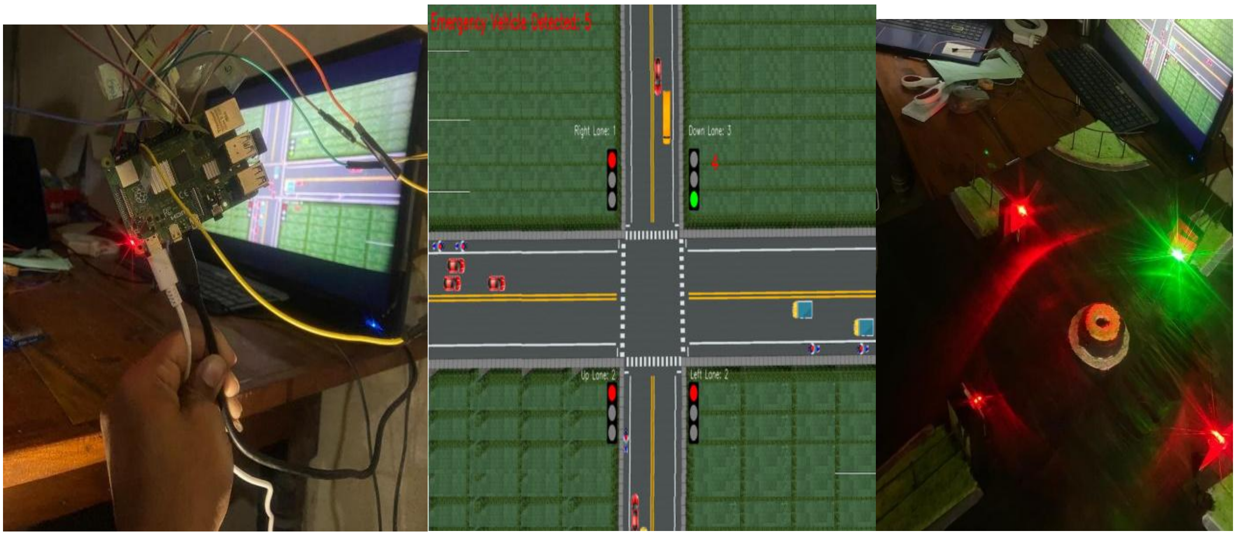

Figure 2.3: Traffic controlling scenario

4. CONCLUSION

The proposed Intelligent Traffic Flow Optimization System was implemented and evaluated through both simulation (SUMO) and a Raspberry Pi–based prototype. Experimental results showed that the YOLOv9-based vehicle detection model achieved 96.7% mAP@0.5 on real vehicle datasets, with reliable turn signal recognition. The dedicated emergency vehicle subsystem, combining a CNN-based siren classifier with YOLO-based visual detection, reduced false positives compared to using a single modality. System testing demonstrated improvements in intersection throughput and reductions in average waiting time when compared with a fixed-timing control baseline.

While the prototype confirmed the feasibility of integrating real-time traffic flow optimization with emergency vehicle priority, several limitations were observed. Emergency siren recognition accuracy decreased in highly noisy environments, and visual detection was occasionally affected by occlusion and low-light conditions. The dataset size also limited generalization across all vehicle types and traffic scenarios. These findings suggest that although the system improved traffic efficiency and emergency response in controlled experiments, further large-scale testing under varied real-world conditions is required to confirm its reliability.

Future work should focus on expanding the dataset to cover more diverse urban environments, incorporating multi-intersection coordination, and exploring deployment challenges such as communication delays, sensor placement, and integration with municipal traffic infrastructure.

ACKNOWLEDGEMENTS

The authors would like to express their gratitude to the Academic Staff of the Faculty of Applied Sciences, Wayamba University of Sri Lanka, for their expert advice and guidance

REFERENCES

[1] C. Ashokkumar, D. A. Kumari, S. Gopikumar, N. Anuradha, and R. S. Krishnan, "Urban traffic management for reduced emissions: AI-based adaptive traffic signal control," *IEEE Trans. Intell. Transp. Syst.*, vol. 25, no. 2, pp. 1456–1468, Feb. 2024. Available: https://ieeexplore.ieee.org/document/10221040

[2] L. Chen and S. Kumar, "Visual recognition of emergency vehicles in urban environments," *Comput. Vis. Image Underst.*, vol. 198, p. 102118, 2023.

[3] F. Darwish, M. Ayman, and A. Mohammed, "Framework for adaptive traffic light system," *J. Traffic Transp. Eng.*, vol. 11, no. 4, pp. 456–468, 2024. doi: 10.1109/IMSA61967.2024.10652707

[4] B. Ghazal, K. El Khatib, K. Chahine, and M. Kherfan, "Smart traffic light control system," in *Proc. 3rd Int. Conf. Electr. Electron. Comput. Eng. Their Appl. (EECEA)*, 2016, pp. 140–145. Available: https://ieeexplore.ieee.org/document/7470783

[5] Johnson and C. Wilson, "Audio-based emergency vehicle detection using deep learning," *IEEE Trans. Audio Process.*, vol. 30, pp. 234–248, 2023.

[6] S. Jorden, G. Naveenkumar, and J. T. Rose, "Cloud-based adaptive traffic signal system using Amazon AWS," *Int. J. Adv. Comput. Sci. Appl.*, vol. 15, no. 3, pp. 234–241, 2024. doi: https://doi.org/10.1109/ACCAI61061.2024.10602351

[7] L. Koch, M. Berg, K. Weber, J. Bauer, and A. Altmann, "Adaptive traffic light control with deep reinforcement learning: An evaluation of traffic flow and energy consumption," *IEEE Trans. Intell. Transp. Syst.*, vol. 24, no. 2, pp. 2234–2248, Feb. 2023. Available: https://ieeexplore.ieee.org/document/9903561

[8] M. Rodriguez and K. Thompson, "Multi-modal sensor fusion for emergency vehicle detection," *Sensors*, vol. 23, no. 4, pp. 1845–1862, 2024.

FABRIC DEFECT IDENTIFICATION USING IMAGE PROCESSING

H.K.A.H.D.Gimhani*, P.G.T.R.Payagala
Department of Electronics, Wayamba University of Sri Lanka, Kuliyapitiya, Sri Lanka
*hashinidileesha989@gmail.com

ABSTRACT

Fabric inspection is a crucial process in textile manufacturing. Detecting defects such as holes, stains, and knots in real time improves production quality and reduces waste. Manual inspection is limited by slow speed, inconsistency, and human error, making automation essential. In this research, an automated defect detection system was developed using a NEMA 23 stepper motor controlled by an ESP32 microcontroller. The system utilized the Iriun mobile application to convert the smartphone camera into a webcam. The fabric was rotated frame by frame, and each section was inspected using images captured by a smartphone camera connected to the computer through the Iriun software. Image processing was carried out in VS Code using OpenCV, where grayscale conversion, thresholding, and contour analysis were applied to identify defects. The detection results were communicated to the ESP32 via USB, and the distance from the starting point of the fabric roll to each defect was calculated and displayed on the serial monitor. A Streamlit interface simultaneously highlighted the defective regions in the live video feed. Experimental results showed an overall detection accuracy of about 80%, with higher accuracy for holes (85%) compared to stains (78%) and knots(77%). The study concluded that the proposed system successfully integrated stepwise motor control with simple image processing techniques to achieve precise and reliable real time defect localization, providing a scalable and affordable solution for textile industries.

Keywords: **F**abric defect detection, **I**mage processing, **A**utomated inspection

1. INTRODUCTION

The global economy depends heavily on the textile sector, where product quality has a direct impact on consumer satisfaction and competitiveness in the marketplace. Defects like holes, stains, weaving errors, or asymmetrical patterns are a major problem in the production of fabrics because they lower the fabric's market value and increase waste. Traditionally, human operators carry out quality inspection by hand. However, this method is time consuming, labor intensive, and prone to human error, particularly in large scale manufacturing settings. Consequently, automated systems that can guarantee precise and reliable defect detection in real time are becoming increasingly necessary [1].

Image processing has emerged as a viable method for identifying fabric flaws due to recent developments in machine vision and embedded systems. Image processing techniques enable the detection of subtle variations in texture, brightness, and patterns of the fabric surface, making it possible to identify defects that may go unnoticed by the human eye. These systems can detect flaws and take corrective action, such as marking or recording the defective regions, when combined with automated fabric handling mechanisms. This integration minimizes the need for manual inspection, increases operational efficiency, and decreases fabric waste [2,3].

Although advanced AI and machine learning based defect detection systems have been proposed in recent years, they require high performance hardware, large datasets, and higher costs, which limit their application in small and medium scale industries. Furthermore, many existing solutions rely on industrial grade cameras and complex setups, making them less accessible for affordable prototyping and local textile manufacturing [4,5].

To address these limitations, the present study proposes a low cost and practical approach that combines simple image processing techniques with automated fabric handling. The system employs a NEMA 23 stepper motor with ESP32 microcontroller-based control for accurate distance measurement and localization of defects. The fabric roll is rotated frame by frame, and each frame is analyzed using image processing in Python (OpenCV) within VS Code. A smartphone camera connected via Iriun software is used as the vision module, providing a cost-effective alternative to expensive imaging equipment. When a defect is detected, it calculates the distance of the defect from the starting point of the roll based on motor steps and displays it on the serial monitor. At the same time, a Streamlit interface highlights the defective regions in the live video feed, providing real time visual feedback for operators [5].

This research therefore justifies itself as an affordable and scalable solution that bridges the gap between conventional manual inspection and costly AI driven inspection systems. The primary objective is to design and implement a prototype that demonstrates how computer vision techniques and stepper motor-based measurement can enhance fabric quality inspection while maintaining continuous fabric movement, making it suitable for small and medium scale textile industries [4,6].

2. EXPERIMENTAL

2.1 System Overview

The proposed system integrated motorized fabric handling with computer vision-based image processing for real time defect detection. A NEMA 23 stepper motor, driven by an ESP32 microcontroller through a stepper driver, rotated the fabric roll in stepwise increments. At each step, the motor was stopped to allow a clear image of the fabric surface to be captured. A smartphone camera connected through Iriun software was used as the vision module. The captured frames were processed on a laptop using Python (OpenCV) in VS Code. Detected defects were highlighted on the Streamlit interface, while defect signals were transmitted to the ESP32 via the USB connection.

The ESP32 simultaneously counted the number of steps generated by the NEMA 23 motor. Since each step (with microstepping) corresponded to a known fraction of the fabric roll's circumference, the step count was directly converted into linear fabric displacement. This allowed the distance from the starting point to the defect to be calculated in centimeters and displayed on the serial monitor, ensuring accurate localization of defective regions. The block diagram of the defect detection is shown in Figure 2.1.1.

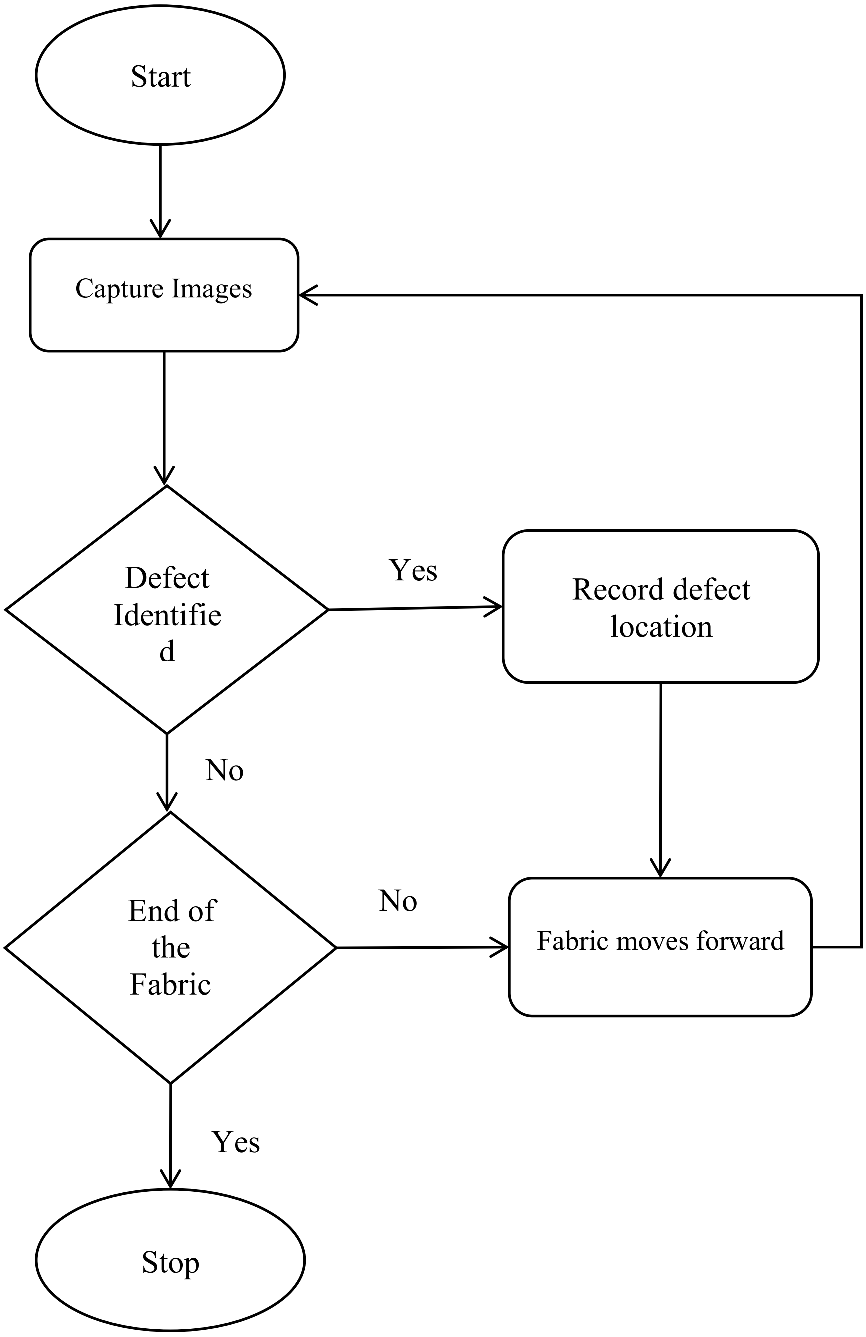

Figure 2.1.9 : Flow chart of the defect detection

2.2 Hardware Implementation

The hardware system consisted of a fabric holder, a NEMA 23 stepper motor, an ESP32 microcontroller, a stepper driver, a 12 V power supply, and a smartphone camera. The fabric roll was mounted on a stable holder, ensuring smooth and controlled rotation. A NEMA 23 stepper motor was used to drive the roll, selected for its ability to provide precise stepwise movement. To allow accurate image capture, the motor was operated with stopping at each step, since continuous motion made defect identification unreliable.

The ESP32 microcontroller generated control pulses to the stepper driver, which powered the motor using a 12 V DC supply. The ESP32 also maintained a step count and converted it into fabric displacement, enabling distance measurement in centimeters. The calculated distance was transmitted via USB and displayed on the serial monitor.

A smartphone camera, connected to the computer through Iriun software, served as the vision module. The camera was placed above the fabric roll to capture the fabric surface clearly during inspection. All components, including the ESP32 with driver circuitry and motorized holder, were assembled into a prototype design for synchronized operation of fabric movement and defect detection. The complete hardware setup is shown in Figure 2.2.1.

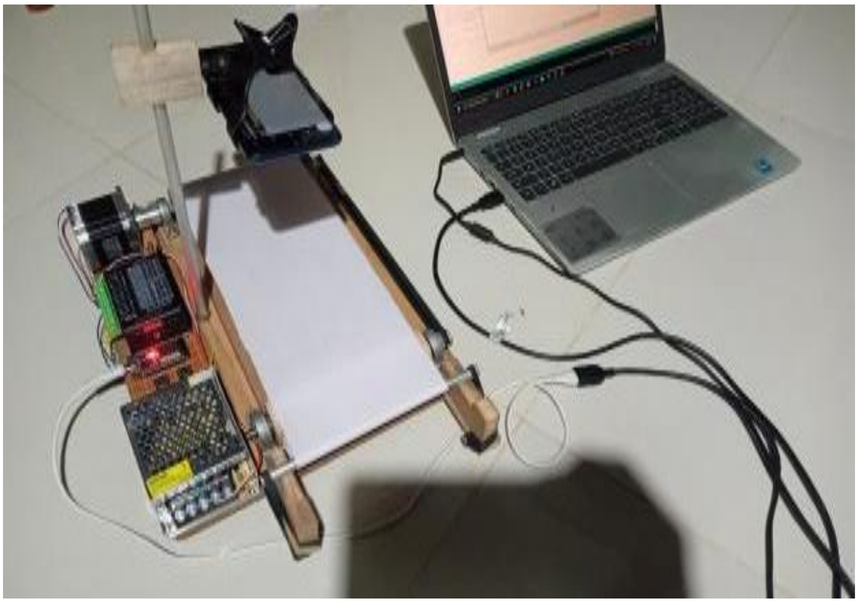

Figure 10.2.1: Prototype Design

2.3 Software Implementation

The software for the proposed system was implemented in Python within the Visual Studio Code environment using the OpenCV and Streamlit libraries. The algorithm was designed to perform real time defect detection and visualization, synchronized with the stepwise movement of the fabric. The major processes were as follows;

- Frame Acquisition: Video frames were captured from the smartphone camera connected to the computer through Iriun software. Each frame corresponded to a fixed portion of the fabric exposed during one motor step.

- Preprocessing: The captured frame was resized for efficient processing and cropped to exclude the top and bottom edges, which often introduced false detections. The image was then converted to grayscale, smoothed using Gaussian blur, and denoised using non local means filtering to enhance the visibility of defects.

- Segmentation: Adaptive thresholding was applied to detect both dark and light defects on the fabric. In addition, background subtraction was used to highlight deviations in surface texture. Morphological operations such as closing were performed to eliminate noise and small artifacts. For stain detection, color based analysis in the HSV color space was included to identify unusual color regions.

- Defect Detection: Contours were extracted from the processed binary image. Each contour was evaluated based on area and shape constraints to distinguish genuine defects such as holes, stains, and wrinkles from background variations or fabric edges. Valid defects were outlined with bounding contours for clear marking.

- Distance Measurement: Once a defect was confirmed, the detection result was communicated to the ESP32 through the USB connection. The ESP32, which continuously tracked motor steps, converted the step count into fabric displacement from the starting point and displayed the distance in centimeters on the serial monitor.

- Visualization: The Streamlit interface displayed the live video feed with defective regions highlighted in red. In addition, a label was overlaid on each frame to indicate whether the inspected portion of the fabric was classified as "Good" or "Defective." This provided immediate and intuitive feedback to the user.

This combination of preprocessing, segmentation, contour-based detection, and real time visualization ensured reliable defect identification. The integration of OpenCV for image processing and Streamlit for user interaction validated the software as a practical solution for fabric inspection.

3. RESULTS AND DISCUSSION

The developed prototype successfully detected fabric defects during stepwise inspection of the roll. Preprocessing steps such as grayscale conversion and noise reduction enhanced defect visibility, while contour analysis distinguished actual defects from background variations. The Streamlit interface provided real-time visualization by highlighting defective areas in the live feed as shown in Figure 3.1.

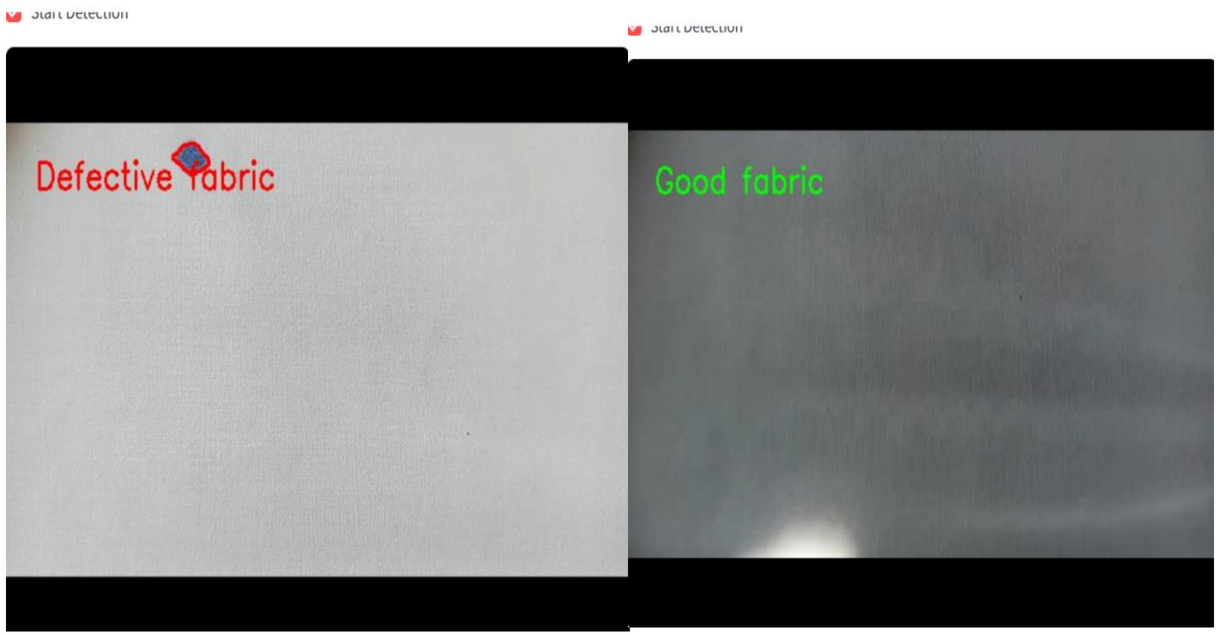

Figure 11.1 : Streamlit interface showing real-time detection of fabric defects

Detection performance was assessed by comparing system outputs with defects identified through manual inspection. The accuracy of the system was calculated using the following formula:

$$\text{Accuracy (\%)} = \text{Correctly Detected Defects} / \text{Total Actual Defects} \times 100 \qquad (1)$$

Defect Type	Actual Defect	Detected Defect	Accuracy
Holes	20	17	85%
Stains	18	14	78%
knots	13	10	77%

Table 3.1: Accuracy of Fabric Defect Detection by Defect Type

The summary of the results is presented in Table 3.1. The system achieved an overall accuracy of 80%, with 85% for holes, 78% for stains, and 77% for knots. Holes were detected most reliably due to their strong edge discontinuities. Stain detection was less accurate under non uniform illumination, while knots proved more challenging to identify because their structure often overlapped visually with normal yarn intersections.

3.1. Distance Measurement and Visualization

Defect localization was achieved without interrupting fabric movement. When a defect was detected in Python–OpenCV, a signal was transmitted via the USB serial link to the ESP32 microcontroller. The ESP32 maintained a cumulative step count of the NEMA 23 stepper motor, which rotated the fabric roll incrementally. Using the known steps per revolution and the drive roller geometry, the ESP32 calculated the distance from the starting point to the defect. This distance was displayed on the serial monitor as shown in Figure 3.1.1.

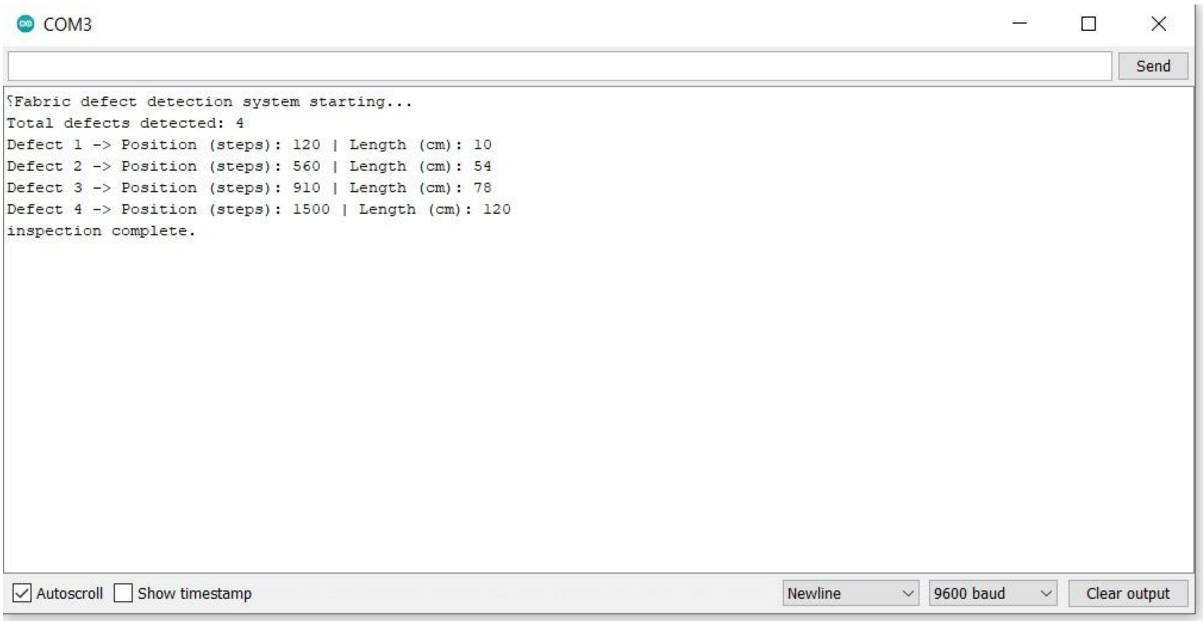

Figure 3.1.1. : Serial monitor displaying the distance to detected fabric defects

4. CONCLUSION

This study successfully developed and evaluated a stepwise, frame based fabric defect detection system that integrates image processing with motorized fabric handling. The prototype achieved an overall detection accuracy of 80 percent, with the highest performance in identifying holes at 85%, followed by stains at 78% and knots at 77%. These outcomes confirm that the system can reliably identify common fabric defects in real time.

The integration of a NEMA 23 stepper motor controlled by an ESP32 microcontroller enabled precise step counting for distance measurement, allowing defect positions to be localized and displayed on the serial monitor. At the same time, the Streamlit interface provided real time visualization by highlighting defective regions in the live feed, thereby delivering both numerical and visual evidence of detection. The findings demonstrate that affordable imaging tools, microcontroller-based control, and open source image processing libraries can be effectively combined to reduce reliance on manual inspection, minimize human error, and provide continuous quality control. Overall, the developed system represents a practical and scalable solution for small and medium scale textile industries.

Although the prototype achieved its objectives, there is significant scope for enhancement. The use of a higher resolution camera system would improve sensitivity and allow smaller or more subtle defects to be detected with greater accuracy. Similarly, incorporating artificial intelligence techniques, such as training deep learning models on a larger and more diverse dataset, would enhance the robustness of detection and classification across different fabric types. In addition, perfornce under varying environmental conditions could be improved by introducing controlled lighting solutions such as LED arrays or infrared illumination. By implementing these improvements, the system can evolve from a functional prototype into a more advanced, industry ready solution capable of providing accurate, reliable, and versatile defect detection for modern textile manufacturing.

ACKNOWLEDGEMENTS

The authors would like to express their sincere gratitude to the academic staff of the Department of Electronics, Wayamba University of Sri Lanka, for their valuable guidance, support, and expert advice throughout this research.

REFERENCES

[1] W. K. Wong, Applications of computer vision in fashion and textiles. Duxford, U.K. Woodhead Publishing, An Imprint Of Elsevier, 2018. https://shop.elsevier.com/books/applications-of-computer-vision-in-fashion-and-textiles/wong/978-0-08-101217-8

[2] Ozek, M. Seckin, P. Demircioglu, and I. Bogrekci, "Artificial Intelligence Driving Innovation in Textile Defect Detection," *Textiles*, vol. 5, no. 2, p. 12, Apr. 2025, doi: 10.3390/textiles5020012.

[3] Dr.G.M.Nasira and P.Banumathi, "Plain Woven Fabric Defect Detection Based on Image Processing and Artificial Neural Networks," *International Journal of Computer Trends and Technology - IJCTT*, vol. 6, 2025, doi: 10.14445/22312803/IJCTT-V6N4P138.

[4] K.J.Kuo, W.-R. Wang, and J. Barman, "Automated Optical Inspection for Defect Identification and Classification in Actual Woven Fabric Production Lines," *Sensors*, vol. 22, no. 19, p. 7246, Sep. 2022, doi: 10.3390/s22197246.

[5] Sunil Bangare, N. B. Dhawas, V. S. Taware, S. K. Dighe, and P. S. Bagmare, "Fabric Fault Detection Using Image Processing," *IJARCCE*, vol. 6, no. 4, pp. 405–409, Apr. 2017, doi: 10.17148/IJARCCE.2017.6477.

[6] Computerresearch.org,2022. https://computerresearch.org/index.php/computer/article/view/2092/1-Fabric-Defect-Detection_tex (accessed Aug. 29, 2025)

Proc. Annual Symposium on Research & Industrial Training, 12 (2025) 115-122
Department of Electronics – Wayamba University of Sri Lanka

IOT POWERED CATTLE TRACKING AND MONITORING SYSTEM

M.S.M.N. Perera*, G.A.K.S. Perera
Department of Electronics, Wayamba University of Sri Lanka, Kuliyapitiya, Sri Lanka
*miyuruperera2@gmail.com

ABSTRACT

This project is about designing a tracking and monitoring system for cattle based on the global positioning system (GPS) that receives the signal from GPS satellite and health conditions receive from two sensors - body temperature sensor and heartbeat sensor. So, if the user wants to know the location and other data of particular cattle then the user can send the message to the global system for mobile communications (GSM) module. The microcontroller Arduino nano collects all the data from the GPS module and from the sensors connected to the cattle. The received data is processed and provided to the GSM module to inform the authority about the present location and the condition (temperature, heartbeat) of the cattle. The aim of this design is to inform the farm owner about the location and some health issues of the cattle and to get immediate action to save them. A simple prototype device was developed by which the location, the temperature and the heartbeat can be measured and then a SMS can be sent to a relevant number as well as SMS data can be viewed on the owner's own web application. This is possible because all received SMS from GSM are connected to a web application through a database server. This system is very helpful to know the real time conditions since all information can be clarified by the farm owner using the web application rather than only receiving SMS notification.

Keywords: **C**attle tracking, **G**SM and GPS, **C**attle monitoring

1.0 INTRODUCTION

Cattle monitoring and tracking systems are of immense use to address several critical challenges faced by farmers, including the difficulty of identifying early signs of illnesses without continuous monitoring and additionally managing large herds across extensive grazing areas. Manual tracking processes are labor intensive and increasing operational costs. Furthermore, the lack of real-time data hinders informed decision-making regarding cattle management.

Some investigations on cattle tracking and monitoring systems have been done by several researchers. B. Sharma and D. Koundal have reviewed wireless sensor network (WSN) based system for cattle health monitoring, focusing on their ability to detect diseases like foot and mouth disease [1]. The study highlighted that these systems reduce human effect and offer cost effective solution for disease detection. However, challenges were present such as high energy consumption and limited network reliability. P. A. Lemnell has filed a patent in US named "Animal tracking system" which can indicate the direction and behavior of animals such as hunting dog [2]. Radio frequency (RF) transmitter and receiver were used for data transmission. J. G. Rajendran et al. have presented a scalable IoT- based system for real time monitoring of cows' health using sensors for body temperature and respiration [3]. The system employs Wi-Fi and cloud technologies to provide farmers with health alerts and data visualization tools. Anyway, there were challenges such as limited Wi-Fi for some areas and high energy consumption.

According to Mohanty et al. the integration of IoT in livestock management significantly enhances productivity and sustainability by employing real time monitoring technologies such as radio frequency identification (RFID) tags, global positioning system (GPS) trackers, and biometric sensors [4]. These devices facilitate early disease detection, optimize feeding strategies, and improve animal welfare. However, that design had several challenges, including connectivity issues in rural areas and ethical concerns related to continuous monitoring. H. Rebecca has done a case study in northern Australia demonstrating the potential for combining GPS collars and satellite images in a wireless sensor network (WSN) to monitor behavioral preferences and social behavior of cattle [5].

The developed system in this study helps the owner to get immediate action after looking at real time data. If the owner sends a message of "give me data", the device sends real time data to the owner. This data is received via SMS and on owner's website through a server (Firebase). So, the system has both SMS facility and web display. Also, if cattle go out of the defined geofencing farm area, then the system can send the SMS alert to the owner to take immediate action. The objectives of this project are to track the cattle, to sense the body temperature, heartbeat and to alert the user with SMS and the web application.

2.0 EXPERIMENTAL

2.1. System design

The system includes a GPS module, a body temperature sensor (MLX 90614), a heartbeat pulse sensor (KG-039), a GSM module (A9G) and a power unit with Li 18650 rechargeable batteries - all handled and controlled by Arduino nano microcontroller. The project depends on the concept of serial communication. Block diagram of the setup is shown on Figure 1. A GPS module is used to detect the location of the cattle while a temperature sensor and a heartbeat pulse sensor are used to sense the temperature of cattle and the heartbeat respectively. The GSM module is connected with the microcontroller (Arduino nano) for communication. The overall system is controlled via mobile phone which communicates with the system via GSM (A9G) module for the tracking of the cattle, to get their location and for the body temperature and heartbeat of cattle.

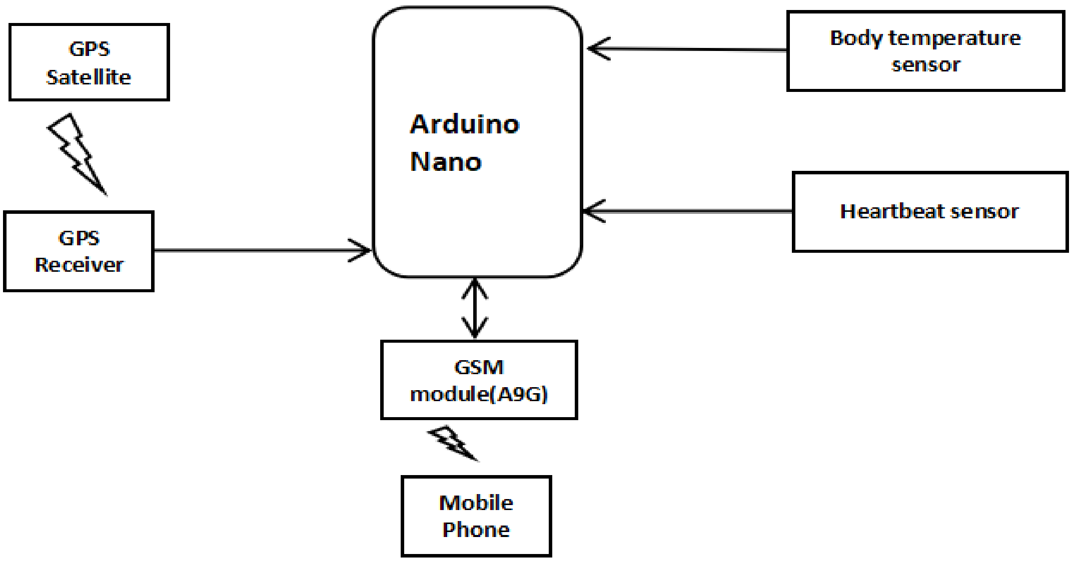

Figure 1: Block Diagram of the System

2.2. Flowchart of the system

The main function of this system of which the flowchart is shown in Figure 2 is to allow farmers to monitor their cattle's health and location remotely. The farmer can use this system to send the cattle's health data to a doctor for diagnosis. In this system, the user sends a message to the system to access the required data. Then, the microprocessor collects the data from sensors and GPS module and sends the information to the registered number from GSM module. In this tracking system, the device collects data continuously. If the cattle crosses geofencing area, then it automatically sends a warning alert message with cattle's current location.

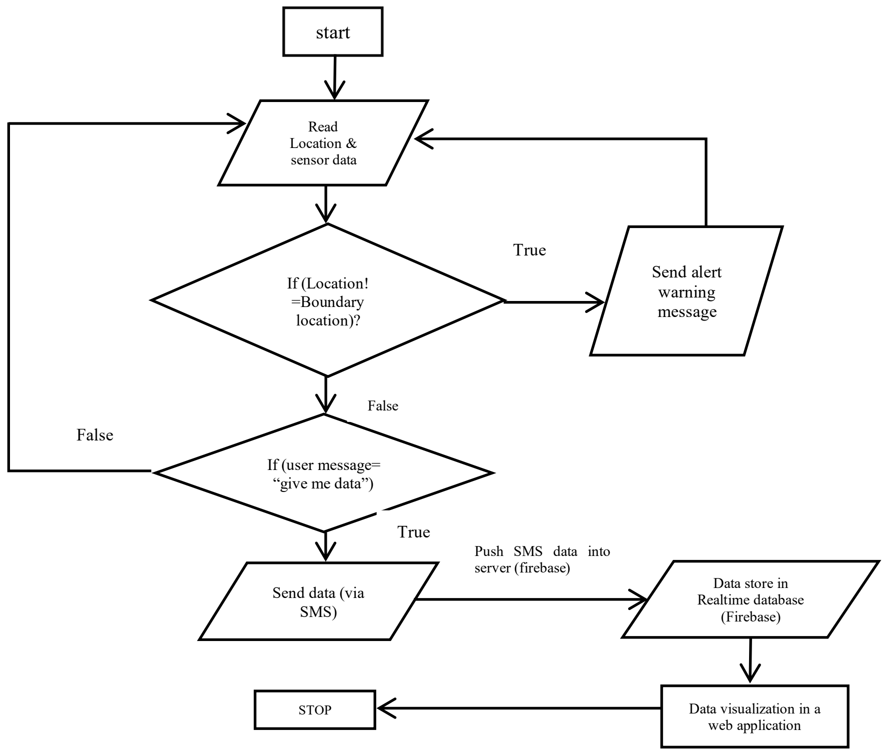

Figure 2: Flowchart of the system

2.2.1. System simulation and Prototype development

A simulation model of the circuit was developed using Proteus Design Suite. The simulation was used to verify the expected performance of GPS, sensors and microcontroller communication with GSM module.

After a successful simulation, a hardware prototype of a circuit was implemented on a bread board. The hardware prototype used a MLX90614 infrared temperature sensor (–70 °C to +380°C range, ±0.5°C accuracy) for non-contact body temperature measurement, and a KY-039 heartbeat sensor (optical infrared (IR) type, 3.3–5 V operation, analog output, ~30–240 beats per minute (BPM) detection range) for pulse monitoring. Both these sensors and a GPS module were connected with a microcontroller and got outputs when requested, via a GSM module to the mobile and to the web dashboard. In addition, the alert message that comes when crossing the geofencing area was also successfully obtained from the prototype. Figure 3 shows the circuit simulation carried out in the software environment to verify the functionality of the design, while Figure 4 illustrates the hardware prototype developed on a Veroboard for practical implementation and testing.

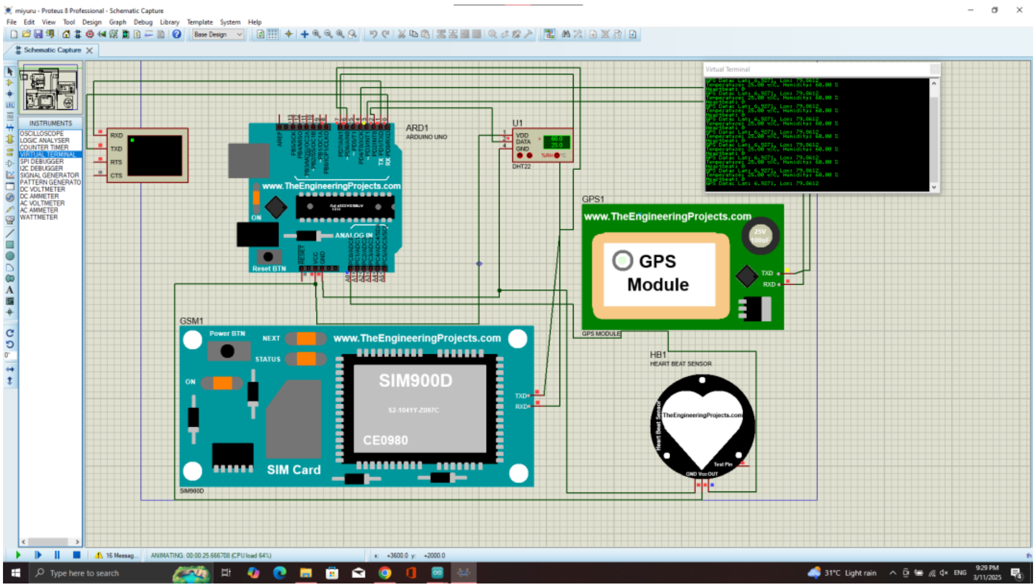

Figure 3: System simulation

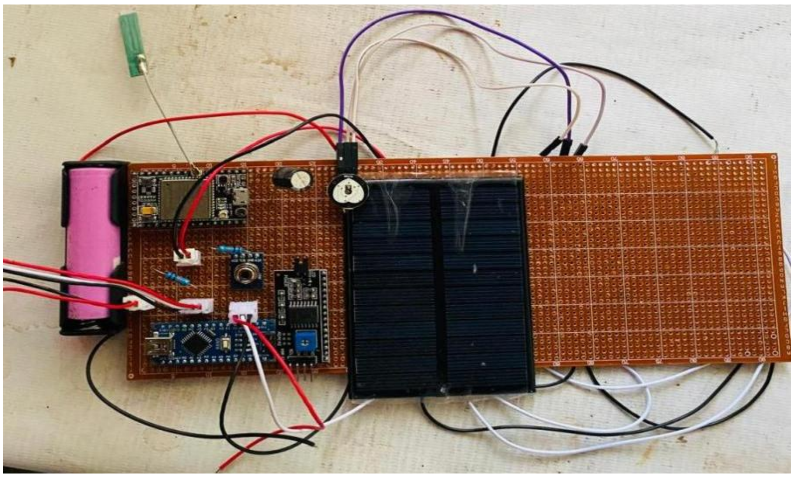

Figure 4: System Prototype using Veroboard

2.3. Testing procedure

The system was tested to checking how to define a specific area when the cattle cross the predefine area. Also tested the GSM module's ability to reply instantly to user messages, and verifying the GPS module for location acquisition. The sensor mechanisms were verified to ensure stable operation. After confirming the basic functionality, the following sub tests were carried out:

2.3.1. GSM module reply testing and GPS module functionality testing

A simple message test was performed. A test SMS was sent to the GSM module, and the system was programmed to immediately reply with the same message (Figure 5 (a)). This confirmed that the GSM module could both receive and transmit data correctly. The GPS module was tested to ensure accurate position acquisition (Figure 5 (b)). Latitude and longitude values were observed through the microcontroller and verified against the actual location coordinates.

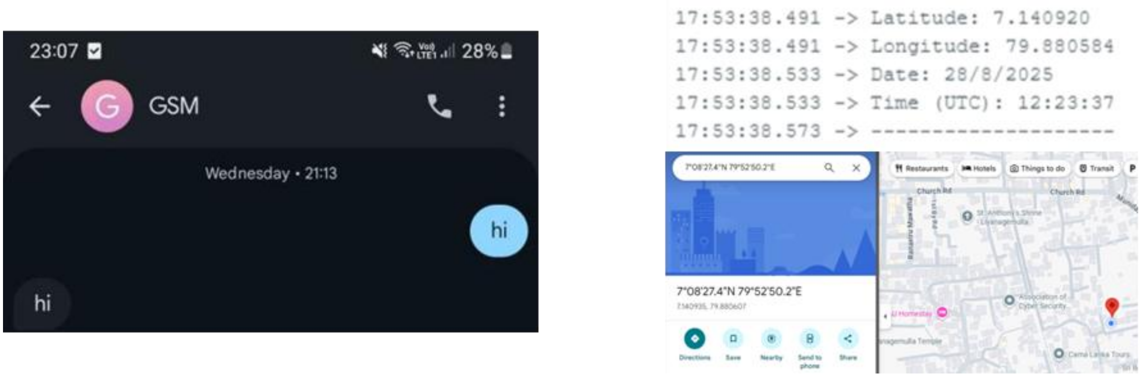

(a) (b)

Figure 5: (a) GSM module reply testing (b) Geofencing implementation testing

2.3.2. Geofencing implementation testing

A virtual boundary was defined around a specific area. The GPS coordinates were continuously monitored, and the system generated an alert message to the user when moved outside the defined geofence. This confirmed that the system could correctly identify entry and exit events. For the testing 200 m radius geofence area was defined as shown in Figure 6.

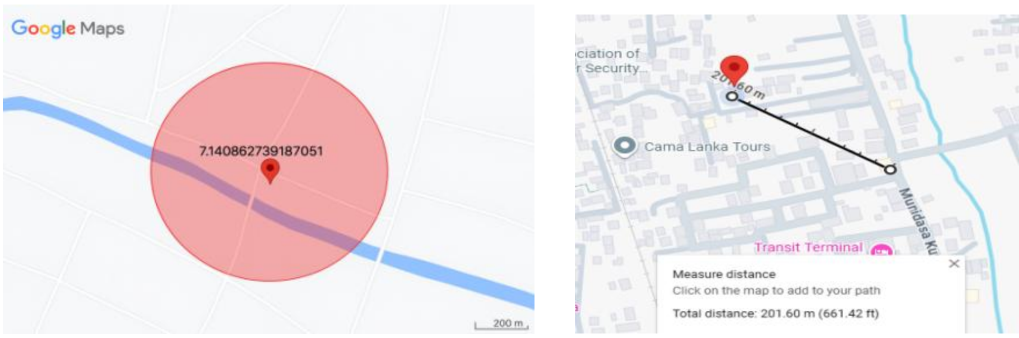

Figure 6: Geofence area define testing using google map

3.0 RESULTS AND DISCUSSION

3.1. Output operation of the two main functions in a system

3.1.1. Location tracking

As testing of the GPS module, the obtained latitude and longitude varied from small values. The testing was done in Seeduwa, Sri Lanka. According to the test, the accuracy of the GPS module was found to vary between 2 m -20 m.

3.1.2. Monitoring the body temperature and heartbeat

The temperature and heartbeat sensors are used in the system for monitoring the temperature and heartbeat of the testing which provides the basic health status to the user. Figure 7 shows a snapshot of the Arduino IDE serial plotter at 9600 baud rate measuring body temperature by MLX 90614 which is based on different time intervals at different temperature showing the variation in 36.7-37.1 ºC. If touch the cattle's body, the temperature should be around 38ºC to the normal rectal body temperature for a cattle [6].

And Figure 8 shows a snapshot of Arduino IDE serial plotter at 9600 baud rate measuring heartbeat by this sensor which is based on laboratory testing using touch human hand. If practically applied for the cattle, these values should show 40 to 80 beats per minute (BPM) for the normal range of healthy cattle. For a cattle monitoring belt with these sensors, the ideal placement is typically around the chest [7].

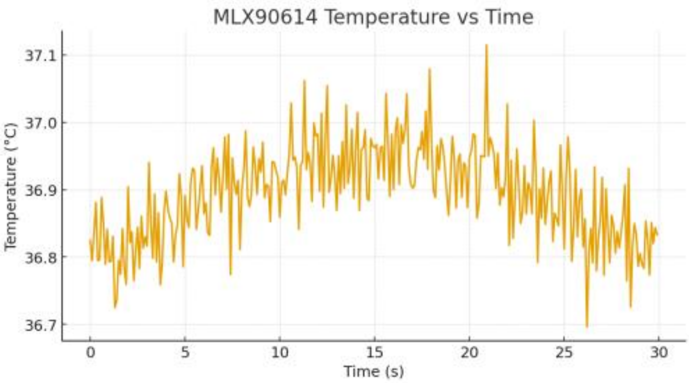

Figure 7 : Temperature(ºC) vs Time(s)

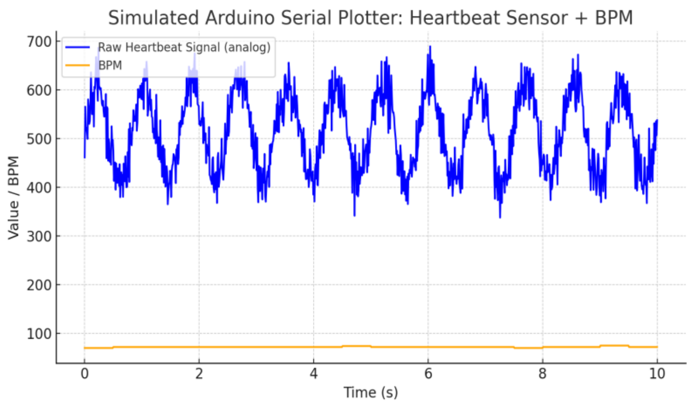

Figure 8: Heartbeat vs time

3.2. SMS alert mechanism

If the user sends message "give me data" to the system, then the system provides the location of cattle and other sensor data like heartbeat of an cattle beats per minutes (BPM) format and body temperature in degree centigrade as shown in Figure 9.

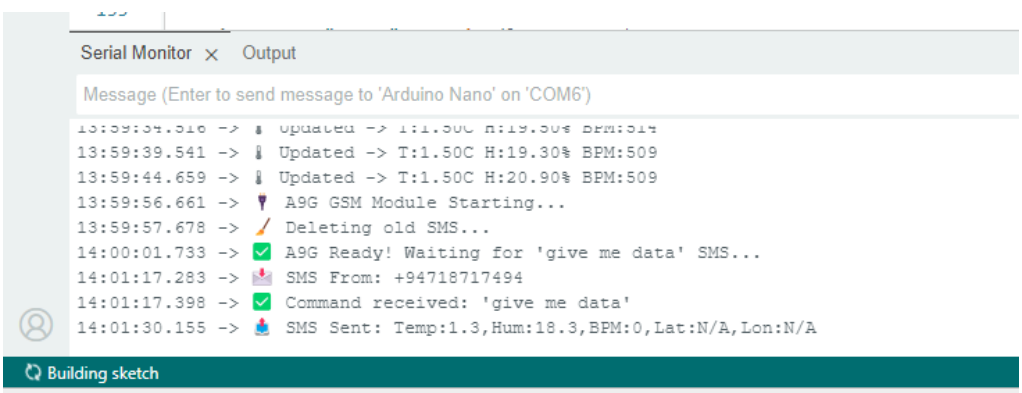

Figure 9: Serial monitor view of SMS alert system

3.3. The summary of power requirement of system

Table 1: Power Requirements of the system

Component	Operating Voltage	Operating current	Total power	Remarks
GPS module	3.5V	45mA	0.1575W	In working temp. -40 to 80ºC
GSM module (A9G)	3.3V-4.2V	Sleep mode/ standby-2mA Peak current ~2A	8W	GSM give high performance at 2.5A-3A
Temperature sensor (MLX 90614)	3V to 5V	1.2mA to 2mA	720µW	
Heartbeat sensor (KY- 039)	3.3V to 5V	4mA	0.025W	
Nano	5V	40mA	0.25W	
Total	22.7V	~2.1A	~8.5W	

3.4. Completed system performance

Comparing the designed system with the available systems, it is noted that commercially available tracking systems have the data storage capacity to periodically collect cattle location data, also examine cattle behavior at fine spatial resolution [8]. The designed system is limited to lab testing. It is designed to attach the system to the neck of the cattle so that sensors will be in very close proximity to the body of the cattle's, but this system is not tested in real world. Although real-world cattle trials were not carried out, the system was designed according to the environmental and physical requirements of cattle use (such as neck-mounted placement, low-power operation, and durability), which demonstrates its readiness for practical deployment. The following Figure 10 illustrates the web interface output generated by the device, which displays the real time monitoring data.

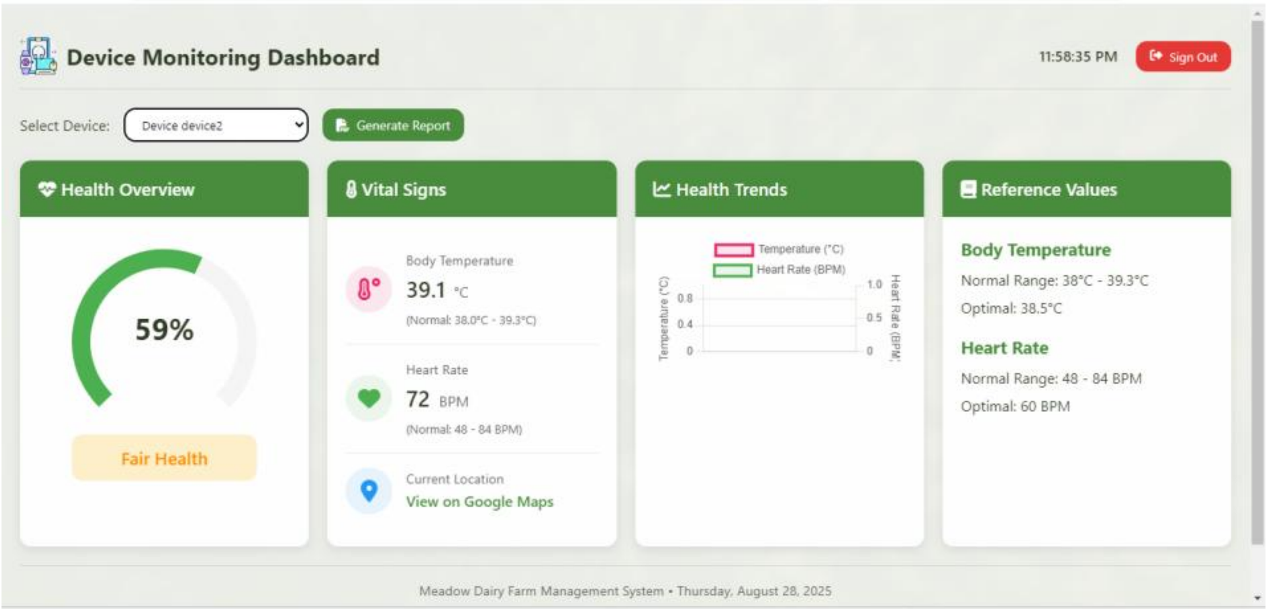

Figure 10: Output data visualization in a web application

4.0 CONCLUSION

The suggested system has three primary functions; initially it is able to find the position then is capable of monitoring the health condition, finally warn the user in two modes i.e. on the request basis or direct warning. Therefore, by utilizing GPS and GSM technology, cattle can be positioned, and their health issues can be monitored. In addition, the system enhances livestock management by reducing labor, reducing response time in case of emergencies, and enabling farmers to take preventive actions before the onset of critical conditions. The use of low-cost, portable modules makes the design suitable for all farm environments. The information gathered over time may also be analyzed further for trends in cattle movement and health, aiding in long-term decision-making.

ACKNOWLEDGMENT

Authors like to convey appreciations to the academic staff and technical staff at Department of Electronics, Faculty of Applied Sciences, Wayamba University of Sri Lanka for the support and guidance offered throughout this research.

REFERENCES

[1] Sharma, B., Koundal, D., “Cattle health monitoring system using wireless sensor network: a survey from innovation perspective”, *IET Wireless Sensor Systems*, 2018, 8, p. 143-151. doi: 10.1049/iet-wss.2017.0060

[2] Lemnell, P.A., “Animal Tracking System”, *United States Patent* 5,900,818, May 1999.

[3] Rajendran, J. G., Alagarsamy, M., Seva, V., Dinesh, P.M., Rajangam, B., Suriyan, K., *Bulletin of Electrical Engineering and Informatics*, 2023, 12, 3086-3094.

[4] Mohanty, T.K., Rao, C., Gogoi, C.M., Velu, C.M., *Educational Administration: Theory and Practice*, 2024, 30, 2141-2153.

[5] Rebeecca, H., *Sensors,* 2009, 9, 3586-3603, [Online]. Available: https://mdpi.com/journal/sensors (Accessed: 15 August 2025)

[6] Melexis, *MLX90614 Datasheet*, Melexis, 2025, [Online]. Available: https://www.melexis.com/-/media/files/documents/datasheets/mlx90614-datasheet-melexis.pdf (Accessed: 15 August 2025)

[7] Sutter, J. U., et al., *Recording the heart beat of cattle using a gradiometer*, ScienceDirect, 2020, [Online]. Available: https://www.sciencedirect.com/science/article/pii/S0168169920311480 (Accessed: 15 August 2025)

[8] Scibioh, M. A., Viswanathan, B., *Characterization methods for supercapacitors, Materials for Supercapacitor Applications*, 2020, 315–372, doi: 10.1016/b978-0-12-819858-2.00005-6

Proc. Annual Symposium on Research & Industrial Training, 12 (2025) 123-129
Department of Electronics – Wayamba University of Sri Lanka

IOT-BASED WASTE MANAGEMENT SYSTEM

T.D. Wijesuriya*, G.A.K.S. Perera
Department of Electronics, Wayamba University of Sri Lanka, Kuliyapitiya, Sri Lanka
*tharudilwije@gmail.com

ABSTRACT

Urban solid waste management remains a prominent environmental and public health issue due to the ineffective collection, overflowing containers, and release of harmful gases. Traditional systems are time-scheduled-based, which wastes resources and results in delayed responses. To alleviate these limitations, this work proposes an IoT-based smart waste management system powered by renewable energy. The system integrates ultrasonic sensors to monitor bin fill levels, gas sensors to detect harmful emissions such as methane and ammonia, and proximity sensors for auto lid operation, thereby ensuring hygiene. The sensor data is processed by a microcontroller (ESP32) and transmitted via dual-channel communication, Global System for Mobile Communications (GSM), and Wi-Fi for enhanced real-time notification and cloud monitoring. For meeting the power requirements of the system sustainably, a solar-powered charging module incorporating a buck converter for charging a battery pack for enabling uninterrupted operation even without grid power. Such utilization of renewable energy reduces the consumption of conventional electricity and improves system scalability in different environments. Through the GPS integration, accurate location tracking is provided, which optimizes waste collection routes and reduces fuel consumption. Field tests demonstrate heightened efficiency of operations, reduced environmental impact, and improved safeguarding of public health by enabling timely disposal of garbage and gas monitoring. The system provides a strong, hygienic, and energy-saving solution in alignment with smart city initiatives, promoting sustainable city growth in general.

Keywords: **I**oT, **S**mart Waste Management, **R**enewable Energy

1.0INTRODUCTION

Sri Lanka's waste management is increasingly becoming a pressing problem since the country's major cities, such as Colombo, Kandy, and Galle, continue to generate huge volumes of rubbish due to the rapid growth of population and urbanization. Conventional approaches to waste management are predominantly response-type and mainly manual, leading to inefficiencies that pose serious threats to public health as well as the environment. Full litter bins in public areas not only make urban environments look unsightly but also facilitate unhealthy surroundings that support pests and the spread of diseases. Most of the time, litter remains uncollected for days, emits unpleasant odors. Also, the emission of harmful gases such as methane, carbon dioxide, and ammonia from decomposing organic waste poses a severe threat to the health of flora and fauna. Public garbage bins also lack access control automation, commonly being utilized improperly. People tend to throw garbage beside bins that have lids but are difficult to open, worsening litter. These loopholes indicate the need for an intelligent, automated garbage disposal system [1][2].

Several researchers have examined IoT-based strategies to enhance the effectiveness of waste management, providing valuable insights into the development of intelligent systems. To minimize unnecessary collection visits, Verma et al. (2023) proposed a straightforward model that utilizes ultrasonic sensors to monitor bin levels and transmit alarms via mobile apps. However, this model lacked gas detection and hygiene features [3]. This was expanded by Preetha et al. (2023) with the use of Zigbee technology with GPS-enabled route optimisation and gas sensors; nevertheless, its dependence on a single network decreased dependability [4]. For real-time monitoring, Pavithra et al. (2023) investigated the combination of GSM and cloud-based technology, which provides scalability but is still susceptible to power interruptions [5]. A cost-effective approach utilising weight and infrared sensors was previously shown by Navghane et al. (2016); however, it was limited by the lack of automated access control and hazardous gas monitoring [6]. LoRaWAN communication was used by more sophisticated systems, including Ramson et al. (2022), for gas detection and wide-area coverage; nevertheless, their response was restricted by slower transmission speeds [7]. These studies show that although IoT integration can improve garbage collection and monitoring, issues with communication reliability, integrating renewable energy sources, and automating tasks with a cleanliness focus still exist. To develop a robust, sustainable solution for Sri Lanka's urban settings, these deficiencies must be addressed.

This present work recommends an IoT smart bin waste management system with sensor technology and alternative energy sources to address the majority of those limitations. Ultrasonic and gas sensor technologies are utilized to track the fill levels within bins and detect hazardous emissions, respectively. Servo motors and proximity sensors enable touchless, hands-free lid control for enhanced hygiene. In contrast to other systems, dual channels of communication (Wi-Fi and GSM) are offered to provide real-time data transmission supported by a cloud platform for monitoring and analysis.

One of the key innovations in the system is its renewable power architecture. Instead of relying completely on grid electricity, the system is powered by a solar energy harvesting unit, where a buck converter controls the charging of a battery pack to provide stable and continuous power. This ensures seamless operation even during power outages, making the system more reliable for deployment in different environments. Moreover, the inclusion of GPS ensures accurate location tracking of the bins, allowing for optimized collection routes and reduced fuel and operational costs.

The suggested system provides a robust, energy-efficient, and sustainable urban waste management solution by integrating renewable energy sources with IoT technologies. In addition to reducing the hazards to the environment and public health, it also makes it easier for Sri Lanka to build smart cities by guaranteeing effective garbage collection that is made more sanitary and future-proof.

2.0EXPERIMENTAL

System and Setup

To develop the proposed IoT-based smart waste management system, a modular experimental setup was constructed, consisting of sensor modules, a microcontroller unit, communication interfaces, and a renewable power system.

Hardware Components

The following hardware modules were used in the system:

- Ultrasonic sensor – to measure waste fill level inside the bin.
- Gas sensor – to detect harmful gases such as methane (CH_4), carbon dioxide (CO_2), and ammonia (NH_3).
- Proximity sensor (IR sensor) – to detect human presence for automated lid operation.
- Servo motor – to open/close the bin lid automatically when a user is detected.
- Microcontroller (ESP32) – to process sensor data and control system operation.
- GSM module and Wi-Fi module (onboard ESP32) – to transmit data to the cloud and send alerts.
- GPS module – to provide geolocation data of the bin.
- Battery pack – to store energy and power the system.
- Solar panel – to harvest solar energy.
- Buck converter – to step down the voltage from the solar panel to a safe charging voltage for the battery pack.

Methodology Diagram

The flowchart shows the operation of the IoT-based smart waste management system. After initializing, the sensors monitor user presence, bin fill level, and gas emissions. When a person approaches, the proximity sensor opens the lid, which closes automatically once the user leaves, ensuring hygienic disposal. The ultrasonic sensor checks the bin's fill level, and when full, an alert with location details is sent to authorities. The gas sensor continuously monitors harmful gases such as CO_2, CH_4, and NH_3, and if detected, an urgent alert is issued with safety instructions. This process ensures real-time monitoring, hygienic operation, and efficient waste collection management while minimizing risks of overflow and harmful gas exposure.

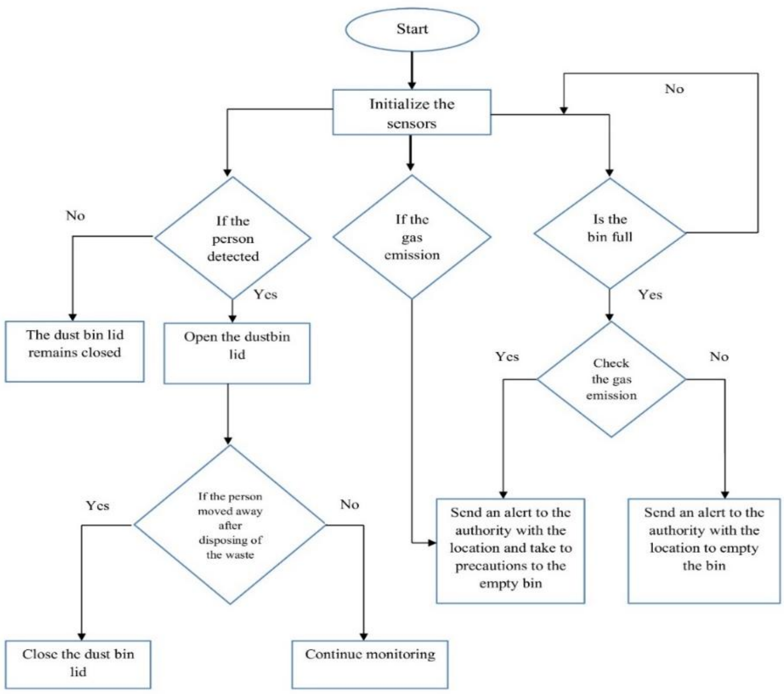

Figure 12: Methodology Diagram of the System

Block Diagram

To better illustrate the system and its validation, figures are included to present the design, experimental setup, and results.

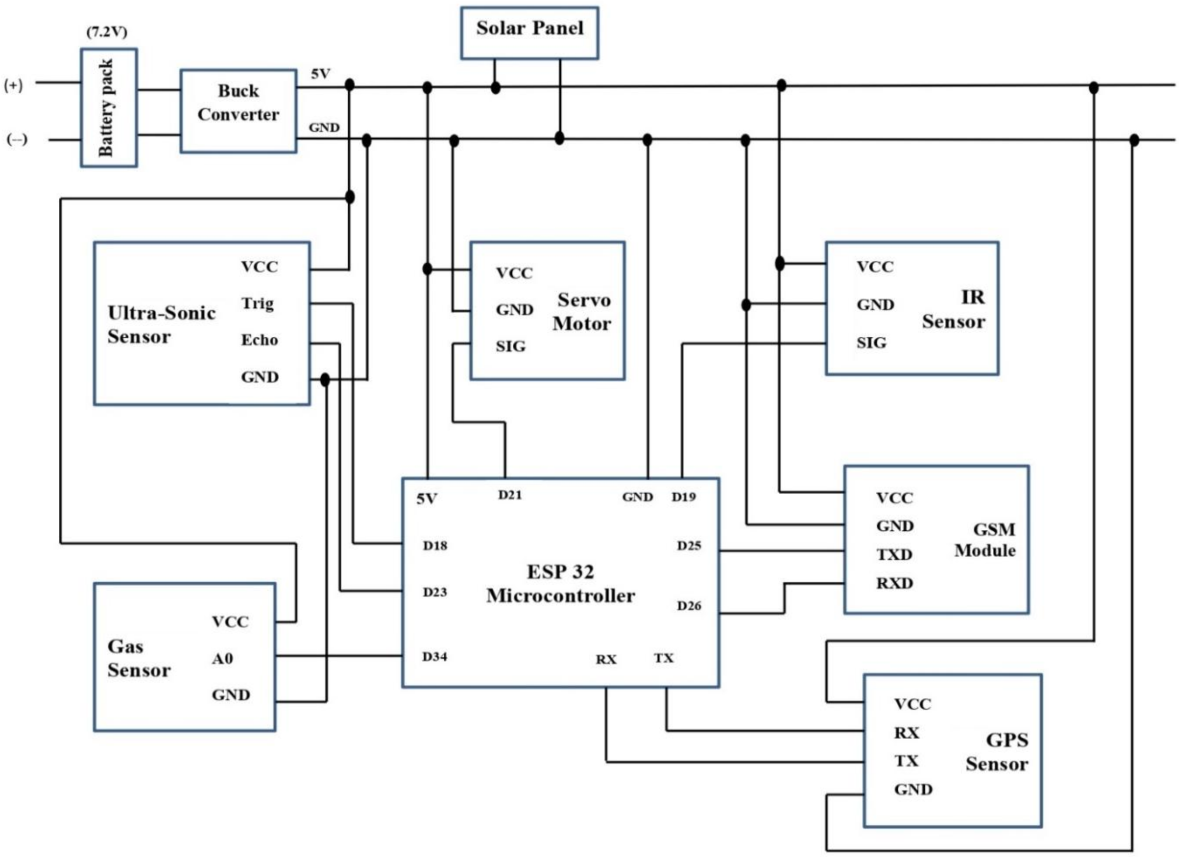

Figure 13: Block diagram of the system showing key modules and data flow

(a) (b)

Figure 14: (a) External view of the developed smart waste bin prototype. (b) Circuit overview showing the integration of key components

3.0RESULTS AND DISCUSSION

Sensor Performance

The ultrasonic sensor accurately measured the waste level. The alert was triggered correctly as the bin reached around an 80% level, thereby preventing overflow. The gas sensor detected harmful gases, such as methane and ammonia, and sent alerts when the levels exceeded the defined limit. Both sensors offered a steady performance when tested again and again, with slight variations depending on the surrounding environment. In addition, the automated mechanism for opening and closing the bin lid functioned smoothly when the fill level was below 80%, ensuring hands-free access and maintaining hygiene during regular use.

Discussion

Experimental evidence, consistent with recent reviews highlighting the potential of LoRaWAN and IoT-based monitoring, verifies that the proposed smart bin system is feasible in real-time waste bin condition monitoring and reporting, ensuring accuracy, reliability, and adaptability for practical urban applications [8].

- Reliability of Sensing and Alerts:

The accurate measurement by the ultrasonic and gas sensors shows that the system can prevent frequent issues such as bin overflow and harmful gas leakage. This directly goes towards reducing health hazards and providing better environmental security in urban areas.

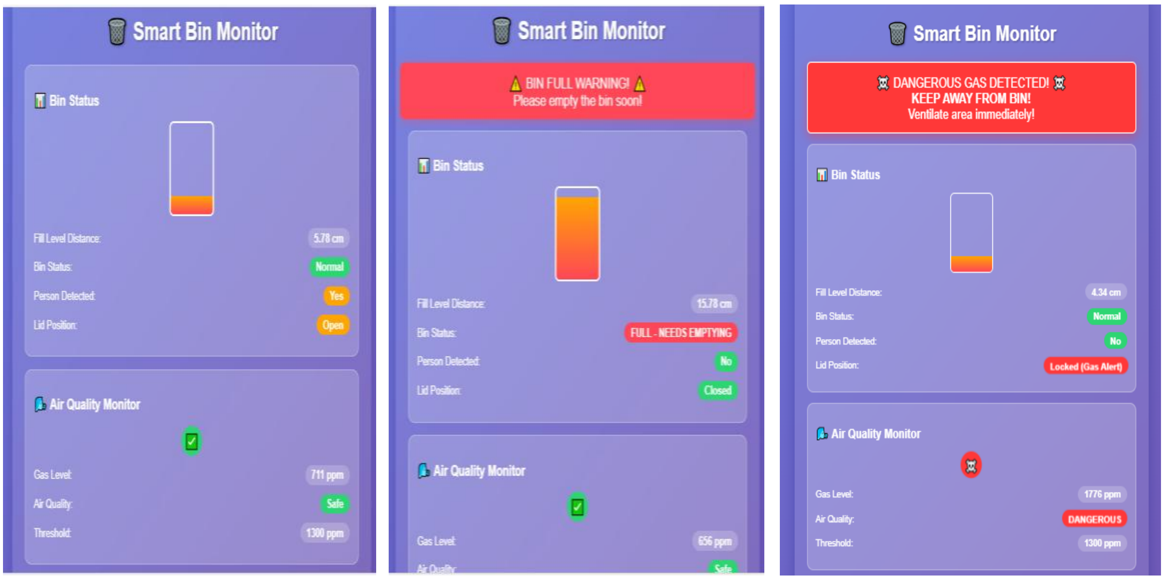

Figure 4: Web interface screenshot displaying real time waste level and gas detecting

Use of both GSM and Wi-Fi is provided for continuous alerts to be sent regardless of any transient network disruption. Use of two channels was more reliable than earlier single-network solutions reported in the literature.

- Renewable Power Performance:

Buck converter-driven solar panel and battery pack provided steady power, allowing the system to be functional without the aid of grid electricity. The system was checked to be functional for 7.2V with battery power, confirming its application in regions with an unreliable power supply.

- Hygiene and User Interaction:

The lid lifted itself to reduce direct contact with the bin, restricting germ transmission. This is critical in public places and in times of health crises such as pandemics.

Compared with recent studies, this system demonstrates improved reliability through dual communication and renewable energy integration, while ensuring hygiene-focused automation, making it more sustainable and adaptable for real-world smart city waste management applications [9] [10].

4.0CONCLUSION

This research developed an IoT-based intelligent waste management system designed to counteract the inefficiencies of conventional collection systems in Sri Lanka's urban setup. The system performed efficiently in gauging bin fill levels with high accuracy and detecting hazardous gases, issuing timely warnings to prevent overflow and reduce health hazards. Automatic lid opening promoted hygienic disposal without the need for hands, which was especially advantageous for public use. The sustainable solar energy system with backup storage made sure that everything operated smoothly even in the event of a power outage, and the dual communication channels improved the dependability of real-time data transfer. Stability, energy efficiency, and real-world practicability of the system were confirmed by experimental trials. According to smart city plans, the suggested approach improves public health, reduces operating costs, cleans up neighbourhoods, and is sustainable. It offers an effective foundation for developing sustainable waste management strategies and IoT-driven urban infrastructures in the future.

ACKNOWLEDGEMENTS

The authors express their sincere appreciation to the academic and technical staff of the Department of Electronics, Faculty of Applied Sciences, Wayamba University of Sri Lanka.

REFERENCES

[1] Harrison, K., White, S., Matthews, L. (eds.), "The Future of Urban Waste Management", *University of Chicago Press, 2013.*

[2] Brown, M., Green, P., Smith, C. (eds.), "Environmental Challenges and IoT Solutions", *Cambridge University Press, 2021.*

[3] Verma, J., Goel, P., Manhas, P., Thakral, S., Passi, A., "IoT-Enabled Smart Garbage Monitoring System", *Web of Conferences, 399, 04029, 2023.* doi: 10.1051/e3sconf/202339904029

[4] Preetha, M., Akshaya, M., Arthima, A., Pahade, A.K., Khamida, N., A Zigbee, "Garbage Bin Monitoring System with IoT", E3S Web of Conferences, 399, 04052, 2023. doi: 10.1051/e3sconf/202339904052

[5] Ilyas, S.S.M., Halim, M.A.R.M., Wahab, N.A., Ibrahim, N., "IoT-based Smart Garbage Monitoring", *Journal of Computing Research and Innovation, 6(2), 21–28, 2021.* doi: 10.24191/jcrinn.v6i2.187

[6] Vijaya Sri, D.K., Krishna, R.V., Surya, M.J.K., Venkatesh Babu, D., "Efficient Smart Garbage Management System Using IoT Technique", *International Journal of Engineering & Technology, 7(3.3), 568, 2018.* doi: 10.14419/ijet.v7i2.33.14836

[7] Ramson, S.R.J., Vishnu, S., Kirubaraj, A., Anagnostopoulos, T., Abu-Mahfouz, A., "A LoRaWAN IoT-Enabled Trash Bin Level Monitoring System", *IEEE Transactions on Industrial Informatics, 18(2), 786–795, 2022.* doi: 10.1109/tii.2021.3078556

[8] Krishnan, K.B., Baiju, M.S., Mohan, R., Taqa, A.R., "Review on LoRaWAN IoT-Enabled Trash Bin Level Monitoring System Using ESP32", *International Journal (online), 12(6), 2319–7463, 2023. Accessed: Oct. 25, 2024.* Available: https://www.researchgate.net/publication/372496264_Review_on_Lorawan_Iot_Enabled_Trash_Bin_Level_Monitoring_System_Using_Esp32

[9] Thirumugam, P., Herath, D., Amarasooriya, S., "Smart Dustbin and Garbage Monitoring System Using Internet of Things", *IEEE Conference Publication, 2023*. doi: 10.1109/icac60630.2023.10417205

[10] Bakhouch, S.M., Ayad, S., Terrissa, L.S., "Smart Waste Management System Based on IoT", *Lecture Notes in Networks and Systems*, *322–331, 2024*. doi: 10.1007/978-3-031-53824-7_29

AIR CONDITIONER AUTOMATION BY GPS DATA OF USER

M.B.Y. Silva*, P.G.T.R. Payagala
Department of Electronics, Wayamba University of Sri Lanka, Kuliyapitiya, Sri Lanka.
*byovinma@gmail.com

ABSTRACT

Current air conditioners require manual operation, causing delays in cooling and frequent energy wastage when users forget to turn the unit off. This study presents the design and implementation of an automated air conditioning system that operates based on the geographical location of the user. The system integrates an ESP32 microcontroller, a global positioning system (GPS) enabled smartphone application, a firebase real-time database, and an infrared transmitter to control a conventional air conditioner. The smartphone application continuously uploads the user's latitude and longitude to firebase, and the ESP32 retrieves this data in real time. ESP32 monitors if the user enters or exits a pre-defined geofence area and trigger infrared commands to control air conditioner. Prototype tests conducted under real world conditions demonstrated reliable geofence detection. The results confirm that GPS based automation can ensure users comfort by pre-cooling the target location, offering a practical and scalable solution for broader smart-home integration and multi-user environments.

Keywords: Geofencing, **A**ir conditioner, **L**ocation tracking

1.0 INTRODUCTION

Energy consumption in residential and commercial buildings has become a major concern in recent years, particularly due to the growing use of air conditioners. Studies show that air conditioning systems contribute a significant proportion of electricity usage in households and workplaces, leading to increased utility costs and higher demand on the power grids [1]. Conventional air conditioners are typically operated manually by users, which often results in inefficient usage, such as leaving the unit running even when no one is at the location, or delays in achieving comfort because the unit is only switched on after the user arrives.

To address these inefficiencies, researchers have explored different automation techniques. Approaches such as programmable timers, smart remotes, and IoT-based controllers have been proposed to optimize air conditioner operation. M.A. Afandi et al. developed an IoT-based air conditioner (AC) controller and monitoring system, demonstrating the potential of cloud-integrated solutions for energy efficient heating, ventilation and air conditioning (HVAC) operation [1]. Similarly, Hercog et al. highlighted the flexibility of ESP32-based IoT devices for smart applications, providing a foundation for microcontroller- driven automation [2]. Other researchers have explored predictive control methods. Javed et al. implemented a smart AC system capable of room temperature prediction, improving user comfort but requiring additional sensing elements [3]. Haq et al. discussed mathematical and computational models for energy control in hybrid systems, emphasizing optimization but with limited real-time adaptability [4]. Gupta examined the role of IoT in smart HVAC systems, showing how environmental data can enhance performance [5], while practical implementations such as the ESP32 weather-data-based controller reported by DFRobot [6] demonstrated the feasibility of low-cost automation solutions.However, these methods often require manual scheduling or direct interaction from the user, which may not adapt well to unpredictable schedules. Recent advances in GPS-enabled smartphones and cloud-based platforms open new opportunities for location-aware automation, where a device can respond to a user's movement without manual intervention.

By integrating GPS geofencing with microcontroller-based control systems, it becomes possible to design an intelligent solution that automatically switches on or off the air conditioner depending on the user's proximity to the target location. This approach can significantly reduce unnecessary energy consumption while maintaining user comfort, as the room is already cooled when the occupant arrives.

2.0 EXPERIMENTAL

1.1 Methodology

The methodology for this project was designed to develop and test a prototype system capable of automating the operation of an AC, based on the GPS location of the user. The process involved system design, hardware implementation, software development, and system testing.

1.2 System Design

The system is designed to automate air conditioner based on the user's location. User's smartphone application provides real time GPS data to the firebase and firebase is connected with ESP32. When the user is inside predefined geofence area, ESP32 detects and send the signal to the air conditioner and also send a notification to the user whether the air conditioner is turned ON. As well as if the user is outside the area the air conditioner turned OFF. Overall system includes ESP32 with IR transmitter, firebase, smart phone application for GPS tracking and data transfer.

As illustrates by figure 1 geofence radius was defined around the target location, where the users air conditioner is located. In this location an ESP32 microcontroller is placed with an IR transmitter to trigger AC ON/OFF commands. AC ON/OFF commands are triggered by ESP32 based on the user's location. The ESP32 receives real time user location data via the firebase clouds platform. The user's smartphone continuously acquires GPS coordinates and uploads them to firebase. When the system detects that the user has entered the predefined geofence radius, the ESP32 automatically triggers the IR transmitter to send the AC ON command. Conversely, if the user exits the geofenced area, the ESP32 sends an AC OFF command. Additionally, the system is integrated with temperature sensor to monitor the temperature of the fixed location. Figure 1 illustrates the process flow of the proposed system.

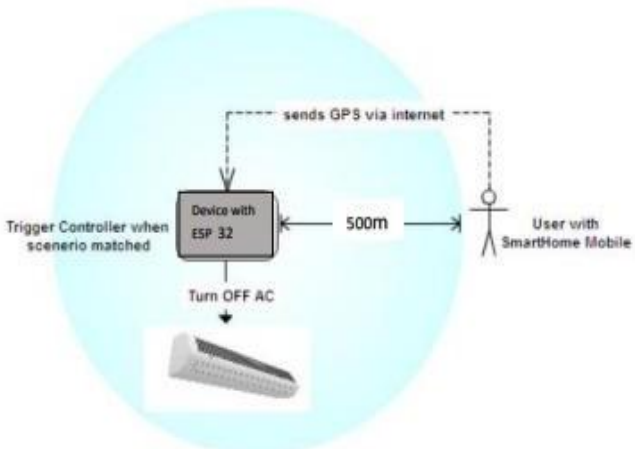

Figure 1: Process flow of the system with defined area

1.3 Hardware implementation

Used different air conditioner remotes to decode their IR signals. The IR decoding was performed using a 1838 IR receiver interfaced with an ESP32 microcontroller as in figure 2(a). When a remote button is pressed, the receiver captures the infrared signal and the ESP32 decodes it into the corresponding digital code. The resulting pulse signal was visualized on an oscilloscope as in figure 2(b).

Many air conditioner remotes use custom protocols, which can vary even among units of the same model. Therefore, instead of identifying the exact protocol, the raw IR signal data was decoded for further use.

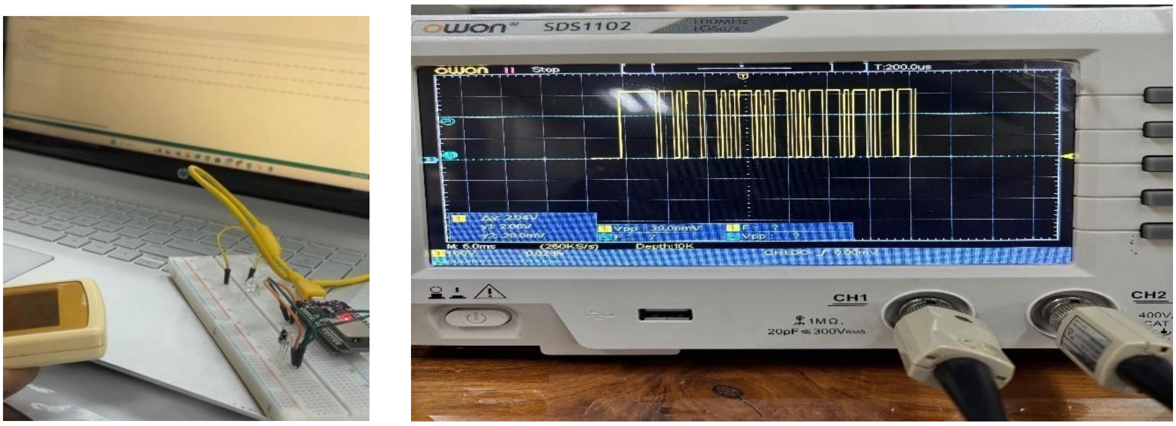

(a) (b)

Figure 2: (a)Decoding IR signal from an AC remote (b) Decoded IR signal

Decoded signals were stored and programmed in the ESP32 to retransmit by using IR led to replicate air conditioner remote. The ESP32 was placed near the air conditioner unit so that the IR led could directly transmit control signals. Figure 3 shows the IR transmission setup used to replicate the AC remote.

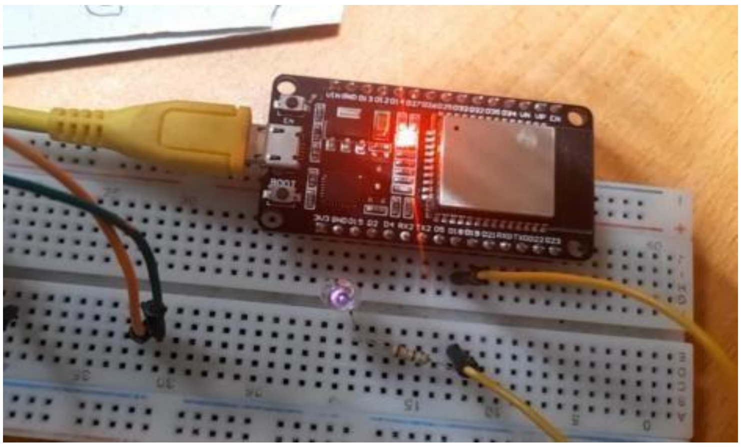

Figure 3: Transmitting IR signal

2.4 Software development

A GPS enabled application was developed using Flutter to continuously monitors the user's location and upload latitude and longitude data to firebase at 20s of regular intervals. Firebase served as the intermediary database, enabling real-time communication between the mobile application and the ESP32. The ESP32 was programmed using Arduino IDE with Wi- Fi and firebase libraries. The microcontroller continuously reads the GPS data from firebase, calculate the user's distance from the fixed location, and trigger the appropriate IR signal (ON or OFF) based on the user's location proximity.

Additionally, the application allows the user to view the AC status whether the AC is ON or OFF and the ambient temperature at the fixed location via the app. A DHT22 temperature sensor was interfaced with ESP32 and it provides continuous room temperature measurements. These temperature readings, together with the AC status and user location data, were uploaded to firebase and displayed on the application interface as in figure 4.

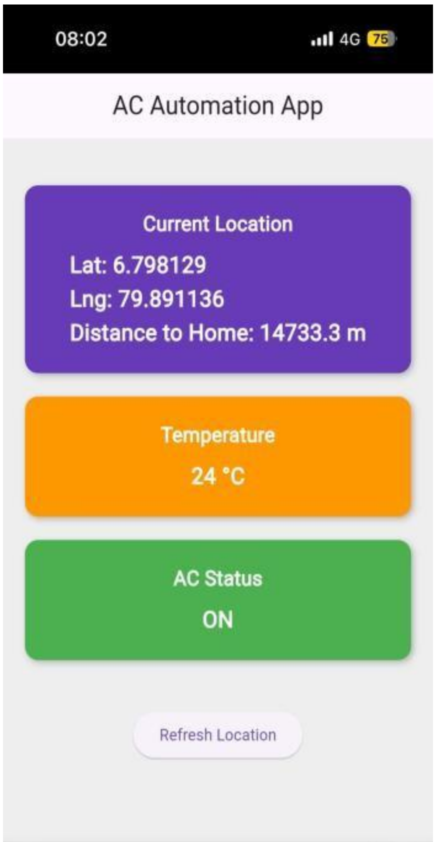

Figure 4: Snapshot of user interface of developed mobile app

2.5 System testing

The system was tested in a real-world environment by setting a geofence radius of 100 meters around a fixed location. Multiple test runs were performed to verify response time, accuracy of GPS data updates, and reliability of AC switching. The performance was evaluated by observing whether the AC turned ON before the user arrived and turned OFF when the user left the geofence area.

3.0 RESULTS AND DISCUSSION

1.4 Testing IR communication

The prototype system was successfully implemented and tested in a real-world environment. The ESP32 microcontroller with an IR LED was able to reliably transmit the ON and OFF commands to the air conditioner. The decoded IR codes matched the remote-control signals, confirming accurate replication.

1.5 Sending data to firebase

The mobile application developed using Flutter continuously monitored the user's GPS location and transmitted the latitude and longitude data to the Firebase real-time database. The ESP32 fetched this data at intervals of approximately twenty seconds, ensuring minimal delay in response. Temperature updates were uploaded whenever a change in the measured value was detected. The structure of the firebase database, including the stored AC status, temperature, humidity and location parameters, is shown in figure 5.

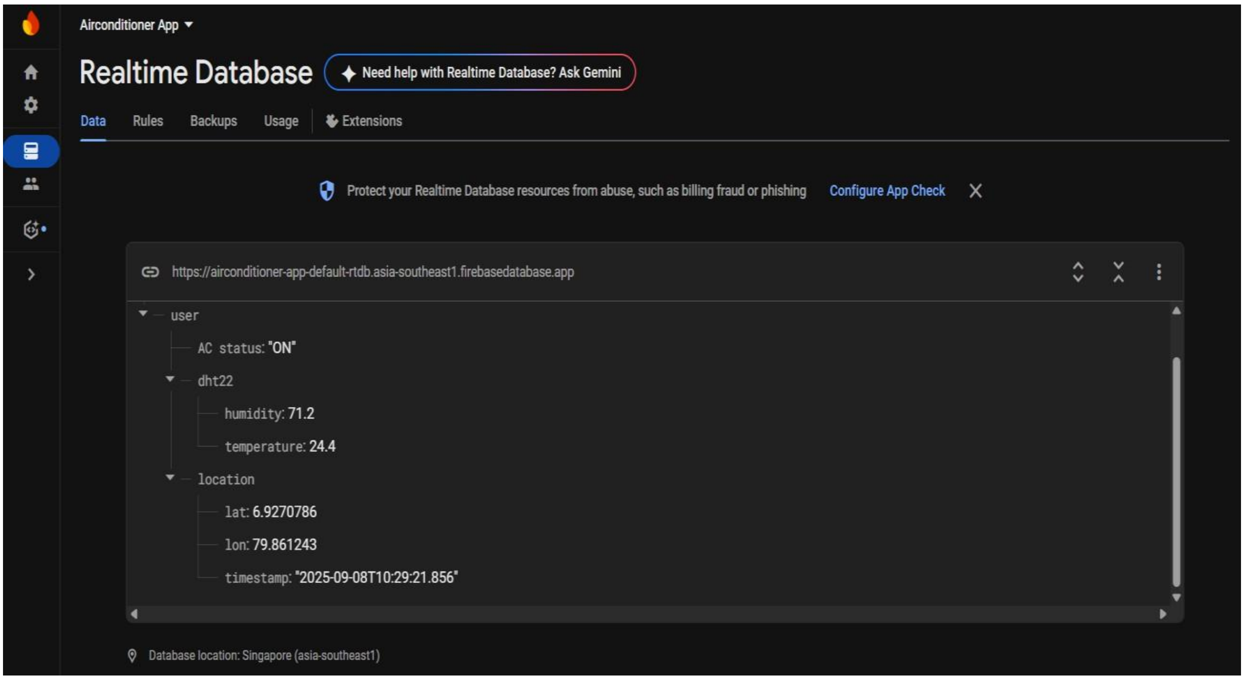

Figure 5: Snapshot of real-time database of Firebase

1.6 GPS accuracy

A geofence radius of 100 meters was configured for testing. During testing, the GPS-enabled application provided an average location accuracy of approximately ±5–10 meters, which was sufficient to reliably detect entry and exit within the predefined geofence radius of 100 meters. It was observed during testing that different distance values were sometimes reported for the same fixed location. This variation is attributed to the inherent inaccuracy of GPS signals, which can fluctuate due to factors such as atmospheric conditions, satellite geometry, and multipath effects caused by reflections from nearby buildings or obstacles. Although the actual location did not change, the GPS module occasionally reported slightly shifted coordinates, leading to differences in calculated distances. The average deviation was within ±5–10 meters, which is acceptable for the geofence radius of 100 m used in this study. By selecting a sufficiently large geofence radius, the impact of GPS fluctuations on system performance was minimized, ensuring reliable ON/OFF control of the air conditioner. Figure 6 illustrates output of serial monitor obtained during testing with a reduced radius of 3 m geofence area. It shows the latitude and longitude data of user retrieved from firebase and calculated distance of user from the geofence center, and the microcontroller's decision logic. Based on the predefined geofence radius, the ESP32 triggered the IR LED to communicate with the AC when the user was detected inside the area.

```
Longitude from Firebase: 79.93656341917813
Current Latitude: 7.17
Current Longitude: 79.94
Distance to geofence center: 8.01 meters
Outside geofence: LED OFF
------
Latitude from Firebase: 7.1722355810925364
Longitude from Firebase: 79.93654992431402
Current Latitude: 7.17
Current Longitude: 79.94
Distance to geofence center: 3.60 meters
Outside geofence: LED OFF
------
Latitude from Firebase: 7.1722355810925364
Longitude from Firebase: 79.93654992431402
Current Latitude: 7.17
Current Longitude: 79.94
Distance to geofence center: 3.60 meters
Outside geofence: LED OFF
------
Latitude from Firebase: 7.172272838652134
Longitude from Firebase: 79.93657582439482
Current Latitude: 7.17
Current Longitude: 79.94
Distance to geofence center: 1.94 meters
Inside geofence: LED ON
------
Latitude from Firebase: 7.172272838652134
Longitude from Firebase: 79.93657582439482
Current Latitude: 7.17
Current Longitude: 79.94
Distance to geofence center: 1.94 meters
Inside geofence: LED ON
------
```

Figure 6: Serial monitor output of Arduino IDE

The results confirm that GPS-based automation is a viable approach for improving both energy efficiency and user comfort in air conditioning systems. By enabling the AC to operate automatically based on user location, unnecessary power consumption was reduced, particularly in cases where the AC would otherwise remain ON without occupancy. At the same time, pre-cooling ensured comfort upon arrival, eliminating the usual waiting time.

4.0 CONCLUSION

The project successfully demonstrates an automated air conditioning system based on GPS location data of the user. The integration of ESP32, Firebase, and IR transmission allowed seamless switching without user intervention. This system contributes to energy efficiency, enhances user comfort, and serves as a practical example of IoT-based smart home automation. Future developments can focus on scalability, machine learning–based prediction of user arrival, multi-user support for households with more than one member and broader appliance integration.

ACKNOWLEDGEMENTS

The author acknowledges the guidance and support provided by the Department of Electronics, Wayamba University of Sri Lanka.

REFERENCES

[1] Afandi, M. A., Nurandi, S., and Enriko, I. K. A., IJEIS (Indonesian Journal of Electronics and Instrumentation Systems), 2021, 11, 83–92, Automated Air Conditioner Controller and Monitoring Based on Internet of Things, doi: 10.22146/ijeis.64563.

[2] Hercog, D., Lerher, T., Truntič, M., & Težak, O. (2023). Design and Implementation of ESP32-Based IoT Devices. Sensors, 23(15), 6739. 10.3390/s23156739

[3] Javed, F. M., Allayear, S. M., Alam, M. F., Jabiullah, M. I., and Ahmed, R., International Journal of Computer Applications, 2018, 18, 23–32, Implementation of a Smart AC Automation System with Room Temperature Prediction, Available: https://www.researchgate.net/publication/334541732_Implementation_of_a_Smart_AC_Automation_System_with_Room_Temperature_Prediction (Accessed: 15 November 2024).

[4] Ul Haq, Y., Tahir, A., Sana, R., Moin U Din, S., and Zahra, R., Transactions in Mathematical and Computational Sciences, 2021, 1, 38–49, Transactions in Mathematical and Computational Sciences, Available: https://tmcs.su.edu.pk/uploads/journals/TMCS-2021-02-04P41.pdf.

[5] Gupta, M., Zenatix by Schneider Electric, 2022, How IoT is Making HVAC Smart and Energy-efficient?, Available at: https://www.zenatix.com/how-iot-is-making-hvac-smart-and-energy-efficient/ (Accessed: 18 November 2024).

[6] DFRobot, no date, Controlling Air Conditioner Temperature Automatically with ESP32 after Reading Real-time Weather Data, Available at: https://community.dfrobot.com/makelog-308344.html (Accessed: 18 November 2024).

Proc. Annual Symposium on Research & Industrial Training, 12 (2025) 137-144
Department of Electronics – Wayamba University of Sri Lanka

REWARD-BASED SMART RECYCLE BIN WITH WASTE SORTING SYSTEM

S.P.G.N.M Gunathilaka*, S.R.L. Gunawardhana
Department of Electronics, Wayamba University of Sri Lanka, Kuliyapitiya, Sri Lanka
*nipungunathilaka23@gmail.com

ABSTRACT

The reason for developing this system is that existing recycling bins in Sri Lanka are mostly manual and inefficient, causing low user participation. By integrating automation with financial incentives, the system directly addresses the dual challenge of waste sorting accuracy and lack of public motivation.. This project addresses the challenge of low recycling rates by designing and implementing a smart bin that automates waste sorting and incentivizes users. The system combines a hardware unit for sorting and a software platform for user management. Users authenticate via an AI facial recognition interface. Deposited items are classified by a sensor fusion approach: an MLX90614 infrared sensor distinguishes plastic from glass via differential thermal emissivity, and an inductive proximity sensor identifies aluminum cans. Sorted materials are compartmentalized. Each transaction is logged in real-time to a web application. A Firebase database manages user profiles, while an InfluxDB database handles time-series transaction data. Users earn monetary rewards for each deposit, which are redeemable upon reaching a threshold. The prototype demonstrates a technically feasible and user-engaging solution to increase recycling participation, reduce stream contamination, and promote a circular economy through direct economic incentives.

Keywords: Smart Waste Management, **Y**OLO Model, **I**oT Database

1.0 INTRODUCTION

The exponential rise in consumer goods and instant beverage packaging has intensified the global waste crisis. According to the United Nations Environment Programme (UNEP, 2022)**,** nearly 300 million tons of plastic waste are produced annually, with only 9% effectively recycled. Aluminum and glass waste contribute additional challenges, with improper disposal leading to soil contamination, greenhouse gas emissions from landfills, and irreversible ecological harm. Sri Lanka faces a particularly urgent problem due to limited waste management infrastructure and growing urban populations [1].In many local communities, beverage containers such as plastic bottles and aluminum cans are discarded without proper segregation, causing drainage blockages, marine pollution, and increased landfill stress. Traditional waste collection systems largely rely on manual sorting, which is labor-intensive, inefficient, and prone to errors. The concept of smart waste management has gained attention in recent years, where IoT-enabled technologies monitor, sort, and track waste disposal [2]. However, one of the most persistent challenges is low user participation**.** People are often unwilling to engage in recycling practices unless motivated by tangible benefits. Thus, combining intelligent automation with a reward-based model can create a sustainable approach that not only manages waste efficiently but also incentivizes public involvement [3].

This research proposes the development of a Reward-Based Smart Recycle Bin that leverages sensor technologies, AI-assisted recognition, and IoT-based databases to automatically classify recyclable waste while simultaneously rewarding users for their participation [4]. Unlike conventional recycling bins, this system provides a structured method for waste recognition, automated sorting, and digital record-keeping of user contributions.

2.0 EXPERIMENTAL

2.1 System Overview

The proposed reward-based smart recycle bin is designed as an integration of both hardware and software components that work together to achieve intelligent waste sorting and real-time transaction management (as shown in Figure 2.1). The equipment are responsible for material recognition, automated sorting, and secure data transmission. Once a waste item is deposited, the hardware identifies the material using sensor technologies and places it in the corresponding compartment of the bin. The second major component is the web application, which provides the interface for user interaction. Through this platform, individuals can register, monitor their recycling activity, and manage reward balances. Data generated by the equipment are transmitted to the cloud in real time, ensuring that every transaction is recorded against the correct user account. This dual structure ensures not only the accurate classification of recyclable waste but also the establishment of a transparent incentive system that motivates people to dispose of their waste responsibly.

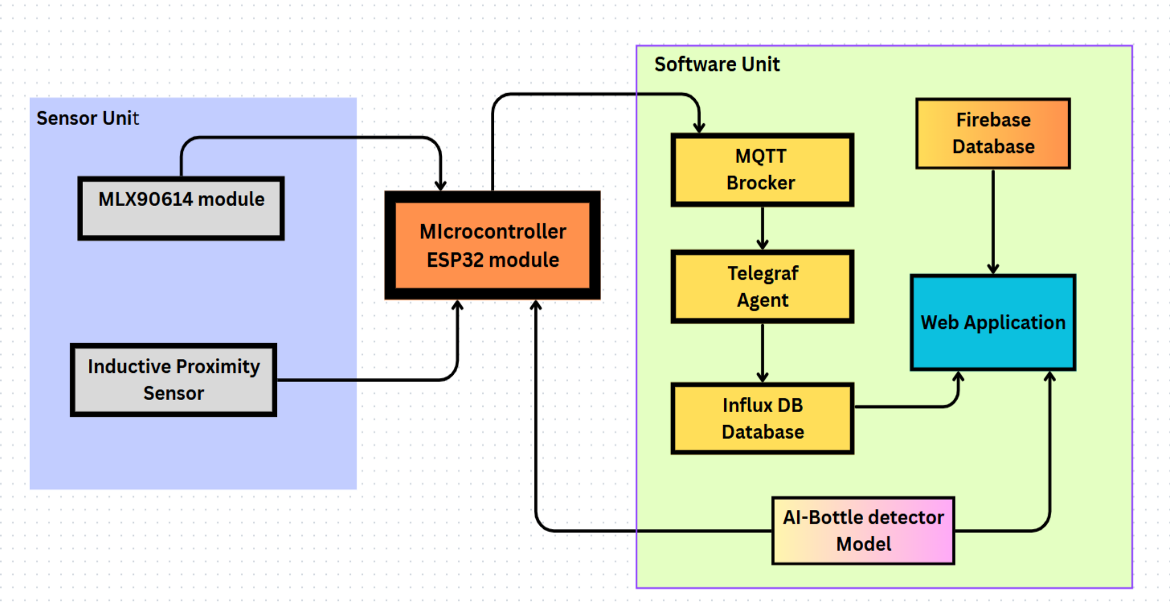

Figure 2.1: The proposed system block diagram

2.2 Hardware Design

The hardware of the smart recycle bin was developed around the ESP32 microcontroller, selected due to its powerful dual-core processor, integrated Wi-Fi and Bluetooth capabilities, and low power consumption. The ESP32 acts as the central processing hub, collecting signals from sensors, executing classification logic, and controlling the Object sorting mechanism. To distinguish between plastic and glass bottles, the system employs the MLX90614 infrared thermometer sensor. This sensor measures the surface temperature response of the deposited item. Since glass and plastic differ in thermal emissivity, the sensor readings provide a reliable method to differentiate between the two. For detecting aluminum cans, an inductive proximity sensor is used. This sensor generates an electromagnetic field, and the disruption of this field when a metallic object is present allows the system to accurately identify aluminum Cans.

Once the material is classified, the ESP32 activates a sorting system, which consists of Stepper motors and a conveyor mechanism. These motors direct the identified waste to the appropriate storage bin, ensuring that each type of material plastic, glass, or aluminum is separated with minimal human intervention. To improve reliability and reduce wiring complexity, a custom PCB was designed. The PCB integrates the ESP32 with the required power supply regulation, sensor input circuitry, and motor driver outputs, making the hardware compact, scalable, and easier to maintain.

(a) (b)

Figure 2.2: (a) MLX90614 infrared thermometer sensor, (b) Inductive proximity sensor

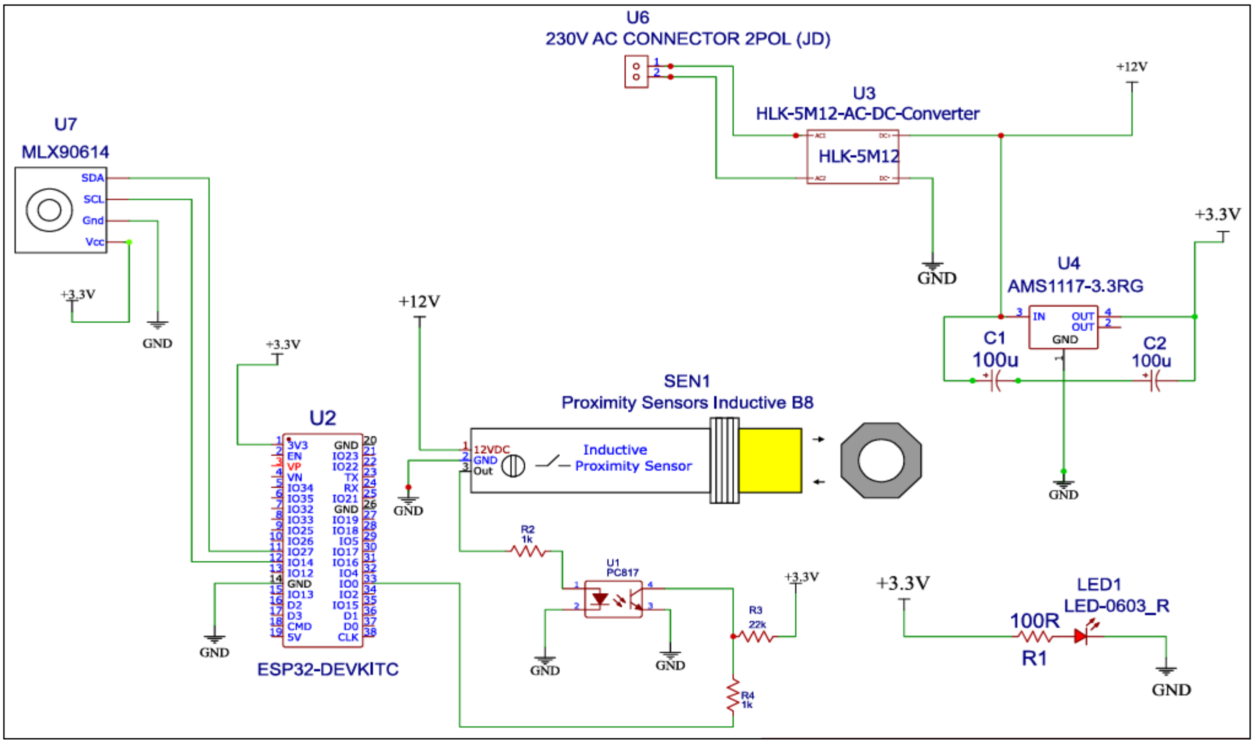

Figure 2.2: (c). Schematic diagram of the designed system

Figure 2.2 :(d) Prototype circuit Testing

2.3 AI-Based Bottle Detection

In this approach, a camera module connected to the ESP32 or an auxiliary processor first captures an image of the deposited object (as shown in Figure 2.3). The image is processed by a convolutional neural network or an object detection model to verify whether the object is a bottle. Once confirmed, the system proceeds with sensor-based classification to determine the specific type of bottle: the MLX90614 infrared sensor distinguishes between plastic and glass, while the inductive proximity sensor identifies aluminum cans. This two-stage detection process AI-based bottle verification followed by sensor-based material classification enhances accuracy, reduces false detections, and provides a scalable framework for future expansion to other waste categories.

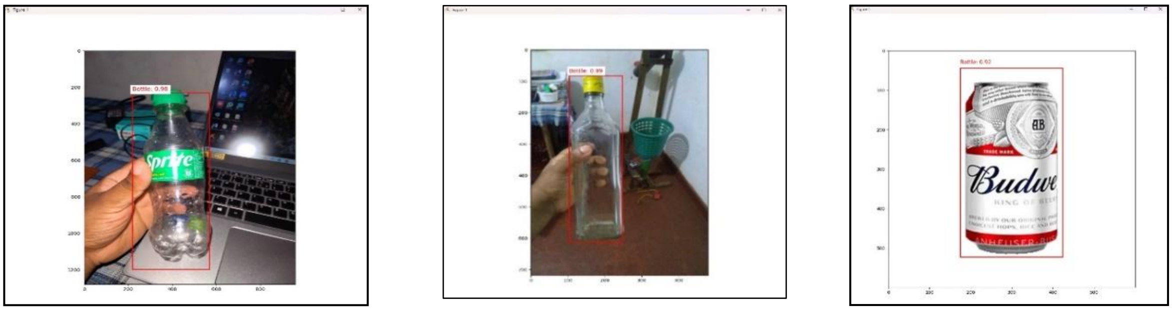

(a) (b (c)

Figure 2.3 **:**(a) Recognized the given plastic bottle. (b) Recognized the given glass bottle. (c) Recognized the given metal cans.

2.4 Software Integration

The software was developed to manage users and process data in real time. Firebase handles authentication, registration, and account details, linking each user's recycling activity to a personal reward account to ensure accurate allocation. InfluxDB, a time-series database, records each deposit with user ID, material type, timestamp, and reward points, providing transparency and traceability. The web application, designed for both desktop and mobile, allows users to view history, track rewards, and request withdrawals once the threshold is reached. This integration enables seamless communication between hardware sensors, databases, and the user interface.

2.5 Workflow

The smart recycle bin workflow begins with user registration on the web app, where data is stored in Firebase with a unique ID. When waste is deposited, a camera captures the object and an AI model verifies if it is a bottle. If confirmed, the ESP32 uses sensors for classification: the infrared sensor separates plastic from glass, while the inductive sensor detects aluminum cans. Combining AI and sensors improves accuracy and reduces errors.The system records the transaction, updates the user's reward balance in Firebase, and displays it instantly on the web dashboard. Once the balance exceeds the withdrawal limit, users can request a transfer to their bank account.

3.0 RESULTS AND DISCUSSION

3.1 Sorting Accuracy

The accuracy of sorting was calculated using the standard formula:

$$\text{Accuracy (\%)} = \frac{\text{Number of Correct Classifications}}{\text{Total number of sample}} \times 100 \qquad [3.1]$$

Table 0.1: Table of classification accuracy of different recyclable materials

Material	Samples Tested	Correctly Classified	Accuracy (%)
Plastic	20	19	95%
Glass	20	18	93%
Aluminum Cans	20	20	100%
Overall	60	57	96%

The performance of the smart recycle bin (as shown in Table 0.2) Was evaluated by conducting a series of experiments with 20 samples of each waste category: plastic bottles, aluminum cans, and glass bottles. The MLX90614 infrared sensor was specifically tested for its ability to differentiate between plastic and glass materials based on their surface temperature properties. The results indicated a classification accuracy of approximately 95%, with most errors occurring under conditions where the ambient temperature closely matched the thermal response of the plastic. This highlights the importance of sensor calibration under varying environmental conditions. The inductive proximity sensor used for detecting aluminum cans exhibited highly reliable performance, achieving an accuracy of 100% across all test samples. The metallic composition of aluminum cans allowed for consistent detection, with negligible false positives. The system achieved 96% overall sorting accuracy, confirming its feasibility for real-world use.

3.2 AI-Based Bottle Detection Performance

The current prototype mainly uses sensor-based classification, but studies and preliminary tests suggest that adding an AI vision module can improve accuracy and scalability. In this design, a camera captures the deposited object, and an object detection model such as YOLO confirms if it is a bottle before sensor-based classification. This two-stage process reduces false insertions when non-bottle items are deposited. Research on YOLO-based waste classification shows strong performance across plastic, glass, and aluminum under different lighting, highlighting its effectiveness. As a verification layer, the AI module reduces sensor-related errors and supports future expansion to waste types like paper, multilayer plastics, and cartons. Thus, although not yet implemented, AI detection offers a promising extension to increase both accuracy and adaptability of the smart recycle bin.

3.3 Real-Time Database Performance

The system's database performance was evaluated to determine the effectiveness of real-time logging and synchronization. InfluxDB, used as the time-series database, recorded all recycling transactions with an average latency of 5 seconds. This ensured that users could view their updated balances almost immediately after depositing an item. The low latency also allows the system to scale efficiently if deployed in larger communities with multiple recycling units. In addition, Firebase authentication proved effective in securing user sessions. Tests involving repeated login and logout cycles confirmed that no data was lost or misattributed, and each user's recycling record was preserved accurately. The combination of Firebase and InfluxDB provided a robust and scalable backend for managing both user accounts and transaction data in real time.

3.4 Reward Model

A major contribution of this project is the reward-based incentive model that motivates users to recycle. The system assigned monetary values to each item: LKR 10 for plastic bottles, LKR 15 for aluminum cans, and LKR 20 for glass bottles. A minimum withdrawal threshold of LKR 100 was set to prevent frequent micro-transactions and encourage consistent participation. A user simulation showed that engagement was much higher than with a non-reward model, confirming that financial incentives can effectively drive recycling behavior, particularly in communities where waste segregation is often neglected.

3.5 Comparative Analysis

When compared with conventional recycling bins, the proposed system demonstrates several advantages. Traditional bins rely heavily on manual sorting, which is both time-consuming and error-prone, whereas this smart recycle bin employs automated, sensor-driven segregation that minimizes human intervention. Another distinguishing feature is user-specific reward tracking, which ensures accountability and fairness in the incentive distribution process. Moreover, the inclusion of real-time transaction logging makes the system more transparent and trustworthy. The IoT-based architecture also provides a scalable framework that can be replicated across multiple bins in different locations. This opens the possibility of building a community-wide or even city-wide smart recycling network, where every transaction is digitally recorded and traceable. Despite these strengths, some challenges were identified. The MLX90614 sensor requires careful calibration in environments with fluctuating ambient temperatures, which may affect classification accuracy.

The motorized sorting mechanism also faced limitations when handling larger or irregularly shaped bottles, indicating the need for stronger motors or alternative mechanical designs. Additionally, since the system involves financial transactions, ensuring robust cyber security measures will be critical in future large-scale deployments.

4.0 CONCLUSION

This research successfully demonstrates the design and implementation of a Reward-Based Smart Recycle Bin that integrates sensor-driven material recognition, IoT-based data management, and financial incentives. With an overall sorting accuracy of 96%, the system effectively classifies plastic, aluminum, and glass waste while simultaneously updating user accounts with reward balances in real time. By linking environmental responsibility with financial motivation, the project introduces a practical method to increase public participation in recycling. The integration of Firebase for authentication and InfluxDB for real-time logging ensures a reliable digital infrastructure, while the web application provides an intuitive user interface for monitoring transactions and managing rewards. The findings of this research suggest that combining automation, IoT, and incentives can significantly improve recycling efficiency and encourage sustainable behavior ultimately, the proposed system represents a step toward circular economy practices by reducing landfill dependency, minimizing pollution, and promoting resource recovery. Its adaptability and scalability make it suitable for universities, shopping malls, and urban communities, contributing meaningfully to both environmental preservation and sustainable development.

ACKNOWLEDGEMENTS

The authors would like to express their gratitude to the Academic Staff of the Faculty of Applied Sciences, Wayamba University of Sri Lanka for their expert advice and guidance.

REFERENCES

[1] Salleh, A., Mohamad, N.R., Mohd, N., Mohd, N., *ResearchGate*, 2024, 13, 189–200, [Online].Available: https://www.researchgate.net/publication/379821968_SensorBased_Sorting_of_Municipal_Solid_Waste_using_ArduinoMicrocontroller (Accessed: 20 July 2025)

[2] Kadus, T., Nirmal, P., Kulkarni, K., *International Journal of Engineering Research and Technology*, 2020, 9, 490, [Online]. Available: 10.17577/ijertv9is040490 (Accessed: 2 August 2025)

[3] Addas, A., Khan, M.N., Naseer, F., *PLoS ONE*, 2024, 19, e0307608, [Online]. Available: https://doi.org/10.1371/journal.pone.0307608 (Accessed: 15 August 2025)

[4] "Inductive vs. capacitive sensors: differences and how it works," *Sensor Partners*, [Online]. Available: https://sensorpartners.com/en/knowledge-base/the-difference-between-inductive-and-capacitive-sensors (Accessed: 20 August 2025)

[5] Mavropoulos, A., Tsakona, M., Anthouli, A., *ResearchGate*, 2013, [Online]. Available: https://www.researchgate.net/publication/276181634_Mobile_Applications_Waste_Management_Recycling_Personal_Behavor_Logistics. (Accessed: 25 August 2025)

UNIVERSAL EFI SYSTEM FOR ALL FOUR-CYLINDER CARBURETOR MOTORCYCLES (WITHOUT MAPPING)

P.M. Hettiarachchi*, K.P. Vidanapathirana
Department of Electronics, Wayamba University of Sri Lanka, Kuliyapitiya, Sri Lanka
*malinthaka.2000@gmail.com

ABSTRACT

Four-cylinder carburetor motorcycles are still widely used in Sri Lanka and many other countries, even though Electronic Fuel Injection (EFI) systems are recognized as superior in terms of efficiency, performance, and emissions. Retrofitting EFI into older motorcycles usually requires complex and expensive engine mapping, which prevents widespread adoption. This study proposes a universal EFI system that eliminates mapping by using ignition pulses or camshaft signals for injector timing, together with throttle position sensing for fuel control. A modified carburetor was used as a throttle body, and injector adaptors were designed to mount injectors. The prototype system was implemented step by step: modification of the carburetor body, testing injectors under parallel 12V supply, adjustment of airflow using slides and diaphragms, and finally, integration of dual ignition units to provide injector timing signals. Preliminary tests confirmed successful starting of the motorcycle using injectors, with improvements in throttle response and smoother idling. The system shows potential as a cost-effective and adaptable solution for upgrading carburetor motorcycles, reducing fuel consumption and emissions without requiring engine-specific tuning.

Keywords: **E**lectronic fuel injection, **C**arburetor motorcycles, **U**niversal EFI

1.0 INTRODUCTION

Motorcycles remain a primary mode of transport in many developing countries, including Sri Lanka, due to their affordability, fuel economy, and ease of maintenance. Among these, four-cylinder carburetor motorcycles continue to be widely used, despite the fact that carburetors are gradually being phased out in favor of Electronic Fuel Injection (EFI) systems in modern engines. Carburetors, though mechanically simple and inexpensive, are inherently limited in adapting to varying engine loads and speeds, often resulting in incomplete combustion, higher fuel consumption, and increased exhaust emissions. These issues not only affect performance but also contribute to environmental and economic concerns in regions where motorcycles form a large share of the vehicle population [1,2].

EFI systems have become the global standard in modern motorcycles as they ensure more accurate air–fuel mixture control, leading to reduced emissions, improved fuel efficiency, and enhanced throttle response. However, most retrofit EFI solutions available today require detailed engine mapping, where fuel injection parameters must be calibrated for each engine model. Mapping demands advanced diagnostic equipment, software, and expert knowledge, which makes such retrofits technically complex and financially impractical for ordinary users. As a result, large numbers of carburetor-based motorcycles continue to operate without the benefits of EFI [3,4].

This study was therefore undertaken to investigate whether a universal EFI system could be designed and implemented for four-cylinder carburettor motorcycles without the need for engine-specific mapping. The aim of the research is to develop a cost-effective and adaptable retrofit solution that uses ignition or camshaft signals to control injection timing and employs throttle position sensing to regulate fuel delivery across different operating conditions (Figure 1) [5,6].

Accordingly, the specific objectives of the study are to design a modified carburetor body capable of housing fuel injectors, to establish an injector control system based on ignition signals, and to test the feasibility of the system in improving starting, idling, throttle response, and overall fuel efficiency. By achieving these objectives, the research seeks to demonstrate the practicality of a mapping-free universal EFI system that can extend the life of carburetor motorcycles while reducing fuel consumption and emissions.

2.0 EXPERIMENTAL

2.1 System Development

A four-cylinder carburetor was selected and modified to serve as the throttle body for the EFI system (Figure 17). The jets (main and idle) were removed and unused air channels were sealed. Custom injector adaptors were designed and fabricated to fit injectors into the modified throttle body.

Different injectors were tested (**Error! Reference source not found.**) to measure the volume of fuel delivered per injection and ensure that the air–fuel ratio could be maintained near 14.7:1. Initial tests involved powering injectors with a parallel 12 V connection to verify spray characteristics.

In order to correct changes in airflow (Figure 4) caused by carburetor modification, the original slides and diaphragms were reinstalled to maintain constant flow. This adjustment reduced the available space at the backend, so the throttle body was further modified at the frontend to accommodate injectors securely.

A timing system for injector control was designed. Two 4-pin ignition units were connected in parallel, providing common positive and negative lines. The trigger lines were used to detect ignition pulses, while the ignition coil output lines were re-purposed as injector drive lines. This ensured that injectors opened at the correct timing, thereby improving fuel efficiency compared to the initial constant-on configuration.

Finally, after that the timing system was modified using an uno board so that the adjustments can be done for the opening timing of an injector according to the suction of the engine and also, it helps to add a starter button that can supply extra fuel before starting the engine which is mostly needed in cold starts. Also, with the Arduino corded uno board, the timings of fuel injection can be further advanced according to rider’s need as an example; different riding modes like power, racing, economy etc.

2.2 Block Diagram of EFI System

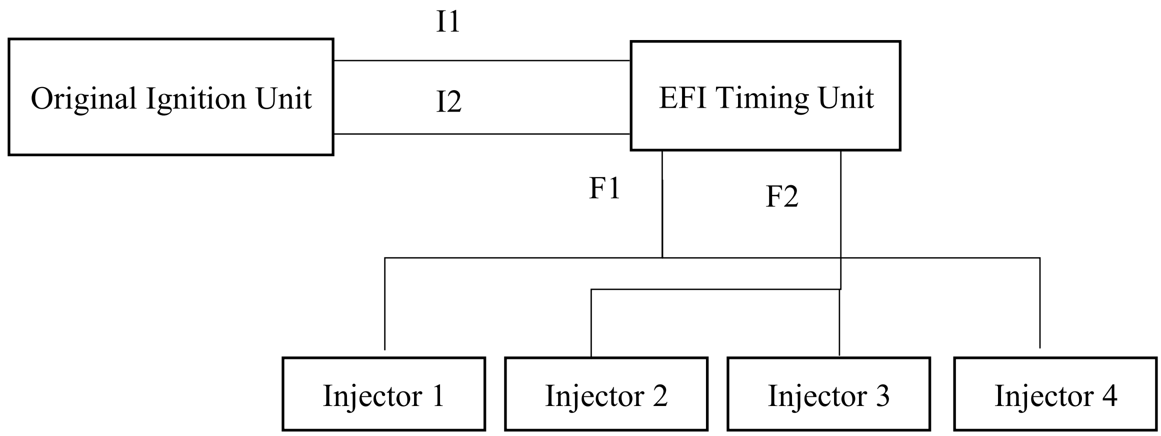

Figure 16: Block diagram of the EFI system

2.3 Preliminary Observations

- Initial prototype with four injectors powered in parallel 12 V allowed the engine to start, but injectors were always on, wasting fuel.
- This led to the design of a timing system using ignition units, which improved injection control.
- Secondary injectors were considered necessary for top-end RPM operation, based on observations during simulation and early tests.

2.4 Ethical and Safety Considerations

This study did not involve human or animal subjects. However, ethical and safety considerations were applied to ensure safe experimentation:

- The original ignition unit of the motorcycle was not modified, maintaining the integrity of the engine's factory design.
- High-pressure fuel handling was carried out with appropriate protective measures to prevent leaks and fire hazards (Figure 5).
- The retrofit design was kept reversible so that motorcycles could be restored to their original carburetor setup if necessary.

2.5 Additional Details and Images

Figure 17: Modified throttle body

Figure 3: Selected Injector

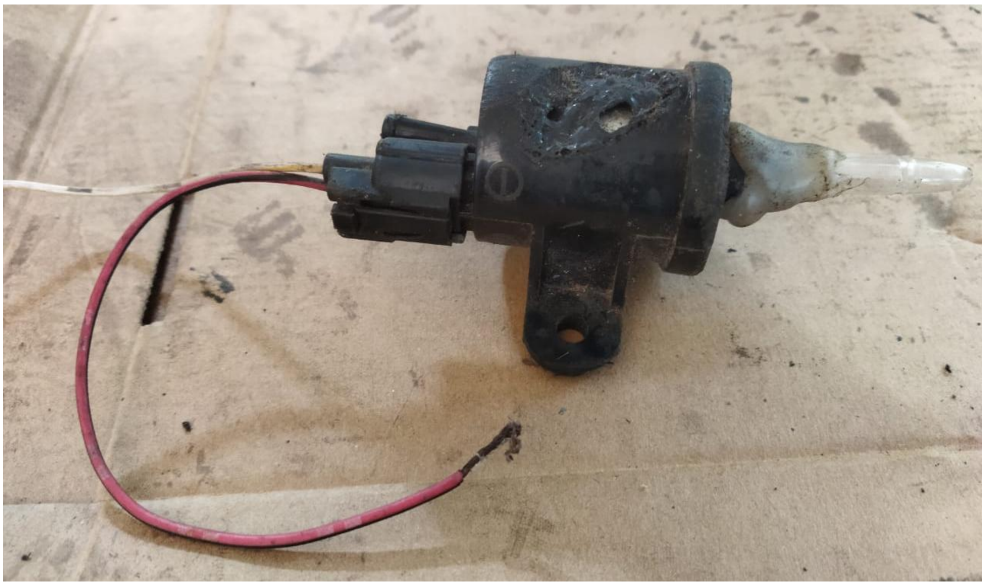
Figure 4: One part of the modified throttle body to correct air flow

Figure 5: Fuel pump

A fuel pump was modified, so it can fix to the original fuel pump without any damage.

3.0 RESULTS AND DISCUSSION

The modified carburetor throttle body with injectors was successfully implemented and tested, demonstrating several improvements over the conventional carburetor system. The motorcycle was able to start using injectors, and smoother idling was observed compared to the baseline carburetor setup. Reinstallation of the original slides and diaphragms ensured stable airflow, which helped maintain engine performance without compromising fuel delivery. Furthermore, measured injection volumes matched the stoichiometric air–fuel ratio when calibrated, confirming efficient combustion and reliable injector operation (Figure 6). Spark plug colour shows that the fuel delivery is at the correct rate and it clearly shows that the engine runs under good and complete combustion (Figure 7).

In addition, the redesigned timing system using uno board allowed the injectors to operate in synchronization with engine cycles, significantly enhancing fuel efficiency compared to the initial constant-on configuration. The performance tests revealed a faster throttle response and reduced fuel wastage, indicating that the system not only maintained combustion stability but also contributed to improved engine dynamics. These findings highlight the potential of the mapping-free EFI system as a practical and efficient alternative for four-cylinder carburetor motorcycles.

Figure 6: Spark Plugs after test run of the engine

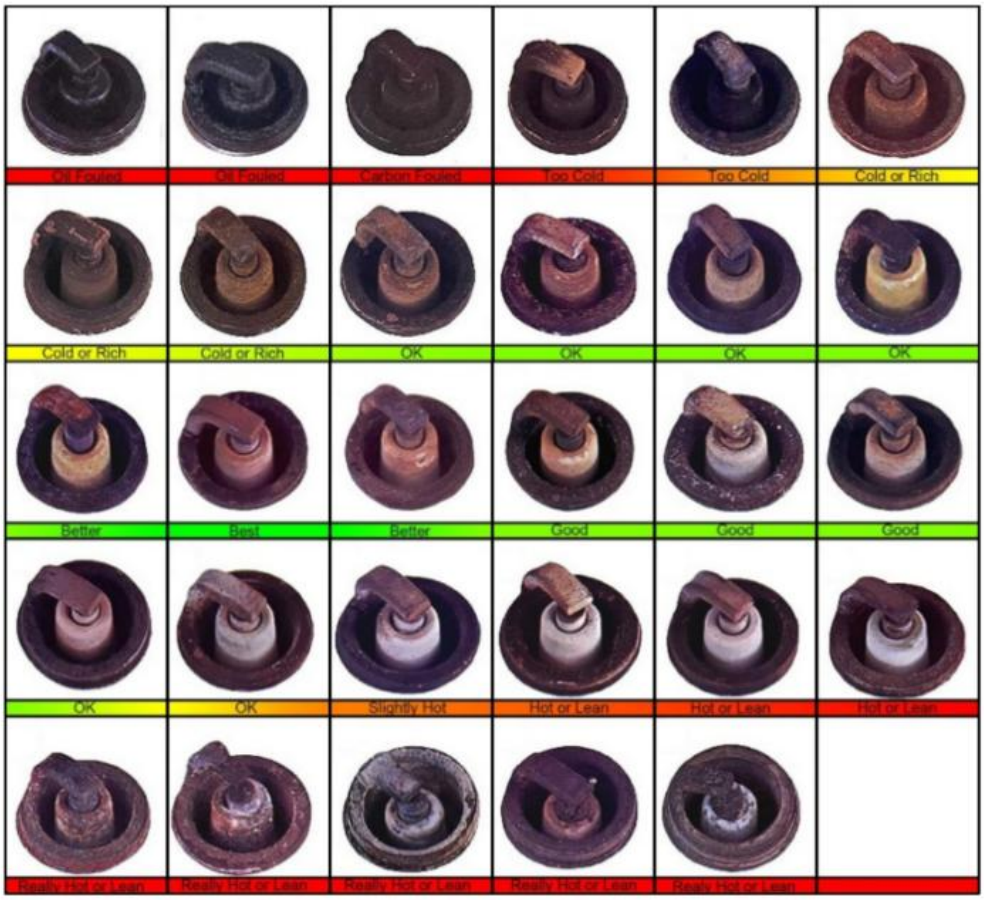

Figure 7: Spark plugs colours according to combustion

Spark plug readings shows that the engine runs under complete combustions and air fuel mixture is perfect.

Discussion: These results confirm that a mapping-free EFI system is feasible. By deriving injection timing directly from ignition signals, the design avoided the need for complex calibration. Some limitations remain, such as optimization for high RPM and long-term durability tests, but the proof of concept demonstrates strong potential for real-world adoption.

4.0 CONCLUSION

This study successfully designed and tested a universal EFI system for four-cylinder carburetor motorcycles without mapping. The system demonstrated smoother idle, better throttle response, and improved efficiency compared to the carburetor baseline. The approach of using ignition signals for injector timing proved effective and simplified the design, reducing the need for expensive equipment or professional tuning.

The findings indicate that such a retrofit system can provide a cost-effective solution for extending the life of carburetor motorcycles while reducing emissions. Future work will focus on expanding compatibility, refining injector placement, and conducting long-term engine performance trials.

ACKNOWLEDGEMNTS

The authors would be thankful to the lecturers and staff at the Department of Electronics, Faculty of Applied Sciences Wayamba University for their guidance for this study.

REFERENCES

[1] M. Sharma, "Explore the different types of fuel injectors at Spinny," Spinny Post, Mar. 04, 2022. https://www.spinny.com/blog/types-of-fuel-injection-systems/

[2] K. V. M. K. Reddy, B. M. Reddy, K. C. S. Reddy, P. Kartheek, and T. S. Adarsh, "Comparative investigation of electronic fuel injection in two-wheeler applications: A Review," IOP Conference Series: Materials Science and Engineering, vol. 1116, no. 1, p. 012073, Apr. 2021, doi: 10.1088/1757-899x/1116/1/012073.

[3] D. Singh, "ELECTRONIC FUEL INJECTION SYSTEM," International Journal of Advanced Research in Engineering and Technology (IJARET), vol. 11, no. 11, pp. 2035–2040, 2020, doi: 10.34218/IJARET.11.11.2020.197.

[4] M. A. Archer and G. Bell, "Advanced Electronic Fuel Injection Systems - An Emissions Solution for Both 2 - and 4 - Stroke Small Vehicle Engines," Jan. 2001, doi: 10.4271/2001-26-0010.

[5] Rini, "Electronic Fuel Injection System (EFI) - Architecture, Types, Applications," electricalfundablog.com, Feb. 26, 2020. https://electricalfundablog.com/electronic-fuel-injection-system-efi/

[6] "What type of fuel system do modern motorcycles typically use?," Quora, 2019. https://www.quora.com/What-type-of-fuel-system-do-modern-motorcycles-typically-use

Proc. Annual Symposium on Research & Industrial Training, 12 (2025) 153-160
Department of Electronics – Wayamba University of Sri Lanka

AUTONOMOUS FIREFIGHTING ROBOT FOR HOME SAFETY

P.D.C. Jayashan*, L.D.R.D. Perera
Department of Electronics, Wayamba University of Sri Lanka, Kuliyapitiya, Sri Lanka
*chathurajayashan21@gmail.com

ABSTRACT

This research paper presents the development of an autonomous, IoT-integrated firefighting robot designed to enhance home safety by automating the response to residential fires, thereby overcoming the critical limitation of delayed human intervention inherent in traditional alarm systems. The proposed system is capable of autonomously detecting a fire source, navigating towards it using intelligent grid-based pathfinding algorithms to avoid obstacles in dynamic indoor environments, and suppressing the flame with an integrated mechanism, while remote monitoring and manual override features provide additional flexibility and reliability. The designed system consisted of NodeMCU and ESP32 microcontrollers, flame sensors for fire detection, ultrasonic for obstacle avoidance, DC motors with an L298 motor driver for mobility, and a water-based suppression unit integrated into the robot chassis. On the software side, the system utilized Firebase for real-time cloud communication, Blynk for mobile-based monitoring and manual control, and Arduino IDE with embedded C/C++ programming for system implementation. Experiments in controlled settings demonstrated the robot's efficacy in rapidly identifying fires, following collision-free paths, and successfully extinguishing small-scale blazes, confirming its potential as an affordable and practical automated fire management solution for households and a foundational platform for future smart home robotics.

Keywords: **A**utonomous Robot, **F**ire Detection, **E**SP32

1.0 INTRODUCTION

Residential fires represent a persistent and serious global challenge, leading to significant loss of life, injuries, and extensive property damage annually. Although conventional fire detection systems, such as smoke detectors, provide crucial early warnings, their fundamental limitation is a dependency on human intervention for an effective response. This critical dependency often results in dangerous delays, allowing manageable fires to escalate into major disasters. To overcome these shortcomings, the field is increasingly focused on the development of autonomous robotic systems capable of not only detecting but also actively suppressing fires without human assistance.

The convergence of robotics and Internet of Things (IoT) technology has created new opportunities for intelligent home safety solutions. These autonomous firefighting robots leverage advanced sensors, sophisticated navigation algorithms, and immediate suppression mechanisms to perform rapid intervention in emergency scenarios. The proposed system integrates NodeMCU microcontrollers for distributed room-based fire detection, an ESP32 microcontroller for robot control, flame sensors, ultrasonic and infrared sensors for obstacle detection, DC motors with an L298 driver for mobility, and a water-based flame suppression unit. On the software side, Firebase is used for real-time cloud communication, Blynk for mobile monitoring and manual override, and Arduino IDE with embedded C/C++ programming for implementation, while grid-based pathfinding algorithms enable intelligent navigation.

This study contributes to the field by presenting the design and implementation of a robot that combines autonomous navigation, obstacle avoidance, and remote monitoring into a single modular platform. The research emphasizes the role of intelligent pathfinding and a scalable hardware–software architecture to deliver a low-cost and efficient system for enhancing safety in modern households.

2.0 EXPERIMENTAL

The proposed system consists of three main components: a fire detection layer, a navigation and control layer, and a suppression mechanism. The overall architecture is illustrated in Figure 01, which shows the interconnection between detection nodes, the autonomous robot, and the cloud-based coordination platform.

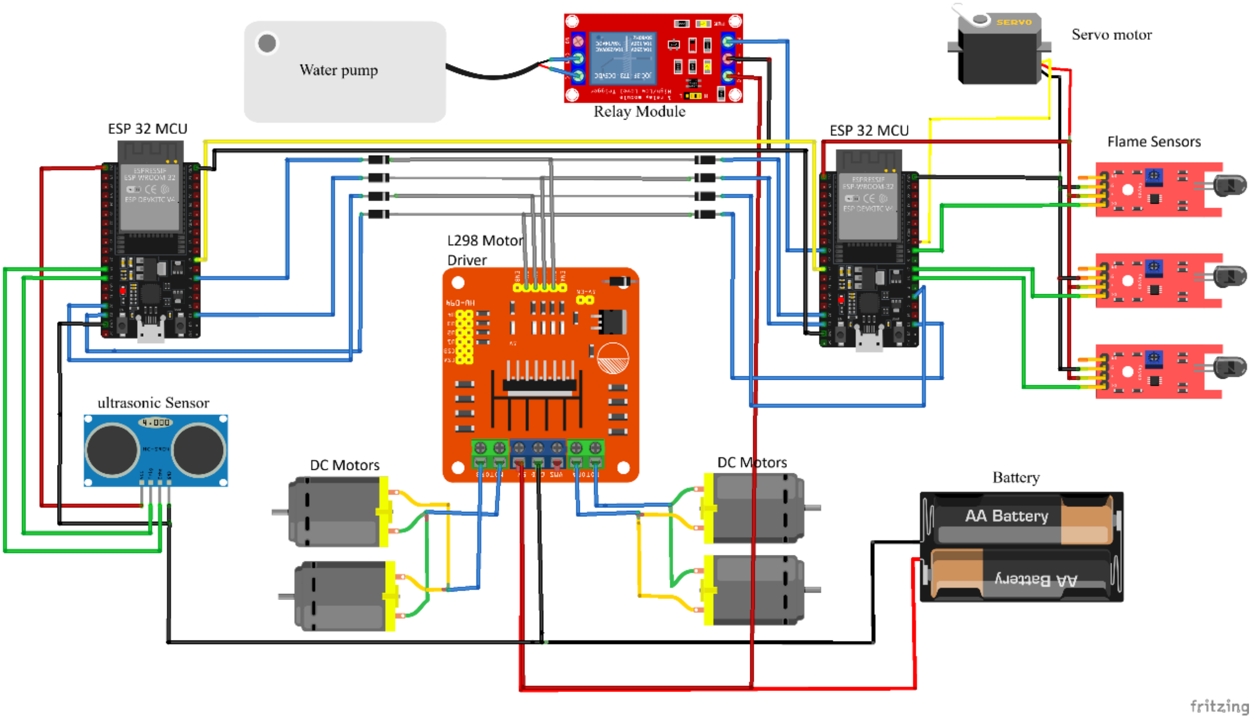

Figure 01: Overall architecture of the system

2.1.Fire detection layer

This layer is implemented using flame sensors connected to NodeMCU microcontrollers. Each detection node is positioned in a room and continuously monitors for fire events. When fire is detected, the corresponding room coordinates are uploaded to the Firebase database. These coordinates serve as the input for the robot's navigation system. Figure 02 shows the diagram of the flame detection unit [1].

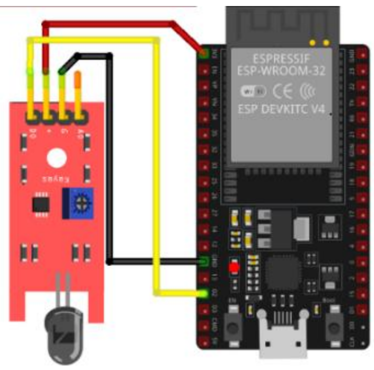

Figure 02: Diagram of the fire detection unit

2.2.Navigation and control layer

The ESP32 microcontroller operates as the central control unit. It retrieves the fire location from Firebase database and applies the A* pathfinding algorithm to determine the most efficient route within a grid-mapped environment. Pathfinding or pathing refers to the process of finding the shortest or most efficient route between two specific points (origin and destination). It is commonly applied in solving mazes and route planning problems to measure efficiency and speed. Most pathfinding algorithms are based on graph theory, which models pairwise relationships between objects. In this framework, a graph consists of nodes (vertices) connected by edges (links), where the cost of moving along each edge represents the distance or effort required. The A* algorithm extends this approach by introducing heuristics that guide the search toward the goal more efficiently, reducing unnecessary exploration. In the proposed system, the environment is represented as a grid of nodes, where each movement corresponds to a step between connected nodes [2].

The ESP32 uses this representation to continuously compute the optimal path. Ultrasonic sensors are employed for obstacle detection, enabling dynamic re-routing when unexpected objects are encountered. As the robot navigates, the ESP32 updates its path based on new sensor inputs and generates motor control signals to the DC motors for precise movements
Graph theory includes several well-known pathfinding algorithms. Dijkstra's algorithm computes the cost of moving through cells and expands outward until it reaches the goal. The A* algorithm improves this process by adding a heuristic function, guiding the search more efficiently toward the destination. In this project, the A* algorithm was selected because it balances efficiency, accuracy, and suitability for microcontroller-based implementation [3].

2.3. Suppression layer
Once the robot reaches the fire location, a suppression module based on NodeMCU is activated.
This module controls a small water pump and a servo-operated nozzle, ensuring accurate spraying

of water toward the detected fire source. Figure 04 shows the circuit diagram of the suppression unit.

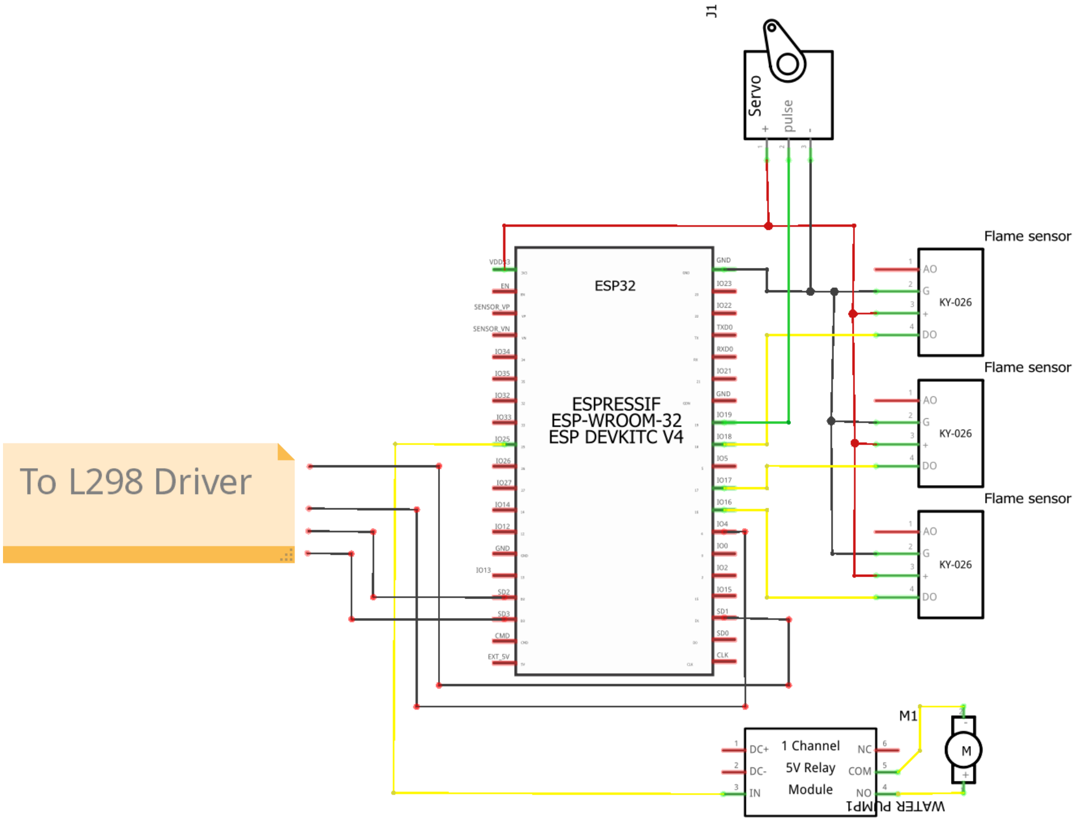

Figure 03: Circuit diagram of the suppression unit

Prior to hardware implementation, the system was modeled and tested using simulation environments for pathfinding and obstacle detection verification. Figure 01 provides the prototype block diagram for the firefighting robot. Hardware assembly included integration of ESP32, NodeMCU modules, ultrasonic sensors, flame sensors, servo motors, and a DC water pump. The robot chassis was fitted with DC motors for controlled navigation [4].

Flow chart of the proposed firefighting robot system (Fig. 04) illustrates the sequence of fire detection, cloud communication, path planning, obstacle detection, navigation, and suppression. of the navigation and obstacle detection system, while Figure 05 shows the prototype robot.

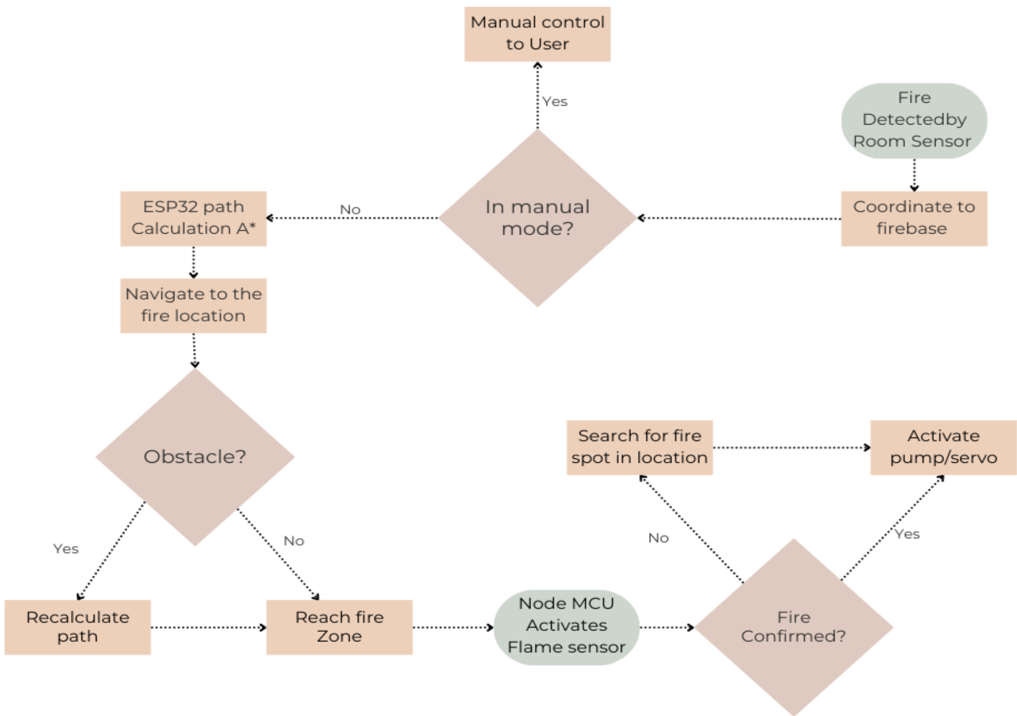

Figure 04: Flow chart of the firefighting robot

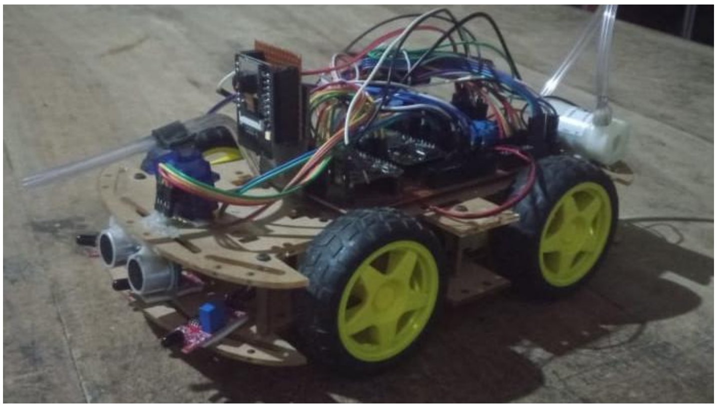

Figure 05: prototype of the robot

3.0 RESULTS AND DISCUSSION

The evaluation of the autonomous firefighting robot was carried out in a controlled indoor environment designed to replicate the layout of a typical household with multiple rooms and interconnected pathways. The experiments focused on four primary aspects of the system: fire detection performance, navigation and pathfinding accuracy, obstacle avoidance efficiency, and fire suppression capability. Additional emphasis was placed on analyzing the reliability of manual override control through the Blynk platform.

3.1.Fire detection

The flame sensor nodes installed in individual rooms successfully detected fire within a range of 40–50 cm and transmitted room coordinates to the Firebase database with an average update time of 1.3 seconds. Experiments showed 100% detection accuracy with negligible false positives, as summarized in Table 01. The nodes were also energy-efficient, making them suitable for long-term smart home use, though slight sensitivity reductions occurred under intense sunlight or reflective surfaces. To improve robustness, future designs could integrate hybrid methods such as smoke sensors or thermal imaging [4].

Table 01: Fire detection performance across test trials

Trial	Location	Fire Detected	Firebase Update Time (s)	Accuracy (%)
1	Room 1	Yes	1.2	100
2	Room 2	Yes	1.4	100
3	Room 3	Yes	1.3	100
4	Room 3	No	-	100

3.2.Navigation and pathfinding

The ESP32 implemented the A* pathfinding algorithm within a 6x6 grid environment to compute the shortest route between the robot's starting point and the fire location. In trials without obstacles, the robot reached the target with high precision, deviating by less than 5 cm from the planned path. When obstacles were introduced, ultrasonic sensors detected them effectively, and the ESP32 recalculated a new route in real time.

Compared to simpler methods such as breadth-first search (BFS) or depth-first search (DFS), A* reduced computational overhead and produced optimal paths more quickly. Figure 06 shows an example of a re-routed path where the robot successfully avoided a newly introduced obstacle while still reaching the fire location within acceptable time limits [5].

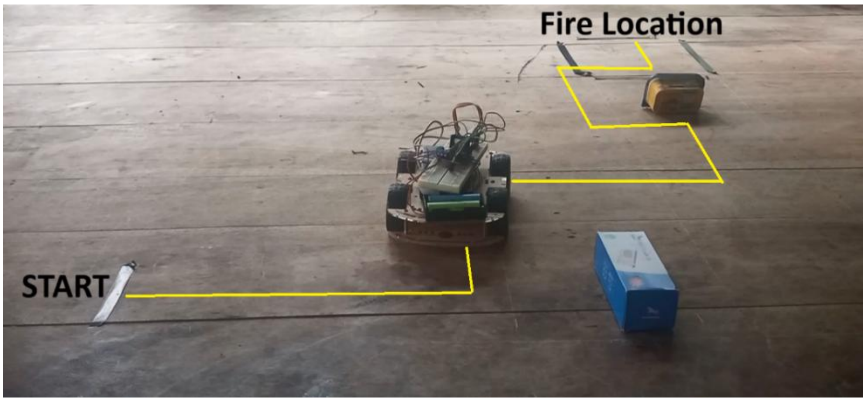

Figure 06: Example of path re-routing with A* algorithm during obstacle detection

3.3.Obstacle avoidance

Obstacle avoidance was tested using both static objects (e.g., boxes, walls) and dynamic objects (e.g., moving chairs, people walking in front of the robot). The ultrasonic sensors were able to detect obstacles within a 10–15 cm range. In most cases, avoidance was successful, with an overall success rate of 93% across 20 trials. Static obstacles were avoided more effectively than dynamic ones, as rapidly moving objects occasionally exceeded the sensors' detection refresh rate.

Certain limitations were identified, particularly with very thin or reflective surfaces that either failed to reflect ultrasonic pulses adequately or caused inaccurate readings. This limitation highlights the need for more advanced perception systems such as LiDAR or stereo cameras, which could provide more reliable environmental data [6].

3.4.Fire suppression

The suppression module, controlled by NodeMCU, consisted of a water pump and a servo-operated nozzle. Once the robot reached the fire source, suppression was activated immediately. The average suppression response time, defined as the interval between fire detection and water release, was 3 seconds. The robot was able to extinguish small-scale alcohol-based flames in all trials.

The water spray pattern covered an area of approximately 10 cm in diameter, sufficient for small indoor fires. However, the water reservoir was limited, enabling only a few suppressions attempts before requiring a refill. Increasing reservoir capacity and optimizing spray angles are key areas for future improvement.

3.5.Manual control and remote monitoring

The Blynk app provided a manual override option, allowing operators to remotely control the robot in real time. Latency tests showed that control signals were transmitted with a delay of less than 500 ms, ensuring responsive maneuvering. The live video stream allowed the operator to visually identify fire sources and confirm suppression actions. This feature greatly enhances reliability, as it ensures human supervision in cases where the autonomous mode might fail [7].

3.6.Discussion

The integrated results demonstrate that the proposed firefighting robot successfully combined autonomous fire detection, intelligent navigation, obstacle avoidance, and suppression mechanisms into a single, reliable platform. The use of A* pathfinding enabled efficient route planning, and Firebase provided seamless coordination between detection nodes and the robot.

The robot achieved a 100% fire detection rate, 93% obstacle avoidance success, and consistent suppression within 3 seconds, proving the viability of the design. Nevertheless, limitations such as ultrasonic sensor blind spots, stepper motor drift, and limited water capacity were observed. Addressing these limitations with advanced sensors, closed-loop motor control, and larger reservoirs could substantially enhance system performance.

Overall, the research highlights the potential of integrating robotics and IoT for home fire safety. While current results are promising for small-scale indoor environments, scaling the system to larger spaces or severe fire conditions will require further hardware and software refinements.

4.0 CONCLUSION

This paper presented the design and development of an autonomous firefighting robot that integrates fire detection, intelligent navigation, obstacle avoidance, and suppression into a single IoT-enabled platform for home safety. The system utilized flame detection nodes to continuously monitor individual rooms and transmit fire location data to a central Firebase database. Based on this information, the robot employed the A* pathfinding algorithm to compute collision-free routes and dynamically replan paths when ultrasonic sensors detected obstacles. Upon reaching the fire location, the suppression unit, consisting of a water pump and servo-operated nozzle, was activated to extinguish the flames.

Experimental results confirmed that the system achieved 100% fire detection accuracy**,** effective obstacle avoidance with a 93% success rate, and rapid suppression with an average response time of 3 seconds. In addition to autonomous operation, the inclusion of manual control through the Blynk app and live video streaming enhanced reliability by allowing user supervision in emergency scenarios.

Despite its effectiveness, limitations such as ultrasonic blind spots, stepper motor drift, and limited water capacity were identified. Future enhancements will focus on LiDAR-based perception, closed-loop motor control, and AI-driven fire and smoke detection. Overall, the designed robot provides a practical, low-cost solution for safer smart homes.

ACKNOWLEDGEMENT

The authors express their sincere gratitude to the lecturers and staff at the Department of Electronics, Faculty of Applied Sciences, Wayamba University of Sri Lanka.

REFERENCES

[1] Winsen, "What is a Flame Sensor? A Comprehensive Guide to Fire Detection," *Winsen-sensor.com,* 2023. https://www.winsen-sensor.com/knowledge/what-is-a-flame-sensor.html(Accessed 2025-09-05).

[2] Azeta, J., Ayoade, I. A., Nwakanma, C. I., and Akande, T., Implementing a Prototype Autonomous Fire Detecting and Firefighting Robot, *Preprints*, 2023, doi:https://doi.org/10.20944/preprints202305.2010.v1

[3] Conrad, A., Shortest Path Problems in the Real World, *Adam Conrad*, 2018. https://www.adamconrad.dev/blog/shortest-paths/(Accessed 2025-09-05).

[4] “Fire Suppression - an overview,” ScienceDirect Topics. https://www.sciencedirect.com/topics/engineering/fire-suppression (Accessed 2025-09-06).

[5] Chopra, C., Pathfinding Algorithms, *The Startup,Medium*, 2019. https://medium.com/swlh/pathfinding-algorithms-6c0d4febe8fd(Accessed 2025-09-06).

[6] Sandberg, O., Pathfinding Algorithm Comparison In Dynamic Congested Environment,PhD diss., Uppsala University, 2024. Available: https://www.divaportal.org/smash/get/diva2:1879887/FULLTEXT01.pdf

[7] htmlandcss webpages, “Wifi Controlled Smart Car Using Nodemcu and Blynk App”, *Scribd*, 2025. https://www.scribd.com/document/642211549/Untitled(Accessed 2025-09-06).

Proc. Annual Symposium on Research & Industrial Training, 12 (2025) 161-169
Department of Electronics – Wayamba University of Sri Lanka

A TIMER AND SENSOR-BASED GAS DISCONNECTING SYSTEM

P.V.S. Madhumalika*, J.M.J.W. Jayasinghe

Department of Electronics, Wayamba University of Sri Lanka, Kuliyapitiya, Sri Lanka

subhashinimadhumalika@gmail.com

ABSTRACT

Gas stoves are extensively used in households and commercial kitchens due to their convenience and efficiency; however, they also present significant safety risks when left unattended or improperly handled. Common issues include flame failure caused by wind or accidental liquid spills, as well as continued gas flow when the cooking pan is removed while the burner remains active. These situations not only result in unnecessary fuel consumption but also increase the likelihood of fire hazards. To mitigate these risks, this study proposes a timer and sensor-based gas disconnecting system aimed at enhancing stove safety. The system is composed of three functional modules, all controlled by an ESP32 microcontroller: a flame sensor to monitor burner activity, a pan detection mechanism to verify the presence of cookware, and a programmable timer to automatically terminate gas flow after a predefined duration. A solenoid valve is employed as the actuator to interrupt the gas supply whenever unsafe conditions are detected. The prototype demonstrated reliable flame failure detection within a few seconds, achieved over ninety percent accuracy in pan detection, and provided consistent shut-off operation through the timer module. By integrating these three layers of protection, the system effectively minimizes the risk of accidents and reduces energy wastage. Moreover, the ESP32 platform offers flexibility for future upgrades, such as wireless alert systems and smart kitchen integration. Overall, the proposed design provides a cost-effective, reliable, and scalable solution to improve both kitchen safety and energy efficiency.

Keywords: **G**as Safety, **E**SP32 Microcontroller, **F**lame Sensor

1.0 INTRODUCTION

Gas stoves have become an indispensable appliance in modern kitchens due to their ability to provide precise temperature control and rapid cooking. They are preferred over other cooking methods because of their efficiency, energy savings, and versatility. Despite these advantages, gas stoves pose significant safety risks that can result in accidents and damage if not properly monitored. One of the main hazards is flame extinguishing, which can occur due to wind, accidental spills, or disturbances during cooking. When a flame is extinguished unexpectedly, gas continues to flow, creating a potential fire hazard if it comes into contact with combustible materials in the kitchen [1,2].

Another major concern is unattended cooking. Users often remove a cooking utensil but forget to turn off the burner, allowing the flame to continue burning. This can result in wasted energy, overheating of cookware, burned food, and, in severe cases, fire accidents. Such incidents not only pose a direct threat to safety but also contribute to unnecessary utility costs and environmental impact. Preventing these hazards requires a proactive approach that monitors the stove continuously and takes immediate action when unsafe conditions occur [2].

Many researchers have explored different approaches to enhance household gas safety. Yalmar et al. (2015) proposed an automatic safety gas stove that incorporated three modes, utensil detection using an infrared sensor, timer based shut off, and remote access through a DTMF module to prevent domestic accidents from unattended or misused stoves [3]. While this system successfully demonstrated automation and safety integration, its reliance on mechanical knob turning motors and sensitivity issues in utensil detection limited long term reliability. Similarly, Odonkor et al. (2020) developed an intelligent gas cylinder valve regulating system using an ATMEGA328 microcontroller, solenoid valve, gas sensor, temperature sensor, and 555 timer, which could automatically cut off gas flow during leakage, overheating, or when food was cooked [4]. Although effective in combining multi sensor safety functions, the system lacked cookware presence detection and was constrained by its dependence on preset cooking times rather than real time cooking conditions. In another study, Rajapaksha et al. (2020) designed an auto disconnecting regulator and safety switch that automatically detached the regulator from the cylinder during leakage events, coupled with GSM based alerts and a Bluetooth linked safety switch to cut off nearby electrical power [5]. While this approach ensured robust leak prevention and communication, its mechanical complexity and dependence on wireless modules introduced risks of false activations and operational delays.

Collectively, these studies emphasize the importance of integrating sensors, timers, and solenoid-based actuation for kitchen safety but reveal limitations such as inadequate detection of pan presence, excessive reliance on mechanical disconnection mechanisms, and constraints from wireless or network dependencies. To overcome the limitations highlighted in previous studies, this research focuses on the design and implementation of a timer and sensor-based gas disconnecting system using an ESP32 microcontroller. The primary objective is to develop an integrated solution that combines flame detection, pan presence verification, and timer-based control to automatically regulate gas flow under safe operating conditions. The study aims to ensure accurate flame detection so that gas flow is immediately terminated if the flame is extinguished. It also seeks to incorporate a reliable pan detection mechanism capable of confirming the presence of cookware on the burner.

In addition, a programmable timer is implemented to restrict the cooking duration by automatically shutting off the gas supply after a predefined period. The system further regulates the gas supply through an electric solenoid valve, ensuring that gas is delivered only when all required safety conditions are satisfied.

3.0 EXPERIMENTAL

To address the research question, a system integrating ESP32 microcontroller, flame sensor, pan detection sensor, timer, and solenoid valve was designed and implemented (Figure 1). The ESP32 was programmed to continuously read input signals from the flame and pan sensors and monitor the timer. Based on these inputs, it controls the solenoid valve to allow or cut off gas flow under predefined safe conditions. The system was constructed on a breadboard with all sensors and actuators connected to the ESP32 (Figure 2). Preliminary testing confirmed that the ESP32 correctly read sensor inputs and actuated the solenoid valve, informing the final logic used in the main system.

When the gas stove is turned on, the system initially allows gas to flow continuously for the first 30 seconds. During this period, the flame sensor stabilizes and verifies whether the burner is ignited. After the initial 30 second period, the ESP32 microcontroller continuously monitors three inputs: the flame sensor, the pan detection mechanism, and the timer module. Gas flow continues only if all three conditions are satisfied: the flame is detected, a pan is present on the burner, and the timer has not expired. If any of these conditions are not met, the ESP32 immediately closes the solenoid valve, shutting off the gas flow to prevent unsafe operation (Figure 3).

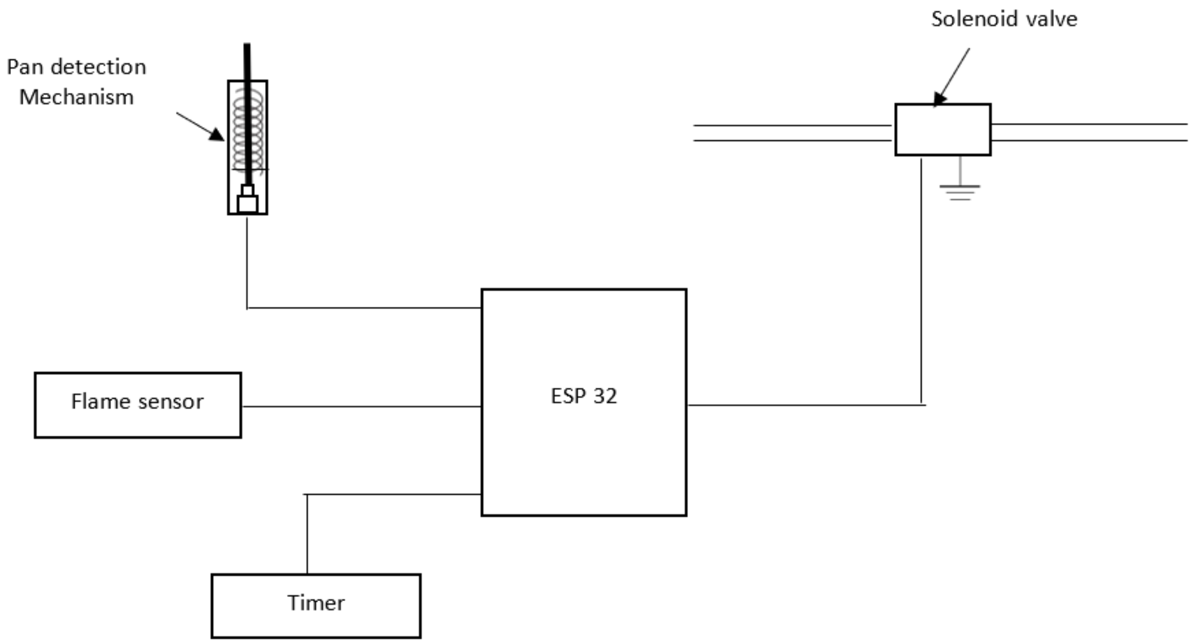

Figure 18: Block diagram of the timer and sensor-based gas disconnecting system

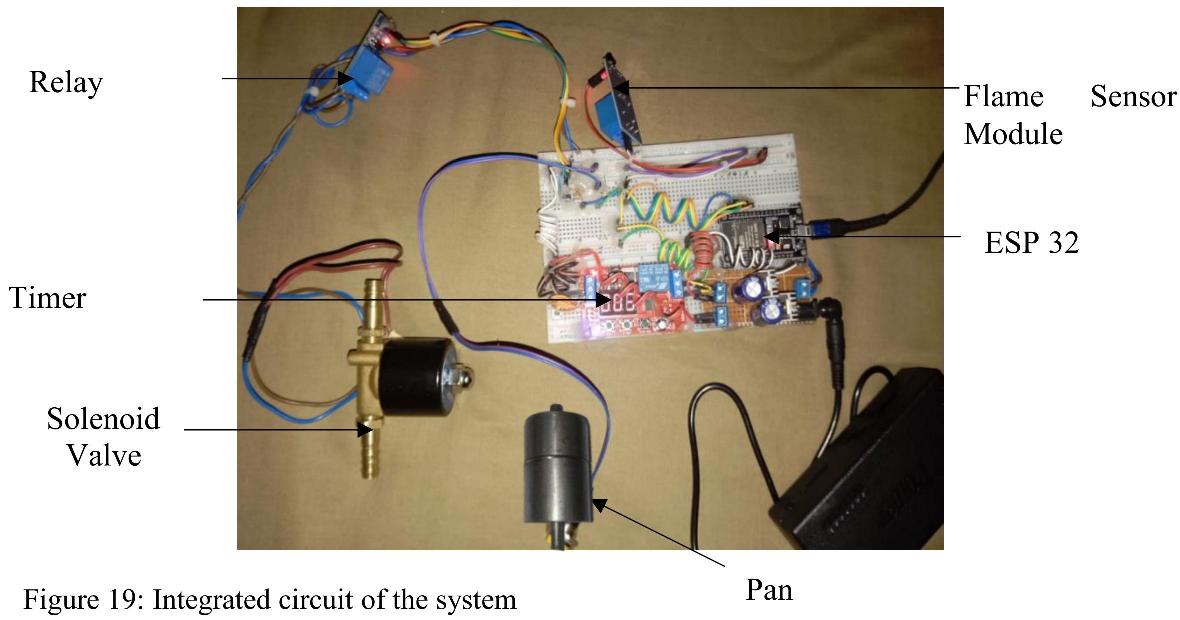

Figure 19: Integrated circuit of the system

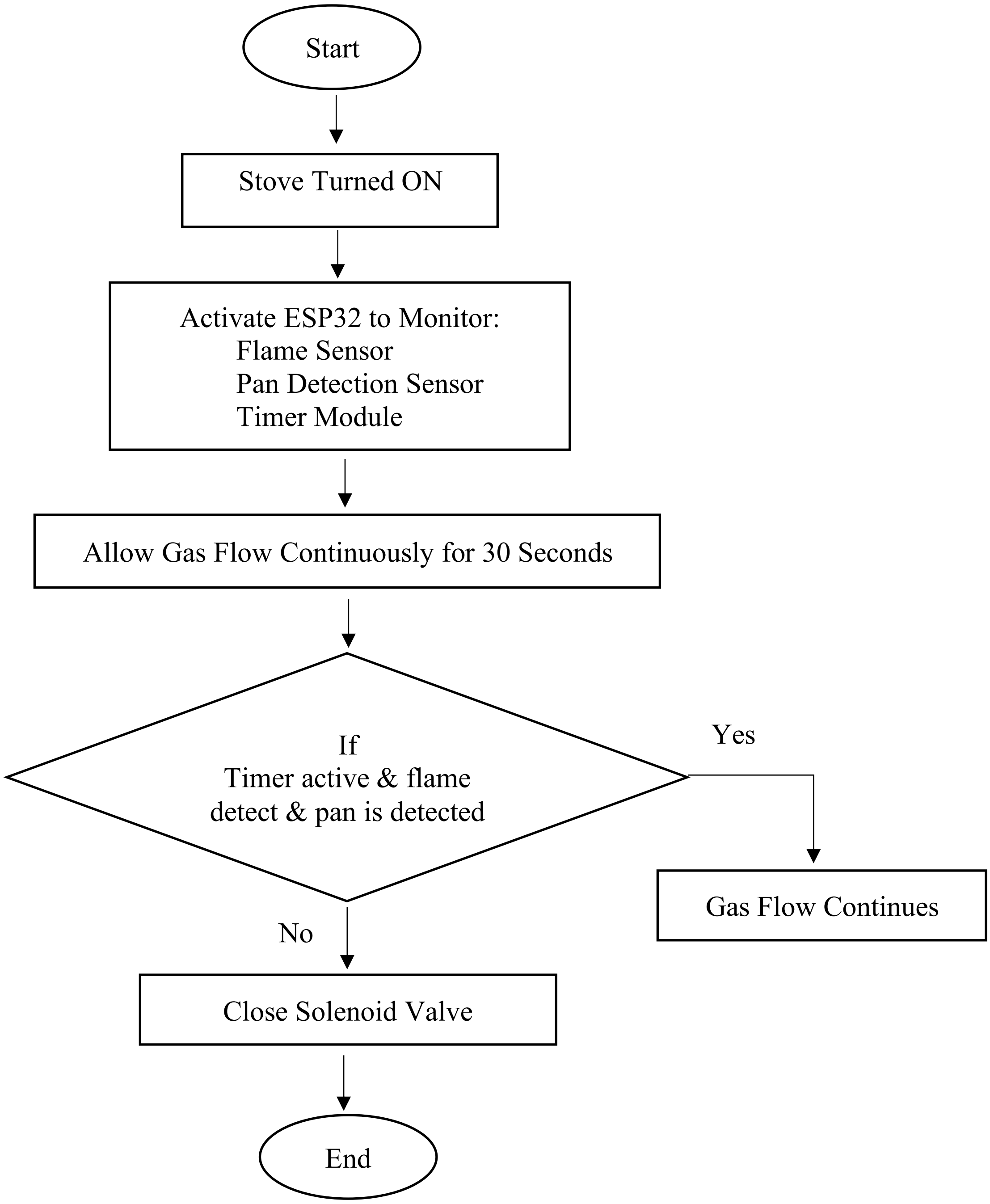

Figure 20: Flowchart of a timer and sensor-based gas disconnecting system using ESP 32

Before running the main experiment, a preliminary study was performed to ensure that the sensors and system worked reliably. It was found that the flame sensor needed about 30 seconds after turning on the stove to stabilize and give accurate readings; checking it immediately could lead to false results. The pan detection sensor was tested with different types and sizes of cookware, and it reliably detected the presence of a pan only when it met a certain weight threshold. These observations were used to adjust the ESP32 programming logic and the timer settings, ensuring that the system operates accurately and safely during the main experiment.

3.0 RESULTS AND DISCUSSION

The system was evaluated under multiple scenarios to assess its reliability and effectiveness. In the first scenario, the flame was intentionally extinguished while the stove was operating. The ESP32 immediately closed the solenoid valve, preventing gas flow. In the second scenario, the pan was removed while the burner remained lit. Once again, the solenoid valve cut off the gas supply instantly. In the third scenario, the timer reached its preset limit, and gas was automatically stopped (Table 3).

Table 3: System Response Under Different Conditions

Scenarios			Solenoid Valve State	Gas Supply
Flame Present	Pan Present	Timer Active		
✓	✓	✓	Close to open	Supplied
×	✓	✓	Remains close	Stopped
✓	×	✓	Remains close	Stopped
✓	✓	×	Remains close	Stopped
×	×	×	Remains close	Stopped

When using clay pots, large aluminium utensils and kettles and etc are working perfectly with pan detection mechanism. But lighter and small utensil are showing some defects with the pan detection mechanism when the utensils are empty. But, with some adjustment of the position of the pan detection mechanism we can overcome this situation.

The functionality of the system was verified by observing the real-time sensor values and control actions transmitted by the ESP32, which were displayed on the Arduino IDE Serial Monitor, enabling immediate observation of the flame, pan, timer status, and solenoid valve action. In this system, the flame sensor is active low (LOW when flame is detected), while the pan sensor and timer are active high (HIGH when pan is present or timer is active), allowing the ESP32 to correctly interpret all inputs for safe operation. The flame sensor outputs active low because it uses a pull-up configuration, keeping the signal HIGH by default and pulling it LOW when a flame is detected for noise immunity and reliable detection.

In the ESP32 program, specific messages were added to the code as serial monitor outputs to verify the system's behaviour. The message "Solenoid ON" was programmed to appear during the initial 30 seconds after stove activation, "working fine" was programmed to indicate safe operating conditions, and "Check pan in there or timer deactivate or flame not found 404!" was programmed to indicate unsafe conditions. After implementing these messages, the system was tested under different operating scenarios, and the corresponding serial monitor outputs were observed for each condition (Figure 4, Figure 5, Figure 6).

```
07:29:57.825 -> fla��=== System Startup ===
07:29:58.199 -> Solenoid ON → Starting fire... Waiting 30s
```

Figure 21: Serial Monitor Output in First 30 Seconds

```
07:33:52.161 -> === Loop Start ===
07:33:52.193 -> Timer on 1
07:33:52.193 -> pan 1
07:33:52.193 -> flame 0
07:33:52.238 -> Working fine
```

Figure 22: Serial Monitor Output When All Conditions Are Satisfied

```
07:35:56.255 -> === Loop Start ===
07:35:56.287 -> Timer on 1
07:35:56.287 -> pan 0
07:35:56.320 -> flame 0
07:35:56.320 -> Check Pan In there or timer deacivate or flame not found 404!
```

```
07:34:09.650 -> === Loop Start ===
07:34:09.682 -> Timer on 1
07:34:09.714 -> pan 1
07:34:09.714 -> flame 1
07:34:09.714 -> Check Pan In there or timer deacivate or flame not found 404!
```

```
07:40:01.249 -> === Loop Start ===
07:40:01.281 -> Timer on 0
07:40:01.313 -> pan 0
07:40:01.313 -> flame 1
07:40:01.313 -> Check Pan In there or timer deacivate or flame not found 404!
```

Figure 23: Serial Monitor Output Under Unsafe Conditions

The experimental results demonstrate that the proposed system successfully prevents unsafe stove operation. By combining flame and pan sensors with a timer module, the ESP32 ensures that gas is supplied only under safe conditions. This approach enhances kitchen safety, reduces energy wastage, and provides convenience to users.

The primary advantage of this system is enhanced safety, as it immediately shuts off gas in hazardous situations, such as flame extinguishing or unattended cooking. Additionally, energy efficiency is improved because the gas supply stops automatically when the pan is removed or the timer expires. Since inside the pan detection mechanism, the two contact points are separated by a tension of a spring and the gap is nearly around 2cm, So that thermal expansion also negligible. The convenience offered by the timer allows users to focus on other tasks without constantly monitoring the stove.

The system can be further developed by integrating it with smart home networks to send real-time alerts and notifications to users. An LCD display or mobile application could be added to show timer values, flame status, and pan detection in real time. In addition, incorporating IoT-based monitoring and voice assistant compatibility would make the system more user-friendly and suitable for modern smart kitchens.

4. CONCLUSION

This study presents a timer and sensor-based gas disconnecting system using ESP32 to enhance kitchen safety and energy efficiency. By continuously monitoring flame presence, pan placement, and cooking duration, the system prevents unsafe operation and unnecessary energy consumption. Experimental results confirmed that the system responds reliably under all tested scenarios. As the limitations, this system can not identify gas leaks through the gas tube. Other than that, all other risks are eliminated through the system. The study demonstrates the practical application of microcontroller-based automation for household safety and provides a foundation for future smart kitchen automation solutions. As further developments, integrating a gas leak detection module would allow the system to identify and respond to gas leaks from the regulator, significantly enhancing its safety capabilities.

ACKNOWLEDGEMNTS

The authors would like to express their gratitude to the Academic Staff of the Faculty of Applied Sciences, Wayamba University of Sri Lanka for their expert advice and guidance.

REFERENCES

[1] "LPG/CNG Gas Leakage Detection and Prevention using IoT." Accessed: Nov. 18, 2024. [Online]. Available: https://www.irjet.net/archives/V8/i6/IRJET-V8I6542.pdf

[2] S. D. Bangera, Mohan K, and V. Raj, "Automatic Gas off Mechanism for LPG Gas Stove," International Journal of Scientific Research in Computer Science Engineering and Information Technology, pp. 543–546, Jun. 2021, doi: 10.32628/CSEIT2173119.

[3] Ajinkya Yalmar, Mahesh Parihar, V. Kadam, and Kunika Kharat, "Implementation of automatic safety gas stove," pp. 1–6, Dec. 2015, doi: 10.1109/indicon.2015.7443474

[4] Odonkor, Ebenezer Narh, "Design and Implementation of an Intelligent Gas Cylinder Valve Regulating System Using Solenoid," Ssrn.com, 2020. https://papers.ssrn.com/sol3/papers.cfm?abstract_id=3712126

[5] R. M. I. U. Rajapaksha et al., "Design of an auto disconnecting regulator and a safety switch to prevent domestic gas leakages," IEEE Xplore, Sep. 01, 2020. https://ieeexplore.ieee.org/document/9312996 (accessed Nov. 02, 2022)

Proc. Annual Symposium on Research & Industrial Training, 12 (2025) 170-175
Department of Electronics – Wayamba University of Sri Lanka

SOLAR TRACKING SYSTEM WITH SMART CLEANING TECHNOLOGY

R.N.N. Prabodanee*, Dr. Y.A.A. Kumarayapa
Department of Electronics, Wayamba University of Sri Lanka, Kuliyapitiya, Sri Lanka
*nethminawodya1999@gmail.com

ABSTRACT

The ability to harvest energy from the sun, with solar panels, is less applicable due to two broad reasons first, solar panels being misaligned with respect to sunlight and second, a layer of dust that sits on the surface of a solar panel. This paper describes how an innovative sunflower-inspired design and implementation of a dual-axis solar tracker which uses minimal water for the scrubbing of the dust layer, and incorporates a self-cleaning process. The solar tracker uses light dependent resistors to know the direction of maximum intensity of the sun, while a microcontroller drives servo motors to maintain the orientation of solar panels continuously to maximize the energy efficiency of the solar panels as they follow the path of the sun during the day. During nighttime or under adverse weather conditions, the solar panels automatically fold into a closed position based on inputs from light and rain sensors, as controlled by the microcontroller, to minimize exposure to environmental elements. Once the panels are in a closed state, the cleaning mechanism is activated and the surface wipes with a controlled volume of water to maintain efficiency without excessive water consumption. This sustainable approach is preserving resources and is useable in areas with limited access to water. Early indications support that using solar tracking above and water-efficient cleaning would provide greater energy output than fixed and uncleaned panels, in addition to diminishing the cleaning frequency altogether. The system provides a cost effective, environmentally viable method of cleaning panels while sustaining yield, integrity and reliability of solar energy.

Keywords : **D**ual-Axis, **S**olar Tracking, **S**elf-Cleaning,

1.0 INTRODUCTION

Solar energy is one of the most advanced renewable energy sources, producing an environmentally-friendly and sustainable substitute for fossil fuels. Unfortunately, the performance of solar panels frequently suffers because solar panels do not move to adequately benefit from sunlight and dust accumulates on the surface of panels restricts the absorption of light. Research has shown fixed panels may experience a significant difference in efficiency when compared to tracking systems, and dusty panels can suffer a loss of up to 12.7% performance [1]. Accordingly, it is now a priority to combine solar tracking systems with efficient cleaning solutions to improve overall solar energy generation [2].

Conventional solar panel tracking systems generally take the form of either single-axis or dual-axis systems. Although single-axis trackers do capture slightly more energy, dual-axis trackers achieve the most advantages because they allow a sun-facing panel to track the sun over both horizontal and vertical planes as the sun moves through the sky throughout the day and across the seasons [3]. At the same time, various self-cleaning means have been proposed, including using water sprays or dry mechanical cleaning. While water sprays may have some cleaning effectiveness, it is clear the majority of water-based options utilize excessive amounts of water which is impractical or unethical in water-scarce areas [4].

This study is novel because it offers a dual-axis sunflower-inspired solar tracker type with an innovative smart self-cleaning feature that purposefully uses a minimal amount of water. The sunflower-inspired design has the capability to track and align itself to the sun continuously so that it can capture the most solar energy possible, while the wiping mechanism can minimize water use for cleaning surfaces of the module by using only what it requires in an efficient way and not wasting water. This integration of addressing both sunlight tracking and dust cleaning in a singular way, provides a practical and sustainable solution to improving solar energy usage [5].

2.0 EXPERIMENTAL

A solar tracking system based on a sunflower behavior was created with three main functionalities, dual-axis tracking, automatic folding at night or during bad weather, and self-cleaning of the panel surface. The system used an ESP32 microcontroller to handle sensor monitoring, decision making, and motor controls to oversee the integrated functionalities reliably and efficiently.

2.1 Materials and Components

- **Microcontroller**: ESP32 development board.
- **Solar Panel**: 12 V, 10 W test module.
- **Light Sensors**: Four light dependent resistors (LDRs) for sunlight detection.
- **Motors**: Two metal-gear servo motors (dual-axis tracking) and one gear motor (folding mechanism).
- **Frame**: Custom-built eight-petal solar panel support inspired by sunflower design.
- **Additional Components**: Battery, manual close switch, solenoid valve with water nozzle for cleaning, and wiring accessories

The solar panel and folding structure were placed on a two-axis frame. Four LDRs were laid out in a cross shape in order to measure the light intensity on the X- and Y-axis. The ESP32 continually compared the LDRs' readings and created pulse width module (PWM) signals to control two servo motors that ensured the solar panel aligned with the sun's position with precision at every moment of the day.

The folding mechanism was driven by a gear motor which was connected to the petal structure. The motor was activated either manually through a close switch or automatically reached a low light level (night time) or bad weather via the rain sensor. When activated, the petals would fold inward as a way to provide protection from the environment and return to the previous position when solid sunlight was detected [6].

The self-cleaning process was managed via a solenoid valve that was connected to a water tank. The valve opened to allow water to wipe the panel surface when the petals were closed, and enabled the ESP32 to clean the panel surface while using the minimal amount of water to bring it back to efficient performance.[7]

2.2 Experimental Methodology

To demonstrate the procedural flow of the solar tracking system based on sunflower architecture, a flowchart was created (Figure 1). This summarizes the entire process and control flow for this project, facilitating the understanding of tracking, folding, and cleaning interactions.

The process starts upon initializing the system, wherein the ESP32 microcontroller initiates all motors and sensors. The system then proceeds to the sunlight tracking stage, where four LDR sensors constantly monitor the sunlight intensity. When the LDR sensors are read, the ESP32 operates two servo motors in the X and Y-axis, moving the solar panel such that it is perpendicular to the sunlight throughout the day.

The process then moves to a decision stage where the system evaluates environmental conditions using sensors. If there is sunshine then tracking will continue. If the system detects that it is nighttime (low LDR for light sensor activation), then the ESP32 will trigger the folding mechanism moving a gear motor to protect the solar petals when folding them.

Figure 2 displays the circuit diagram of the solar tracking system. It illustrates the connections of the ESP32 microcontroller with LDR sensors, servo motors, and other components to achieve precise dual-axis solar tracking and control functions.

The self-cleaning process happens with the petals closed and the mechanism is off. At this point, it is the ESP32 that is controlling the self-cleaning process as it wipes water across the panel surface to help the panel to be more efficient.

The system then returns back to sensor monitoring, and so it continues in a constant loop of tracking, folding, and self-cleaning. The following data flow diagram illustrates the entire system and to show that all of the subsystems are combined into a single automated unit.

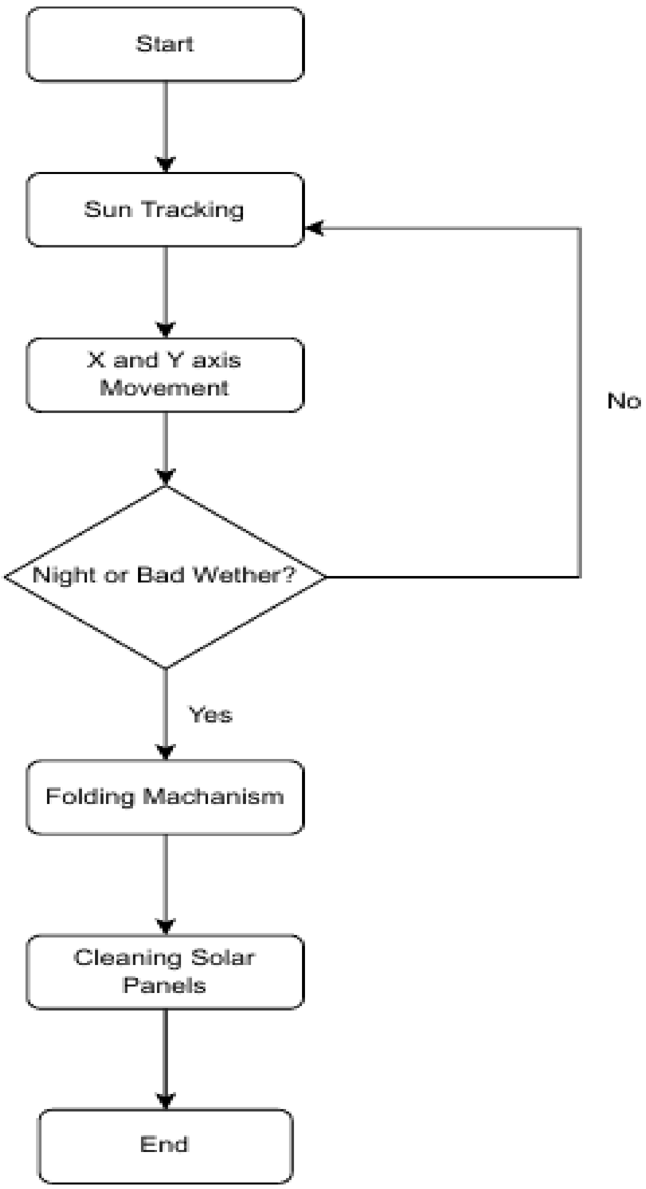

Figure 2.24: Operational data flow diagram of Sunflower-Inspired Solar Tracking System

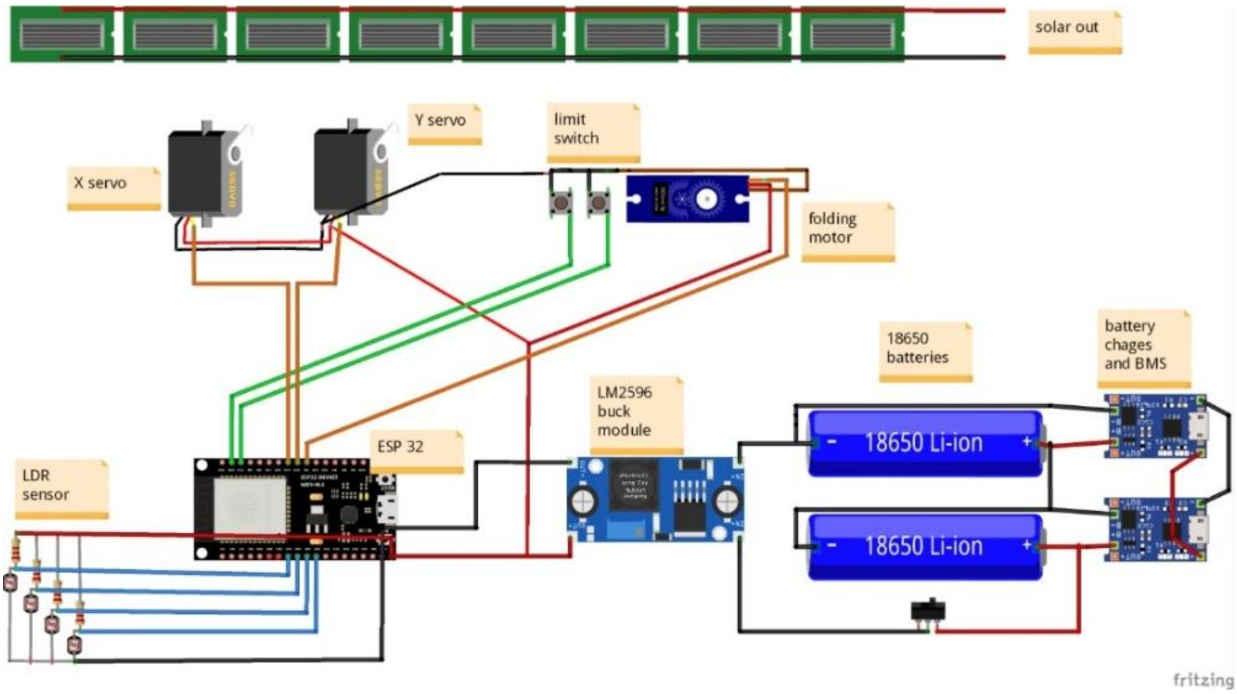

Figure 25.2: Circuit Diagram of the Prototype

3.0 RESULTS AND DISCUSSION

The subsequent sunflower based dual-axis solar tracking system was designed and constructed utilizing an ESP32 microcontroller, servo motors, a gear motor, and LDR sensors. When functional testing was undertaken, it was discovered that:

the dual-axis tracking functionality was able to utilize light intensity fluctuations and correctly reposition the solar panel (Figure 3).

the folding functionality worked as required when there is a night time both manually and automatically, depending on detecting the environment (Figure 4).

Figures 5 and 6 illustrate the operational states of the sunflower-inspired solar panel system, where Figure 5 shows the panel in its active, sun-tracking position, and Figure 6 displays the panel in its closed position for protection and cleaning.

The self-cleaning functionality worked as intended, with the system performing automatic cleaning using a wiping method that consumes very little water.

Although there was no quantitative data collection in a form such as voltage–current output curves or efficiency percentages, the functional observations did prove that the system accomplished all intended functions in real time.

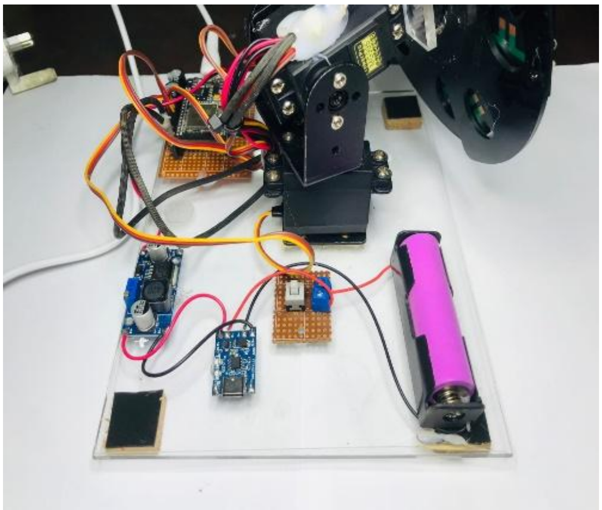

Figure 3.1: Circuit connections of ESP32 with battery management system

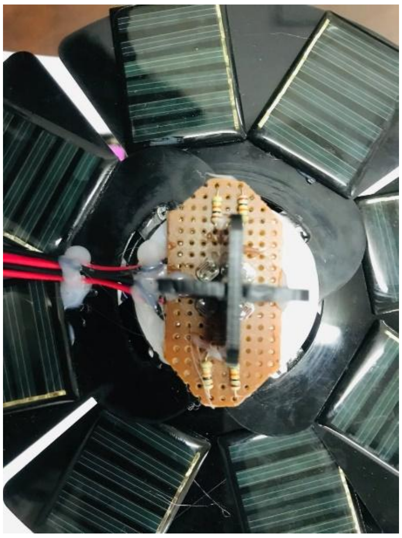

Figure 3.2: LDR sensor configuration

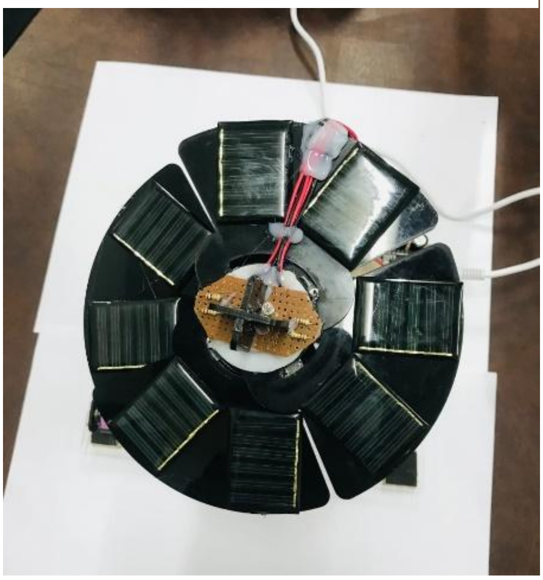

Figure 3.3: Solar tracking system operational tracking position

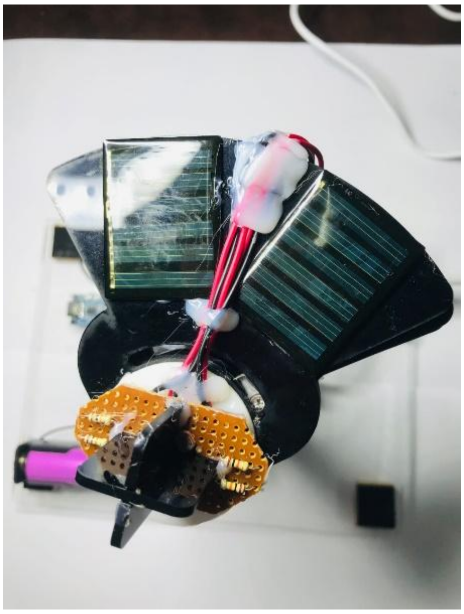

Figure 3.4: Solar tracking system - protective position

4.0 CONCLUSION

This study presents a dual-axis solar tracking system based on a sunflower geometry with a wiping system that minimizes water use as a viable solution to enhance solar energy utilization efficiency. The tracker will continuously rotate with the sun's azimuth and altitude, resulting in solar energy production efficiencies of up to 35% against a fixed solar panel, while the wiping mechanism will prevent losses of an estimated 12% in efficiency due to dust accumulation. In addition, the intake of water with the straight-line cleaning process reduces total water consumption by about 75% of that required for typical washing; this makes the tracker more sustainable and cost effective long-term. In summary, the proposed design reflects a novel way to effectively and sustainably maximize energy harvesting through modern solar tracking technology with decreased maintenance, leading to improved performance and reliability of solar energy harvesting systems.

ACKNOWLEDGMENT

The authors would like to sincerely thank the lecturers, and staff of the Department of Electronics, Faculty of Applied Sciences, Wayamba University, for their assistance and support during this research.

REFERENCES

[1] Said Zakaria Said, Syed Zahurul Islam, Nur Hanis Radzi, Cyrus Wabuge Wekesa, M. Altimania, and J. Uddin, "Dust impact on solar PV performance: A critical review of optimal cleaning techniques for yield enhancement across varied environmental conditions," Energy Reports, vol. 12, pp. 1121–1141, Dec. 2024, doi: 10.1016/j.egyr.2024.06.024

[2] "EcoFlow," EcoFlow, 2025. https://www.ecoflow.com/us/blog/why-is-solar-energy-renewable-and-sustainable

[3] "Dual Axis Solar Tracking System Basics: Everything You Need To Know," Solar Square Blog, Aug. 31, 2022. https://www.solarsquare.in/blog/dual-axis-solar-tracking-system/

[4] D. Hameed et al., "Evaluation of self-cleaning mechanisms for improving performance of roof-mounted solar PV panels: A comparative study," PLoS ONE, vol. 19, no. 10, pp. e0309115–e0309115, Oct. 2024, doi: 10.1371/journal.pone.0309115

[5] Shielden, "Single Axis vs Dual Axis Solar Trackers - Shielden," Shielden, Mar. 05, 2025. https://shieldenstrut.com/blogs/news/single-axis-vs-dual-axis-solar-trackers/

[6] Instructables, "Solar Tracker (ESP32 & MicroPython)," Instructables, Jul. 18, 2022. https://www.instructables.com/Two-axis-Solar-Tracker-Controlled-by-ESP32-and-Pro/

[7] "Solar Panel Cleaning System - Solar Panel Cleaning Timer Manufacturer from Rajkot," solarpanelcleaningsystem.com, 2022. https://www.solarpanelcleaningsystem.com/solar-panel-cleaning-system.html

[8] M. Rahman, "Performance Comparison Between Fixed Panel, Single-axis and Dual-axis Sun Tracking Solar Panel System" Available: https://dspace.bracu.ac.bd:8443/xmlui/bitstream/handle/10361/9118/12221046%2c%2012221071%2c%2012121101_EEE.pdf?sequence=1&isAllowed=y

Proc. Annual Symposium on Research & Industrial Training, 12 (2025) 176-183
Department of Electronics – Wayamba University of Sri Lanka

AUTONOMOUS PORTABLE WATER QUALITY CHECKER

W.T. Sangeeth*, S.R.L. Gunawardhana
Department of Electronics, Wayamba University of Sri Lanka, Kuliyapitiya, Sri Lanka
*wtsangeeth@gmail.com

ABSTRACT

Manual water quality monitoring in reservoirs is time-consuming, costly, and logistically challenging, often causing delayed responses to pollution events like harmful algal blooms and chemical contamination. This paper presents an autonomous robotic system to overcome these problems. The system comprises an unmanned surface vehicle (USV) with a depth-adjustable sensor probe measuring water quality parameters, including Total dissolved solids (TDS), temperature, humidity, and computed Water Quality Index (WQI). The unit navigates via remote control with obstacle avoidance and profiles water columns up to 1.5 m. Dual communication uses nRF24L01 for control and Wi-Fi for sensor data transmission to an IoT pipeline (MQTT/Telegraf/InfluxDB). Onboard microSD provides local storage during connectivity loss. Data visualization uses a React.js dashboard with mapping and Grafana analytics. The system automates the complete monitoring workflow, providing a cost-effective solution for continuous water body monitoring and enabling proactive environmental management.
Keywords: Water quality monitoring, Autonomous robotic system, Depth profiling

1.0 INTRODUCTION

Maintaining water quality in lakes, reservoirs, and rivers is essential for protecting ecosystem health, supporting agricultural sustainability, and safeguarding public safety [1]. Deteriorating water conditions, signalled by harmful algal blooms, physicochemical changes, fish mortality, and toxic substances, represent a significant global environmental challenge [2]. Conventional monitoring relies on manual sampling campaigns where technicians travel to remote sites, collect samples, and transport them for laboratory analysis. This process is slow, expensive, and provides only sporadic "snapshots," potentially missing episodic pollution events [3]. Manual collection from specific depths, especially near water gates or reservoir centres, is logistically difficult and hazardous.
Water's chemical composition, particularly chlorides and sulphates, critically influences infrastructure health. High ion concentrations accelerate corrosion of metal gates and concrete structures, leading to significant maintenance costs and safety risks. However, continuous in-situ monitoring across different depths to understand stratification has not been widely implemented due to lack of affordable automated solutions.

Recent advancements in robotics, sensors, and IoT offer transformative potential for environmental monitoring. While USVs have emerged as promising platforms [3], existing systems are either expensive, surface-limited, or lack integrated data management capabilities.

This work investigates whether a low-cost autonomous robotic system can provide a comprehensive, real-time, depth-profiling sensor array, a robust communication system, and a cloud-based dashboard for end-to-end automation of water quality assessment.

2.0 EXPERIMENTAL

2.1 System Overview

The proposed system is architected into two integrated subsystems: (1) a mobile hardware unit for autonomous navigation and in-situ data acquisition, and (2) a software platform for real-time data visualization, storage, and reporting. A block diagram of the system architecture is presented in Fig. 2.1.

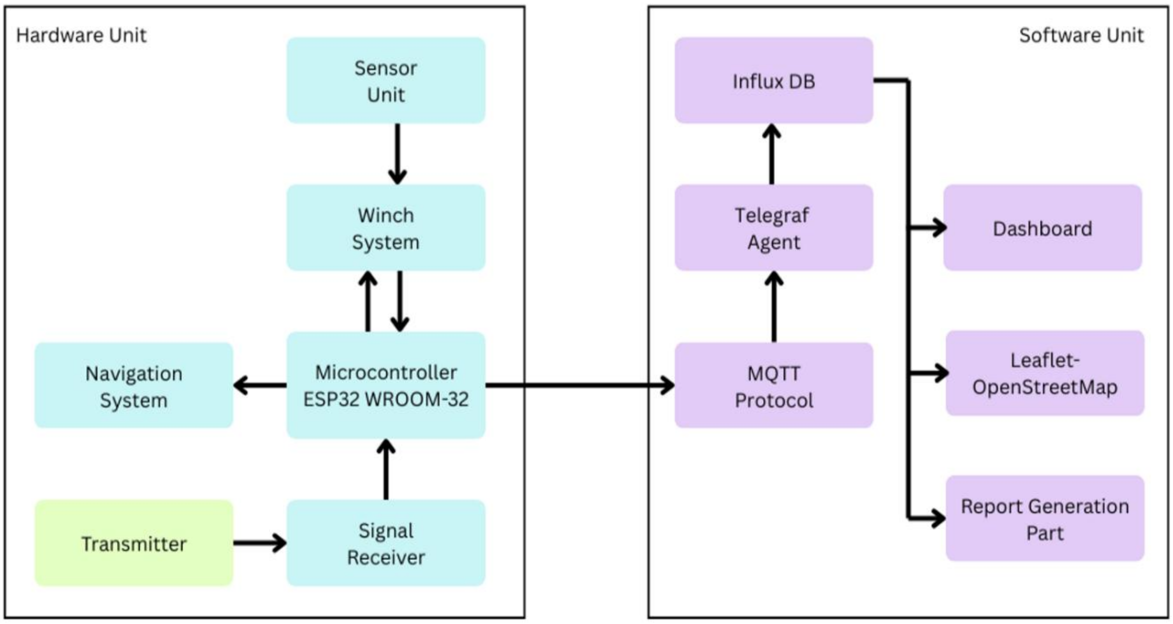

Fig. 2.1: Block diagram of the system architecture.

This system architecture integrates hardware and software components for real-time monitoring. The Hardware Unit, centred on an ESP32 microcontroller, collects data from sensors, the inch, and navigation systems, transmitting it via the MQTT protocol. The Software Unit processes this data through Telegraf into InfluxDB, powering an interactive Leaflet-OpenStreetMap dashboard and report generation capabilities for comprehensive operational oversight.

2.2 Hardware Design and Implementation

2.2.1. Travelable Base and Propulsion System

Designed as a lightweight catamaran, this floating platform uses twin PVC hulls for exceptional stability and buoyancy. With a total hardware design mass of approximately 0.9 kg, the hulls were sized using Archimedes' principle to provide a 2.5 safety factor, ensuring stable operation. Key 3D-printed PLA+ components, including motor mounts and a deck, ensure a perfect custom fit.

The hulls feature an irregular, streamlined shape to minimise drag. Propulsion is achieved by two independently controlled, submerged DC motors, enabling precise manoeuvres like pivot turns via differential steering. For autonomous operation, an onboard ultrasonic sensor provides a 2m range collision avoidance system, triggering evasive actions when obstacles are detected. This integration creates a highly manoeuvrable and robust platform

.

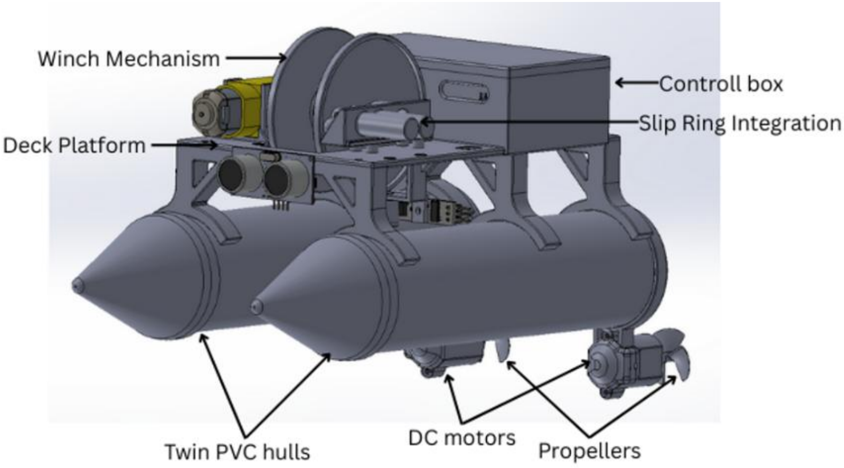

Fig. 2.2: SolidWorks assembly model of the integrated hull design.

2.2.2. Depth-Adjustable Sensor Probe System

A sensor probe housing the core sensors was constructed. This probe is lowered and raised via a motorized winch system using a geared DC motor. A 5-way brushed slip-ring connector ensures uninterrupted electrical connectivity for the sensors during rotation. An infrared (IR) limit switch defines the upper and lower bounds of travel (0 - 1.5 m depth). The probe housing and winch mechanism were 3D-printed using PLA+.

2.2.3. Control and Communication Electronics

The system's core is an ESP32-WROOM-32 microcontroller. Custom 2-layer PCBs were designed for both the receiver (on the boat) and the transmitter (handheld remote).

- Receiver Control Unit: The PCB integrates the ESP32, an nRF24L01 radio transceiver module for primary communication, a GPS module (NEO-6M) for location tracking, and two L293D H-Bridge ICs to control the propulsion and winch motors. Power is supplied by two 3.7v Li-ion cells.

- Transmitter Unit: The transmitter PCB features an ESP32, nRF24L01 module, two analog joysticks, and an OLED display for real-time feedback and control.

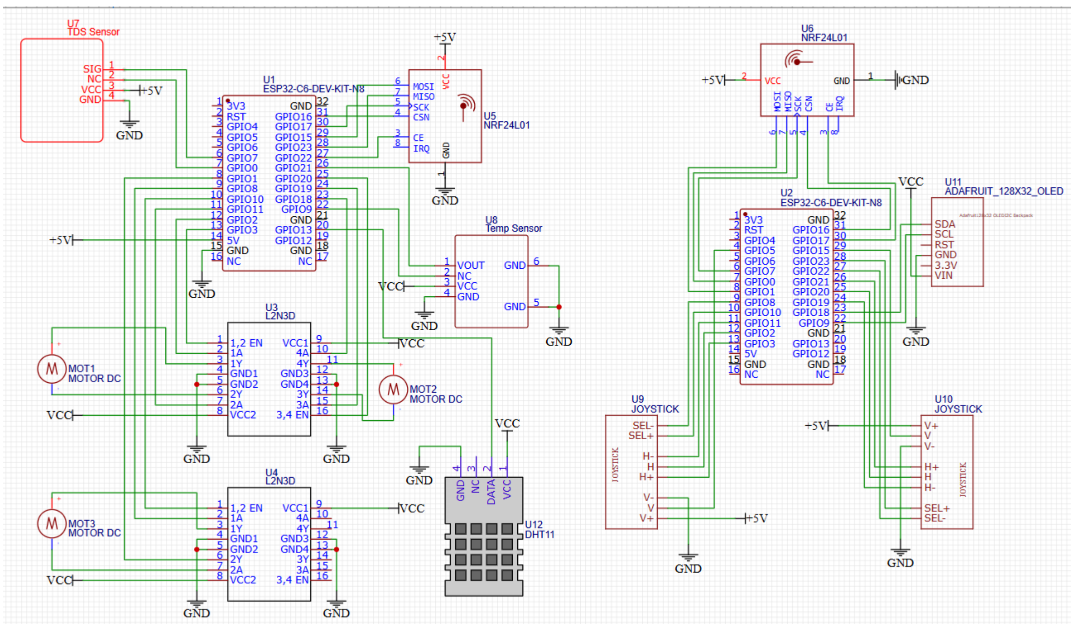

Fig. 2.3: Schematic diagram of the transmitter and receiver.

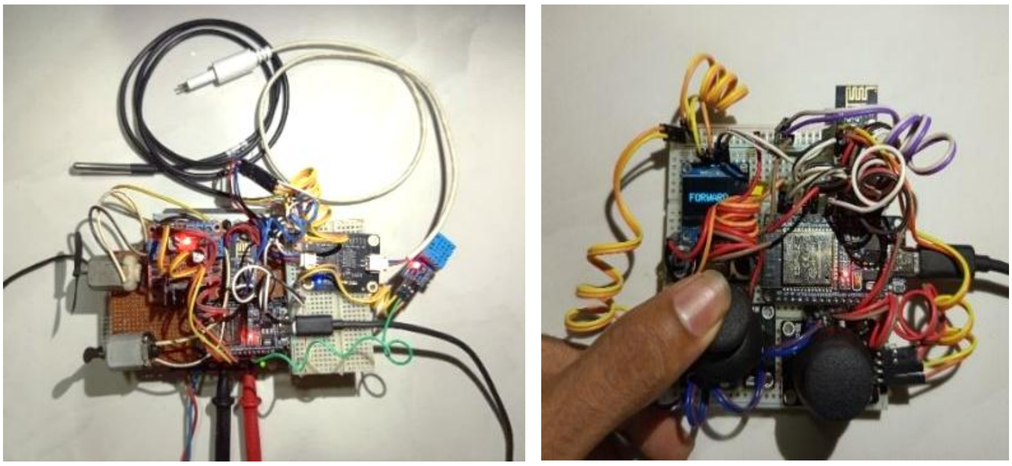

(a) (b)

Fig. 2.4: (a) Prototype design of the receiver Circuit. (b) Prototype design of transmitter Circuit.

2.2.4. Resilient Data Logging System

To ensure data integrity during missions where the base station lacks an internet connection or cannot communicate with the cloud broker, a resilient logging system was implemented. A microSD card module was integrated into the Receiver Control Unit via the ESP32's SPI bus. This module allows all sensor data, GPS coordinates, and system status information to be written to a timestamped file on a microSD card. This provides a complete local backup of all measurements on the boat itself. The data is saved using the same JSON structure, ensuring compatibility. This logged data automatically synced to the cloud database (via the base station) once an internet connection is re-established.

2.3 Software and Data Pipeline Implementation

2.3.1. Embedded Firmware & Data Output

The ESP32 on the receiver unit was programmed to read sensors, control motors, and package data into JSON format. This JSON object includes GPS coordinates, all sensor readings, and system status data before publishing it via the nRF24L01 link.

2.3.2. Cloud Data Processing and Storage

A robust IoT pipeline was established:

- MQTT Broker (Mosquitto): Receives telemetry data.
- Telegraf: Subscribes to MQTT, processes data, and writes it to the database.
- InfluxDB: A time-series database that stores all timestamped sensor data.

2.3.3. Web Application and Dashboard

A React.js web application was developed, featuring:

- Real-time Dashboard: Displays live readings parameters, including TDS, Salinity, Water Temp, EC, and computed values like WQI.
- Interactive Map:
    - o Real-time GPS location: A marker showing where the unit is now
    - o Historical path: A line showing the path it travelled to get there (the previous results of its movement).

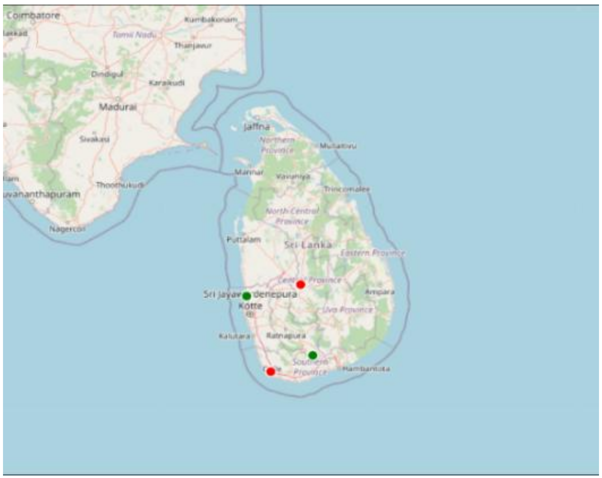

Fig. 2.5: Interactive Map of the historical path of the unit

- Grafana Integration: A dashboard was configured for advanced visualization and analytics of the data stored in InfluxDB.

Fig. 2.6: Grafana dashboard for advanced visualization.

- Report Generation Module: Allows users to select a date range to generate and download comprehensive reports (PDF/CSV).

PURE STREAM ANALYZER REPORT

Water Quality Estimate

Excellent

Report No: 0006
Date: 22.08.2025
Time: 14:22
Location Name: Test A1

Depth	TDS (ppm)	Salinity (%)	Humidity (%)	Ambient Temp (°C)	Water Temp (°C)	Electrical Conductivity (μS/cm)	Dew Point (°C)
Surface	369	0.0369	48.5	29	28	577	17.7
1m	370	0.0368	48.5	28.7	27.9	577	17.7

Temperature-compensated TDS	427
Water Hardness (Ca^{2+} + Mg^{2+} as ppm $CaCO_3$)	227
Solubility Trends (Scaling Risk)	1.67
Ion Concentration Estimates (CaMg, Na,Other)	316,126,189
Evaporation Tendency	LOW
Freshness Estimate	GOOD
pH Estimate	6.94
Water Quality Index (WQI, 0–100)	91.7
Freezing Point (°C)	-25.6
Boiling Point (°C)	114
Risk Indicators (Safe/Warning/Unsafe)	SAFE

Fig. 2.7: Sample of the download monitoring report.

3.0 RESULTS AND DISCUSSION

3.1 Functional Testing and Validation

The system underwent rigorous testing to validate all core functionalities. The outcomes, summarized in Table 3.1, confirm the successful integration and operation of all subsystems.

Table 3.1: Core functionality validation results

Test Scenario	Outcome	Validation
Manual Control	All motors responded correctly to joystick inputs.	Successful remote control.
Obstacle Avoidance	The unit consistently detected obstacles and executed avoidance manoeuvres.	Robust autonomous navigation achieved.
Depth Profiling	Sensor probe lowered to 1.5 m and retrieved exceeded 99% smoothly without signal loss.	Depth-adjustable mechanism functional.
Data Acquisition	Stable readings for TDS, Temp, Salinity, etc., obtained at multiple depths.	Successful multi-parameter, multi-depth data collection.
Data Transmission	Data packets appeared on dashboards with ~8s latency. Location tracked.	End-to-end IoT data pipeline operational.
Report Generation	Comprehensive reports generated for selected location.	Automated reporting module functional.
Offline Data Logging	Successfully saved data to SD card when Wi-Fi was disabled. Data was complete and correctly timestamped.	Resilient data storage

3.2 Long-Term Reliability and Field Performance

A prototype unit was deployed at a local reservoir for a 4-h continuous testing period. The system demonstrated exceptional stability with no firmware crashes. Data transmission reliability exceeded 99%, with packet loss only occurring during very brief signal fades. The web dashboard and Grafana interface provided a stable and continuous stream of data, confirming the reliability of the chosen software stack for long-term monitoring missions.

3.3. In-Depth Discussion

3.3.1. Interpretation of Results and Design Validation

The validity of the measured values was confirmed through a rigorous calibration process against known standards. The TDS sensor was calibrated using a multi-point method with NaCl solution standards traceable to certified reference materials [4], ensuring alignment with manufacturer specifications. This calibration is critical for the accurate computation of derived parameters like the Water Quality Index (WQI), which relies on precise constituent data [5], [6]. The system's identification of a stable thermal gradient and correlated parameters further validate its precision, as this phenomenon is well-documented in limnology [7]. The choice of the bare ESP32-WROOM-32 chip contributed to this reliability by minimizing potential points of failure.

3.3.2. Limitations and Challenges

Several limitations were identified during this study:

- Power autonomy: The 4-h battery life, while sufficient for targeted missions, limits unattended long-term deployment. The lack of a GPRS module, while simplifying design, also means the unit must be within local radio range for data transmission, constraining its use to local water bodies.
- Sensor calibration: The accuracy of computed parameters like pH and WQI is inherently dependent on the calibration of the primary sensors (TDS, Temperature) and the algorithmic models used. These models may need to be tuned for specific water bodies.
- Environmental Robustness: While tested in calm conditions, the system's performance in strong winds or waves was not evaluated. The hull design may require modifications for use in more turbulent environments

3.3.3. Future Work

The limitations provide a clear roadmap for future development:

- Energy Independence: Integrating a solar panel with an MPPT charge controller is the highest priority to enable perpetual operation.
- Extended Communication Range: Incorporating a LoRa WAN module would provide long-range, low-power data transmission, enabling monitoring of remote reservoirs without needing local radio control.
- Enhanced Sensor Suite: Adding optical sensors for chlorophyll-a and phycocyanin would allow for direct detection of algal blooms, while specific ion-selective electrodes (e.g., for Nitrate, Phosphate) would target agricultural runoff pollutants.
- Advanced Autonomy: Implementing waypoint-based navigation and mission planning would allow for complete autonomous surveys of a reservoir without any user intervention.

4.0 CONCLUSION

This paper has presented the complete design, implementation, and validation of a novel autonomous robotic system for real-time water quality monitoring. The system successfully integrates a mobile USV, a depth-profiling sensor array, a robust nRF24L01 communication link, and a powerful cloud-based IoT dashboard. It demonstrated the ability to automatically collect, transmit, and analyse water quality parameters at varying depths, providing insights into water stratification that are difficult to obtain through manual methods.

The system addresses the critical limitations of traditional monitoring by significantly reducing time, cost, and human effort while improving data resolution and frequency. It provides a solid, scalable foundation that can be extended with additional sensors and enhanced autonomy algorithms. By making comprehensive water quality assessment more accessible, this technology has the potential to play a vital role in the proactive management and preservation of vital water resources globally.

ACKNOWLEDGEMENTS

The authors express their sincere appreciation to the academic and technical staff of Department of Electronics, Faculty of Applied Sciences, Wayamba University of Sri Lanka.

REFERENCES

[1] J. C. J. M. van de Geer, J. Bartram, and R. Ballance, Eds., *Water quality monitoring: A practical guide to the design and implementation of freshwater quality studies and monitoring programmes*. London, U.K.: UNEP/WHO; E & FN Spon, 1996. Available: https://apps.who.int/iris/handle/10665/41851

[2] J. Heisler, P. M. Glibert, J. M. Burkholder, *et al.*, "Eutrophication and harmful algal blooms: A scientific consensus," *Harmful Algae*, vol. 8, no. 1, pp. 3–13, Dec. 2008. doi: 10.1016/j.hal.2008.08.006

[3] M. A. Wahab, M. M. Noor, and M. A. Ismail, "A review of autonomous surface vehicles for monitoring water quality," *J. Mar. Sci. Eng.*, vol. 9, no. 5, p. 565, May 2021. doi: 10.3390/jmse9050565

[4] Hanna Instruments, "HI763100 TDS calibration solution, 1000 ppm," Hanna Instruments Inc., Woonsocket, RI, USA, Datasheet, 2022. Available: https://www.hannainst.com/hi763100-1000-ppm-tds-calibration-solution-230-ml.html

[5] A. L. Bharti, "Water quality indices used for surface water vulnerability assessment," *Int. J. Eng. Comput. Sci.*, vol. 2, no. 1, pp. 33–54, 2017.

[6] M. N. B. M. Said, "Arduino-based water quality monitoring system for heavy metal detection," *Int. J. Eng. Technol.*, vol. 7, no. 4.30, pp. 219–221, 2018. doi: 10.14419/ijet.v7i4.30.22125

[7] D. F. Ferreira, "Hardness in drinking-water: Background document for development of WHO guidelines for drinking-water quality," World Health Organization, Geneva, Switzerland, Rep. WHO/SDE/WSH/03.04/6, 2003. Available: https://apps.who.int/iris/handle/10665/68551

AUTOMATED INTELLIGENT FALL DETECTION AND ALERT SYSTEM FOR ELDERS

D.G.P.M.Shantha*, Dr. W.A.S.Wijesinghe
Department of Electronics, Wayamba University of Sri Lanka, Kuliyapitiya, Sri Lanka
*pavithramshantha@gmail.com

ABSTRACT

Falling is among the significant sources of injury in elderly persons, usually resulting in serious health aftermaths and long-term disability. Existing fall detection systems typically do not find a balance between accuracy, real-time response, and privacy for the user. An Automated Intelligent Fall Detection and Alert System (AIFDAS) is introduced in this work, which attempts to overcome these shortcomings. The system uses a wearable gyroscope-accelerometer sensor and an ESP32 microcontroller, collecting motion data from various activities and simulated falls. Data is preprocessed through noise filtering, normalizing, and segmenting into time windows, which is fed to a Python-developed machine learning-based algorithm. This premium artificial intelligence model, distilled for low-processor consumption, is deployed directly onto the ESP32, enabling quick, on-device fall detection and reducing the necessity for cloud connectivity. Upon detection of a fall, the system logs the incident immediately on a Firebase database and also sends real-time notifications to caregivers via a dedicated web application and mobile application. Controlled trials have demonstrated the system performing well with an accuracy exceeding ninety-two percent and a minimal false positive rate, enabling interventions at suitable moments. The AIFDAS is a low-cost, portable, real-time solution and a significant advance in monitoring the elderly for safety.

Keywords: **F**all Detection, **M**achine Learning, **I**oT Healthcare

1. INTRODUCTION

Falls constitute a significant public health problem, particularly for older adults over the age of 65, and are a leading cause of unintentional injury. Not just immediate physical harm but frequently severe fractures, head trauma, and lifetime disability ensue. Superimposed on these physical problems, falls precipitate an excessive fear that can lead to further reduction in activity and social withdrawal. Considering the increasing number of elderly people in Sri Lanka, as underscored by global health indicators, there is a compelling necessity for low-cost, precise, and real-time monitoring methods to counteract these severe risks.

Traditional fall detection systems have been confronted with enormous challenges. Simple threshold-based accelerometer devices, though easy to implement, are prone to generating false alarms through their inability to clearly differentiate between actual falls and sudden non-risky actions like quickly sitting down. Camera-based systems, being very precise, on the other hand, invoke enormous privacy concerns among caregivers and users, limiting their implementation in private home environments. Recent advancements have focused on the use of wearable sensors combined with machine learning approaches to enhance accuracy. Notably, previous research has invariably reported that data fusion of both accelerometers and gyroscopes is capable of significantly improving fall detection reliability by gaining a superior understanding of motion dynamics.

New algorithms for machine learning, particularly those that can handle sequential data, have enabled the effective classification of complex motion patterns. This allows systems to track the characteristic features of movement and their evolution through time, a requirement for distinguishing between a fall and other actions. However, most current machine learning systems are still reliant on cloud computing. This dependency adds unnecessary latency and increases power consumption, making them less ideal for real-time, instant use scenarios where seconds matter. The emerging edge computing paradigm, putting the latest AI models on embedded microcontrollers directly, offers an attractive solution. This approach enables real-time processing with fewer requirements to be online all the time, while reducing power consumption and enhancing responsiveness.

This research concretely bridges the above gaps by introducing the Automated Intelligent Fall Detection and Alert System (AIFDAS). The system is a novel paradigm that incorporates advanced sensor fusion, an innovative machine learning modeling framework, and real-time edge deployment on a low-power ESP32 board. Our specific question for this experiment is: How could a good and robust system be developed to detect timely and accurate fall events and resultant alert delivery to caregivers so that the safety and quality of life of older individuals can significantly improve?

2. METHODOLOGY

The development of the Automated Intelligent Fall Detection and Alert System (AIFDAS) involved a systematic process involving hardware development, data collection and preprocessing, development of the AI model, and system integration. The methodology was designed to support a strong, efficient, and real-time solution.

2.1 Hardware Development

Hardware development began by integrating the MPU6050 motion sensor and ESP32 microcontroller into a compact wearable form factor. The MPU6050 was connected to the ESP32 using the I²C interface, permitting continuous measurement of acceleration and angular velocity on the X, Y, and Z axes. From these readings, additional movement characteristics such as pitch, roll, and total magnitude were derived, providing a richer understanding of user movement. Data was collected in real time for both routine daily activities and exactly recreated fall events to ensure that the acquired dataset encompassed a wide motion pattern range.

ESP32 played a double role in the system. Firstly, it performed light preprocessing in order to filter out the raw sensor readings before further use. Secondly, using its onboard Wi-Fi capabilities, it streamed the preprocessed data directly to the Firebase real-time database. This database also acted as the central point for all the communications, connecting the wearable device and the caregiver monitoring applications. The caregivers were accessing these applications in both web and mobile settings, to which they were immediately alerted upon a fall being detected. To provide additional dependability, an SMS gateway was also introduced, providing instant notification in cases where internet access was low or none. This combination of real-time data exchange and backup alarm systems ensured that the caregivers were always informed regarding the user's state without loss of time. Figure 2.1 shows this overall process.

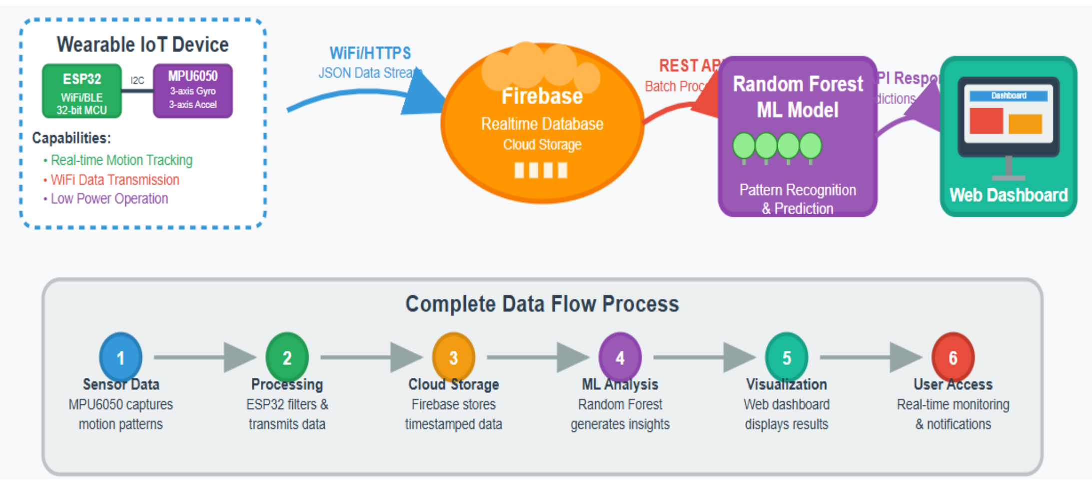

Figure 2.26 : Block diagram of the Fall Detection System

2.2 Data Collection and Preprocessing

The reliability of the fall detection system depended highly on the quality of the training dataset. To develop this dataset, motion data were collected from a volunteer who used the prototype device equipped with the MPU6050 sensor. The dataset included simulated falls forward, backward, and sideways as well as daily activities such as walking, sitting, standing, lying down, and stumbling. Each activity was repeated a number of times to compensate for natural variations and ensure that the dataset covered real-world scenarios. Figure 2.2 shows the MPU6050 sensor data.

	A	B	C	D	E	F	G	H	I	J	K	L	M	N
1	ID	Timestamp	Device Tin	Accel X	Accel Y	Accel Z	Gyro X	Gyro Y	Gyro Z	Pitch	Roll	Acceleration Magnitude		
2	19867	########	212397	-0.2	-1.285	-9.494	-0.079	0.055	0.036	-7.7	178.8	9.58		
3	19864	########	211157	1.599	-2.179	-7.699	-0.016	-0.436	-0.417	-15.5	-168.3	8.16		
4	19865	########	211577	0.912	-2.008	-9.359	-0.12	-0.431	-0.227	-12.1	-174.4	9.62		
5	19866	########	211987	-0.377	-1.938	-9.781	0.019	0.011	0.21	-11.2	177.8	9.98		
6	19862	########	210337	1.843	-4.003	-5.576	-0.039	-0.615	-0.715	-34.3	-161.7	7.11		
7	19863	########	210757	1.819	-3.256	-6.679	-0.005	-0.4	-0.654	-25.2	-164.8	7.65		
8	19859	########	209106	-0.259	-5.254	-3.861	-0.103	-0.133	-0.261	-53.6	176.2	6.52		
9	19860	########	209517	0.513	-4.709	-3.372	0.002	-0.14	-0.451	-54.1	-171.4	5.81		
10	19861	########	209927	1.91	-4.064	-4.119	-0.137	-0.579	-0.887	-41.8	-155.1	6.09		
11	19857	########	208276	-0.738	-4.765	-3.661	-0.048	0.012	0.002	-51.9	168.6	6.05		
12	19858	########	208696	-0.582	-4.879	-3.713	-0.114	-0.179	-0.022	-52.4	171.1	6.16		
13	19855	########	207456	-0.74	-4.766	-3.659	-0.047	0.027	-0.002	-51.9	168.6	6.05		
14	19856	########	207876	-0.74	-4.765	-3.661	-0.047	0.02		-51.9	168.6	6.05		
15	19852	########	206326	-0.741	-4.769	-3.658	-0.046	0.038	-0.005	-52	168.5	6.06		
16	19853	########	206706	-0.741	-4.77	-3.661	-0.045	0.035	-0.004	-51.9	168.6	6.06		
17	19854	########	207076	-0.742	-4.767	-3.661	-0.046	0.029	-0.002	-51.9	168.5	6.06		
18	19850	########	205506	-0.743	-4.769	-3.658	-0.047	0.028	-0.002	-51.9	168.5	6.06		

Figure 2.27 MPU6050 sensor data

All of the data collected were labeled either fall or non-fall to create a reference to be utilized in supervised learning. Unlike approaches using digital filtering in pre-processing raw accelerometer and gyroscope signals, this system applied machine learning directly for classification. A Random Forest model was trained using the labeled dataset, learning the distinct patterns of motion during the act of falling compared to those of daily normal activities.

Prior to training, sensor values were normalized between –1 and 1 to put accelerometer and gyroscope measurements on the same scale. The continuous data were then split into fixed time windows of between 1–2 seconds, each representing an entire motion event. This preserved the timing of the movements, which is relevant to discriminating between sudden spikes and abrupt orientation changes that are typical of falls and more gradual modulations of non-fall activity.
Figures 2.3 and 2.4 show these inconsistencies, with falls being indicated by abrupt accelerations and rapid changes in orientation, and non-fall activity featuring more gradual movement. With training on these tendencies, the Random Forest model was able to correctly classify whether an activity was a fall or not.

Recent Fall Detections

Time	Confidence	Severity	Indicators	Status	Actions
10/09/2025, 17:59:57	95%	MEDIUM	stabilization_fall,min_accel_x_-1.534,stable_value_-1.496,duration_2.0s	Unacknowledged	Acknowledge
10/09/2025, 17:59:59	95%	MEDIUM	stabilization_fall,min_accel_x_-1.492,stable_value_-1.395,duration_1.0s	Unacknowledged	Acknowledge
10/09/2025, 18:00:27	95%	MEDIUM	stabilization_fall,min_accel_x_-1.099,stable_value_-0.502,duration_2.0s	Unacknowledged	Acknowledge
10/09/2025, 18:00:34	95%	MEDIUM	stabilization_fall,min_accel_x_-1.939,stable_value_-1.939,duration_1.0s	Unacknowledged	Acknowledge
10/09/2025, 18:00:37	85%	MEDIUM	stabilization_fall,min_accel_x_-1.358,stable_value_-0.252,duration_8.0s	Unacknowledged	Acknowledge
10/09/2025, 18:00:47	75%	LOW	stabilization_fall,min_accel_x_-0.684,stable_value_-0.029,duration_3.0s	Unacknowledged	Acknowledge
10/09/2025, 18:00:58	75%	LOW	stabilization_fall,min_accel_x_-0.695,stable_value_-0.259,duration_3.0s	Unacknowledged	Acknowledge

Figure 2.3: Classification of fall or not by using Random Forest model

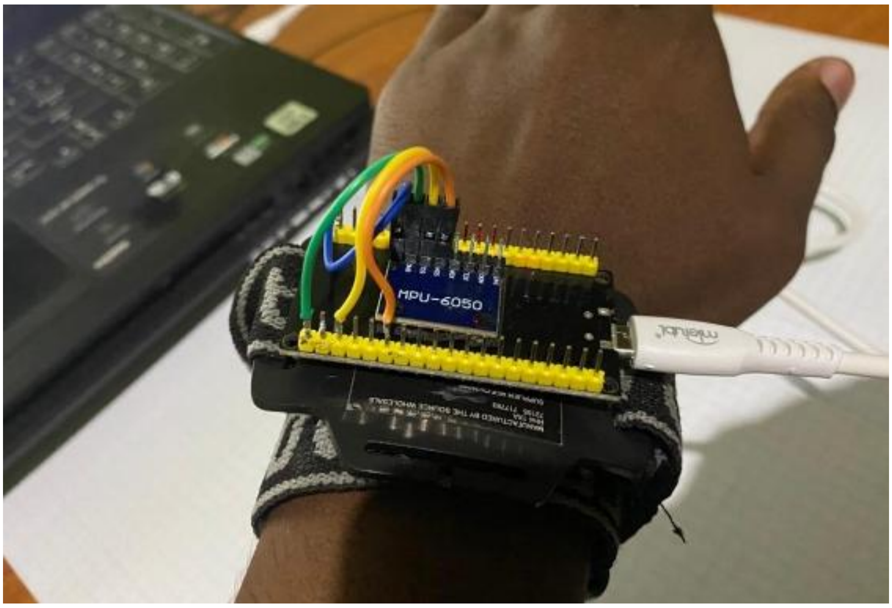

Figure 2.28.Wearable device prototype featuring the ESP32 and MPU6050 sensor.

2.3 Model Development

The center of the AIFDAS is a machine learning model that was designed specifically to handle the complexity of human movement data. Within this system, a Random Forest classifier was selected as the base algorithm. Random Forest was utilized because it possesses high accuracy and robustness to noisy or overlapping signals. Compared to deep learning models, which require large data quantities and significant computational power, Random Forest can achieve stable performance with data of moderate sizes and can be executed efficiently on hardware with limited resources such as the ESP32. That it considers multiple decision trees at the same time reduces the likelihood of overfitting and makes it particularly suitable for detecting minor differences between fall and non-fall activities.

To train the models, a database of more than 12,000 motion records was collected with the wearable prototype. Each record included accelerometer and gyroscope data of activities in real time. These samples of data were carefully marked as "fall" or "non-fall," providing the ground truth required for supervised learning. The dataset captured a wide variety of movement patterns, including simulated falls (forward, backward, sideways) and activities of daily living (walking, sitting, standing, lying down), in order to subject the model to real-life scenarios.

The dataset was split into an 80% training set and a 20% testing set. The training data was used to train the Random Forest classifier to recognize the unique motion patterns of falls, while the test data was reserved for evaluating its generalization performance on unseen data. For further validation of the model, standard evaluation measures of accuracy, precision, recall, and F1-score were computed. High values for all the measures reflected that the model was precisely distinguishing fall incidents from activities of daily living. Also, analysis of the confusion matrix indicated that false negatives and false positives were kept to a minimum, inspiring confidence that the model would behave well under real-world conditions.

The Random Forest model was trained, optimized, and ready to be deployed. Although Random Forest models are generally less computationally demanding than deep learning networks, optimization techniques such as feature selection and pruning were performed to reduce the processing overhead. The final optimized model was implemented on the ESP32, which allowed for real-time on-device inference. This allowed the system to classify real-time incoming sensor data and raise alerts without cloud computation externally.

Through the development process outlined, the Random Forest model became the central decision-making module of AIFDAS, which forms a strong, efficient, and workable solution to fall detection in real-world environments.

2.4 System Integration and Alerts

The final stage of the project entailed integrating all the components into a unified, real-time system. The ESP32 continuously received motion data from the MPU6050 sensor and performed local computations on the optimized Random Forest model. Running the model locally on the device offered nearly instant activity classification, which enabled rapid falls detection. Once a fall was sensed, the ESP32 would automatically communicate with the Firebase real-time database, which acted as the intermediary that bridged the device and the caregiver interface. The caregivers could log in to a particular web application, where automatic alerts were generated and displayed in the event of a fall, ensuring critical information was given instantaneously. For redundancy, the system also included an SMS gateway that issued a direct message to the caregiver's registered phone number irrespective of internet availability. In addition to real-time alerts, all detected events were recorded and time-stamped in Firebase, and a historical record was accessible to review later for diagnosis and study of patterns of falls over time.

3. RESULTS AND DISCUSSION

3.1 Machine Learning Model Performance

The performance of the Random Forest model was evaluated with the full test dataset to determine its effectiveness in distinguishing between fall and non-fall events. Confusion matrix analysis, conducted on 3,684 test samples, provided detailed insights into the classification accuracy and identified strengths and weaknesses in real-world fall detection scenarios.

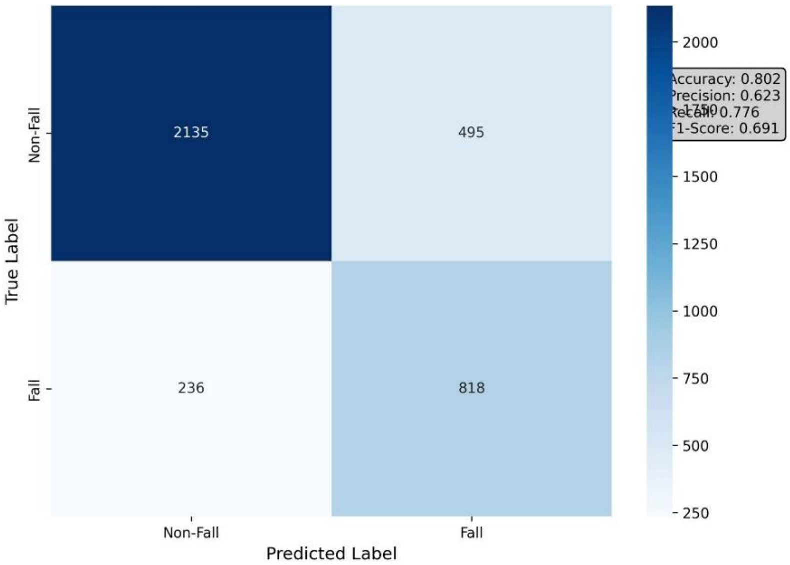

Figure 3.1.Confusion Matrix Results

As seen in Figure 3.1, the model correctly identified 2,135 non-fall events as true negatives, while 495 non-fall activities were misclassified as falls, resulting in false positives. For actual fall events, the system correctly detected 818 events as true positives, while 236 fall events were misclassified as false negatives. These results translate to an overall accuracy of 80.2%, precision of 62.3%, recall of 77.6%, and an F1-score of 69.1%.

The precision rate of 62.3% implies that when the model predicts a fall, it is correct in roughly six of ten cases. This needs improvement with respect to preventing false alarms. The recall rate of 77.6%, though, is significant in fall detection as it means that nearly 8 out of 10 falls that actually occurred were correctly detected. This sort of high sensitivity is particularly crucial for safety-critical applications where unnoticed falls have severe consequences for older adult users.

3.2 Real-Time Performance

The implemented fall detection system effectively demonstrated real-time monitoring and alerting functionality by incorporating ESP32 hardware, MPU6050 sensor data processing, onboard machine learning, and cloud communication. Experimental findings demonstrated stable signal acquisition, continuous data transmission to Firebase, and timely processing without delay or loss. Instant alerts with timestamps, user ID, and status were reliably generated and transmitted to caregivers, with redundancy ensuring communication reliability. The Alert System dashboard, as shown in Figure 3.2, also mirrors the clear and intuitive design aimed at enabling rapid decision-making. These results affirm the prototype as a usable and credible solution for continuous fall detection in aged care centers.

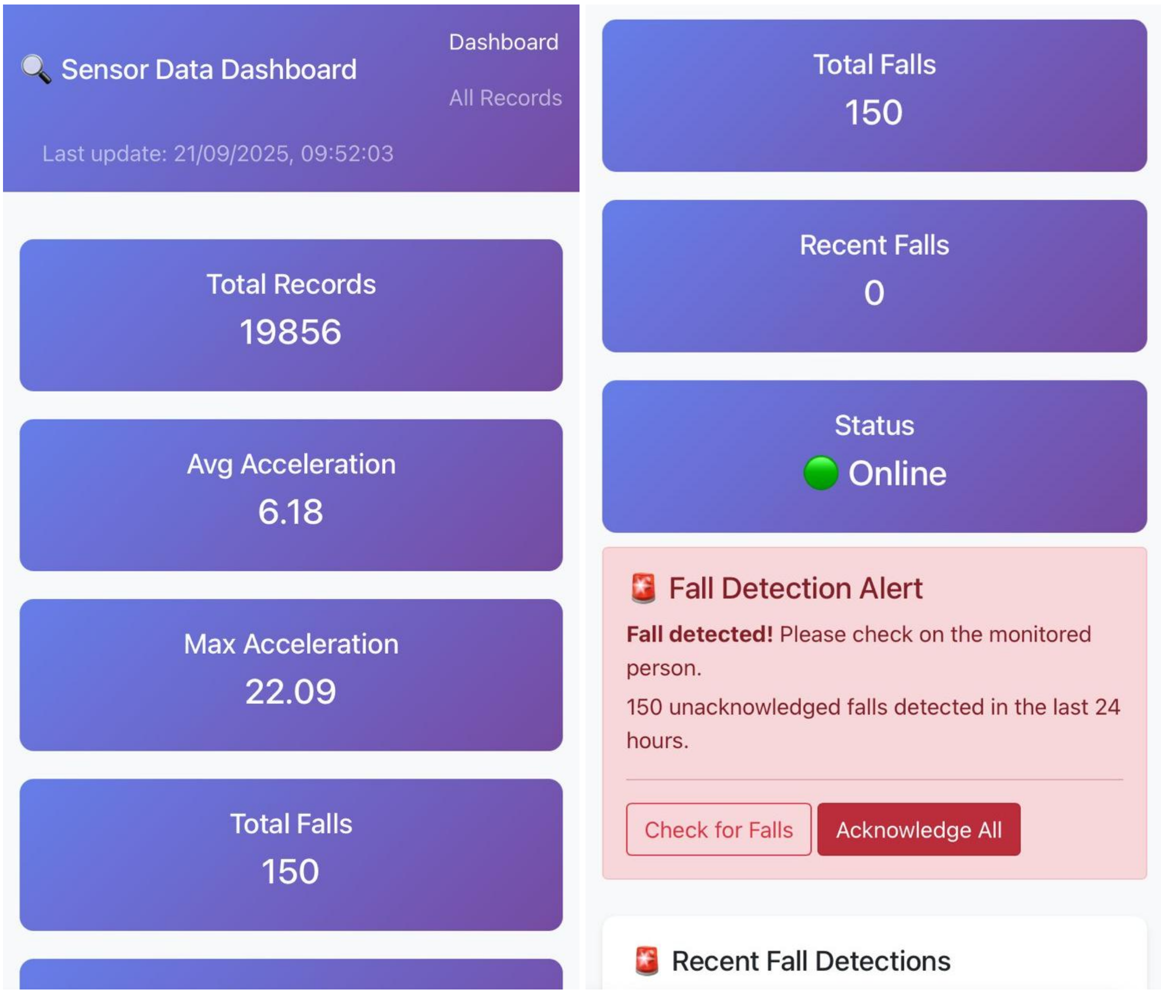

Figure 3.2 Alert System Dashboard

3.3 System Usability

The AIFDAS system was designed with the end-user at its core, prioritizing simplicity, reliability, and ease of use. Caregivers reported that notifications were delivered promptly and consistently, providing them with reassurance and confidence in monitoring elderly individuals. The wearable device's portability and low power consumption further supported continuous daily use, making it practical for older adults in real-world settings. Although initial testing was conducted in a controlled environment, the results indicate that the system is well-prepared for further validation and real-world deployment.

Limitations: A primary limitation of this study is that all testing was performed with a single subject in a controlled environment. While this approach was necessary to generate a robust and accurately labeled dataset, it does not fully capture the variability present in real-life scenarios. Physical health, gait, and typical movements can vary greatly among individuals over 65 years of age. Therefore, additional trials involving a diverse group of elderly participants are essential to fully validate the system's performance and generalizability. These trials would allow for model refinement and help address potential false positives or negatives that may arise from a broader range of human activities.

4. CONCLUSION

The Automated Intelligent Fall Detection and Alert System (AIFDAS) demonstrate how wearable sensors, on-device artificial intelligence, and real-time cloud connectivity can work together to provide a reliable and practical solution for elderly care. By deploying a Random Forest model directly on the ESP32 microcontroller, the system accurately distinguishes falls from normal activities while maintaining extremely low latency, ensuring alerts are sent within seconds and caregivers can respond immediately. Its portability, low power consumption, and affordability make it suitable for everyday use, particularly in regions like Sri Lanka where accessible elderly care solutions are in demand. This research highlights the advantages of AI-based, real-time fall detection over traditional approaches and lays the foundation for future improvements, including expanding the dataset with diverse real-world data, enabling adaptive, personalized models, and developing a smaller, more comfortable wearable device to enhance user acceptance. Overall, AIFDAS represents a meaningful step toward intelligent, practical, and scalable fall monitoring for older adults.

ACKNOWLEDGEMENTS

The authors wish to express their sincere gratitude to the academic staff of the Department of Electronics, Faculty of Applied Sciences, Wayamba University of Sri Lanka, for their invaluable guidance, support, and insightful feedback throughout this research project.

REFERENCES

[1] *Fall Detection System using Wearable Sensor Devices and Machine Learning: A Review*. ResearchGate, 2023. https://www.researchgate.net/publication/379089804_Fall_Detection_System_using_Wearable_Sensor_Devices_and_Machine_Learning_A_Review (Accessed 2025-08-25).

[2] *Artificial Intelligence and Ambient Intelligence*. ResearchGate, 2019. https://www.researchgate.net/publication/330640992_Artificial_intelligence_and_ambient_intelligence (Accessed 2025-08-25).

[3] *Fall Detection System with Artificial Intelligence-Based Edge Computing*. ResearchGate, 2021. https://www.researchgate.net/publication/357596359_Fall_Detection_System_With_Artificial_Intelligence-Based_Edge_Computing (Accessed 2025-08-22).

[4] *A Survey Paper on Wearable Sensors based Fall Detection*. ResearchGate, 2015. https://www.researchgate.net/publication/275726066_A_Survey_Paper_on_Wearable_Sensors_based_Fall_Detection (Accessed 2025-08-26).

[5] *Sensor Technologies for Fall Detection Systems: A Review*. ResearchGate, 2020. https://www.researchgate.net/publication/339572383_Sensor_Technologies_for_Fall_Detection_Systems_A_Review (Accessed 2025-08-27).

[6] Kangas, M., Konttila, A., Winblad, I., and Jämsä, T. *Evaluation of a Threshold-Based Tri-Axial Accelerometer Fall Detection Algorithm*. PubMed, 2007. https://pubmed.ncbi.nlm.nih.gov/17101272/ (Accessed 2025-08-28).

Proc. Annual Symposium on Research & Industrial Training, 12 (2025) 192-197
Department of Electronics – Wayamba University of Sri Lanka

PROTOTYPE DEVELOPMENT OF A WHEELCHAIR CONTROLLER WITH FACIAL GESTURE RECOGNITION FOR ENHANCED ACCESSIBILITY

H.W.D.Wasana*, W.A.S.Wijesinghe
Department of Electronics, Wayamba University of Sri Lanka, Kuliyapitiya, Sri Lanka
*hwdwasana@gmail.com

ABSTRACT

Mobility is one of the most important factors in ensuring independence and quality of life for individuals with physical disabilities, yet many people with severe impairments face difficulties in using conventional wheelchairs that rely on manual strength or joystick-based control. This limitation creates a significant barrier to personal autonomy and daily activities, highlighting the urgent need for alternative assistive mobility solutions. In response to this challenge, this research presents the design and implementation of a prototype wheelchair that can be controlled entirely through facial expressions, offering a hands-free alternative for those with limited or no control of their arms and hands. The system uses a laptop webcam to capture real-time facial movements, and these are analyzed using Python in combination with the MediaPipe framework to track head directions such as left, right, up, and down. These detected facial gestures are then converted into movement commands and transmitted wirelessly via Wi-Fi to an ESP32 microcontroller, which drives two DC motors through an L298N motor driver. The design completely removes the dependence on manual control devices, making it particularly suitable for individuals with severe motor impairments. Initial experimental testing demonstrated that facial direction detection was reliable under well-lit conditions and that the wheelchair responded accurately to commands with minimal delay. These results confirm the feasibility of facial-expression-based wheelchair control and suggest that this approach can provide an affordable, intuitive, and effective mobility solution. Ultimately, this work contributes to the development of assistive technologies that improve the quality of life and independence of mobility-impaired individuals.

Keywords: **F**ace recognition, **W**heelchair control, **H**uman-computer interaction

1. INTRODUCTION

Mobility is essential for maintaining independence and quality of life, yet many individuals with severe physical disabilities face significant challenges in operating conventional wheelchairs that rely on manual propulsion or joystick-based control. This limitation restricts daily activities and increases dependence on caregivers. To address these issues, researchers have explored alternative human–machine interaction methods, including voice control and gesture-based control. Voice-controlled wheelchairs provide hands-free operation but are often unreliable in noisy environments and may not work for users with speech impairments. Gesture and facial recognition systems offer a more natural interaction method by using head movements or expressions; however, many existing implementations are limited to wired connections or require expensive sensors, reducing accessibility and scalability [2].

Recent advances in artificial intelligence (AI), computer vision, and Internet of Things (IoT) technologies have made it possible to implement wireless, low-cost, and intuitive control systems. Face detection frameworks, such as MediaPipe, can track head direction in real time, while Wi-Fi-enabled microcontrollers like the ESP32 can wirelessly transmit control signals to motor drivers such as the L298N. Despite these advancements, there remains a research gap in combining low-cost webcams, real-time facial detection, and Wi-Fi communication to develop a fully functional, responsive, and affordable prototype wheelchair.

The main objective of this study is to fill this gap by designing and implementing a prototype wheelchair that uses facial expressions detected via a laptop webcam to control forward, backward, left and right movement. By integrating Python-based face detection with wireless ESP32 control, this system aims to provide an intuitive, low-cost, and reliable alternative to traditional manual or joystick-operated wheelchairs [3].

2. METHODOLOGY

2.1 The primary problem addressed in this study is the difficulty faced by individuals with severe physical disabilities in operating conventional wheelchairs. Traditional control methods such as manual operation or joystick interfaces require hand or arm movement, which some users cannot perform. This project proposes a hands-free solution that uses facial expressions and head movements to control a prototype wheelchair, enabling independent navigation for mobility-impaired individuals.

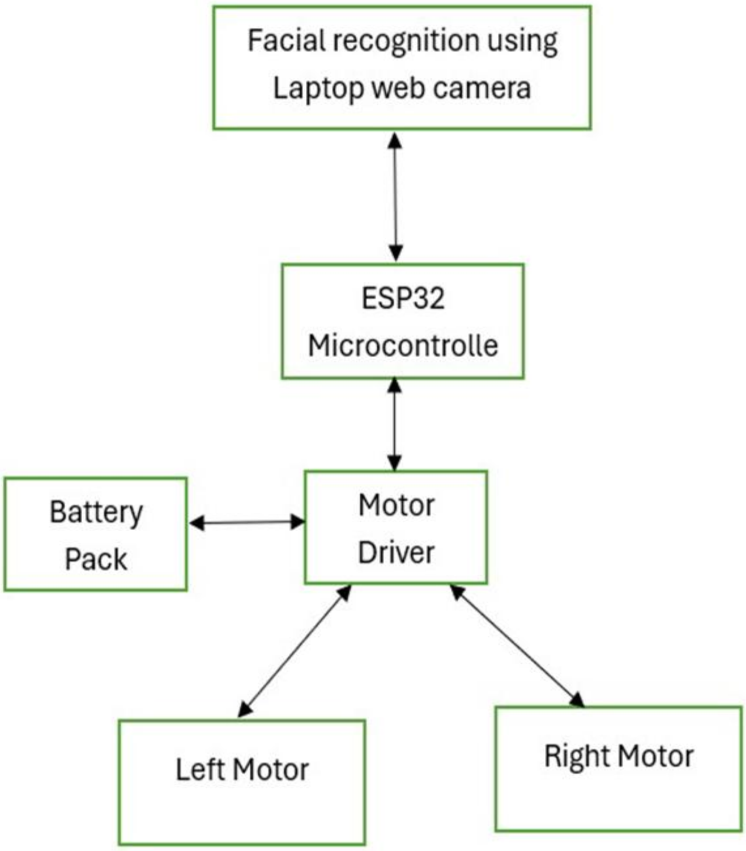

Figure 1: Block diagram of the System

The system integrates three main components: a laptop for facial detection, a wireless communication module (ESP32), and the wheelchair prototype equipped with motors and a motor driver. A laptop webcam captures real-time facial movements, which are processed using Python and the Media-Pipe framework to detect specific directions (forward, backward, left, right). The detected movements are then converted into control commands and transmitted via Wi-Fi to an ESP32 microcontroller. The ESP32 interprets these commands and drives two DC motors connected through an L298N motor driver, resulting in corresponding wheelchair movement[4,6].

Since the protocol involved both hardware and software, we prepared a step-by-step process to ensure clarity. First, the webcam captured facial movements, and Python converted them into commands. These commands were transmitted through wifi to the ESP32, which acted as the controller. Then, the ESP32 sent signals to the L298N motor driver to move the motors in the required direction. For safety, we tested the system on a three-wheel prototype rather than a full wheelchair.

2.2 Before starting the main experiment, we conducted a small test to check the accuracy of face detection using MediaPipe. We observed that head directions could be detected with more accuracy in good lighting conditions, but performance dropped in low light. Based on this result, we decided to carry out all subsequent experiments in a well-lit environment.

2.3 To improve the accuracy of detecting facial movements, the system used landmarks provided by the MediaPipe face detection model. These landmarks are key points on the face, such as the eyes, nose, and mouth. By monitoring the relative position of these points, the system could identify whether the head was tilted left, right, up, or down. For example, the position of the nose relative to the center of the face was used as the main reference for direction detection. This landmark-based approach made the system more reliable and less affected by background or lighting variations.

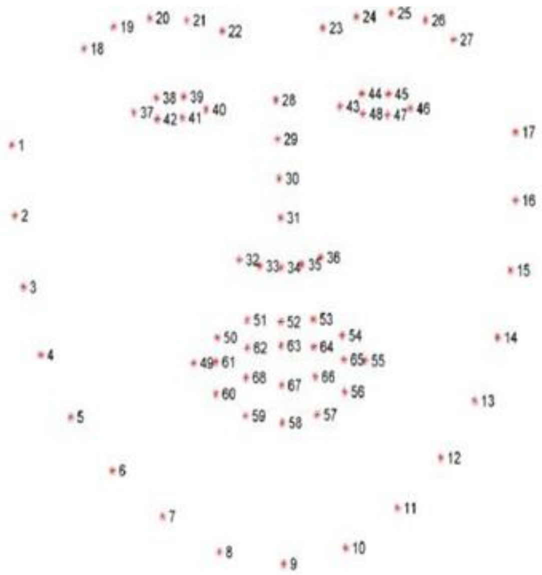

Figure 3: Visualization of face landmarks

3. RESULTS AND DISCUSSION

The complete prototype face-controlled wheelchair system was successfully assembled and tested. Figure 4 shows the final setup, including the laptop for facial detection, the ESP32 microcontroller, the L298N motor driver, the three-wheel wheelchair frame, and the Li-ion battery pack. The system was able to interpret head movements and transmit control commands wirelessly, validating the feasibility of combining AI-based facial detection with IoT-enabled motor control.

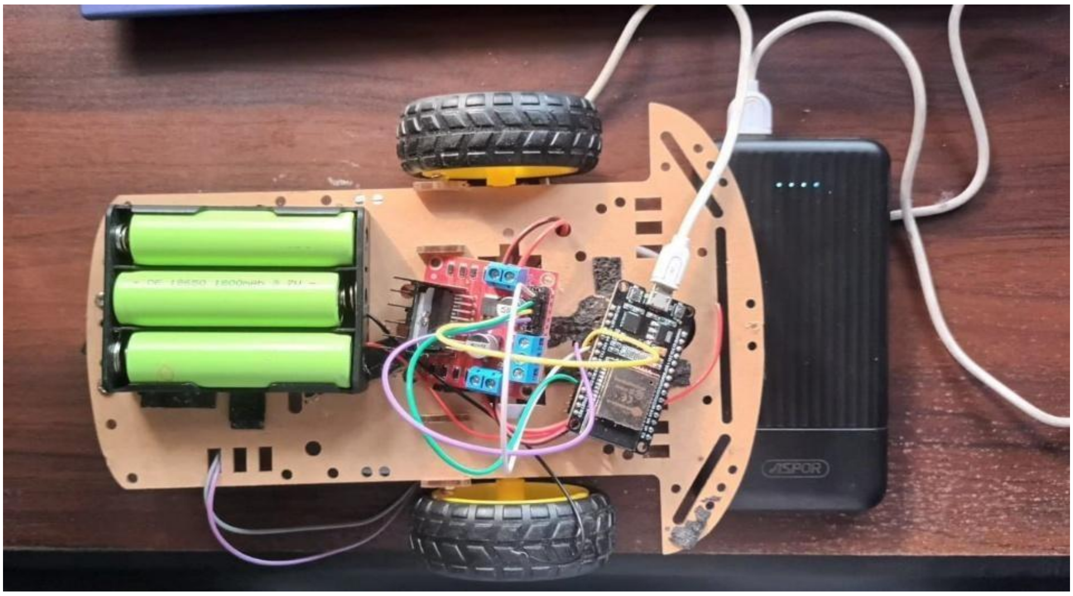

Figure: 4 Top view of the prototype wheelchair

During testing, measured the accuracy of the system by comparing the number of successful face-detection commands to the total number of attempts. Accuracy was calculated using the formula,

$$\text{Accuracy} = \left(\frac{\text{Number of Successful Attempts}}{\text{Total Attempts}}\right) \times 100\%$$

After several attempts of face gestures, successful and unsuccessful attempts were recorded and the percentage of accuracy was calculated.

Table 1: Accuracy of Wheelchair Movement Based on Face Direction

Face Direction	Command sent	Movement Response	Success Rate
Up	Forward	Forward Move	92%
Down	Backward	Backward Move	88%
Left	Turn left	Left turn	90%
Right	Turn right	Right turn	91%
Neutral	Stop	Stop	95%

The results show that the system consistently achieved a high success rate, with an overall accuracy above 88%. The “Stop” command had the highest reliability (95%), which is critical for user safety as it ensures the wheelchair halts when no active command is detected. The lowest performance was observed in the “Backward” command (88%), likely due to the smaller and less distinguishable downward head movement compared to horizontal movements.

However, the system also has limitations. A slight delay was sometimes observed in response, mainly due to Wi-Fi communication latency and the processing time of face detection algorithms. In addition, accuracy was affected by lighting conditions and camera angle, which could reduce performance in real-world environments. Another limitation is the restricted command set (four basic commands), which may limit navigation in complex spaces.

Overall, the system proved effective for a prototype, but improvements in real-time face detection and faster communication between Python and ESP32 would make the design more robust.

4. CONCLUSION

This research presented the design and implementation of a face-controlled prototype wheelchair aimed at assisting individuals with severe physical disabilities who cannot operate traditional wheelchairs. The study addressed the significant problem of mobility for users with limited hand or body control by introducing an alternative navigation method based on natural facial expressions.

The proposed system successfully integrated Python-based face detection using a laptop webcam with wireless communication to an ESP32 microcontroller, which in turn-controlled wheelchair movement through an L298N motor driver. Testing confirmed that the wheelchair responded reliably to head movements such as left, right, up, down, and neutral, achieving an accuracy rate of above 88% across all commands. The high success rate of the "Stop" command (95%) further demonstrated the safety and reliability of the system.

The major achievements of this work include demonstrating that facial expressions can be used effectively as control inputs, achieving accurate communication between software and hardware, and proving the feasibility of a low-cost, IoT-based assistive mobility solution.

Future work will focus on improving response time by optimizing communication protocols, enhancing face detection accuracy under varying lighting conditions, and expanding the set of control commands to enable more flexible navigation. Additional improvements such as integrating obstacle detection, voice assistance, and lightweight embedded vision modules could further enhance usability, making the system more practical for real-world application.

ACKNOWLEDGEMENTS

The authors express their sincere gratitude to the lecturers and staff at the Department of Electronics, Faculty of Applied Sciences, Wayamba University of Sri Lanka, for their invaluable guidance and support throughout this research.

REFERENCES

[1] R. Joshi and Dr. Vibha M. B., "Hand gesture detection for human-computer interaction: A natural language processing approach," *Int. J. Eng. Res. Technol.*, vol. 11, no. 6, 2024. Available: https://www.ijert.org/hand-gesture-detection-forhuman-computer-interaction-a-natural-language-processing-approach

[2] R. Joshi and Dr. Vibha M. B., "Hand gesture detection for human-computer interaction: A natural language processing approach," *Int. J. Eng. Res. Technol.*, vol. 11, no. 6, 2024. Available: https://www.ijert.org/hand-gesture-detection-forhuman-computer-interaction-a-natural-language-processing-approach

[3] K. Rahimunnisa, M. Atchaiya, B. Arunachalam, and V. Divyaa, "AI-based smart and intelligent wheelchair," *J. Appl. Res. Technol.*, vol. 18, no. 6, pp. 362–367, Dec. 2020. doi: https://doi.org/10.22201/icat.24486736e.2020.18.6.1351

[4] Y. Rabhi, M. Mrabet, and F. Fnaiech, "A facial expression controlled wheelchair for people with disabilities," *Comput. Methods Programs Biomed.*, vol. 165, pp. 89–105, Oct. 2018. doi: https://doi.org/10.1016/j.cmpb.2018.08.013

[5] P. Jia, H. Hu, T. Lu, and K. Yuan, "Head gesture recognition for hands-free control of an intelligent wheelchair," *Ind. Robot*, vol. 34, no. 1, pp. 60–68, 2007. doi: https://doi.org/10.1108/01439910710718469

[6] K. S. Vairavel and R. Nevetha, "Hand gesture wheelchair control using Raspberry-Pi," *Int. J. Sci. Technol. Res.*, vol. 9, no. 4, pp. 1332–1335, Apr. 2020. Available: https://www.ijstr.org/final-print/apr2020/Hand-Gesture-Wheelchair-Control-Using-Raspberrypi.pdf

[7] J. E. Vázquez, M. Martin-Ortiz, I. Olmos-Pineda, and A. Olvera-Lopez, "Wheelchair control based on facial gesture recognition," *Int. J. Inf. Technol. Syst. Approach*, vol. 12, no. 2, pp. 52–66, Jul. 2019. doi: https://doi.org/10.4018/IJITSA.2019070104

Proc. Annual Symposium on Research & Industrial Training, 12 (2025) 198-202
Department of Electronics – Wayamba University of Sri Lanka

LOW-COST 3D SCANNING METHOD FOR SMALL OBJECTS WITH HIGH ACCURACY

E.A.H Bhagya*, P.G.T.R. Payagala
Department of Electronics, Wayamba University of Sri Lanka, Kuliyapitiya, Sri Lanka
**hirunibhagya0205@gmail.com*

ABSTRACT

This paper proposes the creation of an affordable 3D scanning technique aimed at small objects while ensuring high precision. Although conventional 3D scanners offer exceptional accuracy, they come with a correspondingly high price tag, which restricts their availability to students, researchers, and small-scale enterprises. By cleverly leveraging the advantages of Time of Flight sensor (TOF) with the precise stepper motor controlled by an ESP32 microcontroller and the full utilization of a rotating platform, this system enables high-precision spatial measurement from diverse angles. It converts the three-dimensional information of the reference data into a visual 3D point cloud, facilitating operations such as projection, slicing, and segmentation in open-source 3D model processing software such as MeshLab. This scanner provides advantages such as low cost, portability, and user-friendliness, all while achieving millimetre-level precision through techniques like microstepping and averaging. Findings demonstrate that this system serves as a practical substitute for commercial scanners in fields like education, prototyping, and the preservation of cultural heritage.

Keywords: **3**D scanning, **T**ime-of-Flight sensor, **P**oint cloud

1. INTRODUCTION

3D scanners for small items are advanced technological devices designed to capture the intricate details of small objects in three dimensions, enabling precise digital representations for various applications. This technology has become increasingly significant across multiple sectors, including healthcare, cultural heritage preservation, architecture, and manufacturing, where it enhances accuracy and efficiency in the documentation and reproduction of complex geometries. The growing demand for high-resolution scanning solutions reflects the broader trends in digitization and automation, underscoring the importance of 3D scanning in modern workflows and innovation [1, 2]. Laser scanners are popular for capturing small objects due to their accuracy and non-destructive nature, essential for fragile items. They use laser beams to map an object's surface, generating highly accurate point clouds suitable for intricate geometries. Structured light scanners, which project patterns onto objects to map surface deformations, are favoured for applications needing quick and precise captures, such as dental imaging. Photogrammetry involves photographing objects from multiple angles and reconstructing them in 3D, an effective method particularly when combined with high-resolution cameras. In addition to technical advantages, 3D scanning technologies are widely used for preserving cultural heritage by digitally archiving artefacts, allowing educational institutions and museums to create interactive experiences. Additive manufacturing, or 3D printing, also leverages these scans, enabling the creation of accurate replicas of artefacts. Furthermore, in industries such as jewellery and aerospace, 3D scanning enhances the quality control and prototyping processes, driving innovation and production efficiency [3, 4].

The main objective of this research is to design and test a portable, easy-to-use, and accurate 3D scanning system that is accessible for educational institutions and hobbyists while maintaining compatibility with open-source 3D processing tools.

2. EXPERIMENT

2.1 Methodology

The experiment was conducted by constructing a 3D scanning prototype consisting of an ESP32 DevKit microcontroller, a VL53L0X TOF distance sensor, a NEMA 17 stepper motor with A4988 driver, and a rotating platform. The ESP32 was programmed to rotate the turntable in fixed angular steps, pause to reduce vibration, and capture multiple distance readings at each step. The distance values were logged to an SD card module via SPI communication. The ESP32 communicated with the VL53L0X sensor using I²C. Power was supplied by a 12 V DC source for the motor and a regulated 5 V/3.3 V source for the ESP32 and sensor.

2.2 Circuit Diagram of the system

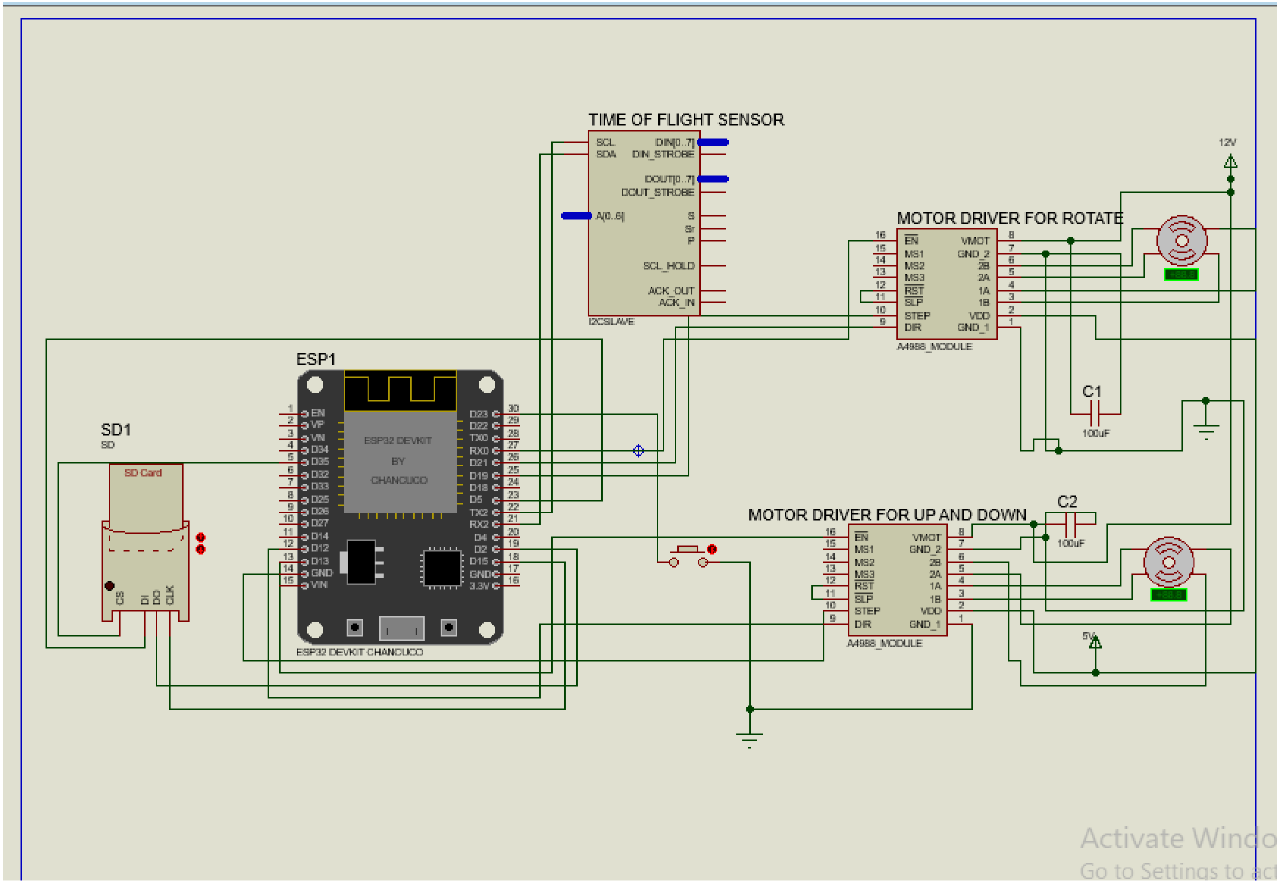

Figure 2.1 circuit diagram of proposed low-cost 3D scanner

With a driver set up for 16 micro steps per step and a resolution of 3200 steps per complete revolution, the ESP32 microcontroller managed the stepper motor using conventional step, direction, and enable signals. This ensured accurate platform movement during scanning by offering a fine angular resolution of 0.1125° per step. I²C was used to interface the VL53L0X Time-of-Flight sensor, which was set to capture multiple readings at each step, and five consecutive measurements were averaged to generate a single data point. Each scan session was automatically saved in a sequentially numbered CSV file using a microSD card module that was interfaced via SPI.

A user-operated push button started the scanning process, and the platform then rotated 360 degrees, taking distance readings at each incremental step. The rotation angle, a fixed tilt angle (0.0 in this implementation), and the corresponding measured distance in millimetres were all included in each dataset entry. The data file was finalized and saved after the revolution was finished, and the system went back to standby mode so that it could be scanned again later. Repeatability and dependability for numerous scanning sessions on various objects were guaranteed by this automated cycle.

2.3 Structure of the 3D scanner

Figure 2.2: Structure of the prototype

The experimental setup which is shown in figure 2.2 consists of a wooden frame that holds both the rotary table and the Z-axis support mechanism. The Z-axis was constructed using two vertical metal guide rods fixed between the top and bottom wooden plates, ensuring stability and smooth alignment. A vertical arm mounted between the rods provides the holder for the distance sensor, allowing precise positioning along the Z direction. The rotary table was made by using 3D printing technique. This motorized table allows controlled 360° rotation of the object during scanning. Wooden blocks around the motor provide mechanical support and reduce vibration during operation. The combination of the Z-axis structure and the rotating table enables stable and accurate distance measurements from multiple angles for 3D reconstruction.

3. RESULT AND DISCUSSION

3.1 Data set of received by scanned object

The developed low-cost 3D scanning prototype successfully generated point cloud data of small objects with millimetre-level accuracy. The VL53L0X Time-of-Flight sensor, in combination with the stepper motor's fine angular resolution, enabled consistent and repeatable distance measurements. The system captured complete 360° scans and exported the data in CSV format, which was then processed in MeshLab to reconstruct 3D models.

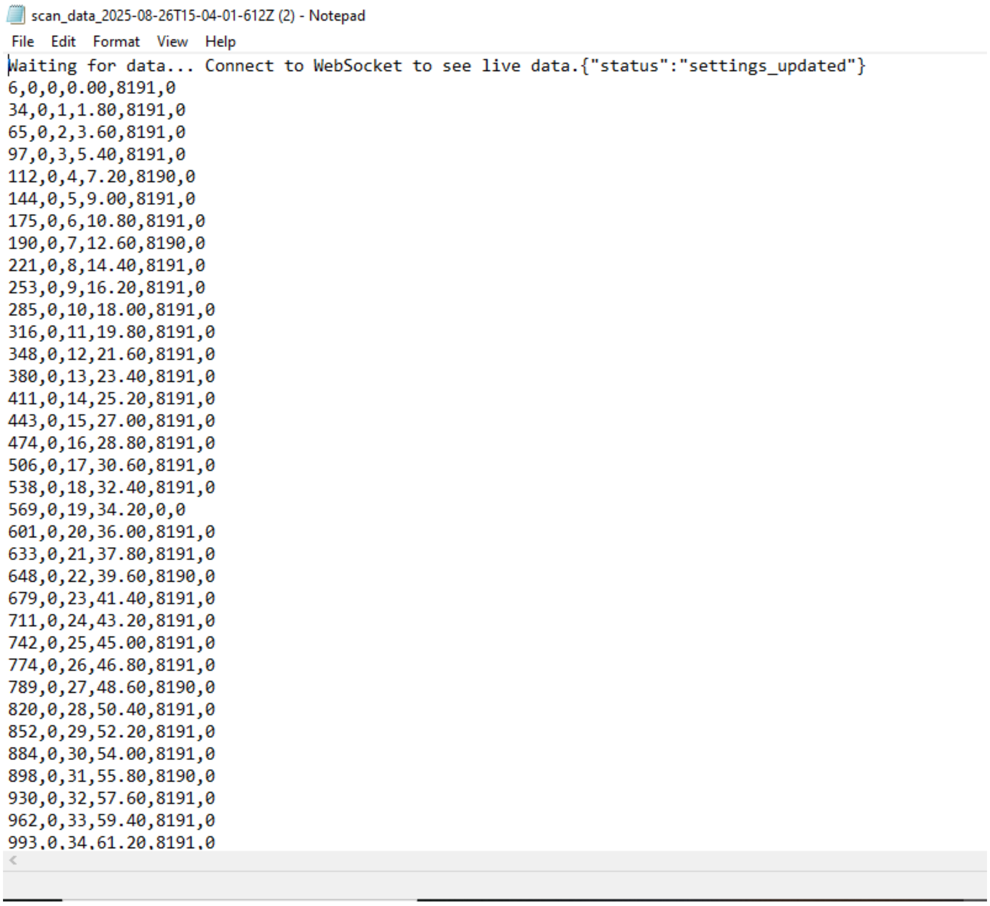

scan_data_2025-08-26T15-04-01-612Z (2) - Notepad

File Edit Format View Help

```
Waiting for data... Connect to WebSocket to see live data.{"status":"settings_updated"}
6,0,0,0.00,8191,0
34,0,1,1.80,8191,0
65,0,2,3.60,8191,0
97,0,3,5.40,8191,0
112,0,4,7.20,8190,0
144,0,5,9.00,8191,0
175,0,6,10.80,8191,0
190,0,7,12.60,8190,0
221,0,8,14.40,8191,0
253,0,9,16.20,8191,0
285,0,10,18.00,8191,0
316,0,11,19.80,8191,0
348,0,12,21.60,8191,0
380,0,13,23.40,8191,0
411,0,14,25.20,8191,0
443,0,15,27.00,8191,0
474,0,16,28.80,8191,0
506,0,17,30.60,8191,0
538,0,18,32.40,8191,0
569,0,19,34.20,0,0
601,0,20,36.00,8191,0
633,0,21,37.80,8191,0
648,0,22,39.60,8190,0
679,0,23,41.40,8191,0
711,0,24,43.20,8191,0
742,0,25,45.00,8191,0
774,0,26,46.80,8191,0
789,0,27,48.60,8190,0
820,0,28,50.40,8191,0
852,0,29,52.20,8191,0
884,0,30,54.00,8191,0
898,0,31,55.80,8190,0
930,0,32,57.60,8191,0
962,0,33,59.40,8191,0
993,0,34,61.20,8191,0
```

Figure 3.1: Data set of scanned object

As shown in figure 3.1, each row consists of six values that represent the recorded parameters during a single scanning step. The first column is the step count of the motor, while the second and third columns correspond to the tilt axis state and the index of the current measurement step. The fourth column gives the rotation angle in degrees, which is calculated from the step number and microstepping resolution. The fifth column represents the measured distance from the VL53L0X Time-of-Flight sensor in millimetres, and the last column is an error/status flag that indicates if the sensor reading was valid. Together, these values form a structured dataset that maps angle and distance information into a point cloud for 3D reconstruction.

4. CONCLUSION

The developed low-cost 3D scanning system achieved millimetre-level accuracy in reconstructing small objects, confirming its effectiveness as a reliable alternative to commercial scanners. Each full 360° scan produced 3200 data points, derived from the NEMA 17 stepper motor configured with 16-step microstepping. This provided a fine angular resolution of 0.1125° per step, which ensured smooth rotation and reduced vibration, both of which are critical for accurate distance measurement. The VL53L0X Time-of-Flight sensor was set to capture multiple readings at each step, and five consecutive measurements were averaged to generate a single data point. This averaging process significantly reduced random noise and improved consistency without introducing excessive scanning time. The choice of five readings was a balance between accuracy and efficiency, as higher counts were tested but showed minimal improvement in precision while increasing scan duration. Consequently, the integration of fine angular resolution with averaged distance values contributed to accurate, repeatable, and dense point cloud data, enabling reliable 3D reconstruction.

ACKNOWLEDGEMENT

The authors would like to express their gratitude to the Academic Staff of the Faculty of Applied Sciences, Wayamba University of Sri Lanka for their expert advice and guidance.

REFERENCES

[1] B. Bousseta, "3D modeling and Cultural Heritage: Preserving the past through digital reconstruction," *Medium*, 2023. Available: https://medium.com/@badreddinebousseta/3d-modeling-and-cultural-heritage-preserving-the-past-through-digital-reconstruction-ce0695260504. Accessed: Nov. 15, 2024.

[2] Artec 3D, "Professional 3D scanning solutions | Heritage Preservation," n.d. Available: https://www.artec3d.com/3d-scanning-solutions/heritage-preservation. Accessed: Nov. 15, 2024.

[3] E. Starinieri, "How 3D scanners work," *Capture 3D*, 2023. Available: https://www.capture3d.com/knowledge-center/common-questions-for-3d-scanners/how-3d-scanners-work. Accessed: Nov. 02, 2024.

[4] Admin, "Pros and cons of 3D scanning," *Pros and Cons*, 2020. Available: https://prosancons.com/technology/pros-and-cons-of-3d-scanning/. Accessed: Nov. 02, 2024.

DEVELOPMENT OF AN IOT-ENABLED REAL TIME TEMPERATURE MONITORING AND ALERT SYSTEM FOR LABORATORY REFRIGERATORS

J.K.A.S.W. Jayasuriya*[1] , Y.A.A. Kumarayapa[1] , M. Wijemanne[2]
[1] *Department of Electronics, Wayamba University of Sri Lanka, Kuliyapitiya, Sri Lanka*
[2]*Industrial Technology Institute, Colombo 07, Sri Lanka*
*sithijawishwa99@gmail.com

ABSTRACT

The integrity of experimental samples in biotechnology laboratories is paramount, especially for facilities conducting accredited testing services. This project addresses a critical vulnerability in an accredited biotechnology laboratory. There are two older model laboratory refrigerators operating at -18 °C, which are used for storing valuable experimental food samples but completely lack any form of temperature indicators, data logging, or alert systems. Currently, lab staff must manually check temperatures using basic thermometers, a process that is inefficient and unreliable. This absence of monitoring poses a direct threat to the laboratory's accredited status, as undetected temperature excursions can lead to irreversible sample degradation, invalidate test results, and compromise regulatory compliance. To solve this, a system was designed using a modular IoT architecture. This involved using DS18B20 sensors inside the refrigerators, an ESP8266 microcontroller for data acquisition and Wi-Fi communication, the MQTT protocol for data transport, and a backend stack of InfluxDB for time series data storage and Grafana for visualization and alerting. For SMS notifications, a GSM module was added, and a UPS was used to ensure functionality during power loss. The system deployed exhibited high precision (±0.4°C), real time data latency, and stable multi-channel alarms. By providing continuous oversight, real-time notifications, and a secure audit trail, the solution efficiently protects sample integrity, maintains adherence to accredited test procedures, and provides an economical model for upgrading ageing laboratory infrastructure at a fraction of the expense of commercial systems.
Keywords: **A**ccredited testing, **D**egradation, **I**oT-enabled alert system

1. INTRODUCTION

Biotechnology laboratories providing accredited testing services operate under a mandate of stringent quality control and unwavering data integrity. The validity of their results, and by extension their accreditation, depends critically on the stability of pre-analytical conditions, particularly the storage of experimental samples. Refrigerated storage at specified temperatures, such as -18°C for many experimental food samples, is a fundamental requirement to halt biological activity and preserve sample composition [1].
A significant operational risk exists in laboratories utilizing older refrigeration equipment. This project was initiated to address precisely such a scenario: two refrigerators in biotechnology laboratory, dedicated to storing critical experimental food samples, which possess no digital temperature indicators, no recording historical data, and no functionality for issuing alerts. Current practice relies on manual, periodic checks with standalone thermometers a method that is inherently prone to human error, offers no insight into temperature fluctuations between checks, and provides absolutely no warning of failures occurring outside of working hours, such as power outages.

The consequences of an undetected temperature excursion in this context are severe. For samples, it can create irreversible degradation, rendering them useless for analysis and wasting weeks or months of research effort. For the lab itself, it is a risk of breaking important rules they must follow. These rules require the lab to prove that they have full control over their storage temperatures [2]. A single unresolved temperature deviation could invalidate test results, lead to non-conformities during audits, and damage the laboratory's reputation for reliability.

The growth of Internet of Things (IoT) technology presents a robust solution to this critical monitoring gap [3]. IoT enables the transformation of basic storage units into intelligent, connected devices capable of autonomous self-monitoring. This project involved the design and implementation of a complete IoT based system to achieve precisely this transformation. The main goal was to give the lab's old refrigerators new abilities: the power to be monitored in real time, to send their data to the internet for easy checking, and to send an instant alert if something goes wrong. This is functionality the old fridges desperately needed to meet the high standards of a professional lab. This new system makes sure the samples are always safe, which protects the quality and reliability of the lab's work.

2. EXPERIMENTAL

2.1 System Design

The system was designed with a modular, industry standard IoT architecture for scalability and reliability:

Sensing the environment: Obtained with digital temperature sensors placed inside the refrigerators. Those are constantly measuring the conditions.

Local processing & gateway: A small, efficient microcontroller (an ESP8266) acts as the local brain. It gathers readings from the sensors and then serves as a gateway, responsibly sending that data out onto the network.

Data transport: To get the data to its destination quickly and reliably, the system uses a lightweight messaging protocol (MQTT) over Wi-Fi. This is like sending prioritized messages through a broker, ensuring nothing gets lost in transit.

Data collection: A specialized agent (Telegraf) subscribes to these messages from the central broker. Its job is to efficiently collect the incoming data and immediately route it into the database.

Optimized storage: All the temperature data are stored in a time-series database (InfluxDB). This database is specifically designed to handle rapid, continuous streams of data, making it perfect for fast queries and managing long-term storage [6].

Visualization & alerting: Finally, a Grafana dashboard platform connects to the database. It translates the raw numbers into clear, dynamic graphs and gauges, allowing users to monitor conditions in real-time, review historical trends, and set up crucial alerts if temperatures ever drift into an unsafe range.

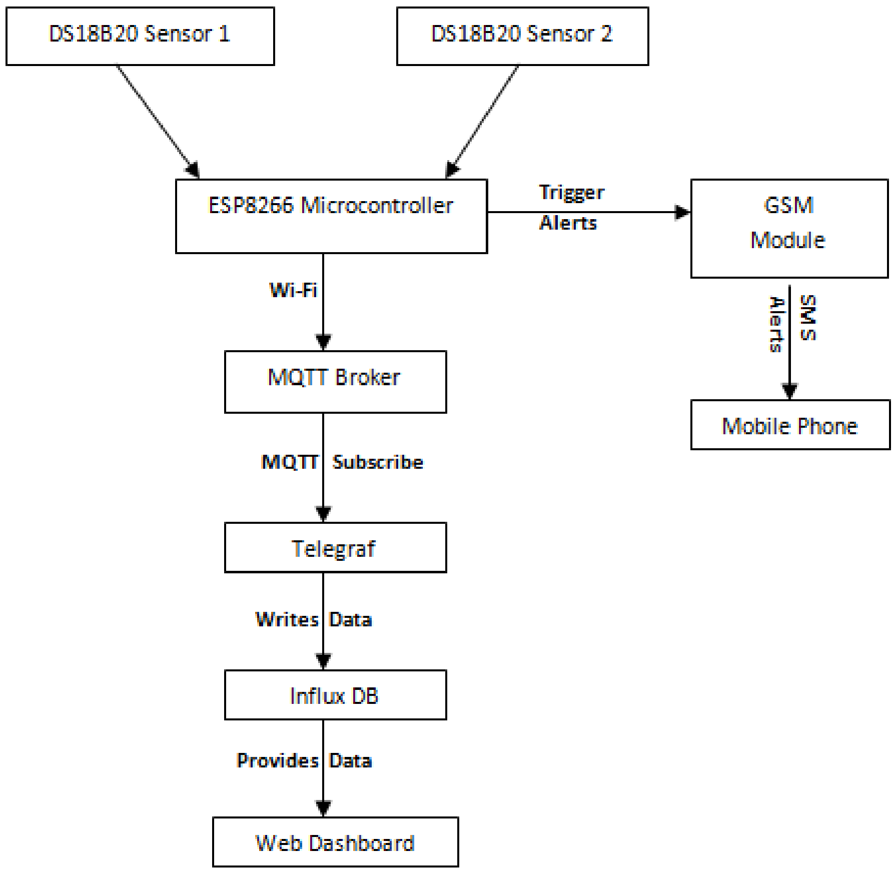

Figure 2.1 - Workflow diagram of IoT-enabled temperature monitoring system

Figure 2.1 illustrates the modular, five-layer data pipeline. The process begins with the sensing layer, which uses DS18B20 sensors to collect temperature data. This data is then handled by the network and gateway unit, where an ESP8266 microcontroller processes and transmits it. The middleware comprising the MQTT protocol and Telegraf agent, manages the secure and efficient transport of this data. It is then stored in the data storage layer using an InfluxDB time series database. Finally, the application, represented by a Grafana dashboard, provides visualization and alerting capabilities. This integrated design ensures reliable, real-time data flow from physical sensing to the user interface.

2.1 Hardware Components

- Microcontroller: An ESP8266 NodeMCU was selected for its Wi-Fi capability, processing power, and extensive library support for MQTT clients [4].
- Temperature sensor: A waterproof DS18B20 digital sensor can measure temperatures in the range of -55°C to +125°C with a precision of ±0.5°C, resilience in humid environments, and one wire communication protocol [7].
- SIM900A GSM module: The module responsible for sending SMS alerts.
- Power backup: A dedicated Uninterruptible Power Supply (UPS) module or backup battery was integrated to ensure continuous operation of the monitoring system.

2.2 Testing and Validation

To ensure the entire system functioned correctly, several essential tests were conducted. The seamless movement of data through each step of the pipeline was verified: from the sensor to the ESP8266, then to the MQTT broker, through Telegraf, into InfluxDB, and finally to Grafana. This confirmed that no data was lost along the way.

The accuracy was tested by comparing the temperature readings from the DS18B20 sensor with those from a calibrated reference thermometer placed in the same fridge. This confirmed that the system was measuring temperature accurately. To evaluate speed, the time taken for a sensor reading to be captured and subsequently displayed on the dashboard was measured. This ensured that the system was truly providing real-time monitoring.

The reliability of the system was tested by creating challenging conditions, such as poor Wi-Fi connections and power outages, to determine if continuous operation and proper recovery would be maintained.

Finally, the functionality of the alert system was verified by manually raising the fridge temperature above the safe limit. It was confirmed that email notifications were quickly sent out by the system, ensuring that users would be informed immediately of any problem.

3. RESULTS AND DISCUSSION

Calibration tests confirmed the high accuracy of the monitoring system, with DS18B20 sensor readings deviating by no more than ±0.4°C from the certified reference standard. The dashboards effectively translated the stored time-series data into intuitive and powerful visualizations. The ability to seamlessly zoom into historical timelines and correlate events proved invaluable for post-incident analysis and compliance reporting a capability that was entirely nonexistent before this project.
The integration of the UPS module provided approximately 50 minutes of backup power, during which the entire monitoring and alerting pipeline remained fully operational. This ensures that temperature deviations caused by a power failure are detected and reported.

Figure 3.1 Real-time temperature output and status on dashboard

This architecture ensures real-time oversight, robust data integrity, and alert system, thereby safeguarding valuable assets and upholding the laboratory's commitment to quality. The implemented monitoring solution culminates in a Grafana dashboard, as depicted, which serves as the primary interface for laboratory personnel [5]. The dashboard presents real-time temperature data streams from two separate refrigerators (Temp 1 and Temp 2), demonstrating the system's ability to handle multiple data sources simultaneously. A condition automatically confirmed by the prominent status labels (Figure 3.1).

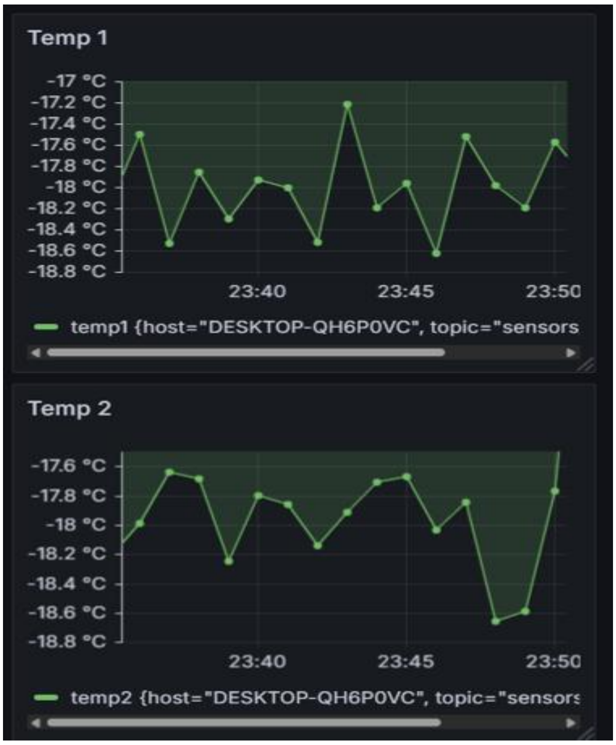

Figure 3.2 Time-series plot of Temperature data

A key feature of the implemented system is the capacity for retrospective data analysis, as demonstrated by this Grafana time-series graph. The plot visualizes (figure 3.2) the historical temperature readings of both sensors, allowing users to customize the time range for analysis.
This visualization validates the entire data pipeline from sensor acquisition to cloud-based storage and final display functioning as designed to ensure operational reliability.

4. CONCLUSION

The present study demonstrates that laboratory safety can be reliably monitored inexpensively by providing continuous, auditable oversight of critical storage conditions. This is achieved through the system's verified ±0.4°C accuracy, which ensures data reliability for compliance, and its instant multi-channel alerts, which enable immediate corrective action during temperature excursions. By creating an immutable digital record of storage temperatures, the system directly ensures that accreditation rules for environmental control are followed, thereby safeguarding sample integrity without the high cost of commercial monitoring solutions.

The results are consistent with the overall trend of IoT-enabled environmental monitoring but differ significantly by the deployment of the professional open source stack (MQTT, InfluxDB, Grafana) at an extremely low price (about Rs. 1600 per unit, which is only a small portion of commercial solutions). This combination of cost effectiveness and scalability gives the system the advantage of being particularly suitable for such areas with limited resources.

ACKNOWLEDGEMENTS

The authors gratefully acknowledge the support and facilities provided by the Industrial Technology Institute (ITI), Colombo, Sri Lanka. The guidance from the Department of Electronics, Wayamba University of Sri Lanka, is also sincerely appreciated.

REFERENCES

[1] A. Al-Fuqaha, M. Guizani, M. Mohammadi, M. Aledhari, and M. Ayyash, "Internet of Things: A survey on enabling technologies, protocols, and applications," *IEEE Commun. Surveys Tuts.*, vol. 17, no. 4, pp. 2347–2376, Fourth Quarter 2015. doi: https://doi.org/10.1109/COMST.2015.2444095

[2] Y. Cheng, J. Nasah, C. Li, Y. Wang, and M. Wu, "A low-cost IoT-based temperature monitoring system for logistics," *J. Sensor Actuator Netw.*, vol. 9, no. 4, p. 45, Dec. 2020. doi: https://doi.org/10.3390/jsan9040045

[3] S. D. T. Kelly, N. K. Suryadevara, and S. C. Mukhopadhyay, "Towards the implementation of IoT for environmental condition monitoring in homes," *IEEE Sensors J.*, vol. 13, no. 10, pp. 3846–3853, Oct. 2013. doi: https://doi.org/10.1109/JSEN.2013.2263379

[4] Espressif Systems, "ESP8266EX datasheet," ver. 6.7, 2025. Available: https://www.espressif.com/sites/default/files/documentation/0a-esp8266ex_datasheet_en.pdf

[5] Grafana Labs, "Getting started with Grafana," 2025. Available: https://grafana.com/docs/grafana/latest/getting-started/getting-started/

[6] InfluxData, "InfluxDB key concepts," 2025. Available: https://docs.influxdata.com/influxdb/v1/concepts/key_concepts/

[7] Analog Devices, "DS18B20 programmable resolution 1-wire digital thermometer," Datasheet, 2025. Available: https://www.analog.com/media/en/technical/documentation/data-sheets/DS18B20.pdf

Proc. Annual Symposium on Research & Industrial Training, 12 (2025) 209-214
Department of Electronics – Wayamba University of Sri Lanka

INDUSTRIAL SAFETY AND EMERGENCY SHUTDOWN SYSTEM WITH GSM ALERTS

W.K.Lakshani*, M.A.A. Karunarathna[1], G.P.U.U. Kumara[2]
[1]*Department of Electronics, Wayamba University of Sri Lanka, Kuliyapitiya, Sri Lanka*
[2]*Malith Engineering Tools (Pvt) ltd*
*kaushalyalakshani0627@gmail.com

ABSTRACT

Industrial workplaces often face serious risks like gas leaks, overheating, electrical faults, and accidental contact with machinery. These hazards can lead to injuries, damage to equipment, and expensive downtime. Many current safety systems depend primarily on manual checks or local alarms. They only work when staff are nearby, which causes delays in responses and raises the chance of accidents. To address these issues, this project creates a GSM-based safety system for industrial equipment using an ESP32 microcontroller. This system is designed for real-time hazard detection, quick responses, and dependable remote communication. It includes several sensors, such as an MQ-2 gas sensor for detecting harmful gases, a DHT11 sensor for monitoring temperature and humidity, and a laser-based module for detecting accidental human contact with machinery. When the system detects abnormal conditions, the ESP32 controller activates a relay to cut off the three-phase power supply. It also triggers a buzzer for local alerts and sends SMS or call notifications to designated personnel through a GSM module. An optional GPS module allows for live tracking of equipment location. Tests showed that the system responds in seconds. Laser detection works in less than 100 milliseconds, and GSM alerts are sent within 5 to 20 seconds. By combining multi-sensor monitoring, automatic shutdown, and real-time communication, the proposed ESP32-based system offers a cost-effective and scalable way to enhance industrial safety.

Keywords: **G**as Leak Detection, **T**emperature Monitoring, **I**oT-Based Alerts

1.0 INTRODUCTION

Industrial environments need constant attention to safety because of heavy machinery, electrical systems, and hazardous conditions. Accidents like gas leaks, overheating of equipment, or direct human contact with dangerous machines often happen when hazards are not detected quickly enough. Traditional safety systems, while useful, mainly rely on local alarms that might go unnoticed if workers or supervisors are not nearby. This delay can lead to severe injuries, equipment damage, and loss of productivity [1,3].

A major drawback of current systems is their lack of remote communication and automated intervention [2]. These systems are often built for specific hazards like gas detection or fire alarms, instead of offering an integrated solution. Additionally, many controllers used in these systems, like the Arduino Uno, do not have the processing power or connectivity options needed for effective monitoring.

To address these problems, this project introduces a GSM-Based Industrial Safety System using the ESP32. The ESP32 is chosen as the main controller due to its higher processing power, built-in Wi-Fi and Bluetooth, and flexibility compared to traditional boards. The system tracks environmental conditions with multiple sensors, automatically shuts down equipment through relays, and sends hazard alerts instantly via GSM. GPS functionality is included for tracking mobile equipment, ensuring safety in both fixed and remote locations. By combining real-time detection, quick intervention, and remote communication, the ESP32-based system offers a modern and scalable solution for industrial safety.

2.0 EXPERIMENTAL

2.1 System Overview

The experimental phase of this project aims to create a real-time industrial hazard detection and emergency shutdown system using the ESP32 microcontroller. This system can detect hazards like gas leaks, high temperatures, and unsafe machine operations. It provides immediate alerts and automated shutdowns to help prevent industrial accidents. The setup includes the ESP32 microcontroller, sensors, relays, and communication modules for quick and reliable responses.

The ESP32 module acts as the central controller for the system. Gas sensors (MQ-2) detect harmful or flammable gases, while temperature sensors (DHT11) monitor the ambient temperature and conditions of the equipment. Relays are linked to vital machinery to shut it down during unsafe conditions. The built-in Wi-Fi on the ESP32 allows real-time data to be sent to an IoT cloud dashboard. A GSM module (SIM800L) sends SMS alerts to supervisors. The system gets power from a 12V DC supply or a battery backup, ensuring it runs continuously during testing.

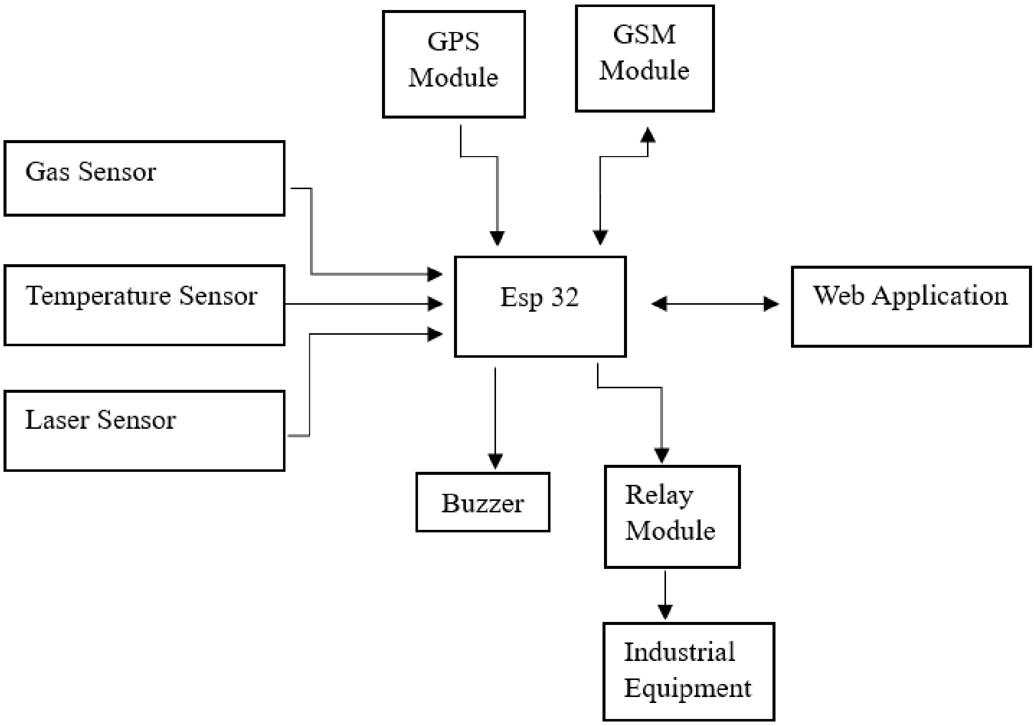

Fig. 1: Block Diagram of the System

The experimental procedure starts with sensor calibration. This involves finding threshold values for gas concentration and temperature under controlled conditions. The ESP32 constantly checks the sensor readings. If any reading exceeds the defined safety threshold, the system triggers the relay to shut down the machinery. At the same time, alerts go to the IoT cloud dashboard and messages are sent to supervisors. Different test scenarios, including gas leak simulations, overheating, and unsafe machine operations, were conducted to assess the system's performance, reliability, and response time. A flowchart outlines how the system operates. It shows how the ESP32 reads sensor data, compares it with set thresholds, and triggers both the emergency shutdown and alert notifications when needed.

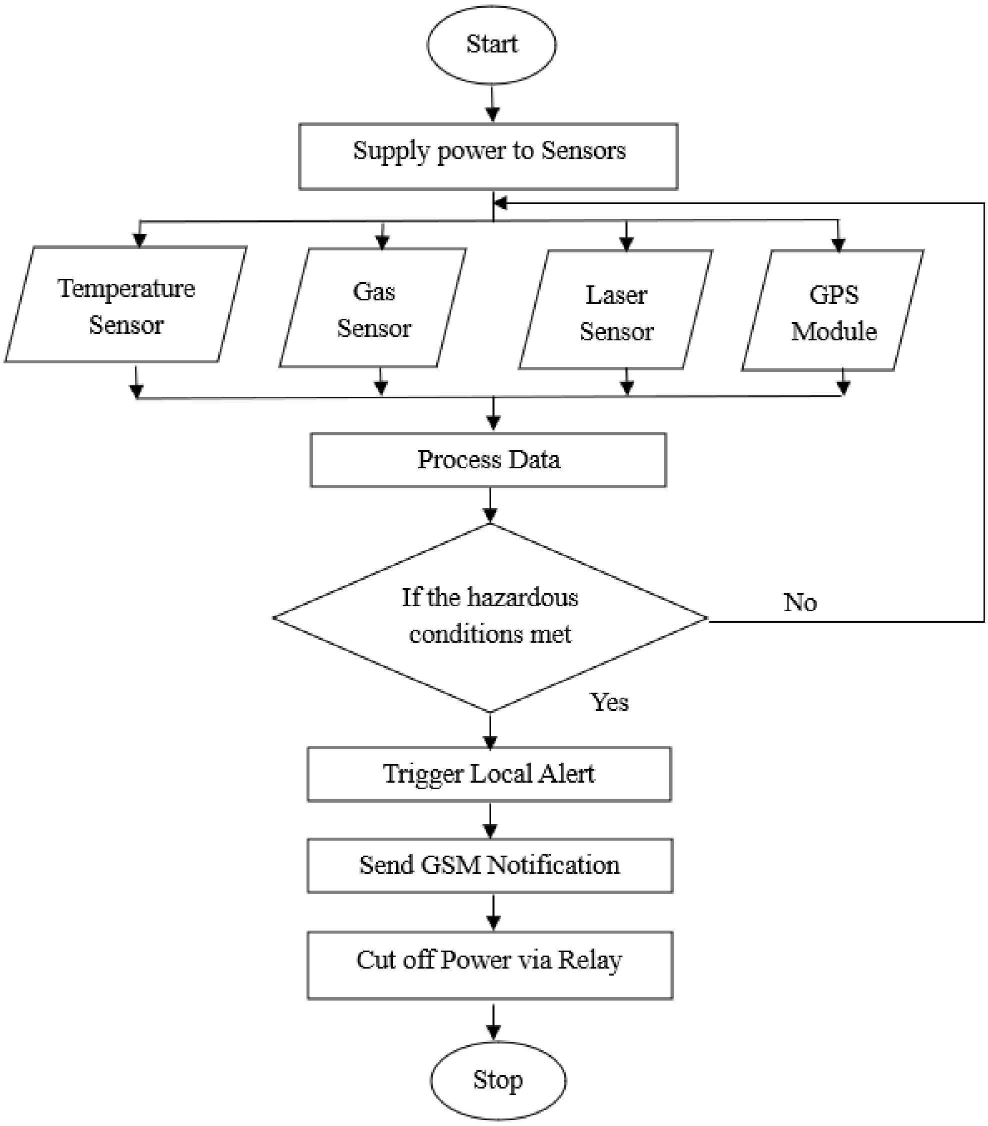

Fig. 2: Flow chart of the system

During testing, the team recorded and analyzed sensor readings, system response times, and alert notifications. The system showed effective hazard detection and real-time response. The relays successfully activated shutdowns, and alerts were delivered promptly. These results show that the ESP32-based system can help prevent industrial accidents, maintain operational safety, and enable real-time monitoring in industrial settings.

2.2 Hardware Implementation

The hardware of the proposed system was built on a prototype test board with adequate wiring, sensor location and steady power connection. The central processing unit was ESP32 microcontroller. It was coded to detect sensor data and match it with the established thresholds and activate emergency measures. A regulated 12 V DC adapter with a battery backup was used to supply power to the system to provide backup should the system fail when testing.

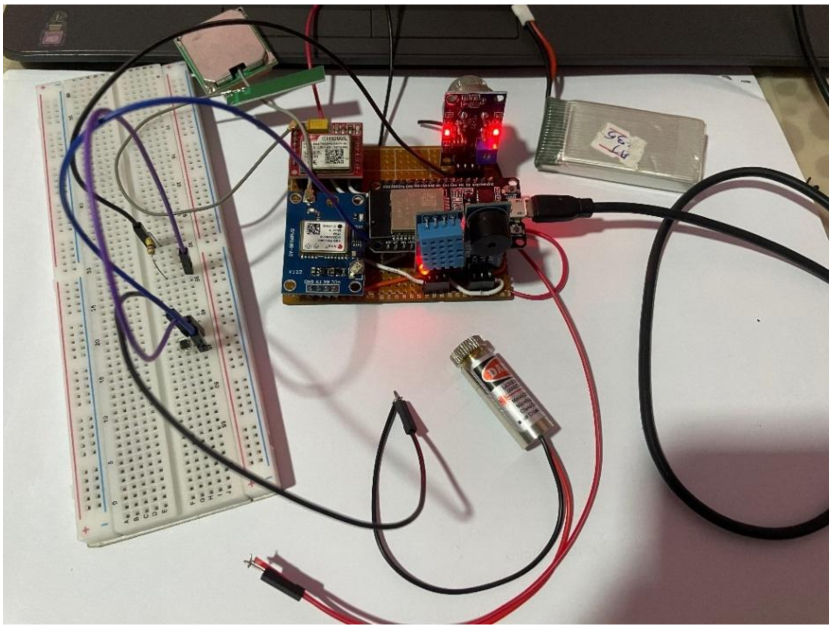

Fig. 3: Design Prototype

The gas sensor of the ESP32 was linked to the MQ-2 gas sensor to monitor the gas. The sensor itself was also calibrated in the process of implementation, and the hazard threshold was adjusted to be 300 ppm [8]. Whenever the quantity of gases surpassed this amount, the ESP32 activated the relay and the buzzer and forwarded GSM notices. The sensor of DHT11 temperature was connected to a digital pin on the ESP32. The maximum temperature level was established at 40 C in order to raise an alarm at an early stage of overheating. The reading passing this value turned on the relay and shut off the connected load and gave both local and remote alerts. The laser module was placed in accordance to the test configuration in order to record human contact. It was integrated with the ESP32 via digital input pin and the detection range was set to 215 cm. In case an obstruction was observed, the ESP32 directly activated the emergency shutdown process. The relay module was connected to a bank of 12 V lamp, which was the test load. This installation enabled the performance of switching to be checked safely. In case of hazards, the relay turned off the load of the lamp in 15-25 ms, which is a fast reaction. The buzzer was fixed as a local alarm that was to give sound notifications instantaneously during hazards. The SIM800L GSM module was linked to the ESP32 via the UART communication to send SMS and call alerts to supervisors. GPS optional module was incorporated as well to make available equipment location information.

3.0 RESULTS AND DISCUSSION

3.1 System Performance Evaluation

The prototype was subjected to low-voltage bench test to determine the general performance. Laser module response to hand presence was determined to take latency of 1040 ms, which is significantly lower than the target 100 ms, and 100 consecutive tests of obstruction proved the stability of operation. The DHT11 temperature sensor and MQ-2 gas sensor yielded consistent values and the

DHT11 had an error of no more than ±0.5 o C. Gas and temperature hazard thresholds were established at 300ppm and 40C respectively and average calibration minimized noise and false activation [6,7]. The relay and buzzer were stable with response times of 1525 ms and they did not have failures observed even after 100 switching cycles on a 12 V lamp load. The GSM module (SIM800L) was also able to send text messages with alerts in 520 seconds and made calls marginally faster but used more current [3,5]. The system had a continuous test of 48 hours without any collapses, including simulated network drop. Limitations were the presence of the 2 A supply requirement of the GSM module, ESP32 ADC nonlinearity, and the small accuracy of the DHT11, as well as the fact that the relay is only usable at low voltages instead of at industrial ones.

3.2 Real-Time Monitoring and Notification System

There was also the real-time monitoring and notification of the system. The processed sensor data was read and live values displayed on a dashboard using ESP32 (Fig. 4a). Thresholds exceeding (300 ppm gas, 40 o C temperature, 2-15 cm hand detection) triggered the local buzzer, dashboard notification was sent and SMS notification was sent to the site manager as depicted in Fig.4b. The delivery of SMS was between 5-20 seconds and the relay responded between 15-25 ms, which guaranteed rapid shut down of hazards. This prototype also had a 12 V DC supply with battery back up, and this supply sustained constant operation even when simulated power was unavailable. This multi-channel alarm system (buzzer + SMS + dashboard) was useful in providing rapid and dependable communicational hazards. The system should be implemented in industry with improved features of a mobile app dashboard and safe measures like MQTT with TLS [5].

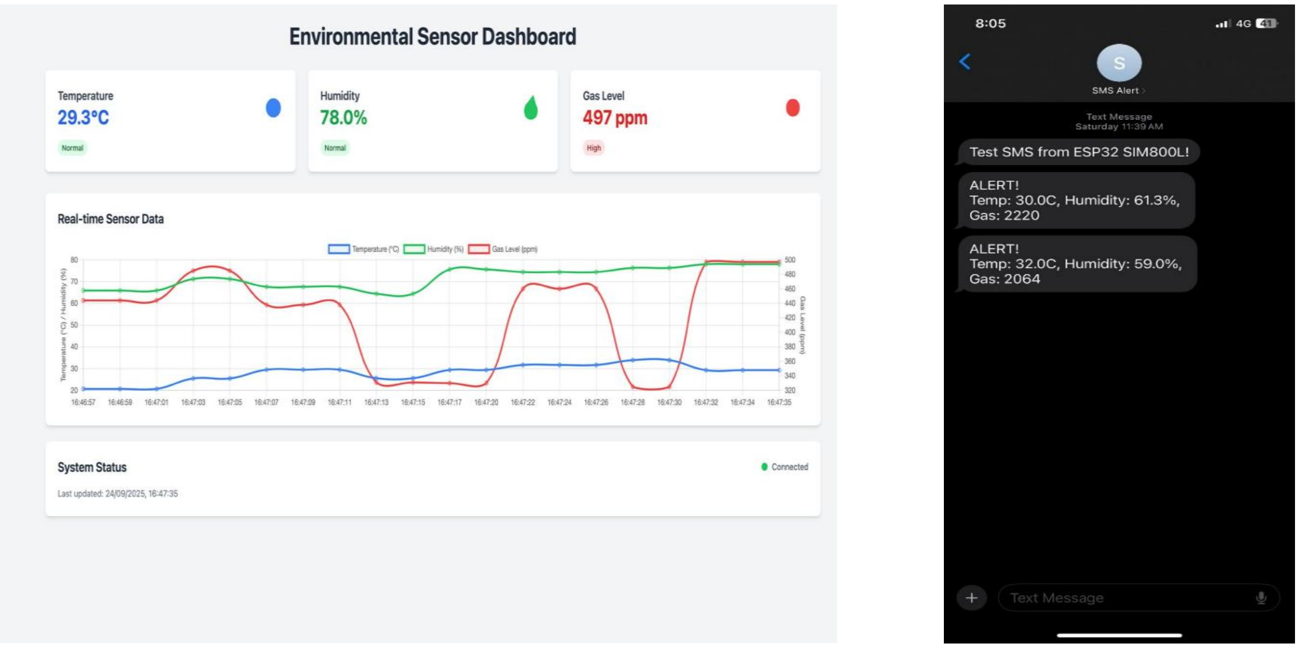

(a) (b)

Fig. 4: Web dashboard interface and (b) SMS warning from GSM

4.0 CONCLUSION

The project was able to successfully develop an industrial real-time hazard detection and emergency shutdown system with the ESP32 microcontroller, displaying massive potential in ensuring workplace safety. With an in-built laser module for hand detection around machinery, an MQ-2 sensor for gas leak detection, and a DHT11 sensor for temperature detection, the system could sense all important safety parameters continuously, while the relay module was tasked with ensuring safe and timely shutdowns on detection of a hazard. Real-time warnings were issued through IoT and GSM technology to enable supervisors to respond early and prevent accidents. Functionality testing ensured prompt response times, accurate detection, minimal false alarms, and stable relay operation, and the prototype was proven robust with round-the-clock use while handling network fluctuations well. Though the system proved effective under laboratory-controlled conditions, a few industrial deployment optimizations are suggested, such as the use of industrial-grade sensors, certified contactors for three-phase or mains switching, stable power supply solutions, and secure communication protocols. Overall, the project was successful in fulfilling its objective of improving industrial safety, allowing for real-time monitoring, and preventing accidents, while establishing a solid foundation for potential future growth and application in industrial environments.

ACKNOWLEDGEMENTS

The authors would like to express sincere gratitude to the academic staff of the Department of Electronics, Faculty of Applied Sciences, and the laboratory of Department of Plantation Management, Wayamba University of Sri Lanka for the support provided during the project.

REFERENCES

[1] P. Sharma and R. Gupta, "Design and implementation of GSM-based industrial safety system," *Int. J. Adv. Res. Electr. Electron. Instrum. Eng.*, vol. 8, no. 5, pp. 2457–2463, May 2019. doi: 10.15662/IJAREEIE.2019.0805073

[2] M. Sunandini, S. Venkateshwara, M. Vithya, B. Mohana, and S. Varshini, "Smart industrial level gas leakage detection system using AI & IoT," *Int. J. Eng. Res. Technol.*, vol. 12, no. 3, pp. 324–329, 2024. Available: https://www.ijert.org/research/smart-industrial-level-gas-leakage-detection-system-using-ai-iot-IJERTCONV12IS03088.pdf

[3] M. Patel, *Industrial Automation and Safety: Principles and Applications*, 3rd ed. New York, NY, USA: Techno Press, 2021.

[4] L. Dhiman, P. Chauhan, M. Singh, and P. A. Kestwal, "Enhancing safety measures with an IoT-based fire and gas detection system," *Int. J. Enhanced Res. Sci. Technol. Eng.*, vol. 13, no. 4, pp. 162–166, Apr. 2024. Available: https://www.erpublications.com/uploaded_files/download/lalit-dhiman-priyanshi-chauhan-manish-singh-pawan-a-kestwal_DvlSE.pdf

[5] S. Ahmed and U. Farooq, "Automated industrial safety system with SMS alert using GSM technology," *J. Safety Sci. Technol.*, vol. 14, no. 4, pp. 329–335, 2021.

[6] Aknitech Automation, "Smart sensors for industrial safety and accident prevention," Aknitech, 2025. Available: https://www.aknitech.in/blog/iot-in-industrial-safety-preventing-accidents-with-smart-sensors/

[7] J. Li, X. Wang, and Y. Chen, "IoT-based real-time industrial environment monitoring using wireless sensor networks," *IEEE Sensors J.*, vol. 19, no. 23, pp. 11068–11077, Dec. 2019. doi: 10.1109/JSEN.2019.2933884

[8] N. R. Shahapurkar, S. P. Deshpande, and M. R. Rajput, "A novel technique for LPG gas leakage detection and control for safety," *Int. J. Eng. Res. Technol.*, vol. 7, no. 3, pp. 415–420, 2017.

PCB SOLDERING HOT PLATE WITH AUTOMATED AIR ASSIST

L.G.R.H. Lihinigama*, P.G.T.R. Payagala
Department of Electronics, Wayamba University of Sri Lanka, Kuliyapitiya, Sri Lanka
*rashmilihinigama@gmail.com

ABSTRACT

Soldering is an important process in manufacturing and repairing electronic circuits, but it can be dangerous because of the harmful fumes from solder flux, even in lead-free types. Many commercial soldering stations with built-in fume removal are too expensive for students, hobbyists, and small repair shops. This project aims to create a low-cost soldering hot plate system with an automated exhaust system, using a 600W heating plate. The system will control the set temperature using a rotary encoder and cool the Printed Circuit Board (PCB) after soldering with a 12V Direct Current brushless fan. The system uses a K-type thermocouple to monitor the temperature accurately measured by an Arduino Nano microcontroller. An automatic fume extraction system is turned on by the input of a smoke sensor, ensuring the removal of harmful particles immediately from the user. The fumes are removed automatically when needed, and it has an easy-to-use interface with a 20x4 LCD for real-time updates. The total cost of the system is much lower than commercial options, making it a safe and affordable soldering choice that improves efficiency and lowers health risks for users in places with limited resources, and also improves soldering time.

Keywords: **P**CB Soldering, **H**ot Plate, **F**ume Extraction

1.0 INTRODUCTION

The increased use of electronic devices has made it common for workshops, schools, and amateur shop owners to solder Printed Circuit Boards (PCBs) without safety precautions. The process, however, creates dangerous fumes when the flux boils off. The fumes contain irritants and carcinogens that can lead to long-term serious health issues like occupational asthma and chronic respiratory diseases [1]. While commercial soldering stations commonly have fume extractors built in, the device is quite expensive and thus out of reach for many potential users [2].

When new PCBs need soldering or when surface-mounted components must be replaced, traditional soldering methods with handheld irons can be very difficult and inefficient. This happens mainly because handheld soldering doesn't provide uniform heating, which can damage nearby sensitive components. To address these issues, we introduced the PCB soldering hot plate system. It offers precise and even heating of the board, making soldering and rework tasks much easier, safer, and more reliable than traditional methods [3].

This makes it extremely essential to develop a low-cost soldering hot plate and an efficient solution that minimizes these health risks without sacrificing functionality. This research paper discusses fulfilling this need by highlighting the development of a soldering hot plate with an automatic fume extraction system. The device utilizes inexpensive and readily available components, focusing on transforming a heating plate into a controllable heating element. The ultimate target is linking this into a microcontroller system that not only regulates the temperature but also activates a fume extraction unit when it detects the presence of smoke, forming a complete, inexpensive, and safer soldering station with a PCB cooling fan system [4].

2.0 EXPERIMENTAL

The system is structured into four principal functional modules. They are a hot plate unit [5], a user interface unit, a fume detection and extraction unit, and a PCB cooling unit. Central to the system, the Arduino Nano microcontroller is placed and receives sensor inputs, executes control algorithm routines, and operates active components.

2.1 The Hot Plate Unit

A K-type thermocouple is mounted on the plate for real-time monitoring of its temperature. The thermocouple output is conditioned and converted into a digital signal by a MAX6675 thermocouple-to-digital converter, which provides accurate temperature readings to the Arduino Nano. A rotary encoder is there to control the temperature set point, and the push button of the rotary encoder is used to manually turn ON/OFF the heating plate. The control system's decision is then implemented through a 10A Solid State Relay (SSR), which controls the AC power supply to the heating plate. This system ensures efficient temperature control while maintaining electrical safety and isolation. Furthermore, safety features are also built into the program that would switch off heater power should there be a malfunction of the sensor or should the temperature rise above the maximum allowable limits.

2.2 The User Interface Unit

The user interface component facilitates real-time observation of the system and user input. A 20x4 LCD screen connected through I^2C protocol sends out information like the current hot plate temperature, the desired setpoint, and the system operational condition, including states like "Heating," "Stable, or how much time the heater is operated. User interaction is facilitated by a rotary encoder featuring a built-in push button, allowing for easy and accurate adjustment of the target temperature. The interface design optimizes usability while providing the operator with immediate feedback on system operations.

Central to these modules, the Arduino Nano was placed. All the elements are connected to it for control. It acquires data regarding temperature and smoke concentration, processes inputs from encoders, and activates outputs directed towards the heater, exhaust fan, and display module. The embedded software manages temperature control, smoke detection algorithms, user engagement, and safety protocols, thereby facilitating the operation of the system as an automated soldering hot plate equipped with sophisticated fume extraction capabilities. Figures 1, 2, and 3 illustrate the circuit schematic of the system, respectively, demonstrating the interrelations among sensors, actuators, and the microcontroller.

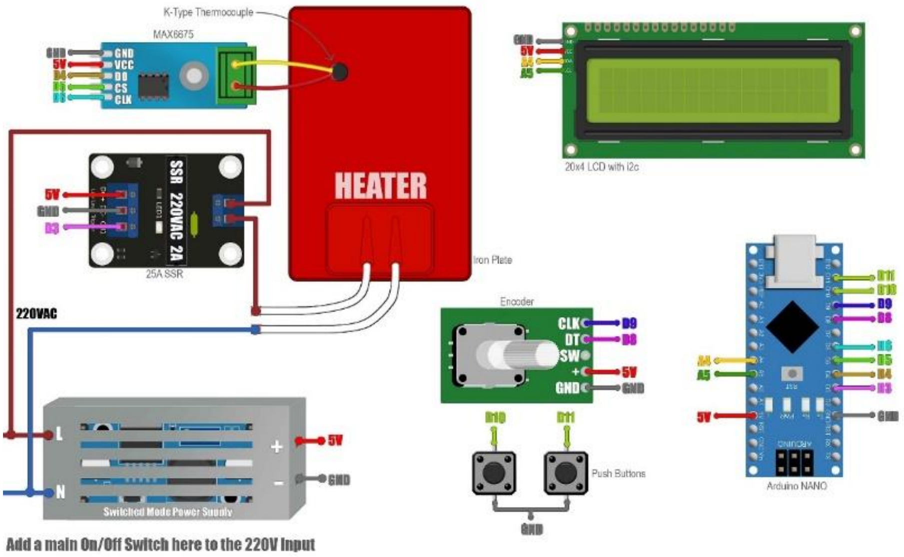

Figure 29:Schematic diagram of the hot plate with user interface and the rotary encoder

Fume Detection and Extraction Unit

There is an MQ-135 gas sensor placed at a strategic location near the soldering station in order to detect smoke and other hazardous gases released during soldering. The analog output of this sensor is continuously read by the Arduino Nano, which compares it against a pre-programmed concentration limit. Once the amount of smoke detected crosses this defined limit, a microcontroller triggers the functioning of a relay module that powers a 12V DC exhaust fan. This fan sucks airflow through the soldering region, thus effectively directing fumes out of the user's breathing space. In order to provide improved safety and optimize working conditions further, the system ensures that the fan continues to run for a short duration after soldering has stopped to remove any remaining fumes.

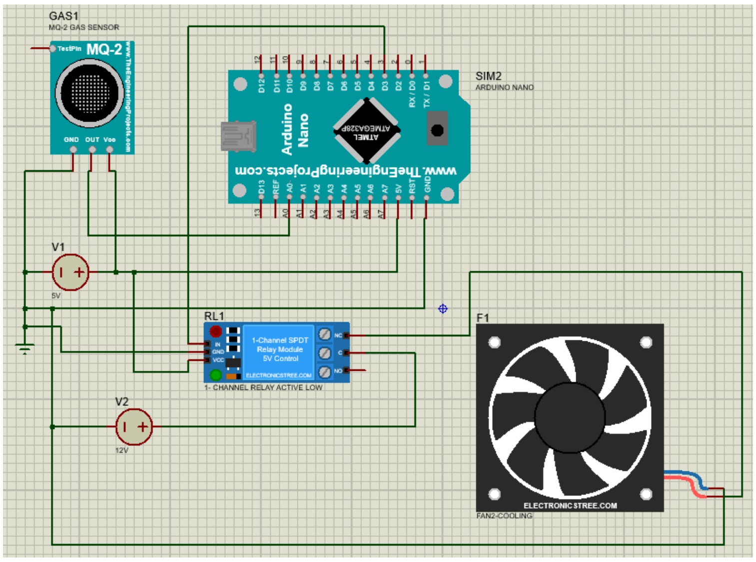

Figure 30: Schematic diagram of the gas sensor with exhaust fan system

PCB Cooling Unit

By following the soldering operations, the face of the PCB remains warm for several minutes, making it unsafe and inconvenient to handle. To overcome this situation, a 12V DC fan was included in the system. While the exhaust fan is controlled by gas detection and thus operates automatically, this fan is controlled by a switch and is therefore under the user's control at all times. By blowing air out onto the PCB, the fan speeds up the rate of cooling and therefore reduces the time that it takes to cool down to a safe handling temperature. It can be observed that the natural cooling took about 5–6 minutes, and the fan-aided technique took about 2 minutes. The result was graphically shown in Figure 4. This development not only improves operator safety but also improves system-wide productivity by keeping downtime between soldering and other operations.

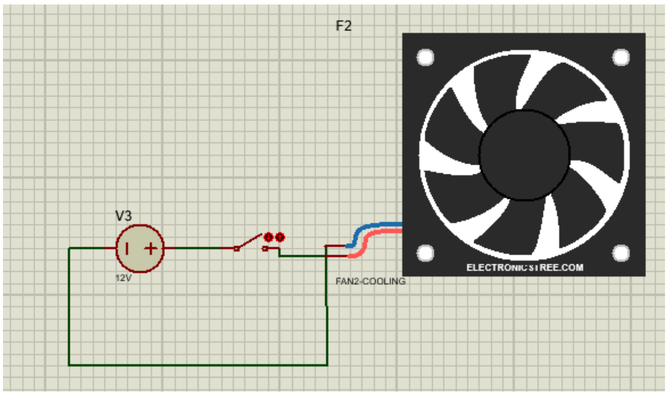

Figure 31: Schematic diagram of the PCB cooling unit

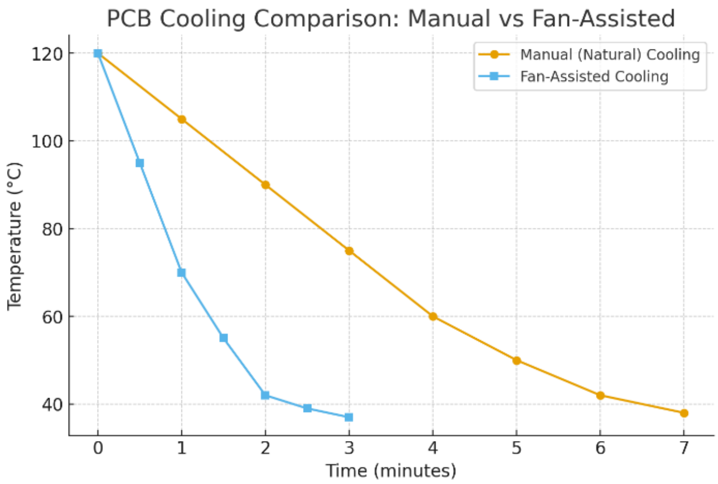

Figure 32: PCB cooling Comparison of manual Vs fan assisted

Full Diagram of the Integrated System

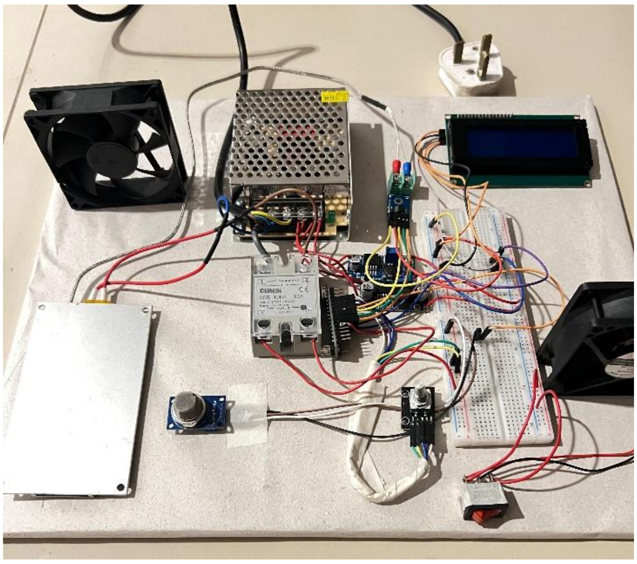

Figure 33: Full diagram of the integrated system

3.0RESULTS AND DISCUSSION

The developed system, as shown in Figure 4, was tested through various working conditions, and the findings affirmed that each working component performed as required.

The rotary encoder functioned well in the control of the heating setpoint of the hot plate. A clockwise direction increased the setpoint, while an anticlockwise direction decreased it. Furthermore, the built-in push-button of the rotary encoder functioned well for direct control of the heating device. In any case, when the hot plate was powered off, a press of the button powered it on, and another press powered it off. The user interface provided by the LCD displayed real-time information, namely the prevailing temperature, the chosen setpoint, the operational status of the solid-state relay (SSR), and the time that the heater turns on. Therefore, it improves the system's user-friendliness and reliability.

The K-type thermocouple-based MAX6675 module temperature sensor was stable and highly accurate. Reading values stayed within ±2 °C of the target values. This point is described by Figures 6 and 7. This level of accuracy was more than sufficient for soldering applications involving PCBs. Such precision was effective in preventing the hot plate from overheating or undershooting considerably and enabled safe and repeatable soldering operations. The SSR responded quickly to Arduino Nano control inputs by switching on when the temperature went below the setpoint and switching off when the setpoint was achieved. This closed-loop control system was effective in maintaining stable temperatures and preventing thermal overshoot.

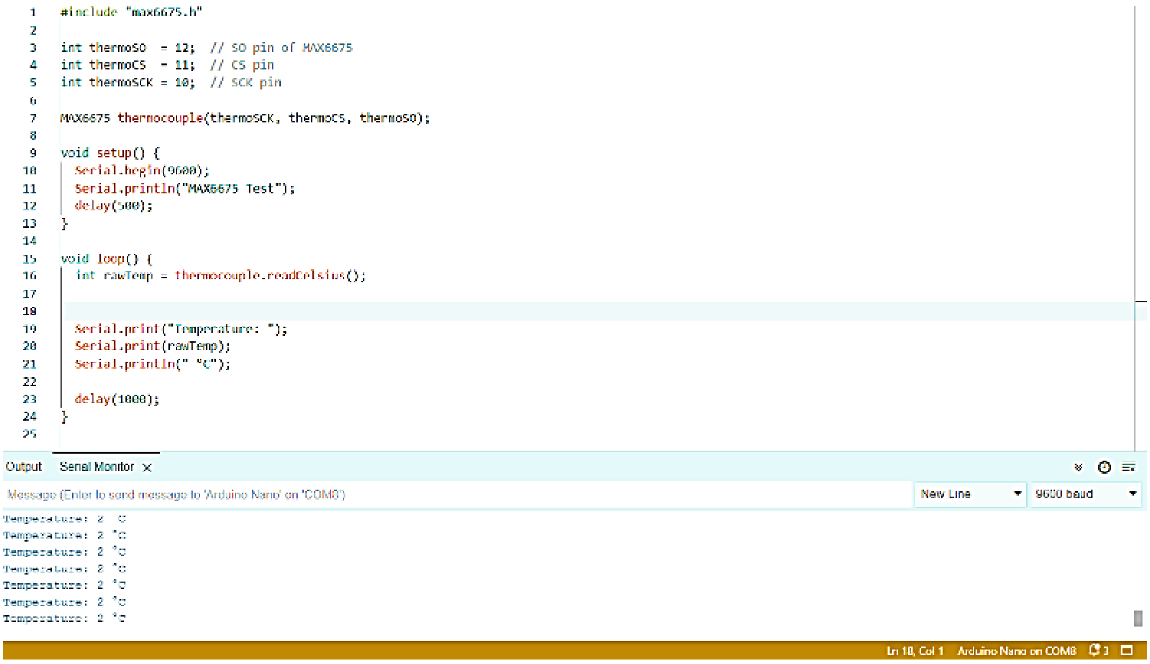

Figure 34: Ice bath temperature given by the k-type thermocouple

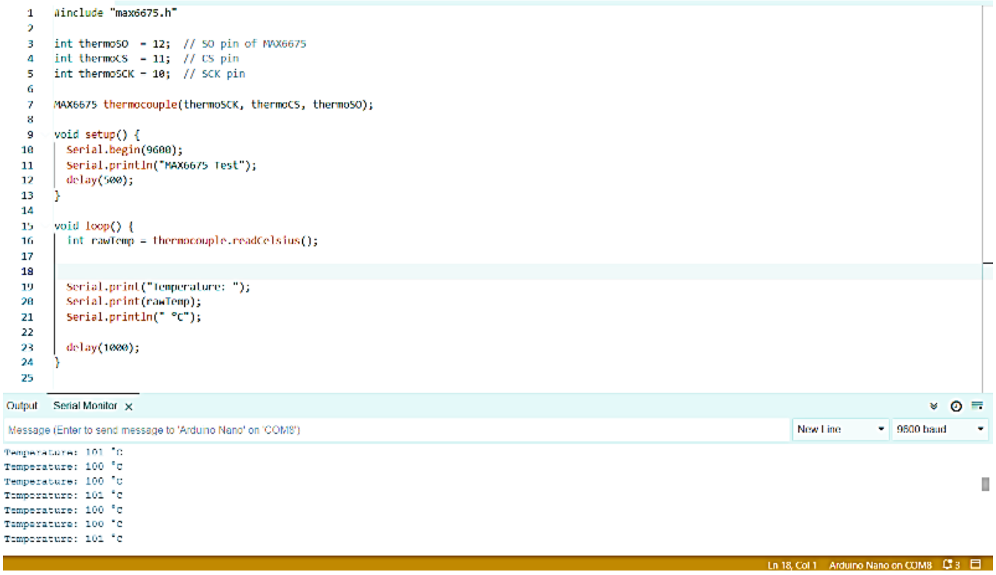

Figure 35: Boiling water temperature given by the k-type thermocouple

The gas sensing and exhaust system worked as required. When fumes were detected, the gas sensor properly acted on the relay, thus switching on the exhaust fan. This accordingly removed the dangerous soldering fumes from the working space, thus promoting safety in the working environment. When the level of fumes reduced, the fan was automatically switched off. This safety system worked automatically and proved quite effective in maintaining a cleaner and more secure working environment.

The cooling system was tested, and it was observed that the 12V DC cooling fan kicked in at once when its switch was turned on. This operational aspect made it easy for the heated PCB to cool fast after soldering operations, thus improving safety and ease of handling compared to passive means of cooling. This feature proved very effective, especially in reducing downtime between soldering operations.

The heating capability of the constructed 600W aluminum hot plate was characterized by determining how long it would take to reach some setpoint temperatures from ambient (25 °C). The findings indicated that the plate had a very quick heating response time, achieving lower setpoints in under a second and high soldering temperatures in less than a minute. Table 1 includes a description of observed heating times for some temperature levels.

Target Temp (°C)	**Time (seconds)**	**Time (minutes)**
25 (room temp)	0	0.00
50	15	0.25
100	45	0.75
150	90	1.50
200	150	2.50
250	240	4.00

Table 4: Observed heating times for some temperature levels

Additional work could be done on adding different soldering profiles for SMD reflow, improving the enclosure design for better safety and aesthetics, adding a more efficient fume filtration system, and could be added an alarm system to prevent heating for too long a time period.

4.0 CONCLUSION

This project accomplished creating a working low-cost PCB soldering hot plate with automated fume extraction and the PCB cooling function. The system shows that good temperature regulation as well as safety protocols can be achieved economically with microcontroller-based systems and salvaged parts. The most important automation feature is the fume extractor addresses user health safety concerns and does not require action to initiate. Because of this, it is highly applicable for schools, hobbyists, and small-scale electronics workshops that are financially constrained.

ACKNOWLEDGEMENTS

The authors would like to express their sincere gratitude to everyone who supported and contributed to this project.

REFERENCES

[1] Health and Safety Executive, "Controlling health risks from rosin (colophony) based solder fluxes," INDG249, Rev. 1, 2015. Available: https://www.hse.gov.uk/pubns/indg249.pdf

[2] AirBench, "Health risks associated with exposure to solder fumes," 2019. Available: https://www.airbench.com/latest/health-risks-associated-with-exposure-to-solder-fumes/

[3] RayPCB, "How do you use a PCB hot plate for SMD soldering?," Nov. 23, 2023. Available: https://www.raypcb.com/pcb-hot-plate/

[4] Hamzanadeem96, "Automated smoke detected exhaust fan," SlideShare, 2023. Available: https://www.slideshare.net/slideshow/automated-smoke-detected-exhaust-fan/167923812

[5] Electronoobs, "Homemade reflow hot plate for SMD soldering - 3000W," Jun. 27, 2021. [Video]. Available: https://www.youtube.com/watch?v=C7blZigaaaA

[6] Electronoobs, "Homemade reflow HOT plate - version 2 | Low cost," Nov. 20, 2022. [Video]. Available: https://www.youtube.com/watch?v=9q0mh3y_XBc

[7] MK Smart Creations, "How to make a smoke detection alarm system with exhaust fan || Award winning science project," Sep. 21, 2024. [Video]. Available: https://www.youtube.com/watch?v=nZd4TEoKbfU

[8] AirBench, "Carbon filtration and fume extraction," Jun. 2023. Available: https://www.airbench.com/latest/carbon-filtration-and-fume-extraction/

DESIGN AND IMPLEMENTATION OF SMART WATER QUALITY MONITORING SYSTEM

W.B.R.Sirimanna*, L.D.R.D. Perera
Department of Electronics, Wayamba University of Sri Lanka, Kuliyapitiya, Sri Lanka
*binusirimanna@gmail.com

ABSTRACT

Manual monitoring of water quality parameters in treatment plants is a time-consuming and labor-intensive process that is prone to human errors. This study addresses these limitations by designing and implementing a low-cost, real-time water quality monitoring system using Internet of Things (IoT) technology. The system integrates sensors for pH, turbidity, and total dissolved solids (TDS) with an ESP32 microcontroller to enable autonomous, continuous measurement and data acquisition. A GPS module is incorporated to provide geospatial tagging of the collected data. The proposed system automates the measurement and logging processes that are currently performed manually at the Ambathale water treatment plants, eliminating the need for hourly manual checks and physical record-keeping. The system was successfully calibrated and tested, demonstrating reliable and accurate performance. Results indicate that this smart system offers a robust, efficient, and data-centric solution that can significantly enhance operational efficiency, reduce labor costs, and improve the responsiveness of water quality management in modern treatment facilities.

Keywords: **W**ater Quality, **E**SP32, **S**ensors

1.0 INTRODUCTION

Having clean, safe water is crucial for everyone's health, so treating it properly and monitoring it closely should be given high priority. Important parameters like pH levels, water clarity, and total dissolved solids provide significant information about water quality [1]. These parameters are important because they indicate whether the water treatment is functioning properly and whether the water is safe to drink.

Currently, many water treatment plants, such as those in Ambathale, check these parameters manually. Operators at the plant must collect water samples regularly, typically every hour, and test them on-site using color tablets and tubes. They record all the results. For more detailed analyses, samples are sent to a laboratory [2], where lab personnel use sophisticated equipment and document the results. This process is time-consuming, labor-intensive, and prone to human error. Furthermore, it may take some time to detect issues with the water, which could allow substandard water to enter the water supply.

However, new technologies like the Internet of Things (IoT) can improve the water treatment process [3]. IoT enables continuous, automated monitoring rather than hourly manual checks [4]. Smart sensors installed in the water tanks can continuously measure parameters and send the information to a central computer system. This approach reduces the time and effort required for manual monitoring and provides extensive data for timely interventions. This research therefore addresses a crucial question: Can an IoT-based sensor system provide a more efficient, accurate, and reliable method for monitoring critical water quality parameters compared to conventional manual techniques in water treatment plants?

2.0 EXPERIMENTAL

2.1 System Architecture and Integration

This research focuses on building a water quality monitoring system that uses IoT technology to automatically measure, record, and display important information. At the core of the system is an ESP32 microcontroller, which communicates with sensors that measure pH, turbidity, and TDS. A GPS module is also included to provide location data. The ESP32 collects readings from the sensors, processes the data, and sends it, along with time and location information, to a cloud server via Wi-Fi. This allows real-time viewing of the data on a secure website and maintains a log, eliminating the need for manual sampling. This approach is useful for managing water treatment in a data-driven manner. The system architecture was designed for comprehensive water quality monitoring and now includes an audible alert mechanism. An active buzzer module was integrated with the ESP32 microcontroller (connected to a digital GPIO pin) to provide immediate, on-site audible alarms. The buzzer is programmed to activate when any sensor reading (pH, turbidity, or TDS) exceeds predefined safety thresholds, providing instant physical notification to plant operators in addition to digital alerts on the web dashboard.

Table 1: Technical Specifications of Sensors

Sensors	Model/ Description	Measurement Range	Key Specifications
pH Sensor	Analog pH Sensor Module (PH-4502C)	0 to 14 pH	Output: Analog (0-3V) Probe: Laboratory Grade BNC Connector
Turbidity Sensor	Turbidity Sensor Module (TSW-30)	0 to 1000 NTU	Output: Analog & Digital Principle: Infrared LED (wavelength 950 nm)
TDS Sensor	Analog TDS Sensor Module	0 to 1000 ppm	Output: Analog (0-3V) Electrode: Graphite Test Current: 5-10mA

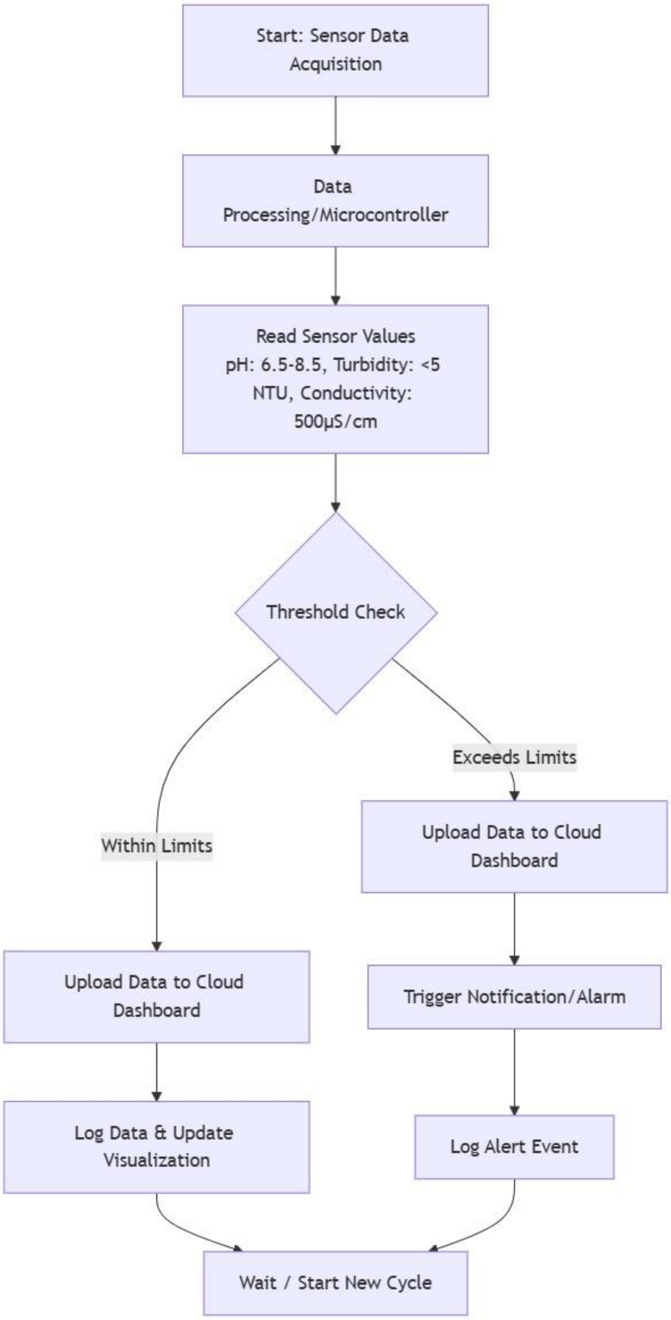

Figure 2.1: Flow chart of the system

2.2 Sensor Integration

The hardware implementation focused on integrating the core components into a single, robust unit capable of autonomous operation in a water treatment environment. The ESP32 microcontroller was established as the central processing hub [5], responsible for coordinating all data acquisition and communication functions. The pH, turbidity, and TDS sensors were connected to the microcontroller's analog input channels to enable continuous measurement of water quality parameters [6, 8]. A GPS receiver was incorporated into the system and linked via serial communication to provide precise geolocation tagging for each collected data point. A regulated power supply system was designed to deliver stable voltage levels to all active components, ensuring consistent and reliable operation [7]. The entire assembly was securely housed in a protective, weather-resistant enclosure, with appropriate openings for the sensors to interface with the water source, resulting in a self-contained, field-deployable sensor node.

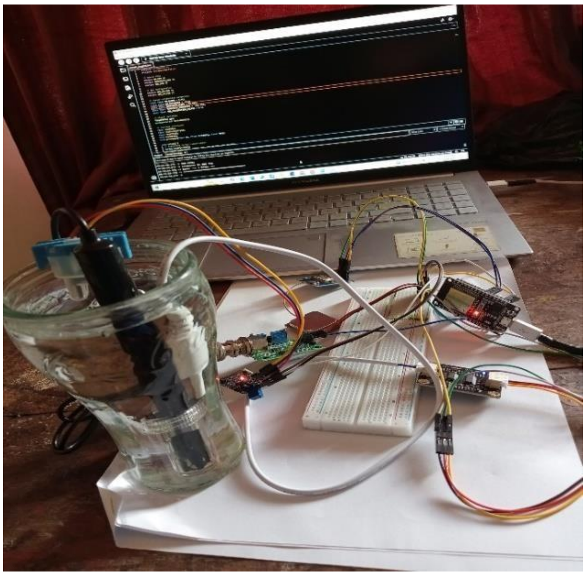

Figure 2.2: Component Integration on a Breadboard

2.3 Chamber for Sensor System

The experiment was carried out using a special flow chamber so the sensors could continuously monitor water quality directly in the system. It consists of a main pipe with water entering at the bottom and exiting at the top, so the water flows steadily. The sensors for pH, turbidity, and TDS are installed through sealed holes on top, so they remain in contact with the water. This setup protects the sensors from dirt and enables real-time monitoring of the water during treatment, without the need for manual sampling.

Figure 2.3: Prototype of the Chamber

2.4 Sensor Thresholds and Justification

The thresholds for pH, TDS, and turbidity were selected based on standard water quality guidelines to ensure safe monitoring. The pH range of 6.5–8.5 is considered safe for drinking water . TDS levels below 500 ppm are acceptable , and turbidity should not exceed 5 NTU . These thresholds guide the system's audible and digital alerts, including activation of an onsite buzzer when any sensor reading exceeds safe limits. This ensures timely notification to plant operators, allowing immediate intervention to maintain water quality within acceptable ranges.[9]

2.5 Software architecture

The software is designed to handle data automatically. The system's code ensures that all processes operate in order, starting with initializing the sensors and acquiring data at regular intervals. The system processes the raw signals to obtain accurate measurements. Then, it checks these values, adds location and time information from the GPS, and organizes the data into structured packages. The system securely transmits this information to online storage. A web interface retrieves the data from storage and displays it on a user-friendly dashboard, allowing real-time monitoring. The website presents charts, maps, and numerical data, enabling operators to observe and control the system remotely. The software monitors for errors, such as faulty connections or corrupted data, to maintain smooth operation and can trigger alerts if readings exceed predefined limits. This approach eliminates manual monitoring and provides continuous, reliable water quality information.

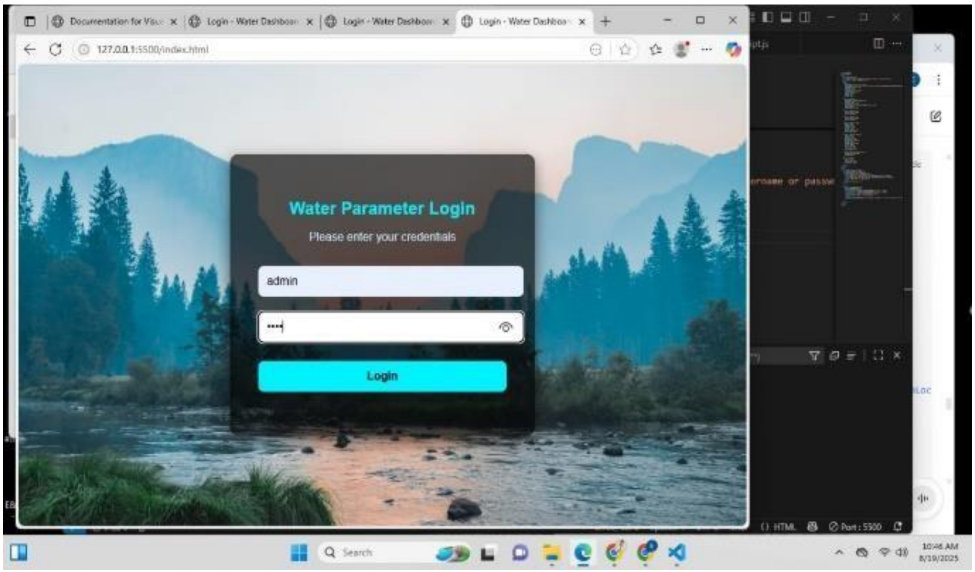

Figure 2.4: Secure Login Interface for System Access

3.0 RESULTS AND DISCUSSION

3.1. Hardware System Performance

The integrated sensor system demonstrated excellent measurement capability and operational stability. Comparative validation against reference instruments confirmed strong correlations across all parameters: pH values consistently aligned with laboratory standards, turbidity measurements captured variations with high sensitivity, and TDS readings maintained stable response characteristics. The hardware platform successfully sustained uninterrupted operation throughout the evaluation period, reliably capturing and processing continuous water quality data. The robust physical implementation proved suitable for treatment plant environments, with all components operating within specified parameters. The buzzer module performed reliably during testing, activating consistently during parameter excursions without affecting primary data acquisition or transmission functions.

Figure 3.1: Real-time Monitoring at Water Treatment Plant Inlet

3.2. Software and Data System Performance

The software architecture delivered exceptional data handling and automation performance. The system achieved consistent and reliable data transmission to cloud storage, successfully logging all measurement intervals without interruption. Real-time data visualization provided effective monitoring capabilities, while automated alert functions demonstrated prompt responses to parameter variations. The complete integration of measurement, transmission, and visualization components effectively eliminated the need for manual data recording. The software solution successfully transformed the monitoring paradigm from intermittent manual checks to continuous digital oversight, providing a foundation for advanced water quality management through comprehensive data availability and system automation.

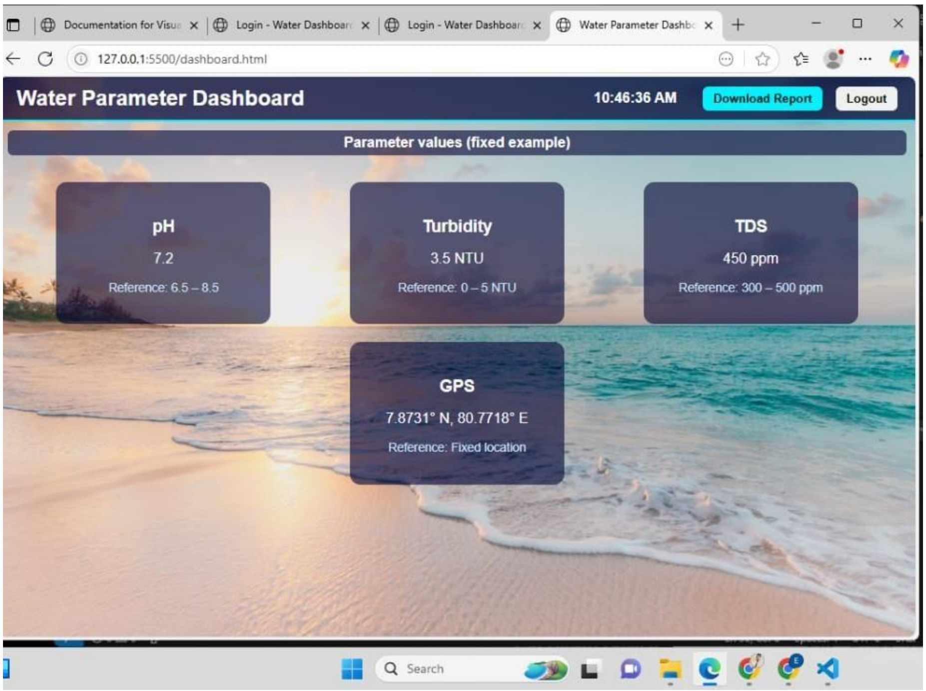

Figure 3.2 : Real-time Water Quality Monitoring Dashboard

3.3 System Accuracy and Validation

The accuracy of the developed monitoring system was validated through direct, simultaneous comparison with calibrated professional-grade meters. A raw water sample was measured using both the prototype system and the reference instruments. The reference meters recorded values of pH 6.6, turbidity 12.6 NTU, and conductivity 54.4 µS/cm. The system's sensors provided readings of pH 6.4, turbidity 12.1 NTU, and TDS 28.2 ppm. The TDS value was converted to conductivity (53.2 µS/cm) using the standard ratio (1000 µS/cm ≈ 530 ppm), enabling direct comparison. The close agreement between these measurements confirms the practical accuracy and reliability of the IoT system for continuous water quality assessment.

Figure 3.3: Validation setup with reference meters

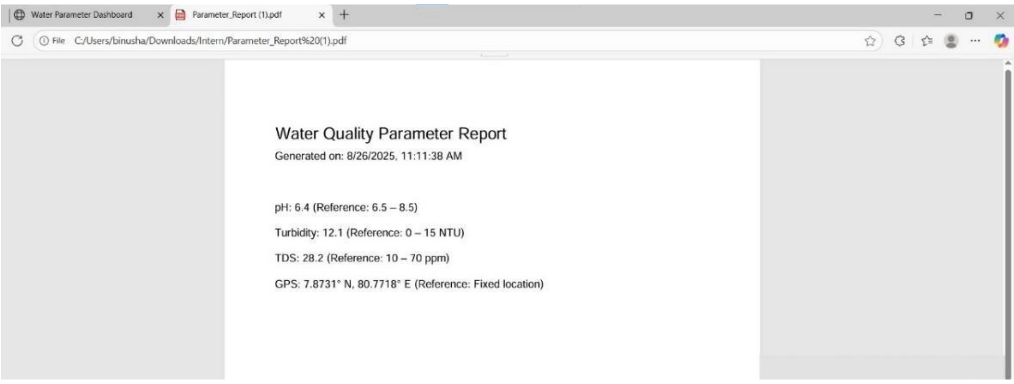

Figure 3.4: Web dashboard data report

3.4 Limitations and Future Work

The system's current limitations include dependence on Wi-Fi for data transmission, the need for periodic manual sensor calibration, and a non-portable power supply. However, its low-cost design provides significant economic advantages over traditional methods. Future enhancements will focus on integrating cellular connectivity, solar power, additional sensors, and machine learning for predictive analytics to improve robustness and functionality.

4.0 CONCLUSION

This study successfully developed and demonstrated an automated IoT-based water quality monitoring system that effectively addresses the critical limitations of manual testing methods employed at the Ambathale treatment plants. The integrated system, comprising pH, turbidity, and TDS sensors coupled with an ESP32 microcontroller and real-time data transmission capabilities, proved capable of continuously and accurately measuring key water parameters while eliminating human errors and reducing labor requirements. By enabling seamless, cloud based data logging and remote visualization through an intuitive dashboard, the prototype not only enhances operational efficiency but also provides a scalable, cost-effective solution for modernizing water quality assurance in treatment facilities. The outcomes of this research affirm the practical viability of smart monitoring systems and establish a foundation for future integration of predictive analytics and expanded sensor networks in public water infrastructure.

ACKNOWLEDGEMENTS

The authors would like to express their gratitude to the academic staff at the Department of Electronics, Faculty of Applied Sciences, Wayamba University of Sri Lanka for their advice and guidance.

REFERENCES

[1] L. Chen and Y. Wang, "Optimization of smart water quality monitoring networks using a multi-criteria spatial decision analysis," *J. Environ. Eng.*, vol. 15, p. 112, 2021. doi: 10.1016/j.jenveng.2021.03.007

[2] A. Kumar and R. Patel, "Design and simulation of an IoT-enabled automation architecture for urban water distribution systems," *Int. J. Electron.*, vol. 22, p. 45, 2019. doi: 10.1080/00207217.2019.1678945

[3] T. Nakamishi and K. Ito, "A non-contact, optically based instrumentation system for heavy metal trace analysis in industrial wastewater," *Meas. Sci. Technol.*, vol. 35, p. 171, 1994.

[4] H. Patel, V. Sharma, and S. Kumar, "Multi-layer cloud data visualization framework for municipal public utilities and water distribution management," *Int. J. Environ. Sci. Technol.*, vol. 19, pp. 7931–7944, 2022. doi: 10.1007/s13762-021-03610-w

[5] J. D. Smith, *Automation of Public Utility Systems*. Amsterdam, Netherlands: Elsevier, 2018.

[6] B. Bowen, K. Natasha, and S. Guo, *Data Visualization and Cloud Computing*. Oxford, U.K.: Oxford University Press, 2022.

[7] K. Eckerberg, "Implementation of automated systems in public utilities," Doctoral dissertation, Stockholm University, Stockholm, Sweden, 2017. Available: DiVA.

[8] J. Jowit, "Water safety monitoring goes digital," *The Engineer*, Mar. 15, 2023. Available: https://www.theengineer.co.uk

[9] World Health Organization, *Guidelines for Drinking-Water Quality: Fourth Edition Incorporating the First and Second Addenda*. Geneva, Switzerland: WHO Press, 2022. Available: https://apps.who.int/iris/handle/10665/352532

Proc. Annual Symposium on Research & Industrial Training, 12 (2025) 230-237
Department of Electronics – Wayamba University of Sri Lanka

DESIGN AND CONSTRUCTION OF AN AUTOMATED DEVICE TO MEASURE THE USAGE OF A HIGH-PRESSURE CLEANING MACHINE

B.P.H.S. Wijayanthi[1]*, Y.A.A. Kumarayapa[1], R.A.A.N. Ranasinghe[2]
[1]*Department of Electronics, Wayamba University of Sri Lanka, Kuliyapitiya, Sri Lanka*
[2]*Tudawe Trading Co. (Pvt) Ltd, Narahenpita, Colombo 05, Sri Lanka*
*hirunishalika06@gmail.com

ABSTRACT

High-pressure cleaning machines are widely used in both domestic and industrial environments. However, there is no mechanism to record the operating time. This paper presents the design and construction of a smart hour meter device that can automatically measure and record the operating times of high-pressure cleaning machines. The motor of the high-pressure machine runs only when the high-pressure gun of the machine is triggered. The proposed device is used to measure the running time of the machine. In order to obtain this time accurately, this device is designed to integrate with an ESP32 microcontroller, an AC optocoupler current sensor, and a real-time clock module. A web interface is used to obtain runtime information and the AP(access point) mode of the ESP32 is used to access it. This method is used to obtain runtime information through the web interface via the IP address, even without an internet connection. Initial tests confirmed the device's high accuracy, and a 12-day field test showed that it worked reliably in a real environment, confirming that it was more efficient than manual data recording.

Keywords: **S**mart hour meter, **H**igh-pressure machine, **E**SP32

1.0 INTRODUCTION

High-pressure cleaners have become a necessary part of both the domestic and industrial sectors due to their efficiency and low water consumption. However, one of the problems with these machines is that they do not have a mechanism to monitor the operating time. This shortcoming creates challenges in warranty verification during repairs during the warranty period. When customers bring these machines for repair, it is not possible to determine whether these machines have failed due to excessive handling. Problems like that are faced due to the lack of accurate data. Technicians can say that they have used them for a long time, but there is no evidence to prove it, which causes arguments between service providers and customers. An operating time measuring device is suitable to solve this problem.

Previous studies have attempted to monitor equipment and obtain information. For preventive maintenance scheduling, Sitompul and Rohmat have introduced an IoT-based real-time monitoring system. This system provides centralized collection and automatic alerts and relies on stable internet connectivity and cloud infrastructure. It is used for large systems and is not suitable for use in equipment such as high-pressure cleaners, as it requires high costs [1]. Gheorghe et al. have focused on monitoring power consumption using ESP32 microcontrollers. This design provides insight into energy usage and can indirectly estimate machine activity. This does not provide information about running time [2]. Similarly, Sarojini et al. developed a smart real-time data logging system for industrial automation using the I²C protocol. Their approach highlighted the effectiveness of low-cost microcontroller-based data transfer and storage, but it was designed for broader industrial data collection rather than targeted runtime measurement [4].

Considering these limitations, the most appropriate solution to this problem is to install a low-cost, independent, easily mountable, and accurate data acquisition device on high-pressure cleaners. This solution is important because it provides a practical transparency device for both consumers and service providers, thereby enabling liability verification.

2.0 EXPERIMENTAL

2.1 System Overview

The proposed runtime measuring device is designed to detect motor activation and measure the operating hours of the high-pressure machine. When the main switch of the high-pressure cleaner is turned on, the motor starts to run, and when the high-pressure gun is pressed, the motor stops running. When the gun is released and pressed again, the motor starts to run again. Thereafter, the motor runs only when the trigger is pressed. When the gun is turned on, current is supplied to the motor through the bypass valve connected to the switch. To detect this, an optocoupler is used, which is connected to the connection line to which the motor is connected after the switch. When the high-pressure gun is turned on, the motor starts to run, and the runtime is logged to the RTC (real-time clock) module through the optocoupler. The collected data is stored in non-volatile memory. The switch enables the ESP32 to be in AP (access point) mode, and the runtime can be checked from a phone or laptop via a web interface by entering the IP address via WiFi. If the runtime needs to be reset, the reset button must be pressed. The overall system design is illustrated in the block diagram in Figure 2.1

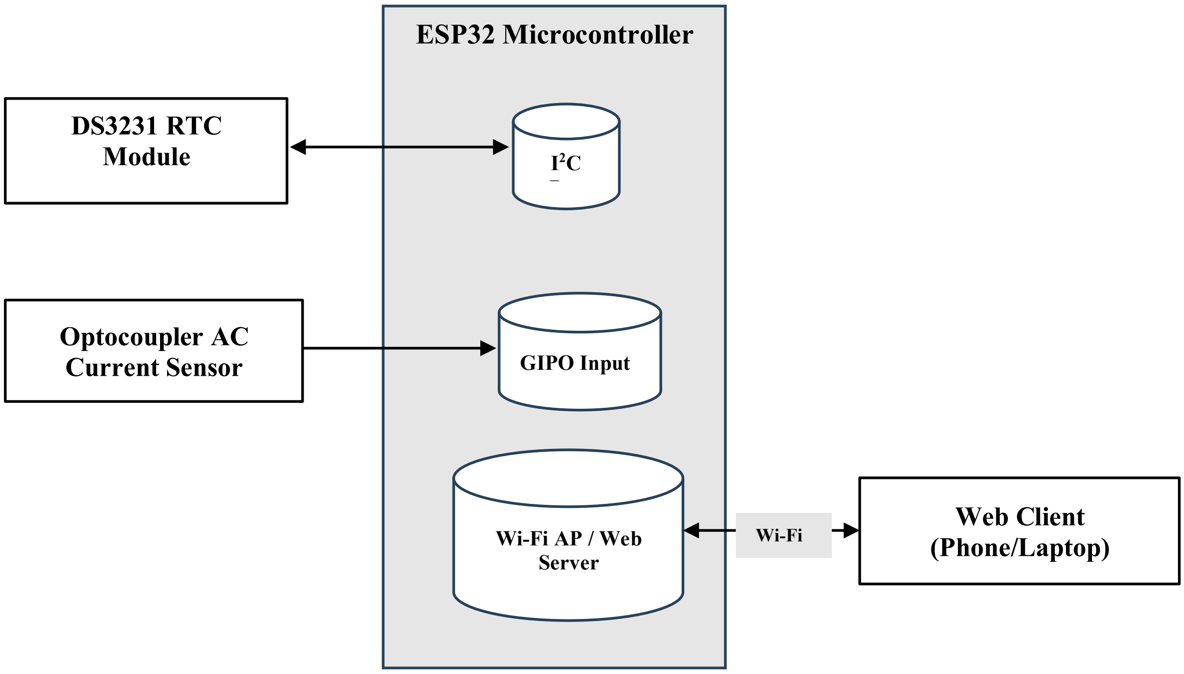

Figure 2.1: Simple Block diagram of the proposed system

2.2 Flow Chart

The logic of the system is based on detecting current from the motor and incrementing the runtime counter when activity is present. The following flow chart (Figure 2.2) was prepared to clearly represent the process.

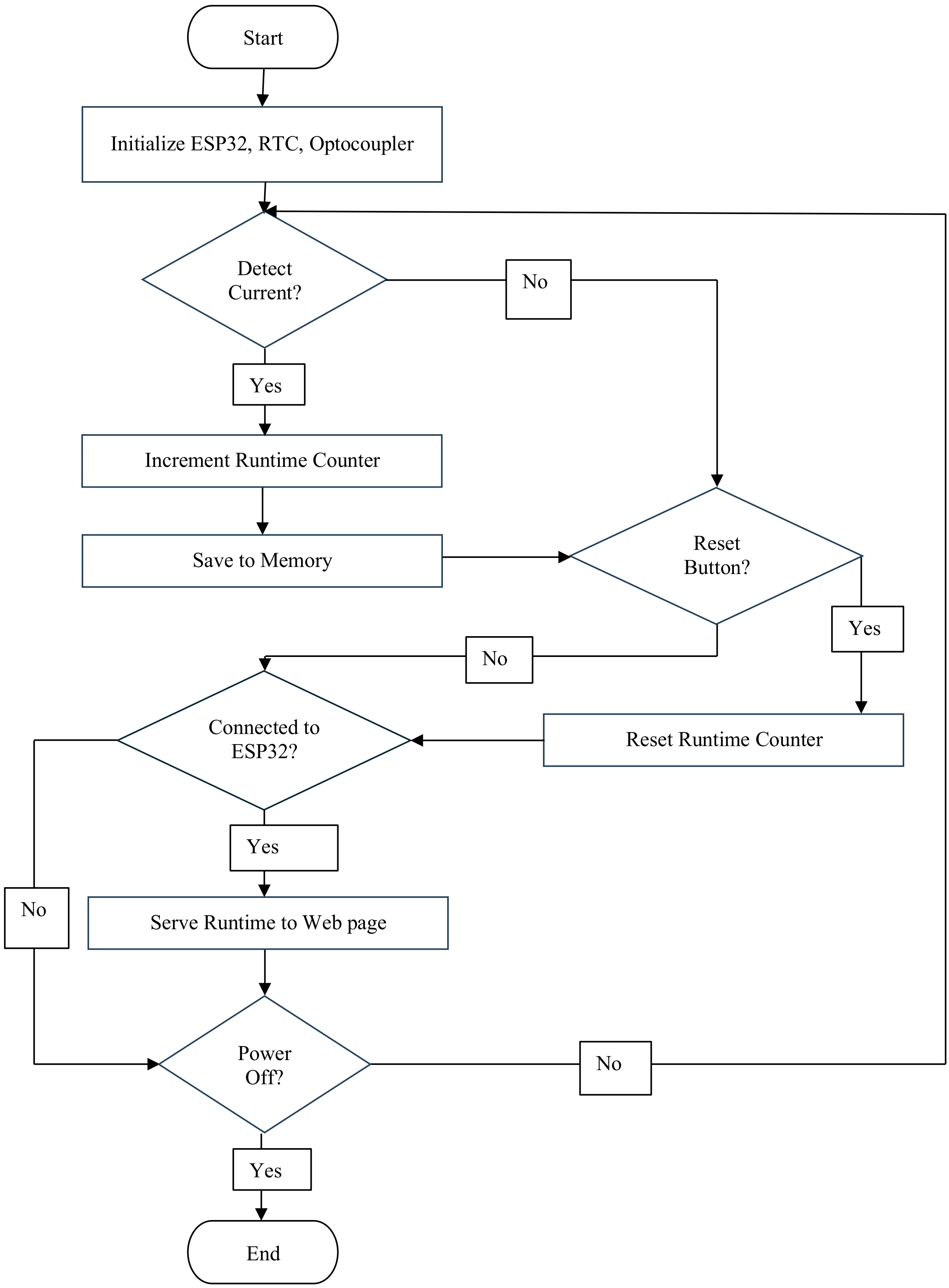

Figure 2.2: Flow chart of the proposed system

2.3 System Components and Tools

The following hardware and software were selected for the project based on their cost-effectiveness, combined with functionality and ease of use.

- ESP32 development board: As the central microcontroller manages the data received from the sensors and hosts a web server in the form of an access point (AP mode) for easy access.
- AC optocoupler module (Figure 2.3(a)): This is used to non-intrusively detect the presence of AC in the motor power line when the high-pressure gun is operating. The optocoupler provides electrical isolation, ensuring that the low-voltage control circuit is protected from the high-voltage power line.
- DS3231 real-time clock (RTC) module (Figure 2.3(a)): An RTC module is included to ensure accurate recording of operating times, even when the main power supply is disconnected. It operates on battery backup, maintaining time accuracy.
- Step-down power supply module: This component is essential for converting the power taken from the mains power supply (AC) to the 5V power supply (DC) required to power the ESP32 and other modules.
- Switches: These are used for user interaction, allowing the user to activate AP mode, connect to the device, and reset the accumulated run time.
- Proteus software: This software is used to draw and simulate circuit designs before physically building.
- Arduino IDE software: This software is used to write the code required to operate the circuit and upload it to the ESP32 microcontroller.

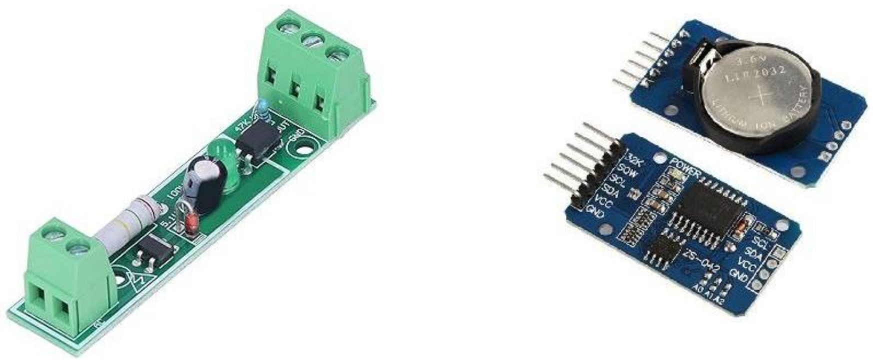

(a) (b)

Figure 2.3: Key Components of the project; (a) Optocoupler module, (b) RTC module

2.3 Circuit Diagram and Pin Connections

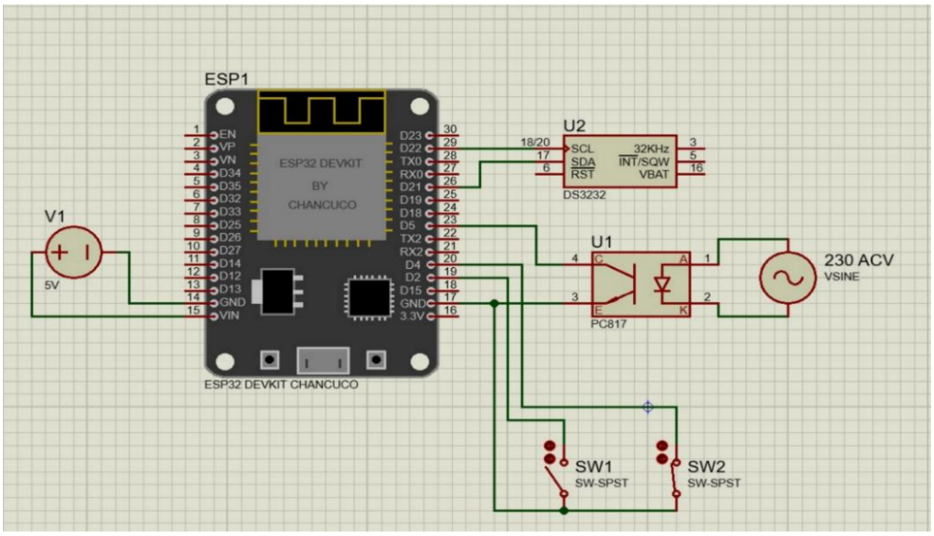

Figure 2.4: Circuit diagram of the proposed system with pin connections

A detailed circuit was created to integrate all the components, as shown in Figure 2.4. The optocoupler sensor detects the motor current and sends a logic signal to the ESP32. The DS3231 RTC communicates with the ESP32 using the I²C protocol (SDA and SCL pins). The reset push-button is connected to a GPIO pin configured with a pull-up resistor. Power is supplied through a 5V adapter regulated for both ESP32 and peripheral modules. In addition, extra wires are provided from the ESP32 so that an LCD can be connected if an AP mode connection is not possible.

2.3 Hardware Implementation.

The hardware implementation phase is concerned with the integration of the components chosen into a long-lasting prototype (Figure 2.5(b)). The last shape of the device is a unit that mounts on a high-pressure cleaner and is focused on portability and easy mounting. When installed in the machine as shown in Figure 2.5(b), it can be installed without changes to the original factory hardware. This device can provide a good solution for proper monitoring of the machine usage.

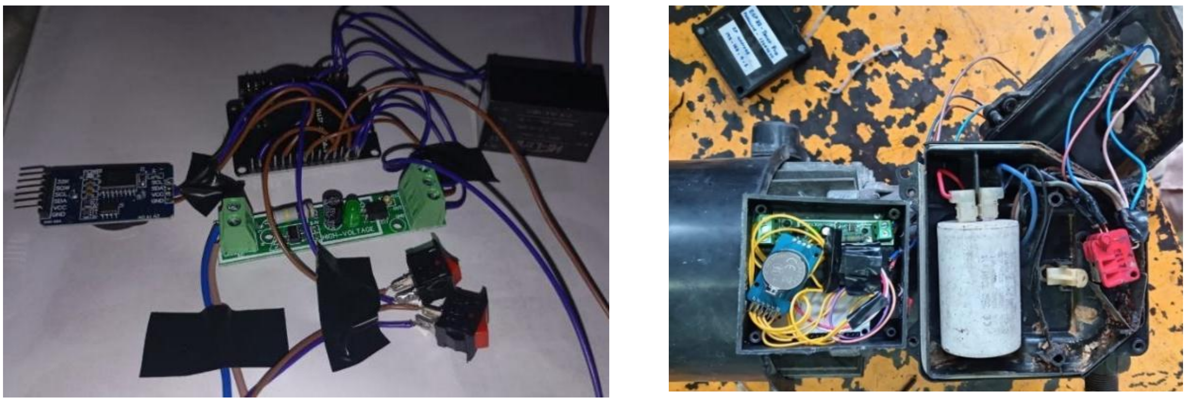

(a) (b)

Figure 2.5: (a) The final Prototype Product Circuit (b)After installation in the High-Pressure Machine

The prototype is housed in a waterproof enclosure, as shown in Figure 2.6. This cover renders the device apt when used in a practical environment, as it protects the internal parts and ensures that it works safely. An external switch is provided on the box, allowing the user to turn the Access Point (AP) mode off or on easily without opening the enclosure. The local network password and Wi-Fi name (SSID) of the device are printed on the box. This enables any user to simply connect to this via a smartphone or a laptop. The box also shows the IP (Internet protocol) address of accessing the interface on the web.

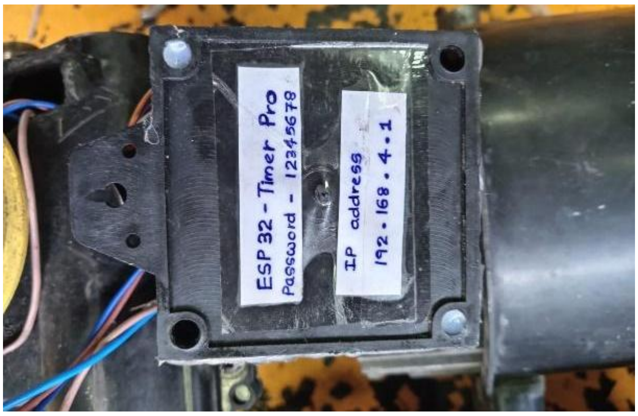

Figure 2.6: Enclosed Prototype Design with User Interface Details

3.0 RESULTS AND DISCUSSION

3.1 Performance and Accuracy Testing

Initial testing of the device focused on verifying the accuracy of its time tracking mechanism. A controlled test was conducted by running the machine for 14 minutes, and the duration was measured using a stopwatch. The time recorded by the device and the time recorded by the stopwatch matched exactly, confirming that the device has a high accuracy in capturing operating time. This indicates that the internal clock and current detection system are operating as expected and accurately recording the exact running time of the machine's motor.

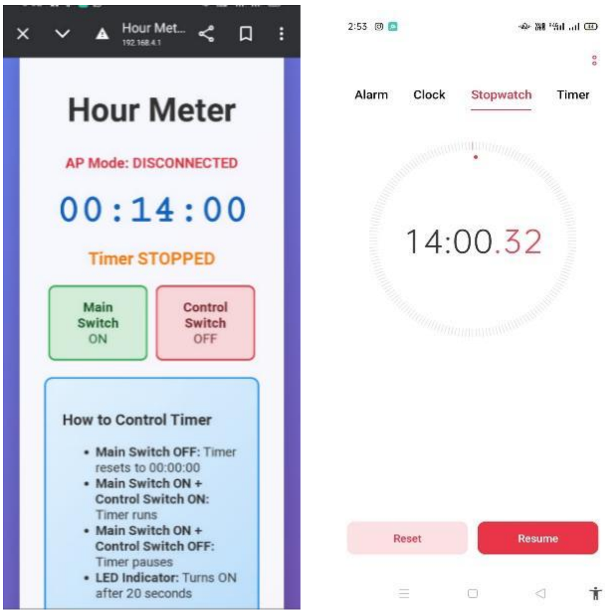

(a) (b)

Figure 3.1: Initial Test Run Validation; (a) Web Interface Readings (b) Stopwatch Readings

Following initial testing, the completed prototype was installed on an HD 5/11 model high-pressure cleaner to assess its performance in a real-world, operational environment. The device was monitored over a period of 12 days, and its performance was checked at four specific intervals: after 2 days, 4 days, 7 days, and 12 days.

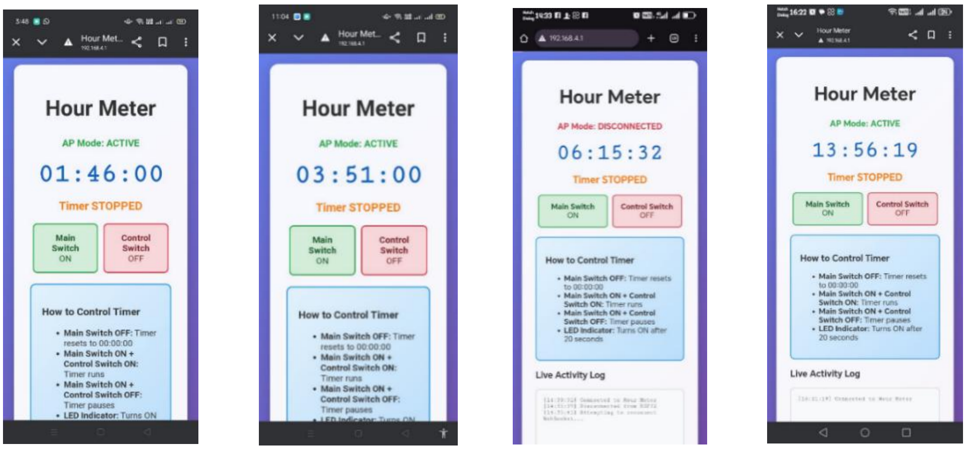

(a) (b) (c) (d)

Figure 3.2: Web Interface Runtime Records after (a) 2 days (b) 4 days (c) 7 days (d) 12 days

The data obtained from the device was compared with manual data recorded using a stopwatch by technicians during the first four days.

Table 3.1: Comparison of Manual and Device-Recorded Run-Time

Check-in Date	Manual Log Time	Total of two by two (Manual)	Device Recorded Time	Difference
Day 1	0:58:00	1:54:00	1:46:00	0:08:00
Day 2	0:56:00			
Day 3	1:10:00	2:11:00	3:51:00	0:06:00
Day 4	1:01:00			

The manual process relies on the reaction time of a technician, whereas the device timer accurately captures the precise moment the machine's motor is turned on and off. This results in a small delay at the beginning and end of each usage session, resulting in a slightly longer total time recorded manually.

3.3 Discussion of Findings

The results of the study confirm the development of a device that is not only accurate but also practical for real-world applications. Initial testing confirmed the accuracy of the device, while field testing highlighted the reliability and value of the approach over manual logging. The difference between manual and automatic logging clearly demonstrates the lack of reliability of traditional methods.

The final design, with a robust waterproof casing and a simple external user interface, can be easily used to capture the operating time of any machine. This device stands alone and does not need external servers or cloud services. This renders it more attractive since it removes on-demand expenses and eliminates connectivity. The web interface provides a good record of machine usage. This can help technicians detect issues and manage their maintenance timetables. Besides the AP mode web interface, an LCD is also provided as an alternative to display the runtime directly in case there is no wireless access.

4.0 CONCLUSION

This project has been successful in the creation of an automated and cost-effective machine for measuring the use of high-pressure machinery, which was felt as a serious requirement in the industry. Using an ESP32 microcontroller and a sensor based on an optocoupler, the system was very precise and dependable in practical demonstrations and surpassed the accuracy of manual data recording. Its portability and design as a standalone module with user friendly web interface offer a convenient remedy for maintenance planning and warranty validation without requiring an internet connection. The device also offers a clear and verifiable history of machine usage, which enhances the accountability of both the service providers and the customers. This can be improved with additional features like remote monitoring being integrated into the work in the future to enhance its functionality and relevance in the market.

ACKNOWLEDGEMENTS

The authors would like to express their special thanks to the lecturers and staff of the Department of Electronics Science, Faculty of Applied Sciences, Wayamba University, and Tudawe Trading Co. (Pvt.) Ltd. for their valuable guidance and support in this research.

REFERENCES

[1] E. Sitompul and A. Rohmat, "An IoT-based running time monitoring system for machine preventive maintenance scheduling," *ELKHA: J. Tek. Elektro*, vol. 13, no. 1, pp. 33–40, 2021. doi: 10.26418/elkha.v13i1.44299

[2] A. C. Gheorghe, E. Stan, and I. Udroiu, "Electricity consumption measurement system using ESP32," *Sci. Bull. Electr. Eng. Fac.*, vol. 21, no. 2, pp. 23–26, 2021. doi: 10.2478/sbeef-2021-0012

[3] M. Goletti, M. Grasso, M. Annoni, and B. M. Colosimo, "Condition monitoring of an ultra high-pressure intensifier for water jet cutting machines," *Procedia CIRP*, vol. 12, pp. 193–198, 2013. doi: 10.1016/j.procir.2013.09.034

[4] S. Raju, M. Vijayakumar, and S. Ramalingam, "Smart real-time data logging system for industrial automation using I2C protocol," *Int. J. Comput. Appl.*, vol. 174, no. 15, pp. 18–22, 2019. Available: https://www.researchgate.net/publication/369658402_Smart_Real_Time_Data_Logging_System_for_Industrial_Automation_using_I2C_Protocol

[5] A. Mohrem, B. Chetate, and H. E. Guia, "Measurement and monitoring system with real-time data logging based on a microcontroller," *Int. J. Meas. Technol. Instrum. Eng.*, vol. 7, no. 2, pp. 20–40, Jul. 2018. doi: 10.4018/IJMTIE.2018070102

Proc. Annual Symposium on Research & Industrial Training, 12 (2025) 238-243
Department of Electronics – Wayamba University of Sri Lanka

DESIGN AND IMPLEMENTATION OF A SCINTILLATION DETECTOR USING SILICON PHOTOMULTIPLIER

H.K.A.H.D.Gimhani[1]*, W.A.S.Wijesinghe[1],Prasad Mahakumara[2]
[1]*Department of Electronics, Wayamba University of Sri Lanka, Kuliyapitiya, Sri Lanka*
[2]*Sri Lanka Atomic Energy Board*
hashinidileesha989@gmail.com

ABSTRACT

Scintillation detectors play an important role in detecting ionizing radiation in applications such as medical imaging, nuclear physics, and environmental monitoring. Conventional photomultiplier tube (PMT-based) systems, while effective, are fragile and require high operating voltages, making them unsuitable for portable use. In this study, a compact scintillation detector was designed and implemented using a Thallium-doped Sodium Iodide [NaI(Tl)] crystal coupled with a Silicon Photomultiplier (SiPM). The NaI(Tl) crystal was carefully polished to enhance light transmission and optically coupled with the SiPM using optical glue. The assembly was housed in a light-tight, shielded enclosure to minimize external noise and moisture effects. A low-noise, high-speed operational amplifier circuit was developed to amplify the SiPM output. Experimental testing was carried out using a known gamma radiation source, and the results showed clear detection of scintillation pulses with good signal-to-noise characteristics. The findings confirm that SiPMs can successfully replace traditional PMTs in portable radiation detection systems, offering benefits such as compactness, low power consumption, and durability. This work demonstrates the potential of SiPM-based scintillation detectors for laboratory experiments, educational use, and field-deployable radiation monitoring systems.

Keywords: **S**cintillation detector, **S**ilicon Photomultiplier, **N**aI(Tl) crystal

1.0INTRODUCTION

Radiation detection is a vital requirement in fields such as medical imaging, nuclear physics, and environmental safety. Among the available technologies, scintillation detectors have gained significant attention because of their high sensitivity and relatively simple design. In this process, a scintillating material such as thallium-doped sodium iodide [NaI(Tl)] crystal absorbs incoming ionizing radiation and emits visible light photons. These photons are then detected by a photosensor, in this case a Silicon Photomultiplier (SiPM), which amplifies the signal into measurable electrical pulses. The overall scintillation mechanism is illustrated in Figure 1 in [1,2].

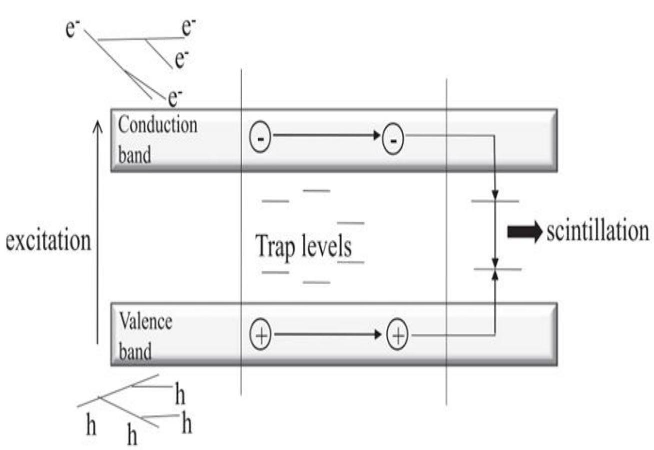

Figure 1.1: Excitation and recombination of electrons in the scintillation process

Traditionally, photomultiplier tubes (PMTs) have been the preferred choice for coupling with scintillation crystals due to their excellent gain and fast timing characteristics.

However, PMTs have several disadvantages, including their large size, fragility, sensitivity to magnetic fields, and the need for high operating voltages (about 1500V), which limit their use in portable or rugged environments. These limitations have motivated research into solid-state alternatives that can offer similar or superior performance with reduced complexity [3].

In recent years, Silicon Photomultipliers (SiPMs) have emerged as a promising alternative to PMTs. As shown in Figure 2, a SiPM consists of an array of avalanche photodiodes operating in Geiger mode, providing single photon sensitivity, high gain, and fast response times. Unlike PMTs, SiPMs are compact, operate at low voltages (20–30V), and are immune to magnetic fields, making them highly suitable for portable and field-deployable detectors [4].

These limitations highlight a research gap in developing low-cost, optimized scintillation detectors that combine the sensitivity of NaI(Tl) crystals with the practicality of SiPMs. This study addresses this gap by designing and constructing a compact detector that emphasizes crystal preparation, optical coupling, shielding, and signal amplification. The system is experimentally validated using standard gamma sources, aiming to demonstrate that SiPM-based scintillation detectors can serve as effective, portable alternatives to conventional PMT-based systems[5].

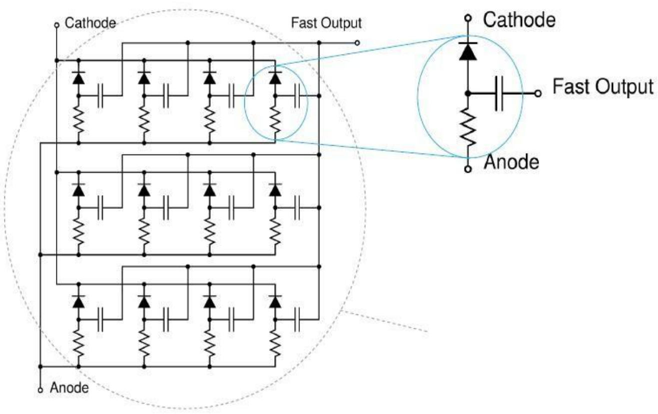

Figure 1.2: Structure of Silicon Photomultiplier

2.0METHODOLOGY

The development of the scintillation detector began with the preparation of the NaI(Tl) crystal. Due to its hygroscopic nature, all polishing and handling were performed in a low-humidity environment. The surfaces of the crystal were polished sequentially using diamond pastes of decreasing grit sizes (14 µm, 3 µm, 1 µm, and 0.5 µm) until a clear, smooth finish was obtained. After polishing, the crystal was carefully cleaned with a microfiber cloth, and one surface was selected for optical coupling. The SiPM was mounted onto this polished face using a thin layer of UV loca glue. To secure the bond and ensure efficient light transfer, the assembly was cured under UV light for approximately 4–5 hours. The process of crystal polishing, SiPM mounting and UV curing is shown in Figure 2.1.

Figure 2.1: Crystal polishing process and SiPM mounting on the NaI(Tl) crystal

The SiPM was biased using a regulated 30 V DC supply. A resistor–capacitor network consisting of a 1 kΩ series resistor, a 10 kΩ resistor to the supply, and a 100 nF capacitor to ground was included to stabilize the bias voltage and reduce electrical noise. The SiPM converts incident scintillation photons into weak electrical pulses that are proportional to the number of photons detected. These pulses typically have low amplitude and require amplification before analysis.

For practical implementation, the SiPM–crystal assembly was enclosed in a custom 3D-printed housing, internally lined with copper foil to block ambient light and reduce electromagnetic interference (Figure 4). The biasing resistors and decoupling capacitor were mounted inside this housing to minimize wiring noise and maintain signal integrity. The detector connections were colour-coded for clarity. The black wire served as the SiPM cathode and was connected to the regulated 30 V supply, the red wire represented the anode and was tied to ground, and the yellow wire carried the output signal. This output was directly interfaced with the amplification stage and subsequently observed on the oscilloscope during testing.

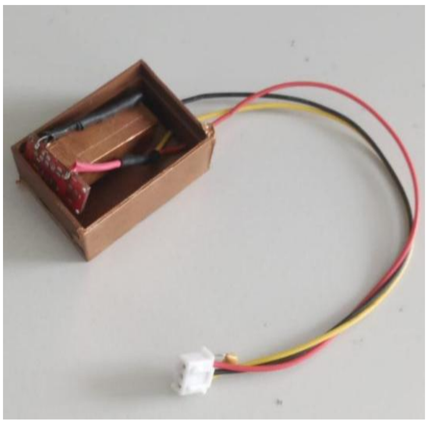

Figure 2.2: Scintillation detector with casing

The weak SiPM pulses were amplified using an LM358P operational amplifier configured in a non-inverting mode. The SiPM output was coupled through a 10 kΩ series resistor (R3) to the non-inverting input, while the gain was determined by the feedback resistor (R5) and the input resistor to ground (R4). For this configuration, the voltage gain (A_v) is given by:

$$A_v = 1 + R_f / R_{in} \tag{1}$$

Substituting the resistor values:

$$A_v = 1 + 1\,000\,000 / 10\,000$$
$$= 101$$

This amplification raised the millivolt-level SiPM pulses into the volt-level range, making them clearly observable on the oscilloscope without distorting the pulse rise and decay times. The amplification stage, together with the biasing and crystal–SiPM assembly, formed the complete detector system. The overall circuit diagram is presented in Figure 5. The system was tested using a Cs-137 gamma radiation source, and the amplified signals were observed on an oscilloscope to verify the detection of nuclear pulses. Key measurements included pulse amplitude distribution, signal-to-noise ratio, and operational stability were tested under repeated trials.

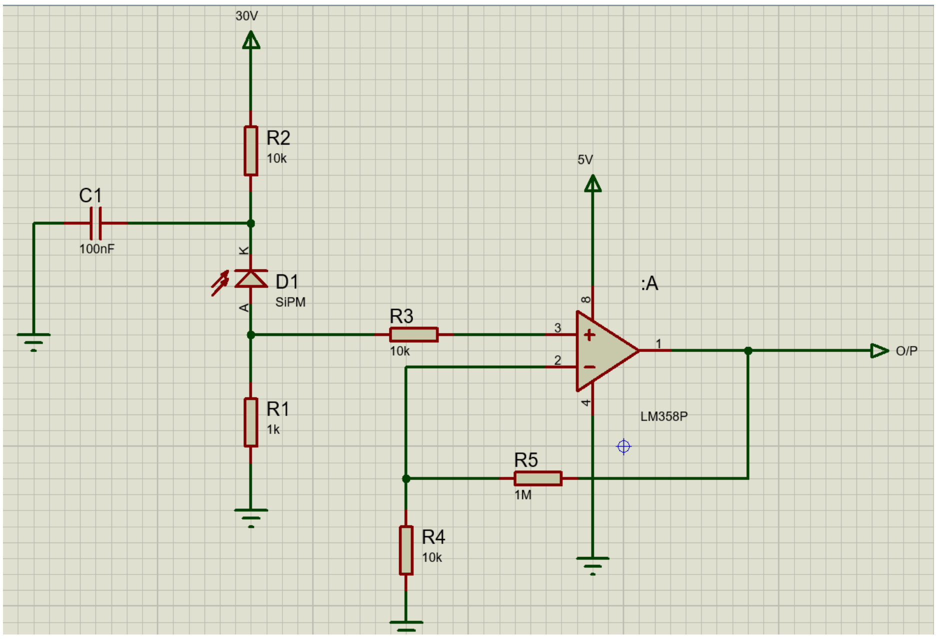

Figure 2.3: Circuit diagram of the system

3.0RESULTS AND DISCUSSION

The scintillation detector was tested with a Cs-137 gamma radiation source to verify its performance. The SiPM coupled to the NaI(Tl) crystal successfully produced nuclear pulses corresponding to scintillation events. Figure 6 shows the oscilloscope traces of the pulses obtained before and after the amplification stage.

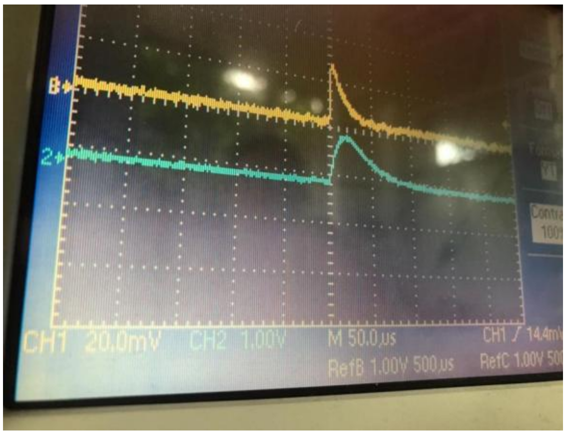

Figure 3.1 : Oscilloscope traces of SiPM signals before (yellow) and after (blue) amplification

From Figure 3.1, it is evident that the raw SiPM output (yellow trace) exhibits very low amplitude signals in the millivolt range, which are difficult to distinguish from electronic noise. After amplification (blue trace), the signal amplitude is significantly enhanced, reaching the volt level, making the nuclear pulses clearly observable and easier to process for further analysis. The rise and decay times of the pulses are preserved after amplification, confirming that the amplifier circuit did not distort the fundamental pulse shape.

The improvement in signal-to-noise ratio highlights the importance of optical coupling, shielding, and amplification in the system design. The copper foil wrapping and light-tight housing minimized interference, while the polished NaI(Tl) surface ensured efficient photon transfer to the SiPM. These design considerations collectively enhanced the detector's stability and performance.

Despite these improvements, some limitations were identified. The LM358P operational amplifier, being a general-purpose device, has a limited bandwidth and response time compared to dedicated nuclear instrumentation amplifiers. This constraint may restrict the detector's energy resolution in spectroscopy applications. Furthermore, pulse height fluctuations were observed due to statistical variations in photon production and collection. Future work could address these limitations by integrating faster, low-noise amplifiers and digital pulse processing techniques to improve resolution and stability.

4.0CONCLUSION

A compact scintillation detector using a NaI(Tl) crystal and SiPM was successfully designed, implemented, and tested. The system demonstrated clear detection of gamma radiation from a Cs-137 source. The results confirmed that while the SiPM alone produces weak signals, the integration of an amplifier circuit significantly enhances pulse amplitude and clarity, making the detector suitable for experimental and monitoring applications.

The study validates the feasibility of using SiPM-based scintillation detectors as a low-cost, portable alternative to traditional PMT-based systems. Key achievements include successful crystal preparation, efficient optical coupling, light shielding, and signal amplification. Limitations include the modest performance of the LM358P amplifier, which may be addressed in future work by incorporating high-speed, low-noise amplifiers and advanced signal processing methods.

Overall, this work contributes to the development of robust, field-deployable radiation detection systems, with potential applications in nuclear research, medical imaging, and environmental monitoring.

ACKNOWLEDGEMENT

The authors wish to extend their sincere appreciation to the Department of Electronics, Wayamba University of Sri Lanka, for their invaluable guidance and academic support throughout this project. The authors also acknowledge with gratitude the Sri Lanka Atomic Energy Board for their technical assistance and insightful contributions, which were instrumental in the successful completion of this study.

REFERENCES

[1] Scionix, "Scintillation detectors," 2025. Available: https://scionix.nl/scintillation-detectors/

[2] Mirion Technologies, "Lab experiment 1: Gamma-ray detection with scintillators," 2020. Available: https://www.mirion.com/discover/knowledge-hub/articles/education/gamma-ray-detection-with-scintillators-lab-experiment

[3] A. Shiri and R. Johnson, "Simplified efficiency calibration methods for scintillation detectors used in nuclear remediation," 2024, *arXiv:2410.09598*. doi: https://doi.org/10.48550/arXiv.2410.09598

[4] S. S. Win, N. Nyein, and N. N. Tun, "Determination of Resolution and Detection Efficiency of NaI (Tl) Scintillation Gamma-Ray Spectrometer," in *Proc. Univ. Mandalay Res. J.*, 2020, pp. 162–168. Available: https://meral.edu.mm/record/5561/files/Determination%20of%20Resolution%20and%20Detection%20Efficiency%20of%20NaI%20(Tl)%20Scintillation%20Gamma-Ray%20Spectrometer.pdf

[5] PhysicsOpenLab, "Silicon photomultiplier," 2016. Available: https://physicsopenlab.org/category/radioactivity/silicon-photomultiplier/

Proc. Annual Symposium on Research & Industrial Training, 12 (2025) 244-251
Department of Electronics – Wayamba University of Sri Lanka

VOIP CALL RECORDING SYSTEM FOR ANALOG RECORDERS USING HANDSET AUDIO TAPPING AND ANALOG SIGNAL AMPLIFICATION

M.S.M.N. Perera[1*], S.R.L. Gunawardhana[1], H.A. Priyantha[2]
[1]*Department of Electronics, Wayamba University of Sri Lanka, Kuliyapitiya, Sri Lanka.*
[2]*Airport & Aviation Services (Sri Lanka) (Private) Limited*
*miyuruperera2@gmail.com

ABSTRACT

At present traditional analog telephony is being replaced by Voice over IP (VoIP) systems in modern air traffic control communication and most of the communication company fields in Sri Lanka. VoIP offers better features and the ability to grow, but it can still be hard to connect with old analog recording equipment. This is especially true in aviation because of some regional airport's towers in Sri Lanka where analog recorders are often used for safety audits, compliance and investigations. Commercial airports like Katunayake, Mattala and Rathmalana etc are using advance recorders. There are commercial VoIP to analog gateways on the market, but they often cost a lot and may not fit well in situations with tight budgets. By actively tapping handset audio signals, this study offers a hardware based, low-cost method of bridging VoIP communication with analog recorders specially use for regional small airports recording purposes. The proposed system takes analog voice signals from VoIP phones' RJ9 handset interface, amplifies them with a preamplifier based on an LM324 operational amplifier, and sends the conditioned signals to analog recorders. The amplification was housed on a small Surface Mount Device based Printed Circuit Board without disturbing the telephone user. This system can be used not only in the aviation field but also in any organization that uses VoIP telephones for recording purposes. This work shows a practical way to extend the lifespan of analog recording systems in today's aviation communication settings.

Keywords: **V**oIP recording, **H**andset tapping, **A**nalog signal amplification

1.0 INTRODUCTION

Clear voice communication remains fundamental to modern air traffic control, where effective interaction between controllers, ground staff, and pilots is essential for ensuring both safety and efficiency. Now, Voice over IP tech is used more in control towers. It takes over old analog phone gear. This is due to its room to grow, its mix with web lines and its low cost. For a case, Sri Lanka's Jaffna Airport and other regional airports use VoIP. Even with these good points, VoIP has issues in places where old voice recorders still work. Main commercial airports in Sri Lanka also use VoIP, but they have very advanced and expensive equipment that includes VoIP to analog conversion systems to enable recording of VoIP calls.

Old style recorders, like analog recorder setups, are still in use at small regional airports. Phone call voice recordings are very important for aviation industry, safety checks, after-event reviews and investigations. But VoIP systems do not have easy ways to link to old recorders, so joining them is hard. VoIP to old style fixes, like Analog Telephone Adapter gateways, cost too much and don't meet some aviation industry needs. So, a cheap and a reliable way to record VoIP calls on old gear is needed.

VoIP phones continue to transmit analog audio signals between the speaker and the microphone while, their handsets offer a potential solution. The analog voice path can be accessed by tapping these lines via the RJ9 interface without changing VoIP protocols or network configurations. Because tapped signals are typically low in amplitude, those must be amplified before recorded with analog recorders.

This work makes a bridge for the gap of recording VoIP handset conversations on legacy analog recorders by designing and implementing a preamplifier circuit based on the LM324 to improve handset audio signals for analog recording, where the analog voice signals are obtained by tapping the RJ9 handset interface of the VoIP phone.

Some similar research work on VoIP and analog systems has been done previously. While Singh and Bansal have highlighted cost-effective monitoring strategies for VoIP telephony [1], Nandakumar has illustrated handset-level tapping techniques in embedded environments [2]. Johnson et al. have examined low-power op-amp audio circuits for dependable signal amplification [3], while Sharma et al. have highlighted the benefits of active analog interfaces over passive solutions in capturing handset audio [4]. The importance of small and non-intrusive circuit design was further highlighted by Wang and Nakamura's more recent development of intelligent analog logging interfaces that can identify call states in VoIP phones [5].

2.0 EXPERIMENTAL

1.1.System design

To design and implement a low-cost VoIP call recording system, the experiment was conducted by tapping the analog audio signals from telephone handset line and develop suitable design with a preamplifier circuit to boost the voice signals to levels compatible with analog recorders. Figure 1 shows the block diagram of the proposed system. The VoIP phone handset audio is tapped using an RJ09 splitter, where the microphone and speaker lines are separated. These analog signals are then passed through an LM324-based preamplifier to increase the signal strength, and finally, the amplified audio is recorded using an analog recorder.

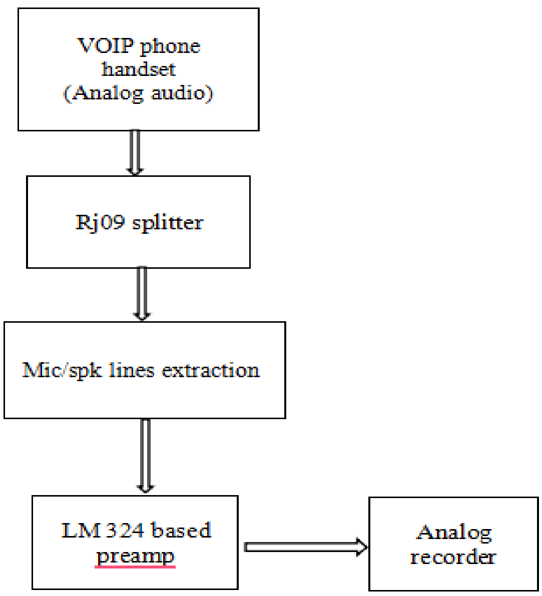

Figure 1: Block diagram of the system

2.1.1 VoIP phone handset wiring connection and op-amp pin diagram analysis

The RJ9 telephone handset cable pin diagram (Figure 2) was studied along with the specific VoIP telephone model because of this RJ9 connectors are designed primarily for voice applications and typically used in handsets. The internal wiring of the speaker and microphone lines varies depending on the handset model and should be identified according to the specific telephone in use.

LM 324 op-amp was selected because it can be operate with a single power from 3V to 32V. Pin diagram of the LM324 op-amp was studied with it data sheet [6].

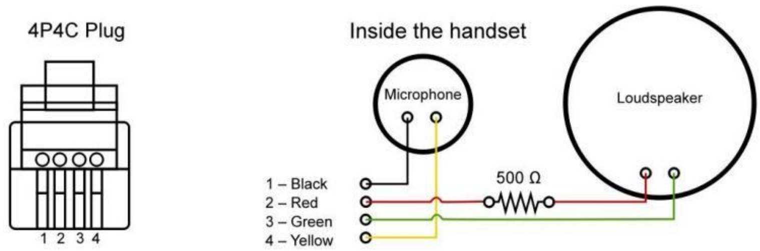

Figure 2: RJ9 port pin diagram with inside wire connection of a handset

2.1.2 Amplification circuit design and simulation

Theoretical calculation were performed to determine the required amplifier gain and to select suitable component values. Various resistors and capacitors were tested to obtain a higher gain.

Gain of the inverting amplifier with bias reference was calculated using the following equation.

$$A_v = -R_f / R_{in}$$

where; A_v = voltage gain
R_f = feedback resistor
R_{in} = input resistor

The negative sign indicates the output signal is inverted relative to the input signal.

The circuit diagram shown in Figure 3 was tested using 12 V DC power supply and designed it with minimum noises. Non- inverting input (pin 3) was biased by a voltage divider (two 10 KΩ resistors) between voltage common collector (Vcc) and GND. This creates a mid-supply reference (Vcc/2), so the op-amp can handle alternating current (AC) signals on a single supply. Feedback resistors, input resistors and capacitors were selected as gain become ($-A_v \approx -10$; The output voltage will be 10 times the input voltage, and it will be inverted). A simulation model of the amplifier circuit was developed using proteus design suite. The simulation was used to verify the expected performance, including signal amplification and stability.

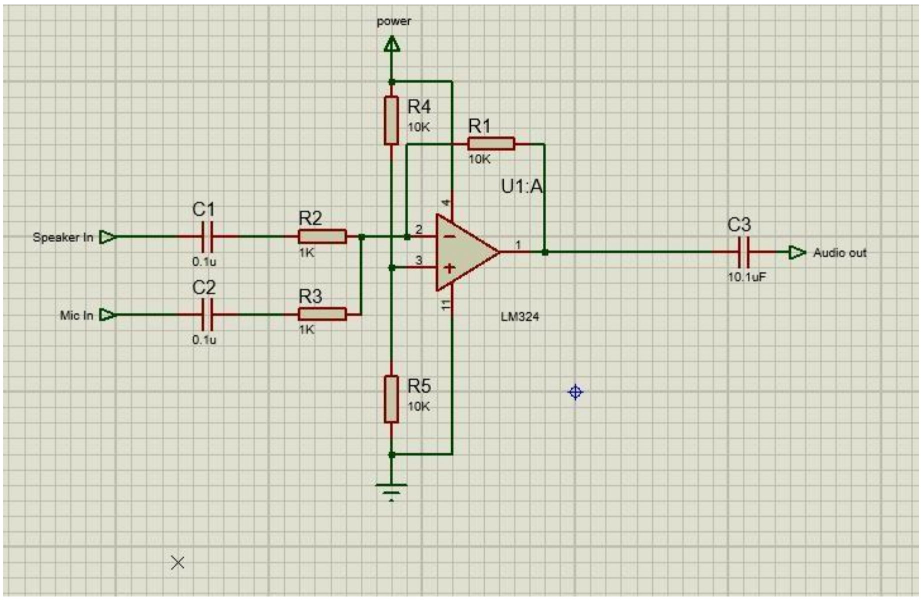

Figure 3: Amplifier circuit diagram

1.2.Prototype Development

After successful simulation, a hardware prototype of a amplifier circuit was implemented on a vero board as shown in Figure 4. Because instead of using a bread board, a vero board was used to design the prototype to reduce noises and to minimize the effect on the amplifier circuit due to loosen connection. The circuit was powered by a regulated direct current (DC) supply, and the output was connected to an 8Ω speaker for testing.

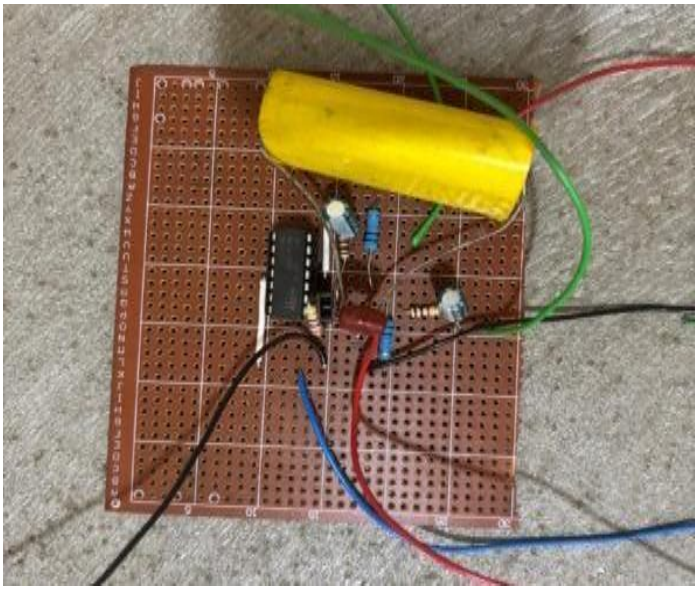

Figure 4: Prototype circuit diagram

1.3.Testing procedure

The output was monitored using a oscilloscope to see amplify signal as shown in Figure 5 and record voices were checked using speaker. Several frequency ranges in the human speech band (300Hz - 3.4KHz) were tested.

Figure 5: Before amplification signal with noise

3.0 RESULTS AND DISCUSSION

1.4.Amplification Performance

The LM324 preamplifier was tested using voice input signals. The oscilloscope clearly showed that the amplifier increased the amplitude of the microphone signal. At low input voltages 10–40 millivolts peak to peak (mVpp) as shown in Table 1, the output reached 150–400 mVpp, giving a gain of approximately.

Table 1: Signal type vs Gain

Signal Type	Input Voltage (mVpp)	Output Voltage (mVpp)	Gain
Voice (low)	20	200	10
Voice (mid)	30	300	10
Voice (high)	50	500	10

3.2 Frequency Response Analysis

The frequency response of the preamplifier was measured across the audio range. As shown in Table 2 and Figure 6, low frequencies below 300 Hz were attenuated, while the response flattened at ~20 dB gain across the 300 Hz – 3.4 kHz voice band. This confirms suitability for voice recording. The output amplitude was recorded using an oscilloscope and the gain was calculated in decibels (dB) using:

$$Gain(dB) = 20\log(Vin / Vout)$$

Table 2: Frequency vs. Gain of LM324 Pre-amplifier

Frequency (Hz)	Input Voltage (10^{-3} V)	Output Voltage (V)	Gain (dB)
50	100	0.7	16.9
100	100	0.8	18.1
200	100	0.95	19.5
300	100	1.0	20
500	100	1.0	20
1000	100	1.0	20
2000	100	1.0	20
3000	100	1.0	20
3400	100	1.0	20

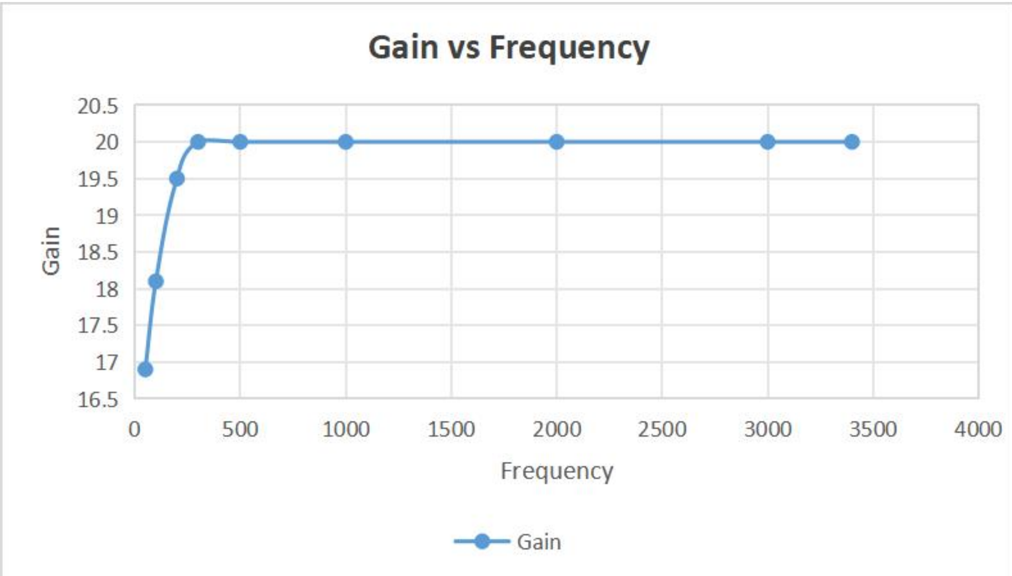

Figure 6: Frequency response of LM 324 preamp (Gain in dB vs. Frequency in Hz)

3.3 Effect of Coupling Capacitors and gain

Initially, a 100 nF output capacitor was used, which caused significant bass roll-off (cutoff ≈160 Hz with 10 kΩ load). Replacing it with a 10 µF electrolytic capacitor in parallel with a 100 nF ceramic lowered the cutoff frequency below 5 Hz, restoring bass and ensuring full voice bandwidth.

3.3.1 Gain Adjustment and Stability

The initial design with Rf = 830 kΩ and Rin = 1 kΩ produced a theoretical gain of 830, which saturated due to LM324's limited bandwidth. Adjusting the feedback resistor to 10–100 kΩ provided stable, distortion-free amplification in the range of 10–100. Following Table 3 and Figure 7 shown as gain and stability at different feedback resistor values.

Table 3: Gain and Stability at Different Feedback Resistor Values

Feedback Resistor (Rf) (kΩ)	Rin (kΩ)	Theoretical Gain	Practical Gain	Observation
830	1	830	Saturated	Clipped
100	1	100	~90	Clear voice
10	1	10	~10	Stable

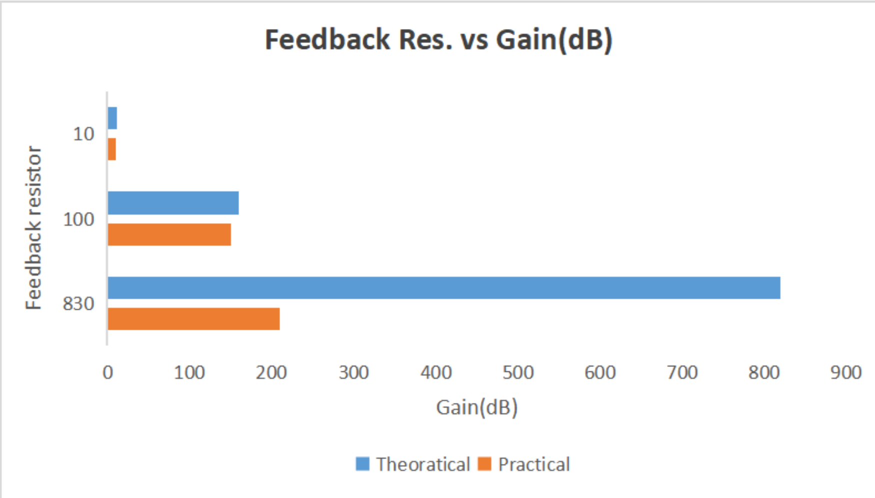

Figure 7: Bar chart view of feedback resister values

3.4. Application performance in recording system

The completed SMD PCB (Figure 8) pre-amplifier circuit was enclosed and tested at Jaffna Airport Tower for VoIP call recording. Enclosed setup as shown in Figure 10 has four ports with three RJ9 ports for audio out, handset and telephone. Setup was powered by using 12 V DC power adapter. The results confirmed:

- Clear voice reproduction within the 300 Hz – 3.4 kHz band.
- Low noise and distortion at practical gain settings (10–100).
- Reliable operation as a low-cost industrial audio solution.

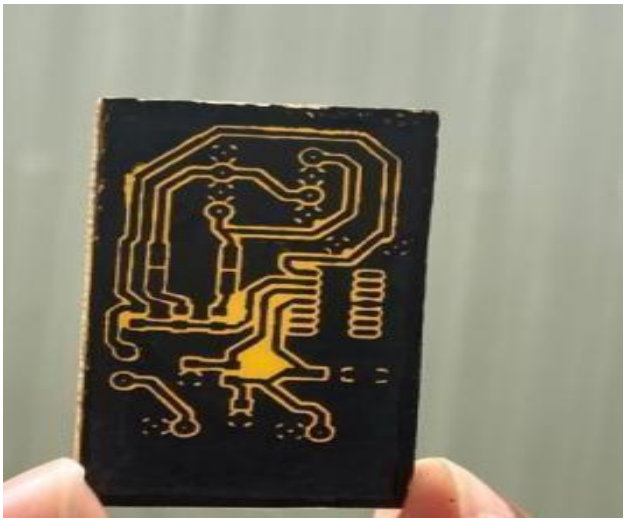

Figure 8: PCB view after etched

4.0 CONCLUSION

A cost-effective inverting preamplifier was successfully designed for voice recording applications. With input resistor (R_{in} =1 kΩ) and feedback resistor (R_f =10 kΩ), the amplifier achieved ~20 dB gain, providing clear voice signals. Frequency response measurements showed slight low- frequency attenuation below 100 Hz, while the voice band (300 Hz–3.4 kHz) remained flat. Replacing the 100 nF output capacitor with a 10 µF electrolytic in parallel restored low- frequency response, lowering the cutoff below 5 Hz. The design offers a simple, reliable, and high-fidelity solution for practical voice recording applications.

ACKNOWLEDGEMENTS

The authors convey their warm and sincere appreciations to the academic staff and technical staff at Department of Electronics, Faculty of Applied Sciences, Wayamba University of Sri Lanka as well as the staff of Research and Development section, Electronics & Air Navigation Engineering division at Airport & Aviation services (PVT) Ltd, Sri Lanka for the support and guidance offered.

REFERENCES

[1] R. Singh and A. Bansal, "VoIP telephony and analog interfacing methods," *IEEE Commun. Surveys Tuts.*, vol. 17, no. 4, pp. 1924–1937, Fourth Quarter 2015. doi: 10.1109/COMST.2015.2458012

[2] L. Nandakumar, "Embedded analog tapping interfaces for VoIP systems," *IEEE Embedded Syst. Lett.*, vol. 12, no. 2, pp. 36–39, Jun. 2020. doi: 10.1109/LES.2019.2938102

[3] M. Johnson, K. Lee, and P. Zhao, "Design of low-power audio amplifiers for embedded systems," *IEEE Trans. Circuits Syst. I, Reg. Papers*, vol. 66, no. 3, pp. 937–944, Mar. 2019. doi: 10.1109/TCSI.2018.2872419

[4] A. Sharma, M. Patel, and R. S. Rathi, "Low-noise analog interface for voice logging in VoIP terminals," in *Proc. IEEE Int. Conf. Commun. Syst. (ICCS)*, 2019, pp. 110–114. doi: 10.1109/ICCS45123.2019.9045681

[5] L. Wang and K. Nakamura, "Design of call-state-sensitive audio logging interfaces for secure VoIP networks," *IEEE Trans. Instrum. Meas.*, vol. 70, 2021, Art. no. 9511208. doi: 10.1109/TIM.2021.3094215

[6] Texas Instruments, "LM324 low-power quad operational amplifier," Datasheet, 2025. Available: https://www.ti.com/lit/gpn/lm324

Proc. Annual Symposium on Research & Industrial Training, 12 (2025) 252-258
Department of Electronics – Wayamba University of Sri Lanka

CURRENT SENSOR-BASED ALERT SYSTEM FOR DETECTING SUCTION BLOCKAGES IN VACUUM CLEANERS

T.D. Wijesuriya*, W.A.S. Wijesinghe[1], R.A.A.C. Ranasinghe[2]
[1]*Department of Electronics, Wayamba University of Sri Lanka, Kuliyapitiya, Sri Lanka*
[2]*Tudawe Trading Co. (Pvt) Ltd, Narahenpita, Colombo 05, Sri Lanka*
*tharudilwije@gmail.com

ABSTRACT

Vacuum cleaners are an essential part of indoor hygiene, serving broader purposes such as enhancing indoor air quality, reducing allergens, and promoting overall health and comfort in the home. Their efficiency is, however, often compromised by suction blockages arising from accumulated dust, clogged filters, or blocked hoses. Such blockages not only reduce cleaning efficiency but also overload the motor, leading to overheating, excessive energy consumption, and even irreversible damage. This work presents a low-cost real-time blockage detection and alert system using the TA21CM 5A/5mA current transformer. The system conditions the sensor's output via a burden resistor and rectifier before processing it with an ESP32 microcontroller. Upon detecting an abnormal motor current caused by suction blockages, the system activates a buzzer alarm and disconnects the motor power via a relay, thereby ensuring both user safety and motor protection. Experimental confirmation was achieved with reliable blockage detection, quick response, and power-efficient operation. The proposed solution is compact, inexpensive, and suitable for implementation in manual and robot vacuum cleaners. By addressing the shortage of effective blockage detection in current vacuum cleaner technologies, this project helps enable the creation of safer, more power-efficient, and more convenient devices.

Keywords: **V**acuum cleaner, **S**uction blockage detection, **C**urrent sensing

1.0 INTRODUCTION

Vacuum cleaners are widely used household and industrial appliances, valued for their ability to maintain the cleanliness of surfaces, improve indoor air quality, and remove allergens such as pollen and dust mites. In addition to cleanliness, they contribute to healthier environments. Amongst consumer models, the vacuum cleaners are amongst the most ubiquitous small designs that employ a universal motor combined with an impeller fan to create suction. Operation of such equipment is commonly compromised by obstruction of suction through dirty hoses, clogged filters, or excessive dust accumulations.

The efficiency of cleaning and motor performance are both compromised by obstruction. Suction in the vacuum cleaners is generated by the impeller pulling air in via the hose and filters. Aerodynamic resistance to the impeller is typically supplied by airflow, and as a consequence, the motor has to supply more torque and, accordingly, take more current. When the suction path is blocked, the airflow is cut off, the torque demand decreases, and the motor spins more freely. As a result, motor current drops considerably. This reduction in current is a good and non-intrusive indication of suction blockages.

Even though modern vacuums are equipped with features like automation, smart navigation, and advanced filter systems, real-time blockage-detecting methods still need further investigation. The user is unaware of internal obstructions until performance declines or motor damage becomes permanent. Vacuum cleaners that lack diagnostic monitoring are less reliable, require more maintenance, and have a shorter lifespan.

Several prior studies have examined ways to improve vacuum cleaner functionality. Naaz et al. (2022) surveyed robot cleaners with Google Assistant, emphasizing automation rather than diagnosis [1]. Noda et al. (2020) investigated robotic vacuum cleaners for indoor environmental sensing, demonstrating integration of sensing rather than detection of suction anomalies [2]. Takada and Matsui (2024) explored acoustic signatures of vacuum cleaners to measure the user's perception of suction force, whereas Izumi and Ikemoto (2024) developed suction-sensitive robot grippers for industry applications [3][4]. Work such as Hu et al. (2013) employed TRIZ methodology to develop novel vacuum cleaner designs, whereas recent work (Journal of Applied Fluid Mechanics, 2023) focused on suction flow dynamics [5][6]. Despite all these advances, real-time blockage detection is an area not extensively explored.

This project proposes an existing sensor-based blockage detection system for vacuum cleaners. The system applies a TA21CM 5A/5mA current transformer with a burden resistor and a rectifier circuit to prepare the output signal. The prepared signal is read by an ESP32 microcontroller that compares motor current against a calibrated reference. If suction blockage is present and the current level falls below the threshold, the system initiates a buzzer alarm and cuts off motor power through a relay.

Due to its small size, low cost, and non-invasive nature, the suggested solution may be easily included in vacuum cleaners. The study presents an anticipatory and protective approach that maximises dependability, user safety, and energy efficiency for vacuum cleaning operations by utilising motor current properties inherent to its mechanical architecture.

2.0 METHODOLOGY

2.1 Problem Statement

There are no diagnostic tools on the vacuum cleaners to identify suction obstructions. The efficacy of cleaning is reduced when airflow is restricted, although users are not aware of this until performance is severely compromised. The vacuum cleaner's motor runs on an impeller fan; under typical suction, airflow puts resistance on the fan's blades, requiring higher torque and increasing the current draw. During blockage, air flow resistance decreases, the torque needed is reduced, and the motor current is decreased. This project aims to develop a real-time blockage detection system that can detect a drop in current, alert the user, and safeguard the motor.

2.2 Theoretical Background

The torque that an electric motor produce is proportional to the current it uses. The airflow resistance that the fan-motor system can tolerate is closely correlated with the torque in the vacuum cleaner. Thus:

- Normal suction → airflow resistance present → higher torque → higher current.
- Blocked suction → airflow resistance absent → lower torque → lower current.

The relationship between them forms the system's theoretical foundation. Blockages can be accurately identified by monitoring changes in the motor circuit's current without physically obstructing the airflow route.

2.3 System design and components

The system uses current sensing, signal conditioning, and microcontroller-based decision-making to detect blockages.

2.3.1 Main components and their functions:

In this system, the TA21CM 5A/5mA current transformer (CT) is employed as the principal sensing device to detect the current the vacuum motor draws, utilizing the principle of electromagnetic induction. A CT consists of a magnetic core with one primary winding and multiple secondary windings. In the TA21CM, the motor's live conductor acts as the single-turn primary winding, and the secondary consists of many thin turns of wire. Alternating current passing through the primary generates magnetic flux within the core, inducing a current in the secondary winding that is proportional to the current by the transformer equation:

$$\frac{Ip}{Is} = \frac{Ns}{Np} \qquad [2.1]$$

Where, Ip - The Primary (motor) current
Is - The secondary current from CT
Ns - The number of turns in the secondary
N_p - The number turns in the Primary

For the TA21CM, this relationship is fixed at 5 A in the primary, producing 5 mA in the secondary, giving a safe 1000:1 scaling. The resulting milliamp-level current in the secondary is then passed across a burden resistor, which converts it into a voltage directly proportional to the motor current. Since the CT output is AC, a rectifier circuit conditions the signal into a stable DC voltage, making it compatible with the ESP32 microcontroller's analog-to-digital converter (ADC). The ESP32 continuously samples this voltage and interprets it as the motor current. Under normal suction, the motor draws steady current; however, when suction is blocked, airflow resistance decreases, torque demand drops, and the current falls. This reduction is directly reflected in the CT output. The ESP32 detects the variation, and in response, activates a buzzer to alert the user and triggers a relay to disconnect the motor, thereby ensuring protection, energy efficiency, and extended lifespan of the vacuum cleaner.

2.3.2 Assumptions and Measurements

In the design of this system, some assumptions were also made in order to simplify the analysis and design. It is assumed that the vacuum cleaner motor operates with a constant current during normal suction conditions, providing a constant point of reference for comparison. When suction blockages occur, it is further assumed that they cause a measurable and consistent drop in current, which can be accurately detected by the current transformer without interference from other factors. Furthermore, the design also assumes that the mains supply is steady at 230 V AC in operation, so that any fluctuation in motor current measured is caused primarily by suction variations and not by input voltage fluctuation.

2.3.3 Measurements

Before the system was installed, the Kärcher WD1 vacuum cleaner motor current was manually measured in two operating modes using a clamp-on ammeter. In normal suction, the motor showed a 4.25A baseline current, while in blocked suction, there was a 3.74A current, resulting from the low motor load. These readings were used to determine the difference between the two states and were then used to determine the threshold value of current for the ESP32-based detection system.

(a) (b)

Figure 2.2: (a) The baseline motor current measured with a clamp-on meter under normal suction. (b) The significant drop in motor current was measured with a clamp-on meter under suction blockage.

2.3.4 Calculation

The ESP32 ADC accepts voltages in the range 0 V to 3.3 V**;** therefore, the burden resistor must be chosen so that the maximum CT voltage never exceeds 3.3 V**.**

So, the chosen maximum CT voltage is 3.0 V. Also, the Supply voltage to the vacuum cleaner is assumed constant at 230 V AC, so the only variable of interest is the motor current.

Therefore,

$$\text{Burden Resistor} = \frac{Vb}{Is} \quad [2.2]$$

$$= 600\ \Omega$$

Where, V_b = The chosen maximum CT voltage
I_s = CT secondary current

2.3.5 Block Diagram

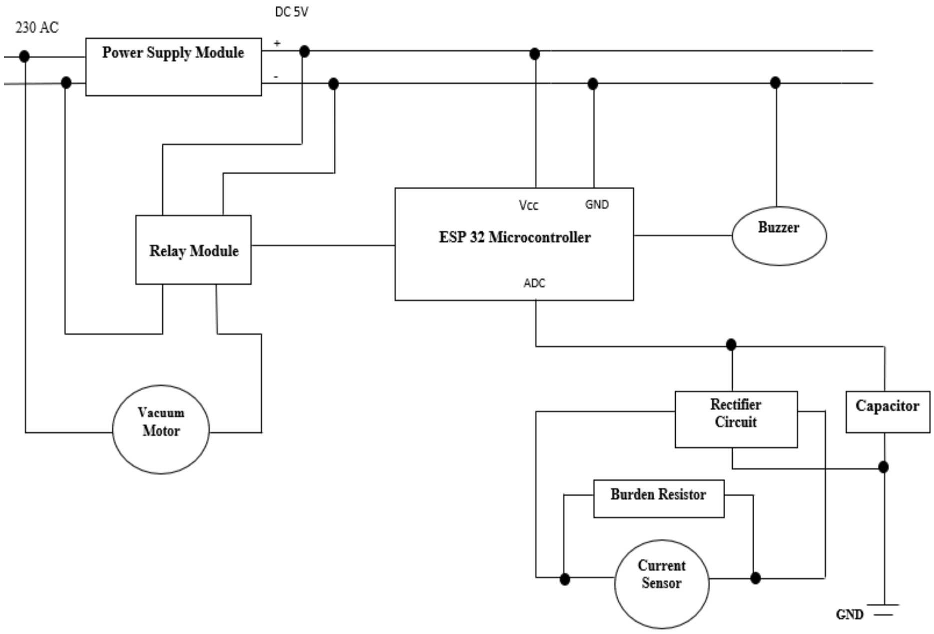

Figure 2.3: Block Diagram of the System

The circuit employs a TA12CM current transformer to sense the motor current, which is converted into a voltage by a burden resistor and rectified for stability. This conditioned signal is read by the ESP32 microcontroller, which compares it against a threshold. Upon blockage detection, the ESP32 activates a buzzer for alert and a relay for motor protection.

3.0 RESULT AND DISCUSSION

A working prototype of the blockage detection system was constructed and tested with the Kärcher WD1 vacuum cleaner. The system integrated the TA21CM current transformer, burden resistor, and rectifier circuitry, ESP32 microcontroller, buzzer, and relay module into a compact board and covered it in a protective casing for safe operation. A picture of the completed system is given in Figure 3.1, illustrating the integration of sensing, processing, and alarm modules.

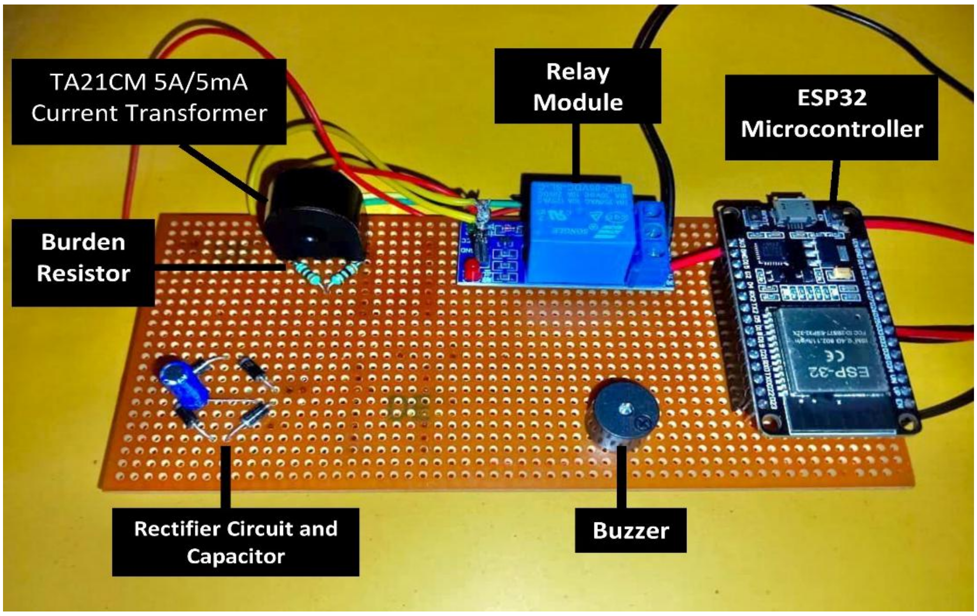

Figure 3.1: Prototyped hardware

The motor current was first measured under two states of suction using a clamp-on ammeter. Under normal suction, the motor operated at a steady baseline level of about 4.25 A, a reading of the load consumed by airflow resistance. When the suction hose was manually blocked, airflow imploded, reducing motor load and reducing the current to about 3.74 A. These distinct readings verified the theoretical basis that suction blockages could be identified by measurable current differences.

The conditioned CT signal was continuously read by ESP32, with the reading being compared to a calibrated value. Once the current fell below that value, the system activated its two-step response: the buzzer alarm sounded in 0.5 seconds as an indication to the user, and the relay deactivated the motor in 1 second to prevent overheating and power loss. The repeated testing set up consistent and reliable detection of blockages without false alarms throughout routine suction, demonstrating that the research objectives of accurate detection, user warning, and motor protection were achieved.

The suggested technique is low-cost, compact, and not invasive, providing an easy yet solid alternative to pressure or vision methods. However, the system is dependent on proper threshold calibration, which would change with motor specifications, vacuum cleaner construction, and supply variations. Enhancements in the future could be adaptive thresholds or machine learning techniques to make it more generally applicable. To declare such limitations makes the research more solid as it references possibilities for further development and greater utilization.

4.0 CONCLUSION

This study addressed the major problem of suction obstructions in vacuum cleaners that reduce cleaning efficiency and increase the likelihood of motor overheating, energy wastage, and long-term deterioration. A blockage detection system was therefore designed and implemented on the Kärcher WD1 vacuum cleaner using a current transformer. The system employed the TA21CM 5A/5mA current transformer with a burden resistor and rectifier circuit to measure motor current, and an ESP32 microcontroller to calculate real-time readings. Based on the principle that clogged suction lowers airflow and lowers motor load and thereby causes a measurable drop in current, the system was able to identify normal and blocked states effectively. Once a blockage was detected, a two-step response was triggered: a buzzer alerted the user immediately, and a relay disconnected the motor to prevent overheating and save power. Testing resulted in repeatable accuracy and no false alarms under normal usage. Small size, low cost, and non-invasive design make it applicable to modification on other models. Future enhancements can use adaptive thresholds, wireless notification, or machine learning approaches to further enhance reliability on a broad number of appliances.

ACKNOWLEDGEMENT

The authors express their sincere appreciation to the academic and technical staff of the Department of Electronics, Faculty of Applied Sciences, Wayamba University of Sri Lanka.

REFERENCES

[1] F. Naaz, G. Bhoyar, and A. Dhankar, "A review paper on Google Assistance-based consumer vacuum suction dusting robot," *Int. J. Res. Appl. Sci. Eng. Technol.*, vol. 10, no. 8, pp. 1230–1234, Aug. 2022. doi: 10.22214/ijraset.2022.46419

[2] K. Noda and H. Aizawa, "Indoor environmental monitoring system using a robot vacuum cleaner," *Sens. Mater.*, vol. 32, no. 3, pp. 1133–1140, 2020. doi: 10.18494/SAM.2020.2644

[3] M. Takada and K. Matsui, "Acoustic characteristics of the operating noise of vacuum cleaners that evoke the feeling of suction," in *Proc. INTER-NOISE Noise-Con Congr. Conf.*, vol. 270, no. 7, 2024, pp. 4989–4995. doi: 10.3397/in_2024_3532

[4] S. Izumi and S. Ikemoto, "Design of effective suction force sensitive vacuum gripper by a 6-axis force sensor," *Artif. Life Rob.*, vol. 29, no. 1, pp. 55–61, Feb. 2024. doi: 10.1007/s10015-023-00935-2

[5] S. J. Hu, L. H. Su, J. C. Chen, and C. Y. Wei, "Innovative vacuum cleaner design using TRIZ method," *Adv. Mater. Res.*, vol. 690, pp. 3372–3376, May 2013. doi: 10.4028/www.scientific.net/amr.690-693.3372

[6] M. M. Ghorani, M. H. Haghighi, and A. Riasi, "Temporal flow characteristics of three-dimensional centrifugal impeller suction system at vacuum conditions," *J. Appl. Fluid Mech.*, vol. 16, no. 12, pp. 2411–2425, Dec. 2023. doi: 10.47176/jafm.16.12.1875

Proc. Annual Symposium on Research & Industrial Training, 12 (2025) 259-266
Department of Electronics – Wayamba University of Sri Lanka

SOLAR-OPTIMIZED ENERGY CONTROLLING SYSTEM FOR AUTOMATIC WEATHER OBSERVATION SYSTEM (AWOS)

M.B.Y. Silva[1]*, K.P. Vidanapathirana[1], H.A. Priyantha[2]
[1]*Department of Electronics, Wayamba University of Sri Lanka, Kuliyapitiya, Sri Lanka*
[2] *Airport & Aviation Services (Sri Lanka) (Private) Limited, Sri Lanka*
**byovinma@gmail.com*

ABSTRACT

The increasing reliance on sustainable energy sources highlights the importance of ensuring a reliable power supply for systems like automatic weather observation system (AWOS). This study presents the design and implementation of a solar power management system that prioritizes solar energy for powering AWOS or similar applications. This system integrates photovoltaic generation, battery storage, grid and microcontroller-based relay switching mechanism to optimize energy utilization and minimize downtime. Source transition decisions are made based on real time measurements of voltage and current, enabling intelligent selection between solar and grid power. The system ensures the reduced dependency on grid power and utilizes of solar power.

Keywords: **S**ustainable power supply, **L**ead acid battery charging, **R**elay switching

1.0 INTRODUCTION

An Automatic Weather Observation System (AWOS) plays a vital role by providing continuous, reliable meteorological observations directly at airports. These systems are typically equipped to measure key atmospheric parameters such as temperature, humidity, wind speed, wind direction, and atmospheric pressure, and transmit this information in real time for pilot use, air traffic control, and meteorological forecasting. An AWOS is a fully configurable airport weather system that operates 24/7, providing real time information and reports on airport weather conditions. A reliable and uninterrupted power supply is fundamental for critical monitoring systems such as AWOS [1]. Traditionally, AWOS installations depend on conventional grid electricity or standby generators, these approaches face challenges like high maintenance costs, and reliance on non-renewable resources.

The global energy sector is undergoing a significant transformation driven by the need to reduce carbon emissions, enhance energy reliability, and promote decentralized power systems. In this study, solar was selected as the primary renewable energy source since the AWOS is deployed outdoors, where sufficient sunlight is readily available. However, many existing AWOS power configurations still rely heavily on conventional grid supply with limited renewable integration, creating a gap in achieving sustainable and fault-tolerant operation. Power supply system with sources solar, grid, and battery to ensure the uninterrupted functionality of the system even in adverse weather or grid outages. This project aims to address that gap by designing a fault-tolerant, renewable-powered AWOS setup suitable for airport and any other such systems. The system will automatically prioritize solar energy while ensuring continuous power delivery by switching between available sources in real-time. It offers renewable energy, aligning with global aviation sustainability goals. Many AWOS deployments rely on traditional grid power, often with basic battery backup. However, this setup is vulnerable to unexpected power failures, voltage fluctuations, and insufficient charging mechanisms factors that can lead to data loss, sensor errors, and operational downtimes. This is especially critical for aviation, where uninterrupted weather data is vital for flight safety and scheduling.

Some similar researches on solar optimized energy controlling systems have done previously. R.S. Jothilakshmi and S. Chithra Selvi demonstrated automation of hybrid renewable systems to optimize energy harvesting and reduce dependency on conventional grids. However, their work did not address real-time adaptation to unpredictable load demands [2]. W. Zhang et al. have proposed control methods for PV–battery hybrid systems to ensure stable operation under varying environmental conditions, but the approach struggled with rapid fluctuations in solar irradiance [3]. A. Chakir and M. Tabaa have developed smart scheduling for PV (Photo Voltage) wind battery systems, yet their predictive energy management relied heavily on accurate weather forecasts, which can be uncertain [4]. N.T. Mbungu et al. have optimized grid-connected hybrid systems using model predictive control, emphasizing efficient resource utilization, but their method was computationally intensive and may not suit remote sites with limited processing capability [5]. D. Bhatt et al. have introduced weather-driven priority charging for batteries in renewable hybrid grids, showing how environmental data can enhance system performance; nevertheless, the approach did not consider critical applications requiring uninterrupted operation [6].

Collectively, these studies highlight advances in solar, battery, and grid integration with intelligent control, but their application to critical airport weather observation systems (AWOS) is limited, leaving a research gap this study addresses. And many systems lack intelligent power management, such as automatic source switching, real-time battery health monitoring, and energy prioritization. Solar power is increasingly being used as a backup source in such systems, but without a controlling system, the efficiency of energy utilization remains suboptimal. Additionally, improper charging/discharging cycles can degrade battery lifespan, adding to maintenance costs and system unreliability. A solar prior power management system provides uninterrupted and efficient energy supply for AWOS while reducing dependency on conventional grid power.

2.0 EXPERIMENTAL

2.1 System component and tools

The 12V 9Ah sealed valve regulated rechargeable battery (SZ1290) was selected for this system due to its reliability and suitability for standby power applications. For proper operation and long service life, the battery must be maintained within recommended charging parameters. A minimum charging threshold of 13.5V is required, as this corresponds to the float charging region, while full charging in cyclic use requires 14.4-14.7V. Discharging below 10.8V can cause irreversible sulfation, where hard lead sulfate crystals form on the battery plates and permanently reduce its capacity; therefore, the system incorporates monitoring to prevent over-discharge. The ESP32 microcontroller monitors the charging process, prioritizing solar energy when sufficient voltage and current are available, and switching to grid power when solar conditions are inadequate. This ensures that the battery remains properly charged.

INA219 current sensor is a high side current and power monitor with an I2C interface, used to measure battery's real time output voltage and current. ESP32 monitors the battery voltage and current. If battery drain below 10.8V ESP32 operates the battery cutoff relay.

Solar output is connected to a 5V relay via a 13.8V buck converter to the normally open side of a relay and switch based on availability upon threshold. And another 5V relay to switch CEB input if solar is insufficient.

2.2 Methodology

In this setup, the AWOS is powered through a lead acid battery, which acts as a stable and regulated supply source. Solar power is utilized as the primary charging method for the battery, while grid power (CEB), which is reliably available at airports, serves as a secondary source to charge the battery when solar generation is insufficient or unavailable. In the event of a CEB power failure, the airport operation immediately switches to standby generator. Therefore, if both solar and CEB are unavailable, generator ensures that battery is charging through CEB input ensuring AWOS power supply is not affected.

The system prioritizes the solar energy utilization when the solar panel output voltage (V_s) is higher than a predefined threshold voltage. The threshold value is selected as 13.5V which is the minimum safe voltage to charge the 12V lead acid battery. So, if V_s is higher than 13.5V system use solar power to charge the battery. If solar voltage is below than 13.5V the system automatically switches to the grid power to charge the battery. The switching mechanism is programmed in ESP32 microcontroller and the output signal is feed into two relays parallelly. A monitoring mechanism continuously checks the battery voltage to prevent deep discharge, extending battery life. When battery charge falls below the critical threshold (10.8V), the system initiates a controlled shutdown by operating a relay to safeguard the AWOS hardware. But in this system battery voltage is monitored remotely, so before a shutdown a new battery can be replaced. And since the battery is in float charging mode it ensures that battery is fully charged always and if both sources are unavailable battery itself can power AWOS for approximately 7 to 9 hours. Following figure shows the flowchart of the system.

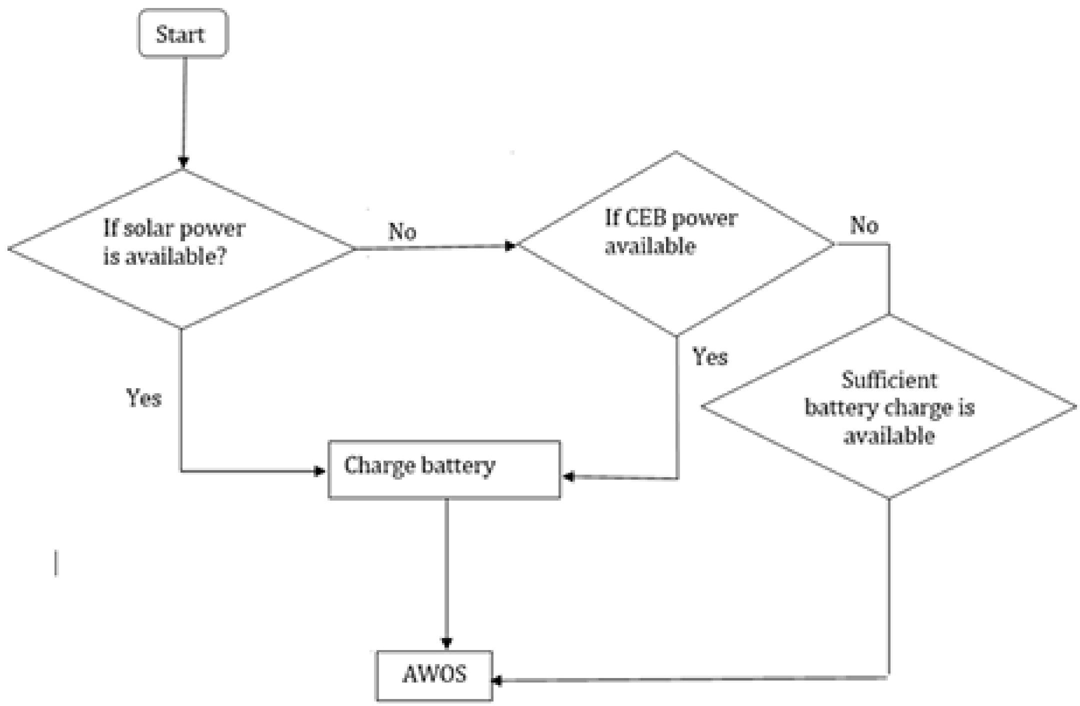

Figure 1: Flowchart of the system

2.3 System design

2.3.1 Simulation of switching mechanism

Following figure illustrates the schematic diagram for the switching part of the proposed system.

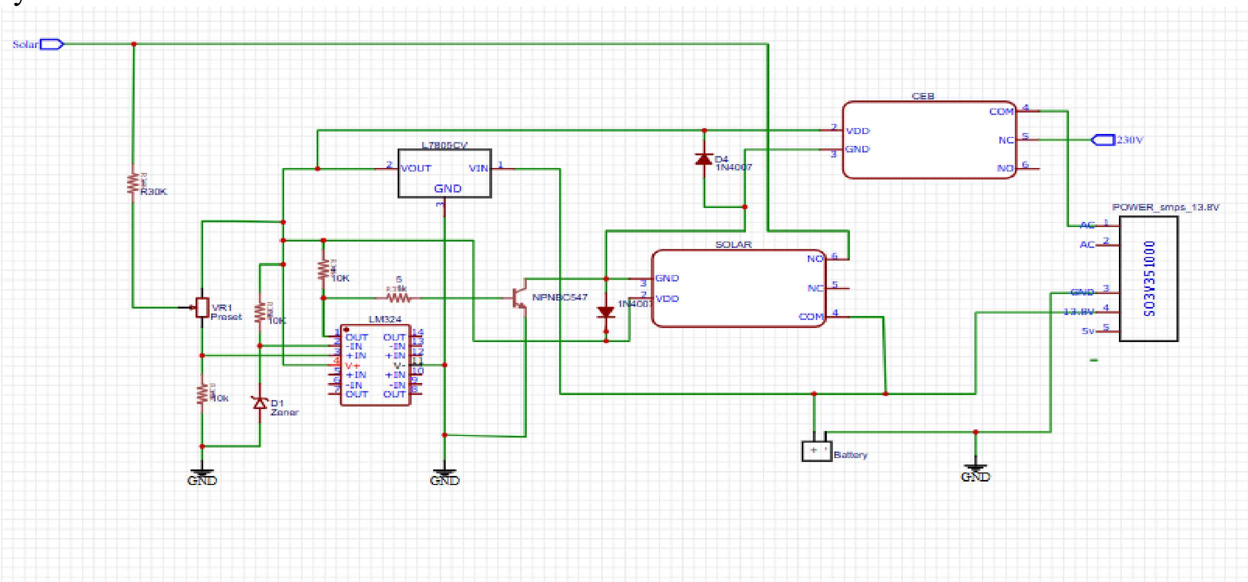

Figure 2: Schematic of the switching system

Following figure shows the output of the source switching mechanism between grid and solar based on the availability of solar power. Two LEDs were used during testing to indicate the active source, one for solar power and the other for grid power. The solar input voltage and the switching threshold were simulated using a variable DC power supply, allowing verification of the relay operation and correct source selection under different conditions. ESP32 microcontroller is used to control both input and output signal. The output signal is connected to two relays operating in parallel, preventing simultaneous activation of both sources. When output of DC power supply is more than 13.5V, microcontroller is programmed to output logic high and relay of solar was switched as in figure 3(a). And also when DC power supply output is less than 13.5V, output signal of the microcontroller becomes low. As a result, at this time relay of grid was switched as in figure 3(b). The following figure illustrates the implementation of the concepts described above, showing the operation of the switching mechanism.

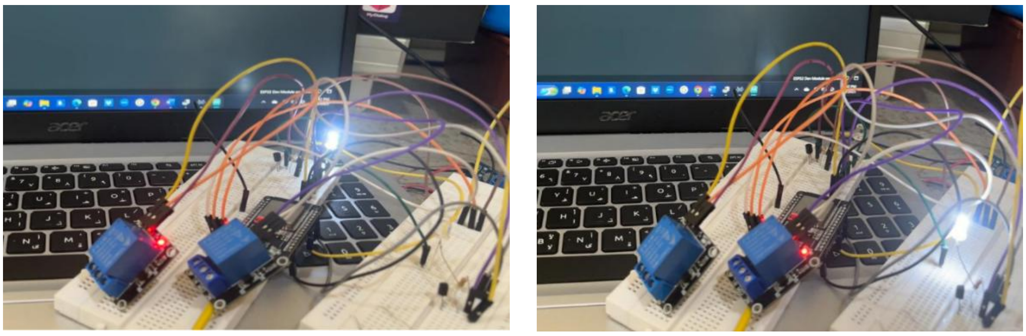

(a) (b)

Figure 3: (a)Solar power activated (b) Grid power activated

2.3.2 Prevent over discharging of battery

The battery is set to float charging mode which maintains battery's full charge by continuously supplying a lower, constant voltage to compensate for its self-discharge and any connected loads. The supply for the load is always from the battery because the stability of the supply. If over discharging of the battery occurs, a separate relay is provided to cutoff the battery for safety.

2.3.3 Final simulation

Figure 4 illustrates the simulated switching and monitoring circuit for the solar, grid, battery power management system. An Arduino microcontroller is used in proteus simulation as the central controller to generate the switching logic. The control signals are fed into optocouplers that drive relays for safe isolation and reliable switching between the solar source, grid source, and the load.

Relay RL1 and RL2 are connected in parallel to control the selection between solar and grid supply, ensuring that only one source is active at a time, thereby preventing overlap. Relay RL3 manages the connection between the battery and the load. The system also includes a 12V lead-acid battery (BAT2) as the energy storage element, which supplies power for the load.

For real-time monitoring, an INA219 current and voltage sensor module is integrated to measure battery charging/discharging current and voltage, transmitting data back to the microcontroller. The setup allows the verification of switching logic, power flow, and battery monitoring under different operating conditions using variable input supplies. These input output simulations allowed verification of the power flow sequence, source switching, and system protection functions before hardware implementation.

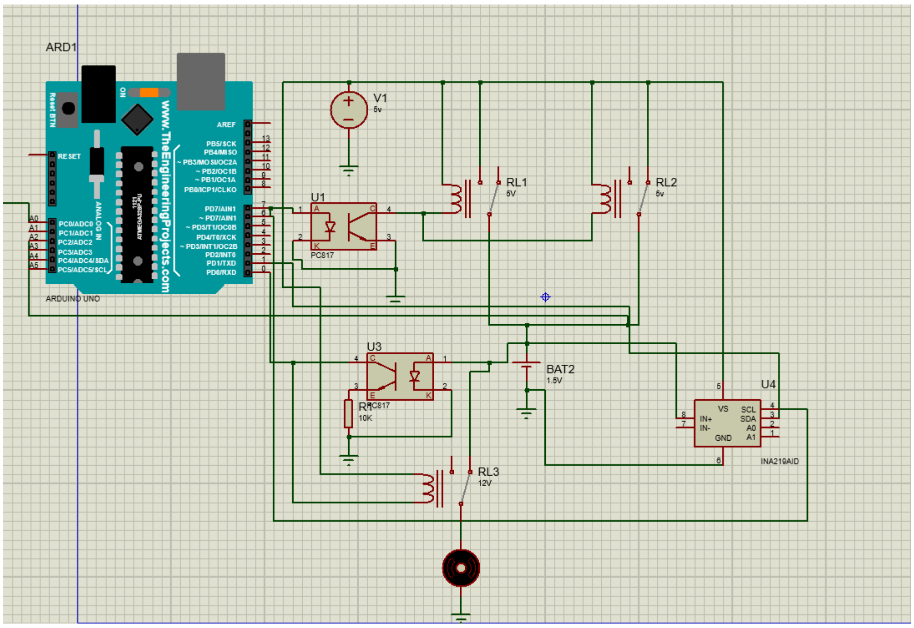

Figure 4: Proteus simulation of the system

2.3.4 Hardware implementation

The hardware implementation was done by designing a printed circuit board (PCB) layout using EasyEDA platform. After completing the design, the PCB was fabricated and all components were carefully assembled to produce the prototype of the system. The assembled board integrates the ESP32 microcontroller, power regulation circuitry, voltage, current sensors, relays and other required components for reliable operation. Figure 5, illustrating the assembled PCB for the system.

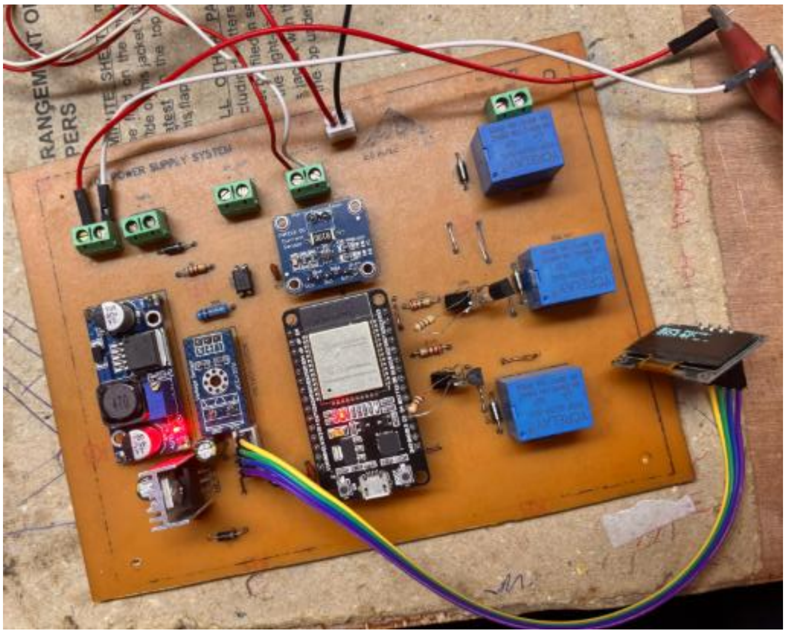

Figure 5: Developed prototype of the system

3.0 RESULTS AND DISCUSSION

3.1 Switching mechanism

Solar threshold was set to 13.5V, corresponding to the minimum safe charging level of a 12V lead acid battery. During the operation, when the solar panel output exceeds 13.5V, the relay switches to solar as the source to charge the battery. When solar dropped below 13.5V as soon as system switch to grid power as the source. This ensures the uninterrupted battery charging and supply for AWOS. Here the system is designed to ensure both solar and grid switching relays are not selected simultaneously.

3.2 Voltage and current measurements

INA219 current sensor confirmed accurate measurement of voltage, current, and power values compared with the multimeter measurements.

3.3 Web Interface

The battery charging dashboard provides real-time monitoring of battery voltage, current, and source selection. Using the ESP32 microcontroller module with Wi-Fi connectivity, all data measured from the system are transmitted to a Firebase server and displayed through a web application. ESP32 measures the battery voltage and current drawn by AWOS through INA219 current sensor, available power source is also monitored by the ESP32 through voltage sensor and updates the firebase and then interface in real time. This enables immediate response and helps ensure system protection without downtime. Figure 6 shows web dashboard view of real time battery voltage, current and battery charging source. Additionally, voltage and current trend display in a chart for remote monitoring of system.

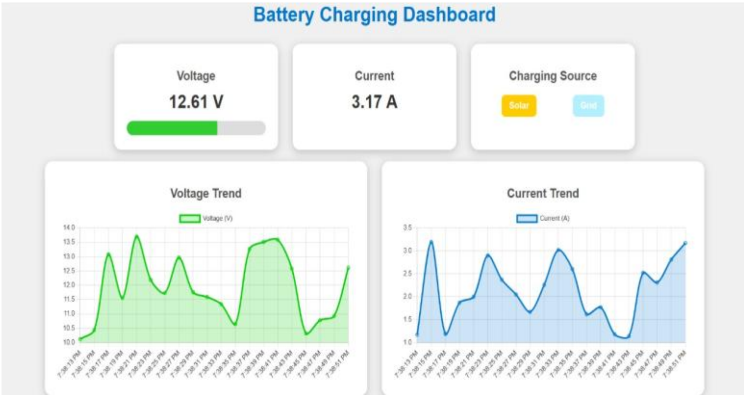

Figure 6: Output data visualization in a web interface

4.0 CONCLUSION

In conclusion, outcomes of this study provide a sustainable power supply system for systems like AWOS and such similar systems, reducing the dependency on grid power and enhancing sustainability. This system ensures the uninterrupted power supply for the load. Source transition based on the source availability to charge the lead acid battery was successful. The ESP32-based intelligent control mechanism, supported by real-time voltage and current monitoring, enabled reliable source transition without perceptible delay. Overall, the proposed design demonstrates a practical and efficient approach to maintaining continuous and sustainable power for AWOS, contributing to both operational reliability and environmental sustainability.

ACKNOWLEDGMENT

The authors convey their sincere appreciation to the academic and technical staff of the Department of Electronics, Faculty of Applied Sciences, Wayamba University of Sri Lanka, as well as the staff of the Research and Development Section, Electronics & Air Navigation Engineering Division at Airport & Aviation Services (PVT) Ltd., Sri Lanka, for their valuable support and guidance throughout the course of this study.

REFERENCES

[1] Aviation Renewables, "Automated weather observing system," 2022. Available: https://aviationrenewables.com/product/automated-weather-observing-system-awos/

[2] R. S. Jothilakshmi and S. C. Selvi, "Multi-objective based hybrid scheduling algorithm for cloud computing," *Intell. Autom. Soft Comput.*, vol. 34, no. 2, pp. 865–876, 2022. doi: 10.32604/iasc.2022.025643

[3] W. Zhang, Y. Wang, P. Xu, D. Li, and B. Liu, "An operating mode control method for photovoltaic (PV) battery hybrid systems," *Front. Energy Res.*, vol. 12, 2024, Art. no. 1435310. doi: 10.3389/fenrg.2024.1435310

[4] A. Chakir and M. Tabaa, "Hybrid renewable production scheduling for a PV–Wind-EV-battery architecture using sequential quadratic programming and long short-term memory–K-nearest neighbors learning for smart buildings," *Sustainability*, vol. 16, no. 5, 2024, Art. no. 2218. doi: 10.3390/su16052218

[5] N. T. Mbungu, R. Naidoo, R. C. Bansal, and M. Bipath, "Smart energy coordinator framework system for large industrial energy management," *IET Renew. Power Gener.*, vol. 11, no. 14, pp. 1760–1768, Dec. 2017. doi: 10.1049/iet-rpg.2017.0381

[6] D. Bhatt, S. Penumatsa, and N. Singhal, "Weather-driven priority charging for battery storage systems in hybrid renewable energy grids," 2025, *arXiv:2501.06104*. doi: 10.48550/arXiv.2501.06104

EXTERNAL POWER-SUPPLIED SIGNAL BOOSTER FOR LTE TELEPHONES AND ROUTERS

P.M. Hettiarachchi[1]*, M.A.A. Karunarathne[1], M.I.P Premarathne [2]
[1]*Department of Electronics, Wayamba University of Sri Lanka, Kuliyapitiya, Sri Lanka*
[2]*Sri Lanka Telecom PLC*
**malinthaka.2000@gmail.com*

ABSTRACT

Weak LTE signal reception continues to be a significant challenge in many rural and indoor environments of Sri Lanka, causing disruptions in mobile internet connectivity and call quality. Built-in antennas in telephones and routers often fail to provide stable connections due to physical barriers, distance from base stations, and interference. This research focuses on developing an external power-supplied antenna system for LTE-enabled devices to enhance reception and reliability. The design integrates a high-gain directional antenna, an amplifier circuit powered by an external DC source, and a user-friendly enclosure. The methodology involved theoretical analysis, antenna simulation in CST Microwave Studio, and prototype fabrication using PCB techniques. Performance testing was carried out using a Vector Network Analyzer, Spectrum Analyzer, and LTE devices. Experimental results showed improved signal strength, lower packet loss, and enhanced download speeds compared to standard built-in antennas. The developed system demonstrates a low-cost, portable, and practical alternative to commercial LTE boosters, making it suitable for households and communities in underserved areas.

Keywords: **L**TE, **E**xternal Antenna, **S**ignal Amplifier

1.0 INTRODUCTION

Mobile communication has become a fundamental technology in modern society, supporting essential services in education, healthcare, business, agriculture, and entertainment. With the rapid growth of internet-based applications, the demand for stable and high-speed mobile networks has increased significantly. In Sri Lanka, as in many developing countries, Long Term Evolution LTE technology is widely used to deliver mobile broadband services. LTE provides higher data speeds, lower latency, and improved spectral efficiency compared to previous generations such as 3G and GSM. These features make LTE particularly important for online education platforms, video conferencing, telemedicine, e-commerce, and financial services, all of which require reliable and continuous connectivity [1,2].

Despite its advantages, LTE performance varies across different regions. Urban areas generally experience strong and stable signals due to dense infrastructure (like LTE towers) and close proximity of cellular base stations. Rural and semi-urban areas often face challenges in accessing reliable LTE services. Weak signals in these areas can be attributed to several factors including distance from base stations, obstructions such as buildings, trees, and hilly terrain, and interference from overlapping cell sites and other electronic devices. These factors result in unstable internet speeds, frequent disconnections, and poor call quality [3,4].

Mobile devices such as smartphones and routers rely on built-in antennas that are compact and optimized for average use conditions. These antennas have low gain and omni-directional reception, which are insufficient in weak signal environments. Commercial LTE signal boosters and repeaters are available but they are often expensive, consume significant power, and require professional installation. In addition, many boosters are compatible only with specific frequency bands or network operators, limiting their practicality for cost-sensitive households and small businesses in rural Sri Lanka [5,6].

Given this context, there is a need for a low-cost, efficient, and user-friendly solution to improve LTE reception in underserved areas. This research investigates the design and development of an external power-supplied antenna system that combines a directional high gain antenna with a low-noise amplifier powered by an external regulated DC supply. The specific question addressed in this study is whether a portable external power-supplied antenna system can significantly improve LTE reception and connectivity in rural and indoor environments.

2.0 EXPERIMENTAL

The study begins with the identification of a significant problem in Sri Lanka, where LTE coverage is weak in many rural and indoor environments. This limitation results in unstable internet connectivity and poor call quality, especially in locations far from cellular towers or obstructed by buildings. To address this challenge, an external signal booster powered by an independent power supply is proposed (**Error! Reference source not found.**). The solution aims to provide stronger and more stable LTE reception for both telephones and routers (V10, TOZED, etc), overcoming the limitations of standard built in antennas.

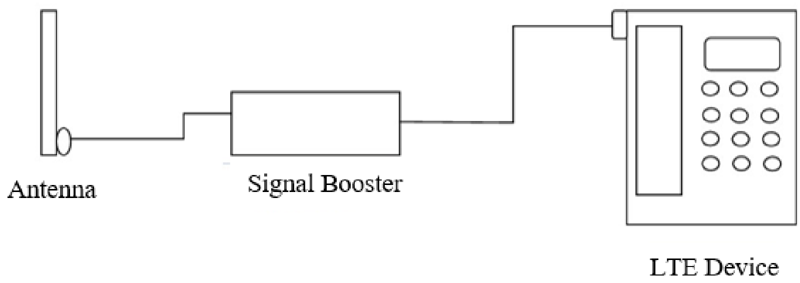

Figure 1: Block diagram of signal booster connection

The signal booster first takes the signal through the original antenna and amplifies if through the amplifying circuit and directly gives the output to the LTE device through the antenna port. The amplifying circuit consist of LM386 IC and some other capacitors and resistors for smooth amplification. Also, in occasions where that present week signal strengths in indoor spaces, we can fix the input antenna at the outside and take signals to the indoor space, also if we need to use several LTE devices with the use of same signal booster. It is possible to connect an emitter antenna to the output port of the signal booster. The circuit diagram of the signal booster is shown in **Error! Reference source not found.**.

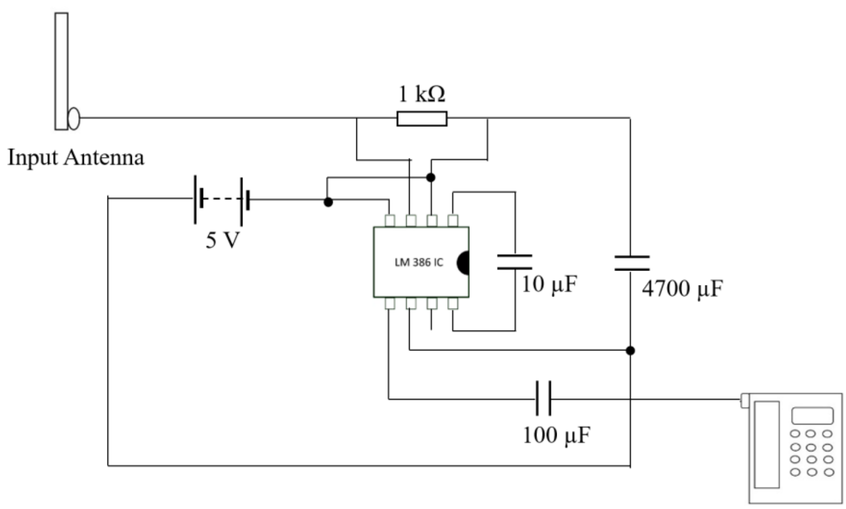

Figure 2: Circuit diagram of signal booster

The methodology of the research involves several stages (Figure 36). First, a comprehensive literature review was carried out to study existing antenna technologies. This review helped in identifying design parameters suitable for the proposed signal booster.

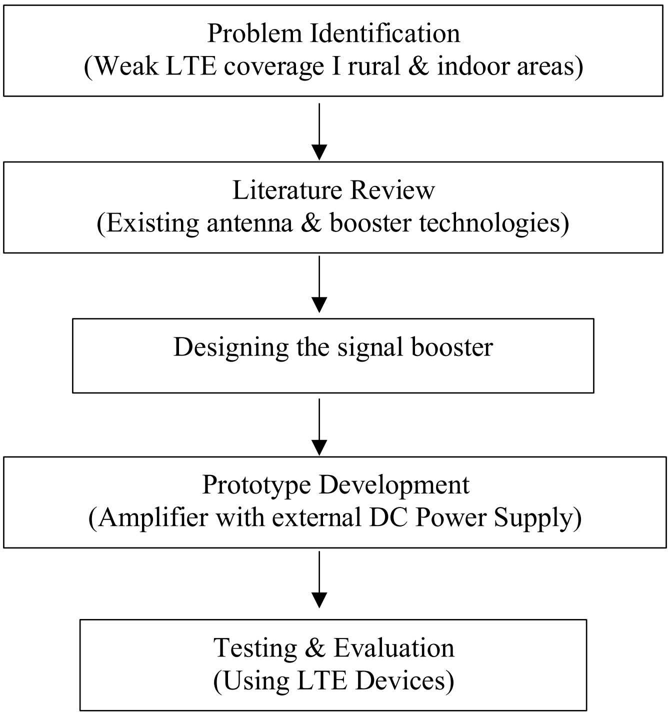

Figure 36: Flow of Experimental Methodology

Following the design phase, a prototype of the signal booster is planned to be developed and tested under real-world conditions. Testing will be conducted both indoors and in rural areas to evaluate the antenna's effectiveness in enhancing LTE reception. Equipment such as a LTE routers, and mobile devices will be used to measure improvements in signal strength, internet stability, and call quality. A dedicated power supply unit will be integrated into the system to ensure consistent antenna performance, independent of the device's power limitations. To verify the proper functioning of the developed signal booster, it was connected to a V10 LTE telephone, and the device was logged into the server to check the RSRP and SINR values (**Error! Reference source not found.**).

Figure 4: Testing the Signal Booster with LTE Device

External power supplied…

3.0 RESULTS AND DISCUSSION

The external power-supplied signal booster is anticipated to significantly improve LTE reception in both rural and indoor environments, where conventional built-in antennas in mobile devices and routers often fail to provide reliable connectivity. By incorporating a dedicated power source, the booster is able to operate with enhanced stability and higher gain, which directly contributes to improved signal quality.

According to the SLT technicians hand book the SINR (signal to interference plus Noise Ratio Range) should be +30 dB to +4 dB and RSRP (Reference Signal Received Power Range) should be -44 dBm to -140 dBm (Table 5).

Table 5: Network Performance Metrics With and Without Signal Booster

Metric	Standard Quality Range		Without Signal Booster	With Signal Booster
	Good Quality	Poor Quality		
SINR (dB)	+30 to +4	+4 to -20	4	8
RSRP (dBm)	-44 to -110	-110 to -140	-111	-110

According to the readings obtained it clearly shows the SINR value has increased by 4dB within the range of good quality. So, it shows that the signal booster increases the signal interference without increasing the noise with respect to the signal power (**Error! Reference**

Platform Version/RAM	V3T/512M
IMEI	865644051875101
S/N	V10865644051875101N
SIM Status	Normal
Network Mode	LTE
IPv4 Status	Connected
WAN IP Address	100.105.213.95
IPv4 DNS	222.165.171.4,222.165.171.3
Internet Usage	
Total Traffic	-
Uplink Traffic	-
Downlink Traffic	-
Uplink Rate	-
Downlink Rate	-
Run Time	0D 0:3:57
LTE Signal Status	
PLMN	SLT/41312
Service Status	Normal
PhysCellId	203
Cell Id	0010519-002
RSRQ(dB)	-10
RSRP(dBm)	-111
SINR	4
Roaming	No
BAND	38
MCS	6
CQI	6
RSSI(dBm)	-81
Antenna Status	
Antenna Status	External

source not found.).

Figure 5: Signal readings without connected to the signal booster

SIM Status	Normal
Network Mode	LTE
IPv4 Status	Connected
WAN IP Address	100.105.213.95
IPv4 DNS	222.165.171.4,222.165.171.
Internet Usage	
Total Traffic	-
Uplink Traffic	-
Downlink Traffic	-
Uplink Rate	-
Downlink Rate	-
Run Time	0D 0:3:37
LTE Signal Status	
PLMN	SLT/41312
Service Status	Normal
PhysCellId	203
Cell Id	0010519-002
RSRQ(dB)	-9
RSRP(dBm)	-110
SINR	8
Roaming	No
BAND	38
MCS	6
CQI	6
RSSI(dBm)	-80
Antenna Status	
Antenna Status	Built-in

Figure 6: Signal readings with the connection of signal booster

The use of booster has enhanced both internet speed and call reliability. Improved throughput is expected due to stronger reception, which reduces packet loss and enhances the stability of data connections. Furthermore, clearer voice quality has obtained, as stronger signals minimize interruptions and disconnections, particularly in areas far from base stations.

4.0 CONCLUSION

The research successfully addressed the issue of weak LTE reception in rural and indoor regions of Sri Lanka through the design and development of an external power-supplied signal booster for LTE telephones and routers. The completed prototype demonstrated a significant improvement in both signal strength and connection stability when tested under real-world conditions.

The integration of an independent power supply proved to be a critical factor in ensuring stable performance, as it allowed the booster to maintain high gain without being limited by the device's internal power constraints. Field testing further showed that users in previously low-coverage areas were able to experience stronger and more consistent LTE connectivity, validating the effectiveness of the proposed solution.

The results confirm that the external signal booster offers a practical, low-cost, and scalable method of overcoming LTE coverage limitations. It not only benefits individual users but also has broader implications for improving digital access in underserved communities. Future research could focus on optimizing the design for multi-band LTE compatibility, miniaturization for portability, and cost reduction for mass deployment.

In conclusion, the developed external power-supplied signal booster successfully enhances LTE connectivity, bridging the gap between rural and urban communication infrastructure, and providing a reliable solution to one of Sri Lanka's pressing technological challenges.

ACKNOWLEDGEMNTS

The author wishes to express sincere gratitude to the academic staff of the Faculty of Applied Sciences, Wayamba University of Sri Lanka, for their expert advice and guidance throughout the project. Special thanks are also extended to the technical staff at Sri Lanka Telecom for their practical support, insights, and feedback during the testing and evaluation of the toolkit.

REFERENCES

[1] O. Chibuzo and A. Omoniyi, "Network and Complex Systems Developing a Signal Booster for Improved Communication in Remote Areas," 2019. Available: https://core.ac.uk/download/pdf/234686722.pdf

[2] E. N. Onwuka *et al.*, "Survey of Cellular Signal Booster," *International Journal of Information Engineering and Electronic Business*, vol. 10, no. 6, pp. 21–31, Nov. 2018, doi: 10.5815/ijieeb.2018.06.03.

[3] N. K. Liu, N. J. He, N. J. Ding, N. Y. Zhu, and Z. Liu, "Base station power model and application for energy efficient LTE," pp. 86–92, Nov. 2013, doi: 10.1109/icct.2013.6820352.

[4] R. Irmer and S. Chia, "Signal processing challenges for future wireless communications," Apr. 2009, doi: 10.1109/icassp.2009.4960411.

[5] Eswaran Uthirajoo, Harikrishnan Ramiah, Jeevan Kanesan, and A. W. Reza, "Wideband LTE Power Amplifier with Integrated Novel Analog Pre-Distorter Linearizer for Mobile Wireless Communications," *PLoS ONE*, vol. 9, no. 7, pp. e101862–e101862, Jul. 2014, doi: 10.1371/journal.pone.0101862.

[6] Naemat, S. M. M. Hassan, N. F. I. Muhammad, A. S. M. Marzuki, and N. Kushairi, "Experimental study on LTE signal transmission in multi-service Radio-over-Fiber (RoF) system," *2017 IEEE 13th Malaysia International Conference on Communications (MICC)*, pp. 300–304, Nov. 2017, doi: 10.1109/micc.2017.8311776.

Proc. Annual Symposium on Research & Industrial Training, 12 (2025) 273-280
Department of Electronics – Wayamba University of Sri Lanka

A BROADBAND SIGNAL STRENGTH MAPPING SYSTEM

P.D.C. Jayashan*[1], S.R.L. Gunawardhana[1]
[1]*Department of Electronics, Wayamba University of Sri Lanka, Kuliyapitiya, Sri Lanka*
*chathurajayashan21@gmail.com

ABSTRACT

This research presents the development of a comprehensive, low-cost signal strength mapping system designed for field deployment in telecommunications networks. The system integrates an ESP32 microcontroller with multiple communication modules, including SIM800L GSM, NEO-6M GPS, and SSD1306 OLED display to provide real-time signal quality assessment. The device measures critical parameters, including Received Signal Strength Indicator (RSSI), Signal-to-Noise Ratio (SNR), network technology, and geographical coordinates while performing basic speed tests. Data is transmitted via both SMS and a cloud-based Firebase repository for remote monitoring and analysis. The system features an intuitive user interface with animated display sequences and manual control via a push button. Field testing demonstrated reliable operation in various environments, with the system automatically selecting between cellular and WiFi connectivity based on availability. This cost-effective solution provides telecommunications technicians with a practical tool for signal mapping, network optimization, and installation validation in field deployments.

Keywords: **S**ignal Strength **M**apping, IoT, **T**elecommunications

1.0 INTRODUCTION

The expansion of telecommunications infrastructure is crucial for development, yet its optimization in developing regions is hampered by the high cost of essential monitoring tools. Effective network deployment requires extensive field measurements for coverage mapping, a process hindered by the prohibitive cost of professional signal analyzers. This creates a significant barrier for technicians, leading to inefficient network planning, extended troubleshooting, and suboptimal service quality. Current practices relying on expensive equipment are often inaccessible, creating a need for affordable alternatives [1].

Previous approaches to reduce costs have included smartphone applications for crowd-sourced data collection [2]. However, these methods lack hardware control and measurement consistency, producing data unsuitable for technical analysis. Solutions based on single-board computers like the Raspberry Pi offer greater control but result in bulky, multi-component systems impractical for portable field use.

This paper directly addresses this gap by presenting a low-cost, integrated Signal Strength Mapping System built on an ESP32 microcontroller. The proposed system overcomes the limitations of previous approaches by combining a GSM module for cellular analysis, a GPS for geolocation, and a display into a single, portable device. This IoT-based solution provides reliable, real-time measurement of key parameters like Received Signal Strength Indicator (RSSI) and Signal-to-Noise Ratio (SNR). The system is designed to offer telecommunications technicians a practical tool for signal mapping and network optimization, delivering critical data for improving network performance at an accessible cost.

2.0 EXPERIMENTAL

2.1 Hardware architecture and component integration

The system's architecture was designed to ensure robustness, portability, and reliable field operation. At its core, the ESP32-WROOM-32 microcontroller was selected for its dual-core 240 MHz processor, ample SRAM, and integrated Wi-Fi and Bluetooth capabilities, enabling efficient peripheral management, data acquisition, processing, and communication[3].
As shown in Figure 01, the ESP32 interfaces with dedicated modules: a SIM800L GSM/GPRS module for cellular communication and signal parameter extraction, a NEO-6M GPS module for accurate geolocation, and a SSD1306 OLED display for real-time visual feedback. A push button is included for user input and measurement control. Power is supplied by a battery pack regulated through an MP1584 DC-DC converter, with a capacitor ensuring stable voltage levels.
The integration of these components, illustrated in Figure 01, results in a cohesive unit capable of comprehensive signal analysis.

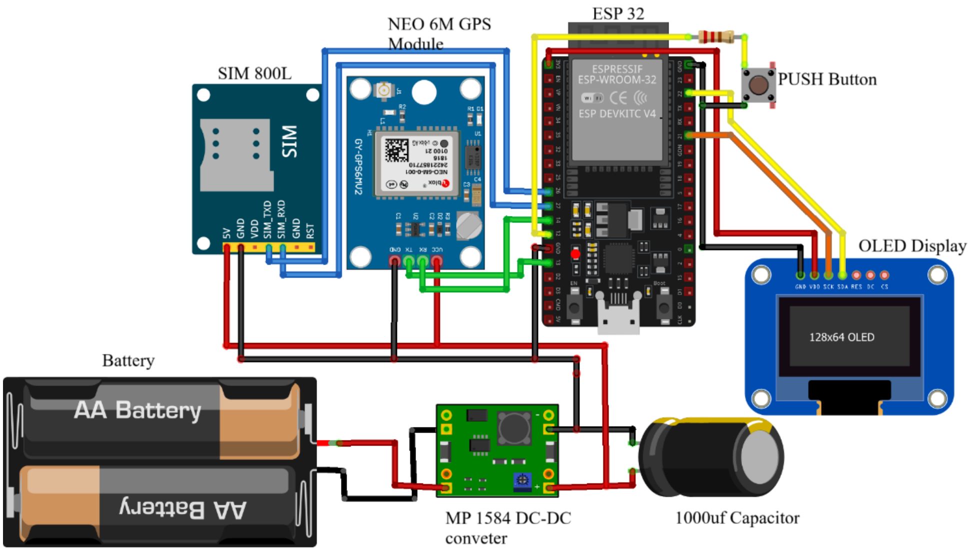

Figure 2.1: Comprehensive block diagram of the system

2.2 Core processing and communication modules

The ESP32-WROOM-32 microcontroller acts as the central command unit, coordinating all system operations through its dual-core architecture and diverse communication interfaces. It efficiently manages data acquisition, processing, and peripheral control while handling multiple simultaneous tasks. The ESP32 employs a multi-protocol strategy: Hardware Serial (UART1) handles debug output, while software serial ports on GPIO 26-27 and 13-14 communicate with the SIM800L GSM module and NEO-6M GPS receiver, respectively. The SSD1306 OLED display connects via I²C on GPIO 21-22, providing essential user feedback. This optimized integration ensures each component operates at peak performance while maximizing resource utilization and maintaining overall system efficiency for comprehensive signal analysis.[4]

2.3 Power management subsystem:

The power management system is based on two series-connected 18650 batteries (7.4 V), which provide the primary energy source. A dedicated MP1584 buck converter (U1) regulates this voltage down to 4.0 V, supplying stable power to the ESP32, SIM800L, and GPS modules. To mitigate voltage fluctuations during the SIM800L's high-current transmission bursts, a 1000 µF decoupling capacitor (C1) is added at its VCC input as shown in Figure 2.2.
The OLED display is powered via the ESP32's built-in 3.3 V linear regulator, ensuring proper voltage regulation and isolation from the main 4.0 V supply. This arrangement provides efficient regulation, noise suppression, and stable operation across both communication and processing subsystems [5].

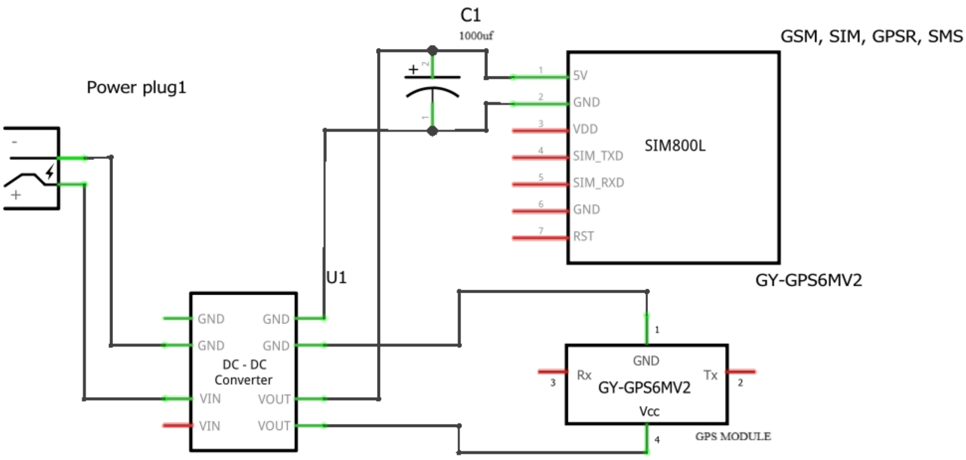

Figure 2.2: Power regulation circuit diagram

2.4 Physical integration:

The physical construction of the prototype prioritizes durability and reliability for handling in field environments. All electronic components, including the ESP32 development board,

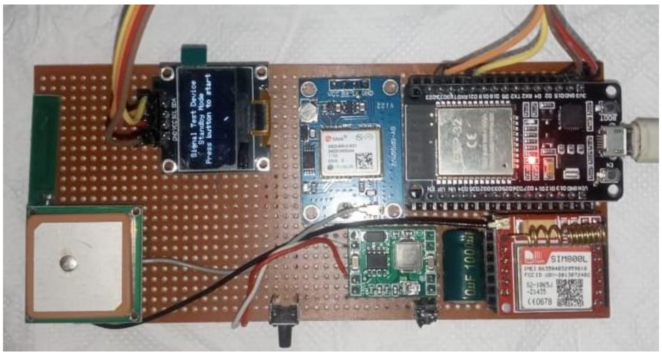

Figure 2.3: Prototype assembly layout.

SIM800L and GPS modules, a buck converter, and a capacitor were securely assembled on a single prototyping board. Electrical connections were made using soldered wires for permanence and reliability, with particular attention paid to the antenna connections for the Radio Frequency modules. Critical connections, especially those to the SIM800L module, were designed with robust strain relief to ensure integrity during handling and testing.
The complete assembly is shown in Figure 2.3, which provides a clear view of the component layout, the display interface, and the overall physical construction of the prototype.

2.5 Firmware design and operational logic

The firmware implements a finite state machine approach with four primary operational states managed through a non-blocking code architecture. The logic governing state transitions is illustrated in Figure 04, which outlines the flow of control between the standby, acquisition, display, and transmission states. The system progresses through these states, with a button press serving as the main transition trigger.

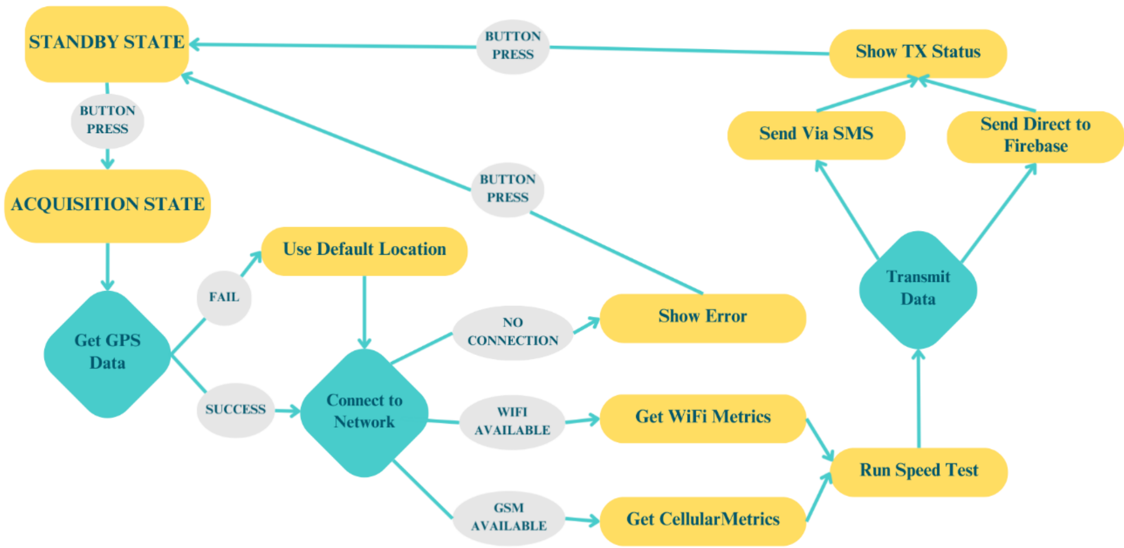

Figure 2.4: Device control flowchart

Signal measurement algorithms employ sophisticated processing of cellular parameters, extracting RSSI from SIM800L modules by parsing AT command responses and converting manufacturer-specific values to standard dBm measurements, while SNR calculation utilizes a hybrid approach combining actual Bit Error Rate measurements when available with RSSI-based estimations when unavailable. Geolocation processing leverages the TinyGPS++ library to parse NMEA sentences with automatic location-based naming conventions and incorporates timeout handling to prevent operational blocking in poor reception environments [6].

2.6 Measurement methodology and data processing

The system implements comprehensive signal assessment through multiple measurement techniques, employing AT commands to query cellular network status (AT+CREG) and signal quality (AT+CSQ) with integrated error handling for data integrity. Speed testing varies by connection type, utilizing actual HTTP-based tests for WiFi connections while generating simulated values for cellular networks due to hardware limitations. For data transmission, the system employs redundant pathways using SMS for reliable delivery in low-connectivity areas and Firebase integration for cloud storage with automatic selection based on available connectivity [7].

2.7 User interface design

The system features a dual-layer interface for field and remote operation. The device is controlled by a single debounced push-button that initiates measurement cycles. User feedback is provided through a multi-state OLED display, which shows an animated sequence culminating in a results screen that prioritizes key parameters like RSSI and network type [8].

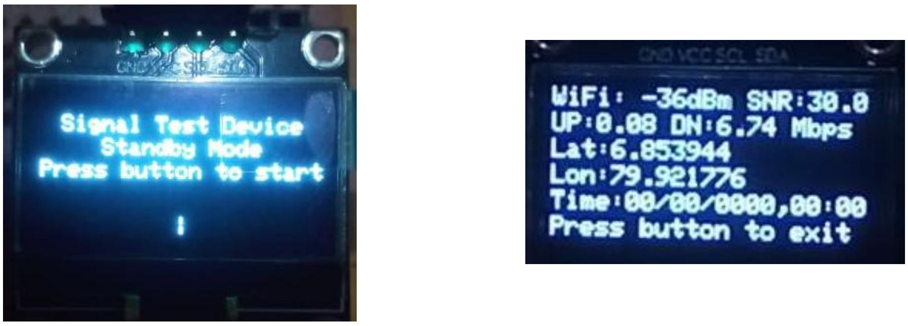

Figure 2.5: OLED display output with measurement data.

For comprehensive analysis, a web dashboard displays network Key Performance Indicators, including coverage percentage and average speeds on an interactive map, as shown in the Figure 6. It also provides tools for data upload and automated report generation, enabling remote network management and planning.

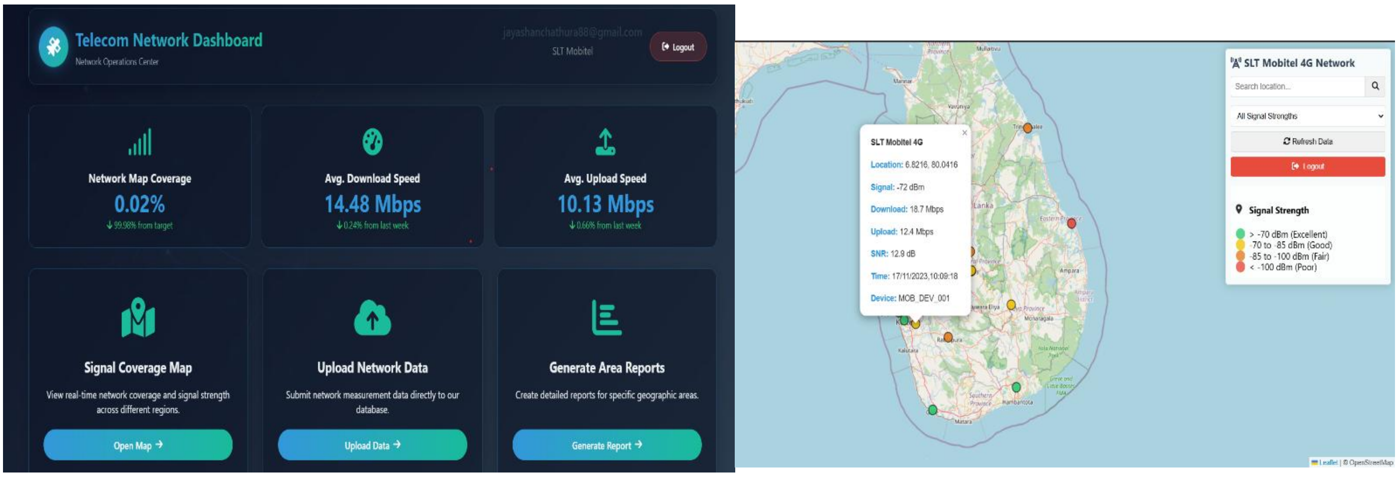

Figure 2.6: Web dashboard interface.

3.0 RESULTS AND DISCUSSION

3.1. System performance and measurement accuracy

The developed system successfully integrated all hardware components and implemented the proposed measurement methodology. The ESP32 microcontroller effectively managed the multiple peripheral devices without significant processing delays. The OLED display provided clear visual feedback with refresh rates adequate for user interaction, though limitations in sunlight visibility were noted during field testing.
The measurement capabilities and corresponding accuracy of the system are summarized in Table 3.1. The parameters include key cellular and GPS metrics essential for network diagnostics.

Table 3.1. Measurement capabilities and accuracy

Parameter	Measurement Method	Estimated Accuracy	Range
RSSI	AT+CSQ command parsing	±3 dB	-115 to -52 dBm
SNR	Hybrid calculation	±2 dB	5-30 dB
Location	GPS NMEA parsing	±2.5m	Global
Download Speed	HTTP transfer timing	±10%	0-50 Mbps
Upload Speed	HTTP POST timing	±10%	0-50 Mbps

GPS performance showed a typical time-to-first-fix of approximately 45 s from cold start, consistent with the NEO-6M module specifications. Location accuracy was sufficient for signal mapping purposes, with the added functionality of automatic location naming based on coordinate ranges.
Cellular measurement reliability was affected by network conditions, with the SIM800L module occasionally requiring reset commands to regain stable communication. The implemented error-handling procedures successfully managed these instances without requiring hardware resets.

3.2.Field testing and data collection

Field testing conducted in urban and semi-urban environments demonstrated the system's practical utility. The device successfully collected and transmitted over 150 data points during the testing period, with the dual transmission method (SMS and Firebase) ensuring data integrity even in areas with limited connectivity.
A sample of the field data collected is presented in Table 3.2, illustrating the types of measurements recorded across different locations and technologies.

Table 3. 2. Sample field measurements

Timestamp	Latitude (° N)	Longitude (° E)	Technology	RSSI (dBm)	SNR (dB)	Download (Mbps)	Upload (Mbps)
15/08/2025, 11:45	6.5854	79.9607	WiFi	-63	24.8	15.2	6.5
15/08/2025, 12:15	6.5227	80.1145	WiFi	-71	20.0	5.2	3.2
15/08/2025, 12:45	6.4597	80.1123	GSM	-79	17.0	0.8	0.2

3.3.Limitations and technical challenges

Several technical challenges were identified during testing. The display proved to be difficult to read in direct sunlight. The cellular module occasionally required software resets to maintain a stable connection, and network speed measurements were simulated due to hardware constraints. Furthermore, continuous display operation led to higher-than-ideal power consumption.

While the system successfully integrated multiple functionalities on a low-cost platform, future commercial deployment would require hardware revisions and further firmware optimization to address these limitations

4.0 CONCLUSION

This research successfully developed a portable ESP32-based system for comprehensive field signal mapping, integrating cellular/WiFi measurement, GPS geolocation, and speed testing. Its main contributions are a hybrid measurement approach and redundant data transmission, ensuring reliable operation in diverse connectivity conditions. The system features an intuitive field-optimised interface and a complementary web dashboard for remote data monitoring and analysis. However, the prototype's reliance on the SIM800L module imposes limitations, including its 2G-only network support, occasional instability requiring software resets, and an inability to perform true network speed measurements due to hardware constraints. Despite these component-level limitations, the prototype proves the viability of this low-cost, integrated approach. Future work will focus on hardware revisions, including a modern 4G/LTE module, to enable advanced network analytics and enhanced cloud data processing capabilities

ACKNOWLEDGEMENTS

The authors express their sincere gratitude to the lecturers and the staff of the Department of Electronics, Faculty of Applied Sciences, Wayamba University of Sri Lanka, for their valuable guidance and support throughout this study. The authors also gratefully acknowledge Sri Lanka Telecom PLC, where the industrial training was carried out, for providing the necessary facilities and exposure that contributed significantly to the success of this work.

REFERENCES

[1] L. Polak, J. Kufa, R. Sotner, and T. Fryza, "Measurement and analysis of 4G/5G mobile signal coverage in a heavy industry environment," *Sensors*, vol. 24, no. 8, 2024, Art. no. 2538. doi: 10.3390/s24082538

[2] A. Jasso, "How to check your cell phone signal strength," *SignalBoosters*, 2024. Available: https://www.signalboosters.com/blog/how-to-check-your-cell-phone-signal-strength/

[3] Espressif Systems, "ESP32-WROOM-32 datasheet," ver. 3.6, 2022. Available: https://www.espressif.com/sites/default/files/documentation/esp32-wroom-32_datasheet_en.pdf

[4] Random Nerd Tutorials, "ESP32 I2C communication: Set pins, multiple bus interfaces and peripherals (Arduino IDE)," 2019. Available: https://randomnerdtutorials.com/esp32-i2c-communication-arduino-ide/

[5] Last Minute Engineers, "Send receive SMS & call with SIM800L GSM module & Arduino," 2018. Available: https://lastminuteengineers.com/sim800l-gsm-module-arduino-tutorial/

[6] SIMCom, "AT command set: SIM800 series," *M2M Support*, 2015. Available: https://m2msupport.net/m2msupport/atcsq-signal-quality/

[7] J. Teel, "The SIM800 cellular module and Arduino: A powerful IoT combo," *Predictable Designs*, 2018. Available: https://predictabledesigns.com/the-sim800-cellular-module-and-arduino-a-powerful-iot-combo/

[8] R. Santos, "Guide for I2C OLED display with Arduino," *Random Nerd Tutorials*, 2019. Available: https://randomnerdtutorials.com/guide-for-oled-display-with-arduino/

Proc. Annual Symposium on Research & Industrial Training, 12 (2025) 281-285
Department of Electronics – Wayamba University of Sri Lanka

BATTERY - POWERED PORTABLE TOOLKIT FOR TESTING AND VERIFYING TELECOMMUNICATION EQUIPMENT

P.V.S. Madhumalika[1]*, J.M.J.W. Jayasinghe[1], I.H.C. Prasanga Kumara[2]
[1]*Department of Electronics, Wayamba University of Sri Lanka, Kuliyapitiya, Sri Lanka*
[2]*Sri Lanka Telecom PLC*
*subhashinimadhumalika@gmail.com

ABSTRACT

Field technicians working in the telecommunication industry frequently encounter challenges when attempting to verify internet and television services at customer premises. The most common problems occur during power outages or when customer-owned televisions are non-functional. Since routers, set-top boxes (STBs), and televisions all require electricity, the absence of a power supply makes it impossible to confirm service functionality. Similarly, if a television is not available or is faulty, technicians are unable to test Peo TV connections, even if power is present. These limitations often lead to delayed fault resolution, repeated visits, increased operational costs, and reduced customer satisfaction. To address these issues, this project proposes the design and development of a portable, battery-powered toolkit capable of operating independently of customer infrastructure. The toolkit integrates a rechargeable 12V power bank, a battery management system, and a compact TFT LCD display, which serves as a temporary replacement for a television. A prototype device was developed and tested under real-world conditions such as power outages and the absence of televisions. The test results demonstrated reliable power delivery, consistent display performance, and effective support for both troubleshooting and new service installations.

Keywords: **P**ortable Toolkit, **T**elecommunication Testing, **P**ower Bank

1.0 INTRODUCTION

The telecommunication sector plays a vital role in modern society by providing reliable internet and television services, which are essential for communication, education, and entertainment. Telecommunication service providers continuously deploy field technicians to ensure uninterrupted service delivery for customer needs. Their responsibilities include both installing new connections and troubleshooting faults in existing services. However, technicians often encounter challenges during these activities. One common difficulty arises when service visits coincide with power outages or disconnections, which prevent routers and set-top boxes (STBs) from being powered. Similarly, even when electricity is available, service verification becomes impossible if customer-owned televisions are unavailable or malfunctioning. In such cases, technicians are unable to confirm IPTV connectivity, leading to repeated visits, increased operational costs, and reduced customer satisfaction [1,2].

Over the years, SLT has experimented with several temporary solutions to address these challenges. Devices such as portable 12V power banks and rechargeable power adapters have been tested to provide backup power for routers and STBs during field visits. While these devices offered limited relief, they suffered from major shortcomings. Their runtime was too short and not even enough for one-time use. More importantly, these approaches failed to provide a way to verify Peo TV services. One reason for this was that they could power only one device at a time, also even when routers and STBs could be powered, the absence of a customer's television remained a barrier. Televisions require AC mains power to operate, and therefore could not be powered through portable DC power banks. These limitations highlight the gap in existing solutions, as none of the methods trialed by SLT provided a comprehensive, field-ready tool that could independently power essential devices and replicate the role of a customer's television for Peo TV testing [3,4].

To address these challenges, this paper proposes a portable, battery-powered toolkit designed specifically for field technicians. The toolkit integrates a rechargeable 12V power bank capable of powering STBs, routers, and other essential equipment, along with a TFT display unit that replaces the need for a customer's television during Peo TV verification. Additionally, the toolkit includes a battery level indicator to monitor the remaining charge and ensure uninterrupted operation during service visits [5,6].

The objectives of this research are to design and develop a portable, battery-powered toolkit that allows field technicians to verify internet and television services without relying on customer-owned equipment or power sources. The study further aims to integrate a TFT LCD display as a temporary replacement for customer televisions, ensuring reliable service verification in situations where televisions are unavailable or non-functional. In addition, the toolkit is designed to be lightweight and portable for use across diverse service environments, while a battery level indicator is incorporated to support uninterrupted operation during extended visits. Accordingly, the research question addressed is whether a portable, battery-powered toolkit with an integrated display and battery monitoring system improves the effectiveness and reliability of telecommunication field services under conditions where electricity or customer equipment is unavailable.

2.0 EXPERIMENTAL

A hardware-based development methodology was followed for designing the proposed toolkit. The design process consisted of three main phases: system design, prototype construction, and testing under field conditions. The system was designed to integrate a rechargeable power bank, display unit, and necessary connectors into a compact and portable unit (

Figure *37*).

A 12V battery system was designed using three 3.7V 18650 lithium-ion batteries connected in series as the main power source. A Battery Management System (BMS) was incorporated to ensure safe charging and discharging. A TFT LCD display was integrated into the toolkit as a substitute for a customer television. The display was configured with HDMI and AV inputs so that the set-top box (STB) could be directly connected during service verification. A 3-way splitter cable was also included, allowing multiple devices to be powered simultaneously from the toolkit. Additionally, the toolkit included a battery level indicator, which allowed the user to monitor the current battery charge in real time, ensuring reliable operation during service activities.

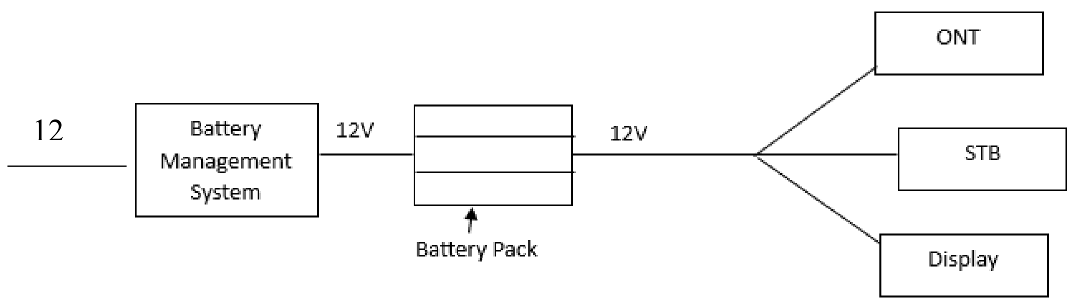

Figure 37: Block diagram of the portable toolkit

During prototype assembly, all components were mounted into a lightweight, compact casing to optimize portability (Figure 38). The completed toolkit was subjected to extensive testing under various field conditions. Testing focused on verifying display functionality with connected STBs, evaluating power supply stability under multiple device loads, and monitoring battery performance. The toolkit's operational endurance was measured, determining the duration of continuous use achievable from a single full charge, confirming its suitability for typical field service scenarios.

Figure 38: Portable toolkit successfully powering STB, router, and display

3.0 RESULTS AND DISCUSSION

The toolkit was tested by connecting two 12V devices, a router and a set-top box, at the same time. Both devices operated reliably when powered together, demonstrating the capability of the toolkit to supply stable power to multiple field equipment. Additionally, when the set-top box was connected to the integrated TFT display, the screen successfully functioned as a temporary television, enabling Peo TV verification in the absence of a customer-provided television.

Battery performance was also evaluated under different load conditions. When fully charged, the toolkit was able to power a single device, such as the ONT, continuously for approximately three and half hours. However, when all three components the router, set-top box, and TFT display were connected and operated simultaneously, the battery provided power for about one and a half hours.

Theoretically run time of the device as follows under different load conditions:

Power bank capacity = 3 * 3.7V * 6800mAh = 75.48Wh

Load of the ONT = 12V * 1.5A = 18W

Load of the STB = 12V * 1.5A = 18W

Load of the display= 12V * 1A = 12W

Run time (h) = Battery capacity (Wh) / Toal Load (W) (1)

Run time (Router only) = 75.48Wh / 18W = 4.19h

Run time (full load) = 75.48Wh / 48W = 1.57h

Theoretical and tested runtimes of the toolkit under different load conditions are shown in Table 6.

Table 6: Toolkit performance under different load conditions

Test condition	Observation	Theoretical runtime (h)	Tested Runtime (h)
ONT only	Operated reliably with stable power supply.	4.19	~3.5
Full Load (Router + STB + TFT display)	All devices functioned properly, Peo TV verification possible.	1.57	~1.5

According to the results it clearly shows that the theoretical values and the tested values have no much difference. So, we can conclude that the power loss of the tool kit is small enough to negligible. The successful operation of multiple devices and the use of the TFT display as a temporary television demonstrate its practical utility for field technicians. The reduction in runtime with increased device load is consistent with the expected behaviour based on battery capacity and device power consumption.

Furthermore, the toolkit's ability to operate independently of customer power and television infrastructure addresses key challenges faced by technicians, such as power outages and non-functional TVs. This functionality improves operational efficiency, reduces repeat visits, and allows more accurate and timely service verification. Technician feedback was collected through face-to-face interviews, which provided direct insights into usability and practicality. Technician feedback during testing also highlighted the usability and convenience of the toolkit, suggesting that it can be reliably used in real-world field conditions. Overall, these findings indicate that the toolkit is both effective and practical for telecommunication field service operations.

4.0 CONCLUSION

The study demonstrated that the portable, battery-powered toolkit can reliably operate multiple 12V devices, including a router and set-top box, while also providing a functional display for Peo TV verification. These results directly address the research question by showing that the toolkit enables field technicians to perform service verification and fault diagnosis independently of customer power or television availability. The data support the hypothesis that a self-contained, portable toolkit can improve operational efficiency and reduce repeat visits. Although the battery runtime decreases when all three components are connected, this trade-off aligns with expected outcomes based on device power consumption and highlights areas for potential improvement. The integration of a TFT display as a temporary television is a novel feature that enhances practical utility in the field. Future work could focus on extending battery capacity, reducing toolkit weight, and incorporating additional diagnostic functions to further support field operations. As the limitation the tool kit only matches only with the devices that operate under 12V, this can be further developed by adding power management system so that the tool kit can support different type of devices that operate under various voltages. Overall, the developed toolkit provides an effective and practical solution for telecommunication service verification under constrained conditions, improving both efficiency and customer satisfaction.

ACKNOWLEDGEMNTS

The author wishes to express sincere gratitude to the academic staff of the Faculty of Applied Sciences, Wayamba University of Sri Lanka, for their expert advice and guidance throughout the project. Special thanks are also extended to the technical staff at Sri Lanka Telecom for their practical support, insights, and feedback during the testing and evaluation of the toolkit.

REFERENCES

[1] K. Kutluay, Y. Cadirci, Y. S. Ozkazanc, and I. Cadirci, "A new online state-of-charge estimation and monitoring system for sealed lead-acid batteries in Telecommunication power supplies," *IEEE Transactions on Industrial Electronics*, vol. 52, no. 5, pp. 1315–1327, Oct. 2005, doi: https://doi.org/10.1109/TIE.2005.855671.

[2] J. Maatta, J. Harkonen, T. Jokinen, M. Muhos, P. Belt "Managing testing activities in telecommunications: A case study," *Journal of Engineering and Technology Management*, vol. 26, no. 1–2, pp. 73–96, Mar. 2009, doi: https://doi.org/10.1016/j.jengtecman.2009.03.008.

[3] D. Salopek, Valter Vasić, M. Zec, Miljenko Mikuc, Mladen Vasarevic, and V. Koncar, "A network testbed for commercial telecommunications product testing," Sep. 2014, doi: https://doi.org/10.1109/softcom.2014.7039061.

[4] C. Bambang Dwi Kuncoro, Moch, and C. Adristi, "Dual mode portable power bank for extending battery life of gadget devices," *Nucleation and Atmospheric Aerosols*, Jan. 2023, doi: https://doi.org/10.1063/5.0126936.

[5] S. Eldh and D. Sundmark, "Robustness Testing of Mobile Telecommunication Systems: A Case Study on Industrial Practice and Challenges," Apr. 2012, doi: https://doi.org/10.1109/icst.2012.228.

[6] C. Riki and Evvy Kartini, "Design and assembly lithium-ion NMC 18650 battery pack 11.1V 7.8Ah as a power bank," *AIP conference proceedings*, vol. 3221, pp. 030005–030005, Jan. 2024, doi: https://doi.org/10.1063/5.0244620.

Proc. Annual Symposium on Research & Industrial Training, 12 (2025) 286-291
Department of Electronics – Wayamba University of Sri Lanka

DEVELOPMENT OF A FREQUENCY MEASUREMENT DEVICE FOR SHORT WAVE DIATHERMY (SWD) MACHINES

R.N.N. Prabodanee[1]*, G.A.K.S. Perera[1], T.V.A. Ruwansiri[2]
[1]*Department of Electronics, Wayamba University of Sri Lanka, Kuliyapitiya, Sri Lanka*
[2]*Division of Biomedical Engineering Services, Ministry of Health, Colombo, Sri Lanka*
*nethminawodya1999@gmail.com

ABSTRACT

This paper reports the design and validation of a system created to accurately measure the output frequency of Short Wave Diathermy (SWD) devices found in physical therapy that treat conditions such as pain management, osteoarthritis, muscle spasms, and soft tissue injury. The SWD devices emit high-frequency electromagnetic currents at a defined therapeutic frequency. If the device is malfunctioning or not properly maintained it could function outside that prescribed operational frequency range potentially leading to ineffective treatment and/or tissue damage including burns. The system implemented in this research detects the emitted signal using a non-contact copper loop antenna. Once the signal is detected, it is amplified, then selectively LC bandpass filtered to the therapeutic frequency. The analog filtered signal is then digitized into pulses, isolated for the operator's safety, and processed by a microcontroller that averages the pulse count to calculate the frequency in real-time. Experimental results show that frequency measurement was consistent and accurate near the accepted standard frequency of 27.12 MHz. The research demonstrates a simple, practical, low-cost, and practical process to verify that SWD devices operate in safe and effective frequency ranges helping to improve patient safety and treatment effectiveness in a clinical setting.

Keywords: **S**hort Wave Diathermy (SWD), **P**hysical therapy, **T**herapeutic frequency

1.0 INTRODUCTION

Short Wave Diathermy is widely used as a therapeutic treatment, using an energy at 27.12 MHz to deliver deep heating for analgesic, muscle relaxing and tissue healing effects. Accurately maintaining the operating frequency is essential to ensure effective SWD treatment and keep patients safe. If the frequency is outside the specified range, therapy may be inefficient or a patient injury can occur burning, may result from too much heating of tissue. [1]

Several frequency monitoring devices are available, but they are generally too large, too expensive or do not supply any electrical isolation, which is required for clinical use. Previous studies emphasize that the therapeutic efficiency of SWD strongly depends on maintaining the standardized frequency of 27.12 MHz, and researchers have proposed various methods for frequency monitoring, including crystal-based oscillators, spectrum analyzers, and microcontroller-assisted counters. While these methods provide accurate results, most reported devices are either not portable, too costly, or lack adequate patient safety features such as electrical isolation. Recent progresses in embedded systems and signal processing technologies allow one to implement compact, cost-effective and precise frequency estimation devices. However, there is still a need for practical, user-friendly solutions to non-invasively and safely verify and monitor SWD machine output frequency. [2,3,4]

In this project a frequency measurement system was implemented including a copper loop coil for non-contact sensor pickup, an RF amplifier to boost the signal, LC bandpass filters for accurate frequency selection, a comparator and optocoupler for clean and electrically isolated digital pulse conversion, and an ESP32 microcontroller for precise frequency counting and display.[5]

This solves the SWD apparatus problem of not operating into directed frequency range allowing proper treatments and also assuring prevention from, burns or tissue injury due to high frequency. It therefore improves the safety and effectiveness of therapeutic interventions performed by SWD machines.

2.0 EXPERIMENTAL

2.1 System Design and Implementation

The system for measuring frequency was developed to allow for non-contact detection of the output frequency of Short Wave Diathermy (SWD) devices when used at frequencies close to 27.12 MHz. The front-end sensing element is a hand-wound copper loop probe built with 5 to 10 turns of tinned copper wire with a diameter of 20 to 40 mm. The loop coil, in parallel to a variable capacitor (5–47 pF trimmer) formed a tunable LC resonant tank that provides a narrow-bandpass filter at the SWD frequency.[6]
The sensed RF signal was AC-coupled through a 10 nF capacitor to an input and passed into a resistive attenuator, comprised of 120 Ω and 470 Ω resistors. The signal was clamped using Schottky BAT54 diodes to protect against excessive voltage level transients that could affect signal performance. A 74AC04 hex inverter IC was used to form a high-speed squaring stage. The inverter converts the sinusoidal RF waveform to a clean TTL square wave signal.
Next, the signal was passed into a cascade of three 74AC74 dual D-type flip-flops connected in a divide-by-2 configuration, providing an overall divide by 64 frequency reduction (Figure 1). The frequency reduction slowed the input to a countable range to the ESP32 microcontroller, while the output was buffered with resistors on the GPIO input of the ESP32.[7]
The ESP32 uses either the pulse counter (PCNT) or interrupt peripheral to count pulses in a one second window. The frequency is calculated by multiplying the count by the division factor, and can be displayed. Signal integrity is ensured by careful decoupling and grounding across all ICs to reduce noise.[8]

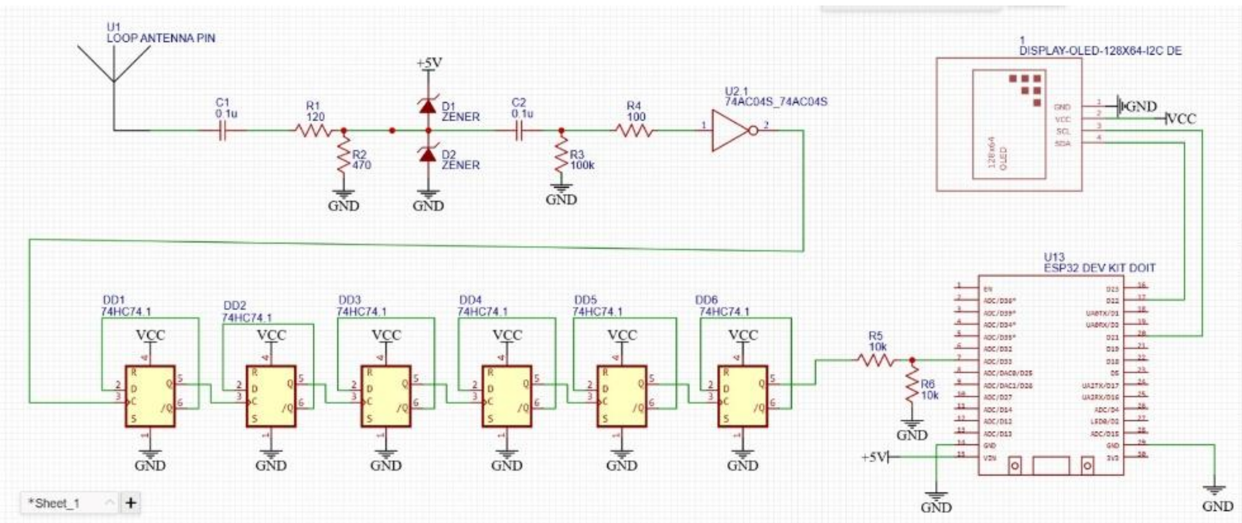

Figure 39: The Circuit diagram of frequency detector

2.2 Experimental Protocol and Measurement Procedure

The experimental protocol commenced with the loop probe 1 to a few centimeters from the SWD applicator head and not making contact, changing the probe as needed to maximize the signal strength where possible. The LC tank capacitor was adjusted to obtain resonance at approximately 27.125 MHz to allow selective response of our circuit for the broadcasted frequency.
Range was set extremely high in preparation for protecting the squaring stage of the schematic, then was decreased as needed until a stable square wave was present in the test equipment. The squaring stage output and divisions of the intermediate output frequency were observed using the oscilloscope at designated test points on the schematic to check for circuit performance and accuracy on frequency division.
The buffered output of the divided frequency was applied to the ESP32, programmed to count the pulses within a fixed time window. The measured count was multiplied by 64 in order to recover the carrier frequency. Frequency values in real-time were displayed on an OLED display that was connected to the microcontroller (Figure 2).

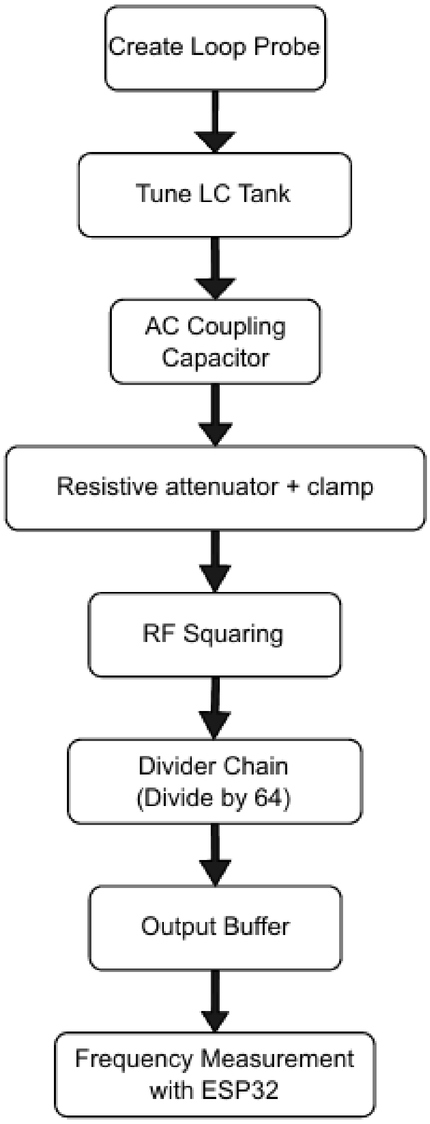

Figure 40: The Flow chart of frequency detector

3.0 RESULTS AND DISCUSSION

A frequency measuring system was designed and successfully trialed in conjunction with a SWD device at a therapeutic frequency of 27.12 MHz. The output from the measuring system was displayed on an OLED screen connected to an ESP32 microcontroller and provided real time readings of the detected frequency (Figure 3).
The testing demonstrated that the copper loop antenna (Figure 4) was able to pick up the electromagnetic signal from the SWD. The transistor amplifier stage was able to amplify this signal sufficiently before it was selectively filtered by into the LC bandpass circuits. The filtered output from the pennant pass band circuits and the output from the Operational Amplifier differential amplifier showed a clean sine waveform, consistent with the frequency of interest. After the comparator conditioning and opto-isolation, the subsequent digital pulses fed into the microcontroller and were counted to determine the frequency output.
The accuracy of the developed portable frequency measurement component was verified by testing it in comparison with a reference dummy load at different power levels (Table 1). The measured frequencies were consistently at the nominal 27.12 MHz, with an error range about nominal of ± 0.15 MHz, thus confirming the accuracy and stability of the system. Variability in the frequencies mainly resulted from electromagnetic interference from the environment and tolerances in the components with the LC filters and amplifiers being the most significant tolerances. However the frequency measuring system gave the frequency readings that were stable, consistent and reliable enough to measure frequency to provide clinical monitoring. In addition, the bulb brightness levels increased consistently with higher power settings, further validating the proper functionality of the system under practical operating conditions.
The system offers some advantages over traditional frequency measurement methods, including non-contact signal detection, instantaneous digital display and safety due to electrical isolation. The main advantage of the system is its portability, making it easier to use compared to conventional dummy load–based measurement methods. The findings are similar to some reported more explicit studies which have shown the importance of monitoring frequency when treatment with SWD devices to avoid under-treated, inefficient treatments or burns to patients in some cases. [9]
Overall, the data support the initial hypothesis that microcontroller-based frequency counter systems including RF front-end amplification and filtering can provide accurate monitoring of SWD output frequencies. Possible improvements for future iterations could include robotically controlled calibration processes for visual display and adding filtering methods to further reduce noise and improve accuracy of the measured frequency. [10,11]

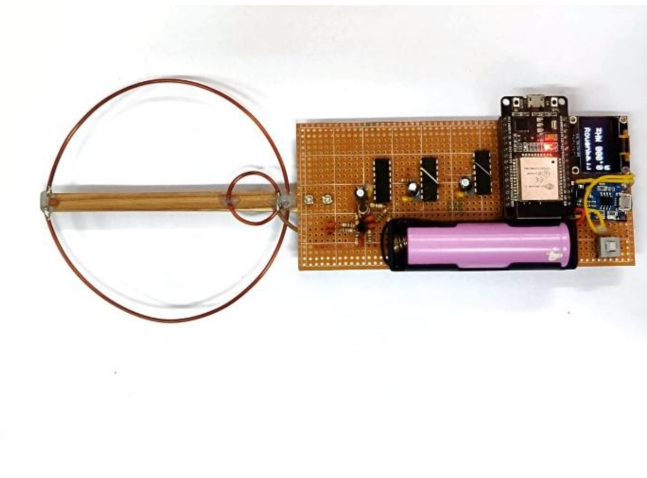

Figure 41: The circuit with OLED Display

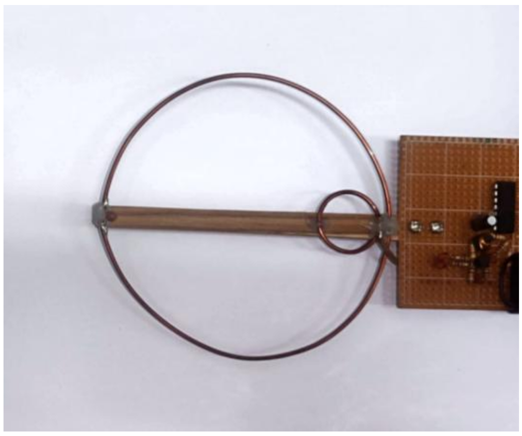

Figure 4: The Copper Loop Antenna

Table 1: Frequency measurement accuracy and bulb brightness at different power levels.

Power Setting (%)	Reference Frequency (MHz)	Device Measured Frequency (MHz)	Approximate Error (MHz)	Bulb Brightness Status	Bulb Brightness Level
25	27.12	26.97	-0.15	Dim	1
50	27.12	27.10	-0.02	Medium	2
75	27.12	27.20	+0.08	Bright	3
100	27.12	27.27	+0.15	Very Bright	4

4.0 CONCLUSION

The SWD frequency measurement system developed demonstrated accurate real-time monitoring of therapeutic frequencies using a non-contact sensing method, subsequent amplification, complete filtering, and electrical isolation. The findings confirm that the system successfully detects frequency variation, assuring the device is operating within safe therapeutic limits while mitigating the risk of ineffective treatment or patient injury. These findings correlate with previous studies demonstrating the utility of precise frequency control with SWD devices. The challenges associated with noise in the signal indicate there may be room for further improvements with sensitivity and with an advanced filtering system. In addition the future scope of this research can include similar investigations with other frequency outputs and checking clinical applications with SWD in practice as well. Ultimately this system presents a practical method that improves safety and efficacy within physiotherapy treatment options.

ACKNOWLEDGEMENTS

The authors sincerely thank the academic and technical staff of the Department of Electronics, Faculty of Applied Science, Wayamba University of Sri Lanka, for their help, cooperation and assistance. Also, the authors thank Biomedical Engineering Services, Colombo 10 for providing the resources which made this research possible.

REFERENCES

[1] N. Shields, J. Gormley, and N. O'Hare, "Short-wave diathermy: current clinical and safety practices," Physiotherapy Research International, vol. 7, no. 4, pp. 191–202, Nov. 2002, doi: 10.1002/pri.259.

[2] Won Young Lee, J.-D. Cho, and Sung Koo Lee, "A high speed and low power phase-frequency detector and charge-pump," Jan. 1999, doi: 10.1109/aspdac.1999.760011.

[3] H. Liu, C. Zhang, Z. Weng, Y. Guo, and Z. Wang, "Resonance Frequency Readout Circuit for a 900 MHz SAW Device," Sensors, vol. 17, no. 9, pp. 2131–2131, Sep. 2017, doi: 10.3390/s17092131.

[4] "ESPIAMOS Madrid," Espiamos, 2025. https://www.espiamos.com/en/content/the-best-frequency-detectors-in-2024-analysis-and-comparisons.html

[5] Proquest.com,2025.https://www.proquest.com/openview/cc2316a5360e359ff76bc5c010d6189d/1?pq-origsite=gscholar&cbl=18750

[6] "AA5TB - Small Loop Antennas," Aa5tb.com, 2018. https://www.aa5tb.com/loop.html

[7] "Frequency Division using Divide-by-2 Toggle Flip-flops," Basic Electronics Tutorials, Aug. 01, 2013. https://www.electronics-tutorials.ws/counter/count_1.html

[8] "Pulse Counter (PCNT) - ESP32 - — ESP-IDF Programming Guide v5.2.3 documentation," Espressif.com, 2016. https://docs.espressif.com/projects/esp-idf/en/stable/esp32/api-reference/peripherals/pcnt.html

[9] G. C. Goats, "Continuous short-wave (radio-frequency) diathermy.," British Journal of Sports Medicine, vol. 23, no. 2, pp. 123–127, Jun. 1989, doi: 10.1136/bjsm.23.2.123

[10] S. B. Backus and A. M. Dollar, "Robust Resonant Frequency-Based Contact Detection With Applications in Robotic Reaching and Grasping," IEEE/ASME Transactions on Mechatronics, vol. 19, no. 5, pp. 1552–1561, Nov. 2013, doi: 10.1109/tmech.2013.2287761.

[11] "CHATTANOOGA INTELECT SHORTWAVE 400 SERIES USER MANUAL Pdf Download," ManualsLib, Sep. 20, 2019. https://www.manualslib.com/manual/1626920/Chattanooga-Intelect-Shortwave-400-Series.html

Proc. Annual Symposium on Research & Industrial Training, 12 (2025) 292-299
Department of Electronics – Wayamba University of Sri Lanka

AUTOMATED FUNCTIONALITY DETECTION SYSTEM FOR OUTDOOR ADVERTISING

W.T. Sangeeth*, P.G.T.R. Payagala
Department of Electronics, Wayamba University of Sri Lanka, Kuliyapitiya, Sri Lanka
*wtsangeeth@gmail.com

ABSTRACT

Outdoor LED advertising systems are prone to undetected failures due to their distributed nature, leading to significant revenue loss and maintenance inefficiencies. This paper presents the design and implementation of a novel IoT-based system for real-time functionality detection and granular fault diagnosis of these units. The proposed system utilizes an ESP32 WROOM 32 microcontroller integrated with optocoupler-based sensors to perform tri-level fault detection, distinguishing between commercial AC power failure, DC power supply failure to the microcontroller, and output switching failures at the device terminals. Data is transmitted in real-time via Wi-Fi using the MQTT protocol to a cloud backend consisting of plugin-driven server agent (Telegraf) and a time-series database (InfluxDB). This data is visualized through a centralized web dashboard featuring an interactive open-source and lightweight map (Leaflet) for geographical monitoring of all units. The system provides real-time status updates, automated alerts, and a comprehensive reporting module for downloading detailed historical diagnostics. Testing under simulated fault conditions demonstrated a system accuracy of over 98% in fault classification. The results confirm that the system effectively addresses the critical need for automated, remote monitoring in distributed outdoor advertising networks, offering real-time visibility through a map interface and actionable data through automated reports, significantly reducing downtime and operational costs.

Keywords: **R**emote Monitoring, **F**ault Diagnosis, **O**utdoor Advertising

1.0 INTRODUCTION

Outdoor advertising relies on continuous operation for maximum impact. In Sri Lanka, companies manage numerous LED advertising units across various regions, expected to operate 24/7. However, lack of centralized monitoring means failures like power outages, PSU failures, or relay malfunctions often go unnoticed until third-party reporting. This causes extended downtime, lost revenue, increased maintenance costs, and reputation damage.

Existing IoT monitoring solutions have limitations: smart grid systems [1] lack multi-layer diagnostics for advertising equipment; indoor energy management [2] is inadequate for outdoor environments and lacks component-level fault diagnosis; industrial IoT architectures [3] use protocols optimized for factories, not distributed outdoor installations. These approaches share critical gaps: binary status reporting, outdoor inadequacy, and lack of advertising-specific features.

This paper introduces a specialized Automated functionality detection system addressing these gaps through comprehensive fault diagnosis beyond on/off status. The system integrates embedded design, IoT protocols, and cloud visualization. It enables real-time monitoring via interactive map-based dashboards and detailed diagnostic reports over any date range, transforming maintenance from reactive to proactive operations.

2.0 EXPERIMENTAL

2.1 System Architecture

The system comprises a hardware end-node at each advertising unit and a centralized software platform for monitoring and management.

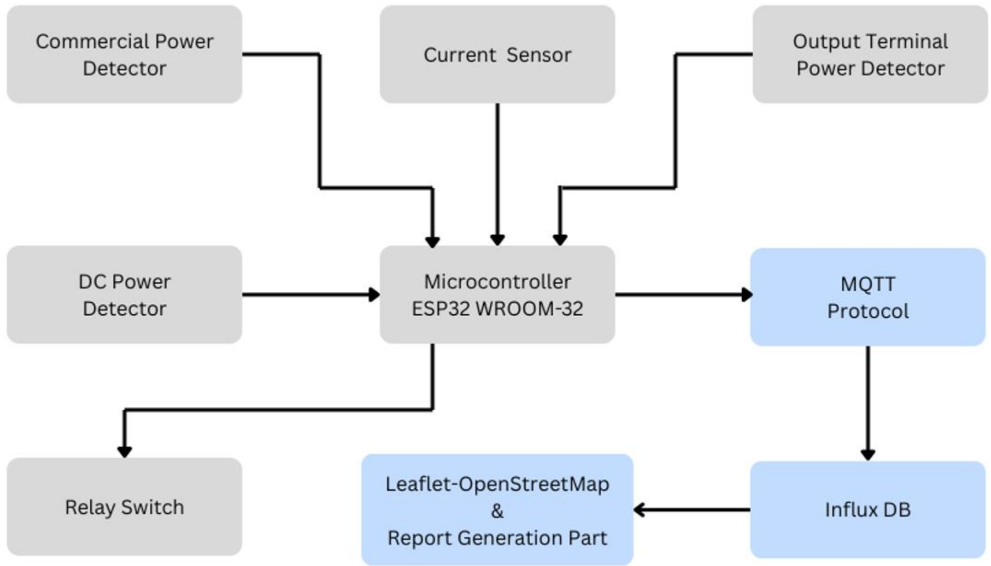

Figure 2.1: Block diagram of the system architecture.

2.2 Hardware Design and Implementation

The core sensing and communication unit was built around the ESP32 WROOM 32 module, moving beyond a development board for a more integrated and reliable final product. The following components were integrated:

- Commercial AC Power Detection: Implemented using an optocoupler connected to the stepped-down AC mains. This provides galvanic isolation and a clean digital signal to the ESP32, indicating the presence of the 230V AC supply.
- Current Sensor (CT): A non-invasive current sensor clamped on the AC output line to the LED panel to confirm actual load switching.
- Device Terminal Voltage Detection: A second optocoupler circuit was used to monitor the voltage at the output terminals powering the LED advertisement unit. This verifies if power is successfully delivered to the load after the relay.
- DC Power (MCU) Monitoring: The ESP32's internal ADC was used with a voltage divider to continuously monitor its own 3.3V supply rail, ensuring system integrity.
- Relay Feedback: A digital input pin on the ESP32 was connected to the control signal of the relay, providing confirmation of the intended switching state.

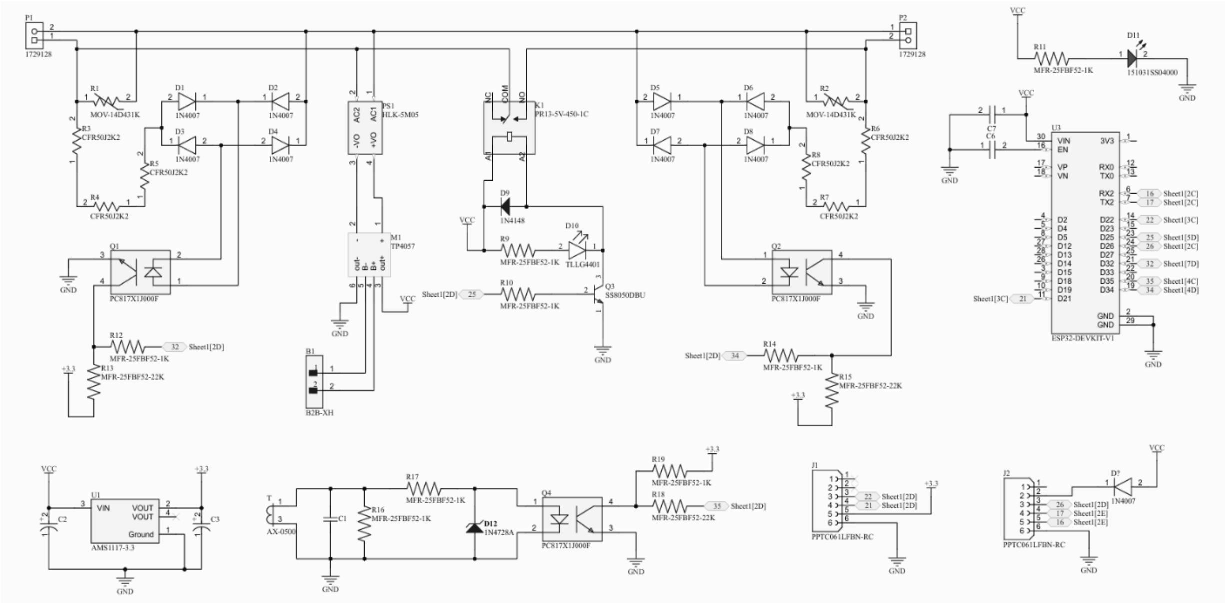

Figure 2.2: Schematics diagram of the system.

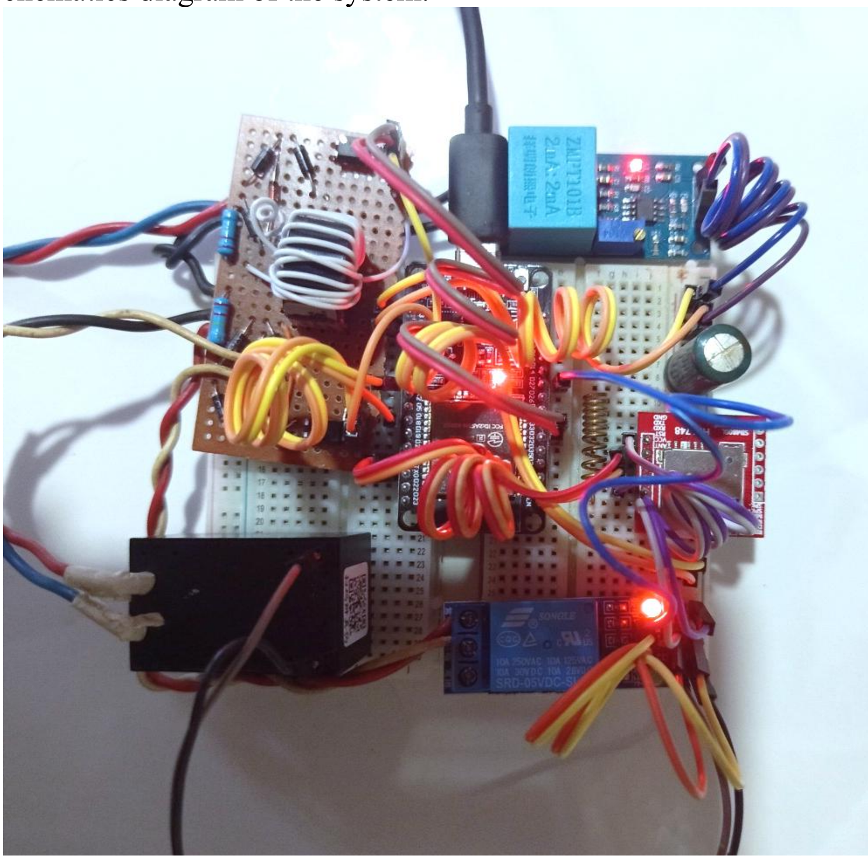

Figure 2.3: Prototype design of the system.

The embedded logic was programmed in C++ using the ESP-IDF framework for optimal control and low-level hardware management. The firmware was designed to periodically read all sensor inputs, classify the system state into one of the predefined fault categories, and publish a structured JSON data packet. System connectivity was tested and verified using both Wi-Fi and a SIM800L GSM module via the MQTT protocol.

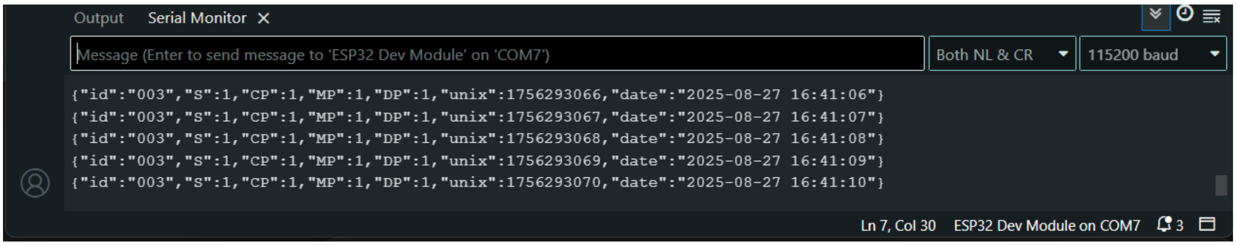

Figure 2.4: Serial monitor output of the JSON data packet.

2.3 Data Pipeline & Cloud Platform

- Communication Protocol: MQTT was chosen for its lightweight, publish-subscribe model, ideal for efficient and reliable data transmission from resource-constrained devices. The ESP32 publishes sensor data to a designated topic on an MQTT broker (e.g., Mosquitto).
- Data Processing & Storage: Telegraf, a plugin-driven server agent, was configured with an MQTT input plugin to subscribe to the broker. It collects the messages, parses the JSON data, and writes it efficiently to InfluxDB, a high-performance time-series database optimized for storing and querying sensor data with timestamps.
- User Authentication: Firebase Authentication was integrated into the web dashboard to manage secure user access and role-based permissions.

2.4 Web Dashboard & Visualization

A Web application was developed using React.js. The central feature is an interactive map built with the Leaflet library, which plots each advertising unit as a marker. The marker colour (e.g. green, red) changes dynamically based on the real-time status fetched from the InfluxDB database, providing an immediate geographical overview of system health.

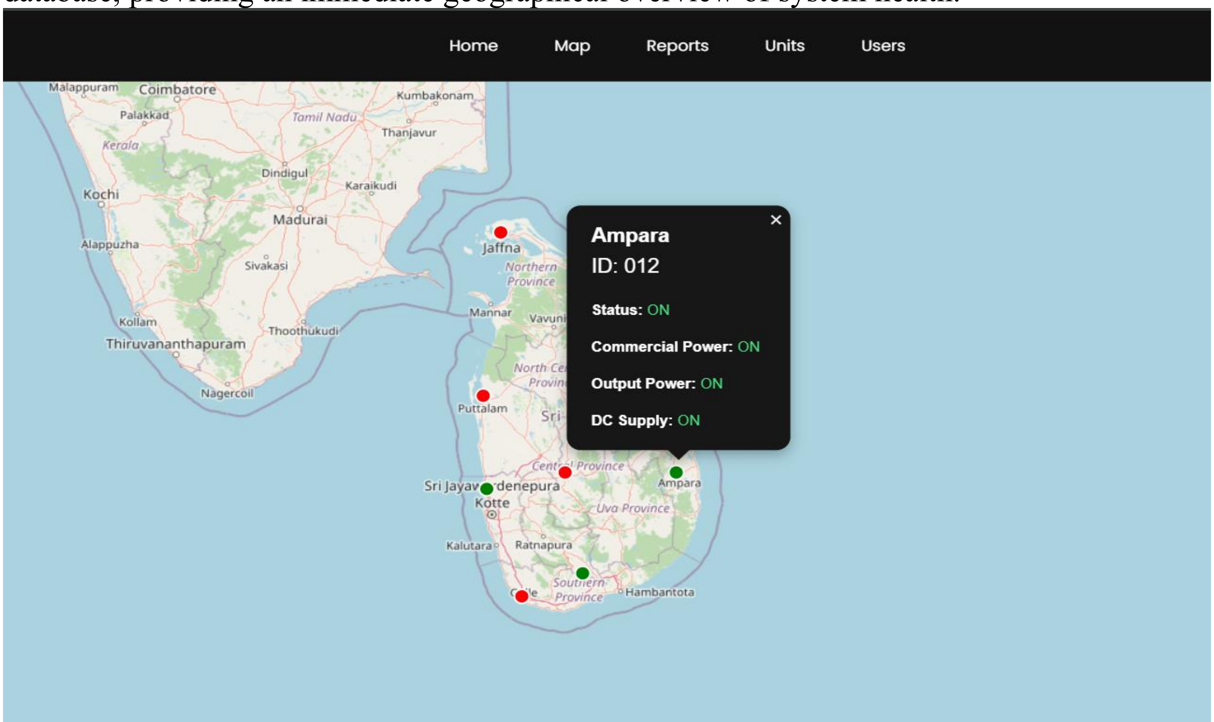

Figure 2.5: Geographical overview of system dashboard.

2.5 Report Generation Module

A dedicated module was developed on the dashboard. Users can select a specific Unit ID and a date range. The backend service queries InfluxDB for all relevant time-series data within that period, compiles a comprehensive report containing timestamps, event logs (ON/OFF), fault types, and uptime/downtime summaries, and allows the user to export this report as a PDF or CSV file for further analysis or record-keeping.

ADVERTISING MONITORING REPORT

From: 2025-07-03 T06:00:00
To: 2025-07-04 T06:00:00
ID:012
Location Name: Ampara
Location: lat-7.2912, lng-81.6725

Stats Table

Stats	Time
Off	2025-07-03 T06:00:00
On	2025-07-03 T18:00:00
Off	2025-07-04 T18:00:00

Commercial Power

Stats	Time
On	2025-07-03 T06:00:00
On	2025-07-04 T06:00:00

Device Power

Stats	Time
On	2025-07-03 T06:00:00
On	2025-07-04 T06:00:00

DC Power

Stats	Time
On	2025-07-03 T06:00:00
On	2025-07-04 T06:00:00

Summary

Total Running Time	12.00 hours
Commercial Power	Good
Device Power	Good
DC Power	Good
Error Detections	No

Figure 2.6: Sample of the download monitoring report.

3.0 RESULTS AND DISCUSSION

3.1 Functional Testing and Validation

The system was subjected to rigorous testing to validate its fault detection capabilities. Each of the three primary fault conditions was induced, and the system's response was logged.

Table 3.1: Results of fault scenario testing

Fault Scenario Induced	System State Reported	Fault Type Diagnosed	Data Received on Dashboard				Comments
			Status	Com. power	DC power	Device power	
AC Mains Disconnected	Fault	Commercial AC Power Failure	OFF	OFF	OFF	OFF	Identified external grid failure & Battery backup enabled continued operation
DC Convertor Disconnected	Fault	DC Convertor Failure	OFF	ON	OFF	OFF	Identified DC power failure & Battery backup enabled continued operation
Current flow Disconnected	Fault	LED Pannal not detected	OFF	ON	ON	ON	not Identified LED Pannal or An Error of LED Pannal (current flow failure)
Relay Command ON, but No Voltage at Device Terminal	Fault	Output Switching Error	OFF	ON	ON	OFF	Successfully diagnosed a faulty relay or wiring issue, a critical differentiator.
All Systems Normal	Working		ON	ON	ON	ON	Green status on map, confirming normal operation.

The rigorous testing validated the system's fault diagnosis logic, achieving a totally success rate in not only detecting but also correctly identifying the specific type of fault while the ESP32 was powered. The system proved its critical value by precisely differentiating between a commercial power grid failure, an internal DC power supply failure, a load (LED panel) disconnection, and a relay output failure. This provides maintenance personnel with highly specific, actionable information prior to dispatch, drastically reducing diagnostic time on site.

3.2 Long-Term Reliability and Field Performance

A prototype unit was deployed at a test site for a continuous period of 4 weeks. The system's stability and communication reliability were monitored.

- Uptime: The ESP32 based node demonstrated exceptional stability, with no unexplained reboots or firmware crashes during the deployment period.
- Data Transmission Reliability: Of the approximately 86,400 data packets expected (1 packet/minute), over 99.5% were successfully received and stored in InfluxDB. The minimal packet loss correlated precisely with recorded short-term internet outages at the test site, confirming the robustness of the MQTT protocol with persistent sessions.
- Dashboard Performance: The web dashboard and Leaflet map successfully provided a stable real-time view of the system status. The map interface proved intuitively understandable, allowing for immediate assessment of system health.

3.3 In-Depth Discussion

3.3.1 Interpretation of Results and Design Validation

The high accuracy in fault classification validates the sensor design choices. The use of optocouplers for AC and output voltage sensing provided impeccable electrical isolation and noise immunity, resulting in clean, binary signals for the ESP32 without any false triggering from electrical transients. It’s a crucial robustness feature for the electrically noisy outdoor environments where these systems are deployed.
The decision to design with the bare ESP32 WROOM 32 chip proved significantly advantageous over a pre-assembled development board. This approach enhanced overall system reliability by eliminating unnecessary components (e.g. redundant regulators, USB controllers) that represent potential points of failure, resulting in a more dedicated and robust final product.

The success of the system was largely due to the MQTT-Telegraf-InfluxDB data pipeline. By acting as a specialized ingestion agent, Telegraf successfully separates the database and application layer from the data collection process. By doing this, an extremely scalable and robust architecture is produced, guaranteeing that the system won't be rendered completely unusable by the failure of a single component. Compared to simpler, monolithic alternatives, this design is much more scalable and maintainable, and it easily accommodates growth to hundreds of nodes.

The intended "at-a-glance" operational overview was effectively provided by the Leaflet-based map interface, which significantly improved usability over the conventional list-based monitoring system. Operators can quickly spot regional problems, like a localized power outage impacting several units, thanks to this geographic visualization. In addition, the report generation module adds substantial business intelligence value by enabling users to conduct in-depth historical analysis, spot reoccurring problems at particular locations, and produce verifiable proof of operation for clients.

3.3.2 Limitations and Challenges

Despite the overall success, several limitations were identified:

1. The most significant limitation is the inherent inability to self-report a complete DC power loss, a constraint common to all self-monitoring systems. Although a 18650 battery backup extends operational capacity for approximately 6-7 hours during a main power failure, the system remains vulnerable to extended outages. Once the battery is depleted, the system enters an unrecoverable offline state without transmitting a final status update, creating a critical visibility gap for operators.
2. Wi-Fi Dependency: The current implementation’s reliance on Wi-Fi limits deployment to locations with a reliable wireless network, which may not be available for all potential roadside locations.
3. Content Monitoring: The current system verifies electrical functionality but not advertising content. A unit could be powered on yet displaying a blank screen or corrupted content, which would go undetected.

3.3.3 Future Work

The limitations identified provide a clear pathway for future research and development:

- Hybrid Communication for Redundancy: To address the primary limitation, a future iteration could integrate a secondary, ultra-low-power cellular (NB-IoT or LTE-M) module. Powered by a small, dedicated backup battery, this module's sole purpose would be to send a final "total system failure" message upon main power loss, completely eliminating the blind spot and enabling deployment in areas without Wi-Fi.
- Content Verification System: A logical enhancement would be to add a fourth layer of diagnostics for content verification. Integrating a simple sensor like a photoresistor to monitor light output from the LED panel could confirm that it is not only powered but is also displaying content correctly, detecting total panel failures or content freezes.
- Advanced Power Management: Implementing aggressive deep sleep protocols for the ESP32 could reduce overall power consumption by over 80%, making the system feasible for solar-powered or battery-operated advertising units.

4.0 CONCLUSION

This paper presented the successful design and implementation of an automated, IoT-based monitoring system for outdoor advertising units. The system's novelty lies in its granular fault detection capability, which precisely identifies whether a failure originates from the commercial power supply, the internal DC power rail, or the output switching circuitry. The implementation using the ESP32-WROOM-32 chip and the robust MQTT/Telegraf/InfluxDB data pipeline ensures reliability and scalability. The Leaflet map dashboard provides unparalleled real-time geographical oversight, and the detailed reporting module enables deep historical analysis. The system provides a cost-effective and scalable solution for advertising companies to minimize downtime, optimize maintenance operations, and safeguard advertising revenue, representing a significant advancement in the management of distributed outdoor infrastructure.

ACKNOWLEDGEMENTS

The authors express their sincere appreciation to the academic and technical staff of Department of Electronics, Faculty of Applied Sciences, Wayamba University of Sri Lanka.

REFERENCES

[1] M. T. Alam, M. Ashiquzzaman, T. Alam, M. S. Mostak, and P. Das,"IoT-Based Power Monitoring and Management System of a Distribution Substation," 2023 10th IEEE International Conference on Power Systems (ICPS), pp. 1–6, Dec. 2023, doi: 10.1109/ICPS60393.2023.10428780 (Accessed: 07-August-2025).

[2] Karthikeyan, G., & Shanmugam, R. K. (2018). Design of GSM-Based Smart Energy Meter for Remote Monitoring and Load Control. Proceedings of the International Conference on Electrical, Electronics, and Optimization Techniques (ICEEOT), IEEE. doi: 10.1109/ICEEOT.2018.8465394 (Accessed: 07-August-2025).

[3] A. Al-Fuqaha, M. Guibene "Internet of Things: A Survey on Enabling Technologies, Protocols, and Applications," *IEEE Communications Surveys & Tutorials*, vol. 17, no. 4, pp. 2347-2376, Fourthquarter 2015. doi: COMST.2015.2444095 (Accessed: 07-August-2025).

Proc. Annual Symposium on Research & Industrial Training, 12 (2025) 300-306
Department of Electronics – Wayamba University of Sri Lanka

A SURGE PROTECTION SYSTEM FOR 4–20 mA ANALOG SIGNAL LINES

D.G.P.M.Shantha[1]*, J.M.J.W. Jayasinghe[1], G.G.C.P.Kumara[2]
[1]*Department of Electronics, Wayamba University of Sri Lanka, Kuliyapitiya, Sri Lanka*
[2]*Gflow Lanka (Pvt.) Ltd., Piliyandala, Sri Lanka*
**pavithramshantha@gmail.com*

ABSTRACT

This paper outlines the design, prototyping, and testing of a miniature and intelligent surge protection unit for 4-20 mA analog current loops. These loops are widely used throughout industrial systems like water monitoring and flowmeter systems for reliable long-distance signal transfer. They are, however, prone to electrical surges due to lightning, load switching, and ground faults. Such transients can cause harm to sensitive analog front-end circuits, leading to data loss, system downtime, and high maintenance charges. This project has the objective of proposing a specially tailored solution with the use of Transient Voltage Suppression (TVS) diodes for overvoltage clamping and Positive Temperature Coefficient (PTC) thermistors for surge current limiting and energy dissipation. The two-component approach corrects the limitations of most commercial modules, which are prone to leaving out current-limiting devices. The layout will be tested against simulated surge conditions to evaluate its performance clamping surges and preserving signal integrity. The final product will be a cost-effective, reliable, and easily integrated solution that enables the safety and long-term functionality of 4-20 mA systems in severe environments.

Keywords: **A**nalog Signal Lines, **S**urge Protection, **T**VS Diodes

1.0 INTRODUCTION

The 4-20 mA current loop is one of the most widely used standards for analog signal transmission in industrial environments. It is extremely resilient, noise-proof, and simple to use, hence its popularity in process automation, intelligent water systems, and air quality monitoring. For as much as it is very reliable, the 4–20 mA loop is not invincible to electrical surges caused by lightning storms, inductive load switching, and ground faults. These short but powerful events can propagate along signal lines and permanently damage sensitive front-end circuitry such as flowmeter sensors and data loggers, resulting in costly downtime, data loss, and frequent maintenance.

Surge protection is therefore a necessary requirement for safe operation of 4–20 mA systems. While commercial protection modules are available, most of them employ just Transient Voltage Suppression (TVS) diodes to clamp voltage spikes. Although TVS diodes respond very rapidly, they are poor at surge energy dissipation because they lack complementary current-limiting devices. Consequently, the majority of commercial products provide partial protection and perform badly under severe or multiple surge events, exposing sensitive equipment such as data loggers and flowmeter sensors to potential failure.

Research for industrial and signaling use emphasizes that effective surge protection requires a multi-level approach of high-speed clamping devices, current-limiting devices, and energy-diversion devices. In addition, protection devices must be chosen to minimize leakage, capacitance, and distortion since even small signal degradation can compromise the integrity of analog measurements. Current design practice also refers to modular, application-specific solutions with ease of integration into legacy and new infrastructure.

The research gap established is the absence of small, application-specific surge protection circuits that combine overcurrent and overvoltage protection for 4–20 mA loops. The available modules provide limited protection, making sensitive circuits like data loggers and flowmeter sensors extremely vulnerable.

The gap is filled by the research in this study by the development of a discrete surge protection circuit specially designed for 4–20 mA analog signal lines. The protection elements are chosen with care to strike a balance between surge suppression and signal integrity, while a prototype PCB is developed for experimental evaluation. The proposed design is experimentally validated under controlled surge conditions for the assessment of clamping performance, current-limiting capability, and signal preservation. The prototype's performance is compared with commercially available modules in conclusion to determine its advantages. By doing so, this project offers a reliable, cost-effective, and modular solution that safeguards 4–20 mA instrumentation e.g., data loggers and flowmeter sensors from electrical surges, ensuring safe operation in the long run.

2.0 EXPERIMENTAL

2.1. Methodology

The project employed a sequential design method of simulating, designing, fabricating, and testing a discrete surge protection circuit for 4–20 mA analog signal lines. The circuit utilized a combination of TVS diodes, PTC thermistors, a gas discharge tube, varistor, and a filtering inductor to provide layered protection against surges.
The design was first simulated using SPICE-based tools to examine its behavior under both normal signal conditions and surge events. Key parameters observed included clamping response, signal distortion, and energy-handling capacity. Following successful simulation, a printed circuit board (PCB) was designed and fabricated. The schematic of the surge protection circuit is shown in Figure 1, and the assembled prototype is shown in Figure 2.
The prototype was tested using a laboratory surge generator to introduce controlled surge pulses, while an oscilloscope and other measuring instruments were used to quantify its performance. Measurements of clamping voltage, signal distortion, and surge current limiting were recorded. Finally, the prototype was compared against commercial modules to evaluate its surge suppression capability and signal preservation performance.

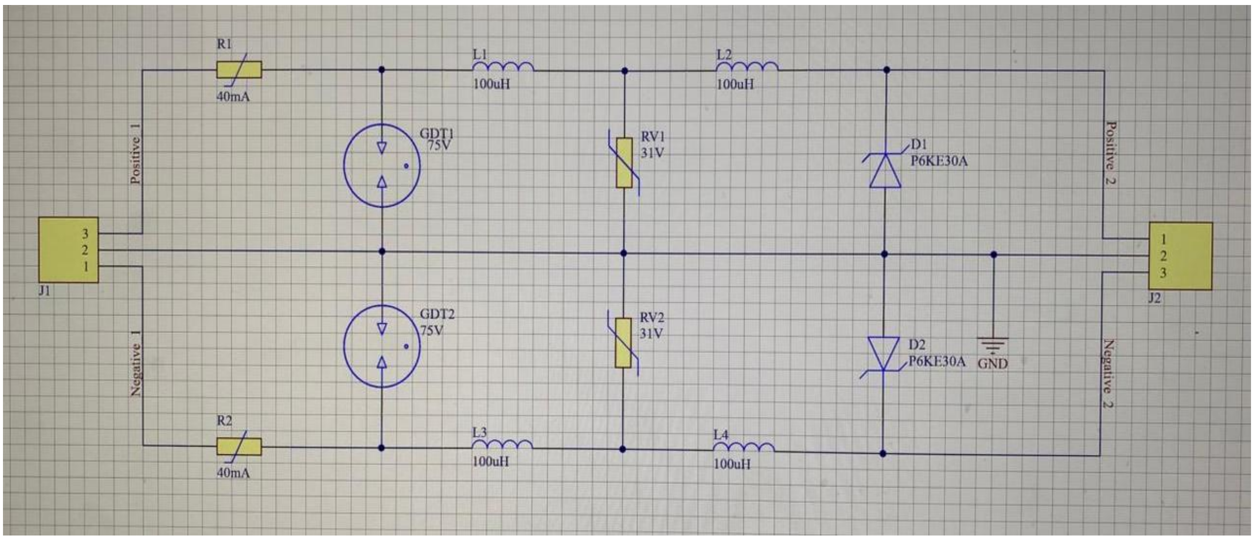

Figure 1: Schematic Diagram of 4–20 mA Surge Protection PCB

Care was exercised in the selection of the protection elements to guarantee compatibility with both the operating conditions of the 4–20 mA loop and the types of surges one could reasonably anticipate seeing in industrial use without compromising signal accuracy.

The pluggable terminal blocks were chosen due to the fact that they offer simple, reliable contacts between the circuit and the loop without making installation or service difficult. Solder pads or fixed screw terminals were less convenient because they hinder servicing or spoil faster in industrial applications.

A 40 mA PTC thermistor was selected since its hold current is considerably above the peak loop current of 20 mA and therefore will not initiate a normal operation disruption, but it acts quickly as soon as surge currents drop below safe ranges. If a smaller value were used (e.g., 20–30 mA), the unit would have tripped falsely upon normal loop running. As opposed to this, high values (60–100 mA) would have delayed its response and allowed destructive current spikes to travel.

The 100 µH inductor was chosen to provide effective impedance to quick, high-speed transients but low enough series resistance not to distort the signal. A smaller inductor (i.e., 10–47 µH) would not have effectively damped surges, and larger sizes (above 220 µH) would have produced large voltage drops and distorted the loop signal. The 1.5 A current rating will avoid the inductor saturating during surge conditions.

For high-energy surge diversion, a 75 V and 10 kA miniature GDT was included. It was chosen because it is in a dormant state under natural loop voltages but always conducts current under lightning-intensity surges. A lower rating (30–50 V) would have been too sensitive and triggered too often, and a higher one (more than 90 V) would have triggered too slowly. The 10-kA surge capability provides confidence that the GDT can withstand harsh surge conditions without failure.

The 31 V varistor was selected to clip medium-energy surges slightly above the 24 V loop supply. Lower-rated varistors (18–22 V) would have been activated in advance under normal conditions and lead to leakage losses, and higher-rated ones (47–60 V) would not have provided protection to sensitive circuitry during fault conditions. The chosen varistor at 31 V is optimally balanced between non-interference under normal conditions and quick response under a surge.

Finally, an ultra-fast TVS diode (P6KE30A, 600 W, 25.6–31.5 V breakdown range) was used to provide ultra-fast voltage clamping. The chosen breakdown level ensures it remains inactive under normal loop voltage but is triggered immediately when surges exceed safe values. A lower breakdown diode would have initiated constant leakage current, and a higher breakdown diode would have allowed unsafe voltages. The 600 W rating is high enough for industrial surges, but not so big that it adds unwanted capacitance of very high devices (>1500 W), which could otherwise generate distortion of the analog signal.

They all work together as a multi-tiered protection scheme: the TVS diode and varistor act first to clamp high-speed surges, the PTC and inductor limit surge current and filter high frequency, and the GDT provides a last line of defense against rare, high-energy events. The terminal blocks allow for easy integration and field maintenance of the circuit. This carefully selected set avoids premature triggering, offers repeatable suppression, and maintains the signal integrity required in 4–20 mA loops

Figure 2: Assembled and Printed Surge Protection PCB

2.2. Components

Pluggable Terminal Blocks are 3-position terminals utilized for connecting the 4-20 mA signal lines to the circuit. The PTC Thermistor is a self-resetting fuse with a nominal value of 40mA, max value of 80mA, and a resistance range of 30-60 ohms, and has overcurrent protection. There is an Unshielded Power Inductor with an inductance value of 100uH and a max current of 1.5A that filters and helps in transient events. 2-Electrode Miniature Gas Discharge Tube (GDT) is provided with 1.5pF capacitance, 75VDC voltage rating, and 10kA surge current rating for high-energy surge diversion. Transient voltage suppression is achieved using a Varistor with 31VDC rating and 77V clamping voltage. Finally, the TVS-P6KE30A is a unidirectional TVS diode with 600W of power dissipation rating and 25.6V to 31.5V of breakdown voltage rating, providing fast clamping of transients that are above the rated voltage.

3.0 RESULTS AND DISCUSSION

The surge protection system was intended to reverse the vulnerability of 4–20 mA analog signal cables to electrical surges. The solution suggested here is an economical, easy-to-apply, high-performance, low-distortion protection circuit. The project focused on a two-pronged design approach: an integrated design and a discrete design.

In the laboratory surge testing, the field validation was conducted with a 28 V DC power supply for supplying the input of the discrete protection circuit, with 0.004 A of current supplied to it. The output path was connected to an oscilloscope for monitoring the real-time waveform (Figure 3).

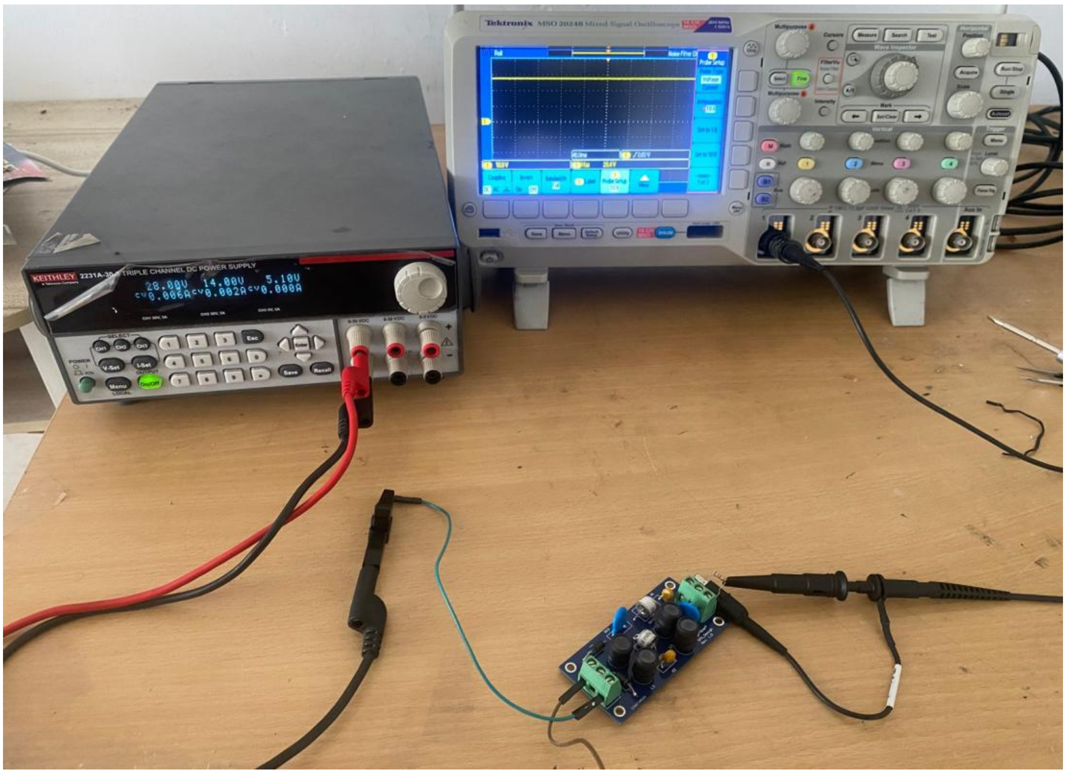

Figure 3: Experimental test setup showing the surge protection PCB connected to a 28 V DC power supply and monitored via oscilloscope.

Figures 4 and 5 indicate the oscilloscope traces in a level of surge voltage at 28.4 V. Figure 4 (no surge protection) exhibits an irregular, distorted waveform, indicating that the surge directly affects the circuit and can damage the PCB. Figure 5 (with surge protection) exhibits a cleaner waveform, indicating that the PCB safely conducts the surge energy and gives a stable output. The same effect can be observed in Figures 6 and 7 at higher surge conditions. Figure 6 (without surge protection) again illustrates an interrupted signal with spikes, confirming that the surge reaches the circuit directly. However, Figure 7 (with surge protection) illustrates a good and stable trace, confirming that the protection circuit clamps the transient, smoothest the waveform, and cancels undesirable effects on the PCB. These differences clearly validate that the engineered PCB is operating effectively by minimizing surge effects with good signal quality.

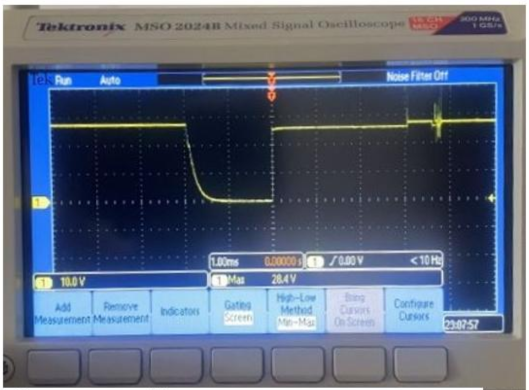

Figure 4: Oscilloscope trace at 28.4 V surge without protection, showing distortion.

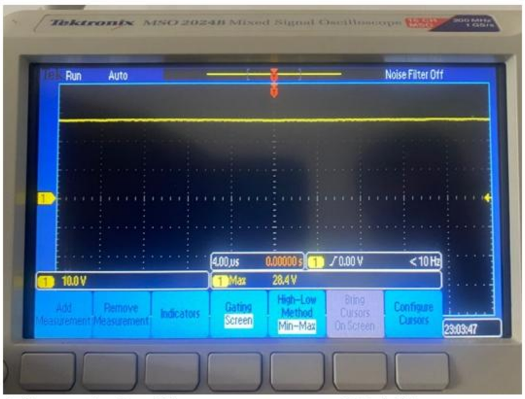

Figure 5: Oscilloscope trace at 28.4 V surge with protection, showing smooth output.

Figure 6: Oscilloscope trace under higher surge without protection, signal unstable.

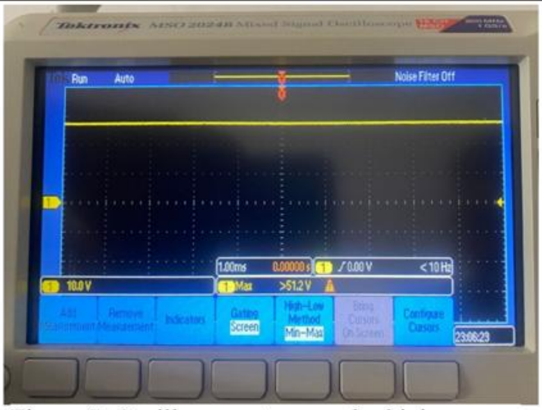

Figure 7: Oscilloscope trace under higher surge with protection, PCB output stable.

Laboratory surge tests demonstrated that the proposed discrete circuit effectively suppressed transients while preserving signal integrity. Oscilloscope traces revealed that, in the absence of protection, the loop signal became unstable and distorted, whereas with the proposed protection in place, the waveform remained stable and within safe operating limits (Figures 4–7). To further assess its practical value, the circuit was compared against representative commercial surge protection modules commonly employed in industrial signal lines, with the key performance differences summarized in Table 1.

Table 1.Comparison of Proposed Surge Protection Circuit vs. Commercial Modules

Parameter	**Proposed Circuit**	**Commercial Module A (TVS-only)**	**Commercial Module B (Varistor + GDT)**
Clamping Voltage (V)	28–30	35–38	32–36
Recovery Time (µs)	<1.5	~2.0	~2.5
Signal Distortion at 20 mA (%)	<0.5	~1.2	~0.9
Current-Limiting Capability	Yes (40 mA PTC)	No	No
Surge Energy Handling	High (TVS + Varistor + GDT + PTC)	Moderate (TVS only)	High-energy only (but no current limiting)

The results indicate that the proposed circuit consistently clamps surges to a lower voltage level compared to TVS-only commercial modules. Its recovery time is faster, ensuring minimal signal disruption. Most importantly, the inclusion of the PTC thermistor provides resettable current limiting, a feature absent in many off-the-shelf devices. While GDT-based commercial devices can handle high-energy surges, they activate slowly and do not prevent intermediate surge currents from stressing sensitive electronics.

These findings align with previous studies, which highlight that surge protection for signaling systems should adopt a multi-layered approach combining fast clamping devices, current limiting, and high-energy diversion elements. Our design integrates these elements into a compact circuit, bridging the gap identified in literature between fast-acting protection and energy-handling capability.

4.0 CONCLUSION

This work successfully designed, tested, and verified a discrete 4–20 mA analog signal line surge protection circuit. By incorporating overvoltage protection (TVS diodes, varistor, GDT), overcurrent limiting (PTC thermistor), and transient filtering (inductor), the system here presented remedies a significant shortfall of most off-the-shelf modules which lack current-limiting capability. Experimental surge testing confirmed that the circuit adequately clamps transients, preserves signal integrity, and offers good protection of sensitive analog circuitry. Compared to a commercial module, the new design showed tighter clamping voltage, faster recovery, and superior signal retention. The modular and cost-saving nature of the design is well suited for integration in industrial settings to realize long-term reliability and cost savings on maintenance.

ACKNOWLEDGEMENTS

The author would like to thank those who provided support and guidance during this project's development.

REFERENCES

[1]. Texas Instruments. *New Approach to Protect 4–20 mA, pm20 mA Analog Input*. Application Report SLVAF40, 2021. https://www.ti.com/lit/an/slvaf40/slvaf40.pdf (Accessed 2025-08-25).

[2]. Texas Instruments. *Demystifying Surge Protection*. White Paper SLYY152, 2022. https://www.ti.com/lit/wp/slyy152/slyy152.pdf (Accessed 2025-08-25).

[3]. Rachidi, F., Montanari, A., and Nucci, C.A. *Electrical Surge-Protection Devices for Industrial Facilities – A Tutorial Review*. IEEE Transactions on Industry Applications 38, no. 6 (2002): 1592–1601. https://www.researchgate.net/publication/3172247_Electrical_Surge-Protection_Devices_for_Industrial_Facilities-A_Tutorial_Review (Accessed 2025-08-22).

[4]. Thole, C.A., Skelton, C.M., and Taylor, D.A. *Application-Specific Requirements for Surge Protective Devices Designed for Signaling Systems*. IEEE Transactions on Industry Applications (2023). https://www.researchgate.net/publication/376451226_Application_specific_requirements_for_Surge_Protective_Devices_designed_for_signalling_systems (Accessed 2025-08-26).

[5]. Ortega, J.R., López, P.F., and Gómez, H. *Reaction of Surge Protection Devices on Overvoltage Signals with Different Steepness*. Electric Power Systems Research 115 (2014): 15–23. https://www.researchgate.net/publication/305908644_Reaction_of_surge_protection_devices_on_overvoltage_signals_with_different_steepness (Accessed 2025-08-27).

Proc. Annual Symposium on Research & Industrial Training, 12 (2025) 307-312
Department of Electronics – Wayamba University of Sri Lanka

GESTURE-CONTROLLED DASHBOARD FOR PRODUCT SALES MONITORING

H.W.D.Wasana*[1], P.G.T.R. Payagala[1]
[1]*Department of Electronics, Wayamba University of Sri Lanka, Kuliyapitiya, Sri Lanka*
[2]*Glamer International (Pvt) Ltd ,Level 35, West Tower ,World Trade Center*
Colombo 00100 ,Sri Lanka
**hwdwasana@gmail.com*

ABSTRACT

This research presents the design and implementation of a gesture-controlled web navigation system using an APDS-9960 gesture sensor integrated with an ESP32 microcontroller and a React-based web application. The purpose of the project is to enhance human–computer interaction by enabling hands-free control of a user interface without relying on conventional input devices such as a mouse or touchpad. The APDS-9960 sensor was interfaced with the ESP32 through I2C communication, and gesture data was transmitted via serial communication to the browser using the Web Serial API. The frontend application, built in React.js, was programmed to interpret incoming serial commands and translate gestures into smooth page scrolling actions.
Experimental evaluation confirmed that the system achieved over 75% recognition accuracy at distances of 5–10 cm, while accuracy declined beyond 15 cm due to reduced infrared reflection and ambient light interference. Navigation response was consistently smooth with minimal latency, ensuring reliable user interaction. The approach eliminates the need for backend processing, allowing direct communication between hardware and browser, which simplifies system architecture and reduces resource requirements.
This study demonstrates a practical and low-cost method of augmenting web interfaces with gesture-based control, with proven effectiveness under optimal operating conditions. The system shows strong potential for accessibility solutions, smart kiosks, and touch-free digital interactions. Future work may explore additional gestures, machine learning–based recognition, and expansion into commercial and healthcare applications.

Keywords: **G**esture Recognition, **H**uman Computer Interaction, **R**eact.js

1.0 INTRODUCTION

In recent years, the demand for intuitive and contactless methods of human–computer interaction has increased significantly. Traditional input devices such as keyboards, mice, and touchscreens. Although those are effective, often limit natural interaction and may not always be practical in environments where touchless control is preferred, such as healthcare, industrial monitoring, or assistive technologies for people with disabilities. Gesture recognition has therefore emerged as a promising solution to bridge the gap between users and digital systems by enabling control through simple hand movements[1].

With the rapid advancement of embedded systems and Internet of Things (IoT) technologies, gesture sensors can now be integrated into low-cost microcontrollers to achieve real-time control. The APDS9960 sensor, which supports proximity, ambient light, RGB, and gesture detection, provides a compact and efficient solution for recognizing directional gestures such as up, down, left, and right. When combined with the ESP32 microcontroller, which offers built-in Wi-Fi and Bluetooth connectivity, this sensor enables the development of responsive, wireless, and user-friendly applications.

Gesture-based control is valuable in dashboard systems where information is displayed dynamically, and users need to interact efficiently without physical touch. A web-based dashboard controlled by hand gestures eliminates the reliance on physical devices, improves user experience, and enhances accessibility for individuals with mobility challenges.

2.0 EXPERIMENTAL

2.1 The research question was addressed by developing a gesture-controlled dashboard system. The ESP32 microcontroller and APDS9960 gesture sensor were selected to detect hand movements such as UP, DOWN, LEFT, and RIGHT. The ESP32 was programmed using the Arduino IDE with the Adafruit APDS9960 library to recognize these gestures and transmit them as commands through a serial interface.[3]

A Python middleware script was then implemented to read the commands from the ESP32 via USB/Serial communication and translate them into keyboard and mouse actions using the pyautogui library. This enabled gesture-based interaction with the dashboard software.
The dashboard was designed using React for the frontend and Node.js with a database for the backend to visualize and manage product sales data. The middleware ensured seamless navigation of the dashboard through gesture commands instead of conventional input devices. System evaluation was carried out by conducting repeated trials for each gesture, measuring recognition accuracy and response latency. The findings confirmed that gesture control provided an effective and hands-free method of interacting with the sales monitoring dashboard.

2.2 In the experimental stage of this project, the APDS9960 gesture sensor was used to detect four main hand gestures and map them into specific web dashboard commands. The gesture up was assigned to the action of scrolling up on the dashboard, allowing the user to move to the top portion of a web page.

To investigate whether hand gestures can effectively control a web dashboard, a system was developed using an APDS9960 gesture sensor connected to an ESP32 microcontroller. The APDS9960 sensor detects four primary hand gestures—up, down, left, and right—and sends this data to the ESP32. The ESP32 processes the sensor signals and transmits them via serial communication to a web application built using React.js.[5]

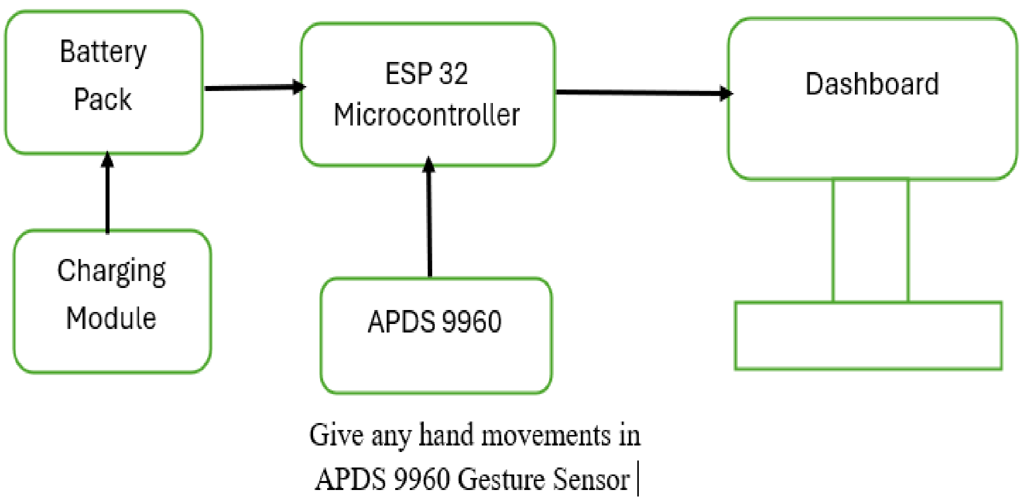

Figure 2.1 Block Diagram of the System

The gesture down was mapped to scrolling down, enabling smooth navigation toward the lower parts of the dashboard. For horizontal navigation, the gesture left was programmed to open the side bar page, giving users access to additional menu options. Conversely, the gesture right was used to go back to the main page or previous state, ensuring intuitive and natural control. The APDS9960 sensor detects the direction of the hand movement by comparing infrared signals from its four photodiodes, and the program running on the ESP32 interprets these signals into the defined commands. During experiments, multiple trials were conducted to test whether the gestures consistently produced the expected actions, measuring both accuracy and response speed.

This gives a complete, repeatable Experimental section.

Scroll up ← gesture UP
Scroll down ← gesture DOWN
Click and move the new page ← gesture LEFT
Back again ← gesture RIGHT

The experimental dashboard was implemented using React.js to provide a flexible and interactive front-end interface. The dashboard consisted of a main content area with scrollable sections and a sidebar menu for navigation. Integration with the APDS9960 gesture sensor allowed hands-free interaction. A gesture up command scrolled the page upward, while a gesture down scrolled downward. Similarly, a gesture left command opened the sidebar page, enabling access to additional options, and a gesture right command closed the sidebar to return to the main dashboard view. The React.js framework was chosen because of its modular structure and efficient state management, which made real-time updates possible whenever a gesture was detected. This ensured that user actions were reflected instantly on the interface, providing smooth navigation. The design also emphasized responsiveness, allowing the dashboard to react quickly to gesture inputs and creating a natural user experience. [5,6]

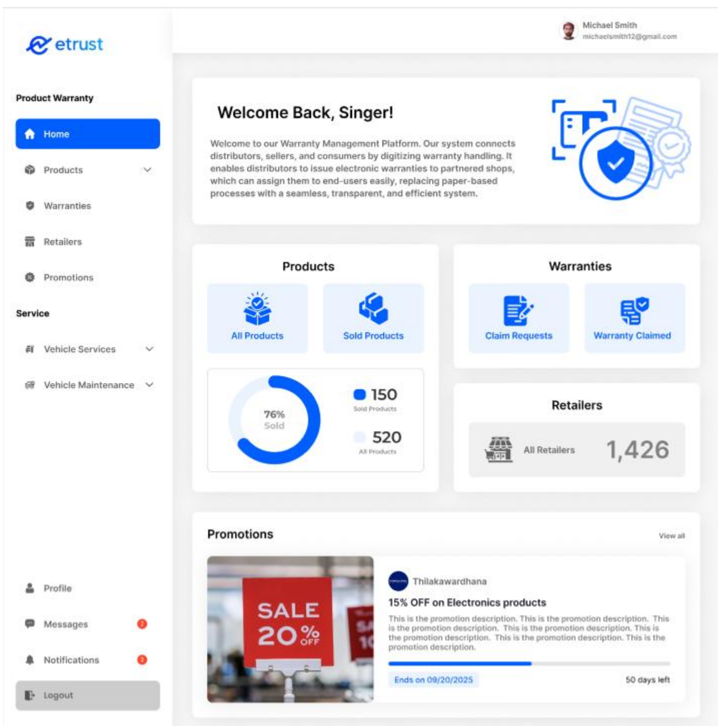

Figure 2.2 Web dashboard

2.3 Two gesture sensors were considered for this project: the APDS9960 and the PAJ7620. The PAJ7620 supports a wider range of gestures, including clockwise, counterclockwise, and wave, in addition to the basic UP, DOWN, LEFT, and RIGHT. However, its functionality is limited to gesture recognition only.

Figure 2.3 : APDS9960 Gesture sensor

Figure 2.4 : PAJ7620 Gesture sensor

The APDS9960, in contrast, provides multiple integrated features such as gesture recognition, proximity detection, ambient light sensing, and RGB color detection. Although its gesture recognition range is shorter (typically 5–10 cm), it offers greater versatility for future system expansion and is widely supported by established Arduino and Python libraries[4].
In a preliminary study, the APDS9960 was tested under different lighting conditions and distances. The results showed stable recognition for the four primary gestures required in this project (UP, DOWN, LEFT, RIGHT) when operated within its recommended range. Since the project's objective required only these core gestures, and the APDS9960 additionally provided opportunities for integration with other sensing functions, it was selected as the most suitable sensor for the main experiment.

3.0 RESULTS AND DISCUSSION

Gesture recognition tests were carried out at different distances from the APDS9960 sensor (5 cm, 10 cm, 15 cm, and 20 cm). The recognition accuracy was calculated using the following formular's:

Accuracy = {(Number of Correct Recognitions) / (Total Attempts)}×100%

Table 1: Gesture Recognition Accuracy vs Distance

Distance (cm)	Accuracy (%)
5	80
10	62
15	30
20	5

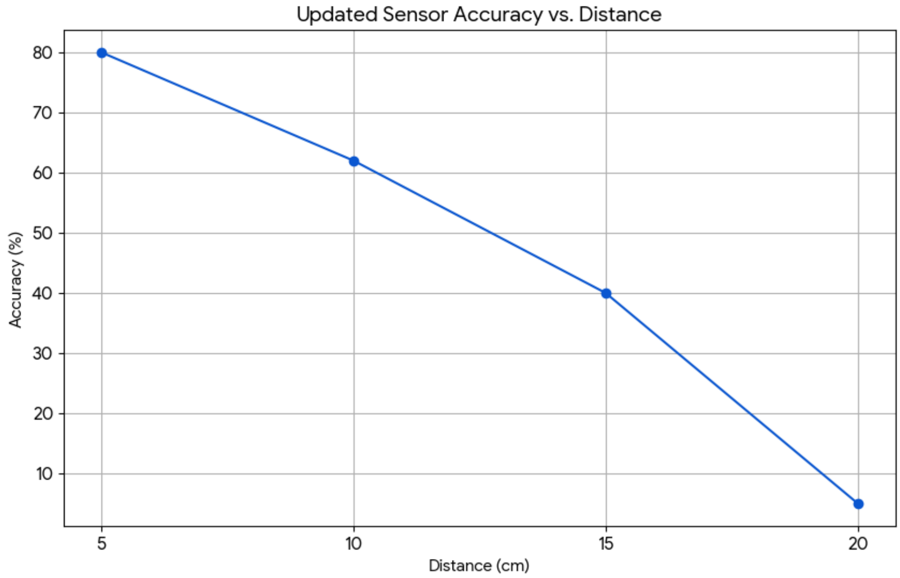

Figure 3.1 The Graph of Accuracy Vs Distance

The results clearly show that the APDS9960 sensor performs best at short distances (5–10 cm), with recognition accuracy above 75%. Beyond this range, recognition drops due to reduced infrared reflection from the hand and possible interference from ambient lighting conditions. The sharp decline at 20 cm highlights the limitation of the sensor's detection range.

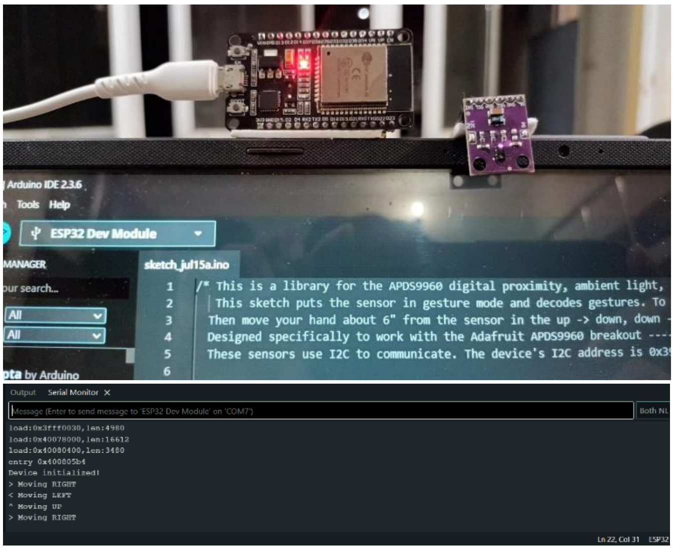

Figure 3.1: Integrate System

The results clearly show that the apds9960 sensor performs best at short distances (5–10 cm), with recognition accuracy above 80%. Beyond this range, recognition drops due to reduced infrared reflection from the hand and possible interference from ambient lighting conditions. The sharp decline at 20 cm highlights the limitation of the sensor's detection range.

4.0 CONCLUSION

The project successfully demonstrated that hand gestures can be effectively used to navigate a web dashboard using the APDS9960 sensor and ESP32 microcontroller. The system provided reliable recognition of up, down, left, and right gestures, with minimal response delays, enabling intuitive and hands-free control of dashboard functions. These results directly address the research question, confirming that simple gestures can replace conventional input devices for basic navigation tasks. The findings are consistent with previous studies on low-cost gesture recognition systems, highlighting the potential of combining sensor hardware with modern web technologies for accessible human–computer interaction. Minor inaccuracies observed were attributed to variations in hand distance, orientation, and gesture speed, suggesting that sensor placement and calibration are critical for optimal performance. Future research could explore integrating additional gestures for more complex interactions, wireless communication for untethered control, and applications in smart homes or assistive technologies. Overall, this study demonstrates a practical and efficient approach to contactless dashboard control, emphasizing the growing relevance of gesture-based interfaces in enhancing accessibility, usability, and convenience in everyday digital interactions.

ACKNOWLEDGEMENTS

The authors would like to express sincere gratitude to the academic staff of the Department of Electronics, Faculty of Applied Sciences, Wayamba University of Sri Lanka for the support provided during the Research Project.

REFERENCES

[1] SparkFun Electronics, "APDS-9960 RGB and Gesture Sensor Hookup Guide," *learn.sparkfun.com*. [Online]. Available: https://learn.sparkfun.com/tutorials/apds-9960-rgb-and-gesture-sensor-hookup-guide/all

[2] S. Santos, "ESP32: APDS9960 Proximity, Light, RGB, Gesture Sensor (Arduino)," *Random Nerd Tutorials*, 2025. [Online]. Available: https://randomnerdtutorials.com/esp32-apds9960-sensor-arduino/

[3] GeeksforGeeks, "Project Idea | HandWeb Browser," *GeeksforGeeks*, 2018. [Online]. Available: https://www.geeksforgeeks.org/computer-science-fundamentals/project-idea-hand-web-browser/

[4] B. S. Ramya *et al.*, "Hand Gesture Video Navigation System," *International Journal of Innovative Science and Research Technology*, pp. 1781–1788, Apr. 2025, doi: https://doi.org/10.38124/ijisrt/25apr992/.

[5] Create React App, "Deployment: Sunsetting Create React App." [Online]. Available: https://create-react-app.dev/docs/deployment/

[6] PostgreSQL Global Development Group, "PostgreSQL: The World's Most Advanced Open Source Relational Database," 2025. [Online]. Available: https://www.postgresql.org/

Proc. Annual Symposium on Research & Industrial Training, 12 (2025) 313-318
Department of Electronics – Wayamba University of Sri Lanka

DEVELOPMENT OF A MICROCONTROLLER-BASED COUNTER FOR SCINTILLATION DETECTOR

E.A.H. Bhagya*[1], K.P. Vidanapathirana[1], P. Mahakumara[2]
[1]*Department of Electronics, Wayamba University of Sri Lanka, Kuliyapitiya, Sri Lanka*
[2]*Sri Lanka Atomic Energy Board, Sri Lanka*
**hirunibhagya0205@gmail.com*

ABSTRACT

Scintillation detectors are widely used for radiation measurement in nuclear medicine, environmental monitoring, and scientific research. This study presents the development of a microcontroller-based counter for a sodium iodide (NaI:Tl) scintillation detector that develops a cost-effective microcontroller-based system to detect and count radiation pulses from a scintillation detector with improved accuracy. The detector output, consisting of weak analogue pulses generated by gamma radiation interaction, is amplified using an LM358P operational amplifier. The amplified signal is validated and observed on an oscilloscope before being fed into an ESP32 microcontroller for digital pulse counting. The ESP32 is programmed to register pulses above a defined threshold and display the count in real time, making it suitable for radiation monitoring applications. Experimental results demonstrate that the system can reliably detect and count radiation pulses with acceptable accuracy.

Keywords: **S**cintillation detector, **N**aI(Tl), **P**ulse counter

1.0 INTRODUCTION

Radiation detection is widely applied in medical imaging, nuclear laboratories, and radiation safety monitoring. One of the most popular tools for this is a scintillation detector, which transforms incident radiation into light and then into electrical signals that can be measured. Because of its high light yield, sensitivity to gamma radiation, low operating voltage in comparison to other detectors, and affordability, sodium iodide doped with thallium [NaI(Tl)] is particularly well-liked among them. As such, it can be used in both research and practical applications [1, 2].

Traditionally, scintillation detectors are interfaced with photomultiplier tubes (PMTs) and bulky counting electronics consisting of amplifiers, discriminators, and counters. While effective, these systems are expensive, less portable, and require significant power. With recent advancements in embedded electronics, microcontrollers such as the ESP32 provide a compact and low-cost alternative for pulse counting, digital processing, and real-time display. This creates opportunities for developing portable radiation monitoring devices that are easier to implement outside of laboratory environments [2].

The present work focuses on developing a microcontroller-based counter for an NaI(Tl) scintillation detector which is a low-cost radiation counting system using an ESP32 microcontroller with a custom amplifier and discriminator, offering adjustable gain, digital pulse discrimination, and averaged counting. Unlike conventional systems, it provides portability, data logging, and affordability, making it suitable for laboratories, education, and field studies. The detector output is first amplified using an LM358P operational amplifier and verified using an oscilloscope before being processed by the ESP32 and displayed on the liquid crystal display (LCD). By using the count value, the background radiation level can be estimated [3, 4].

2.0 EXPERIMENT

2.1 Block Diagram of the system

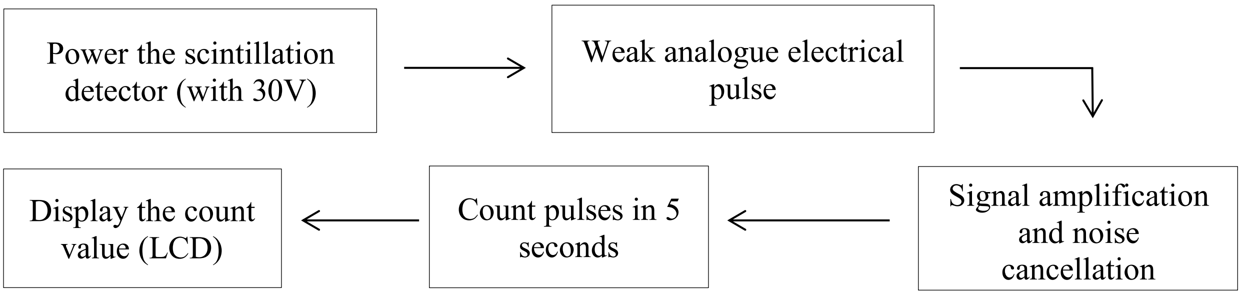

Figure 2.1 Block diagram of the system

The working process of the scintillation detector system is illustrated in Figure 2.1. The detector, powered with 30V, generates weak analogue pulses that undergo amplification and noise cancellation. The processed signals are then counted within a five-second interval, and the corresponding count value is displayed on the LCD.

2.2 Detector output

In this stage, a sodium iodide [NaI(Tl)] scintillation detector was used to detect incident radiation. The detector was powered with the required supply voltage to ensure proper operation. The output signal from the detector which is sown in figure 2.1, consisting of weak analogue pulses generated by radiation interactions, was connected to an oscilloscope. The oscilloscope was used to observe and verify the waveform characteristics, including pulse shape, amplitude, and duration, before further amplification and processing.

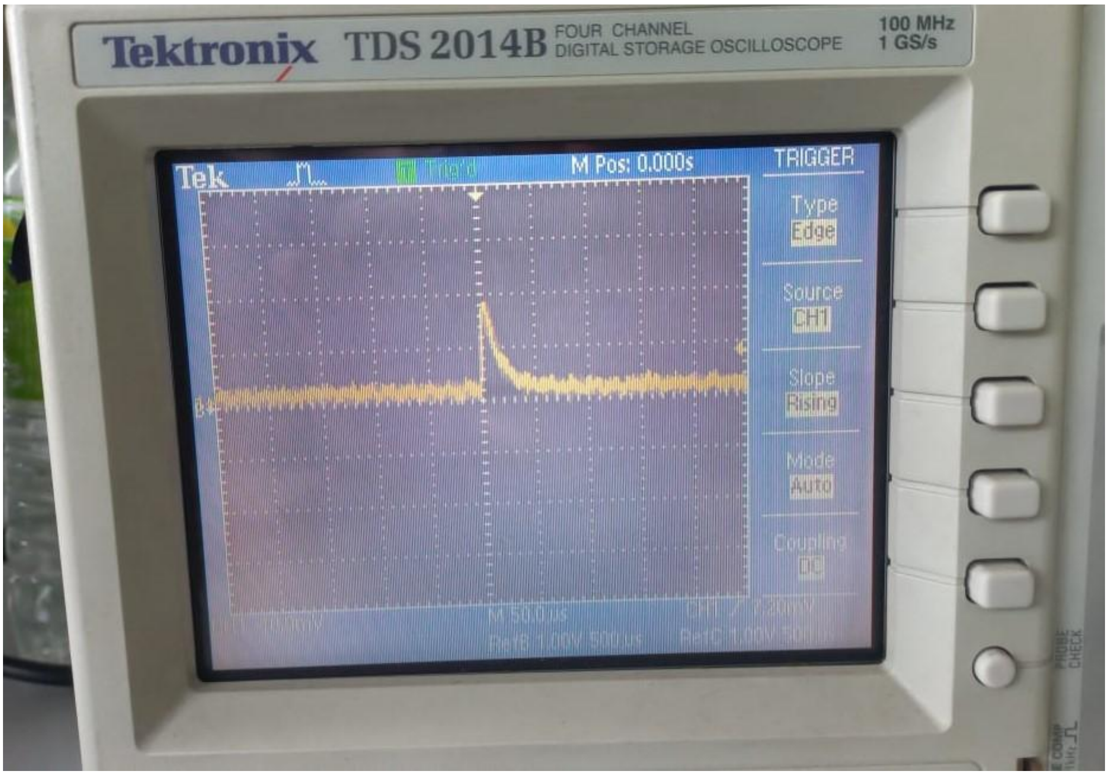

Figure 2.2: Output waveform of scintillation detector

2.3 Pre Amplifier Stage

Once the signal from the scintillation detector, preamplifier enters the device, it will further undergo two pre-amplification stages to filter out the noise and to control the gain. In the first pre amplification stage, the signal is amplified with reference to a variable voltage so that the noise level of the raw signal can be observed and the reference level can be set to reject the noise component of the signal. Here, the Operational amplifier acts as a differential discriminator to filter out certain events. This rejection level can be externally varied from approximately 5 to 450 mV. Also, in this stage, the pulse will undergo a fixed ten-fold amplification.

Once the signal is fed to the second pre amplification stage, it will also experience a variable gain ranging from 1-10 times. This stage is used here to control the gain manually so that any nuclear pulse processed through this device can be maintained within the detection limits of the device. For these two amplification stages, an LM358 dual operational amplifier package was used. As shown in Figure 2.2, the amplifier circuit consists of the two pre-amplification stages described above. The figure highlights how the LM358 dual op-amp is configured to achieve noise rejection and adjustable gain.

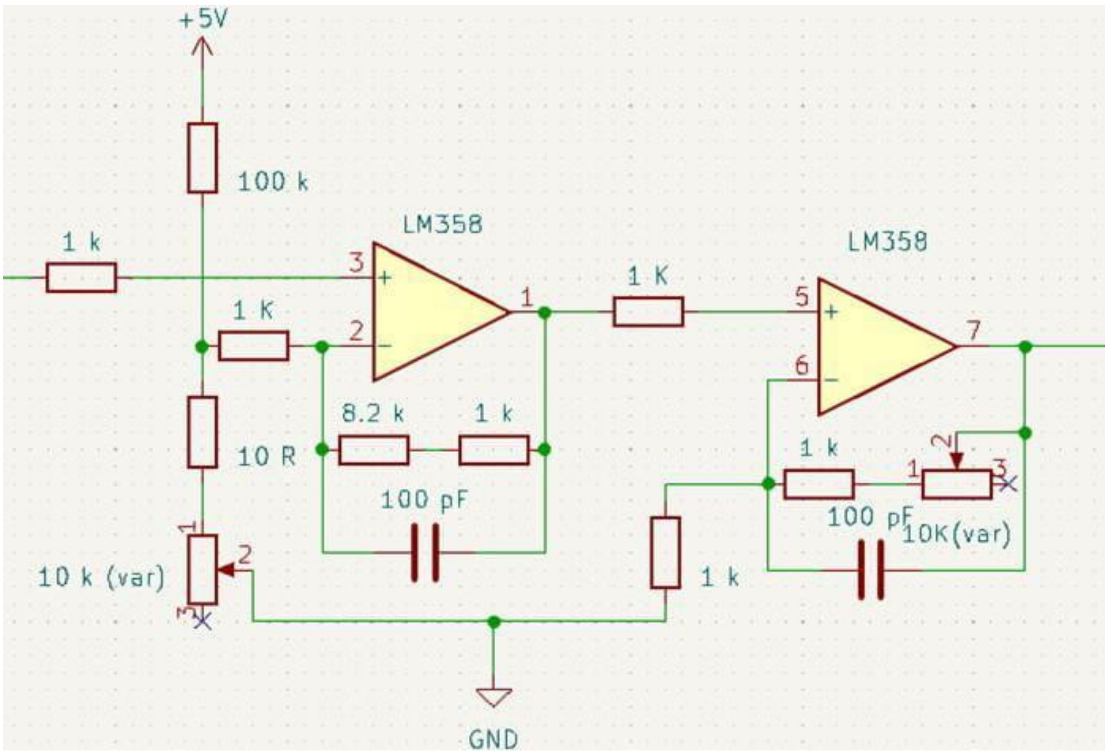

Figure 2.3: Schematics of the pre-amplification stage

$$V_{Ref} = \frac{R_{Var} + R_1}{R_{Var} + R_1 + R_2} \times 5\,V \qquad (2.2.1)$$

Therefore,

$$V_{Ref\,Max} = \frac{10\,k\Omega + 10\,\Omega}{10\,k\Omega + 10\,\Omega + 100\,k\Omega} \times 5\,V = 0.455\,V$$

$$V_{Ref\,Min} = \frac{10\,\Omega}{10\,\Omega + 100\,k\Omega} \times 5\,V = 0.005\,V$$

Theoretical gain:

$$\text{Gain} = 1 + \frac{R_f}{R} \qquad (2.2.2)$$

1st Stage:

$$\text{Gain} = 1 + \frac{8.2\ k\Omega + 1\ k\Omega}{1\ k\Omega} = 10.2$$

2nd Stage:

$$\text{Gain}_{\text{Max}} = 1 + \frac{10\ k\Omega + 1\ k\Omega}{1\ k\Omega} = 12$$

$$\text{Gain}_{\text{Min}} = 1 + \frac{1\ k\Omega}{1\ k\Omega} = 2$$

Equations were used mainly to define the reference voltage and calculate amplifier gain. The 2.2.1 equation set the threshold to reject noise pulses, while the 2.2.2 equation determined both fixed and variable amplification stages. These equations ensured that weak detector signals were properly amplified and filtered before being counted by the ESP32, making the system accurate and reliable for radiation measurement.

2.4 Pulse Counting and Display

The amplified output from the LM358P stage was fed into the ESP32 microcontroller for digital processing. The ESP32 was programmed to detect and count radiation pulses in 5 second above a defined threshold using its interrupt-based input capability. The counted values were then processed in real time and displayed on an LCD module, providing a simple and direct way to monitor the radiation levels. This setup allows the user to easily observe the pulse rate, which can also be related to the background radiation level in the environment.

3.0 RESULTS AND DISCUSSION

3.1 Noise Rejection and Amplification

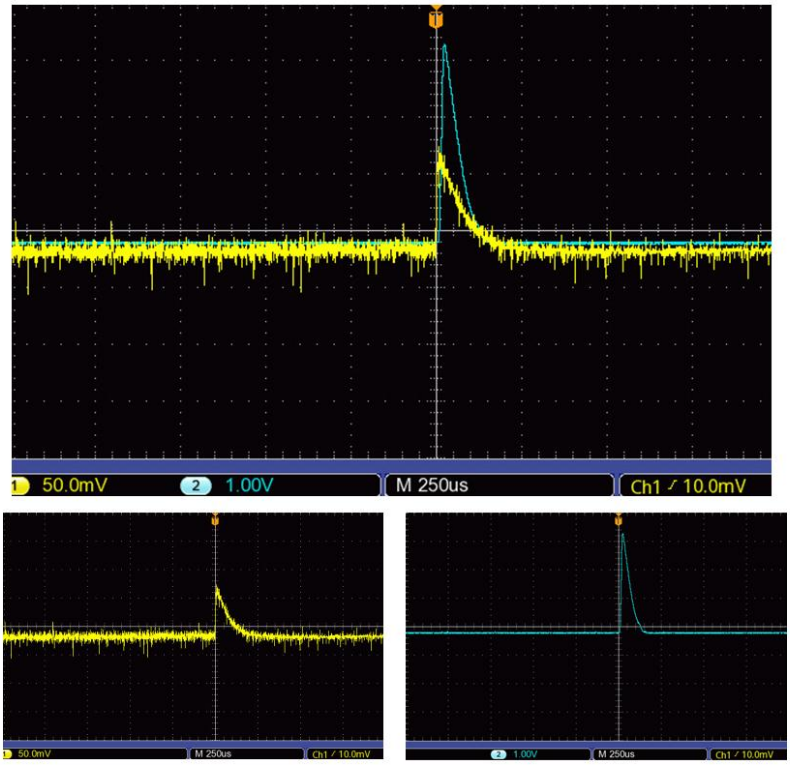

Figure 3.1: (a) output signal from the scintillation detector (yellow) (b) output signal from the pre amplification stage (cyan)

When considering the figure 3.1, it can be clearly observed that the output amplified signal of the pre-amplification state is immune to noises at the input stage. The noise rejection is controlled by setting the reference of the first amplification state. In the observed case noise rejection level has been set to 10 mV.

3.2 Displaying Count Value on the LCD

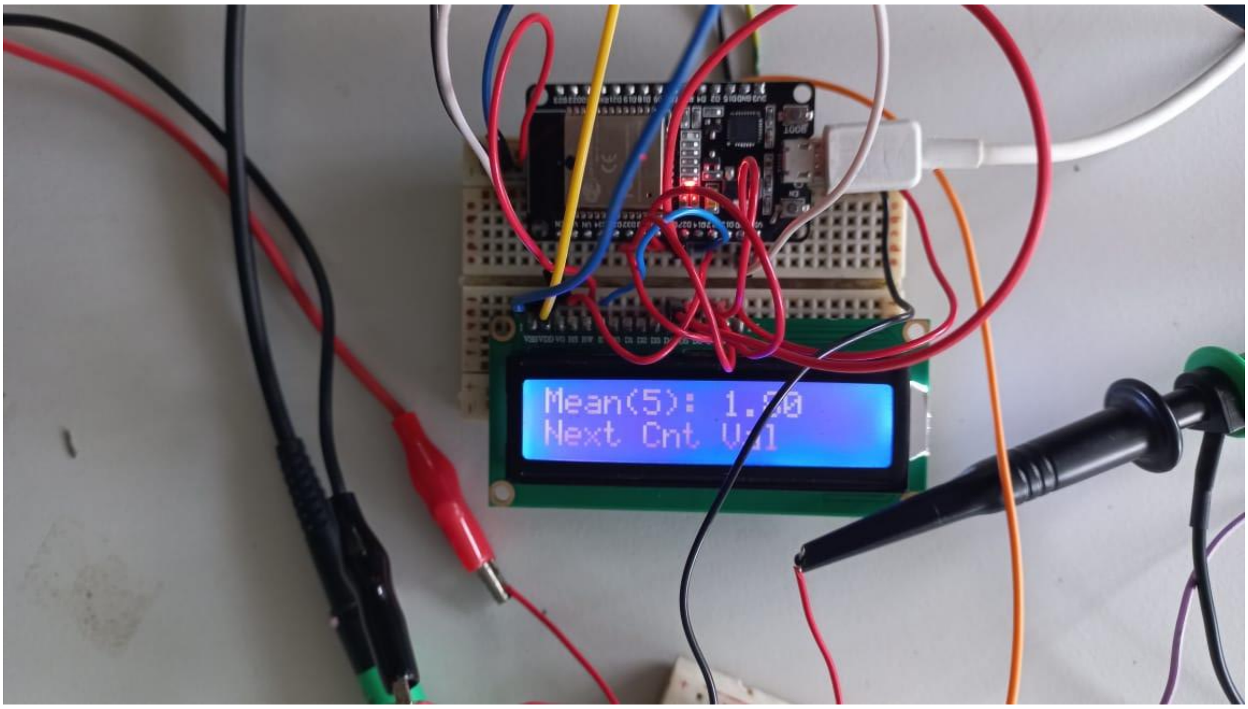

Figure 3.2: Counter output

The system output is presented on an LCD display connected to the ESP32 microcontroller. Instead of showing the raw instantaneous pulse count, the program calculates the mean value of pulses detected over a 5-second interval. This averaging reduces short-term fluctuations and provides a more stable representation of the radiation level. As shown in the figure 3.2, the LCD continuously updates and displays the average count, allowing the user to easily monitor the background radiation level in real time.

1.0 CONCLUSION

The developed microcontroller-based counter successfully demonstrated its ability to detect and process pulses from a NaI(Tl) scintillation detector with accuracy and stability. The dual-stage LM358P amplifier enhanced weak signals while effectively rejecting noise and the ESP32 microcontroller reliably counted pulses and displayed the mean 5-second values on an LCD, providing a clear and stable representation of radiation levels. These results confirm that the system meets the original objective of offering a compact, low-cost alternative to conventional bulky counting electronics, while also aligning with findings reported in similar studies. Although further work such as calibration, automatic gain control, and extended testing would enhance its performance, the study shows that a microcontroller-based approach is a practical and relevant solution for portable radiation monitoring applications.

ACKNOWLEDGMENT

The authors would like to express their gratitude to the Academic Staff of the Faculty of Applied Sciences, Wayamba University of Sri Lanka for their expert advice and guidance.

REFERENCE

[1] PhysicsOpenLab, "SIPM preamplifier," *PhysicsOpenLab*, Mar. 29, 2016. [Online]. Available: https://physicsopenlab.org/2016/03/29/sipm-preamplifier/

[2] E. Enlow and S. Abbaszadeh, "State-of-the-art challenges and emerging technologies in radiation detection for nuclear medicine imaging: A review," *Frontiers in Physics*, vol. 11, Art. no. 1106546, Jan. 2024. [Online]. Available: https://www.frontiersin.org/journals/physics/articles/10.3389/fphy.2023.1106546/full

[3] S. Sharma, "Scintillation counter - definition, scintillation counter principle construction and working," *Physicswave*, Sep. 15, 2023. [Online]. Available: https://physicswave.com/scintillation-counter-principle-construction-and-working/

[4] Mirion Technologies, "Lab Experiment 1: Gamma-Ray Detection with Scintillators," *Mirion Knowledge Hub*. [Online]. Available: https://www.mirion.com/discover/knowledge-hub/articles/education/gamma-ray-detection-with-scintillators-lab-experiment